SYNTHESIS AND *IN VITRO* EVALUATION OF LIPID SIGNALING MODULATORS

Dissertation

zur Erlangung des Doktorgrades

der Naturwissenschaften

vorgelegt beim Fachbereich

Biochemie, Chemie und Pharmazie

der Johann Wolfgang Goethe-Universität

in Frankfurt am Main

von

Estel·la Buscató Arsequell

aus Barcelona

Frankfurt am Main (2013)

(D30)

vom Fachbereich Biochemie, Chemie und Pharmazie der

Johann Wolfgang Goethe-Universität als Dissertation angenommen.

Dekan: Prof. Dr. Thomas Prisner

Gutachter: Prof. Dr. Dieter Steinhilber

Jun. Prof. Dr. Ewgenij Proschak

Datum der Disputation:

“It was like a new world opened to me, the world of science, which I was at last permitted to know in all liberty.”

Marie Curie (1867-1934)

Table of contents

Abbreviations

5-HEDH	5-hydroxyeicosanoid dehydrogenase
5-HETE	5-hydroxyeicosatetraenoic acid
5-HpETE	5-hydroperoxyeicosatetraenoic acid
5-oxo-ETE	5-oxo-eicosatetraenoic acid
5-LO	5-lipoxygenase
15-LO	15-lipoxygenase
15-PGDH	15-hydroxyprostaglandin dehydrogenase
AA	arachidonic acid
ABL	V-abl, Abelson murine leukemia viral oncogene homolog 1
ADP	adenosine diphosphate
AKBA	3-*O*-acetyl-11-keto-boswellic acid
AML	acute myelogenous leukemia
AMP	adenosine monophosphate
ATP	adenosine triphosphate
BCL-2	B-cell lymphoma 2
BCR	break point cluster
BSA	bovine serum albumin
C1P	ceramide-1-phosphate
cAMP	cyclic adenosine monophosphate
CerS	ceramide synthase
CLP	coactosin-like protein
CML	chronic myeloid leukemia
CNS	central nervous system
COPD	chronic obstructive pulmonary disease
COX	cyclooxygenase
$cPLA_{2\alpha}$	cytosolic phospholipase $A_{2\alpha}$
CTP	cytidine triphosphate
CYP	cytochrome P450
CysLT	cysteinyl leukotriene
CysLT1RA	CysLT1 receptor antagonist
DAG	diacylglyceride
DBD	DNA binding domain
DHA	docosahexaenoic acid
DHET	dihydroxyeicosatrienoic acid
DHOME	dihydroxyoctadecenoic acid
D-MAPP	(1*S*, 2*R*)-D-*erythro*-2-(N-myristoylamino)-1-phenyl-1-propanol
EC_{50}	half maximal effective concentration
EDTA	ethylene diamine tetraacetate
EGFR	epidermal growth factor receptor
EH	epoxide hydrolase
eNOS	endothelial nitric oxide synthase
EP	PG receptor
EPA	eicosapentaenoic acid
EPOME	epoxyeicosadecenoic acid
ER	endoplasmatic reticulum
ERK1/2	extracellular signal-regulated kinase ½
FAP	familial adenomatous polyposis
FDA	Food and Drug Administration
FGF_2	fibroblast growth factor 2
FLAP	5-LO activating protein
fMLP	N-formyl-leucyl-phenylalanine
GC	glucocorticoid

GI	gastrointestinal tract
GPCR	G-protein coupled receptor
GPx	glutathione peroxidase
GSH	glutathione
HPLC	high performance liquid chromatography
HWB	human whole blood
EET	epoxyeicosatrienoic acid
HDL	high-density lipoprotein
HETE	hydroxyeicosatetraenoic acid
IBD	inflammatory bowel disease
IC_{50}	half maximal inhibitory concentration
IL	interleukin
K_a	affinity constant
LBD	ligand binding domain
LC-MS/MS	liquid chromatography coupled to tandem mass spectrometry
LDH	lactate dehydrogenase
LDL	low-density lipoprotein
LM	lipid mediators
LO/LOX	lipoxygenase
LOOH	lipid hydroperoxide
LPA	lysophosphatidic acid
LPC	1-O-alkyl-lysophosphatidylcholine
LPS	lipopolysaccharide
LSC	leukemia stem cells
LT	leukotriene
LTA_4	leukotriene A_4
LTB_4	leukotriene B_4
LTC_4	leukotriene C_4
LTD_4	leukotriene D_4
LTE_4	leukotriene E_4
LT	leukotriene
MAPEG	membrane-associated proteins in eicosanoid and glutathione metabolism
MAPK	mitogen-activated protein kinase
mEH	microsomal epoxide hydrolase
MDR	multi-drug resistance protein
MetS	metabolic syndrome
mPGES-1	microsomal PGE_2 synthase-1
MS	mass spectrometry
NBDNJ	N-butyldeoxynojirimycin
NDGA	nordihydroguaiaretic acid
NDSAID	non-steroidal anti-inflammatory drug
NF-κB	nuclear factor κB
NO	nitric oxide
NOE	N-oleoylethanolamine
NSAID	non-steroidal anti-inflammatory drug
OAG	1-oleoyl-2-acetyl-sn-glycerol
PAF	platelet activating factor
PAI-1	plasminogen activator inhibitor-1
PBS	phosphate buffered saline
PC	phosphatidylcholine
PDMP	1-phenyl-2-decanoylamino-3-morpholino-propanol
PG	prostaglandin
PGB_1	prostaglandin B_1
PGD_2	prostaglandin D_2

PGE_2	prostaglandin E_2
$PGF_{2\alpha}$	prostaglandin $F_{2\alpha}$
PGG_2	prostaglandin G_2
PGH_2	prostaglandin H_2
PGHS	prostagladin H_2 synthase
PGIS	PGI_2 synthase
PGI_2	prostacyclin
PK	pharmacokinetic
PKA	protein kinase A
PKC	protein kinase C
PKCζ	protein kinase C ζ
PLA_2	phospholipase A2
PMNL	polymorphonuclear leukocytes
PPAR	peroxisome proliferator activated receptor
PPRE	peroxisome proliferator response element
PUFA	polyunsaturated fatty acid
RAF	proto-oncogene serine/threonine-protein kinase
RBL-1	rat basophilic leukemia-1
RE	response elements
ROS	reactive oxygen species
RXR	retinoid X receptor
S1P	sphingosine-1-phosphate
$S1P_1$	S1P receptor
SDS PAGE	sodium dodecyl sulfate polyacrylamide gel electrophoresis
sEH	soluble epoxide hydrolase
sEHI	soluble epoxide hydrolase inhibitor
sEHp	soluble epoxide hydrolase phosphatase
SEM	standard error of the mean
SL	sphingolipid
SMase	sphingomyelinase
SPPARM	partial and selective PPAR modulators
SPT	serine palmitoyl transferase
TGF-α	transforming growth factor-β
TNF-α	tumor necrosis factor alpha
TP	thromboxane receptor
TRPV4	transient potential cation channel, subfamily V member 4
TZD	thiazolidinedione
TXA_2	thromboxane A_2
UTP	uridine-5'-triphosphate
VEGF	vascular endothelial growth factor
WST-1	water soluble tetrazolium salts

Introduction

1. Lipid mediators

Lipids are the major components of the cellular membranes[1] of all organisms. Due to the physicochemical properties (amphipathic, hydrophobic) of lipid molecules, the structure of cellular membrane is a lipid bilayer. Lipids are the most efficient source of energy and excessive storage[2] while decreased lipid use results in energy misbalance and can lead to the development of metabolic syndrome[3]. Lipid molecules can also function as intercellular signaling molecules in different processes such as immune self-defense and homeostasis maintenance. Because of these properties, lipid mediators (LM) can be regarded as local hormones or autacoids, whose information cannot be directly read out from the genome but genes, encoding a particular group of proteins that are essential for their biosynthesis (enzymes), transport (transporters) and signal transduction (receptors) can be indirectly manipulated. LMs[4] play an important role in the regulation of cell proliferation and differentiation, the reproductive, gastrointestinal and cardiovascular systems, as well as inflammatory[5,6] and immune responses[5]. Dysregulation of LMs has been linked to various diseases such as inflammation, infertility, atherosclerosis, ischemia, metabolic syndrome, allergy, degenerative[7] diseases and cancer[8,9]. LMs are produced locally through specific biosynthesis pathways in response to extracellular stimuli. They are exported extracellularly, bind to the corresponding G protein-coupled receptors (GPCRs)[10] to transmit signals to target cells, and are then sequestered through specific enzymatic processes.

LMs can be structurally divided into three classes. Class 1 includes arachidonic acid (AA)-derived eicosanoids comprising prostaglandins (PGs), leukotrienes (LTs), thromboxanes (TXs) and their relatives. The importance of this field was recognized with the award of the Nobel Prize in physiology and medicine in 1982 to John R. Vane, Sune K. Bergström, and Bengt I. Samuelsson[11] for their collective work[12] on the biochemistry and physiologic activities of AA metabolites. Class 2 includes lysophospholipids, platelet-activating factor (PAF), lysophosphatidic acid (LPA) and sphingosine-1-phosphate (S1P) latter discussed in ceramide metabolism (chapter 4.1). Endocannabinoids can also be classified in this group, since the hallmark endocannabinoid, 2-arachidonoyl-glycerol, has a glycerol backbone. Class 3

represents newly identified anti-inflammatory LMs derived from ω-3-polyunsturated fatty acids (PUFAs), such as resolvins (derived from eicosapentaenoic acid (EPA) and protectins (derived from docosahexaenoic acid (DHA)).

1.1 Eicosanoids

Eicosanoids consist of several large families derived from polyunsaturated fatty acids (ω-3, ω-6 fatty acids). They are generated via the oxidation of 20-carbon chain fatty acids. Prostanoids and LT are generated by cyclooxygenases (COX) and lipoxygenases (LO) respectively[13] (Figure 1). Five major bioactive prostanoids are known, namely PGE_2, PGD_2, PGI_2, and thromboxane A_2 (TXA_2)[14]. COX catalyzes the incorporation of two oxygen molecules into AA (previously released from membrane glycerophospholipids by various phospholipases A_2 (PLA_2)[15] subtypes[16]) to form PG endoperoxides, which are converted into various types of PGs by terminal PG synthases. Two isoforms[17,18] have been identified from COX enzymes: a constitutive form (COX-1) and an inducible form (COX-2). Aspirin[19] inhibits the activity of both enzymes through acetylation. PGD_2 has been related to the regulation of sleep[20], allergy[21] and adiposity[22] and TXA_2 is involved in thrombosis[23], platelet aggregation and atherosclerosis. PGE_2 is associated with many pathological events such as inflammation[24], fever, pain and cancer[25] through its receptors EP1 to EP4[26]. PGE_2 is formed from AA by COX-1 and COX-2-catalyzed formation of prostaglandin H_2 (PGH_2) and further transformation by PGE synthases. The isomerization of the endoperoxide PGH_2 to PGE_2 is catalyzed by three different PGE synthases, cytosolic PGE synthase (cPGES) and two membrane-bound PGE synthases, mPGES-1 and mPGES-2[27].

Bioactive LTs, including LTB_4 and cysteinyl LTs (LTC_4, LTD_4 and LTE_4) are critical LMs involved in asthma[28] and they are produced by lipoxygenases[29]. In mammals, six different types of LO are named according to the carbon position at which a single oxygen molecule is incorporated: 5-lipoxygenase (5-LO), 8/12-lipoxygenase, two types of 12-lipoxygenase (12*S* and 12*R*) and two types of 15-lipoxygenase (15-LO1 and 15-LO2). 5-LO is a dioxygenase that catalyzes the incorporation of oxygen and subsequent dehydration to produce the unstable allylic epoxide LTA_4 which is further converted to LTB_4 or LTC_4 by LTB_4 hydrolase or LTC_4 synthase respectively[6,30]. LTB_4 is a chemoattractant and regulator of immune responses whereas cysteinyl-LTs are major components of the inflammatory reaction through CysLT receptors[31,32]. LT are

important LMs in processes such as inflammation, allergy, bronchoconstriction[33] and cancer[34].

Although PG and LT are the best known eicosanoids, AA is also a substrate for another enzymatic pathway, the cytochrome P450[35] (CYP) system[36]. This pathway consists of two main branches: ω-hydroxylases which convert AA to hydroxyeicosatetraenoic acids (HETEs) and epoxygenases that convert AA to four regioisomeric epoxyeicosatrienoic acids (EETs; 5,6-EET, 8,9-EET, 11,12-EET and 14,15-EET). HETEs are involved in inflammation and vascular function[37].

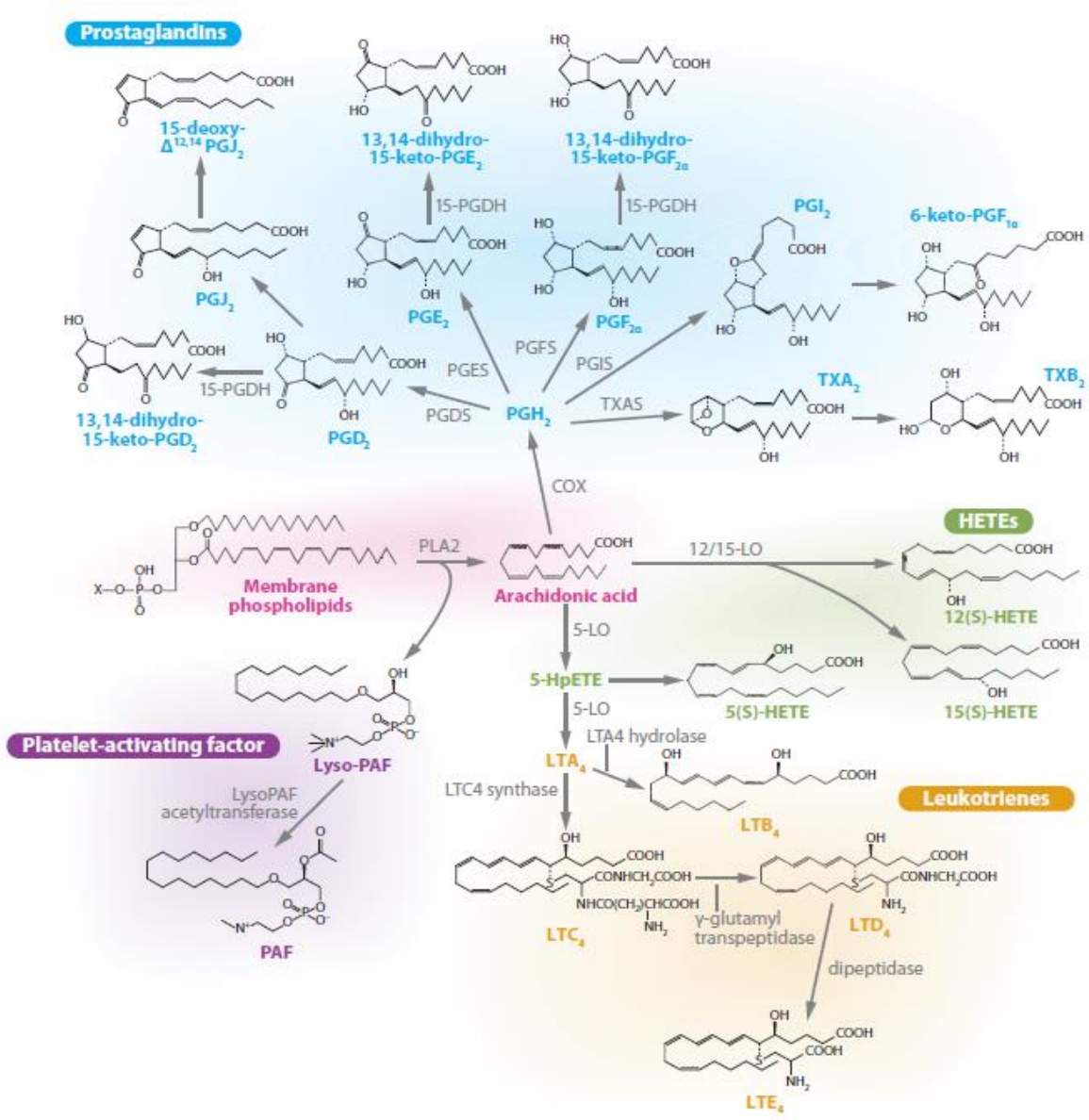

Figure 1. Biosynthetic pathways of eicosanoids and PAF[4].

EETs are hydrolyzed (Figure 2) to the less biologically active[38] dihydroxyeicosatrienoic acids (DHETs) by soluble epoxide hydrolase (sEH). EETs[39,40] can act in a paracrine or autacrine manner, inducing vasodilatory and anti-inflammatory effects in blood vessels, are beneficial in lowering blood pressure, and protect the brain and myocardium from ischemia. Moreover, EETs stimulate tube formation and renal epithelia cell proliferation[41] and survival[42], pointing out the clinical relevance of targeting enzymes metabolizing these LMs. Latter the biological effects of EETs are discussed in chapter 3.2.

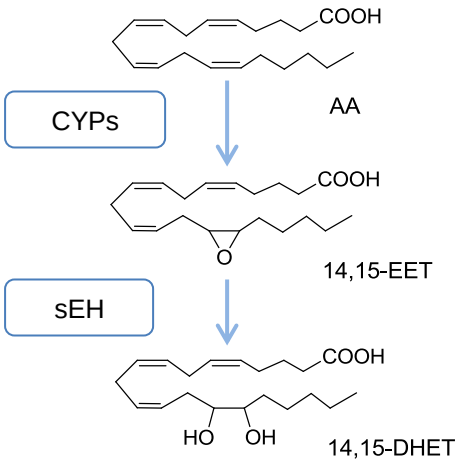

Figure 2. AA metabolism to 14,15-DHETs.

1.2 Lysophospholipids

PAF is produced from 1-O-alkyl-lysophosphatidylcholine (LPC) by LPA_2 followed by its acetylation by LPC acyltransferase 2[43]. It is a particular LM in inflammation and allergy[44,45]. LPA is produced extracellularly from LPC by autotaxin and it is degraded by a class of lipid phosphates[46] (possibly sEH phosphatase domain, discussed in chapter 3.1). LPA is involved in brain development, neuropathic pain and pulmonary fibrosis. S1P is structurally similar to LPA[47] and both have relatively long half-lives (minutes to hours), it is synthesized by sphingosine kinase[48] (1 and 2) and it regulates different biological processes such as anaphylaxis[49], cancer[50] and lymphocyte egress[51] from both primary and secondary lymphoid tissues through binding to S1P receptor ($S1P_1$). Modulation of $S1P_1$ through the use of agonism, leads to an immunosuppressive[52,53] response. A crosstalk between S1P and eicosanoids has been found since S1P

stimulates the induction of COX-2[54], while ceramide-1-phosphate (C1P)[55] (further discussed in chapter 4) is important for PLA_2 activation at the Golgi membrane.

1.3 ω-3 PUFA derivatives

Discovered by Serhan[56] and Bazan, these ω-3 LMs such as resolvins, protectins, maresins and lipoxins (derived from ω-6 AA) have recently attired the attention due to their critical role in inflammation[57,58]. Biosynthesis of these anti-inflammatory LMs from PUFAs involves 15/5-LO and other enzymes like COX-2 (Figure 3).

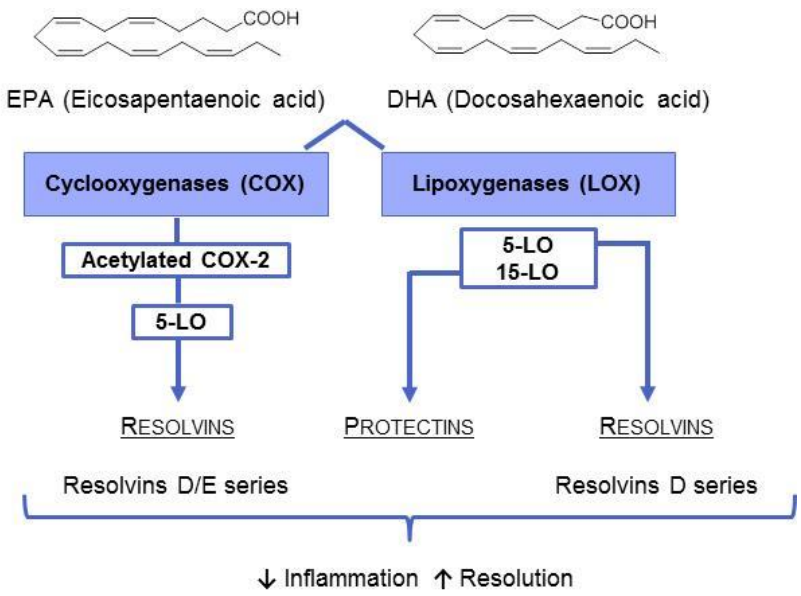

Figure 3. Bioactive eicosanoids derived from the ω-3 family.

1.4 Receptors for lipid mediators

Nearly 350 different GPCRs have been identified. From this large number, 30 correspond to lipid receptors[10]. On the basis of homology with TP (thromboxane receptor[59], the first cloned) seven additional PG receptors[60] have been discovered. The most well-known are EP receptors that have been related to PGE_2 recognition. Regarding LT receptor, LTB_4 is the most potent chemotactic compound for neutrophils, eosinophils and macrophages, it binds to BLT_1 and BLT_2, latter can also bind other HETEs[61]. Also for the monohydro(pero)xylated eicosanoids (5-HpETE and for 5-oxo-ETE, Figure 6), the existence of specific GPCRs (called OXE[62] receptors) have been described. The cannabinoid receptors CB_1 and CB_2 also interact with lipid ligands. CB_1 expressed in central nervous system and CB_2 primarily in immune cells they bind bile

acids, lysophosphatidylserine, or lysophosphatidylinositol; they can also bind EETs in a low micromolar range: 20 µM for 5,6-EET[63]. As a last group, nuclear receptors as LM receptors[64] can be found, that interact together to modulate some pathophysiological state of cellular system. In certain cases, certain PG and their metabolites[65] bind to nuclear receptors such as peroxisome proliferator-activated receptors (PPAR). Nuclear receptors are further discussed in chapter 3.3.

1.5 Lipid mediators in health and diseases

LMs have been historically considered terminal mediators[66], causing symptoms like fever, pain, edema, muscle contraction and inflammation. However, recent studies have revealed that LMs play a fundamental role as signaling molecules[67–73]. Moreover enzymes and receptors involved in LM signaling have been and are still being targeted pharmacologically to alleviate the symptoms of various diseases (asthma, allergy, etc.). A discussion of the pathophysiological roles of LMs[66] is beyond the scope of this study and therefore the main focus is the relationship of LMs in cancer.

1.5.1 Lipid mediators in cancer

Epidemiological data supports that about 20% of cancer deaths are linked to inflammation and chronic infections[74]. As an example, inflammatory bowel diseases can lead to colorectal cancer[75,76]; prostatitis can lead to prostate cancer[77]. Most precancerous and cancerous tissues have the typical hallmark of inflammation[78]: cytokines and chemokines. Tumor growth[79–83] requires intercellular communication that is conducted by several soluble factors like vascular endothelial growth factor (VEGF), fibroblast growth factor 2 (FGF_2), transforming growth factor-β (TGF-β), tumor necrosis factor-α (TNF-α), interleukin-1 (IL-1) and oxygen free radicals. One of the main focuses of this work is to synthesize inhibitors of enzymes producing LMs with an important role in cancer, nevertheless with special emphasis on eicosanoids. Animal studies provide evidence that activation[84,85] of COX and LO pathways during chronic inflammation and carcinogenesis results in aberrant metabolism of AA, which may be one mechanism for the contribution of dietary fats to carcinogenesis.

Moreover, COX and PG have been demonstrated to be involved in tumorigenesis[86], tumor progression, metastasis and angiogenesis. PGE_2 is the most common PG found in different human cancers including colon, lung, breast, head and neck cancers. The up-regulation[87] of PGE_2 is associated with poor prognosis[88]. Cancer patients with

tumors having increased COX-2 expression exhibit decreased survival rates. Recent studies have evaluated the role of PG and COX in tumor progression under hypoxic conditions[89,90] and moreover, COX-2 is up-regulated by hypoxia in human vascular endothelial cells. Genetic deletion of microsomal PGE_2 synthase 1 (mPGES-1), which generates PGE_2, results in suppression of intestinal cancer growth by 66-95%[91]. In addition to inhibition of PG production to overcome tumor growth, another strategy is the overexpression of eicosanoid metabolizing enzymes like 15-hydroxyprostaglandin dehydrogenase[92] (15-PGDH), responsible for the degradation of PGE_2. 15-PGDH is down-regulated[93] in numerous human cancers. Lack of 15-PGDH expression in these tumors results in increased endogenous PGE_2 levels. PGE_2 up-regulates B-cell lymphoma 2 (BCL-2)[94], an antiapoptotic protein, and induction of nuclear factor κB (NF-κB). It has been demonstrated the effective anti-tumor activity of COX-2 inhibitors in inflammation-associated cancers, like colorectal carcinoma[95,96]. Celecoxib reduced the adenoma size and number in patients with familial adenomatous polyposis[97,98] (FAP). Two clinical trials (NCT00151476, NCT00685568) demonstrated significant reduction of adenoma growth but they were terminated due to cardiovascular toxicity[99] and death. Nevertheless, the Food and Drug Administration (FDA) approved celecoxib for the treatment of colon and rectal polyps in patients with FAP that did not have atherosclerotic disease.

The LO pathway has also an important role in tumor progression[100] and survival[101,102]. LOs mediate invasion of intrametastatic[103] lymphatic vessels and lymph node metastasis in mammary carcinoma. Abundance of 5-LO mRNA[104] has been investigated in human brain tumors, the increased expression of 5-LO has been linked with the progression and development of pancreas, breast, kidney cancers[100]. LTB_4 can promote the growth of melanoma. Moreover, a LTB_4 antagonist, LY29311[105]1 inhibited colon cancer growth and induced apoptosis *in vitro*. Another metabolite produced by 5-LO, 5-HETE can stimulate the proliferation of prostate cancer cells and act as survival factor when added exogenously[106]. The combination of COX-2 and 5-LO inhibitors inhibited tumor growth in several tumor models[107–109] (lung, colon, skin and pancreas). This inhibition[110] was accompanied by the down-regulation of LTB_4 and PGE_2, which stimulate both epithelial and stromal cells to produce VEGF and FGF-2. These angiogenic products induce COX-2 and in turn PGE_2 and PGI_2 creating a feedback loop. 12-HETE has been shown to be involved in cancer cell growth, inhibition of 12-LO blocks cell proliferation and induces apoptosis (Figure 4). Moreover, 12-LO is highly expressed in ovarian cancer[111] patients. Another LO that contributes to

inflammation and cancer development is 15-LO-1[112,113], which is expressed in cancers like Hodgkin lymphoma and colorectal cancer. While 5-HETE and 12-HETE have pro-tumorigenic activity, HETEs such as 8-HETE and 11-HETE are reported to have anti-tumor activity. 8*R*-LO[114] has been identified as an anti-tumorigenic, tumor suppressing enzyme and its metabolite 8-HETE induces growth inhibition in premalignant epithelial cells.

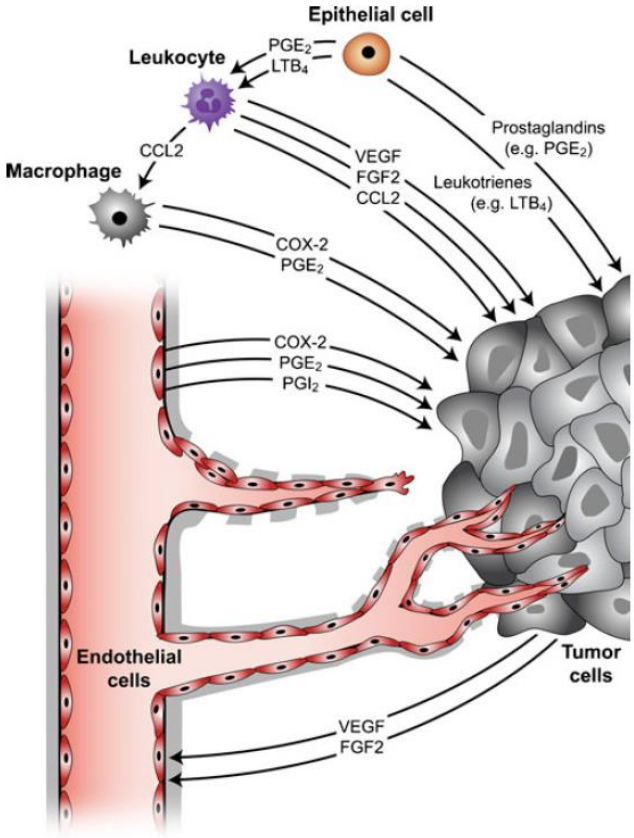

Figure 4. Eicosanoids in cancer and the tumor environment[115]. PGE_2 and LTB_4 stimulate to produce VEGF and FGF-2 in an autocatalytical loop.

Most of LO-derived HETEs[116] inhibit apoptosis, stimulate angiogenesis and enhance proliferation. 20-HETE produced by the CYP ω-hydroxylation pathway is a pro-inflammatory mediator that stimulates IL production: IL-8, 12, 4 and PGE_2. 20-HETE has pro-angiogenic activities[117] and plays an important role in VEGF dependent angiogenesis.

5-LO gene (*Alox5*) has recently attired the attention as possible target gene to treat leukemia, in particular chronic myeloid leukemia (CML). CML[118] is the first malignancy to be linked to a genetic abnormality, a chromosomal translocation: t(9:22) known as

the Philadelphia chromosome. As a result part of the BCR[119] ("breakpoint cluster region") gene from chromosome 22 is fused with the ABL (V-abl, Abelson murine leukemia viral oncogene homolog 1) gene on chromosome 9. The resultant abnormal protein is a tyrosine kinase that can be inhibited by tyrosine kinase inhibitors such as imatinib, dasatinib or nilotinib. *Alox5* gene resulted to be a critical regulator for leukemia stem cells (LSCs) in BCR-ABL induced CML[120]. In the absence of *Alox5* gene, BCR-ABL failed to induce CML in mice. This deficiency did not cause impairment in the function of normal hematopoietic stem cells, highlighting *Alox5* and the corresponding gene product 5-LO as a possible treatment for CML stems cell that are not sensitive to BCR-ABL kinase inhibitors. Moreover, Chen *et al*. demonstrated[121,122] that treatment with zileuton[123] (a well-known 5-LO inhibitor, approved by the FDA) suppressed leukemia stem cells in CML mice, inhibited *Alox5* function and coadministration with imatinib had a better therapeutic effect that zileuton or imatinib alone[a]. An *in vitro* study also supports the role of *Alox5* in CML, with the study of CML blast cell in culture with 5-LO inhibitors which reduced cell proliferation[124].

2. Leukotriene signaling

LTs are part of the lipid signaling that uses information in an autocrine or paracrine form to regulate immune responses and other pathophysiological processes[125]. They are expressed[126] in leukocyte, macrophagues and other tissues[126,127] and cells in response to immunological and nonimmunological[127] stimuli. LT production is normally accompanied by the production of histamine and PGs. Nevertheless LTs are three to four orders of magnitude more potent and with longer half-times comparing to histamine[128]. LOs metabolize AA into the corresponding 5-, 8-, 12- and 15-HETE and in the context of tumor development they can be divided into pro-tumor (5-HETE, 12-HETE) and antitumor LTs (15-HETE). In this work 5-LO inhibitors have been extensively studied and discussed in the following chapter.

[a] University of Massachusetts Medical School, Phase I Study to Evaluate the Safety of Zileuton (Zyflo) in Combination With Imatinib Mesylate (Gleevec) in Patients With Chronic Myelogenous Leukemia, Clinical trial identifier:NCT01130688

2.1. 5-lipoxygenase

AA appears in the cell as an esterified phospholipid in the *sn*-2 position[129]. To increase intracellular levels of AA for the LT biosynthesis a phospholipase is required to release the fatty acid. Typically, PLA_2 a cytosolic PLA_2 group[15] IV ($cPLA_{2\alpha}$)[130] is in charge of starting the LT machinery. Mice deficient in this enzyme are unable to synthetize LT regardless[131] which stimuli was used. $cPLA_{2\alpha}$ possesses in its amino terminal part, a putative Ca^{2+}- dependent phospholipid binding. As mentioned before, $cPLA_{2\alpha}$ is activated by C1P and by phosphorylation of Ser505. It hydrolyzes the ester bond by a so-called "serine protease" mechanism in which the Ser228-Asp549 dyad plays a major role and Arg200 a secondary.

5-LO is a dioxygenase (EC 1.13.11.34) that catalyzes the incorporation of both atoms of molecular oxygen into AA (previously released by $cPLA_{2\alpha}$ and transferred via 5-LO activating protein (FLAP)[132,133] in two steps[134,135]: in a concerted reaction to give the hydroperoxide 5(*S*)-hydroperoxy-6-*trans*-8,11,14-*cis*-eicosatetraenoic acid (5-HpETE) which accounts a pseudoperoxidase activity, as well as the following dehydration to the unstable epoxide LTA_4[11,136]. The second step is a pseudolipoxygenation and it involves the abstraction of hydrogen at C-10 followed by a radical migration to C-6 and rearrangement (Figure 5). The radical combines with the 5(*S*)-hydroperoxy group which leads to a dehydration.

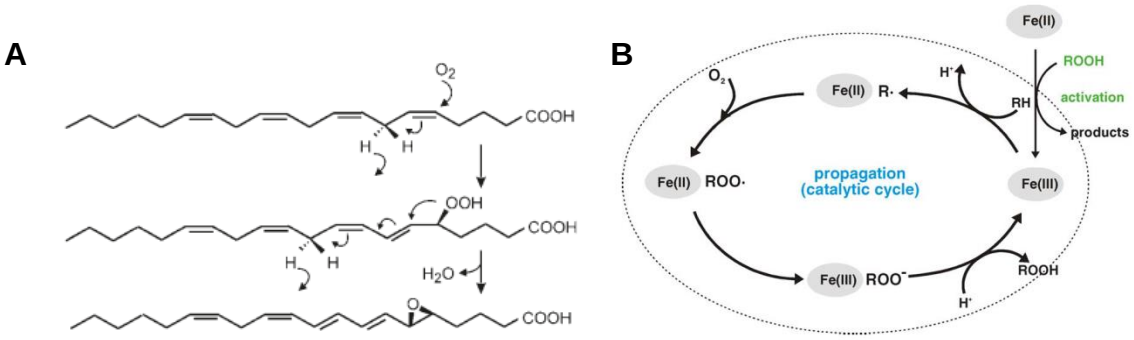

Figure 5. A. Biosynthesis of LTA_4 from AA[137]. **B.** Catalytic cycle involving lipid peroxides (LOOH)[138].

The subsequent conversion of LTA_4, by LTA_4 hydrolase leads to LTB_4, and/or the conjugation with glutathione (GSH) by LTC_4 synthase yields the LTC_4, depending on the cell type and the enzymes present[6,30]. In addition to the conversion to LTA_4, the 5-HpETE can be reduced to the resultant alcohol 5-HETE[139] (Figure 6).

5-HETE can be further oxidized by 5-hydroxyeicosanoid dehydrogenase (5-HEDH) obtaining 5-oxo-eicosatetraenoic acid (5-oxo-ETE) a highly potent granulocyte chemoattractant[140], eliciting a response time higher than PAF and 30-40 times higher than LTB_4 and LTD_4.

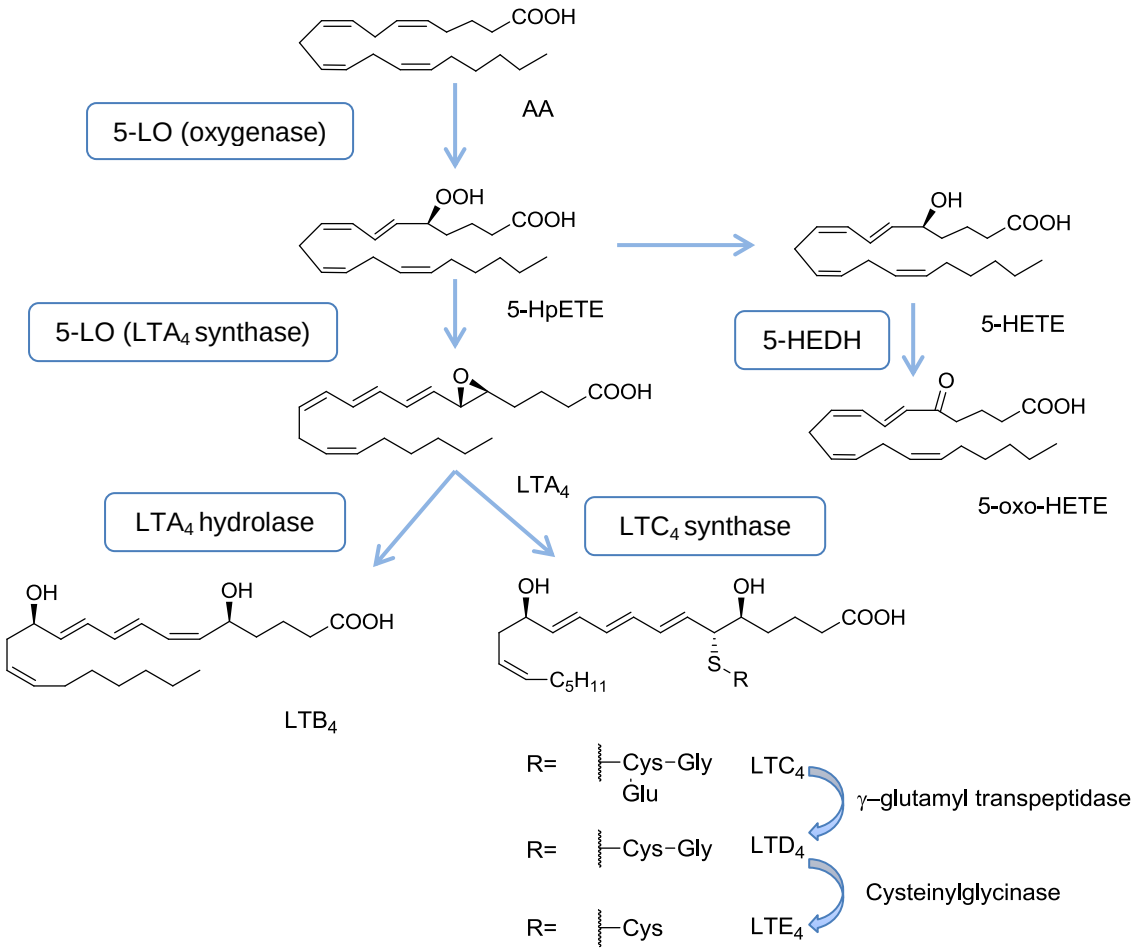

Figure 6. LTs biosynthesis.

The human 5-LO (Figure 7) consists of 673 aminoacids with a molecular weight of 78 kDa. 5-LO can form dimers[141] and the recently resolved crystal structure of the stable form of the 5-LO (PDB: 3o8y)[142] has revealed two distinct domains: the N-terminal regulatory domain so called “C2-like” domain (114 amino acids, 115-663), which in 5-LO confers Ca^{2+}-dependent membrane[143,144] binding (18–21 amino acids), and the larger catalytic domain. The C2-like domain, organized in a β-sandwich is important[145] for the membrane, Ca^{2+} and diacylglycerides[146] binding. The binding site for cellular membrane or phosphatidylcholine (PC) is defined by three tryptophan residues[147] (Trp13, 75 and 102). The catalytic domain (121-673) is primarily α-helical and harbors

the non-heme catalytic iron[142]. The iron is coordinated[148] by three conserved histidines (His 367, 372, and 550), as well as the main-chain carboxylate of the C terminus (Ile673) forming a 2-His-1-carboxylate-triade.

Two other amino acids in 5-LO, Glu376 and Gln558 are functionally important and they were discovered through mutagenic studies. 5-LO has an ATP binding site located between the C2-like domain (Lys73 to Lys83) and the catalytic domain (Phe193 to Phe209) in the dimeric form. In the inactive form of the enzyme, the iron is Fe^{2+} (ferrous) and the enzyme is not capable of converting AA to the corresponding LTs. Fe^{2+} has to be oxidized by lipid hydroperoxides (LOOH) to the active Fe^{3+} to perform the catalytic cycle[149] (Figure 5). 5-LO activity is strongly stimulated by Ca^{2+}, which binds to the C2-like domain and thus increases the affinity for binding AA[150] to facilitate membrane association and binding to PC vesicles and appears to reduce the requirement of 5-LO for activating LOOH.

The enzyme 5-LO is a soluble enzyme that can reside in either in the cytoplasm or the nucleus[151]. The subcellular location of 5-LO is regulated, with nuclear import commonly leading to increased LT biosynthesis[152] (Figure 9). 5-LO can be found[153,154] in blood leukocytes (granulocytes), monocytes/macrophagues, mast cells, B-lymphocytes and dendritic cells but not in platelets, endothelial cells and erythrocytes.

2.1.1. 5-LO regulation

It has been shown that 5-LO activity can be regulated by several cellular stimuli (Figure 9). Stimulation by relevant agonist such as Ca^{2+}-mobilizing agents (ionophores) and soluble agonists (previously described PAF, formyl-methionyl-leucyl-phenylalanine (fMLP)). 5-LO activity is strongly dependent of FLAP[148] in intact cells, *in vitro* 5-LO can be activated in the absence of FLAP[150,155]. FLAP is a protein without known catalytic activity that belongs to the MAPEG family (membrane-associated proteins in eicosanoid and glutathione metabolism) and it is expressed in the nuclear envelope where it facilitates the transfer of AA from $cPLA_{2\alpha}$ to 5-LO.

2.1.1.1. Ca^{2+} regulation

Native 5-LO purified from human leukocytes[156] is activated by Ca^{2+} in a 2:1 stoichiometry. Ca^{2+} binds to the N-terminal C2-like domain and increases the affinity of 5-LO towards AA and also towards activating LOOH. It stimulates 5-LO translocation to the nuclear membrane and causes binding to PC. Nevertheless, in homogenates of

human polymorphonuclear leukocytes (PMNL) and rat basophilic leukemia-1[157] cells (RBL-1) 5-LO product formation is detected in the absence of Ca^{2+}. Activation of 5-LO by Ca^{2+} requires the presence of PC or coactosin-like protein[158] (CLP) that promotes the LTA_4 synthase function of 5-LO.

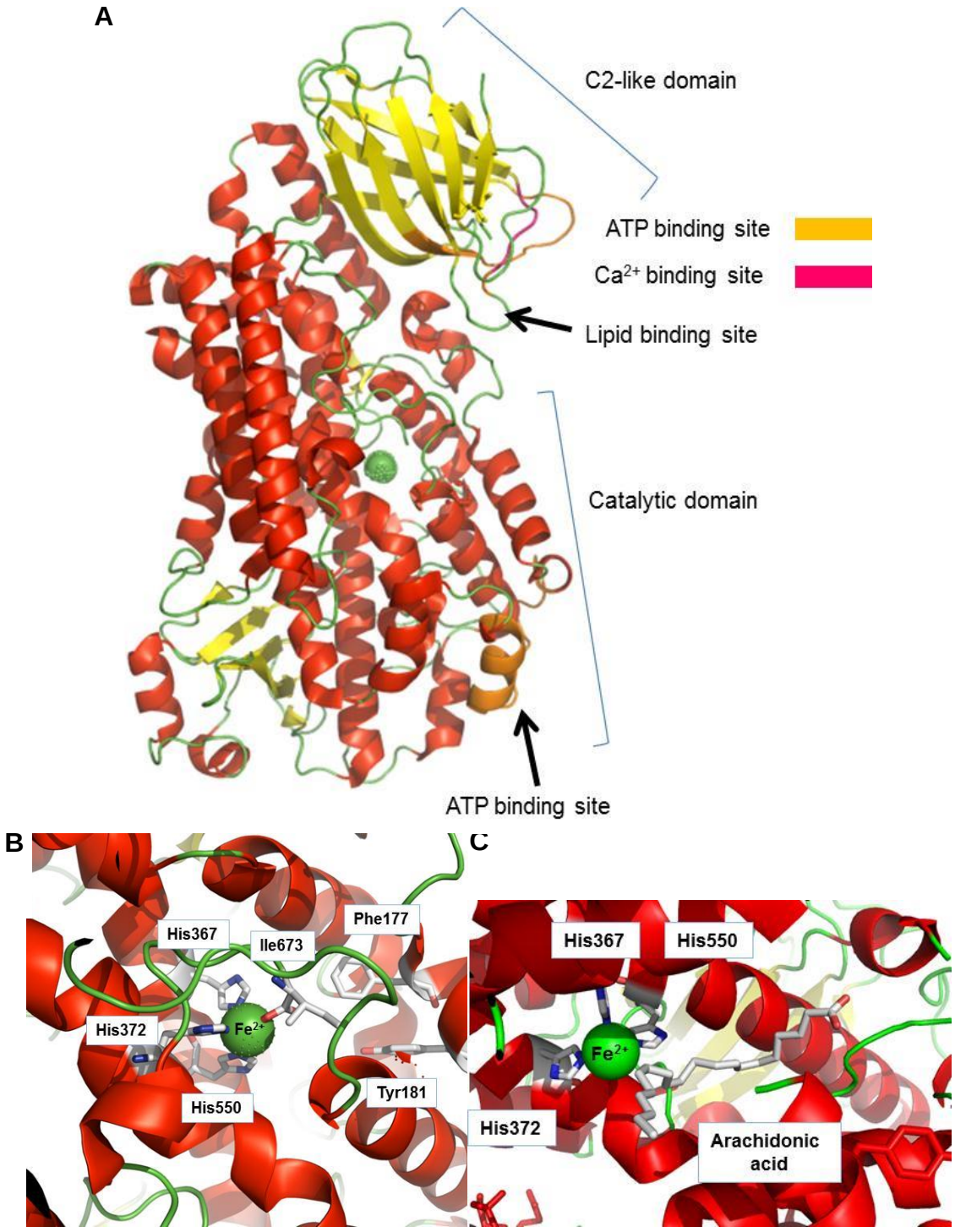

Figure 7. A. Crystal structure of "stable" 5-LO published by Gilbert *et al.*
B. Catalytic center of 5-LO in the catalytic domain. **C.** 5-LO cocrystallized with AA (3v99)[159].

2.1.1.2. ATP regulation

The mechanism of ATP activation is unclear and it involves the binding of the nucleotide to 5-LO. 5-LO is the only LO whose catalytic activity is stimulated by ATP and in a less extent by other nucleotides (ADP, AMP, cAMP, CTP and UTP)[160]. ATP has a K_a value of 31 µM, the activation is Ca^{2+}-dependent and leads to a typical two to six fold activation. The stoichiometry is equimolar, and 5-LO[161] has two binding sites (Figure 7). The amino acids involved are Trp75 and Trp201.

2.1.1.3. Regulation by phosphorylation

Several kinases such as p38 mitogen-activated protein kinase (MAPK), other MAPK activated protein kinases and extracellular signal-regulated kinase (ERK) 1/2 have been identified as kinases[162,163] that phosphorylate 5-LO (Figure 8). The p38 MAPK-regulated MAPK-activated protein kinase (MK)-2/3 and ERK1/2 can phosphorylate the enzyme at Ser271 and Ser663 *in vitro* which is connected to the nuclear import[148,163,164] and therefore with an increased LT production. However, protein kinase A (PKA), that phosphorylates 5-LO at Ser523, has a effect[165] in decreasing 5-LO catalytic activity and prevents the nuclear import of the enzyme to the nucleus. Recent publications[159] showed that after mimicking phosphorylation at Ser663 by mutating the Ser663 to an Asp, 5-LO activity was shunted to a 15-LO activity, suggesting that phosphorylation of 5-LO at Ser663 could not only down-regulate LT biosynthesis[137] but stimulate lipoxin production in cells lacking 15-LO.

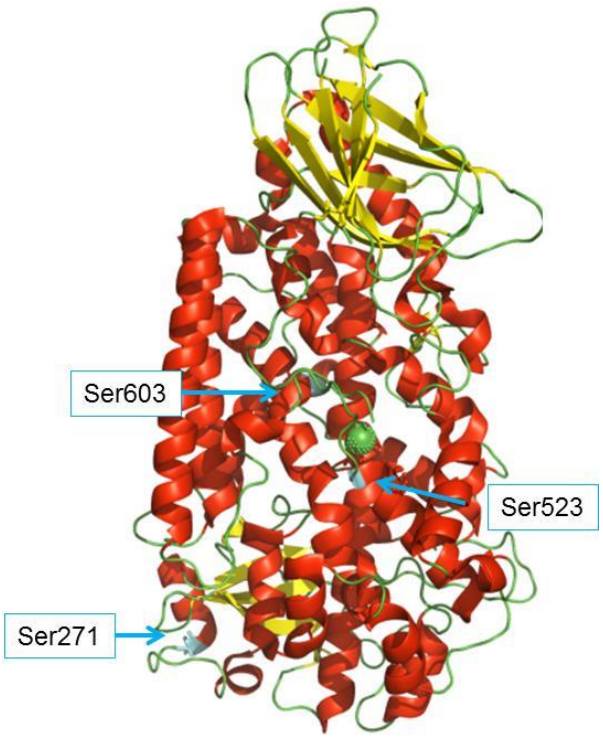

Figure 8. Phosphorylation sites of 5-LO.

2.1.1.4. Regulation by lipids

5-LO is regulated by membrane preparations[166] (phospholipids). Synthetic PC vesicles act as a stimulatory factor for 5-LO. Like many C2 domains, C2 like domain induces Ca^{2+}-induced membrane association. Binding of 5-LO to synthetic PC lysosomes is mediated by three Trp residues (Trp13, Trp75 and Trp102). Diacylglicerides like 1-oleoyl-2-acetylglycerol (OAG)[146] stimulate 5-LO product formation in the absence of Ca^{2+}, probably by acting at a phospholipid binding site located within the C2-like domain.

2.1.1.5. Regulation by other factors

Serio *et al.* showed another[167] pathway to induce LT biosynthesis, prolonged exposure to the bacterial component, lipopolysaccharide (LPS) increased FLAP gene transcription, mRNA expression, protein expression and LT biosynthesis in human monocyte like THP-1 cell line. Other agents include growth factors[164], cytokines, phorbol esters or Epstein-Barr virus which may enhance AA availability, increasing the expression of FLAP or elevating Ca^{2+} levels.

Several glutathione peroxidases like monocyte-derived soluble protein can inhibit the 5-LO and this effect is suppressed[144] by adding a glutathione peroxidase inhibitor.

Gender-related differences in LT biosynthesis and 5-LO have been recently observed in human whole blood (HWB) and neutrophils due a regulation of 5-LO by androgens[168]. In cells from females, 5-LO product formation was 1.8 fold higher in female cells than in cells from males. Moreover, 5α-dihydrotestosterone repressed LT biosynthesis in female cells down to the level of male cells.

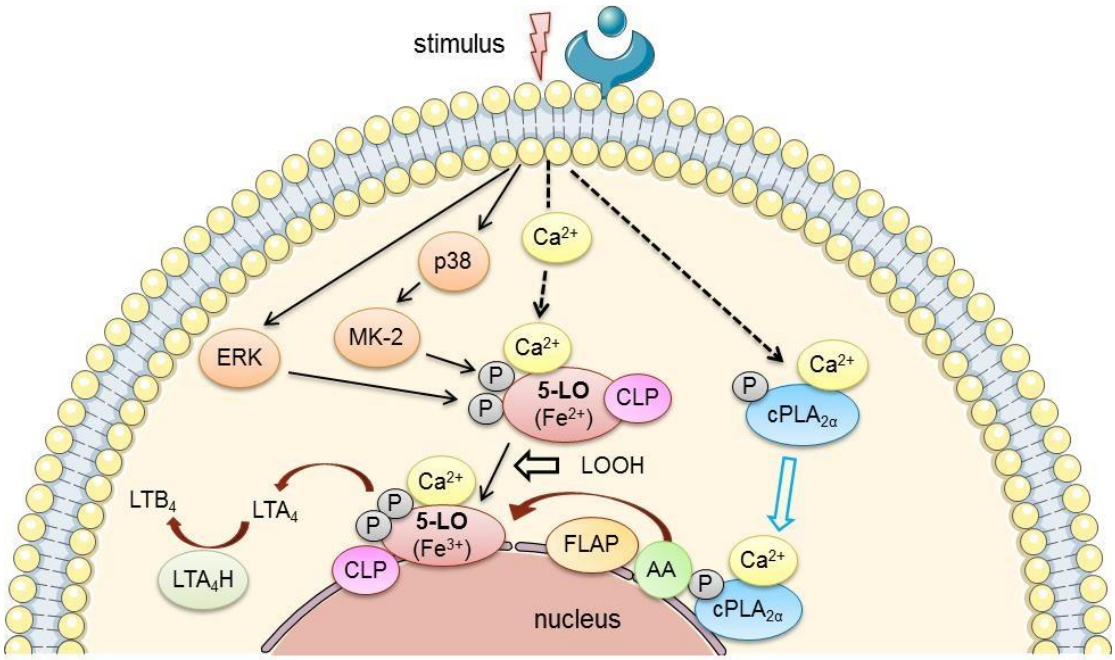

Figure 9. Cellular regulation of 5-LO.

2.1.2. Development of 5-LO inhibitors

As mentioned before, in the inactive form of the enzyme, the iron is ferrous (Fe^{2+}) and has to be oxidized by LOOH to the active Fe^{3+} to perform the catalytic cycle. This principle has been used to develop 5-LO inhibitors. They are classified into four groups: redox-active, non-redox type, iron ligand inhibitors and diverse inhibitors[169] (Figure 10).

2.1.2.1. Redox-active

The first class involves reducing agents that reduce Fe^{3+} required to catalyze the incorporation of molecular oxygen into AA. As an example: many natural plant derived agents such as nordihydroguaretic acid (NDGA), caffeic acid, coumarins and several polyphenols, e.g. AA-861, commercial available phenidone, BW-755C[170] (Burroughs-

Wellcome). They show high potency *in vitro* but they lack an appropriate oral bioavailability, interact with several redox cellular reactions and exert severe side effects (like methemoglobine formation[171]) due to the production of reactive radical species.

2.1.2.2. Iron ligands

The second class of 5-LO product biosynthesis inhibitors are the iron ligand inhibitors, which are represented by hydroxamic acid[172] or N-hydroxyurea that chelates the active site iron and possess weak reducing properties. BWA4C[173] and (±)-1-(1-Benzo[b]thien-2-ylethyl)-1-hydroxyurea also called zileuton[174] (Zyflo®) (Abbott) was the first 5-LO inhibitor that entered the US[123] market in 1997 for the chronic treatment and prophylaxis of various clinical phenotypes of asthma. Nevertheless, zileuton exhibits liver toxicity that is unrelated to the inhibition of 5-LO and short half-life[175,176] requiring a large dose four times a day, thus its clinical use is limited. Nevertheless, zileuton showed in clinical trials beneficial effects in rheumatoid arthritis, inflammatory bowel disease (IBD), psoriasis and allergic rhinitis[177].

ABT-761[178] (VIA-2291) is a structural optimization (introduction of a rigidity element) that improved the potency five-fold as well as the oral bioavailability. It has been recently investigated in several clinical trials in cardiovascular diseases (vascular inflammation[b] and acute coronary syndrome)

2.1.2.3. Non-redox type

Non-redox type inhibitors compete with AA[179] for binding to 5-LO without any redox properties, and due to their chemical diversity, it is unclear whether they bind or not to the active site of the protein (AA substrate-binding cleft) or in allosteric cleft of the protein, for example the C2-like domain. They compete with AA or LOOH for binding to 5-LO[180]. Representatives of this third class are ZD 2138[181] and CJ-13,610 (Pfizer)[179]. They reduce acute inflammatory responses but they have lower potency depending on the physiological stimulus. They are also called active site-directed inhibitors and

[b] Tallikut Pharmaceuticals, Clinical Study Protocol No. VIA-2291-01, A Phase 2 Randomized, Double-blind, Parallel-group, Placebo-controlled, Dose-ranging Study of the Effect of VIA-2291 on Vascular Inflammation in Patients After an Acute Coronary Syndrome Event, NCT00358826

some of them lack of selectivity, display poor efficiency and oral bioavailability like ICI211965[182] (methoxyalkyl thiazoles).

2.1.2.4. Diverse 5-LO inhibitors

A novel 5-LO inhibitor has been described, although it has not a defined mechanism, AKBA[183] (3-*O*-acetyl-11-keto-boswellic acid) had appropriated inhibitory potency but failed to inhibit LT formation *in vivo*.

Another strategy to develop 5-LO inhibitors is to target FLAP that is required to metabolize AA released by $cPLA_2$. FLAP inhibitors like MK-886[184] and AM103[185]. MK-886[186] shows an interaction with LTC_4 synthase and with mPGES-1 that point out its lower selectivity in the AA cascade. Another early compound was Bay-X1005[187,188], which was tested in clinical trials for treatment of myocardial infarction. A major pharmacological strategy is the dual inhibition of the 5-LO/COX pathway to overcome several side effects. Celecoxib is a known 5-LO/COX-2 dual inhibitor that reduced the blood level of LTB_4[189]. It has been published[180] that the inhibition of 5-LO product formation is dependent on the enzyme stimulation. Especially in the presence of high concentration of exogenous AA, the inhibition of LT biosynthesis cannot be accomplished.

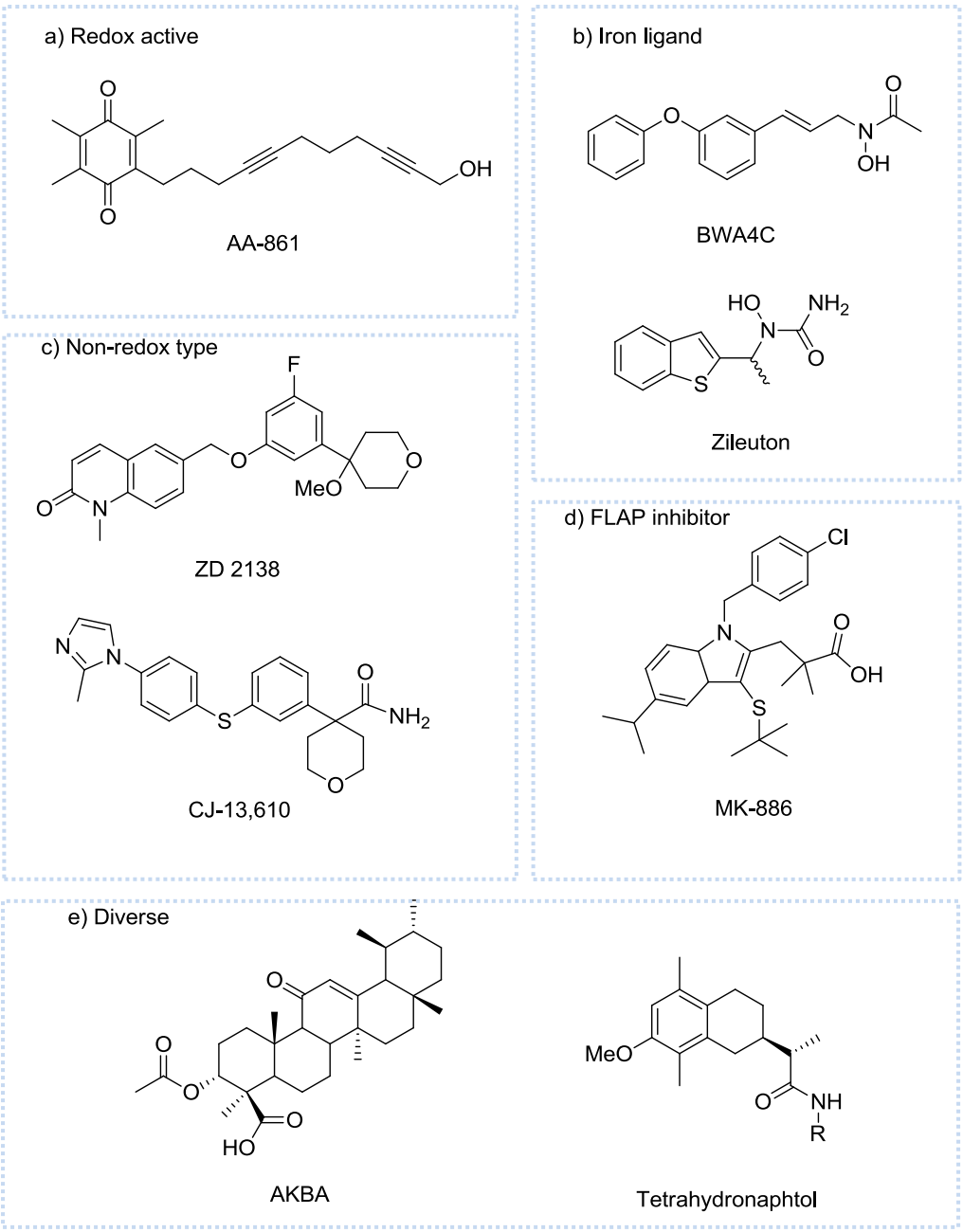

Figure 10. 5-LO four types of inhibitors: redox active, iron ligand, non-redox type, diverse and FLAP inhibitors as different strategy[c].

Consequently, there is a need for the design and development of new direct inhibitors of 5-LO that exhibit a high potency *in vivo* irrespective the mode of activation.

[c] Structures mentioned in text but not appearing in Figure 10 are depicted in the Appendix.

2.1.3. Leukotriene biosynthesis and roles in disease

LTs are mainly produced by stimulated leukocytes[190]. Epithelial and endothelial cells can also generate LTB_4, LTC_4 and LTD_4 at inflammatory sites through transcellular metabolism by which these cells use LTA_4 that is released from immune cells (neutrophils) as endothelial and epithelial cells express LTA_4 hydrolase[191]. The chemotactic and chemokinetic agent LTB_4 leads to recruitment of T-lymphocytes and causes phagocytosis[32,31]. Cys-LTs play an important role in asthma and allergic rhinitis, chronic inflammation, vascular permeability[192] and regulation of adaptive immune response. The combined action of 5-LO and 12-LO or 15-LO can lead to lipoxins that act as stop signals for inflammatory responses[193]. 5-LO plays an important role in acute and chronic inflammation, asthma, rhinitis, atherosclerosis and arthritis[194].

LTs, in general, are involved in asthma, allergic rhinitis, glomerulonephritis, rheumatoid arthritis, IBD, sepsis, cancer [d] and atherosclerosis (Figure 11). LTs metabolizing enzymes are highly expressed in the wall of human abdominal aortic aneurysms[195]. Moreover, genetic variants in the genes of the 5-LO pathway have been associated with the risk of development of acute myocardial infarction and stroke[196]. Eicosanoids are increased in infectious exacerbations of chronic obstructive pulmonary disease (COPD)[e]. They are also elevated in the airways of stable COPD patients compared to healthy subjects[197].

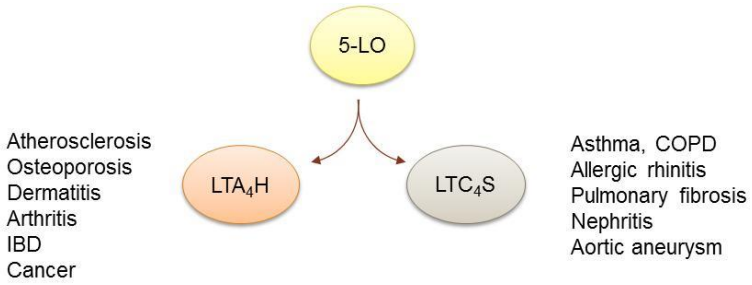

Figure 11. Diseases associated with overproduction of LTs.

[d] National Cancer Institute, Randomized Phase II Study of Eicosanoid Pathway Modulators and Cytotoxic Chemotherapy in Advanced Non-Small Cell Lung Cancer, NCT00070486
[e] National Heart, Lung, and Blood Institute (NHLBI), Antileukotriene Therapy for COPD Exacerbations, NCT00493974

3. EET signaling

In response to endothelial cell activation, AA can be converted by CYP epoxygenases to EETs which have potent vasodilator and anti-inflammatory properties[198–200]. EETs are produced primarily by endothelial cells or other types like astrocytes or cardiomyocites. Alteration in EET pathway is described in various animal models of cardiovascular diseases such as hypertension, blood pressure elevation, endothelial dysfunction and end-organ damage. EETs have several activities both as paracrine and autocrine mediators. EETs and their diols DHETs are PPAR*α* agonists, further discussed in chapter 3.3.1.1. The regioisomers of EETs activate several other enzymes[201] like tissue plasminogen activator, PI3 kinase, PKA and their glycerol derivatives activate cannabinoid receptors CB_1 and CB_2. On the contrary, EETs inhibit other signaling pathways like TXA_2 signaling, L-type calcium channels and cardiac sodium channels and diminish inflammation by inhibiting NF-κB[202]. Many vascular effects of EETs are modulated by nitric oxide[203]. EETs are mainly further metabolized by sEH discussed in the next chapter.

3.1. Soluble epoxide hydrolase

Epoxide hydrolases (EC 3.3.2.7-11) catalyze the hydrolysis of epoxides to the corresponding vicinal 1,2-diols. Two mammalian epoxide hydrolase[204] (EH) enzymes microsomal (mEH) and sEH have been fully characterized over the past 30 years in the field of xenobiotic metabolism. Both enzymes belong to the family of *α/β* hydrolase fold[205], two tyrosines residues which place the epoxide within the active site distinguish epoxide hydrolases from other members of this family.

mEH is highly expressed[206] in liver, lungs, kidneys, intestine, brain, prostate and testes and its expression is inducible by a number of compounds (e.g. phenobarbitone). Classically it plays an important role in xenobiotic metabolism due to its broad substrate selectivity and prominent expression in the liver mEH also metabolizes numerous endogenous fatty acids epoxides[207] such as epoxystearic acid.

sEH is encoded by the human gene EPHX2 and it is expressed as a homodimeric enzyme consisting of two 62 kDa monomers. The N-terminal domain is a phosphatase domain capable of hydrolyzing lipid phosphates such as LPA[208]. C-terminal domain contains the hydrolase catalytic center and both domains are separated by a proline rich linker (Figure 12). The C-terminus of sEH transforms four regioisomers of EETs:

5,6-, 8,9-, 11,12- and 14,15-EETs to the corresponding[209] DHETs, by which the biological effects of EETs are diminished. sEH is located in the cytosol and peroxisomes.

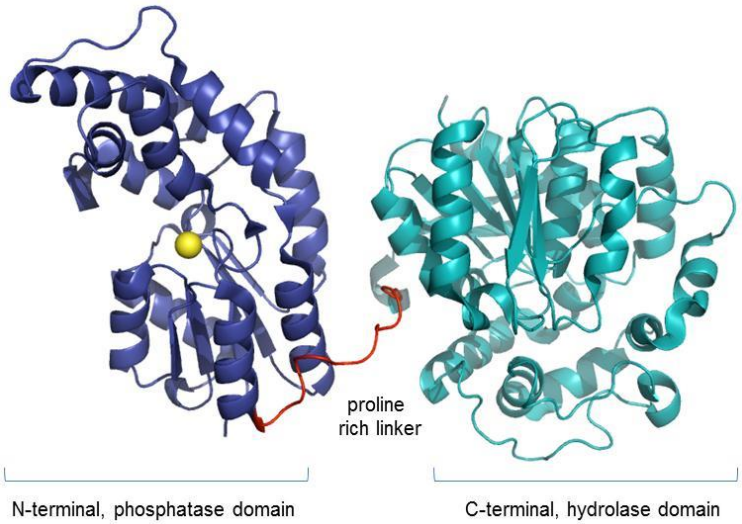

Figure 12. Monomer of sEH.

EETs are preferred substrates of sEH and 14,15-EET is the regioisomer that is hydrolyzed with the highest V_{max} (9.03 µmol/min/mg protein) and most potent K_m (5 µM)[210]. sEH is also able to metabolize[211,212] epoxyeicosadecenoic acids (EPOMEs) to the more toxic and inflammation inducing dihydroxyoctadecenoic acids (DHOMEs).

The catalytic mechanism of oxirane ring opening follows via an S_N2-type reaction where the epoxide is activated by general acids Tyr381 and Tyr 465 with simultaneous nucleophilic attack by Asp333 to form an alkylenzyme intermediate. A water molecule activated by His523 attacks the intermediate, forming a tetrahedral intermediate which collapses to release the diol[213]. Favored sEH substrates are *trans*-substituted[214] over *cis*-substituted epoxides. The amino acid residues forming the catalytic triad of the sEH are Asp333/His523/Asp494 (Figure 13).

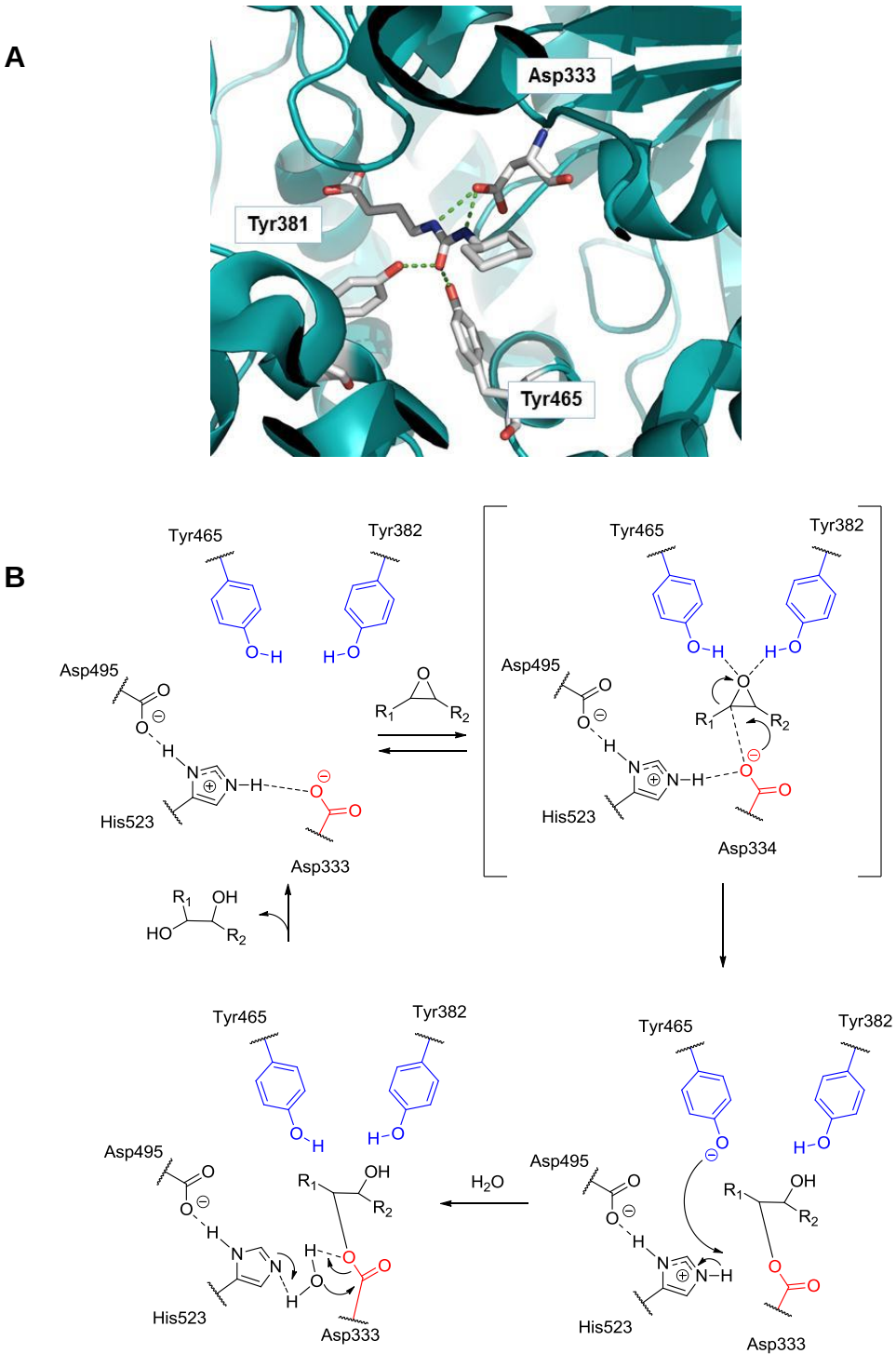

Figure 13. A. Catalytic center of sEH hydrolase domain (1zd3) with 4-((cyclohexylamino)carbonyl)aminobutanoic acid. **B.** Catalytic mechanism.

The N-terminal domain shows phosphatase activity. This class of phosphatase belongs to the family of the haloacid dehalogenase, class IV, a group that uses Asp as nucleophile; this group comprises a number of phosphatases, dehalogenases and other hydrolases. sEH phosphatase (sEHp) reveals[215] an hexacoordinated Mg^{2+}, the

first step is a nucleophilic attack by Asp9 on the phosphoester group and protonation of the leaving group. In a second step, the phosphoenzyme intermediate (acylphosphate) is hydrolyzed via a nucleophilic attack by an activated water molecule[216] (Figure 14).

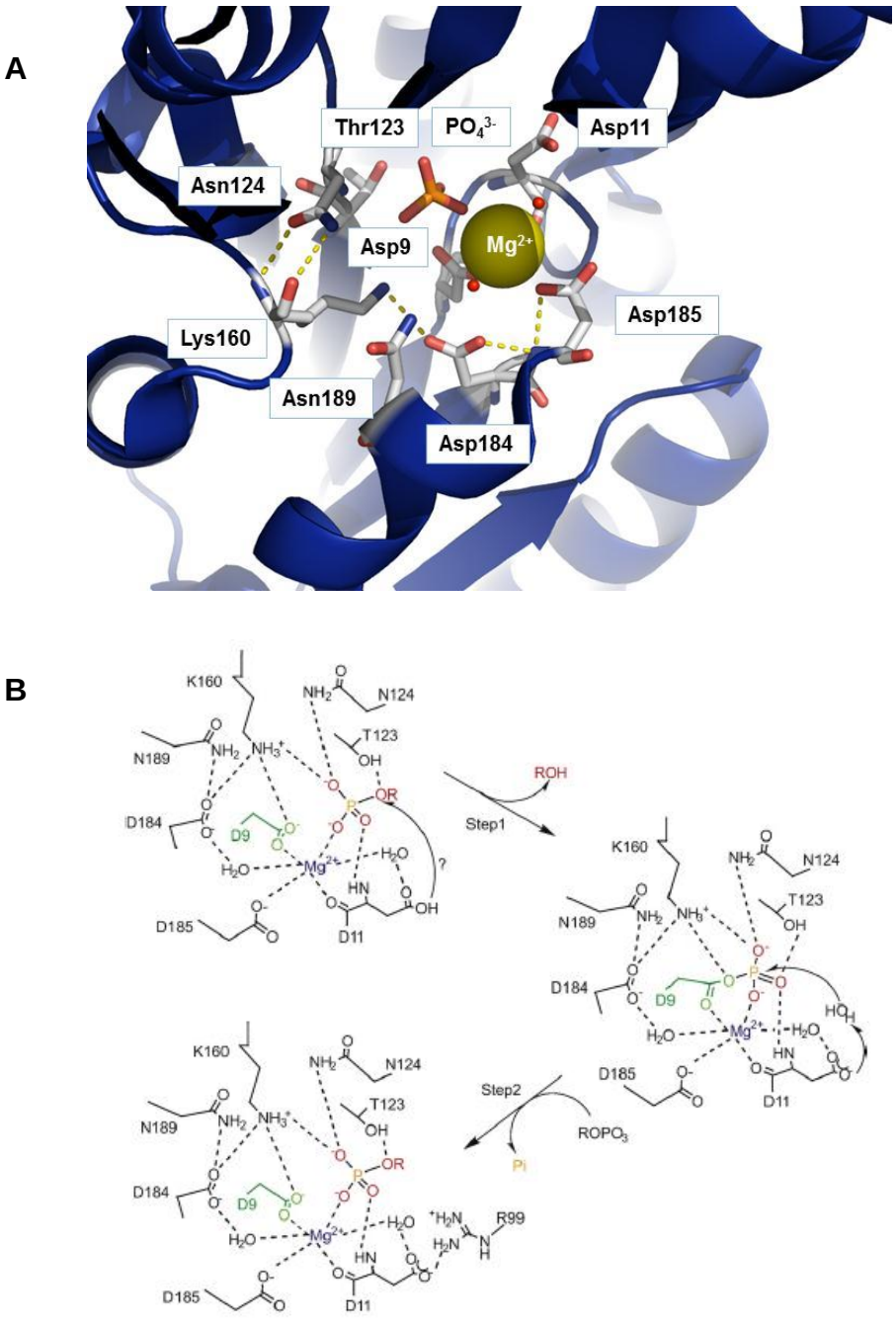

Figure 14. A. Catalytic center of sEHp. **B.** Proposed mechanism of sEHp by Cronin and coworkers[216].

In contrast to sEH hydrolase domain, little is known about the biological role of sEHp, Hou *et al.* postulated an important role in the regulation of the endothelium nitric oxide

synthase (eNOS) activity[217]. Endothelium-derived nitric oxide (NO) is a regulator of vascular tone, controlled by eNOS. Dysregulation of this enzyme has been related to hypertension[218]. More recently, opposite functions of the phosphatase activity and EH activity were reported (Table 1) in the regulation of cholesterol levels[219]. Oguro *et al.* determined that both domains[217] are important for cell growth but the phosphatase domain was necessary for VEGF expression. Overexpression of a sEH mutant mice lacking phosphatase activity did not decrease VEGF expression, indicating that lipid signaling molecules may be the substrates for the sEHp, which activate the growth of cells. sEHp is able to dephosphorylate LPA[220], nevertheless the phosphatate activity towards S1P was lower in comparison to LPA indicating that sEH can selectively hydrolyze LPAs. $cPLA_2$ also produces lysophospholipids which are converted to LPA by autotaxin, moreover $cPLA_2$ releases AA that is necessary to produce EETs, substrates of sEH hydrolase; this last finding suggests the possibility of an interesting interaction of the both different domains of sEH.

Table 1. Biological functions of the different domains of sEH.

	sEH phosphatase	sEH hydrolase
Cholesterol regulation	-/- → significant lowering	-/- → 40% increase of cholesterol
VEGF expression	important	irrelevant
Cell growth	important	important

3.1.1. Development of sEH inhibitors

The main strategy to develop sEH inhibitors is to mimic the reaction intermediates or transition states, as observed for other *α/β* hydrolases fold enzymes. Therefore, various ureas, amides and carbamates (with the appropriated substituents) have been developed as successful sEH inhibitors (sEHIs)[221]. Trp334 niche and Phe265 can accommodate a variety of functional groups of sEHIs (Figure 15). The binding pocket exists as an L-shaped hydrophobic tunnel.

Structure-activity relationships show that the secondary urea as central pharmacophore must have a relative small substituent such as phenyl, hexyl, or cyclohexyl on one side; nevertheless a large group can be tolerated on the other side of the molecule[222]. This strategy has been developed in the case of 12-(3-adamantan-1-ylureido)dodecanoic

acid (AUDA)[223], known as sEHI of reference but lacking of the desired pharmacokinetic properties and susceptible to cellular metabolism.

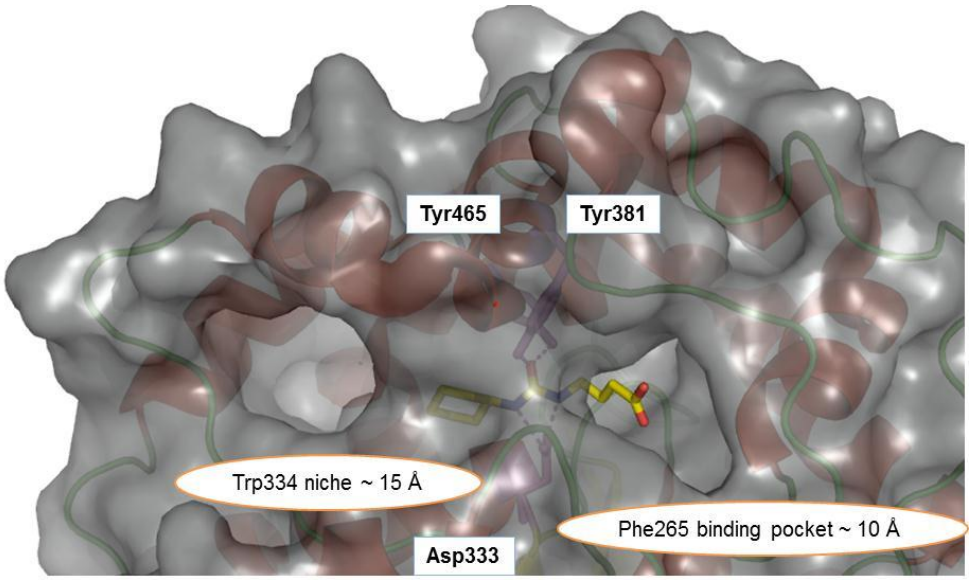

Figure 15. X-ray cocrystal structure of human sEH showing the binding pocket (1zd3)[213].

Compounds like AUDA are potent and competitive inhibitors with low nanomolar K_i values, but the lack of solubility in water implies the use of common formulation solvents or the incorporation of a second pharmacophore: polar functional groups (carbonyl, ester, ether, sulfonamide or amide) in a 7 Å distance that typically improved pharmacokinetic (PK) properties while maintaining potency (Figure 16).

Another strategy to improve physical properties like solubility is to conformationally constrain the substituted ureas. For example piperidine moiety[224] was identified to rigidify the linker between the primary and secondary pharmacophores or spirocyclic ureas with high oral exposure and low clearance. The main problem of compounds carrying an adamantyl moiety is the rapid hydroxylation of these substances that are not suitable for *in vivo* studies[225]. Nicotinamide moiety was discovered by researchers at Boehringer Ingelheim in a high-throughput screening[226]. Pyridine ring binds to a unique site in the Trp334 niche and the diphenyl group takes advantage of the large binding pocket, nevertheless the compound does not have optimal PK properties (poor absorption)[226]. A novel pyrazole aniline derived amide was discovered by the same company with the desired pharmacokinetic properties, co-crystallized (3otq)[227] sEH with the inhibitor showed that one pyridyl group was facing solvent, therefore it improved the solubility and the other group interacts with Trp336 as π-π stacking.

Novel sEHIs were identified as a rigidified urea structure that exhibited the same interactions as urea inhibitors: Tyr381 and Tyr465 interact with the nitrogen of the benzisoxazole and the substituted amino group with Asp333. This novel class of compounds exhibited better potency and improved PK properties with a relative low molecular weight (<400 g/mol).

Despite of the current research and development of sEHIs with high potency, selectivity, oral exposure and high therapeutic index with few side effects in animals; only one compound has been analyzed[228] in a clinical trial (AR9281) for the treatment of patients with mild to moderate hypertension and impaired glucose tolerance. The clinical outcome of this trial was the lack of efficacy of AR9281 to treat hypertension or diabetes.

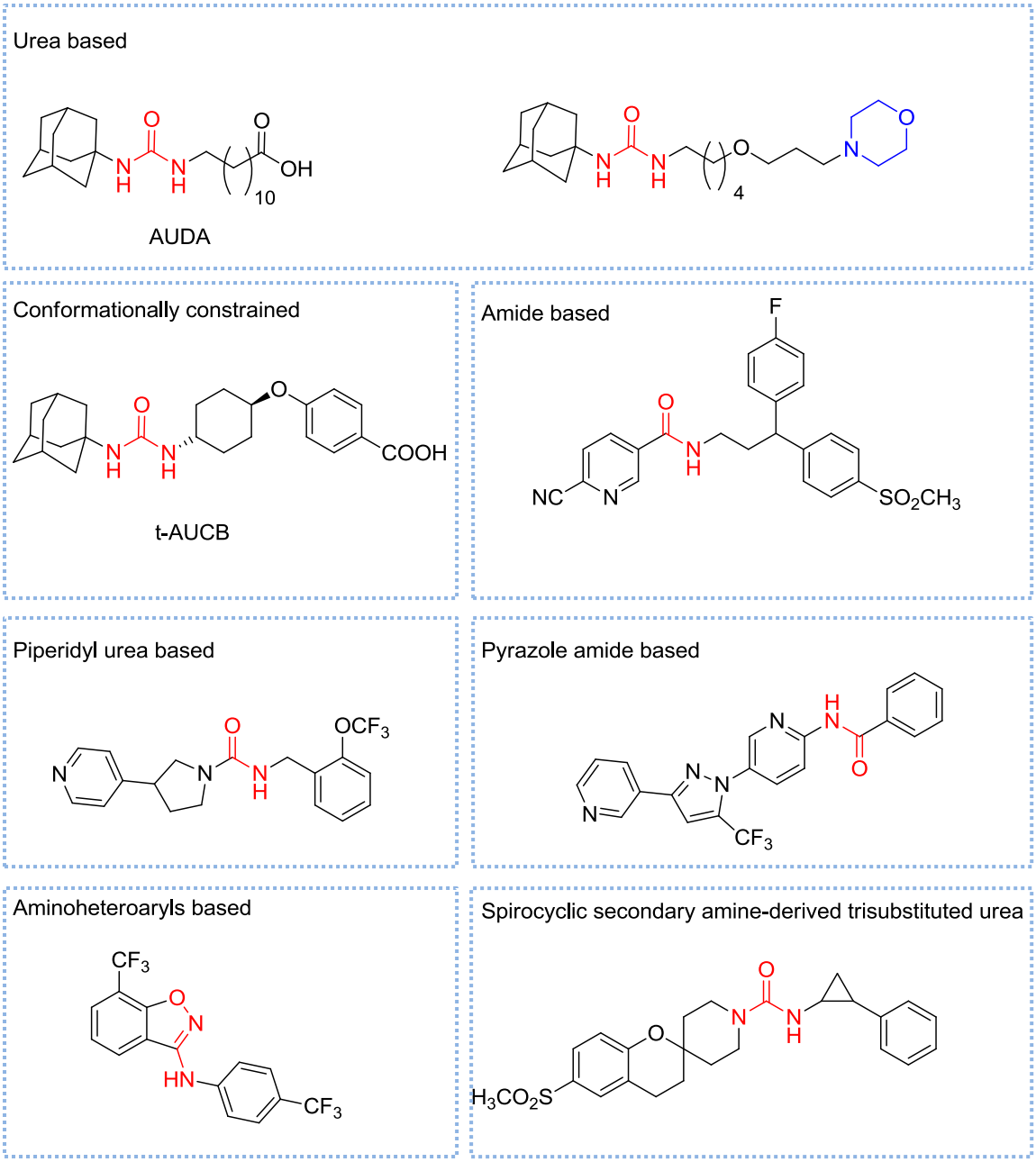

Figure 16. sEH inhibitors developed by several pharmaceutical companies with different pharmacophores (depicted in red), secondary pharmacophore introduced to improve PK properties is depicted in blue.

sEHIs have been tested in several animal diseases[221] with promising results. In the field of inflammation, deletion of sEH genes reduced the inflammatory response to endotoxin pointing out the role of sEH in inflammation. The first evidence of EETs role in inflammation was the fact that 11,12-EET prevents the TNF-α induced activation of NF-κB expression in mice[229] (chronically active in many inflammatory diseases[230]). Moreover sEH inhibitors may synergize with classical anti-inflammatory drugs including COX and LO inhibitors[231].

Another field that attired the attention of sEHI development concerns cardiovascular diseases. Inhibition of sEH[232–234] protects against hypertension, atherosclerosis and cardiac hypertrophy. EETs have been shown to reduce blood pressure in spontaneous hypertensive rats[235]. They regulate blood pressure by acting on vascular tone in arteries as well as by acting on the kidney through enhanced natriuresis (sodium excretion). Low EET levels and high sEH levels have been associated with cardiac hypertrophy[236]. They also modulate blood clotting, specifically 11,12-EET and 14,15-EET reduce platelet aggregation through membrane hyperpolarization. It has been proposed that sEHIs could improve the safety[237] of coxibs (a class of NSAIDs); that caused a higher incidence of strokes by decreasing platelet stability by shifting to an increase of 20-HETE as a consequence of COX-2 inhibition. sEHIs are able to return this ratio to a normal level after COX-2 inhibition[237]. Another therapeutic area of interest for sEHIs is the neuropathic and inflammatory pain[238]. An sEHI (APAU, 1-(1-acetylpiperidin-4-yl)-3—adamantylurea) showed[239] similar efficacy in comparison to morphine in a pain alleviation model. They synergize with COX and 5-LO inhibitors and in a pain model after LPS exposure they appeared to be similar for Vioxx (a class of coxib, NSAID). The main advantage of these inhibitors is, in comparison with gabapentin (used in the treatment of neuropathic pain), the fact that sEHI do not cause changes in behavior or coordination often associated with opioids[240]. sEHIs have been successfully used in the treatment of angiotensin II-dependent hypertension[241], smoke-induced chronic obstructive pulmonary disease (COPD)[242], share cardioprotective properties[243], ameliorate metabolic syndrome[244].

3.2. EET signaling in cancer

EETs are produced by CYP epoxygenases, epoxidation can occur at any of the four double bonds of AA resulting in the four regioisomers mentioned before[245]. EETs are synthesized in the endothelium and active large-conductance Ca^{2+}-activated K^+ channels, causing hyperpolarization of the vascular smooth muscle and vasorelaxation[246]. Therefore, they are called endothelium derived hyperpolarization factors. 14,15-EET interacts with transient potential cation channel, subfamily V member 4 (TRPV4)[247]. The mechanism[248] was rather unclear and Behm *et al.* showed that the three remaining EET regioisomers might function as thromboxane receptor (TP) antagonists with K_i value of 3.3 µM (for 14,15-EET). This ability is in concordance

with the fact that EETs function as anti-inflammatory agents possible through a prostanoid pathway mediated inflammatory process, inhibiting NF-κB mediated inflammation[249]. In summary, EETs have beneficial effects on inflammatory and vascularization processes, nevertheless in the recent five years, it has been postulated that EETs play critical[250] roles in cellular proliferation, angiogenesis and migration. EETs have been shown to promote endothelial cell[251] migration via eNOS, MEK/MAPK and PI3-K. 11,12-EET and 14,15-EET promote angiogenesis[41] via sphingosine kinase 1 or through Src, PI3K/AKt signaling and also enhancing the effects of VEGF angiogenesis. Moreover, Panigrahy *et al.* recently published[252] that EETs stimulate multiorgan metastasis and tumor dormancy escape in mice (Figure 17). They demonstrated that using genetic and pharmacological manipulation of endogenous EET levels led to a promotion of primary tumor growth and metastasis. Furthermore, sEH pharmacological inhibition with sEHI (discussed in chapter 3.1.1), elevated EETs levels[253], accelerated primary tumors and revealed an increase in the number of tumor cells expressing VEGF.

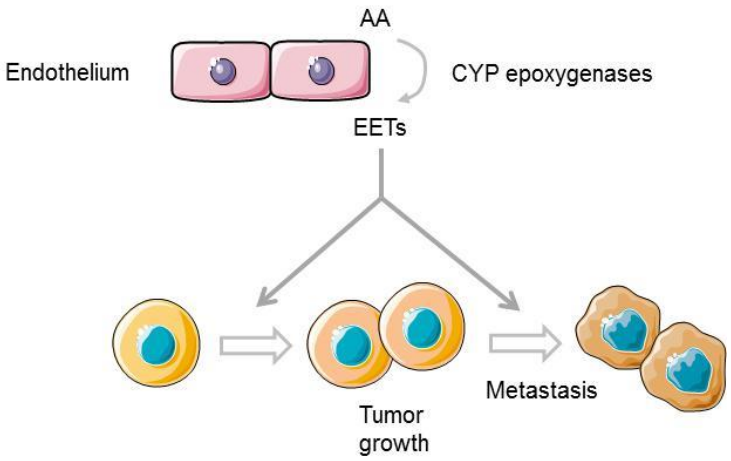

Figure 17. Schematic representation of how EETs can affect tumor growth.

Nevertheless, they had no significant effects on basal endothelial migration but increased VEGF-mediated endothelial migration. Systemic administration of sEHI stimulated lung, liver, and axillary lymph node metastasis in murine models. In summary, EETs promote metastasis by triggering secretion of VEGF by the endothelium, which is critical for EET cancer stimulating activity. They represent a novel class of LM that act as a double-edged sword in cardiovascular diseases (due to their beneficial effects) and cancer (due to recent concerning publications). The

postulated mechanism[254] for EETs to promote tumor growth is via EGFR/PI3K/Akt and EGFR/MAPK pathways[255] to promote cancer cell survival (Figure 18).

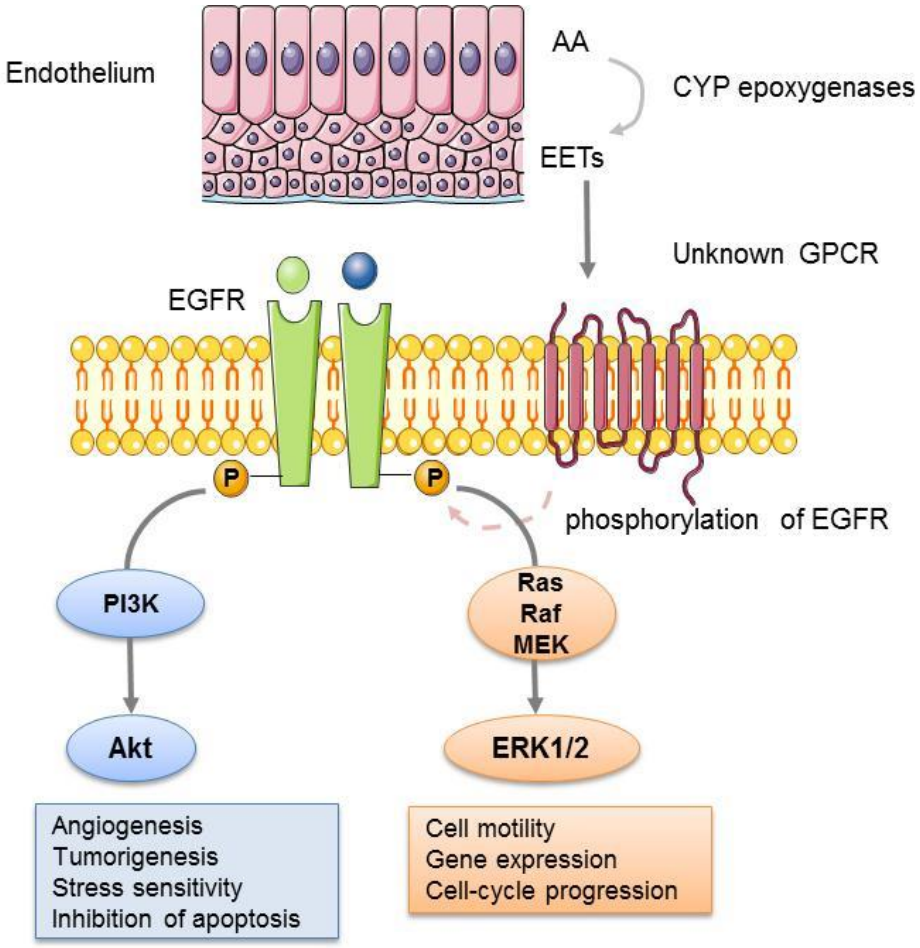

Figure 18. EETs downstream signaling pathways in cancer.

Angiogenesis is mainly produced by VEGF, expression of VEGF gene is enhanced under hypoxic conditions and controlled by hypoxia inducible factor 1 (HIF-1). HIF-1[256] is composed by HIF-1α and Arnt. Under hypoxia, HIF-1α dimerizes with Arnt and binds to the hypoxia response element in the promoter region of genes such as *VEGF*. The addition of EETs or overexpression of CYP epoxygenases induced *VEGF* expression[257].

3.3. Nuclear receptors

Nuclear receptors[258,259] are proteins located inside the cells that are able to detect steroid and thyroid hormones (Figure 19). They contain three major domains[260]: a variable amino-terminal domain, a highly conserved DNA-binding domain (DBD)[261],

and a less conserved carboxyl-terminal ligand binding domain (LBD). The superfamily is sub-divided into three classes. Class 1 is the steroid receptor family, and includes the progesterone receptor, the estrogen receptor, the glucocorticoid receptor, the androgen receptor and the mineralocorticoid receptor. Class 2, or the thyroid/retinoid family[262], includes the thyroid receptor, vitamin D receptor, the retinoic acid receptor and the PPAR. PPARs[263] are members of the nuclear steroid hormone receptors superfamily[264] that transduce a variety of nutritional and inflammatory signals. Class 3 corresponds to the orphan receptors[265].

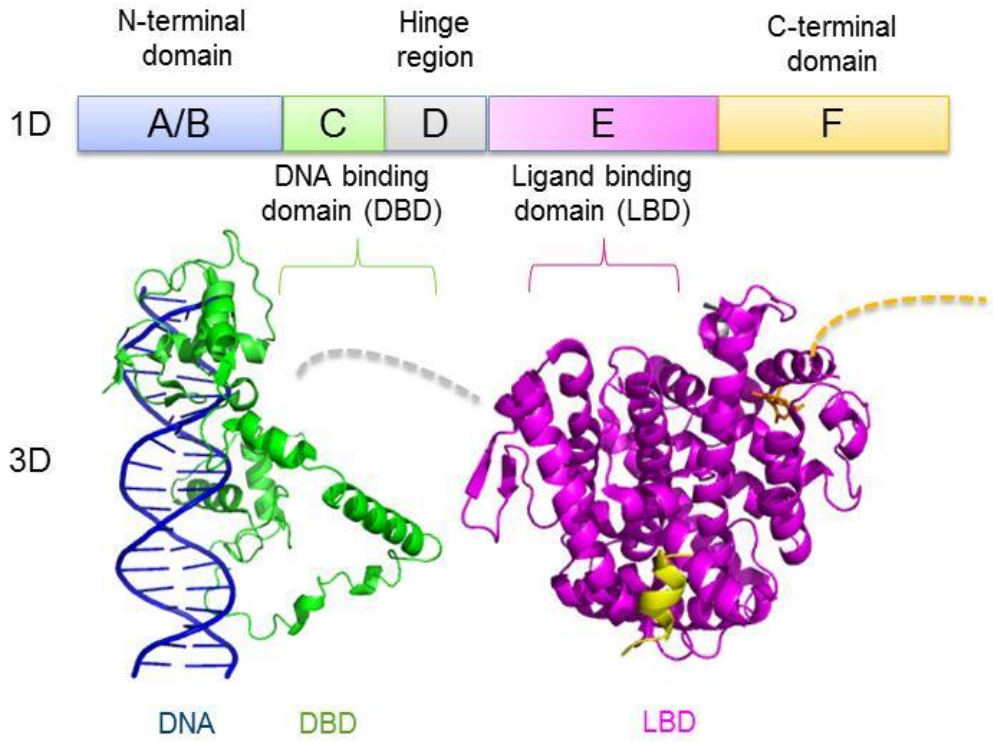

Figure 19. DBD contains two zinc fingers that binds to specific DNA sequences and N-terminal domains containing the activation function 1 (AF-1) whose action is independent of the presence of a ligand.

3.3.1. Peroxisome proliferator-activated receptors

Similar to other nuclear hormone receptors, PPAR acts as a ligand activated transcription factor. Upon binding with a ligand, PPAR heterodimerizes with retinoid X receptor (RXR)[266], bind to the response elements (RE) arranged as direct repeats spaced by one nucleotide, termed peroxisome proliferator response elements (PPREs) and regulates the expression of target genes. The PPAR/RXR complex (Figure 20) can be activated by the ligand of either receptor[267], and the simultaneous binding of both ligands is more efficient. PPARs play an important role in cell proliferation[268] and

inflammation signaling. Among these functions PPARs contribute to regulation of glucose, lipid and cholesterol metabolism and are the ideal target to treat metabolic syndrome[269]. There are three known subtypes of PPAR receptors depending on their expression in tissues[270]: PPAR*α*, *γ* and *β/δ*. They all share structural and functional organization similar to that of other nuclear receptors.

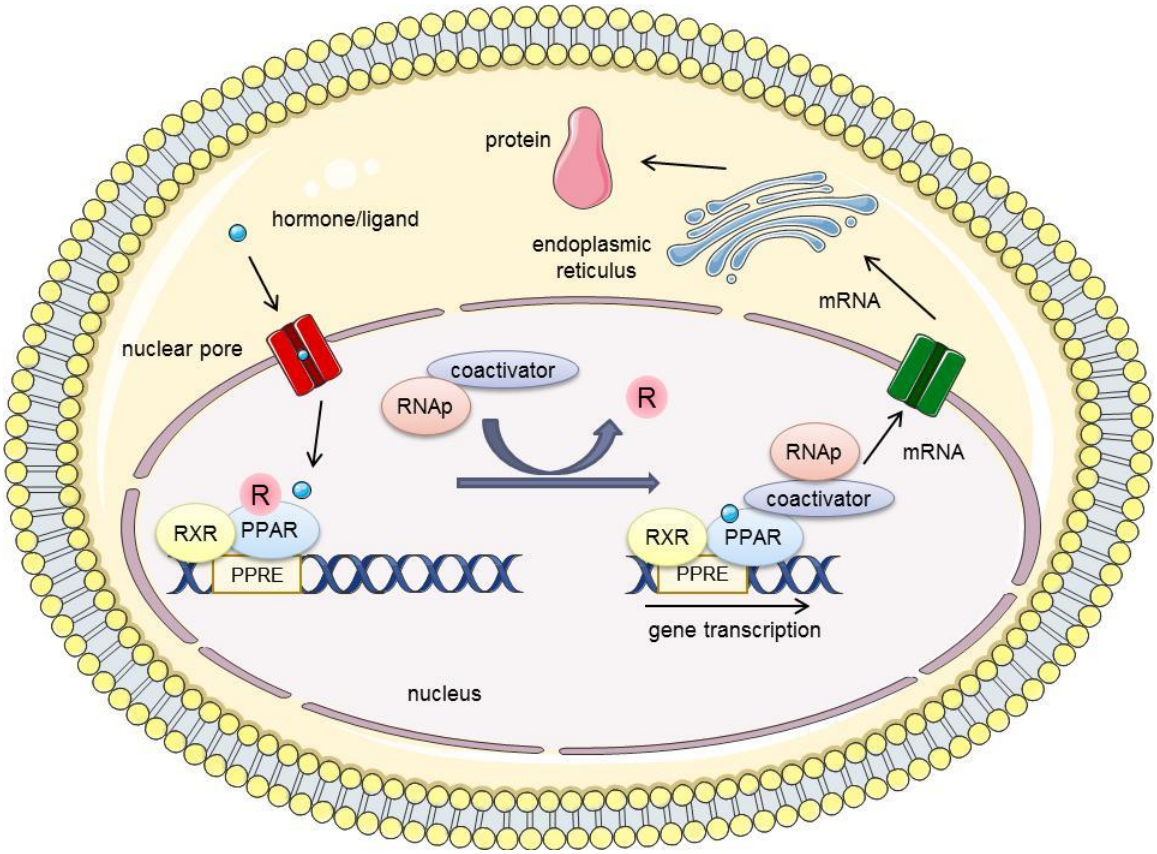

Figure 20. Mode of action of PPAR in the cell: repressor (R), RNA polymerase (RNAp).

Regarding their selectivity, compounds that activate any of PPARs are reported as agonists, antagonists, partial and selective PPAR modulators (SPPARMs), dual agonists, and PPAR*α,γ*, *β/δ* pan-agonists. PPAR*α* is expressed at high levels in liver where it promotes fatty acid oxidation, ketogenesis, lipid transport and gluconeogenesis[271]. This receptor regulates lipid metabolism and modulates inflammation by its effect on genes which control reverse cholesterol transport. PPAR*α* is the molecular target mainly of hypolipidemic fibrates[272] including clofibrate[273] and bezafibrate[273]. PPAR*α* agonists are used in the treatment of dyslipidemia associated with atherosclerosis and dyslipidemia primarily associated with type 2 diabetes mellitus. The second subtype PPAR*γ* is the most widely investigated due to its important role in adipogenesis[274], where PPAR*γ* activation[275] leads to the generation of

adipocyte-specific genes[276]. PPAR*γ* also participates in glucose homeostasis, cell cycle regulation, inflammation, atherosclerosis[275], apoptosis and carcinogenesis[277]. PPAR*γ* is also activated by synthetic ligands including the thiazolidinedione class (TZD) like pioglitazone and rosiglitazone of clinically used anti-type 2 diabetic drugs[278] (Figure 21). Simultaneous activation of PPAR*γ* and PPAR*α* alters the tissue distribution of fatty acids by stimulating their uptake and use in adipose tissue, liver and skeletal muscle. Whereas PPAR*γ* agonists increase adiposity and body-weight gain[279], it has been reported that PPAR*α* agonists decrease food intake[280] and fat depots induced by PPAR*γ* agonist treatment. Dual combination of PPAR*α/γ* ligands exerts complementary activities and has been used as new therapy for the treatment[281] of diabetes type 2 and metabolic syndrome[282].

PPAR*δ* can be ubiquitously found in all kind of tissues but it is the highest expressed PPAR subtype in brain and the cerebral vasculature. PPAR*δ* stimulates fatty acid oxidation in heart and skeletal muscle, and plays a role in cell differentiation, placental development, cancer, wound repair, and atherosclerosis. The main representative of PPAR*δ* agonist is L-165041[283] that shares the L-shape needed for PPAR*δ* activation. As previously showed, PPAR plays an important role in different processes for the cell and therefore compounds that activate selectively PPAR subtype can lead to novel clinical therapeutic effects.

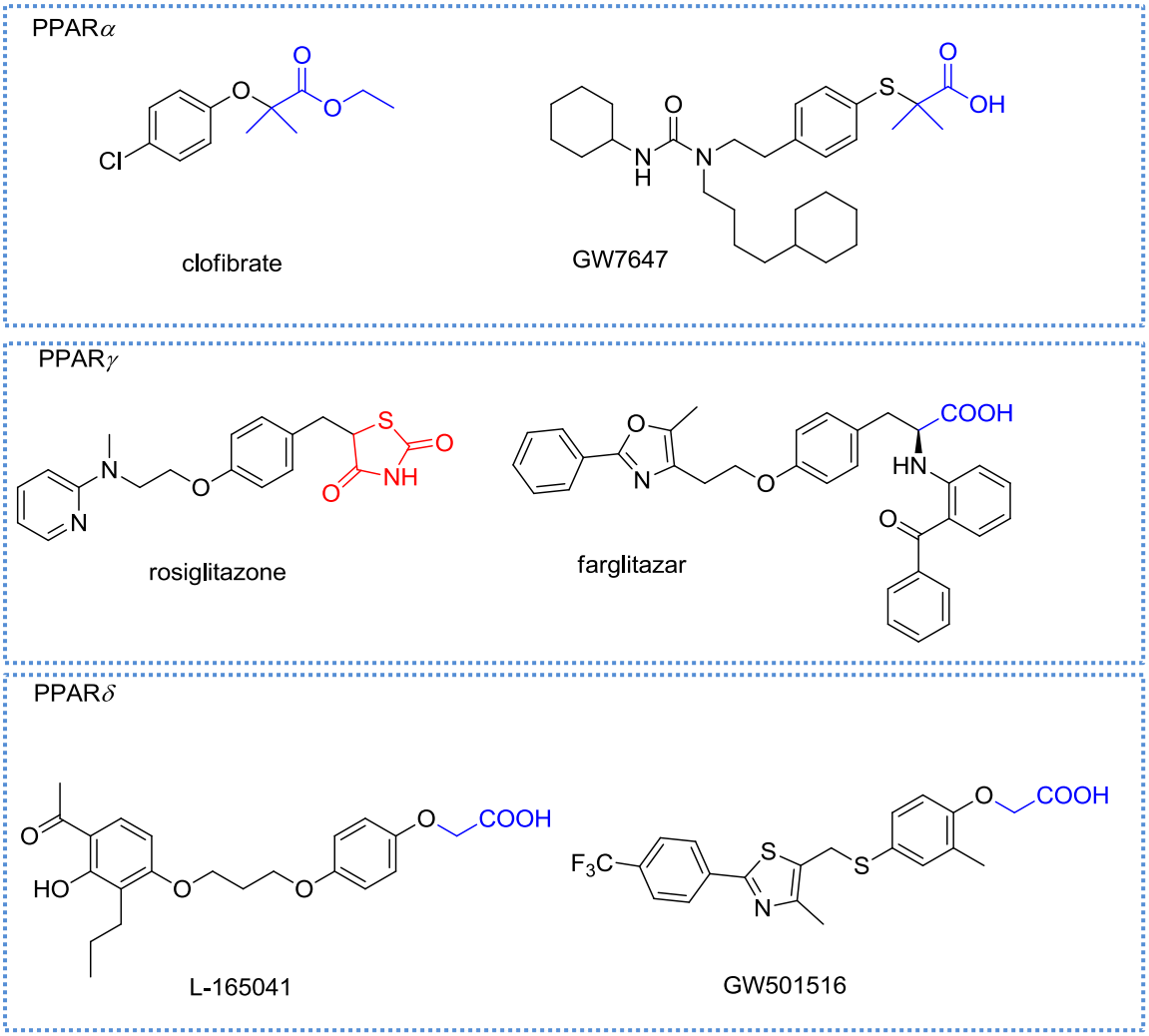

Figure 21. Known PPAR*α,γ,δ* agonists.Depicted in blue acidic head group identified as PPAR general pharmacophore. Depicted in red thiazolidinedione group.

3.3.1.1. PPAR endogenous ligands

The diversity and high concentrations of agents required for receptor activation led to the hypothesis that PPAR activators work by either being metabolized[284] in the cell to an active form or by inducing the release or biosynthesis of endogenous PPAR ligands.

As an example of natural ligands[285], PGI_2 can transactivate PPAR*δ* and PGD_2 dehydration product 15-deoxy-Δ12,14-PGJ_2 is a natural ligand for PPAR*γ*[286]. PGE_2 can also indirectly activate PPAR*δ* in certain contexts[287]. The specific action of each PG is tissue dependent. LTB_4 a natural inflammation mediator is a PPAR*α* ligand. Krey *et al.* showed that another AA metabolite that strongly activates PPAR*α* is 8(*S*)-HETE that stereoselectively activates the receptor over its 8(*R*)-enantiomer[64]. A search for natural ligands revealed that PPAR*α* is activated by long-chain fatty acids such as DHA and

EPA, linoleic acic, linolenic acid and AA[288]. Competition binding assay revealed the last three to be ligands for PPAR*α* and PPAR*γ* in the micromolar range[288]. Moreover EPA has been co-crystallized into the LBD of PPAR*δ* (pdb:1gwx)[289].

3.3.2. Role of PPAR in metabolic syndrome

The metabolic syndrome (MetS)[290] is a cluster of symptoms mainly consisting[291] of the so-called "Deadly Quartet'' of hyperglycemia, hypertriglyceridemia, hypertension, and obesity. Due to its complex nature, the current treatment strategies[292] of MetS require multiple pharmacological compounds regulating lipid and glucose homeostasis as well as blood pressure and coagulation. MetS is a clustering of factors with an increased risk for atherosclerotic cardiovascular disease and diabetes[293]. This clustering has also been related with non-alcoholic fatty liver disease[294], sleep apnoea and some forms of cancer[295]. The symptoms[295] commonly occurring on patients with MetS are: obesity (body fat is concentrated around the waist; obesity is defined by having a waist circumference of 102 cm for men and 89 cm for women), increased blood pressure (systolic 130 mm Hg or more, diastolic 85 mm Hg or more), high blood sugar level (fasting test 100 mg/dL) and high cholesterol (150 mg/dL of triglycerides, 1.7 mmol/L HDL and less than 40 mg/dL for men and 50 mg/dL for women). Up-to-date treatment for MetS is a patient lifestyle change of the to increase physical activity, initiation of drug therapy with statins to reduce LDL, diuretics to decrease blood pressure to treat diabetes type 2 and to handle obesity are currently being used (Table 2). Certainly, evidence exists[296] to support the notion that the diet, exercise, and pharmacologic interventions may inhibit the progression of metabolic syndrome to diabetes mellitus.

MetS is increasing in prevalence[297], paralleling an increasing epidemic of obesity. In the United States, data from a 1999-2000 survey showed that the age-adjusted prevalence of metabolic syndrome among adults aged 20 years or older had risen from 27% (data from 1988-1994) to 32%.

Table 2. Treatment currently used in patients with MetS.

Class of medication[f]	Drug	Mode of action
Antidiabetics, biguanidines	• Metformin (insulin-sensitizing agent)	Reduces hepatic glucose output, increases glucose uptake and triggers weight reduction.
Antidiabetics, TZD	• Rosiglitazone (Avandia) • Pioglitazone (Actos)	• Stimulates glucose uptake and lowers insulin plasma levels. • Improves cell response to insulin.
Lipid lowering agents, statins	• Atorvastatin (Lipitor) • Fluvastatin (Lescol)	Statins are (3-hydroxy-3-methylglutaryl coenzyme A [HMG-CoA] reductase inhibitors that affect the lipid profile.
ACE inhibitors	• Captopril • Enalapril	They prevent the conversion of angiotension I to angiotensin II, a potent vasoconstrictor.
Lipid lowering agents, other	• Fenofibrate (Lipofen) • Niacin (Niacor)	These agents are used to iprove lipid profile, fenofibrate increases VLDL catabolism.
Antiplatelet agents, cardiovascular	• Aspirin	Strong inhibitor or PG synthesis and platelet aggregation (improves thrombosis).

Nevertheless, the combination of several drugs for individual risk factors can decrease the efficacy and enhance the toxicity of each drug. Therefore, there is a strong unmet medical need in reliable and efficient drugs targeting multiple symptoms of MetS over the long term, thereby minimizing problems with polypharmacy[298].

3.3.3. PPAR modulators and sEH inhibitors in the treatment of MetS

An important part of this work was the development of dual modulators inhibiting sEH and activating PPAR as a possible strategy to treat MetS, due to the important role of sEH in the metabolic syndrome. Moreover, sEH inhibitors have been shown to reduce symptoms of diabetes in several models[299]. *Trans*-4-[4-(3-adamant-1-ylureido)-cyclohexyloxy]-benzoic acid (t-AUCB) alleviated the signs of MetS *in vivo* including glucose, insulin and lipid abnormalities; furthermore inhibition or deletion of sEH prevents hyperglycemia, promotes insulin secretion, reduces islet apoptosis and decreases adipogenesis[300,301]. This inhibitor increased systolic blood pressure, cardiovascular and hepatic structural and functional dysfunction. Kim *et al.* showed that

[f] www.reference.medscape.com

treatment with EETs decreased adipocyte differentiation via increasing levels of heme-oxygenase-1 and adiponectin (involved in glucose regulation and fatty acid oxidation)[300]. Nevertheless the absence of a theoretical mechanism of action in treating diabetes caused the failure of AR9281[228] (Arête Therapeutics) in phase II trial to improve blood markers of metabolic syndrome[302].

Based on this knowledge sEH has attired the attention as a possible target to treat metabolic syndrome[301] in conjunction with selective PPAR activation.

PPARs and sEH are related through the modulatory action of sEH substrates and metabolites on PPAR. Recent publications showed that EETs are PPAR*γ* and PPAR*α* ligands[303,304]. Competition and direct binding assays revealed that EETs bind to the ligand-binding domain of PPAR*γ* specifically 14,15-EET (K_i = 3 ± 1 nM)[305]. Furthermore, latest publications discovered that DHETs have a higher potency to activate PPAR*α*[304] suggesting that DHETs may have additional vascular actions as a result of its effect on PPAR*α*.

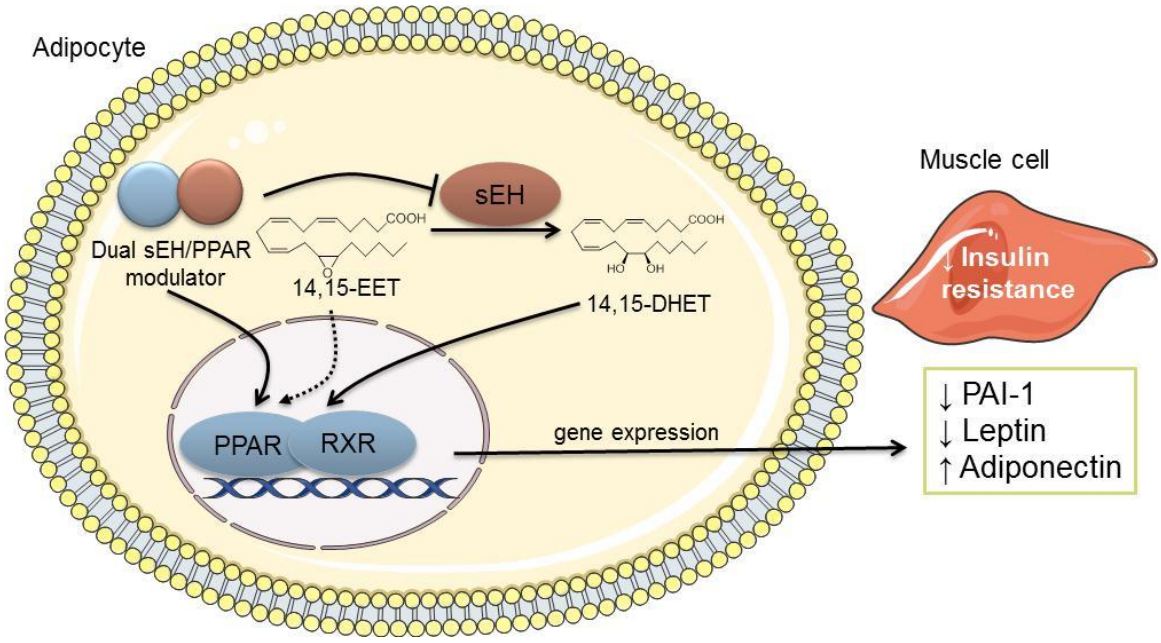

Figure 22. Mode of action : sEH inhibitor leads to a decrease DHETs which may lead to a decreased PPAR activation. This effect is compensated by sEH/PPAR dual modulation. PPAR activation leads to a decrease in plasminogen activator inhibitor-1 (PAI-1)[306], leptin and to an increase in adiponectin.

Figure 22 summarizes the expected mode of action of dual acting compounds which should lead to increased EETs level due to sEH inhibition and substitute the beneficial activation of PPAR by DHETs. Fang *et al.* discovered an activation of PPAR*α* by

substituted urea-derived sEHIs after cellular metabolism[284]. The described compounds experienced β-oxidation that reduced their ability to inhibit sEH but contributed their ability to bind and activate PPAR*α*. Further development of compounds inhibiting sEH and selectively activating PPAR could lead to agents with beneficial action on hyperglycemia, hypertriglyceridemia and hypertension which can serve as a starting point for development of polypharmacological compounds for treatment of metabolic syndrome[307].

4. Sphingolipid signaling

Within the past decade, sphingolipids (SL)[308], a family of biologically active compounds, found in eukaryotic cell membranes, emerged as active participants in the regulation of key biologic functions that regulate the proliferation, survival, and death of cells[309]. Exogenous application of ceramide is cytotoxic, and exposure of cells to radiation or chemotherapy is associated with increased ceramide[310] levels due to enhancement of the *de novo* synthesis, catabolism of sphingomyelin, or both. SLs contain a long-chain sphingoid base (such as sphingosine), an amide linkage to a long-chain fatty acid and one of different polar head groups (Table 3).

Table 3. Types of SLs.

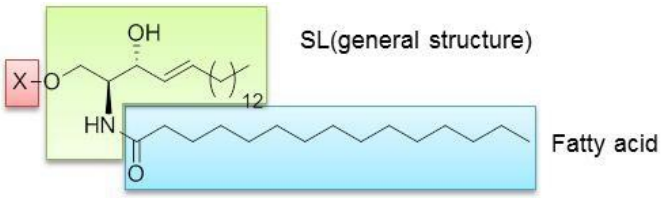

Name of SL	Name of X
Ceramide	H
Sphingomyelin	Phosphocholine
Neutral glycolipids, glucosylcerebroside	Glucose
Lactosylceramide	Di-, tri-, or tetrasaccharide
Ganglioside	Complex oligosaccharide

The head group defines the various SL classes, with a hydroxyl group found in ceramides, phosphatidylcholine in sphingomyelin and carbohydrates in the several glycosphingolipids. It has been long assumed that SLs, concentrated in the cell

membrane, to have only structural roles in the cell. However the rapid actuation of sphingomyelinase (SMase)[311] to different stimuli pointed out the existence of a SL signaling pathway[3,69,312–314].

4.1. Ceramide metabolism

Ceramide can be metabolized to less toxic forms by glycosylation, acylation, or by catabolism to sphingosine, which is then phosphorylated to the anti-apoptotic S1P (Figure 23). Glycosylceramide synthase overexpression has been shown to enhance resistance to doxorubicin or imatinib, suggesting that ceramide metabolism or catabolism might enhance cancer chemotherapy[315]. Combination of chemotherapeutic compounds and modulators of ceramide action and/or metabolism demonstrated increased anti-tumour activity in preclinical models with minimal toxicity for non-malignant cells[316].

While ceramide has been proposed as a messenger for events as diverse as differentiation, senescence, proliferation and cell cycle arrest, most research has focused on apoptosis[317–321]. Evidence supporting ceramide as messenger for apoptosis induction is based on data obtained from many different cell systems[322,323]. Moreover, agonist- and stress-induced increases in ceramide levels precede biochemical and morphologic manifestations of apoptosis in many systems. Incubation of cancer cells in the presence of SL analogues[324] (like B13, adamantyl-ceramide, C_{18} and thiouracil-ceramide) triggered caspase activation and apoptosis. The mechanisms by which SLs induce caspase activation[325] likely involve mitochondrial events such as cytochrome *c* release since overexpression of Bcl-2 or Bcl-xL counteracts SL cytotoxic effects[326].

Ceramide can be formed *de novo*, involving serine palmitoyl transferase (SPT), (dihydro)ceramide synthase (CerS 1-6). The genes encoding CerS are also name Lass (longevity assurance)[327,328]. The biological functions of these Lass-generated ceramides in regulating cell growth and/or pathogenesis have been investigated. Defects in the Lass-1 dependent generation of C_{18}-ceramide were implicated in the pathogenesis and/or progression of squamous cell carcinomas of the head and neck[329].

Specifically, it has been shown that the majority of these tumours contained lower levels of C_{18}-ceramide compared to their normal counterparts, suggesting that defects in the Lass-1/C_{18}-ceramide pathways might be important for tumour progression.

Interestingly, it has been demonstrated that the levels of C_{16}-ceramide are significantly up-regulated in some tumors[330], compared to their normal adjacent tissues. These data suggest that endogenous ceramides with different fatty acid chain lengths might have distinct biological functions. For example, while C_{18}-ceramide induces anti-proliferative responses, C_{16}-ceramide might exert pro-survival responses[331].

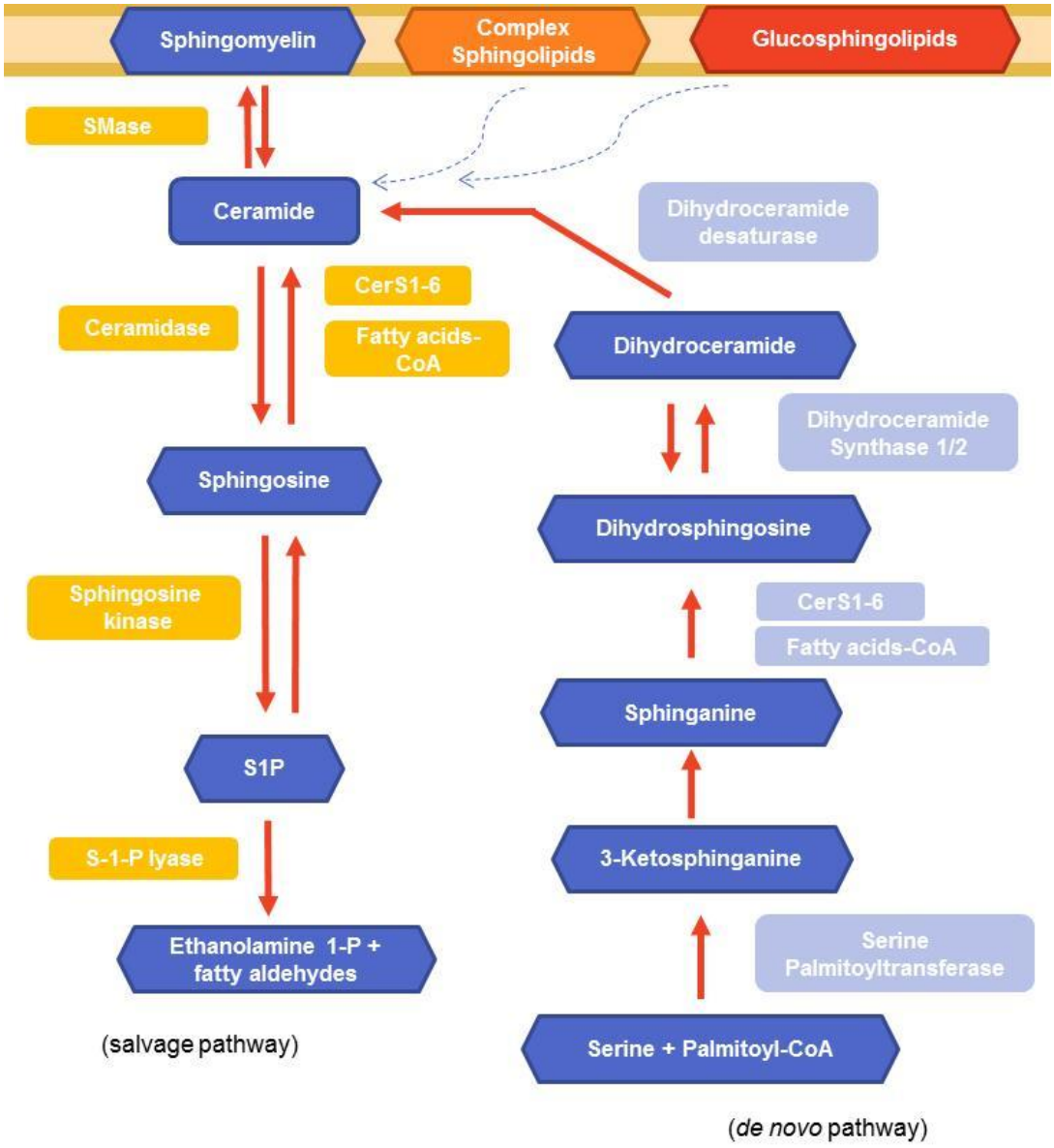

Figure 23. *De novo* and salvage pathway to biosynthesize ceramide.

There are three main pathways for ceramide synthesis. *De novo* synthesis takes place at the endoplasmic reticulum and it involves the condensation of L-serine with palmitoyl-CoA by SPT generating 3-ketosphinganine. After the action of 3-oxosphinganine reductase, sphinganine is obtained which is further acetylated yielding

dihydroceramide by ceramide synthase. The last step is the conversion of dihydroceramide to ceramide by dihydroceramide desaturase[332].

The salvage pathway involves the degradation of complex SLs to form ceramides and afterwards sphingosine. Alternatively, sphingosine can be phosphorylated to obtain S1P which is cleaved by S1P-lyase to obtain phosphatidylethanolamine and fatty aldehydes[333].

A third pathway involves SMase (acid, neutral or alkaline) which hydrolyses sphingomyelin, yielding ceramide. Ceramide levels also may be elevated by inhibiting acid, neutral, or alkaline ceramidase yielding sphingosine. Ceramide, sphingosine and S1P have emerged as key LM and ceramidase plays an important role in maintaining a balance between their pro- or anti-apoptotic functions.

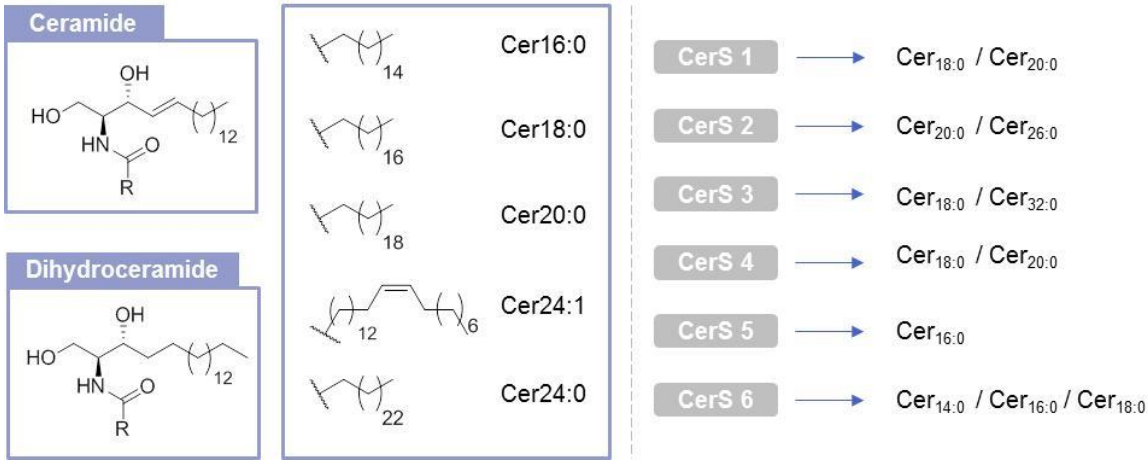

Figure 24. Ceramide structure and fatty acids alkylic chain.

All CerS have similar values for K_m for sphinganine (1.8-4.8 µM)[334] but differ in their selectivity for acyl-CoAs based on different fatty acids[335] (Figure 24).

The expression of the different CerS is tissue specific. In particular, CerS1 is highly expressed in brain, skeletal muscle and testis, whereas CerS2 (kidney, liver), CerS3 (testis, skin) and CerS4-6 are low expressed in other tissues[336–339]. Decreased levels of endogenous ceramide, caused by the overexpression of one of its metabolizing enzymes, results in the development of multidrug resistance phenotype in many cancer cells. Increased levels of glycosylated ceramide have been found in resistant tumor-cells suggesting that shunting to glycosylation may decrease the cytotoxic effects of chemotherapy[316].

More interesting is the fact that biosynthesized ceramides have opposite effects when triggering apoptosis or promoting cell survival. Treatment of cells with different apoptosis inducing agents like ionizing radiation, UV light, TNF-α, VEGF or chemotherapeutic agents (etoposide, vincristine, daunorubicin, doxorubicin, fludarabine, placlitaxel, fenretinide, etc)[310] leads to an accumulation of ceramide and therefore they are called "tumor suppressor" LMs. Chemotherapy-mediated increase results from the stimulation *de novo* pathway of ceramide biosynthesis increase in SMase activity or disruption of ceramide catabolism. Ceramide mediates antiproliferative responses by regulating its down-stream targets like cathepsin D, ceramide-activated phosphatase and kinases such as the kinase suppressor of Ras, MAPK, RAF (proto-oncogene serine/threonine-protein kinase), protein kinase C ζ (PKCζ) and MAPK/ERK. Down-stream indirect targets of ceramide are caspases, c-Myc and telomerases[340].

Hartmann *et al.* showed in MCF-7 breast cancer cells and HCT-116 human colon cancer cells that overexpression[331] of CerS4 and CerS6 inhibits cell proliferation by the up-regulation of long chain ceramides $C_{16:0}$, $C_{18:0}$ and $C_{20:0}$. On the other hand, up-regulation of CerS2[341] and therefore increase on $C_{24:0}$ and $C_{24:1}$ promotes cell proliferation. Moreover an increase of long chain ceramides[342] is accompanied by the induction of apoptosis (Figure 25). The balance between $C_{16:0}$ and $C_{24:0}$/$C_{24:1}$ ceramides is important for induction of apoptosis in several cancer cell lines. CerS5 plays an important role in sphingosine salvage pathway[343] signaling and in the response to cellular stress.

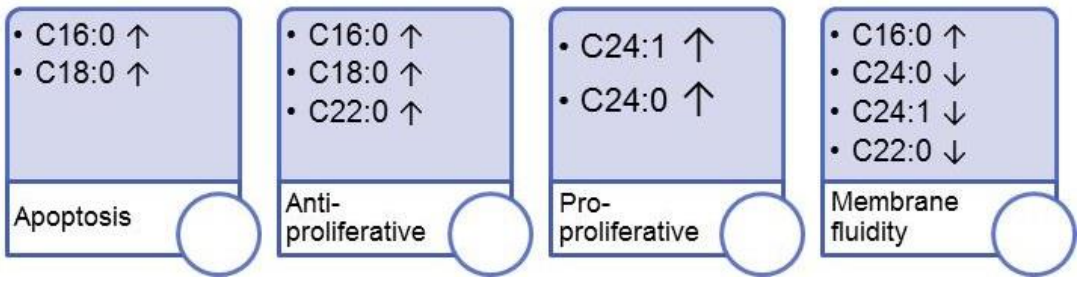

Figure 25. Chain length-specific function of ceramides[341] (according to Grösch *et al.*).

4.1.1. Sphingolipids analogues and inhibitors of ceramide metabolism

As a potential therapy for the treatment of cancer[330] in conjunction with chemotherapeutic agents, SL enzymes play an important role and the discovery of SL analogues and/or ceramide metabolism inhibitors (Figure 26) is essential to success.

Potential drug targets in the sphingomyelin pathway[344] are SPT, CerS, ceramidase, glucosylceramide synthase and sphingosine kinase as the key enzymes[345].

As SPT inhibitors that impair the condensation of serine and palmitoyl CoA to produce 3-ketodihydrosphingosine include sphingofungins, lipoxamycin and myriocin, which are natural products are really selective[346,347].

Catabolism of ceramide occurs by the action of ceramidases which hydrolyze the amide bond to yield the sphingosine moiety and fatty acids. They can be classified depending on the optimum pH of reaction into acidic, neutral and alkaline[348]. The main representative of neutral/alkaline ceramidase inhibitor is (1*S*, 2*R*)-D-*erythro*-2-(N-myristoylamino)-1-phenyl-1-propanol (D-MAPP) and N-oleoylethanolamine (NOE) as acidic ceramidase inhibitor[349,350].

Known inhibitors of CerS include sphingosine analogues such as fumonisin B_1[351], AAL toxin, australifungin (a product of the fungus *Sporormiella australis*) and the synthetical FTY720[352] (fingolimod) a myoricin analogue currently in clinical trials for the treatment of multiple sclerosis[353,354].

For example as glucosylceramide synthase inhibitors two classes can be found: ceramide analogues such as 1-phenyl-2-decanoylamino-3-morpholino-propanol (PDMP)[355] and iminosugars like N-butyldeoxynojirimycin (NBDNJ)[356]. Both inhibitors classes are the most efficient SL metabolism inhibitors.

There are a large number of compounds structurally not related to SMases that act as inhibitors, probably by inducing proteolytic degradation. As an example, desipramine has been used to inhibit ceramide formation[357]. Amitriptyline, a tricyclic antidepressant too, only inhibits the acidic SMase[358].

In general SL metabolism inhibitors (Figure 26) are often natural products with difficult synthesis (because of several stereocenters) and poor pharmacological properties with the exception of sphingosine kinase inhibitors having more “drug like” chemical structures like thiazoles, pyrazoles and coumarines[359].

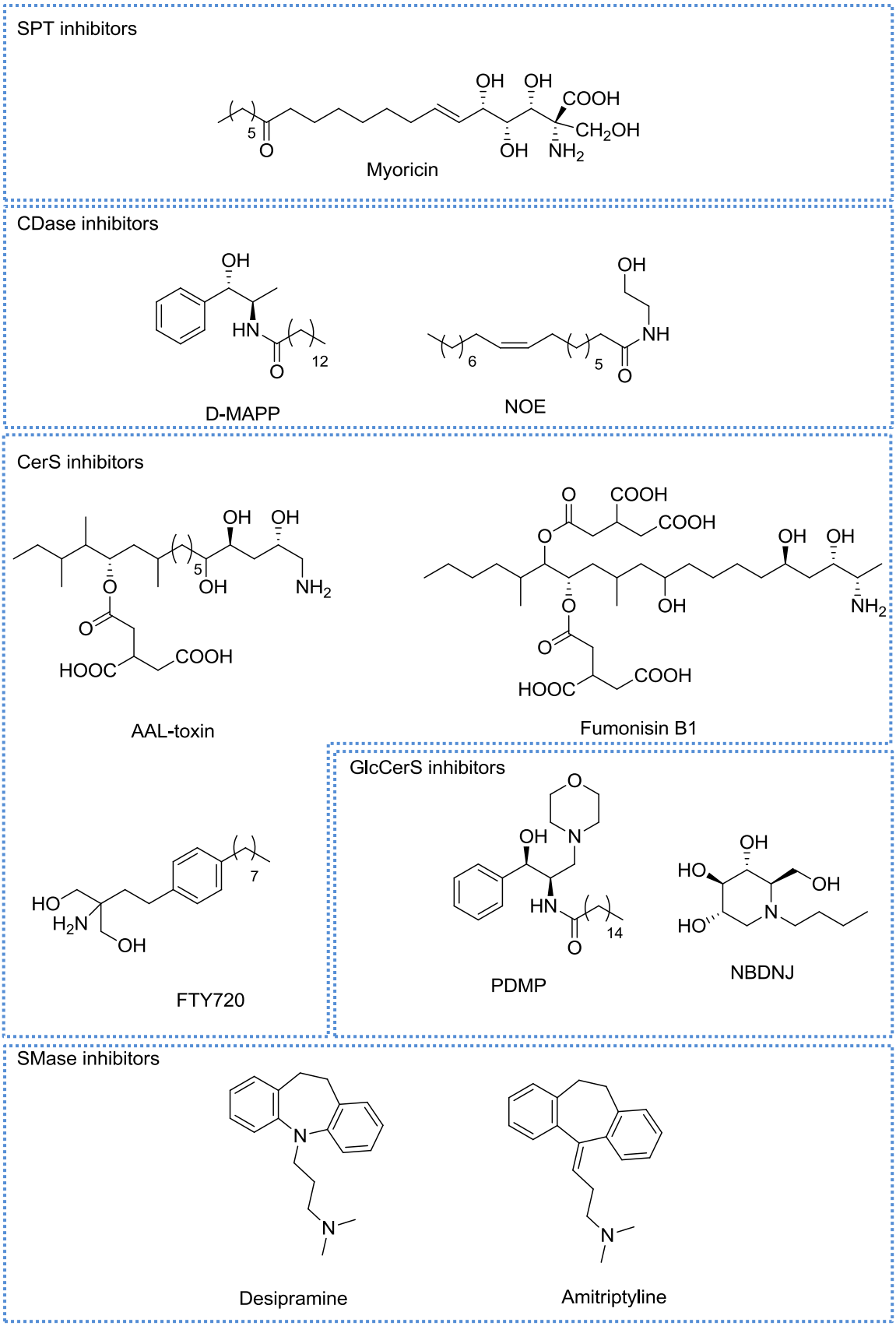

Figure 26. Inhibitors of ceramide metabolism.

4.2. Crosstalk between arachidonic acid and sphingolipid metabolism

A number of research groups demonstrated that AA was released[36] from cells undergoing apoptosis induced by TNF-α and that $cPLA_2$ activity was necessary for cell death[360]. A number of hypotheses have been postulated to explain the contribution of AA and $cPLA_2$ in cell death. For example AA might activate the neutral SMase causing production of ceramide and apoptosis. Alternatively LO pathway has been suggested to be important for TNF-α induced apoptosis[361]. AA has been reported to be toxic in different cell lines like A-549, MCF-7, HeLa, HepG2 (when they are not overexpressing CYP)[360].

Chen *et al.* demonstrated that AA induced apoptosis[36] in BM3 cells via activating neutral SMase, after blocking AA-induced apoptosis by adding the SMase inhibitor scyphostatin. The blockade of this effect provided direct evidence that unesterified AA induces apoptosis through the activation of neutral SMase resulting in conversion of sphingomyelin to ceramide.

Remarkably, it has been recently published that an increase in ceramide results from blockade of the COX, LO, and CYP metabolic pathways[362] which have AA as a substrate, would result in elevated levels of AA, and subsequent increases in ceramide/apoptosis resulting from increased function of neutral SMase. Specifically, it is postulated that a combination of agents blocking COX-1 (e.g. indomethacin, ketoprofen), COX-2 (celecoxib), 5-LOX (e.g. AA-861, ketoconazole) and/or the p450 pathway (miconazole) would have a synergistic effect on clinical glioma cell killing by either radiation, or chemotherapeutic therapy[363] (Figure 27). Kwon *et al.* demonstrated that exposure of cultured cortical neurons to AA (50 µM) yielded apoptosis which was attenuated by LO inhibitors or CYP450 inhibitors rather than COX inhibitors[364].

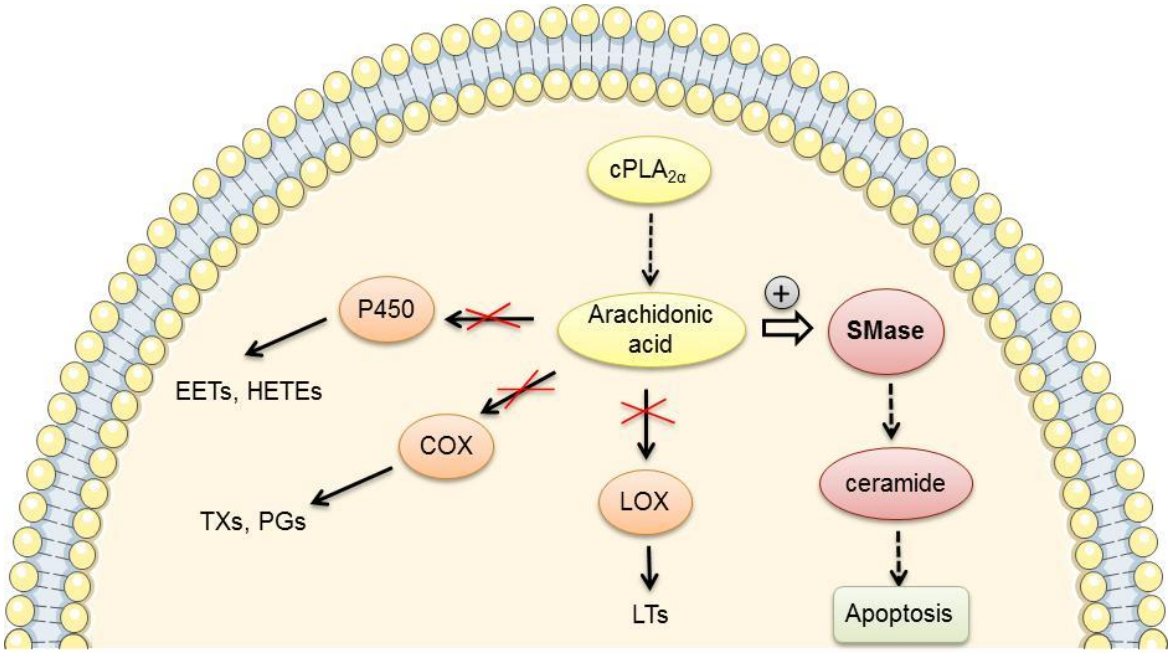

Figure 27. Postulated mechanism by Omahen *et al.* augmentation of cell apoptosis by blockage of AA metabolism.

Moreover, overexpression of LO, and its metabolites has been shown in many tumours, including meningiomas and malignant gliomas, natural LO inhibitors such as the boswellic acids induce apoptosis in high grade gliomas[365]. It would appear that investigating the efficacy of COX/LO/CYP inhibition[366] in augmenting currently accepted cytotoxic therapies for malignant tumours has the potential to produce clinically relevant results. Furthermore, exposure of cultured cortical neurons to AA (50 µM) yields neuronal apoptotic cells through[364] LO and CYP pathway rather than COX.

5. Affinity chromatography as a tool for target identification

To understand the regulation of complex cellular events like lipid signaling, functional analysis of each protein involved in the signaling cascade is required[367].

Identification of novel validated targets remains a top priority in modern drug discovery[368]. Chemical proteomics[369,370] is a powerful approach to discovery new targets or to elucidate possible side effects of a lead candidate. Unlike the traditional target-based drug discovery that starts from the identification and validation[371] of a target that is often poorly validated and fails to give the full picture of a disease, chemical proteomics cannot be realized without the establishment of reliable mechanism for target indentation by performing a phenotypic screening (Figure 28).

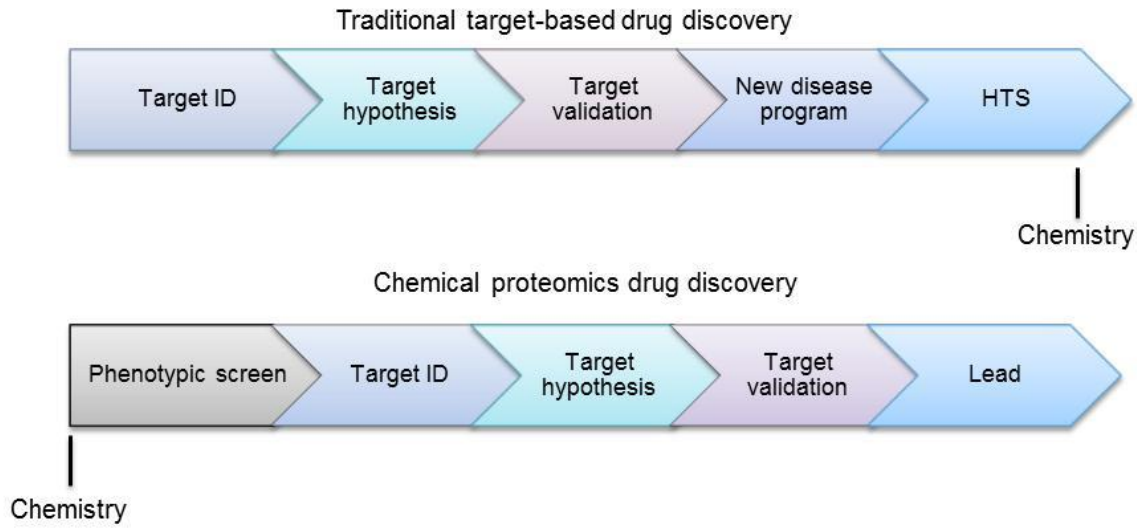

Figure 28. Conventional target-based drug discovery versus chemical proteomics approach.

Failures in drug development programs were related to unspecified mechanism of action, poor PK properties and safety issues. Chemical proteomics has also been used to discover new targets for known drugs, allowing the expansion into new disease indications and the understanding of off-target liabilities. Chemical proteomics is a key approach for target identification and one of the most powerful methods for detecting interactions between a compound and target proteins[372].

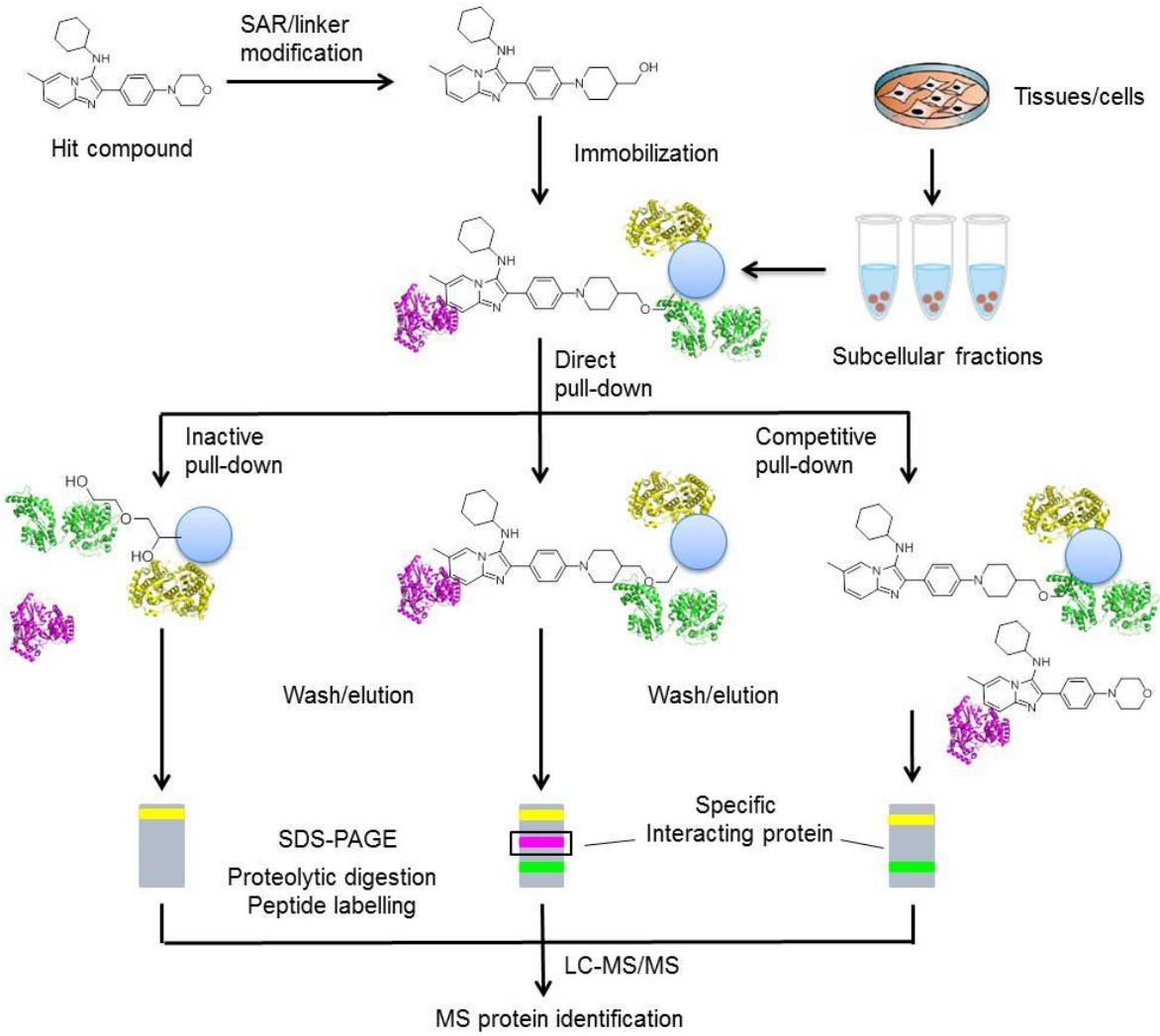

Figure 29. Drug-affinity chromatography strategy followed in this work to unravel off-target effects.

It combines drug-affinity chromatography and mass spectrometry (MS) analysis for protein identification. The affinity beads contain via suitable linker (Figure 29) and functional group the desired small molecule to be used for obtaining bound proteins[373]. A protein bond to the affinity beads is washed and then eluted with the free compound. In the case the small molecule is not soluble in a buffer system the beads are inactivated in loading buffer and analyzed by SDS-PAGE and the bands of interest are then cut off proteolitically digested and analyzed by LC-MS/MS[374–378].

Aims and objectives

Lipid signaling cascades are a complex, interconnected and self-regulated systems. Targeting one or more enzymes implicated in several pathophysiological conditions of the cell could lead to alleviation of symptoms of various diseases. LMs are basically involved in inflammation but they play an important role in diseases such as cancer, pain, atherosclerosis, metabolic syndrome, auto-immune responses (rheumatoid arthritis, multiple sclerosis), Alzheimer's disease, etc. Since cancer has been referred as a chronic inflammation that acts as a key regulator of tumor promotion and progression including evasion from apoptosis, enhanced angiogenesis and metastasis; targeting LMs involved in inflammation such as eicosanoids and ceramide metabolism could lead to a therapy to treat cancer related malignancies[86].

The main objective of the present thesis is the synthesis of lipid signaling modulators and their evaluation *in vitro* as therapeutic strategy to overcome pathophysiological conditions (cancer, metabolic syndrome) where LMs play an important role. AA metabolism and ceramide signaling are related[379] through the fact that AA induces apoptosis by activating the neutral SMase pathway. In this regard, it has been suggested that COX and LO inhibitors may be cancer-preventive not only by inhibiting specific antiapoptotic AA metabolites but also by facilitating accumulation of AA which promotes neutral SMase activity and increases the proapoptotic ceramide[36].

Material and Methods

The following methods can be found in the different publications resulted from this PhD thesis.

Method	Paper
Chemical synthesis	Paper I, III, IV, V, VI
sEH purification and activity assay	Paper V, VI
Annexin V/PI staining	Paper V
Log *P* measurement	Paper IV

1. Experimental methods

1.1 Chemistry

The structures of the synthesized compounds were confirmed by ^{1}H, ^{13}C NMR and mass spectrometry (ESI). The purity of the synthesized compounds was determined by HPLC or combustion analysis and was found > 95%. Starting materials and solvents were purchased from Sigma-Aldrich, Apollo Scientific, Alfa Aesar or Acros Organics and were reagent grade and were used without further purification. Products were purified using a Varian 971-FP Flash Purification System on silica gel with 50 µm particle size. Thin layer chromatography was performed on Merck aluminium backed plates, precoated with silica (0.2 mm, $60F_{254}$), which were developed using UV fluorescence (254 nm). ^{1}H and ^{13}CNMR spectra were measured in DMSO-d_6 or MeOH-d_4 on a Bruker AV 250 (250 MHz for ^{1}H-NMR and 63 MHz for ^{13}C-NMR), Bruker AMX 400 (400 MHz) (75 MHz for ^{13}C-NMR) and Bruker AV300 (282 MHz for ^{19}F-NMR). Chemical shifts (δ) are reported in parts per million (ppm) using tetramethylsilane (TMS) as internal standard. All coupling constants (J) are given in Hertz and the splitting patterns are designed as follows: s (singlet), d (doublet), dd (doublet of doublets), t (triplet), dt (doublet of triplets), q (quartet), and m (multiplet) Mass spectra were obtained on an Electrospray-Ionization Fisons (VG Platform II) spectrometer measuring in the positive- or negative-ion mode (ESI-MS system). High resolution mass spectra were measured by a MALDI LTQ Orbitrap XL spectrometer from Thermo Scientific. Combustion analysis was performed by the microanalytical laboratory of the Institute of Organic Chemistry and Chemical Biology, Goethe University Frankfurt, on an Elementar Vario Micro Tube CHNO rapid elemental analyzer. HPLC analysis was

performed using LC2020 (Shimadzu, Duisburg, Germany) on a Kinetex 2.6 µm C18 100 Å, 100 x 2.1 mm (Phenomenex, Aschaffenburg, Germany). This method included a water/methanol gradient run of 5-95% and detection at 254 nm and 280 nm.

1.2. Cell culture

Cell lines were obtained from the *Deutsche Sammlung von Mikroorganismen und Zellkulturen* (DSMZ). HeLa, MCF-7 and A549 cell lines were grown in Dubelcco's modified Eagle's medium (DMEM) containing 10% fetal calf serum (FCS), 100 units/mL each of penicillin and streptomycin and 1 mM sodium pyruvate. HepG2 was grown in DMEM containing 10% FCS, 0.1 mM non-essential aminoacids and 100 units/mL each of penicillin and streptomycin. U937 and A498 cell lines were grown in RPMI 1640 medium containing 10% inactivated FCS and 100 units/mL each of penicillin and streptomycin. Capan-2 cell line was grown in McCoy's 5A medium containing 10%FCS and 100 U/mL each of penicillin and streptomycin. All cell lines were grown at 37°C in an atmosphere containing 5% CO_2. Cells were count using a Neubauer chamber and trypan blue as staining dye.

Table 4. Cell lines used in this work.

Cell line	Morphology	Doubling time	Cell type
Capan-2	Adherent, epithelial-like cells growing in uniform monolayers	50-70 h	Pancreas adenocarcinoma
HeLa	Epithelial-like cells growing in monolayers	aprox. 48 h	Cérvix carcinoma
U937	Single cells in suspension	30-40 h	Histiocytic lymphoma
HepG2	Adherent, epithelial-like cells growing in monolayers and in small aggregates	50-60 h	Hepatocellular carcinoma
A549	Epithelial cells, growing adherently as monolayer	40 h	Lung carcinoma
A498	Epithelial-like, adherent cells growing as monolayers	>60 h	Kidney carcinoma
MCF-7	Epithelial-like cells growing as monolayers	50 h	Breast adenocarcinoma

1.2.1. WST-1 assay

Cell viability in Capan-2, A549 and MCF-7 was determined using the water soluble and stable tetrazolium salt WST-1 (Roche, Mannheim, Germany) which is cleaved to a

soluble formazan by a complex cellular mechanism that occurs primarily at the cell surface. This bioreduction is largely dependent on the glycolytic production of NAD(P)H in viable cells. Therefore, the amount of formazan dye formed directly correlates to the number of metabolically active cells in the culture. Cells were seeded into 96-well plates to a density of 3-5 x 10^3 cells/100 µL well (Capan-2, A549, MCF-7). After 48 h of growth to allow attachment of cells to the wells, compounds were added at various concentrations (0.3-30 µM) with a maximal DMSO concentration of 1%. After 48 h of growth, 10 µL containing WST-1 reagent was added and incubated at 37°C during 30 min. Cell viability was assessed using a microplate reader (infinite M200, Tecan Group Ltd., Crailsheim, Germany) according to the manufacturer's protocol (absorbance of the formazan product at 450 nm with a reference wavelength at 620 nm). Results are expressed as a percentage relative to vehicle-treated control (1% DMSO was added to untreated cells).

1.3. Affinity chromatography

- Preparation of sepharose beads:

28 mg of epoxy sepharose beads 6B (GE Healthcare) were soaked in distilled water (5 ml) and washed several times with distillated water (10 ml). Compound **19**, was solved in 1 ml coupling buffer (1 M Na_2CO_3/1,4-dioxane (1:1), pH 13) and added to the sepharose beads (to achieve 200 µmoles ligand per ml medium). The reaction was stirred on an orbital shaker at 40°C during 16 h at 450 rpm. Modified beads were washed with coupling buffer (2 x 10 ml) to remove excess of ligand. To block any remaining active groups, negative beads and modified beads were stirred at 50°C, during 4 h and 450 rpm with 1 M ethanolamine, pH 8.0. The beads were washed with at least three cycles of alternating pH (4.0 and 8.0). Each cycle consisted of a wash with 0.1 M acetate buffer pH 4.0 containing 0.5 M NaCl followed by a wash with 0.1 M Tris-HCL buffer pH 8.0 containing 0.5 M NaCl. For pull down assays, purified recombinant 5-LO was incubated with the negative and modified beads, o/n at 4°C. Afterwards, centrifugation at 2,400 x *g*, 5 min, 4°C and three washing steps with 1 ml PBS/EDTA 1 mM, 1 ml PBS/EDTA 1 mM with 0.5 M NaCl and 1 ml PBS/EDTA 1 mM.

In the case of celecoxib and DMC, same procedure was used.

When lysate cells were used, lysate was applied directly to the beads or pre-incubation with negative beads at 4°C during 4 h followed prior to direct application.

- Lysis buffer:

Lysis buffer for PMNL (EP6 experiment): 50 mM HEPES, pH 7.4, 200 mM NaCl, 1 mM EDTA, 1% Triton X-100, 2 mM PMSF, 10 µg/ml leupeptin, 120 µg/ml STI, sonicated (3 x 10 sec, MS 72, Sonoplus HD 200, Bandelin electronic) and centrifugated (2,400 x *g*, 10 min, 5°C)

Lysis buffer for MCF-7 cells (celecoxib, dimethycelecoxib experiments): 137 mM NaCl, 25 mM MOPS, 0.1% Triton X-100, 15 mM EGTA, 100 µM PMSF, 2 µg/ml Leupeptin, 0.1 mM Na_3VO_4, 15 mM $MgCl_2$, sonicated (3 x 10 sec, MS 72, Sonoplus HD 200, Bandelin electronic) and centrifugated (2,400 x *g*, 10 min, 5°C)

Lysis buffer for HeLa cells (celecoxib, dimethycelecoxib experiments): 50 mM HEPES, pH 7.4, 200 mM NaCl, 1% Triton X-100, 100 µM PMSF, 20 µM leupeptin.

HeLa cells (6 x 10^6 cells) were seeded in normal growth media and allowed to attach for 24h at 37°C, 5% CO_2. To start the stimulation, medium was replaced by DMEM medium containing TNF-α (5 ng/ml) and IL-1β (1 ng/ml) during 16 h to overexpress COX-2, sonicated (3 x 10 sec, MS 72, Sonoplus HD 200, Bandelin electronic) and centrifugated (5,000 x *g*, 10 min, 4°C).

In all cases, prior SDS-PAGE, beads/eluted fractions were heated at 95°C during 5 min in loading buffer (250 mM Tris-HCl, pH 6.8, 5 mM EDTA, 50% glycerol, 10% SDS, 0.05% bromophenol blue, 10% β-mercaptoethanol).

1.4. SDS-PAGE and Western Blotting

Protein extracts (equal amount) were separated by 10% SDS-polyacrylamide gel electrophoresis (SDS-PAGE) and were electrophoretically blotted onto a nitrocellulose membrane (GE Healthcare). Membranes were dried prior being incubated overnight in Odyssey blocking buffer. Afterwards, membranes were treated (5 ml, 1:1000) with the primary antibody against COX-2 (anti-human COX-2, mouse, monoclonal in 1:1 PBS/blocking buffer + 0.1% Tween-20) at 4°C overnight. Membranes were washed four times with PBS/0.2% Tween-20 and were treated (5 ml, 1:5000) with a secondary antibody (anti-mouse, IRDye680 or IRDye800 conjugated). After several washing steps with PBS/0.2% Tween-20, the blots were visualized on an Odyssey Infrared Imaging System.

1.5. Statistics

Data are expressed as mean values with S.E. All IC_{50} and EC_{50} values are means with S.E. or S.D. of the IC_{50} or EC_{50} values obtained from measurements at five different concentrations of the compounds in three to five independent experiments. IC_{50} and EC_{50} values were determined using a sigmoidal dose response (variable slope) equation from GraphPad Prism® (GraphPad Software, LaJolla, USA) software. Data were analyzed taking a *P*-value < 0.001 as significant (n=3) (one way ANOVA and Dunnett's *post hoc* test).

Results and discussion

Paper I: Rörsch, F.; Buscató, E.; Deckmann, K.; Schneider, G.; Schubert-Zsilavecz, M.; Geisslinger, G.; Proschak, E.; Grösch, S. Structure–activity relationship of nonacidic quinazolinone inhibitors of human microsomal prostaglandin synthase 1 (mPGES 1). *Journal of Medicinal Chemistry* **55**, 3792–3803 (2012).

Paper II: Hieke, M.; Rödl, C. B.; Wisniewska, J. M.; Buscató, E.; Stark, H.; Schubert-Zsilavecz, M.; Steinhilber, D.; Hofmann, B.; Proschak, E. SAR-study on a new class of imidazo[1,2-*a*]pyridine-based inhibitors of 5-lipoxygenase. *Bioorganic & medicinal chemistry letters* **22**, 1969–75 (2012).

Paper III: Wisniewska, J. M.; Rödl, C. B.; Kahnt, A. S.; Buscató, E.; Ulrich, S.; Tanrikulu, Y.; Achenbach, J.; Rörsch, F.; Grösch, S.; Schneider, G.; Cinatl, J.; Proschak, E.; Steinhilber, D.; Hofmann, B. Molecular characterization of EP6, a novel imidazo[1,2-*a*]pyridine based direct 5-lipoxygenase inhibitor. *Biochemical pharmacology* **83**, 228–40 (2012).

Paper IV: Buscató, E.; Wisniewska J. M.; Rödl C. B.; Brüggerhoff, A.; Kaiser A.; Rörsch, F.; Kostewicz E.; Schubert-Zsilavecz M., Grösch, S.; Steinhilber D., Hofmann B. and Proschak, E., Structure activity relationship and *in vitro* pharmacological evaluation of imidazo[1,2-*a*]pyridine-based inhibitors of 5-lipoxygenase. *Future Medicinal Chemistry* (2013), *in press*.

Paper V: Buscató E.; Büttner, D.; Brüggerhoff, A.; Klingler, F.-M.; Weber J.; Scholz, B.; Živković, A.; Marschalek, R.; Stark, H.; Steinhilber D., Bode, H.B.; Proschak E.; From a multipotent stilbene to soluble epoxide hydrolase inhibitors with antiproliferative properties. *ChemMedChem* (2013), *in press*.

Paper VI: Buscató, E.; Blöcher, R.; Lamers, C.; Klingler, F.-M.; Hahn, S.; Steinhilber, D.; Schubert-Zsilavecz, M.; Proschak, E. Design and synthesis of dual modulators of soluble epoxide hydrolase and peroxisome proliferator-activated receptors. *Journal of medicinal chemistry* **55**, 10771-5 (2012).

1. Paper I: *Structure–activity relationship of nonacidic quinazolinone inhibitors of human microsomal prostaglandin E2 synthase-1 (mPGES-1)*

Background and rationale: mPGES-1 is an inducible enzyme of the AA cascade and mainly coupled to the expression of cyclooxygenase-2 (COX-2). mPGES-1 is a member of the MAPEG family an exhibits glutathione-dependent PGE synthase activity.[380] Proinflammatory stimuli such as lipopolysaccharide (LPS) upregulate the protein level of both enzymes. The major product, prostaglandin E_2 (PGE_2), plays an important role in the mediation of pain,[381,382] fever,[383] the development of various cancer types (including intestinal tumors and prostate and lung cancers,[86] and several inflammatory diseases like rheumatoid arthritis[384]. mPGES-1 deletion modulates evoked pain inflammation and ameliorates the experimental autoimmune encephalomyelitis which is thought to be a model of multiple sclerosis. PGE_2 production is inhibited by nonsteroidal anti-inflammatory drugs (NSAIDs), specifically selective and nonselective COX-inhibitors. To overcome the side-effects observed when inhibiting COX enzymes, inhibition of mPGES-1 might improve the pharmacological profile of current analgesic, anti-inflammatory, and antipyretic medication due to a reduction of side effects as compared to known NSAIDs.

Enzyme inhibition can be accomplished following two aproaches, down-regulation of mPGES-1 expression or inhibition of the enzyme activity. Often inhibitors of the human mPGES-1 failed to inhibit on the rat enzyme *in vitro* resulting the performance of preclinical animal models impossible[385]. In a previous study, several scaffolds (quinoline, quinazolinone) were identified as mPGES-1 inhibitors using a multistep virtual screening protocol[386]. Quinazolinone (FR20) provided the structure for an extensive structure-activity relationship.

Results: The inhibitors were synthesized in a two step approach starting with a multicomponent reaction between 5-iodoanthranilic acid, carboxylic acid and a benzylic amine to yield 2,3-disubstituted-3*H*-iodoquinazolin-4-one which reacted in a copper-catalyzed related Golberd reaction with an aromatic amide to yield the desired quinazolinone structure. This compound set includes variations at three residue positions with (halogenated) aromatic and heterocyclic groups (like thiophene) as well as aliphatic side chains. It turned out that variations at R_1 in most cases considerably reduced the activity compared to the initial scaffold. Only aromatic residues with an *o*-chloro-substitution were tolerated, which points to the importance of a hydrophobic

interaction with the *o*-chlorine atom in contrast to unsubstituted phenyl moiety and *o*-fluor. Moreover, a reduced inhibition was observed when R_1 is an aliphatic residue; larger substituents like phenethyl further impaired activity. Bioisosteric replacement of the *o*-substituted phenyl-residue R_1 by a thiophene resulted in a less potent inhibitor. Apparently, the R_2 residue may be exchanged for a smaller substituent without losing potency. Simplification of the [1,1′-biphenyl]-4-ylmethyl-group to a benzyl-group, is also tolerated, with no detrimental effect on activity. Variations of the R_3 residue were only possible for some derivatives: methyl and a benzyl residues yielded comparable activities, while a replacement with cyclopropyl abolished inhibition. Therefore it was concluded R_1 is critical for the activity of this class of inhibitors, while R_2 and R_3 play a minor role (Figure 30). Regarding *in vitro* eicosanoid profiling, neither COX-1 nor COX-2 were affected at 1 µM concentration. Whole blood eicosanoid screening revealed a distinct profile for each compound including many fatty acids of the three major AA subcascades: the prostanoids, leukotrienes, and HETEs.

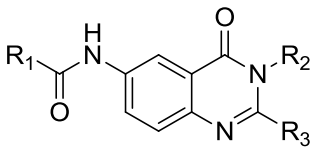

Figure 30. Quinazolinone scaffold.

2. Paper II: *SAR-study on a new class of imidazo[1,2-a]pyridine-based inhibitors of 5-lipoxygenase*

2 Paper III: *Molecular characterization of EP6, a novel imidazo[1,2-a]pyridine based direct 5-lipoxygenase inhibitor*

3 Paper IV: *Structure activity relationship and in vitro pharmacological evaluation of imidazo[1,2-a]pyridine-based inhibitors of 5-lipoxygenase*

Background and rationale: LTs also play a prominent role in chronic inflammation and in regulation of the adaptive immune response[387]. Still also anti-inflammatory properties of the 5-LO have recently been shown as the enzyme is involved in the biosynthesis of the resolvins, agents that trigger mechanisms of natural resolution of inflammation,[388] based on the multiple pathophysiological actions of LTs, there are,

increasing therapeutic indications for 5-LO inhibitors including acute and chronic inflammation, asthma and rhinitis, atherosclerosis and arthritis,[194] however its contribution to carcinogenesis is under debate[101,102]. The other major LOs, 12-LO, 15-LO1 and 15-LO2 are also discussed in this context and 15-LO activity is reported to have tumor suppressive effects[112,113]. Zileuton (Zyflo®) is the only 5-LO inhibitor that entered the US market in 1997 for the chronic treatment and prophylaxis of various clinical phenotypes of asthma. It has also been tested in the treatment of allergic rhinitis with promising results. Nevertheless, zileuton exhibits liver toxicity and an unfavorable pharmacokinetic profile with a short half-life;[175,176] as a consequence its clinical use is limited. Thus, there is a need for the design and development of new inhibitors of 5-LO. Potential drug candidates should exhibit high efficacy *in vitro* and *in vivo*; as well as desired pharmacological properties such as high selectivity for 5-LO low hepatotoxicity and good oral bioavailability.

Results: Within these three publications, an initial structure-activity relationship of imidazo[1,2-*a*]pyridine based inhibitors was described. This scaffold derived from a virtual screening for cyclooxygenase (COX)/5-LO dual inhibitors[389]. Several inhibitors were synthesized by means of the multicomponent reaction Gröbke Blackburn Bieynammé. In the first publication, different inhibition studies in a cell-based and study cell-free assay, led to a heterocyclic scaffold, which after medicinal chemistry, directed to the lead structure EP6. The initial EP6 lead compound was pharmacologically evaluated in the second publication and Wisniewska[390] *et al.* could conclude that EP6 suppresses 5-LO activity in intact PMNL with an IC_{50} value of 0.16 µM and it exhibits full inhibitory potency in cell free assays (IC_{50} = 0.05 µM for purified 5-LO). The efficacy of EP6 is not affected by the redox tone or the concentration of exogenous AA and interacts with the regulatory domain of 5-LO, the C2-like domain. EP6 suppressed 5-LO activity independently of the inflammatory stimulus or the activation pathway. The main drawback of EP6 was its inactivity in human whole blood assays due to its poor solubility and high plasma binding (98%). In the third publication, an extensive SAR (Figure 31) is described with the optimization of our *in vitro* pharmacologically evaluated lead compound (EP6). Several parts of the structure were chemically modified: small substituents at different positions of the imidazo[1,2-*a*]pyridine core and diverse functionalities at the eastern phenyl moiety. Although it was not possible to introduce a solubility group without impairing the 5-LO inhibitory activity, combination of small polar groups lead to a more favorable solubility and *in vitro* metabolic stability.

Furthermore, the cytotoxic potential of the initial lead structure could be abolished. This study demonstrated that imidazo[1,2-*a*]pyridines are a versatile scaffold for the development of novel, direct and selective 5-LO inhibitors with a favorable pharmacokinetic and toxicological profile.

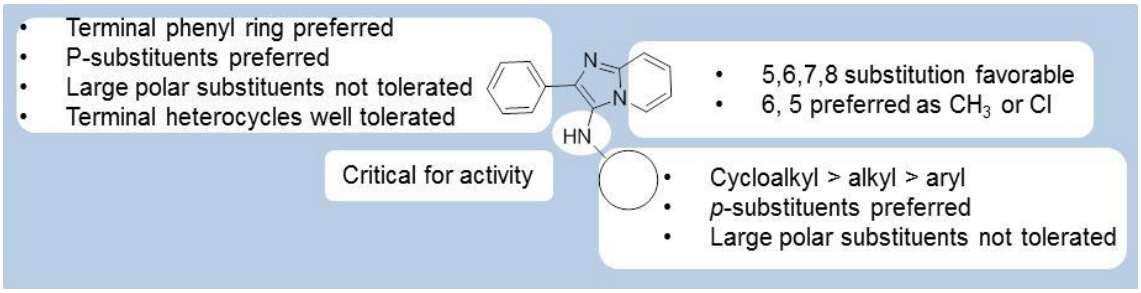

Figure 31. Summary of the structure-activity relationship of imidazo[1,2-*a*]pyridine as 5-LO inhibitors.

3. Paper V: *From a multipotent stilbene to soluble epoxide hydrolase inhibitors with antiproliferative properties*

Background and rationale: sEH is in the focus of pharmaceutical research for numerous indications including cardiovascular disorders, diabetes and inflammatory processes[219,222,391–393] Although several inhibitors reached clinical trials (AR9281, in patients with mild to moderate hypertension) no clinical outcome has been reported. Several publications have stressed the possible role of EETs and sEH in cancer growth and metastasis which is rather ambiguous.[394] EETs promote metastasis by triggering secretion of VEGF by the endothelium, which is critical for EET cancer stimulating activity. The postulated mechanism[254] for EETs to promote tumor growth is via EGFR/PI3K/Akt and EGFR/MAPK pathways[255] to promote cancer cell survival. In this study, it has been intended to discover chemical compounds exhibiting cytotoxic profile and simultaneously target sEH. Moreover, polypharmacological compounds (e.g. sorafenib) have gained a special attention in the field of cancer treatment due to the complexity of pathways involved in cancer pathogenesis[395–397]. The principle of addressing multiple targets by polypharmacological compounds can be transferred to cancer treatment.[398] In this study we intended to discover chemical compounds exhibiting cytotoxic profile and simultaneously target soluble epoxide hydrolase.

Results: an initial screening a small library of compounds isolated from entomopathogenic bacteria, namely *Photorhabdus* and *Xenorhabdus* lead to the

discovery that one of the metabolites, the pluripotent isopropylstilbene (IPS) from *Photorhabdus*[399] exhibited the desired properties by inhibiting sEH with an IC_{50} of 10 µM. After an in-house screening of a small collection of compounds exhibiting the stilbene scaffold (chalcones and resveratrol analogues), the scaffold (*E*)-styryl-1*H*-benzo[*d*]imidazole was identified as a potential new sEH inhibitor. Compounds were synthesized in two steps: condensation of a substituted *o*-phenyldiamine with the appropriated (*E*)-cinnamic acid and the cyclization of the resulting amide in the presence of hydrochloric acid. Synthesized compounds exhibited IC_{50} values ranging from 0.6-32.1 µM, resulting *ortho*-substituted compounds (on the styryl moiety) in the highest inhibition (Figure 32). The structure-activity relationship of the compounds on sEH was rather flat, which correlated with the possible binding mode proposed by the molecular docking study. The effect of most potent compounds on cell viability was evaluated on several cancer lines (HepG2, HeLa, MCF-7, A498 and U937), resulting in EC_{50} values ranging from 1.1 to 21.8 µM. In conclusion, following a natural product-inspired design approach[400] the desired biological activity of a bacterial secondary metabolite was transferred to a synthetic compound series. The natural product inspired drug design extends the valuable role of natural products as drugs and drug precursors to templates for fully synthetic bioactive molecules.

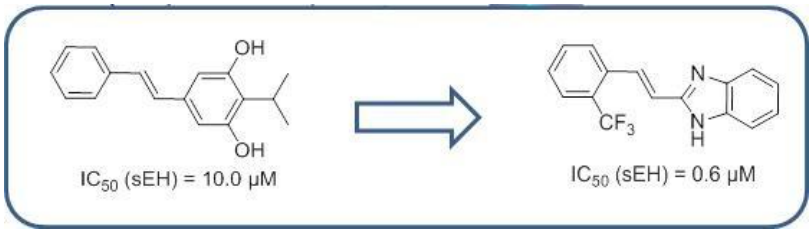

Figure 32. Natural product-inspired design of stilbene-derived sEH inhibitors.

4. Paper VI: *Design and synthesis of dual modulators of soluble epoxide hydrolase and peroxisome proliferator-activated receptors*

Background and rationale: MetS treatment is to change lifestyle of the patient to increase physical activity and initiation of drug therapy. Nevertheless, the combination of several drugs for individual risk factors can decrease the efficacy and enhance the toxicity of each drug. Therefore, efficient drugs targeting multiple symptoms of MetS over the long term are needed, thereby minimizing problems with polypharmacology[298]. Simultaneous activation of PPARγ and PPARα alters the tissue distribution of fatty

acids. Whereas PPAR*γ* agonists increase adiposity and body-weight gain[279], it has been reported that PPAR*α* agonists decrease food intake[280] and fat depots induced by PPAR*γ* agonist treatment. Dual agonism of PPAR*α/γ* ligands exerts complementary activities and has been used as new therapies for the treatment of diabetes type 2[281] and metabolic syndrome[282]. On the other hand sEH ameliorates MetS[244] and sEH knockout models as well as sEH inhibitors prevent hyperglycaemia, promote insulin secretion, reduce islet apoptosis and decrease adipogenesis[300,401]. Based on this knowledge sEH has attired the attention as possible target to treat metabolic syndrome[244] in conjunction with selective PPAR activation.

Results: In the present work novel compounds that are able to inhibit sEH and activate PPAR, regardless their metabolism, were presented. Compounds were synthesized via a combinatorial approach: phase transfer catalysis was used to obtain the *N*-alkylated products. These were reduced on Raney nickel remaining the corresponding amines which reacted with several isocyanates yielding the equivalent urea derivatives. Eventually, ester derivatives were hydrolyzed to obtain the carboxylic acids and therefore introduce the PPAR pharmacophore. Compounds were connected through a diethylphenyl linker between the pyrrole ring and the urea (sEH pharmacophore). Compounds exhibited IC_{50} values ranging from 23 nM to 2 µM on sEH; EC_{50} 2-5 µM on the different PPAR subtypes. Several subtype of PPAR agonists were developed, yielding pan-modulators, α/γ agonists or selective agonists.

5. Synthesis of 5-LO inhibitors

5.1 Synthesis of NO-NSAIDs

Besides of the three publications presented in this thesis, another type of 5-LO inhibitors have been developed and synthesized. The first group of compounds are NO-NSAIDs that have been proposed as 5-LO inhibitors (Dr Steinbrink, PhD thesis: "*Identification and characterization of sulindac sulphide as a novel type of 5-lipoxygenase inhibitor with clinical relevance*"). NO-NSAIDs consist of a conventional NSAID moiety linked, in most cases, via a spacer to an NO-releasing moiety in this case a $–ONO_2$ (nitrate) group. They are a new class of anti-inflammatory and analgesic drugs and have been investigated in cancer[402]. The combination of balanced inhibition of the two main COX isoforms with release of NO confers to NO-NSAIDs reduced gastrointestinal more safety. It is suggested that the NO, which is released as the

compounds are metabolized, may counteract the consequences of the NSAID-induced decrease in gastric mucosal prostaglandins[403].

The synthesis (Figure 33) of NO-sulindac and NO-naproxen started with an esterification of the carboxylic acids of sulindac and naproxen[404] using 1,4-dibromobutane as spacer and K_2CO_3 as a base and it was refluxed during 3h to obtain (*Z*)-4-bromobutyl 2-(5-fluoro-2-methyl-1-(4-(methylsulfinyl)benzylidene)-1*H*-inden-3-yl)acetate (**2**) and (*S*)-4-bromobutyl 2-(6-methoxynaphthalen-2-yl)propanoate (**5**) in 53% and 50% yield respectively.

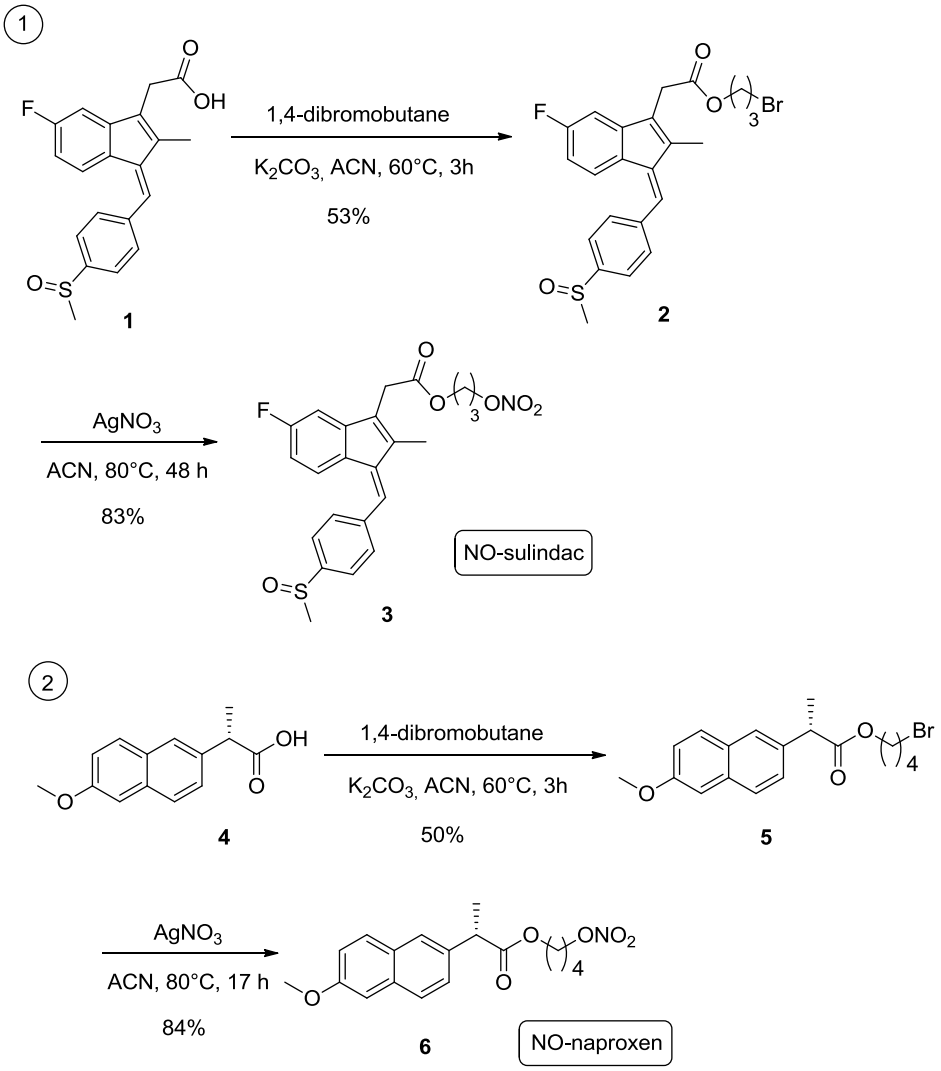

Figure 33. Synthesis of NO-sulindac (**3**) and NO-naproxen (Naproxcinod) (**6**).

The last step consisted of nucleophilic substitution using silver nitrate to obtain the nitrate derivatives: NO-sulindac (**3**) and NO-naproxen (**6**) in 50% and 84% yield respectively. Both compounds were tested[g] on several systems: on intact PMNL, recombinant purified 5-LO and human whole blood. Examinations on PMNL could evoke inhibition of 5-LO only by the NO-derivative and not by the corresponding NSAIDs. NO-sulindac inhibited 5-LO product formation with an IC_{50} value of 2 µM, whereas NO-naproxen inhibited 5-LO product formation in intact PMNL by 61% at 50 µM; naproxen did not exhibit any inhibition (Figure 34). A dose-dependent inhibition was observed in the case of NO-sulindac. BWA4C was used as positive control.

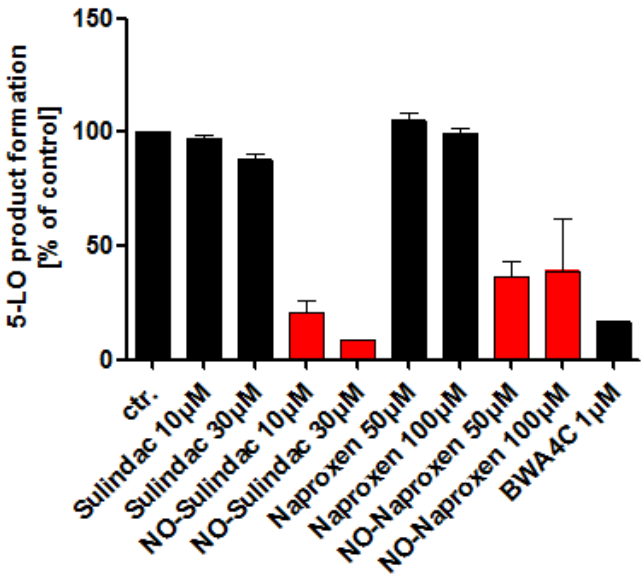

Figure 34. 5-LO product formation in PMNL (cell-based assay). 5 x 10^6 intact cells (PMNL) were preincubated with NSAIDSs respectively NO-derivatives at 4°C with concentrations indicated for 15 min. Samples were then stimulated with 2.5 µM A23187 (calcium ionophore) and supplied with 20 µM AA. Analysis of 5-LO products by HPLC was performed n=3. Values are expressed as mean + SEM.

Regarding purified 5-LO, sulindac did not affect 5-LO product formation whereas NO-sulindac led to an IC_{50}= 1 µM pointing out the importance of the NO releasing moiety (depicted in red, Figure 35). In the case of NO-naproxen the inhibition was lower (40% at 50 µM).

[g] All test were performed by Dr Steinbrink at the Pharmaceutical Chemistry Department, Goethe University Frankfurt am Main in the group of Professor Dr Steinhilber.

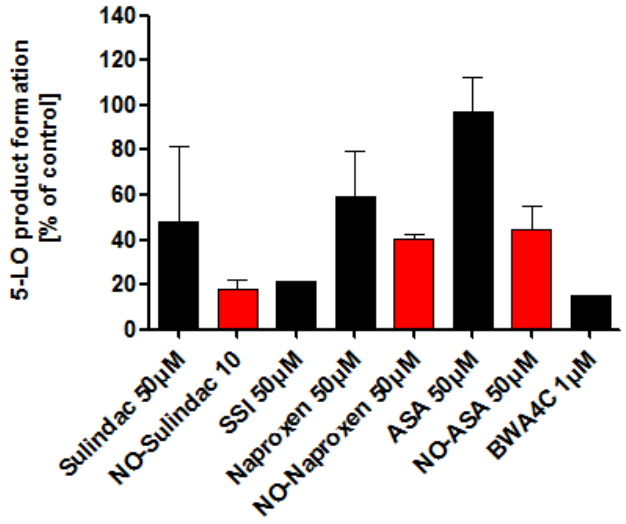

Figure 35. 5-LO product formation on recombinant purified 5-LO. Recombinant 5-LO protein was incubated with the indicated concentrations for 15 min at 4°C. 5-LO activity was started by the addition of 2 mM Ca^{2+} and 20 µM AA. Analysis of 5-LO products by HPLC was performed n=3. Values are expressed as mean + SEM.

HWB, experiments were carried out using as physiological stimulus: LPS and fMLP. 5-LO product formation (LBT_4 and 5(*S*)-HETE) were inhibited by 50% at 100 µM concentration of both NO-sulindac and NO-naproxen (Figure 36). The concentrations tested were higher than in the previous experiments in order to see inhibitory effects despite of protein plasma binding. In summary, NO-sulindac, NO-napoxen and NO-ASA (NO-aspirin) represent a new class of 5-LO inhibitors that could circumvent the undesired effects of COX inhibition and additionally reduce inflammatory processes.

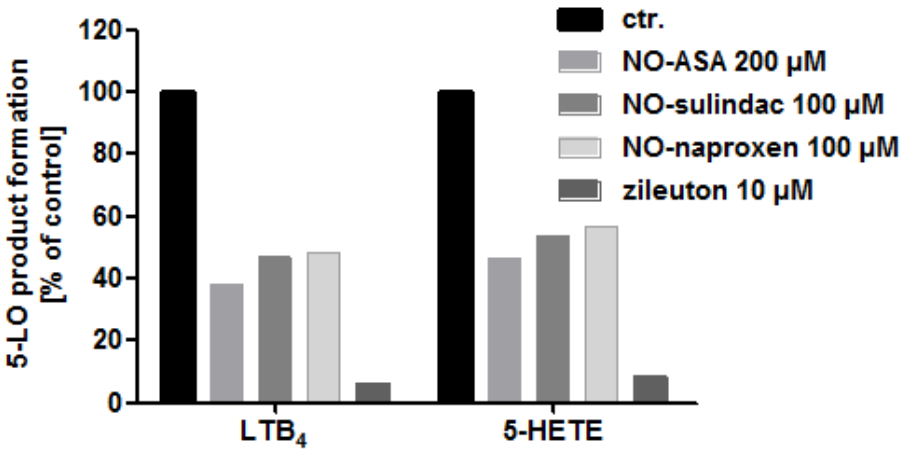

Figure 36. 5-LO product formation (LTB4 and 5(*S*)-HETE in HWB. Venous whole blood freshly from healthy volunteers was preincubated (30 min) with compounds at the concentrations given

at 37°C. After adding 10 mg/ml LPS and 1 µM fMLP reaction was performed for 1h at 37°C and stopped by cooling the samples on ice. LT levels were measured by LC-MS/MS (n=1).

5.2 Synthesis of CJ 13,610

5-LO is involved in the regulation of leukemia stem cells (LSC) activity after having found that 5-LO activity is indispensable for the induction of a CML-like disease by BCR/ABL *in vivo*[121,405]. Both, genetic targeting of 5-LO in Alox$^{-/-}$ mice and pharmacological targeting by a selective 5-LO inhibitor, abolished the leukemogenic potential of BCR/ABL. In this model 5-LO has been identified as a critical regulator of LSC in the CML-like disease. CJ 13,610[179] is a non-redox type 5-LO inhibitor that has been synthesized to prove: if the effects of 5-LO targeting the LSC in CML, are extendible to the LSC in acute myelogenous leukemia (AML) and whether 5-LO is involved in the regulation of the Wnt-signaling[406] (important pathway in the maintenance of cancer stem cells), in order to better understand how NSAID inhibit Wnt-signaling and the aberrant self-renewal of LCS in AML and CML.

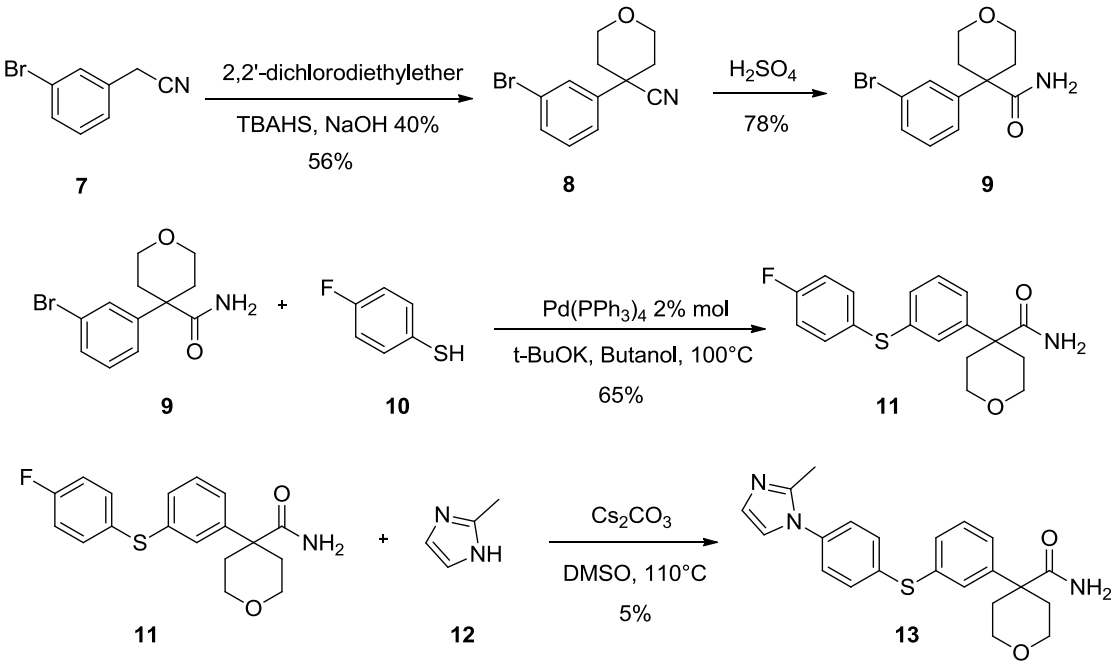

Figure 37. Synthesis of CJ 13,610 (**13**) (Pfizer).

The synthesis[407–410] followed a four step approach (Figure 37). A tetrahydropyran ring was introduced in 3-bromophenylacetonitrile (**7**) catalyzed by tetrabutylammonium sulphate (TBAHS) to obtain the desired product 4-(3-bromophenyl)tetrahydro-2*H*-

pyran-4-carbonitrile (**8**) in 56% yield. Subsequent hydrolysis using concentrated H_2SO_4 led to 4-(3-bromophenyl)tetrahydro-2*H*-pyran-4-carboxamide (**9**) in 78% yield that was used in a palladium (0) catalyzed cross-coupling involving a 4-fluorothiophenol and 4-(3-bromophenyl)tetrahydro-2*H*-pyran-4-carboxamide (**9**) and $Pd(PPh_3)_4$ to yield 4-(3-((4-fluorophenyl)thio)phenyl)tetrahydro-2H-pyran-4-carboxamide (**11**) in 65% yield. Introduction of a 1-methylimidazole group led to the desired product (**13**) in only 5% yield due to a complicated purification by LC-MS[h].

Roos *et al.* showed[i] that the pharmacological inhibition of 5-LO suppresses the aberrant stem cell capacity of hematopoietic stem and progenitor cells *in vitro* and *in vivo*. These effects were seen not only with CJ-13,610 but also using zileuton. Therefore, suppression of aberrant stem cell capacity should result from the drugs ability to specifically target 5-LO and not derive from pleiotropic effects. Taken together it has been established that the pharmacological inhibition of 5-LO is a novel approach of stem cell therapy in leukemia, by targeting the Wnt-signaling.

6. Affinity chromatography experiments

6.1 EP6 pull down assay

Pull down experiments were carried out to elucidate the possible off-targets effects when using EP6 as a 5-LO inhibitor. Wisniewska *et al.* recently published that EP6 affected the cell viability of U937 cells (lacking 5-LO expression) resulting in a EC_{50} = 14 µM[411]. The reduction of cell viability seems to be an 5-LO independent mechanism and a potential anticancer effect. Imidazo[1,2-*a*]pyridine scaffold have been already identified as topoisomerase Iiα inhibitors[412] and this target could possible the off-target effect observed on U937 cell line. In order to elucidate the possible mechanism, affinity chromatography combined with mass spectrometry was used. Since the second SAR of imidazo[1,2-*a*]pyridine pointed out that the secondary amine was necessary to inhibit

[h] The synthesis was performed according to Pfizer (EP1029865 A2, 2000, US6194585 B1, 2001).

[i] Submitted manuscript: *5-lipoxygenase as a novel principle of stem cell therapy in acute myeloid leukemia,* Jessica Roos, Claudia Oancea, Maria Heinßmann, Hannelore Held, Astrid S. Kahnt, Estel.la Buscató, Ewgenij Proschak, Dieter Steinhilber, Thorsten J. Maier, and Martin Ruthardt

5-LO product formation, an analogue of EP6 was synthesized by modifying the morpholine ring to introduce a functional group to be coupled to the sepharose beads.

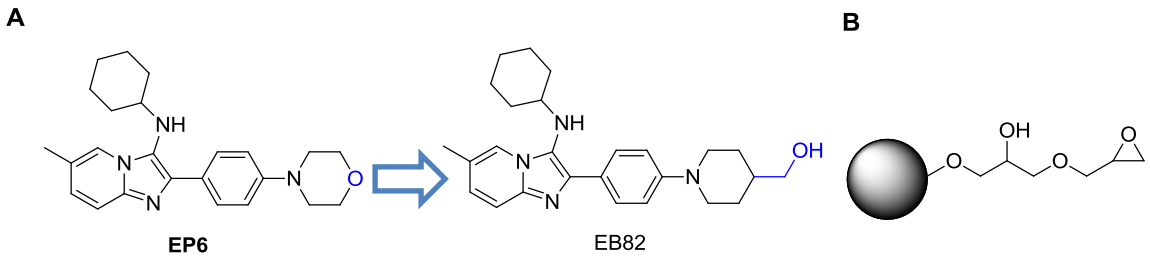

Figure 38. A. EB82 (**19**) analogue of EP6. **B**. Epoxy-activated Sepharose 6B.

The sepharose used was an epoxy-activated Sepharose 6B (GE Healthcare) that has an epoxy linker to be coupled to different chemical groups. Ligands (small molecules to be investigated) can be coupled through hydroxyl, amino or thiol groups. A hydroxyl group was chosen due to synthetical accessibility. The synthesis of EB82 (**19**) started by generating the aldehyde (**16**) necessary to perform Gröbke-Bienaymé multicomponent reaction[413]. 4-fluorobenzaldehyde (14) was treated with piperidin-4-ylmethanol (**15**) to yield 4-(4-(hydroxymethyl)piperidin-1-yl)benzaldehyde (**16**) in 35%. This intermediate was used to perform the next reaction to obtain EB82 (**19**) in 53% yield (Figure 38).

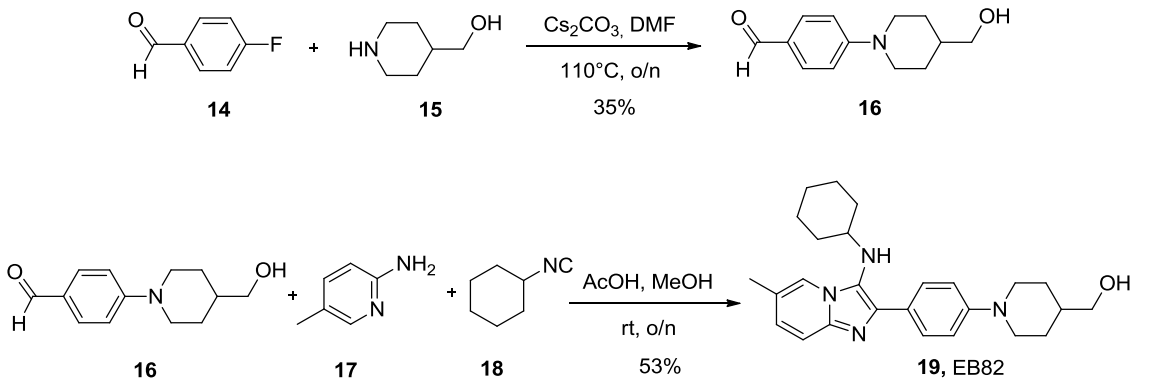

Figure 39. Synthesis of EP6 analogue (**19**) to perform pull down assays.

To evaluate if this chemical modification affected the affinity of this compounds towards 5-LO, the inhibitory activity of EB82 on PMNL[j] cells (Figure 40) was measured. EB82 (**19**) exhibited an IC_{50} = 0.34 µM. EP6 had a similar inhibitory potency (IC_{50} = 0.16 µM) and therefore the chemical modification did not affect the affinity.

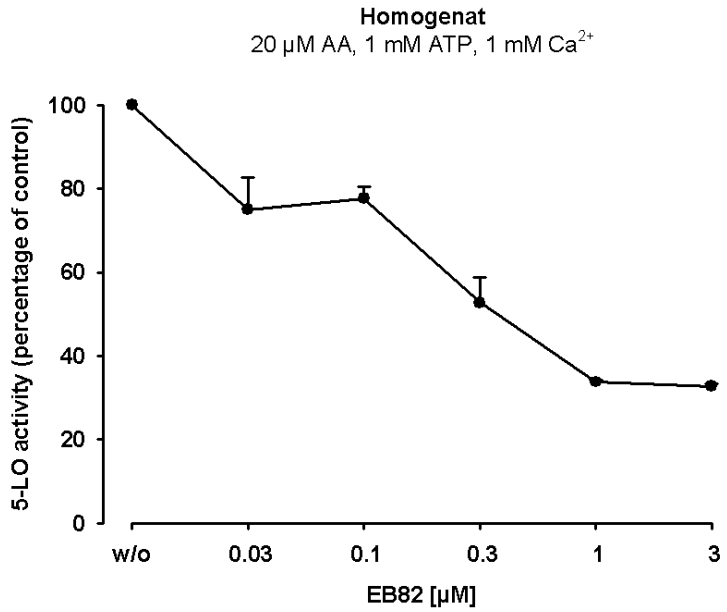

Figure 40. Inhibitory activity of EB82 (**19**) on PMNL cells. 5-LO activity assay was performed with homogenates of 7.5 x 10^6 PMNL. Homogenates were incubated in PBS/EDTA 1 mM and 1 mM ATP and the reaction was started with 20 µM AA and 2 mM $CaCl_2$. The inhibitory activity of EB82 (19) was measured as % of control (DMSO). 100% of control corresponds to 50.55 ± 18.5 ng 5-LO product/10^6 PMNL. Product formation was analyzed by HPLC (n=3, ± SEM).

In order to discriminate specific binding proteins from nonspecific binders, parallel experiments were performed: incubation with negative beads (previously cleaved with ethanolamine to remove active epoxides). In this pull-down mode, the specific binding proteins were removed while the nonspecific binding proteins remain. In order to assess if the modified beads are chemically modified and the analog (**19**) shows specific binding, recombinant 5-LO was incubated with negative and positive beads (Figure 41).

[j] Test on PMNL/pull down assays were performed by/with Dr Wisniewska (Pharmaceutical Chemistry department, Goethe University Frankfurt am Main)

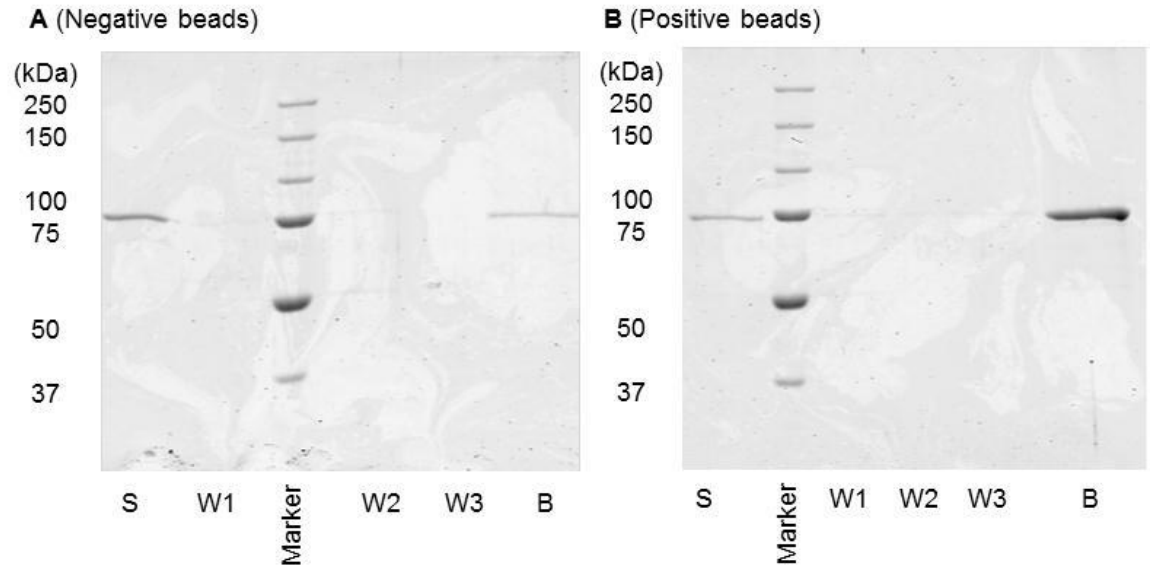

Figure 41. 10% SDS-PAGE with Coomassie staining, comparison of negative or unmodified beads (A) with coupled beads with EB82 (**19**) (B) and their affinity towards 5-LO (recombinant, purified, 0.25 µM). Marker used: All Blue. S: supernatant of the centrifugation after incubation with 5-LO, W1: wash step with PBS/EDTA 1 mM, W2: wash step with PBS/EDTA 1 mM and 0.5 M NaCl, W3: wash step with PBS/EDTA 1 mM, B: beads after boiling at 95°C during 5 min in loading buffer 2x.

After coupling of beads with compound **19** (3 µM), different concentrations of 5-LO were tested (0.25, 0.5, 1, 3 and 6 µM). Unspecific binding could be detected nevertheless; it was lower in comparison with positive beads (modified with compound **19**). Therefore, the experiment was repeated with the PMNL lysate. Lysates were incubated at 4°C with the beads and they were analyzed on a 10% SDS-PAGE. Several specific interactions (Figure 42) could be detected and after comparing the intensity of the different bands, they were cut off and analyzed after a tryptic digestion by MALDI-TOF MS in the group of Professor Karas. However, proteins could not be detected due to a high content of lipid membrane.

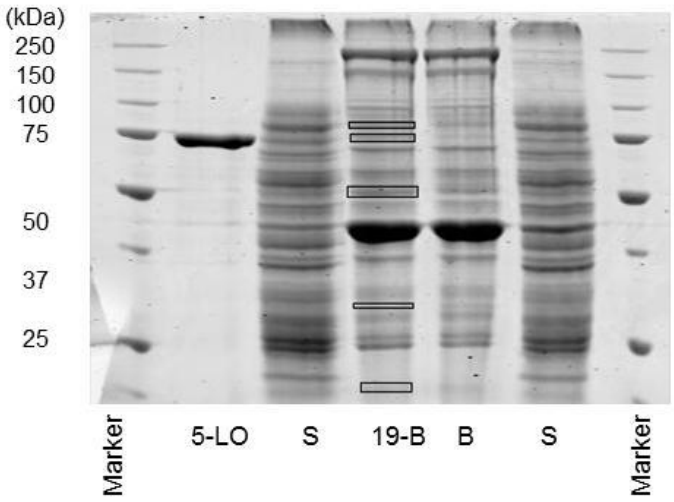

Figure 42. 10% SDS-PAGE stained with Coomassie. 1 x 10^8 PMNL were lysated and the supernatant was incubated with positive beads (19-B) or negative beads (B). Afterwards, beads were washed with the same washing steps (W1, W2, W3) and boiled in loading buffer 2x during 5 min. S: supernatant after lysis and centrifugation, 19-B: proteins that interact with positive beads (after boiling in loading buffer 2x), B: proteins that interact with negative beads (after boiling in loading buffer 2x), marker used: All Blue.

6.2 Celecoxib and dimethylcelecoxib pull down assay

Celecoxib (Celebrex®, Onsenal, Pfizer) and dimethylcelecoxib (DMC) belong to the drug family COXIBS, selective COX-2 inhibitors. Whereas celecoxib represents a potent COX-2 inhibitor, DMC is not active on COX-2[414]. Both compounds decreased tumor cell viability with IC_{50} of 73 and 53 µM respectively (A549)[415]. The mechanism has not been yet explained[416–421], several hypothesis have been proposed[422] and therefore pull down experiments have been performed to explain the off-target effect observed in these compounds (Figure 43).

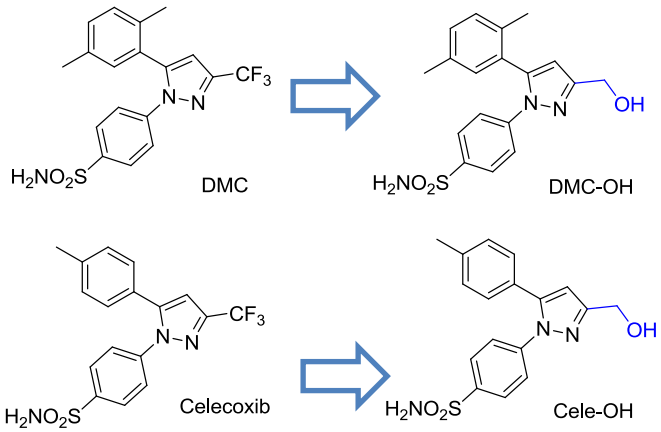

Figure 43. DMC and its analogue DMC-OH, Celecoxib and its analogue Cele-OH.

The synthesis followed to produce both free ligands and compounds to be coupled was already published[414] by Penning *et al.* The first step involved an Claisen condensation between acetophenones (**19**, **24**) and 2,2,2-trifluoroacetate (**20**) using 1.2 eq NaOMe in MeOH to obtain 1-(2,5-dimethylphenyl)-4,4,4-trifluorobutane-1,3-dione (**21**) and 4,4,4-trifluoro-1-(*p*-tolyl)butane-1,3-dione (**24**) in 53% and 54% (Figure 44).

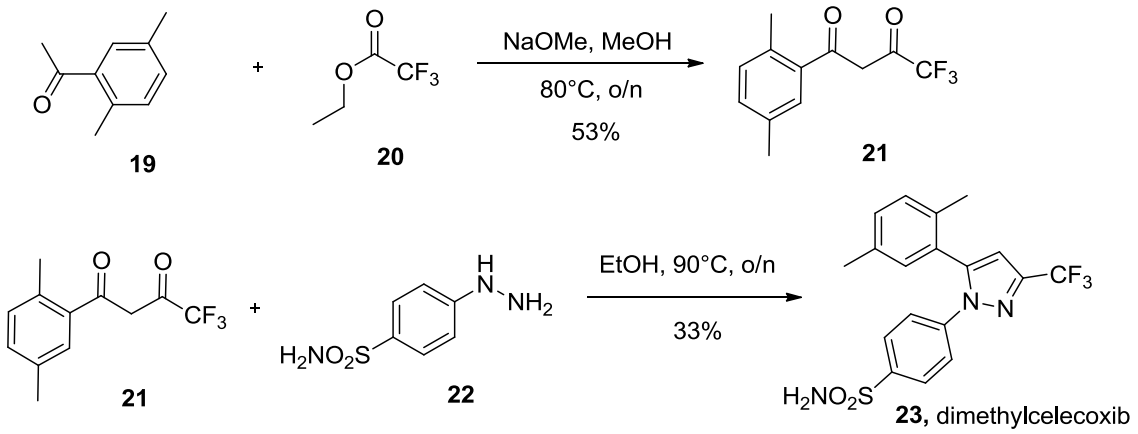

Figure 44. Synthesis of DMC, overall yield 18%.

The next step involved the reaction of the 1,3-dicarbonyl adducts (**21** and **24**) with 4-hydrazinylbenzenesulfonamide-HCl (**22**) to yield the desired 1,5-diarylpyrazole: 4-(5-(*p*-tolyl)-3-(trifluoromethyl)-1*H*-pyrazol-1-yl)benzenesulfonamide (**25**) in 8% yield after separation of isomers and 4-(5-(2,5-dimethylphenyl)-3-(trifluoromethyl)-1*H*-pyrazol-1-yl)benzenesulfonamide (**23**, DMC) in 33% yield (Figure 44 and Figure 45).

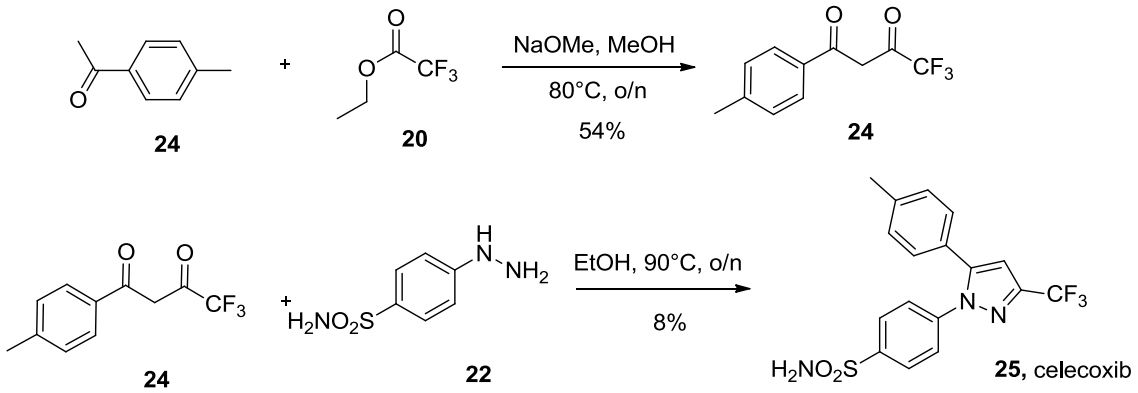

Figure 45. Synthesis of celecoxib, overall yield 4%.

To synthesize celecoxib and DMC analogues, a similar synthetic approach has been used but introducing a -CH_2OH moiety to facilitate the coupling to the beads. The first step involved a Claisen condensation between acetophenone (**19**) and 2,2,2-trifluoroacetate (**20**) using 1.2 eq NaOMe in MeOH using ultrasound bath to obtain (*E*)-1-(2,5-dimethylphenyl)-3-hydroxy-3-methoxyprop-2-en-1-one (**27**) in 72% yield.

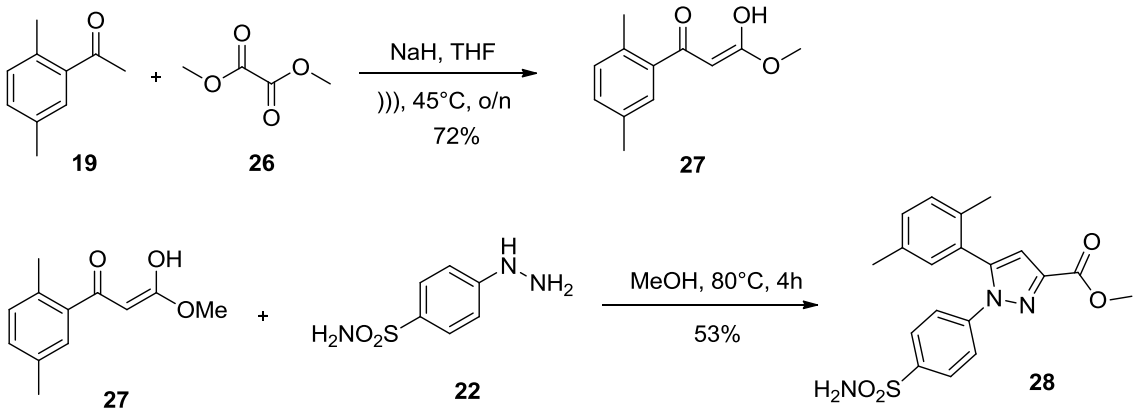

Figure 46. Claisen condensation and 1,5-diarylpyrazole formation (**28**).

The 1,3-dicarbonyl adduct reacted with 4-hydrazinylbenzenesulfonamide-HCl (**22**) to yield methyl 5-(2,5-dimethylphenyl)-1-(4-sulfamoylphenyl)-1*H*-pyrazole-3-carboxylate (**28**) in 53% that underwent reduction with $LiAlH_4$ to obtain the alcohol 4-(5-(2,5-dimethylphenyl)-3-(hydroxymethyl)-1*H*-pyrazol-1-yl)benzenesulfonamide (**29**, Cele-OH) in a moderated yield (43%). Cele-OH was synthesized by Andreas Lill (research group Professor Stark) using the same procedure.

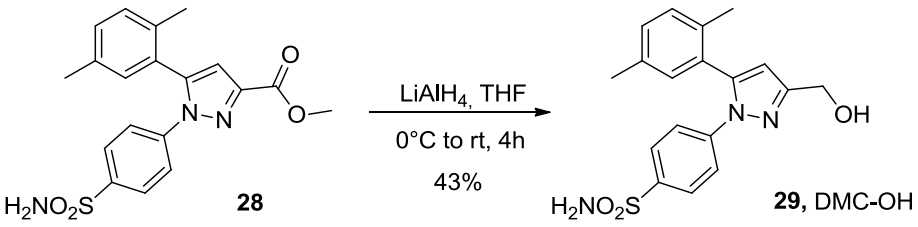

Figure 47. Reduction of 28 with $LiAlH_4$ to yield (**29**).

All synthesized compounds were evaluated using recombinant enzymes: COX-1 and COX-2. Figure 48 shows that COX-1 was not inhibited neither by DMC nor by DMC-OH, the same holds true for COX-2 inhibition, where DMC inhibited COX-2 at 80 µM by 50.6% inhibition and DMC-OH by 41% (Figure 49).

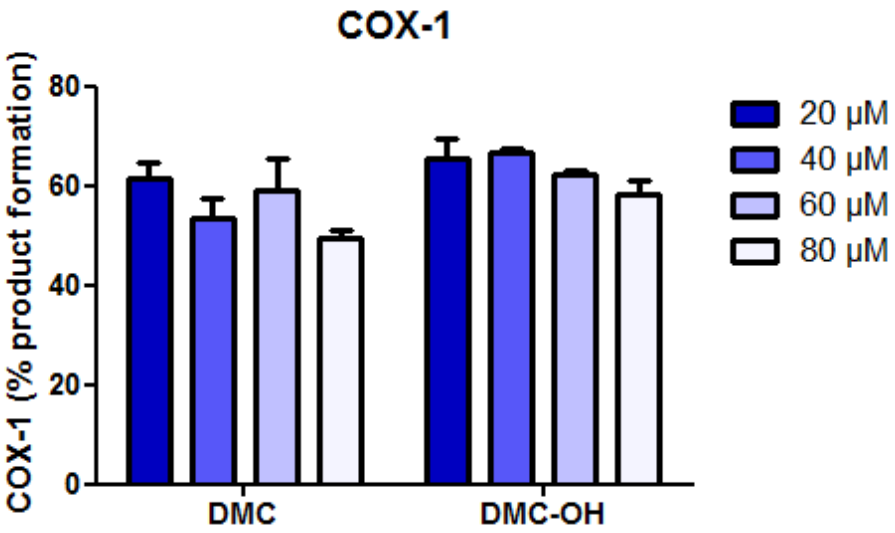

Figure 48. COX-1 assay was performed by Klaus Deckmann at the Institute for Clinical Pharmacology, Uniklinik Frankfurt (Research group: Dr Grösch) using a COX inhibitor screening assay kit (Caymann Chemicals) that includes ovine COX-1 and human recombinant COX-2. $PGF_{2\alpha}$ and PGE_2 were measured by LC-MS/MS and added (n=3, mean ± SEM). SC-560 was used as positive[423] control obtaining 23 ± 16.1 % inhibition at 1 µM.

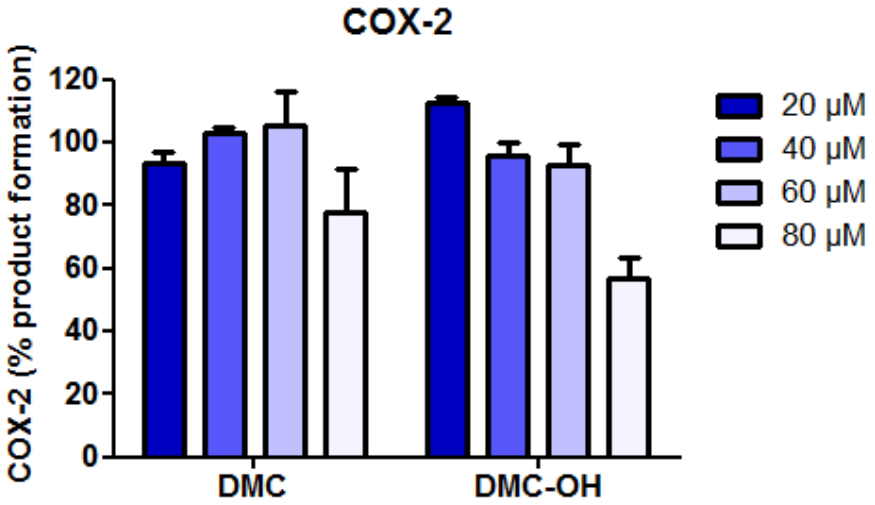

Figure 49. COX-2 assay was performed by Klaus Deckmann at the Institute for Clinical Pharmacology, Uniklinik Frankfurt (Research group: Dr Grösch) using a COX inhibitor screening assay kit (Caymann Chemicals) that includes ovine COX-1 and human recombinant COX-2. $PGF_{2\alpha}$ and PGE_2 were measured by LC-MS/MS and added (n=3, mean ± SEM).

As expected celecoxib inhibited only COX-2, e.g. at 0.1 µM (30.1% inhibition) and its analogue showed a dose-response behavior nevertheless with less potency (Figure 50 and Figure 51).

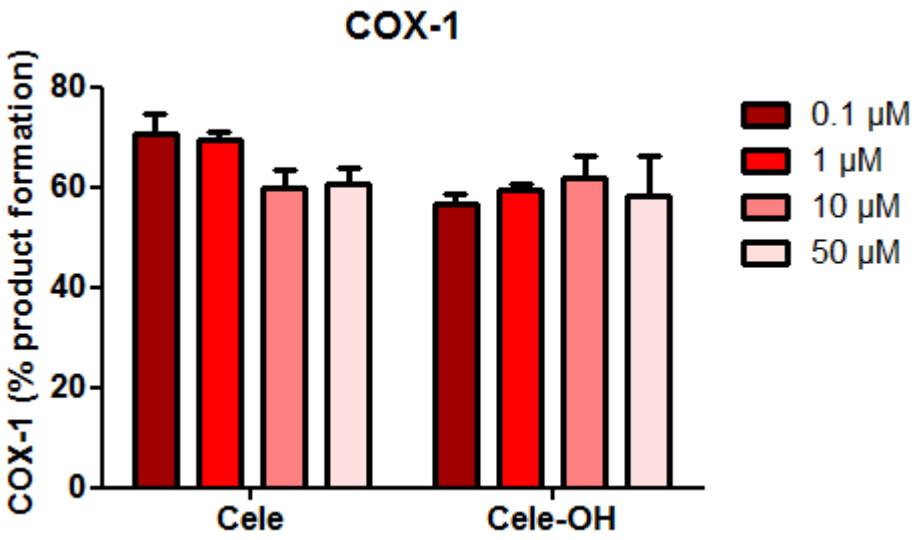

Figure 50. COX-1 assay was performed by Klaus Deckmann at the Institute for Clinical Pharmacology, Uniklinik Frankfurt (Research group: Dr Grösch) using a COX inhibitor screening assay kit (Caymann Chemicals) that includes ovine COX-1 and human recombinant COX-2. $PGF_{2\alpha}$ and PGE_2 were measured by LC-MS/MS and added (n=3, mean ± SEM). SC-560 was used as positive[423] control obtaining 23 ± 16.1 % inhibition at 1 µM.

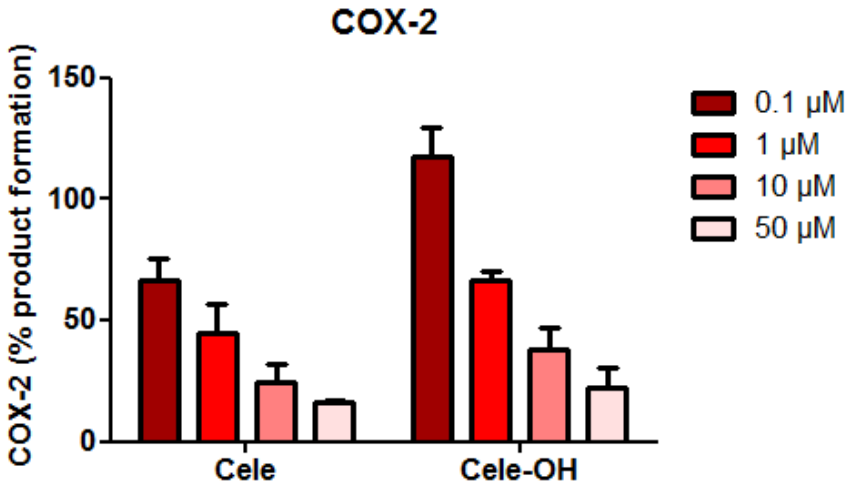

Figure 51. COX-2 assay was performed by Klaus Deckmann at the Institute for Clinical Pharmacology, Uniklinik Frankfurt (Research group: Dr Grösch) using a COX inhibitor screening assay kit (Caymann Chemicals) that includes ovine COX-1 and human recombinant COX-2. $PGF_{2\alpha}$ and PGE_2 were measured by LC-MS/MS and added (n=3, mean ± SEM). SC-560 was used as positive[423] control obtaining 23 ± 16.1 % inhibition at 1 µM.

The next step was to evaluate the synthesized compounds and their analogues on a cell viability assay to confirm that the chemical modification (Figure 43) did not affect the biological properties of the compounds.

Compounds (celecoxib, Cele-OH, DMC and DMC-OH) were incubated with HeLa cells and the cell proliferation in a WST-1 assay was evaluated. DMC was the only compound which affected the cell viability of this cell line resulting in an IC_{50} = 50 µM. The time of incubation (24 h) was less than published in the literature and therefore, the effect observed with other cell lines is not to be observed in this assay. Nevertheless, celecoxib did not show a dose-response behavior in relationship with the concentration and therefore this experiment should be repeated in the future.

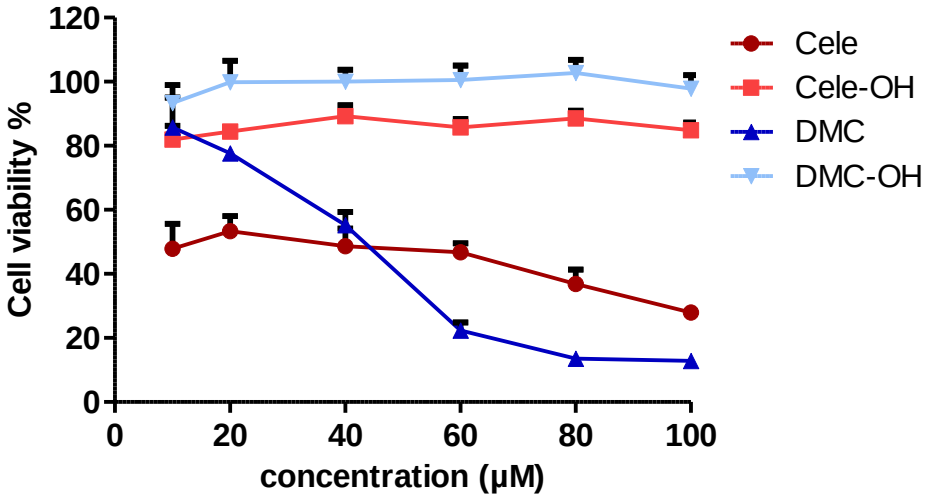

Figure 52. Cell viability was measured using WST-1 assay (Roche) on HeLa cells, incubation time 26h. This experiment was performed by Klaus Deckmann at the Institute for Clinical Pharmacology, Uniklinik Frankfurt (Research group: Dr Grösch) (n=3, mean ± SEM).

Two different experiments were performed with the coupled beads to DMC-OH and Cele-OH. In the first experiment, modified beads were placed in a syringe and lysate MCF-7 cells (supernatant) was applied to the beads, washed with PBS and proteins attached to the beads eluted with free ligands: DMC and celecoxib. Figure 53 and Figure 54 show the SDS-PAGE resulted from analyzing all the fractions in both cases. Probably due to the poor solubility of celecoxib and DMC, proteins were not eluted. Consequently, experimental setup was changed and in the second experiment, to prove that DMC-OH and Cele-OH were coupled to the beads, COX-2 should habe been detected to confirm the affinity of COX-2 towards the modified beads.

HeLa cells were stimulated with TNF-α (5 ng/ml) and IL-1β (1 ng/ml) to overexpress COX-2 and lysated. Supernatant was applied directly to the beads (Figure 55) or pre-

incubated with negative beads 1h at 4°C (Figure 56) to eliminate unspecific binding of COX -2 to the sepharose (polysaccharide polymer material extracted from seaweed).

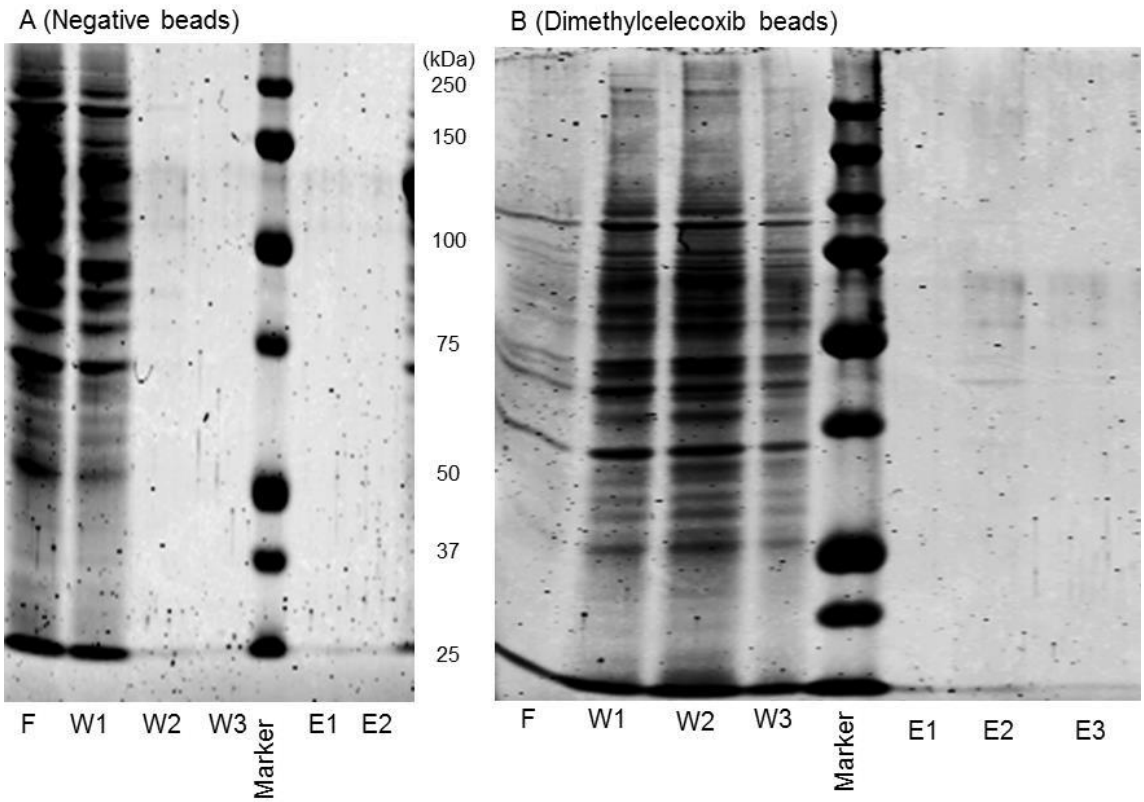

Figure 53. 10% SDS-PAGE stained with Coomassie. 7 x 10^7 MCF-7 were lysated and the supernatant applied to the negative and DMC-OH placed in a syringe. After several washing steps, proteins were eluted with 500 µL of 2.5 mM DMC. F: flow through, W1, W2, W3: washing steps with PBS, E1, E2: elution with DMC (2.5 mM), marker used: All Blue.

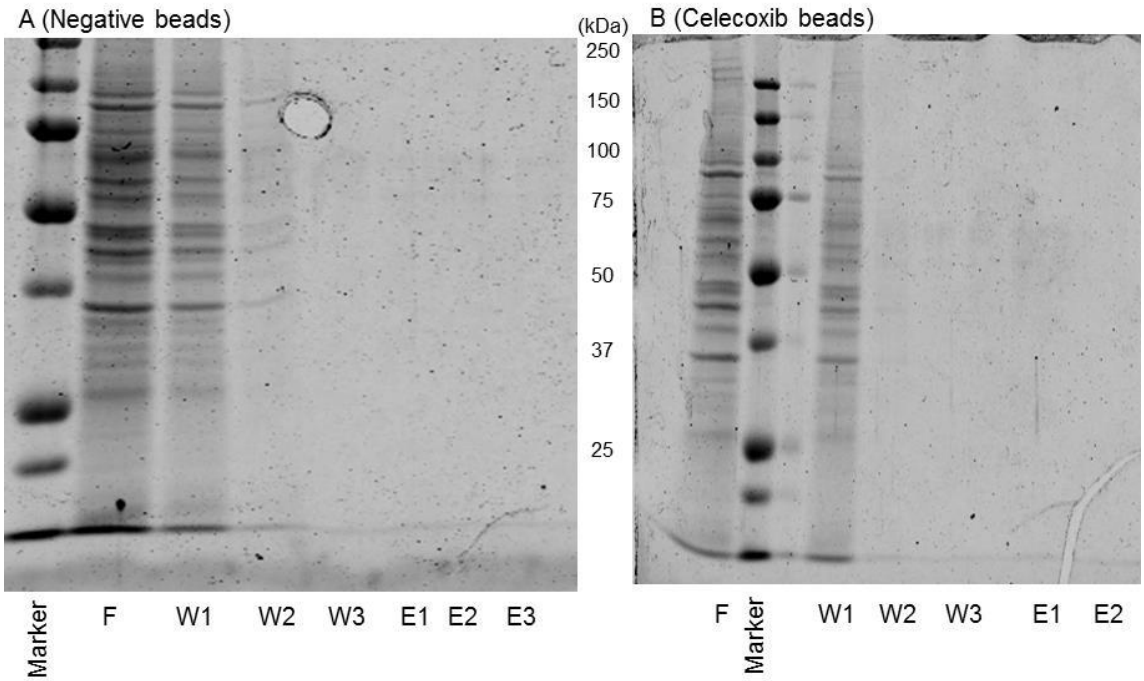

Figure 54. 10% SDS-PAGE stained with Coomassie. 7 x 10^7 MCF-7 were lysated and the supernatant applied to the negative and Cele-OH placed in a syringe. After several washing steps, proteins were eluted with 500 µL of 2.5 mM celecoxib. F: flow through, W1, W2, W3: washing steps with PBS, E1, E2: elution with celecoxib (2.5 mM), marker used: All Blue.

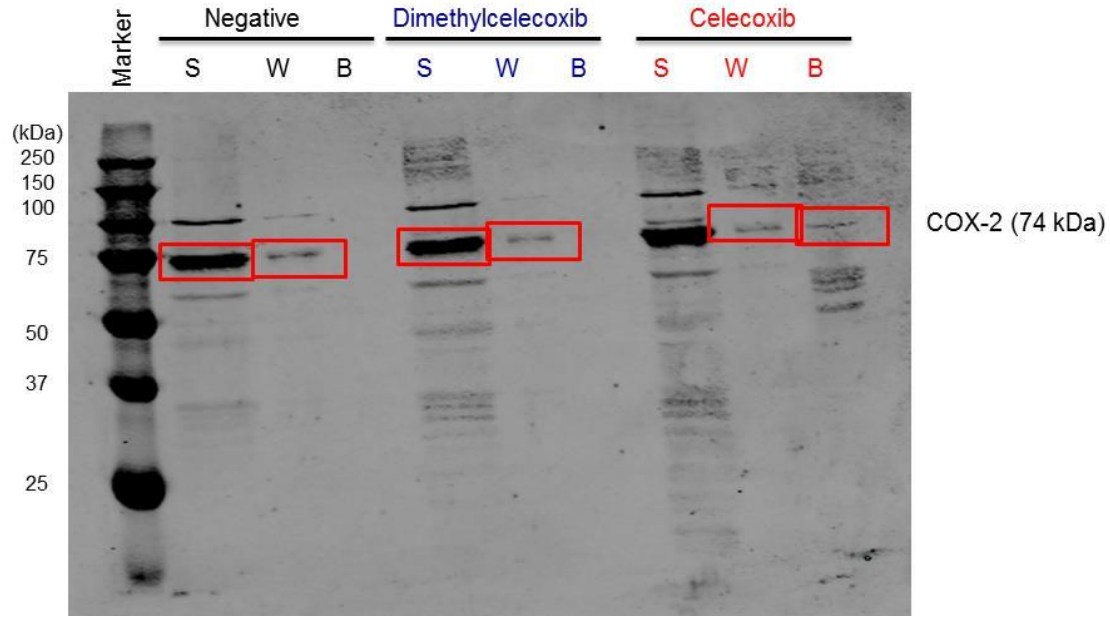

Figure 55. Western blot of a 10% SDS-PAGE treated with an anti-COX-2 antibody (Caymann Chemicals). HeLa cells (6 x 10^6 cells) were stimulated with TNF-α (5 ng/ml) and IL-1β (1 ng/ml) to overexpress COX-2. Supernatant were incubated at 4°C o/n with DMC-OH and Cele-OH beads. Beads were in 100 µl (2x loading buffer + 10% β-mercaptoethanol) boiled during 5 min at 95°C. S: supernatant after centrifugation, W: washing step with PBS, B: beads. In blue: beads coupled to DMC-OH in red: beads coupled to Cele-OH.

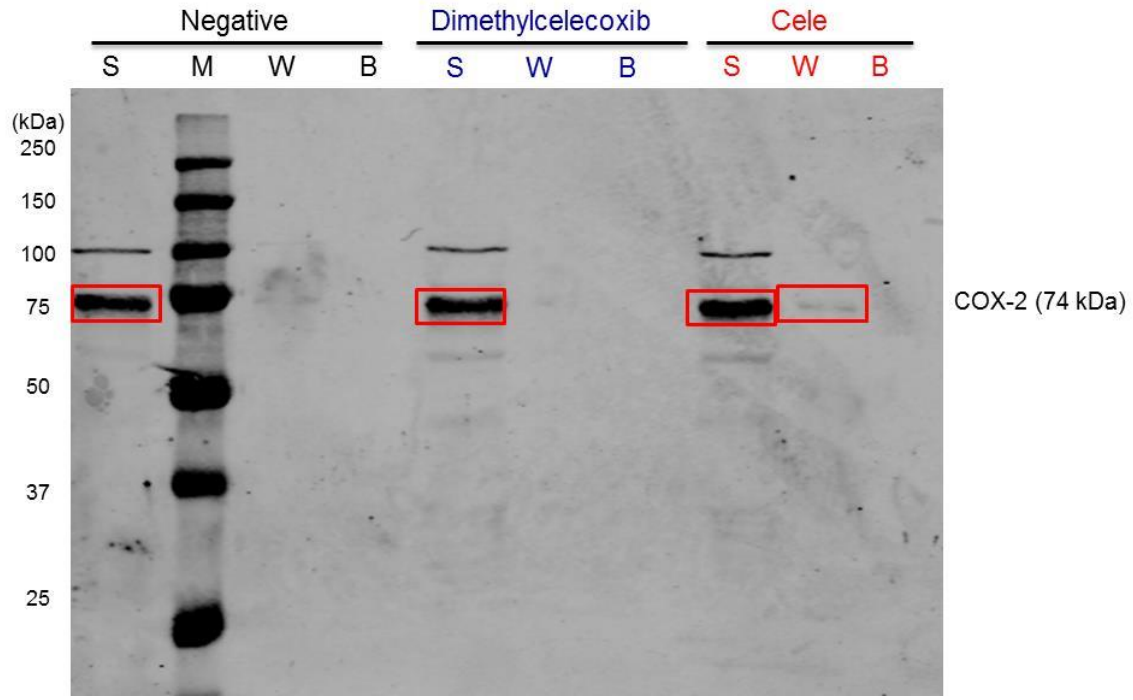

Figure 56. Western blot of a 10% SDS-PAGE treated with an anti-COX-2 antibody (Caymann Chemicals). HeLa cells (6 x 10^6 cells) were stimulated with TNF-α (5 ng/ml) and IL-1β (1 ng/ml) to overexpress COX-2. Supernatants were incubated in negative beads during 1h at 4°C prior to incubation at 4°C o/n with DMC-OH and Cele-OH beads. Beads were in 100 µl (2x loading buffer + 10% β-mercaptoethanol) boiled during 5 min at 95°C. S: supernatant after centrifugation, W: washing step with PBS, B: beads. In blue: beads coupled to DMC-OH in red: beads coupled to Cele-OH.

Supernatant, the fraction resulting from washing and the unmodified and modified beads were separated on a 10% SDS-PAGE and transferred to a nitrocellulose membrane to detect via Western Blott COX-2, using a monoclonal anti-COX-2 antibody. COX-2 could not be detected in the supernatant or the first washing step of Cele-OH and as expected of DMC-OH (DMC is not active on COX-2 and therefore it should not show affinity towards the enzyme) and that meant that the beads were not efficiently modified with the compounds. This could probably due to a problem with the pH of the coupling method or the lower reactivity of the $–CH_2OH$ alcohol with the epoxide group on epoxide sepharose beads. This problem could be solved by changing the linker by a amine ($-CH_2NH_2$) or thiol ($-CH_2SH$) or by changing the coupling conditions.

7. Synthesis of ceramide metabolism modulators

The only available inhibitors or modulators of ceramide metabolism are often lipidic structures containing one or two C_{18} alkylic moiety linked via a 2-aminobutane-1,3-diol moiety. The main strategy to produce ceramide metabolism modulators is to mimic the structural group, found in all main sphingolipids, and link it to a lengthy alkyl chain. The resulted structure is often difficult to be synthesized (several stereocenters) and possess poor pharmacological properties regarding Lipinski's rule of 5[424]: high lipophilicity. Therefore, pharmacological tools are needed to regulate abnormal tumour growth. The main idea of this work was to design a novel synthesis route to produce ceramide metabolism modulators that possess adequate "drug like" properties such as solubility, metabolic stability and, on the top of that, easy chemical accessibility. All compounds share structural similarities: a 3-aminopropane-1,2-diol that mimics the central core of ceramide (Figure 57).

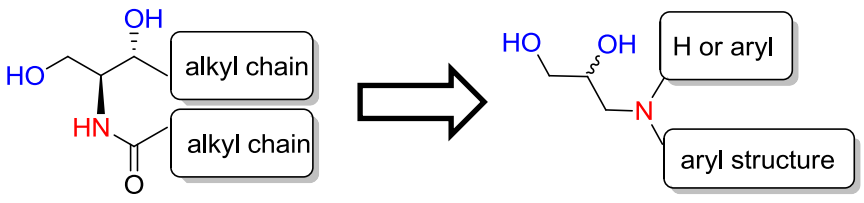

Figure 57. Simplification of the structure to produce "drug like" modulators of ceramide metabolism.

Synthesis started with the production of the key intermediate: (2,2-dimethyl-1,3-dioxolan-4-yl)methanamine (**32**[k], the main chemical structure that mimics the sphingoid base. In this chapter, the synthesis and *in vitro* evaluation of compounds EB72 (**35**) and EB143 (**38**) is presented.

EB72 (**35**) (1-(4-chlorophenyl)-3-(2,3-dihydroxypropyl)urea) is a derivative synthesized in two steps: the first step involves (Figure 58) a reaction among the main building block **32** (obtained via a *p*-TsOH catalyzed reaction between 3-amino-1,2-propandiol (**30**) and 2,2-dimethoxypropane (**31**)) and 4-chlorophenylisocyanate (**33**) obtaining 1-(4-chlorophenyl)-3-((2,2-dimethyl-1,3-dioxolan-4-yl)methyl)urea (**34**) which underwent hydrolysis yielding the desired 1,2-diol: 1-(4-chlorophenyl)-3-(2,3-dihydroxypropyl)urea, EB72, **38** (overall yield 61%).

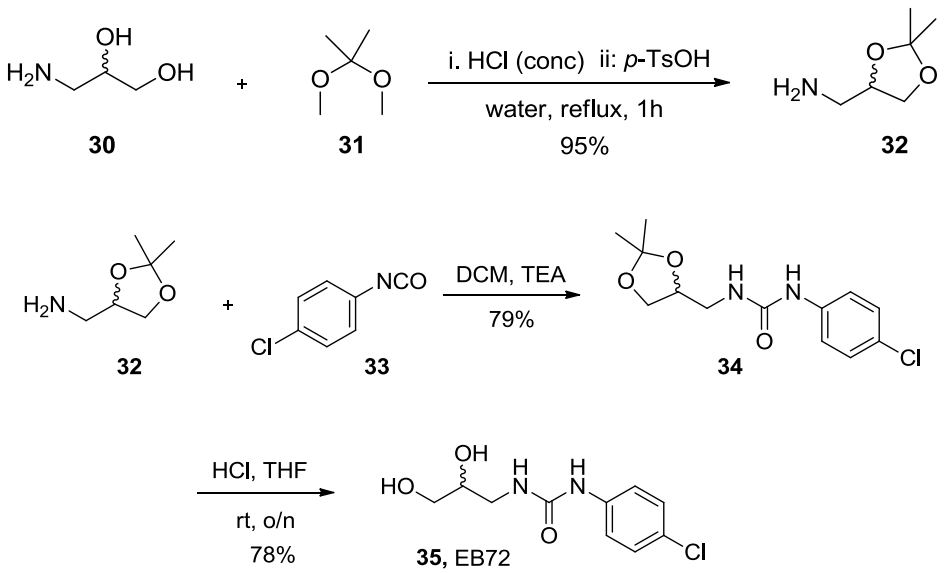

Figure 58. Synthesis of EB72 (**35**) ((1-(4-chlorophenyl)-3-(2,3-dihydroxypropyl)urea).

Compound **35**, was evaluated in an *in vitro* assay to measure the ceramide synthase activity: the microsomal fraction of HCT-116 as well cell lysates of HCT-116 cells, which overexpress CerS2, CerS4 or CerS6 were isolated. Palmitoyl-CoA, steraryl-CoA, nervonyl-CoA or lignoceryl-CoA were used for the assay (Figure 59). The inhibitors were incubated for 10 min at 37°C and the reaction started with different acyl-CoAs and afterwards the sphingolipids were analyzed by LC-MS/MS. For the *in vitro* cell viability

[k] The synthesis was performed according to Abbott Laboratories (WO2008/76356 A1, 2008).

assay, HeLa (cervical cancer), a WST-1 assay was used to determine the viability and proliferation rate of the cells after 48 h incubation with the inhibitor (Figure 60).

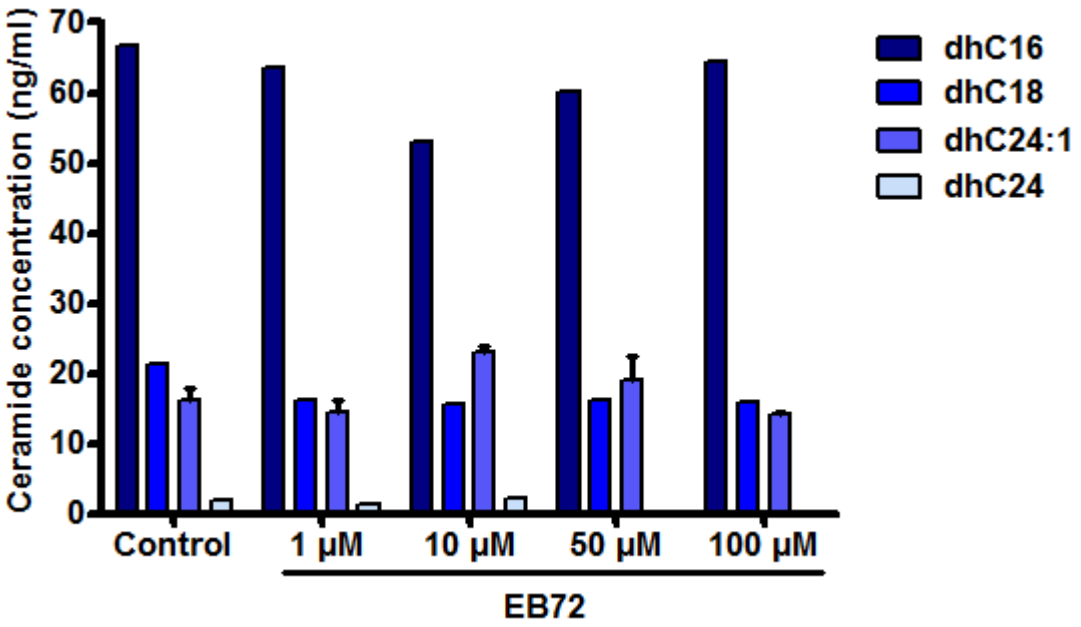

Figure 59. For quantitation of sphingolipids, HCT-116 cells were stimulated with 10 ng/ml TGF-β. The cells were harvested and the sphingolipids were extracted via liquid-liquid extraction with methanol as described previously[422] and analyzed by LC-MS/MS (n=3, ± SEM).[I]

[I] Ceramide levels were measured by Sina Fuchs at the Institute for Clinical Pharmacology, Uniklinik Frankfurt (Research group: Dr Grösch) (n=3, mean ± SEM).

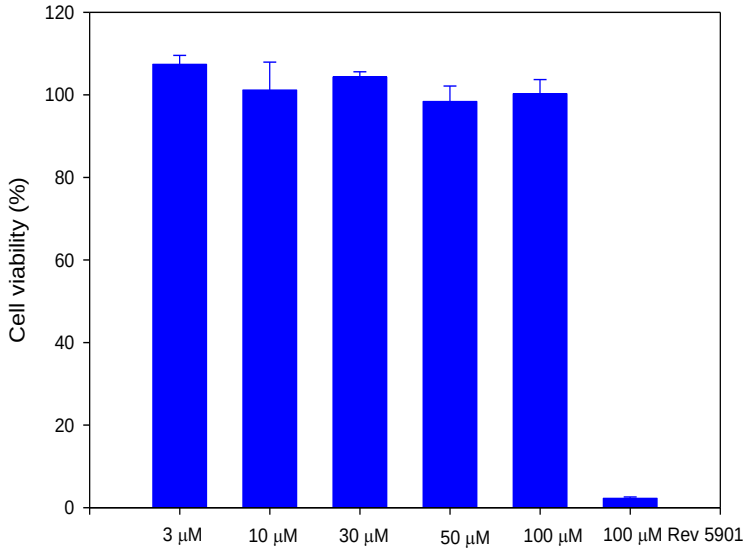

Figure 60. Cell viability was measured using WST-1 assay (Roche) on HeLa cells, incubation time 48h. This experiment was performed by Dr Astrid Khant at the Pharmaceutical Chemistry department, Goethe University (Research group: Professor Steinhilber) (n=3, mean ± SEM). Positive control used: Rev5901[425].

EB72 (**35**) did not affect the cell viability of HeLa cells, but it was tested in the ceramide synthase assay to evaluate its possible effect on ceramide metabolism. Neither of the sphingolipids levels were affected by the inhibitor showing that a bigger and more lipophilic structure is needed. In the case of cell viability, the structure is possibly to hydrophilic to enter inside the cells, and therefore cannot reach the apoptosis machinery.

Second compound synthesized is less hydrophilic and thus should be able to enter into the cell membrane. The synthesis (Figure 61) of EB143, **38** (3-((3-methoxy-4-((4-(trifluoromethyl)benzyl)oxy)benzyl)amino)propane-1,2-diol) involves three steps which were: firstly 3-methoxy-4-((4-trifluoromethyl)benzyl)oxy)benzaldehyde (RC3, **36**) was produced following a typical ether synthesis with 1-(bromomethyl)-4-(trifluoromethyl)benzene and vanilline[m] followed by reductive amination of the main

[m] Synthesis of compound 36 was done by Roberto Carrasco Gómez at the group of Professor Schubert-Zsilavezc, Pharmaceutical Chemistry department, Goethe University, Frankfurt am Main.

building block **32** with the latter in 82% yield. The obtained product underwent hydrolysis yielding EB143, **38** (36% overall yield).

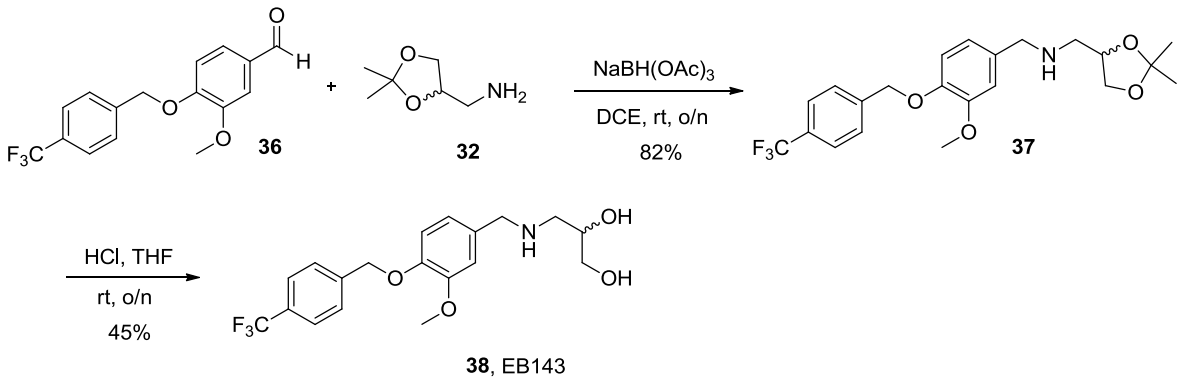

Figure 61. Synthesis of EB 143, 38 (3-((3-methoxy-4-((4-(trifluoromethyl)benzyl)oxy)benzyl)amino)propane-1,2-diol).

After synthesising compound **38**, it was evaluated *in vitro* in two different assays: a cell-based assay using HCT-116 cells (colorectal carcinoma) (Figure 63), cells were incubated with the inhibitors over various period of time. The sphingolipids were extracted with methanol and determined by liquid chromatography coupled to tandem mass spectrometry (LC-MS/MS) analysis ($C_{16:0}$-dhCer, $C_{18:0}$-dhCer, $C_{24:0}$-dhCer, $C_{24:1}$-dhCer and Sph). The second assay (Figure 62) was used to measure the ceramide synthase activity. The inhibitors were incubated for 10 min at 37°C and the reaction started with different acyl-CoAs and afterwards the sphingolipids were analyzed by LC-MS/MS. For the *in vitro* cell viability assay, HeLa (cervical cancer), a WST-1 was used to determine the viability and proliferation rate of the cells after 48 h incubation with the inhibitor (**64**).

SL levels of most all SL were affected by the inhibitor **38** specially $dhCer_{16:0}$ and $dhCer_{24:1}$ but not $dhCer_{18:0}$ or $dhCer_{24:0}$. Ceramide levels are increased and not decreased (inhibition), this pointed out a possible cytoxicity of compound **38** which increased levels in a dose-response manner. Compound **38** is not a ceramide synthase inhibitor and affected the cell viability of cells HCT-116 and HeLa (EC_{50} =50 µM) (Figure 64). In a cell-based assay the x-fold increase is lower but did not follow a dose-response manner, confirming that EB143, **38** is a cytotoxic compound that does not inhibit ceramide synthase or affect ceramide metabolism but in an apoptotic mechanism. Further chemical modifications should be taken into consideration to

modulate this effect. These compounds may target other ceramide metabolism enzymes.

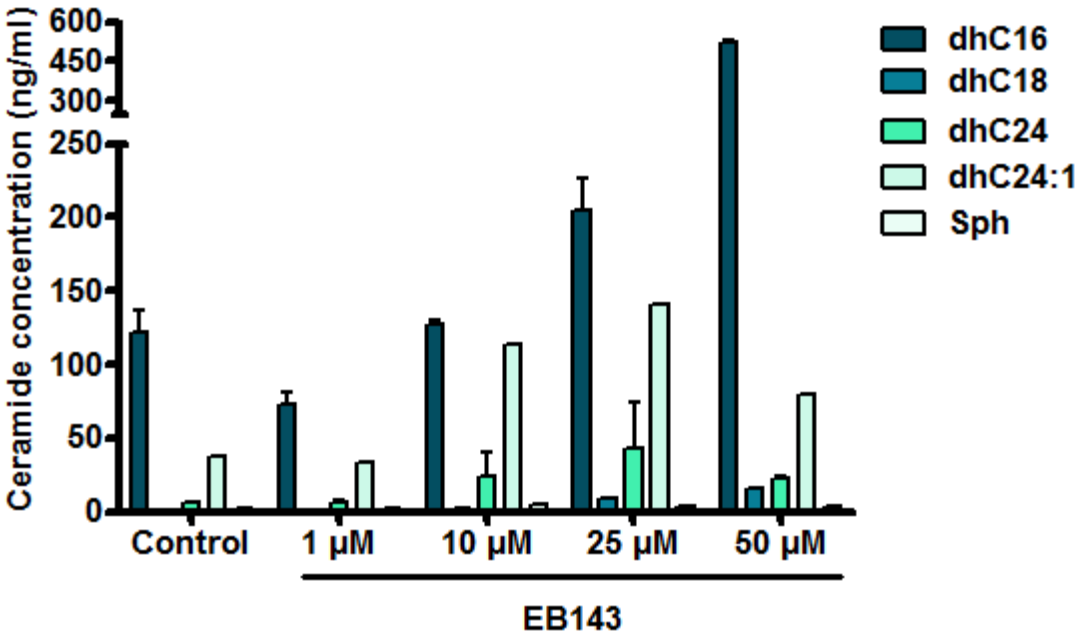

Figure 62. *In vitro* ceramide synthase assay. HCT-116 cells were lysated and 100 µg protein incubated with (15 µM sphinganine, 50 µM acyl-CoA in 20 mM HEPES and 2 mM $MgCl_2$ (pH 7.4). Palmitoyl-CoA was used for the assay. The products were measured using LC-MS/MS (n=3, ± SEM).

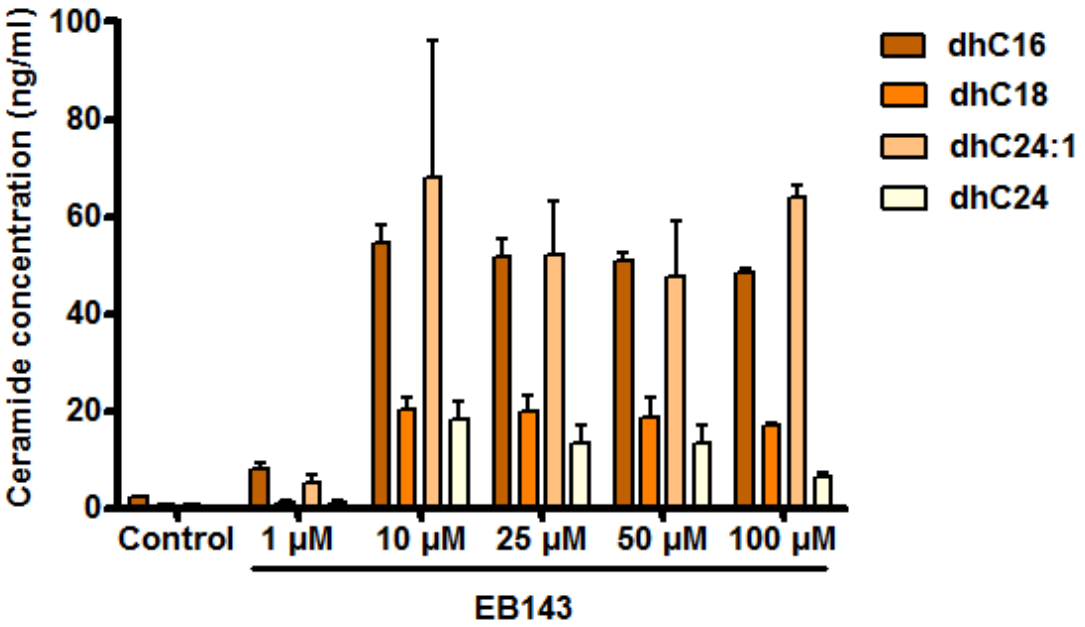

Figure 63. For quantitation of sphingolipids, HCT-116 cells were stimulated with 10 ng/ml TGF-β. The cells were harvested and the sphingolipids were extracted via liquid-liquid extraction with methanol as described previously[422] and analyzed by LC-MS/MS (n=3, ± SEM).

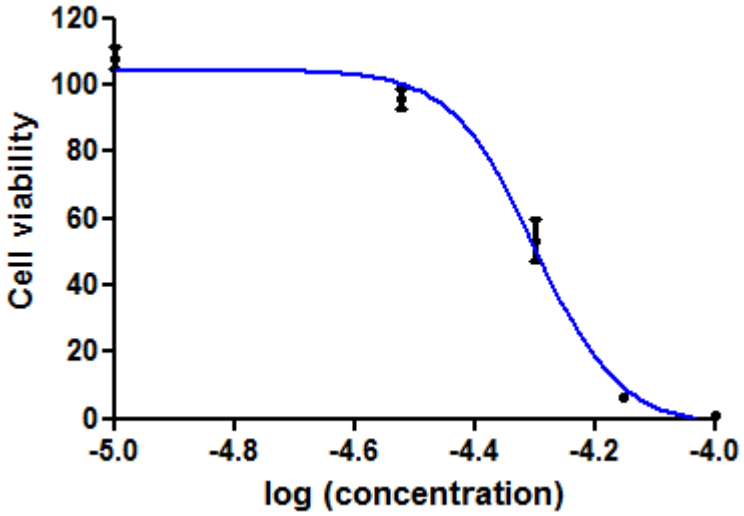

Figure 64. Cell viability was measured using WST-1 assay (Roche) on HeLa cells, incubation time 48h. (n=3, mean ± SEM).

8. Evaluation of 5-LO inhibitors on ceramide metabolism

It has been suggested that COX and LO inhibitors may be cancer-preventive not only by inhibiting specific antiapoptotic AA metabolites but also by facilitating accumulation of AA which promotes neutral SMase activity and increases the proapoptotic ceramide[36]. In this chapter several 5-LO inhibitors, two synthesized (5-LO inhibibitor 1 and 5-LO inhibitor 2, Figure 65) and zileuton were tested on several cancer cell lines (A459, Capan-2, MCF-7) and ceramide levels were measured.

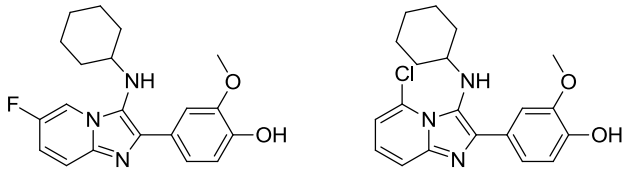

5-LO inhibitor 1 (Inh 1) 5-LO inhibitor 2 (Inh 2)

Figure 65. 5-LO inhibitor 1 (4-(3-(cyclohexylamino)-6-fluoroimidazo[1,2-*a*]pyridin-2-yl)-2-methoxyphenol) and 5-LO inhibitor 2 (4-(5-chloro-3-(cyclohexylamino)imidazo[1,2-*a*]pyridin-2-yl)-2-methoxyphenol).

EB143, and celecoxib were used as substance control because they have been previously characterized[422]. The first experiment was to measure the level of all ceramide and compare them with vehicle (DMSO) (Figure 66). Different cells lines were incubated with the inhibitors over 4h. The sphingolipids were extracted[n] with methanol and determined by liquid chromatography coupled to tandem mass spectrometry (LC-MS/MS) analysis ($C_{16:0}$-Cer, $C_{18:0}$-Cer, $C_{24:0}$-Cer, $C_{24:1}$-Cer)[331].

[n] Ceramide levels were measured by Daniela Hartmann at the Institute for Clinical Pharmacology, Uniklinik Frankfurt (Research group: Dr Grösch) (n=2, mean ± SEM).

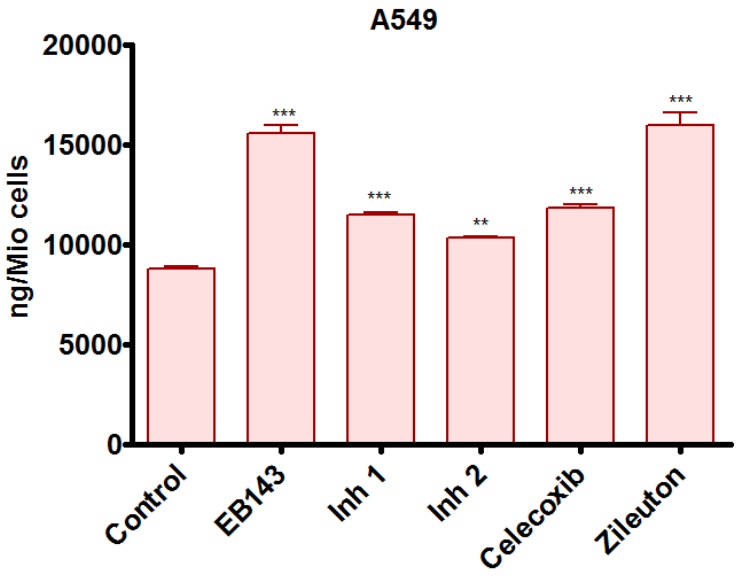

Figure 66. For quantitation of sphingolipids, A549 were incubated with EB143, 5-LO inhibitor 1, 5-LO inhibitor 2, celecoxib, Zileuton at 50 µM during 4h. The cells were harvested and the sphingolipids were extracted via liquid-liquid extraction with methanol as described previously[422] and analyzed by LC-MS/MS (n=3, ± SEM).

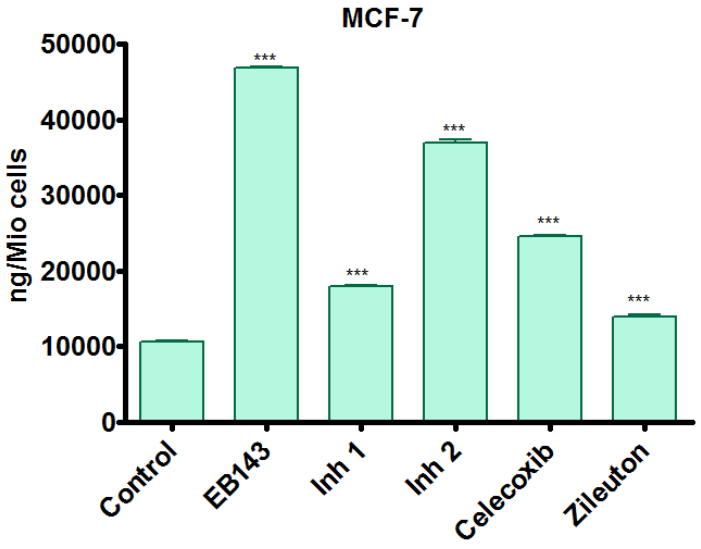

Figure 67. For quantitation of sphingolipids, MCF-7 were incubated with EB143, 5-LO inhibitor 1, 5-LO inhibitor 2, celecoxib, Zileuton at 50 µM during 4h. The cells were harvested and the sphingolipids were extracted via liquid-liquid extraction with methanol as described previously[422] and analyzed by LC-MS/MS (n=3, ± SEM).

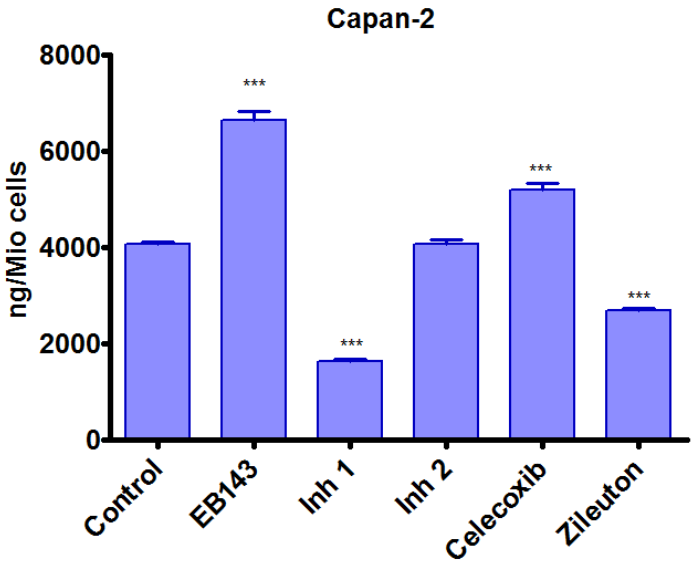

Figure 68. For quantitation of sphingolipids, Capan-2 were incubated with EB143, 5-LO inhibitor 1, 5-LO inhibitor 2, celecoxib, Zileuton at 50 µM during 4h. The cells were harvested and the sphingolipids were extracted via liquid-liquid extraction with methanol as described previously[422] and analyzed by LC-MS/MS (n=3, ± SEM).

In all cases, EB143 (**38**) affected the ceramide levels by increasing them in all cancer cell lines and confirming its cytotoxic profile (Figure 66-Figure 68). Celecoxib significantly increased the total ceramide levels, which had been already published by several research groups[422,426,427]. These two compounds served as positive controls. Regarding 5-LO inhibitors, they exhibited different behavior: 5-LO inhibitor 1, increased total ceramide levels on MCF-7, A549 but decreased on Capan-2. 5-LO inhibitor 2, increased in all cases ceramide levels but on Capan-2 cells. Zileuton increased ceramide levels moderately on MCF-7, significantly on A549 and decreased on Capan-2.

In order to distinguish between a cytotoxic effect of the compounds or a direct interaction with ceramide biosynthesis, which already occurred with inhibitor EB143, cell viability of the different compounds, was assessed in two different concentrations on all tested cancer cell lines (10 and 100 µM). Cytotoxicity profile of EB143 was again confirmed (Figure 69-Figure 71) and 5-LO inhibitors (1 and 2) affected the cell viability of Capan-2 and MCF-7 cell lines but not in the case of A549. Zileuton was only slightly cytotoxic when using Capan-2 cells, this might be due to the low rate of division of Capan-2 cells (more than 72h).

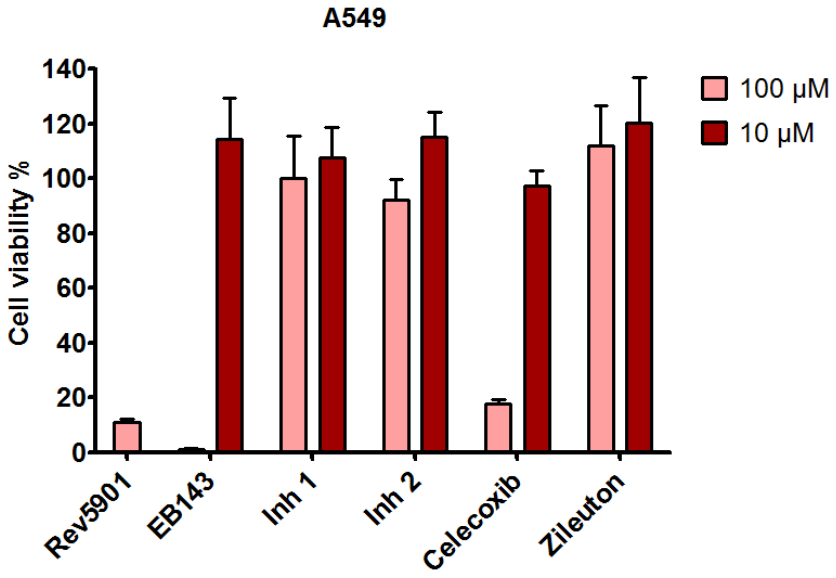

Figure 69. Cell viability was measured using WST-1 assay (Roche) on A549 cells, incubation time 48h. (n=3, mean ± SEM). Rev5901 was used as a positive control.

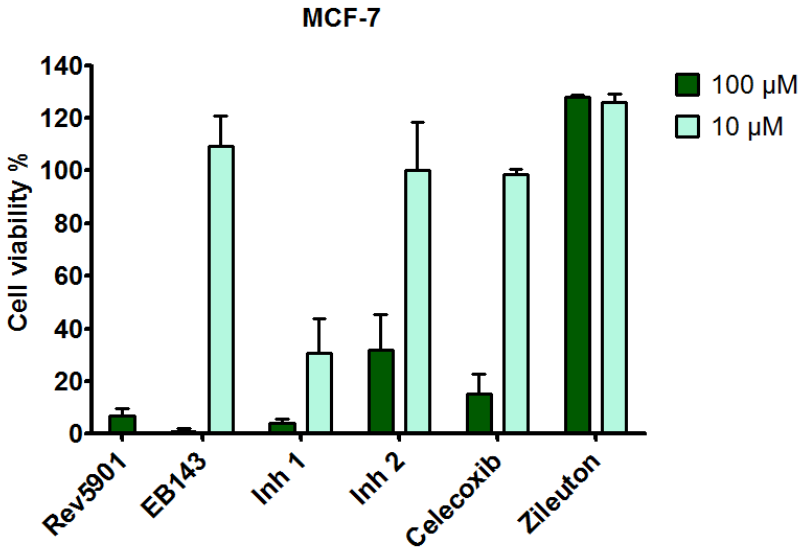

Figure 70. Cell viability was measured using WST-1 assay (Roche) on MCF-7 cells, incubation time 48h. (n=3, mean ± SEM). Rev5901 was used as a positive control.

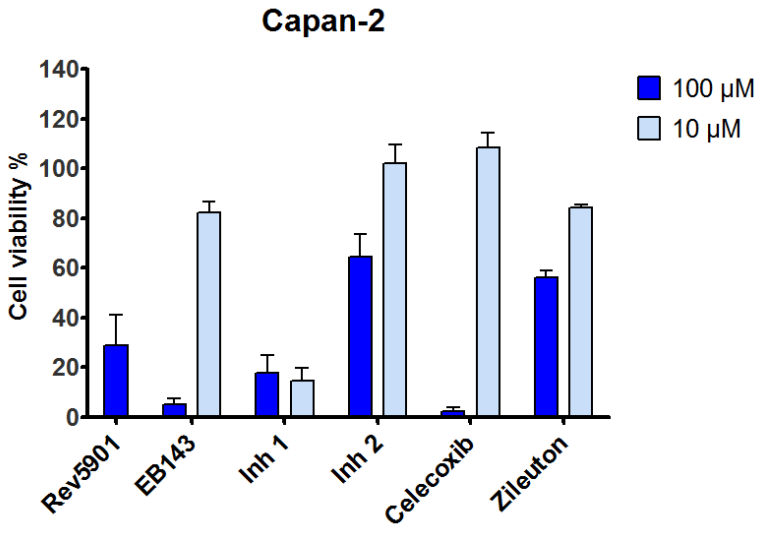

Figure 71. Cell viability was measured using WST-1 assay (Roche) on Capan-2 cells, incubation time 48h. (n=3, mean ± SEM). Rev5901 was used as a positive control.

Due to the fact that Capan-2 does not express 5-LO they were discarded for further investigations (Table 5). After analyzing this results, A549 were selected to work with and try to prove the hypothesis postulated by Omahen[363]. In the next experiment A549 cells were incubated 4h with 5-LO inhibitors and their sphingolipids levels were measured after extraction and LC-MS/MS analysis.

Table 5. Enzyme expression on different used cancer cell lines.

	Capan-2	MCF-7	A549
5-LO	-	+	+
COX-1	+	+	+
COX-2	+	+	+

5-LO inhibitor 1 and 5-LO selectively increased Cer-$C_{24:0}$ levels compared to control (Figure 72 and Figure 73), this ceramide has been proposed as prosurvival sphingolipid.

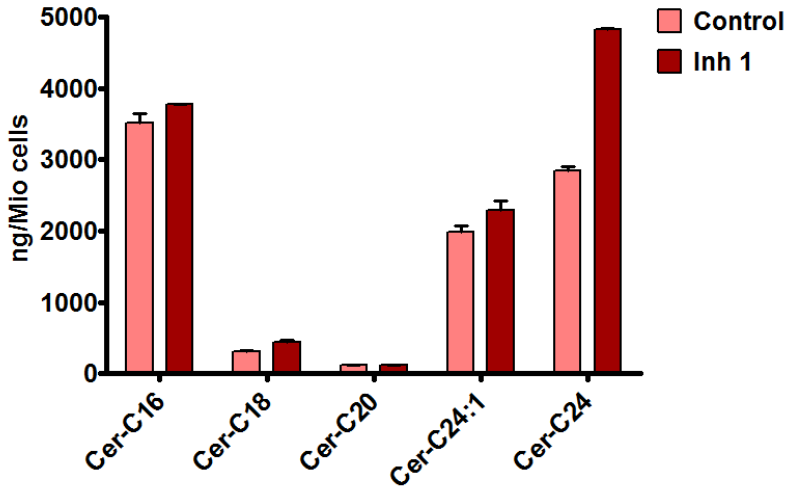

Figure 72. For quantitation of sphingolipids, A549 were incubated with 5-LO inhibitor 1 at 50 µM during 4h. The cells were harvested and the sphingolipids were extracted via liquid-liquid extraction with methanol as described previously[422] and analyzed by LC-MS/MS (n=2, ± SEM).

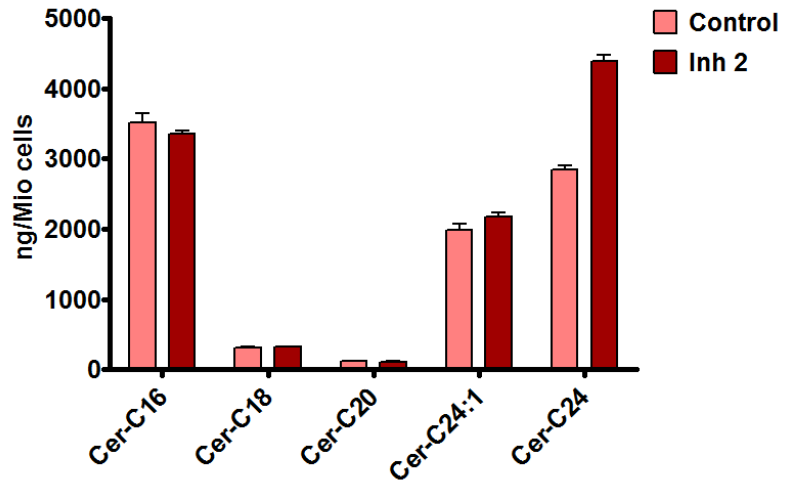

Figure 73. For quantitation of sphingolipids, A549 were incubated with 5-LO inhibitor 2 at 50 µM during 4h. The cells were harvested and the sphingolipids were extracted via liquid-liquid extraction with methanol as described previously[422] and analyzed by LC-MS/MS (n=2, ± SEM).

Zileuton increased Cer-$C_{16:0}$ and $Cer_{24:1}$ levels, but decreased Cer-$C_{24:0}$ (Figure 74). The balance between $C_{16:0}$ and $C_{24:0}$/$C_{24:1}$ ceramides is important for induction of apoptosis is several cancer cell lines and therefore zileuton acts as 5-LO inhibitor that increases AA levels which could lead to increase of ceramide and therefore apoptosis. The observed increase of Cer-$C_{16:0}$ may be a consequence of induction of the key enzymes of the sphingolipids pathway CerS and/or SPT. mRNA and protein expression of CerS and SPT in A549 cells after zileuton treatment should be investigated in order to confirm this hypothesis.

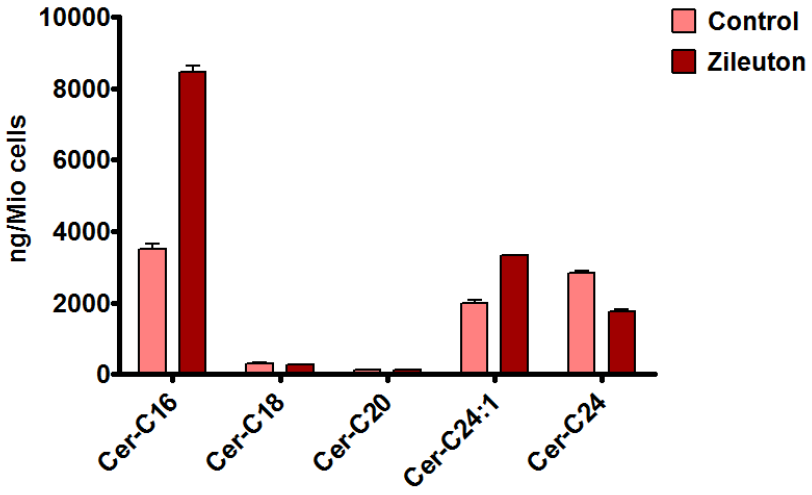

Figure 74. For quantitation of sphingolipids, A549 were incubated with zileuton at 50 µM during 4h. The cells were harvested and the sphingolipids were extracted via liquid-liquid extraction with methanol as described previously[422] and analyzed by LC-MS/MS (n=2, ± SEM).

Ceramides are either synthesized via salvage pathway or *de novo* synthesis. For this purpose, an inhibitor of SPT transferase was used (myoricin, 150 nM) which only blocks the *de novo* synthesis. Amitryptiline and desipramine induce the degradation of the acid SMase and the down-regulation of acid ceramidase[428] leading to a partial inhibition of the salvage pathway. A549 cells were incubated with 5-LO inhibitors in the presence of absence of myriocin (150 nM), amitryptiline (20 µM) and desipramine (20 µM). Regarding 5-LO inhibitor 1, myoricin alone is able to reduce $C_{24:0}$ levels below the control, a similar effect occurred when incubation the cell with 5-LO inhibitor 1 and myriocin. On the contrary, treatment of 5-LO inhibitor 1 together with either amitryptiline or desipramine led to an increase in ceramide levels. This last result should not be taken into consideration (Figure 75). Inconsistent results were obtained when repeating the same experiment with 5-LO inhibitor 2 (Figure 76). A selective increase on $C_{24:0}$ could not be observed.

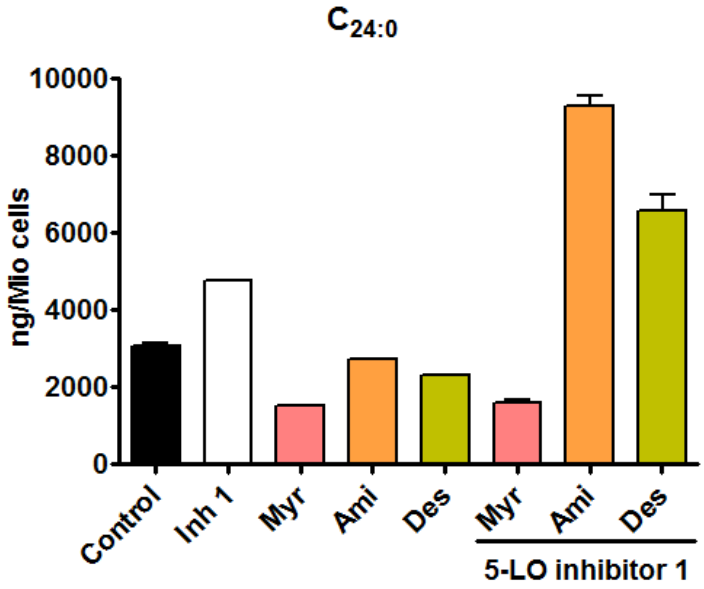

Figure 75. Cer-$C_{24:0}$ levels. For quantitation of sphingolipids, A549 were incubated with 5-LO inhibitor 1 at 50 µM with/without myoricin 150 nM, amitryptiline 20 µM and despramine 20 µM during 4h. The cells were harvested and the sphingolipids were extracted via liquid-liquid extraction with methanol as described previously and analyzed by LC-MS/MS (n=2, ± SEM).

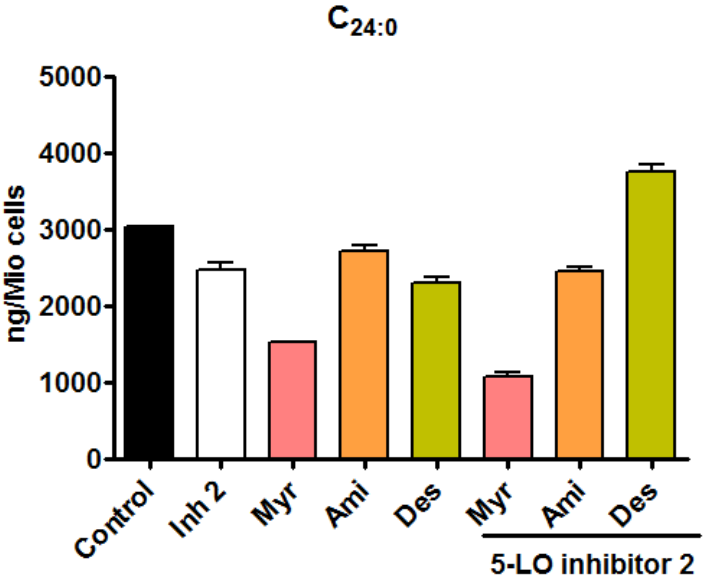

Figure 76. Cer-$C_{24:0}$ levels. For quantitation of sphingolipids, A549 were incubated with 5-LO inhibitor 2 at 50 µM with/without myoricin 150 nM, amitryptiline 20 µM and despramine 20 µM during 4h. The cells were harvested and the sphingolipids were extracted via liquid-liquid extraction with methanol as described previously and analyzed by LC-MS/MS (n=2, ± SEM).

Regarding zileuton, myoricin alone is able to reduce $C_{24:1}$ levels below the control, a similar effect occurred when incubation the cell with zileuton and myriocin. Moreover, treatment of zileuton together with either amitryptiline or desipramine led to a decrease in Cer-$C_{24:1}$ levels but the inhibition was not complete indicating that probably the *de novo* pathway has an important role (Figure 77). A similar behavior was observed with Cer-$C_{16:0}$ levels (Figure 78).

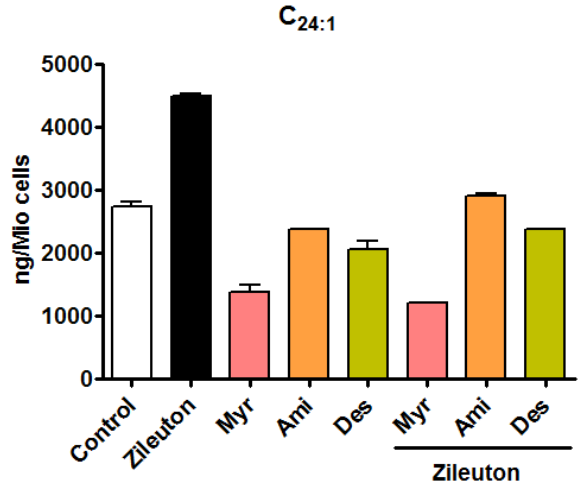

Figure 77. Cer-$C_{24:1}$ levels. For quantitation of sphingolipids, A549 were incubated with zileuton at 50 µM with/without myoricin 150 nM, amitryptiline 20 µM and despramine 20 µM during 4h. The cells were harvested and the sphingolipids were extracted via liquid-liquid extraction with methanol as described previously and analyzed by LC-MS/MS (n=2, ± SEM).

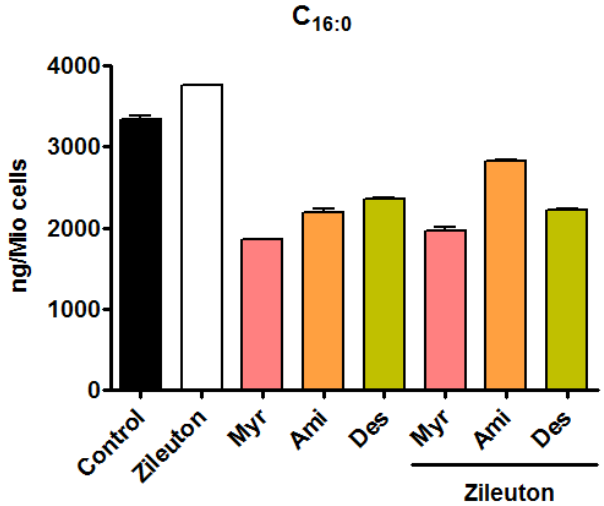

Figure 78. Cer-$C_{16:0}$ levels. For quantitation of sphingolipids, A549 were incubated with zileuton at 50 µM with/without myoricin 150 nM, amitryptiline 20 µM and despramine 20 µM during 4h. The cells were harvested and the sphingolipids were extracted via liquid-liquid extraction with methanol as described previously and analyzed by LC-MS/MS (n=2, ± SEM).

Summary

Lipid mediators have been referred as bioactive lipids, whose change in lipid levels resulted in functional or pathophysiological consequences. They are in the focus of biological research, nevertheless this is a late recognition due to the many difficulties of working with bioactive lipids due to their properties: hydrophobic, unstable and they occur in only in small quantities. Liquid chromatography and mass spectrometry have facilitated the work with them. Especially in this field, cardiovascular diseases and inflammatory mediated diseases and cancer are pathophysiological events where LMs are deregulated. Additionally, if the modulation of one LM pathway is not sufficient to overcome a disease, the combination of targeting two or more pathways could be effective. Needless to say, lipid signaling cascades are complicated pathways and possible shunting into other pathways when inhibiting or genetically deleting enzymes should be taken into consideration.

The first part of this work has focused on enzymes that metabolize eicosanoids, like mPGES-1 and 5-LO. mPGES-1 is an important enzyme metabolizing PGH_2 and one of the key players of the AA cascade. Its product, PGE_2 plays an important role in different inflammatory processes. Inhibition of the mPGES-1 might be a promising step to circumvent COX dependent side effects of NSAIDs. The class of quinazoline compounds around the lead structure FR20 has been investigated on isolated human and murine enzyme, in HeLa cells and in different human whole blood (HWB) settings to establish the possible effects of these compounds on eicosanoid profiling. Novel compounds with inhibitory activities in the submicromolar range (IC_{50}: 0.13 µM - 0.37 µM on isolated enzyme) were obtained which were also effective in cells and HWB. Furthermore, pharmacological profiling of toxicity and lipid screening with LC/MS-MS revealed that compounds also reduce PGE_2 levels in intact cells and whole blood; they do not impair cell viability but lack the ability to inhibit the murine mPGES-1 enzyme. This problem could be overcome by means of chemical synthesis varying the scaffold (quinoline, quinazoline) or introducing biosteric replacement in the phenyl moieties.

5-LO is a relevant enzyme that plays an important role in eicosanoid signaling in particular in leukotriene biosynthesis. Leukotrienes are involved in asthma, allergic rhinitis, glomerulonephritis, rheumatoid arthritis, sepsis, cancer and atherosclerosis. Moreover, genetic variants in the genes of the 5-LO pathway have been associated with the risk of development of acute myocardial infarction and stroke. Eicosanoids are

increased in infectious exacerbations of chronic obstructive pulmonary disease (COPD). They are also elevated in the airways of stable COPD patients compared to healthy subjects. Therefore, 5-LO has attired the scientific community as a possible therapeutic target to treat the several disease conditions listed before. In this study an extensive evaluation of imidazo[1,2-*a*]pyridines as a suitable lead structure for novel 5-LO targeting compounds was presented Within the three publications, 5-LO inhibitory activity of synthesized compounds was investigated in intact PMNL, a cell-free assay, in human whole blood and rodent cells to both elucidate structure-activity relationships and compounds were *in vitro* pharmacological evaluated. Chemical modifications for lead optimization via straight forward synthesis were used to combine small polar groups (hydroxy, and methoxy groups) which led to a suitable candidate with desired *in vitro* pharmacokinetic profile in terms of solubility and intrinsic clearance without showing any cytotoxicity. More than 70 imidazo[1,2-*a*]pyridine derivatives have been synthesized, resulting in more than 50 active compounds. Although it was not possible to introduce a solubility group without impairing the 5-LO inhibitory activity, combination of small polar groups lead to a more favorable solubility and *in vitro* metabolic stability. Overall, the development of 5-LO inhibitors with high efficacy and selectivity *in vivo* will provide a possible treatment for patients having one of the diseases where leukotriene biosynthesis plays an important role.

Other types of 5-LO inhibitors have been synthesized during this work, NO-NSAIDs can be postulated as novel 5-LO inhibitors that could circumvent the undesired side-effects of inhibiting COX isoforms (ulcer perforation, gastrointestinal bleeding and in some cases death). It is suggested that NO group is released *in situ* or after compounds are metabolized. NO-NSAIDs maintain the same anti-inflammatory properties by inhibiting 5-LO in clinical relevant concentrations. NO-NSAIDs are currently under clinical trial for the treatment of diseases where inflammation plays an important role. Synthesis of NO-NSAIDs is straightforward and can be applied for most NSAIDs recently published. Among them, the most promising candidate is NO-sulindac that was able to inhibit 5-LO product formation in intact PMNL, purified 5-LO and HWB in micromolar concentration. Additional experiments regarding their mechanism are currently being performed.

The present study could show that dual inhibitors are an interesting approach that is practicable. It has been used in the recent years to overcome side-effects and diseases concerning more pathophysiological conditions. MetS is an example of a conjunction of

symptoms: hyperglycemia, hypertriglyceridemia, hypertension and obesity. Due to its complex nature, the current treatment strategies of MetS require multiple pharmacological compounds regulating lipid and glucose homeostasis as well as blood pressure and coagulation. This study describes the first synthesis of dual sEH/PPAR modulators as potential agents for treatment of MetS. Following a combinatorial approach, an acidic head group known as a pharmacophore important for PPAR*α/γ* dual agonistic activity was combined with different hydrophobic urea derivatives in order to introduce an epoxide mimetic (sEH pharmacophore). The resulting compounds yielded high inhibition of sEH and different patterns of PPAR agonistic activity. This study demonstrates that the pharmacophores of PPAR agonists and sEH inhibitors can be easily combined, resulting in a simplified blueprint of a dual sEH/PPAR modulator. Further *in vivo* pharmacological evaluation studies are needed in order to evaluate, which pattern of PPAR activation shows the most promising profile for treatment of metabolic syndrome.

Another example of dual pharmacology has been presented in this work. Natural products derived compounds were able to target sEH and exhibit promising antiproliferative properties. The principle of addressing multiple targets by natural products can be transferred to synthetic multi-target ligands. In conclusion, several (*E*)-styryl-1*H*-benzo[*d*]imidazoles were synthesized and evaluated on recombinant sEH after an initial hit (IPS) that lead to potent sEH inhibitors exhibiting antiproliferative activities. Following the natural product-inspired design, the desired biological activity from a bacterial secondary metabolite has been enhanced and transferred to a synthetic compound series. The resulting compounds were accessible via an easy synthetic route and offered a possibility to investigate the structure-activity relationships. The natural product inspired drug design extends the valuable role of natural products as drugs and drug precursors to templates for fully synthetic bioactive molecules. Simplification of natural products by means of chemical synthesis could lead to an interesting field in the treatment of cancer.

Affinity chromatography has been used to unravel unknown- and off-target effects which either contribute to the biological effect of the inhibitor or that counteract or lead to undesired side-effects. During this PhD work, two main projects related to this technique have been established. In the first one, related to an imidazo[1,2-*a*]pyridine inhibitor (EP6), it has been shown that epoxide-sepharose is a reliable material in order to couple compounds bearing an alcohol. Coupling of an analogue of EP6 to the

sepharose has been accomplished and affinity towards 5-LO was demonstrated. The challenging step is to discern from unspecific protein binders and analysis via SDS-PAGE separation and mass spectrometry. Further experiments using other cell types or improving SDS-PAGE analysis (e.g. 2D gel analysis) should be useful to unravel EP6 off-target effect. During the second project related to off-target effects of celecoxib and DMC, the main problem was the coupling of the functional group to the sepharose. Affinity towards COX-2 could not be demonstrated pointing out the inefficient coupling method. Higher pH values during coupling reaction should be tested in further experiments. Nevertheless, affinity chromatography is a useful technique to unravel cellular mechanisms.

Sphingolipid metabolism is also a recent area that attired the attention of cancer researchers, due to their important roles in cell proliferation and apoptosis. Ceramide metabolism inhibitors were synthesized and evaluated on different assay systems in order to assess their efficacy on several cancer lines. Remarkably, 2,2-dimethyl-1,3-dioxolan-4-yl)methanamine (**32**) was a useful scaffold to mimic the sphingoid base. This key intermediate was used to produce ceramide analogues that could enter the cell and target apoptosis machinery. EB143 (**38**) increased ceramide levels in an *in vitro* ceramide synthase assay in a dose-response manner meaning that ceramide synthase was not inhibited but the ceramide *de novo* synthesis was activated. This effect was due to the fact that EB143 is a cytotoxic compound with an interesting antiproliferative profile. Further chemical modifications should be carried out to modulate this effect.

COX and LO inhibitors are cancer-preventive not only by inhibiting specific antiapoptotic AA metabolites but also by facilitating accumulation of AA which promotes neutral SMase activity and increases the proapoptotic ceramide. Several 5-LO inhibitors have been evaluated on several cancer lines and sphingolipid levels were measured in order to obtain a relationship. A549, Capan-2 and MCF-7 cells line were incubated with synthetic 5-LO inhibitors and zileuton. Compounds were cytotoxic to all cancer cell lines except from A549. Needless to say, zileuton did not exhibit a cytotoxic profile. Synthetic 5-LO inhibitors were able to modify ceramide levels but were useless when coincubating with sphingolipid metabolism inhibitors (myoricin, amitryptiline etc.) and inconsistent results were obtained. On the contrary, zileuton selectively increased Cer-C_{16} levels and in less extend Cer-$C_{24:1.}$ When using a SPT inhibitor (myoricin) alone was able to reduce $C_{24:1}$ and Cer-$C_{16:0}$ levels below the control, a similar effect occurred

when incubation the cells with zileuton and myriocin. Interestingly, treatment of zileuton together with either amitryptiline or desipramine led to a decrease in Cer-$C_{24:1}$ and levels Cer-$C_{16:0}$ but the inhibition was not complete indicating that probably the *de novo* pathway has an important role. Further investigations on mRNA level should be carried out in order to discern which CerS is activated.

The main objective of the present thesis was the synthesis of lipid signaling modulators and their evaluation in vitro as therapeutic strategy to overcome pathophysiological conditions (cancer, metabolic syndrome, etc). It has been accomplished on many relevant targets like 5-LO, mPGES-1, sEH and PPAR and these lipid signaling modulators could be used in the treatment of diseases conditions where lipid mediators play an important role.

Zusammenfassung

Lipidmodulatoren (LMs) sind wichtige Mediatoren von physiologischen und pathophysiologischen Vorgängen. Die physikochemischen Eigenschaften bioaktiver Lipide erschweren ihre Erforschung, allerdings hat der Fortschritt auf den Gebieten der Flüssigkeitschromatographie und Massenspektrometrie die Analytik der LMs und damit auch die Aufklärung ihrer Rolle in pathophysiologischen Vorgängen ermöglicht. Zu diesen zählen kardiovaskuläre Erkrankungen, Entzündungsprozesse und Krebs - pathophysiologische Abläufe, bei denen Lipidmodulatoren dysreguliert sein können.

Der erste Teil dieser Arbeit beschäftigte sich mit Enzymen, die Arachidonsäure und ihre Metabolite umwandeln. Die mPGES-1 ist ein wichtiges Enzym der Arachidonsäurekaskade und sein Produkt, Prostaglandin E_2 (PGE_2) spielt eine wichtige Rolle bei verschiedenen Entzündungsprozessen. Inhibition der mPGES-1 könnte ein vielversprechender Schritt sein, die COX-abhängigen Nebenwirkungen von NSAIDs (Perforation von Darmgeschwüren sowie gastrointestinale Blutungen) zu umgehen. Eine Klasse von Quinazolin-Verbindungen rund um die Leitstruktur FR20 wurde an isoliertem menschlichen und murinen Enzym, in HeLa Zellen sowie unter verschiedenen Bedingungen im menschlichem Vollblut untersucht, um die möglichen Wirkungen der Verbindungen auf das Eicosanoid-Profil zu ermitteln. Neuartige Substanzen mit inhibitorischem Potential im submikromolaren Bereich (IC_{50}: 0.13 µM - 0.37 µM an isoliertem Enzym) wurden synthetisiert, die ebenfalls in Zellen sowie im Vollblut aktiv waren. Weiterhin zeigten das pharmakologische Profiling der Toxizität und ein Lipid Screening mittels LC/MS-MS, dass die Substanzen ebenfalls den PGE_2 Spiegel in intakten Zellen sowie im Vollblut senken können und gut zellgängig sind, allerdings nicht in der Lage sind die murine mPGES-1 zu inhibieren. Dieses Problem könnte durch die Variation des Grundgerüsts (Quinolin oder Quinazolin) oder durch Einführung bioisoteren Ersatzes der Phenylgruppe gelöst werden.

Neben der mPGES-1 spielt das Enzym 5-lipoxygenase (5-LO) ebenfalls eine wichtige Rolle in der Eicosanoid-Signaltransduktion, speziell bei der Leukotrien-Biosynthese. Leukotriene sind an der Entstehung von Asthma, allergischer Rhinitis, Glomerulonephritis, rheumatoider Arthritis, Sepsis, Krebs und Atherosklerose beteiligt. Weiterhin wurden Varianten in den Genen des 5-LO Signalweges mit einem Risiko zur Entwicklung eines akuten Myokardinfarkts oder Schlaganfalls verbunden. Erhöhte

Eicosanoidspiegel zeigen sich bei infektiösen Verschlimmerungen der chronisch obstruktiven Lungenerkrankung (COPD). Auch bei stabilen COPD-Patienten sind die Eicosanoidspiegel höher als bei gesunden Menschen. Aus diesen Gründen ist die 5-LO ein interessantes Target für Therapieansätze bezüglich der eben genannten Krankheiten.

In drei Publikationen wurde die Inhibition der 5-LO an intakten PMNLs, einem zellfreien Assay, in menschlichem Vollblut (HWB) und in Nagerzellen untersucht, um Struktur-Aktivitätsbeziehungen aufzuklären und sie pharmakologisch *in vitro* zu evaluieren. Chemische Modifikationen zur Optimierung der Leitstruktur wurden mittels organischer Synthese eingeführt. Die Kopplung kleiner, polarer Gruppen (Hydroxyl- und Methoxy-Gruppen) brachte Verbindungen hervor, welche das gewünschte pharmalogische Profil hinsichtlich ihrer Löslichkeit, der intrinsischen Clearance und der Zytotoxizität aufwiesen. Die vorliegende Arbeit zeigt eine umfassende Evaluierung der Imidazo[1,2-*a*]pyridin als Leitstruktur neuartiger 5-LO-Inhibitoren. Über 70 Imidazo[1,2-*a*]pyridin-Derivate wurden synthetisiert, von denen mehr als 50 die 5-LO inhibierten. Obwohl es nicht möglich war, eine löslichkeitsfördernde Gruppe einzuführen ohne das Inhibitionspotential zu senken, gelang es doch durch die Kombination von kleinen, polaren Gruppen die Löslichkeit sowie die metabolische Stabilität *in vitro* zu verbessern. Die Entwicklung neuer 5-LO-Inhibitoren mit hoher Wirksamkeit und Selektivität *in vivo* bietet einen vielversprechenden Ansatz zur Behandlung von Patienten mit Krankheiten, bei denen die Leukotrien-Biosynthese eine Rolle spielt.

Im Rahmen dieser Arbeit wurden weiterhin NO-NSAIDs synthetisiert, die ebenfalls die 5-LO inhibieren, ohne die unerwünschten Nebenwirkungen durch Inhibition der COX-Isoformen hervorzurufen. Es wurde postuliert, dass nach der Metabolisierung der Verbindungen die NO-Gruppe *in situ* freigesetzt wird. NO-NSAIDs weisen antientzündliche Eigenschaften auf indem sie in klinisch relevanten Konzentrationen die 5-LO inhibieren. Momentan befinden sie sich in klinischen Studien zur Behandlung von Krankheiten, die mit Entzündungsprozessen verbunden sind. Die Synthese der NO-NSAIDs ist unkompliziert und kann für die meisten bekannten NSAIDs durchgeführt werden. Von den synthetisierten Verbindungen ist NO-Sulindac am aussichtsreichsten, da es in mikromolaren Konzentrationen die 5-LO-Produktbildung sowohl in intakten PMNL, als auch bei rekombinanter 5-LO und im Vollblut inhibierte. Zusätzliche Experimente bezüglich des Wirkmechanismus werden momentan

durchgeführt. Weiterhin soll die Wirksamkeit von NO-Sulindac in Entzündungsmodellen *in vivo* bestätigt werden.

Eine weitere Studie konnte zeigen, dass duales Targeting ein interessanter und praktikabler Ansatz ist, der in den letzten Jahren verwendet wurde, um Nebenwirkungen zu vermindern und Krankheiten zu therapieren, die mehrere pathophysiologische Faktoren betreffen. Das Metabolische Syndrom (MetS) ist ein Beispiel für das parallele Auftreten der folgenden Symptome: Hyperglykämie, Hypertriglyzeridämie, Bluthochdruck und Fettleibigkeit. Aufgrund dieser Komplexität erfordert die aktuelle Behandlungsstrategie des MetS eine Gabe mehrerer Wirkstoffe zur Regulierung der Lipid- und Glukose-Homöostase, sowie zur Regulierung des Blutdrucks und der Blutgerinnung. Diese Studie beschreibt die erste Synthese von dualen sEH/PPAR Modulatoren als mögliche Wirkstoffe zur Behandlung des MetS. Einem kombinatorischen Ansatz entsprechend wurde eine azide Kopfgruppe (Pharmakophor von PPAR*α/γ* dual Agonisten) mit verschiedenen hydrophoben Harnstoffen kombiniert, die als Epoxid-Mimetikum dienen (Pharmakophor der sEH). Die synthetisierten Verbindungen zeigten starke Inhibition der sEH und unterschiedliche Muster bei der agonistischen Aktivität an PPAR. Es konnte gezeigt werden, dass die Pharmakophore von PPAR-Agonisten und sEH-Inhibitoren leicht kombiniert werden konnten, um ein vereinfachtes Modell für duale sEH/PPAR Modulatoren zu erhalten. Allerdings sind weitere *in vivo* Studien nötig, um heraus zu finden, welches PPAR Aktivationsmuster den vielversprechendsten Ansatz zur Behandlung des MetS bietet.

Als weiteres Beispiel für Polypharmakologie sind Verbindungen zu nennen, die von Naturstoffen abgeleitet wurden, und in der Lage sind, sowohl die sEH zu inhibieren als auch antiproliferativ zu wirken. Ausgehend von diesen Naturstoffen und dem ursprünglichen Hit Isopropylstilben wurden multi-target Liganden synthetisiert. Die (*E*)-styryl-1*H*-benzo[*d*]imidazole erwiesen sich als Inhibitoren der sEH mit antiproliferativen Eigenschaften. Dem Naturprodukt-inspiriertem Aufbau der Substanzen entsprechend, zeigten sie die gewünschte biologische Aktivität, die sich aufgrund ihrer Ähnlichkeit zu den bakteriellen Sekundärmetaboliten vermuten lässt. Die Styryl-Verbindungen sind über eine einfache Syntheseroute zu erhalten, was die Möglichkeit bot, die Struktur-Aktivitätsbeziehungen zu untersuchen. Der verfolgte Ansatz zeigt die Bedeutung von Naturprodukten als wichtige Wirkstoffe beziehungsweise als Ausgangspunkt, um Wirkstoffe mit hoher Bioaktivität zu erhalten.

Die Vereinfachung von Naturstoffen durch chemische Synthese könnte neue Möglichkeiten zur Behandlung von Krebs eröffnen.

Die Affinitätschromatographie ist eine Methode, um unbekannte Effekte zu untersuchen, welche die biologische Wirkung eines Inhibitors verstärken oder schwächen können, sowie unerwünschte Nebenwirkungen hervorrufen. In dieser Arbeit wurde die Affinitätschromatographie in zwei Projekten angewendet. Da die Epoxid-Sepharose ein geeignetes Material ist, um Verbindungen zu immobilisieren, die eine Alkoholgruppe tragen, wurde ein Imidazo[1,2-*a*]pyridin-Analogon (EP6) erfolgreich daran gekoppelt, um die Affinität von EP6 auf die 5-LO zu demonstrieren. Der schwierige Schritt dabei ist die Unterscheidung zwischen spezifischer und unspezifischer Proteinbindung sowie die Analyse mittels Massenspektrometrie nach der Auftrennung im SDS-PAGE. Diese Experimente wurden mit unterschiedlichen Zelltypen sowie optimierten SDS-PAGE-Methoden (z.B. 2D Gelanalyse) durchgeführt, um die unspezifischen Wechselwirkungen mit EP6 abzutrennen. In einem zweiten Projekt sollten die die Nebenwirkungen von Celecoxib und Dimethylcelecoxib (DMC) untersucht werden. Das Hauptproblem war dabei die Kopplung der funktionellen Gruppen an die Sepharose. Da keine Affinität der Substanzen bezüglich der COX-2 gezeigt werden konnte, muss davon ausgegangen werden, dass die Immobilisierung der Substanzen nicht funktioniert hat. Höhere pH-Werte während der Kopplungsreaktion müssen in weiteren Experimenten getestet werden. Dennoch ist die Affinitätschromatographie eine interessante Technik, um zelluläre Mechanismen aufzuklären.

Der Sphingolipid(SL)-Metabolismus ist ebenfalls ein Gebiet, das aufgrund seiner Bedeutung bei Zellproliferation und Apoptose die Aufmerksamkeit von Krebsforschern auf sich zieht. Inhibitoren des Ceramid-Metabolismus wurden synthetisiert und in verschiedenen Assay-Systemen auf ihre Effizienz bezüglich unterschiedlicher Krebslinien evaluiert. Bemerkenswerterweise ist 2,2-Dimethyl-((1,3-dioxolan-4-yl)methanamin (**32**) ein geeignetes Mimetikum der Sphingoid-Base. Diese entscheidende Zwischenerkenntnis wurde genutzt, um Ceramid-Analoga zu synthetisieren, die zellgängig sind und in die Apoptose eingreifen. EB143 (**38**) erhöhte den Ceramid-Spiegel in einem *in vitro* Ceramid-Assay dosisabhängig, was darauf schließen lässt, dass nicht die Ceramid-Synthase inhibiert, sondern die Ceramid *de novo* Synthese aktiviert wurde. Dieser Effekt resultiert aus den zytotoxischen Eigenschaften von EB143 und seinem interessanten, antiproliferativen Profil. Weitere

chemische Modifikationen sollten vorgenommen werden, um diesen Effekt ergänzend zu modulieren.

Inhibitoren von COX und LO sind krebspräventiv sowohl durch die Inhibition spezifischer, antiapoptotischer Arachidonsäure(AA)-Metabolite, als auch durch die Erleichterung der Anhäufung von AA, was die Aktivität der neutralen SMase fördert und den Spiegel an proapoptotischen Ceramiden erhöht. Diverse 5-LO-Inhibitoren wurden an verschiedenen Krebs-Zelllinien untersucht und die SL-Spiegel gemessen, um eine Beziehung herzustellen. Die Zelllinien A549, Capan-2 und MCF-7 wurden mit den synthetisierten 5-LO-Inhibitoren und Zileuton inkubiert. Zileuton zeigte selbstverständlich kein zytotoxisches Profil, jedoch wirkten alle anderen Inhibitoren zytotoxisch auf alle Zelllinien außer A549. Die synthetisierten 5-LO-Inhibitoren waren in der Lage die Ceramidspiegel zu modulieren, allerding nicht oder nur inkonsistent, wenn sie mit Inhibitoren des SL Metabolismus (Myoricin, Amitryptilin, etc.) coinkubiert wurden. Zileuton hingegen erhöhte selektiv die Cer-C_{16}-Spiegel und in geringerem Maß auch von Cer-$C_{24:1}$. Die Verwendung eines SPT-Inhibitors (Myoricin) zeigte eine Reduktion der $C_{24:1}$- und Cer-$C_{16:0}$-Spiegel unter die Kontrolle. Ein ähnlicher Effekt zeigte sich bei der Inkubation der Zellen mit Zileuton und Myriocin zusammen. Interessanterweise zeigte die Behandlung von Zileuton zusammen mit entweder Amitryptilin oder Despiramin eine Absenkung der Cer-$C_{24:1}$- und Cer-$C_{16:0}$-Spiegel, was die Vermutung der Aktivierung des *de novo* Pathways nicht komplett stützt. Weitere Experimente auf mRNA-Ebene sollten durchgeführt werden, um zu unterscheiden, ob die CerS aktiviert wird.

Das Hauptziel der vorliegenden Arbeit war die Synthese und *in vitro* Evaluierung von Modulatoren verschiedener Lipid-Signaltransduktionskaskaden als Ansatz zur Behandlung pathologischer Physiologien (Krebs, Metabolisches Syndrom usw.). Für viele klinisch relevante Targets wie 5-LO, mPGES-1, sEH und PPAR wurde dies erfolgreich durchgeführt, so dass die synthetisierten Modulatoren einen Nutzen zur Behandlung diverser Krankheiten bieten können, bei denen Lipid Mediatoren beteiligt sind.

References

1. Sonnino, S. & Prinetti, A. Membrane domains and the “lipid raft” concept. *Current medicinal chemistry* **20**, 4–21 (2013).

2. Hamer, I., Van Beersel, G., Arnould, T. & Jadot, M. Lipids and lysosomes. *Current drug metabolism* **13**, 1371–87 (2012).

3. Hla, T. & Dannenberg, A. J. Sphingolipid signaling in metabolic disorders. *Cell metabolism* **16**, 420–34 (2012).

4. Shimizu, T. Lipid mediators in health and disease: enzymes and receptors as therapeutic targets for the regulation of immunity and inflammation. *Annual review of pharmacology and toxicology* **49**, 123–50 (2009).

5. Isobe, Y., Kato, T. & Arita, M. Emerging roles of eosinophils and eosinophil-derived lipid mediators in the resolution of inflammation. *Frontiers in immunology* **3**, 270 (2012).

6. Samuelsson, B., Dahlén, S. E., Lindgren, J. A., Rouzer, C. A. & Serhan, C. N. Leukotrienes and lipoxins: structures, biosynthesis, and biological effects. *Science (New York, N.Y.)* **237**, 1171–6 (1987).

7. Reitz, C. Dyslipidemia and the risk of Alzheimer’s disease. *Current atherosclerosis reports* **15**, 307 (2013).

8. Allaj, V., Guo, C. & Nie, D. Non-steroid anti-inflammatory drugs, prostaglandins, and cancer. *Cell & bioscience* **3**, 8 (2013).

9. Yang, Y., Tang, L.-Q. & Wei, W. Prostanoids receptors signaling in different diseases/cancers progression. *Journal of receptor and signal transduction research* **33**, 14–27 (2013).

10. Im, D.-S. New intercellular lipid mediators and their GPCRs: an update. *Prostaglandins & other lipid mediators* **89**, 53–6 (2009).

11. Samuelsson, B. Leukotrienes: mediators of immediate hypersensitivity reactions and inflammation. *Science (New York, N.Y.)* **220**, 568–75 (1983).

12. Raju, T. N. The Nobel chronicles. 1982: Sune Karl Bergström (b 1916); Bengt Ingemar Samuelsson (b 1934); John Robert Vane (b 1927). *Lancet* **354**, 1914 (1999).

13. Bergstroem, S. & Samuelsson, B. Prostaglandins. *Annual review of biochemistry* **34**, 101–8 (1965).

14. Bergström, S., Carlson, L. A. & Weeks, J. R. The prostaglandins: a family of biologically active lipids. *Pharmacological reviews* **20**, 1–48 (1968).

15. Burke, J. E. & Dennis, E. A. Phospholipase A2 structure/function, mechanism, and signaling. *Journal of lipid research* **50 Suppl**, S237–42 (2009).

16. Hui, D. Y. Phospholipase A(2) enzymes in metabolic and cardiovascular diseases. *Current opinion in lipidology* **23**, 235–40 (2012).

17. Pairet, M. & Engelhardt, G. Distinct isoforms (COX-1 and COX-2) of cyclooxygenase: possible physiological and therapeutic implications. *Fundamental & clinical pharmacology* **10**, 1–17 (1996).

18. Needleman, P. & Isakson, P. C. The discovery and function of COX-2. *The Journal of rheumatology. Supplement* **49**, 6–8 (1997).

19. Vane, J. R. & Botting, R. M. Mechanism of action of aspirin-like drugs. *Seminars in arthritis and rheumatism* **26**, 2–10 (1997).

20. Urade, Y. & Hayaishi, O. Prostaglandin D2 and sleep/wake regulation. *Sleep medicine reviews* **15**, 411–8 (2011).

21. Takahashi, G. *et al.* The potential role of prostaglandin D2 in nasal congestion observed in a guinea pig model of allergic rhinitis. *International archives of allergy and immunology* **158**, 359–68 (2012).

22. Elias, E. *et al.* Central nervous system lipocalin-type prostaglandin D2-synthase is correlated with orexigenic neuropeptides, visceral adiposity and markers of the hypothalamic-pituitary-adrenal axis in obese humans. *Journal of neuroendocrinology* **23**, 501–7 (2011).

23. Yuhki, K., Kashiwagi, H., Kojima, F., Kawabe, J. & Ushikubi, F. Roles of prostanoids in the pathogenesis of cardiovascular diseases. *International angiology : a journal of the International Union of Angiology* **29**, 19–27 (2010).

24. Akaogi, J., Nozaki, T., Satoh, M. & Yamada, H. Role of PGE2 and EP receptors in the pathogenesis of rheumatoid arthritis and as a novel therapeutic strategy. *Endocrine, metabolic & immune disorders drug targets* **6**, 383–94 (2006).

25. Greenhough, A. *et al.* The COX-2/PGE2 pathway: key roles in the hallmarks of cancer and adaptation to the tumour microenvironment. *Carcinogenesis* **30**, 377–86 (2009).

26. Reader, J., Holt, D. & Fulton, A. Prostaglandin E2 EP receptors as therapeutic targets in breast cancer. *Cancer metastasis reviews* **30**, 449–63 (2011).

27. Samuelsson, B., Morgenstern, R. & Jakobsson, P.-J. Membrane prostaglandin E synthase-1: a novel therapeutic target. *Pharmacological reviews* **59**, 207–24 (2007).

28. Papierniak, E. S., Lowenthal, D. T. & Harman, E. Novel therapies in asthma: leukotriene antagonists, biologic agents, and beyond. *American journal of therapeutics* **20**, 79–103 (2013).

29. Scoggan, K. A., Jakobsson, P. J. & Ford-Hutchinson, A. W. Production of leukotriene C4 in different human tissues is attributable to distinct membrane bound biosynthetic enzymes. *The Journal of biological chemistry* **272**, 10182–7 (1997).

30. Funk, C. D. Prostaglandins and leukotrienes: advances in eicosanoid biology. *Science (New York, N.Y.)* **294**, 1871–5 (2001).

31. Yokomizo, T., Izumi, T., Chang, K., Takuwa, Y. & Shimizu, T. A G-protein-coupled receptor for leukotriene B4 that mediates chemotaxis. *Nature* **387**, 620–4 (1997).

32. Goodarzi, K., Goodarzi, M., Tager, A. M., Luster, A. D. & Von Andrian, U. H. Leukotriene B4 and BLT1 control cytotoxic effector T cell recruitment to inflamed tissues. *Nature immunology* **4**, 965–73 (2003).

33. Philteos, G. S., Davis, B. E., Cockcroft, D. W. & Marciniuk, D. D. Role of leukotriene receptor antagonists in the treatment of exercise-induced bronchoconstriction: a review. *Allergy, asthma, and clinical immunology : official journal of the Canadian Society of Allergy and Clinical Immunology* **1**, 60–4 (2005).

34. Greene, E. R., Huang, S., Serhan, C. N. & Panigrahy, D. Regulation of inflammation in cancer by eicosanoids. *Prostaglandins & other lipid mediators* **96**, 27–36 (2011).

35. Spector, A. A. Arachidonic acid cytochrome P450 epoxygenase pathway. *Journal of lipid research* **50 Suppl**, S52–6 (2009).

36. Chen, J.-K., Capdevila, J. & Harris, R. C. Cytochrome P450 Epoxygenase Metabolism of Arachidonic Acid Inhibits Apoptosis. *Molecular and Cellular Biology* **21**, 6322–6331 (2001).

37. Chen, L., Ackerman, R. & Guo, A. M. 20-HETE in neovascularization. *Prostaglandins & other lipid mediators* **98**, 63–8 (2012).

38. Zhao, X. & Imig, J. D. Kidney CYP450 enzymes: biological actions beyond drug metabolism. *Current drug metabolism* **4**, 73–84 (2003).

39. Inceoglu, B., Schmelzer, K. R., Morisseau, C., Jinks, S. L. & Hammock, B. D. Soluble epoxide hydrolase inhibition reveals novel biological functions of epoxyeicosatrienoic acids (EETs). *Prostaglandins & other lipid mediators* **82**, 42–9 (2007).

40. Nithipatikom, K. & Gross, G. J. Review article: epoxyeicosatrienoic acids: novel mediators of cardioprotection. *Journal of cardiovascular pharmacology and therapeutics* **15**, 112–9 (2010).

41. Webler, A. C. *et al.* Epoxyeicosatrienoic acids are part of the VEGF-activated signaling cascade leading to angiogenesis. *American journal of physiology. Cell physiology* **295**, C1292–301 (2008).

42. Fisslthaler, B. *et al.* Cytochrome P450 2C is an EDHF synthase in coronary arteries. *Nature* **401**, 493–7 (1999).

43. Shindou, H. *et al.* A single enzyme catalyzes both platelet-activating factor production and membrane biogenesis of inflammatory cells. Cloning and characterization of acetyl-CoA:LYSO-PAF acetyltransferase. *The Journal of biological chemistry* **282**, 6532–9 (2007).

44. Honda, Z., Ishii, S. & Shimizu, T. Platelet-activating factor receptor. *Journal of biochemistry* **131**, 773–9 (2002).

45. Kihara, Y. *et al.* Dual phase regulation of experimental allergic encephalomyelitis by platelet-activating factor. *The Journal of experimental medicine* **202**, 853–63 (2005).

46. Umezu-Goto, M. *et al.* Autotaxin has lysophospholipase D activity leading to tumor cell growth and motility by lysophosphatidic acid production. *The Journal of cell biology* **158**, 227–33 (2002).

47. Takabe, K., Paugh, S. W., Milstien, S. & Spiegel, S. “Inside-out” signaling of sphingosine-1-phosphate: therapeutic targets. *Pharmacological reviews* **60**, 181–95 (2008).

48. Bandhuvula, P. & Saba, J. D. Sphingosine-1-phosphate lyase in immunity and cancer: silencing the siren. *Trends in molecular medicine* **13**, 210–7 (2007).

49. Olivera, A. Unraveling the complexities of sphingosine-1-phosphate function: the mast cell model. *Prostaglandins & other lipid mediators* **86**, 1–11 (2008).

50. Heffernan-Stroud, L. A. & Obeid, L. M. Sphingosine kinase 1 in cancer. *Advances in cancer research* **117**, 201–35 (2013).

51. Cyster, J. G. & Schwab, S. R. Sphingosine-1-phosphate and lymphocyte egress from lymphoid organs. *Annual review of immunology* **30**, 69–94 (2012).

52. Hla, T. & Brinkmann, V. Sphingosine 1-phosphate (S1P): Physiology and the effects of S1P receptor modulation. *Neurology* **76**, S3–8 (2011).

53. Chiba, K. & Adachi, K. Discovery of fingolimod, the sphingosine 1-phosphate receptor modulator and its application for the therapy of multiple sclerosis. *Future medicinal chemistry* **4**, 771–81 (2012).

54. Kawamori, T. *et al.* Sphingosine kinase 1 is up-regulated in colon carcinogenesis. *FASEB journal : official publication of the Federation of American Societies for Experimental Biology* **20**, 386–8 (2006).

55. Lamour, N. F. *et al.* Ceramide 1-phosphate is required for the translocation of group IVA cytosolic phospholipase A2 and prostaglandin synthesis. *The Journal of biological chemistry* **284**, 26897–907 (2009).

56. Serhan, C. N. *et al.* Maresins: novel macrophage mediators with potent antiinflammatory and proresolving actions. *The Journal of experimental medicine* **206**, 15–23 (2009).

57. Cortina, M. S., He, J., Li, N., Bazan, N. G. & Bazan, H. E. P. Neuroprotectin D1 synthesis and corneal nerve regeneration after experimental surgery and treatment with PEDF plus DHA. *Investigative ophthalmology & visual science* **51**, 804–10 (2010).

58. Hersberger, M. Potential role of the lipoxygenase derived lipid mediators in atherosclerosis: leukotrienes, lipoxins and resolvins. *Clinical chemistry and laboratory medicine : CCLM / FESCC* **48**, 1063–73 (2010).

59. Flesch, D., Merk, D., Lamers, C. & Schubert-Zsilavecz, M. Novel prostaglandin receptor modulators - Part II: EP receptor modulators; a patent review (2002 - 2012). *Expert opinion on therapeutic patents* **23**, 233–67 (2013).

60. Davì, G., Santilli, F. & Vazzana, N. Thromboxane receptors antagonists and/or synthase inhibitors. *Handbook of experimental pharmacology* 261–86 (2012).doi:10.1007/978-3-642-29423-5_11

61. Toda, A., Yokomizo, T. & Shimizu, T. Leukotriene B4 receptors. *Prostaglandins & other lipid mediators* **68-69**, 575–85 (2002).

62. Cooke, M., Di Cónsoli, H., Maloberti, P. & Cornejo Maciel, F. Expression and function of OXE receptor, an eicosanoid receptor, in steroidogenic cells. *Molecular and cellular endocrinology* (2012).doi:10.1016/j.mce.2012.11.003

63. Snider, N. T., Nast, J. A., Tesmer, L. A. & Hollenberg, P. F. A cytochrome P450-derived epoxygenated metabolite of anandamide is a potent cannabinoid receptor 2-selective agonist. *Molecular pharmacology* **75**, 965–72 (2009).

64. Krey, G. *et al.* Fatty acids, eicosanoids, and hypolipidemic agents identified as ligands of peroxisome proliferator-activated receptors by coactivator-dependent receptor ligand assay. *Molecular endocrinology (Baltimore, Md.)* **11**, 779–91 (1997).

65. Capobianco, E., White, V., Higa, R., Martínez, N. & Jawerbaum, A. Effects of natural ligands of PPARgamma on lipid metabolism in placental tissues from healthy and diabetic rats. *Molecular human reproduction* **14**, 491–9 (2008).

66. Narumiya, S. & FitzGerald, G. A. Genetic and pharmacological analysis of prostanoid receptor function. *The Journal of clinical investigation* **108**, 25–30 (2001).

67. Nakanishi, M. & Rosenberg, D. W. Multifaceted roles of PGE(2) in inflammation and cancer. *Seminars in immunopathology* **35**, 123–37 (2013).

68. Jacobi, D., Stanya, K. J. & Lee, C.-H. Adipose tissue signaling by nuclear receptors in metabolic complications of obesity. *Adipocyte* **1**, 4–12 (2012).

69. Podbielska, M., Krotkiewski, H. & Hogan, E. L. Signaling and regulatory functions of bioactive sphingolipids as therapeutic targets in multiple sclerosis. *Neurochemical research* **37**, 1154–69 (2012).

70. Bieberich, E. It's a lipid's world: bioactive lipid metabolism and signaling in neural stem cell differentiation. *Neurochemical research* **37**, 1208–29 (2012).

71. Hermanson, D. J. & Marnett, L. J. Cannabinoids, endocannabinoids, and cancer. *Cancer metastasis reviews* **30**, 599–612 (2011).

72. Furuya, H., Shimizu, Y. & Kawamori, T. Sphingolipids in cancer. *Cancer metastasis reviews* **30**, 567–76 (2011).

73. Maceyka, M., Harikumar, K. B., Milstien, S. & Spiegel, S. Sphingosine-1-phosphate signaling and its role in disease. *Trends in cell biology* **22**, 50–60 (2012).

74. Ranjha, R. & Paul, J. Micro-RNAs in inflammatory diseases and as a link between inflammation and cancer. *Inflammation research : official journal of the European Histamine Research Society ... [et al.]* (2013).doi:10.1007/s00011-013-0600-9

75. Monteleone, G., Pallone, F. & Stolfi, C. The dual role of inflammation in colon carcinogenesis. *International journal of molecular sciences* **13**, 11071–84 (2012).

76. Okayama, H., Schetter, A. J. & Harris, C. C. MicroRNAs and inflammation in the pathogenesis and progression of colon cancer. *Digestive diseases (Basel, Switzerland)* **30 Suppl 2**, 9–15 (2012).

77. Sfanos, K. S. & De Marzo, A. M. Prostate cancer and inflammation: the evidence. *Histopathology* **60**, 199–215 (2012).

78. Gasparoto, T. H. *et al.* Inflammatory events during murine squamous cell carcinoma development. *Journal of inflammation (London, England)* **9**, 46 (2012).

79. Girard, N. Other signalization targets. *Targeted oncology* (2013).doi:10.1007/s11523-012-0246-5

80. Efferth, T. Signal transduction pathways of the epidermal growth factor receptor in colorectal cancer and their inhibition by small molecules. *Current medicinal chemistry* **19**, 5735–44 (2012).

81. Kalimuthu, S. & Se-Kwon, K. Cell survival and apoptosis signaling as therapeutic target for cancer: marine bioactive compounds. *International journal of molecular sciences* **14**, 2334–54 (2013).

82. Vartanian, A. A. Signaling pathways in tumor vasculogenic mimicry. *Biochemistry. Biokhimiia* **77**, 1044–55 (2012).

83. Claesson-Welsh, L. & Welsh, M. VEGFA and tumour angiogenesis. *Journal of internal medicine* **273**, 114–27 (2013).

84. Vendramini-Costa, D. B. & Carvalho, J. E. Molecular link mechanisms between inflammation and cancer. *Current pharmaceutical design* **18**, 3831–52 (2012).

85. Hyde, C. A. C. & Missailidis, S. Inhibition of arachidonic acid metabolism and its implication on cell proliferation and tumour-angiogenesis. *International immunopharmacology* **9**, 701–15 (2009).

86. Wang, D. & Dubois, R. N. Eicosanoids and cancer. *Nature reviews. Cancer* **10**, 181–93 (2010).

87. Cebola, I. & Peinado, M. A. Epigenetic deregulation of the COX pathway in cancer. *Progress in lipid research* **51**, 301–13 (2012).

88. Ke, H.-L. *et al.* Cyclooxygenase-2 (COX-2) up-regulation is a prognostic marker for poor clinical outcome of upper tract urothelial cancer. *Anticancer research* **32**, 4111–6 (2012).

89. Camacho, M. *et al.* Hypoxia upregulates PGI-synthase and increases PGI_2 release in human vascular cells exposed to inflammatory stimuli. *Journal of lipid research* **52**, 720–31 (2011).

90. Cook-Johnson, R. J. *et al.* Endothelial cell COX-2 expression and activity in hypoxia. *Biochimica et biophysica acta* **1761**, 1443–9 (2006).

91. Nakanishi, M. *et al.* Genetic deletion of mPGES-1 suppresses intestinal tumorigenesis. *Cancer research* **68**, 3251–9 (2008).

92. Lou, L.-H. *et al.* 15-PGDH is reduced and induces apoptosis and cell cycle arrest in gastric carcinoma. *World journal of gastroenterology : WJG* **18**, 1028–37 (2012).

93. Lehtinen, L. *et al.* 15-Hydroxyprostaglandin dehydrogenase associates with poor prognosis in breast cancer, induces epithelial-mesenchymal transition, and promotes cell migration in cultured breast cancer cells. *The Journal of pathology* **226**, 674–86 (2012).

94. Kataoka, K., Takikawa, Y., Lin, S. De & Suzuki, K. Prostaglandin E2 receptor EP4 agonist induces Bcl-xL and independently activates proliferation signals in mouse primary hepatocytes. *Journal of gastroenterology* **40**, 610–6 (2005).

95. Garcia Rodriguez, L. A., Cea-Soriano, L., Tacconelli, S. & Patrignani, P. Coxibs: pharmacology, toxicity and efficacy in cancer clinical trials. *Recent results in cancer research. Fortschritte der Krebsforschung. Progrès dans les recherches sur le cancer* **191**, 67–93 (2013).

96. Dovizio, M. *et al.* Effects of celecoxib on prostanoid biosynthesis and circulating angiogenesis proteins in familial adenomatous polyposis. *The Journal of pharmacology and experimental therapeutics* **341**, 242–50 (2012).

97. Huang, K. *et al.* Clinical characteristics and outcomes in familial adenomatous polyposis patients with a long-term treatment of celecoxib: a matched cohort study. *Familial cancer* **10**, 303–8 (2011).

98. Lynch, P. M. *et al.* The safety and efficacy of celecoxib in children with familial adenomatous polyposis. *The American journal of gastroenterology* **105**, 1437–43 (2010).

99. Sands, G., Shell, B. & Zhang, R. Adverse events in patients with blood loss: a pooled analysis of 51 clinical studies from the celecoxib clinical trial database. *The open rheumatology journal* **6**, 44–9 (2012).

100. Pidgeon, G. P. *et al.* Lipoxygenase metabolism: roles in tumor progression and survival. *Cancer metastasis reviews* **26**, 503–24 (2007).

101. Steinhilber, D. *et al.* 5-lipoxygenase: underappreciated role of a pro-inflammatory enzyme in tumorigenesis. *Frontiers in pharmacology* **1**, 143 (2010).

102. Park, S.-W., Heo, D.-S. & Sung, M.-W. The shunting of arachidonic acid metabolism to 5-lipoxygenase and cytochrome p450 epoxygenase antagonizes the anti-cancer effect of cyclooxygenase-2 inhibition in head and neck cancer cells. *Cellular oncology (Dordrecht)* **35**, 1–8 (2012).

103. Kerjaschki, D. *et al.* Lipoxygenase mediates invasion of intrametastatic lymphatic vessels and propagates lymph node metastasis of human mammary carcinoma xenografts in mouse. *The Journal of clinical investigation* **121**, 2000–12 (2011).

104. Boado, R. J., Pardridge, W. M., Vinters, H. V & Black, K. L. Differential expression of arachidonate 5-lipoxygenase transcripts in human brain tumors: evidence for the expression of a multitranscript family. *Proceedings of the National Academy of Sciences of the United States of America* **89**, 9044–8 (1992).

105. Hennig, R. *et al.* LY293111 improves efficacy of gemcitabine therapy on pancreatic cancer in a fluorescent orthotopic model in athymic mice. *Neoplasia (New York, N.Y.)* **7**, 417–25 (2005).

106. Ghosh, J. & Myers, C. E. Arachidonic acid stimulates prostate cancer cell growth: critical role of 5-lipoxygenase. *Biochemical and biophysical research communications* **235**, 418–23 (1997).

107. Chen, X. *et al.* Overexpression of 5-lipoxygenase in rat and human esophageal adenocarcinoma and inhibitory effects of zileuton and celecoxib on carcinogenesis. *Clinical cancer research : an official journal of the American Association for Cancer Research* **10**, 6703–9 (2004).

108. Rioux, N. & Castonguay, A. Inhibitors of lipoxygenase: a new class of cancer chemopreventive agents. *Carcinogenesis* **19**, 1393–400 (1998).

109. Wenger, F. A. *et al.* Effects of Celebrex and Zyflo on liver metastasis and lipidperoxidation in pancreatic cancer in Syrian hamsters. *Clinical & experimental metastasis* **19**, 681–7 (2002).

110. Ye, Y. N. *et al.* Dual inhibition of 5-LOX and COX-2 suppresses colon cancer formation promoted by cigarette smoke. *Carcinogenesis* **26**, 827–34 (2005).

111. Guo, A. M. *et al.* Role of 12-lipoxygenase in regulation of ovarian cancer cell proliferation and survival. *Cancer chemotherapy and pharmacology* **68**, 1273–83 (2011).

112. Kelavkar, U. P. & Cohen, C. 15-lipoxygenase-1 expression upregulates and activates insulin-like growth factor-1 receptor in prostate cancer cells. *Neoplasia (New York, N.Y.)* **6**, 41–52

113. Cimen, I., Astarci, E. & Banerjee, S. 15-lipoxygenase-1 exerts its tumor suppressive role by inhibiting nuclear factor-kappa B via activation of PPAR gamma. *Journal of cellular biochemistry* **112**, 2490–501 (2011).

114. Kim, E. *et al.* An antitumorigenic role for murine 8S-lipoxygenase in skin carcinogenesis. *Oncogene* **24**, 1174–87 (2005).

115. Panigrahy, D., Greene, E. R., Pozzi, A., Wang, D. W. & Zeldin, D. C. EET signaling in cancer. *Cancer metastasis reviews* **30**, 525–40 (2011).

116. Moreno, J. J. New aspects of the role of hydroxyeicosatetraenoic acids in cell growth and cancer development. *Biochemical pharmacology* **77**, 1–10 (2009).

117. Guo, M. *et al.* 9L gliosarcoma cell proliferation and tumor growth in rats are suppressed by N-hydroxy-N'-(4-butyl-2-methylphenol) formamidine (HET0016), a selective inhibitor of CYP4A. *The Journal of pharmacology and experimental therapeutics* **317**, 97–108 (2006).

118. Yeung, D. T. & Hughes, T. P. Therapeutic targeting of BCR-ABL: prognostic markers of response and resistance mechanism in chronic myeloid leukaemia. *Critical reviews in oncogenesis* **17**, 17–30 (2012).

119. Druker, B. J. *et al.* Efficacy and safety of a specific inhibitor of the BCR-ABL tyrosine kinase in chronic myeloid leukemia. *The New England journal of medicine* **344**, 1031–7 (2001).

120. Graham, S. M., Vass, J. K., Holyoake, T. L. & Graham, G. J. Transcriptional analysis of quiescent and proliferating CD34+ human hemopoietic cells from normal and chronic myeloid leukemia sources. *Stem cells (Dayton, Ohio)* **25**, 3111–20 (2007).

121. Chen, Y., Hu, Y., Zhang, H., Peng, C. & Li, S. Loss of the Alox5 gene impairs leukemia stem cells and prevents chronic myeloid leukemia. *Nat Genet* **41**, 783–792 (2009).

122. Chen, Y., Li, D. & Li, S. The Alox5 gene is a novel therapeutic target in cancer stem cells of chronic myeloid leukemia. *Cell cycle (Georgetown, Tex.)* **8**, 3488–92 (2009).

123. Carter, G. W. *et al.* 5-lipoxygenase inhibitory activity of zileuton. *The Journal of pharmacology and experimental therapeutics* **256**, 929–37 (1991).

124. Anderson, K. M. *et al.* Selective inhibitors of 5-lipoxygenase reduce CML blast cell proliferation and induce limited differentiation and apoptosis. *Leukemia Research* **19**, 789–801 (1995).

125. Werz, O. & Steinhilber, D. Therapeutic options for 5-lipoxygenase inhibitors. *Pharmacology & therapeutics* **112**, 701–18 (2006).

126. Folco, G. & Murphy, R. C. Eicosanoid transcellular biosynthesis: from cell-cell interactions to in vivo tissue responses. *Pharmacological reviews* **58**, 375–88 (2006).

127. Bozza, P. T. *et al.* Eosinophil lipid bodies: specific, inducible intracellular sites for enhanced eicosanoid formation. *The Journal of experimental medicine* **186**, 909–20 (1997).

128. Snyder, D. W. & Fleisch, J. H. Leukotriene receptor antagonists as potential therapeutic agents. *Annual review of pharmacology and toxicology* **29**, 123–43 (1989).

129. Schaloske, R. H. & Dennis, E. A. The phospholipase A2 superfamily and its group numbering system. *Biochimica et biophysica acta* **1761**, 1246–59 (2006).

130. Mahadevappa, V. G. & Powell, W. S. The metabolism of arachidonic and eicosapentaenoic acids in human neutrophils stimulated by A23187 and FMLP. *Journal of cellular biochemistry* **40**, 341–52 (1989).

131. Uozumi, N. *et al.* Role of cytosolic phospholipase A2 in allergic response and parturition. *Nature* **390**, 618–22 (1997).

132. Miller, D. K. *et al.* Identification and isolation of a membrane protein necessary for leukotriene production. *Nature* **343**, 278–81 (1990).

133. Woods, J. W. *et al.* 5-lipoxygenase and 5-lipoxygenase-activating protein are localized in the nuclear envelope of activated human leukocytes. *The Journal of experimental medicine* **178**, 1935–46 (1993).

134. Panossian, A., Hamberg, M. & Samuelsson, B. On the mechanism of biosynthesis of leukotrienes and related compounds. *FEBS letters* **150**, 511–3 (1982).

135. Maas, R. L., Ingram, C. D., Taber, D. F., Oates, J. A. & Brash, A. R. Stereospecific removal of the DR hydrogen atom at the 10-carbon of arachidonic acid in the biosynthesis of leukotriene A4 by human leukocytes. *The Journal of biological chemistry* **257**, 13515–9 (1982).

136. Ford-Hutchinson, A. W., Gresser, M. & Young, R. N. 5-Lipoxygenase. *Annual review of biochemistry* **63**, 383–417 (1994).

137. Haeggström, J. Z. & Funk, C. D. Lipoxygenase and leukotriene pathways: biochemistry, biology, and roles in disease. *Chemical reviews* **111**, 5866–98 (2011).

138. Werz, O. & Steinhilber, D. Development of 5-lipoxygenase inhibitors--lessons from cellular enzyme regulation. *Biochemical pharmacology* **70**, 327–33 (2005).

139. Huwyler, J., Bürgin, M., Zeugin, T. & Gut, J. Transformation of 5-hydroperoxyeicosatetraenoic acid into dihydroxy- and cysteinyl-leukotrienes by rat hepatocytes: effects of glutathione. *Molecular pharmacology* **39**, 314–23 (1991).

140. Erlemann, K.-R. *et al.* Regulation of 5-hydroxyeicosanoid dehydrogenase activity in monocytic cells. *The Biochemical journal* **403**, 157–65 (2007).

141. Häfner, A.-K. *et al.* Dimerization of human 5-lipoxygenase. *Biological chemistry* **392**, 1097–111 (2011).

142. Gilbert, N. C. *et al.* The structure of human 5-lipoxygenase. *Science (New York, N.Y.)* **331**, 217–9 (2011).

143. Hammarberg, T., Reddy, K. V., Persson, B. & Rådmark, O. Calcium binding to 5-lipoxygenase. *Advances in experimental medicine and biology* **507**, 117–21 (2002).

144. Bürkert, E. *et al.* The C2-like beta-barrel domain mediates the Ca2+-dependent resistance of 5-lipoxygenase activity against inhibition by glutathione peroxidase-1. *The Journal of biological chemistry* **278**, 42846–53 (2003).

145. Allard, J. B. & Brock, T. G. Structural organization of the regulatory domain of human 5-lipoxygenase. *Current protein & peptide science* **6**, 125–31 (2005).

146. Hörnig, C. *et al.* 1-Oleoyl-2-acetylglycerol stimulates 5-lipoxygenase activity via a putative (phospho)lipid binding site within the N-terminal C2-like domain. *The Journal of biological chemistry* **280**, 26913–21 (2005).

147. Michel, A. A. Y., Steinhilber, D. & Werz, O. Development of a method for expression and purification of the regulatory C2-like domain of human 5-lipoxygenase. *Protein expression and purification* **59**, 110–6 (2008).

148. Peters-Golden, M. & Brock, T. G. 5-lipoxygenase and FLAP. *Prostaglandins, leukotrienes, and essential fatty acids* **69**, 99–109

149. Rådmark, O. P. The molecular biology and regulation of 5-lipoxygenase. *American journal of respiratory and critical care medicine* **161**, S11–5 (2000).

150. Reid, G. K. *et al.* Correlation between expression of 5-lipoxygenase-activating protein, 5-lipoxygenase, and cellular leukotriene synthesis. *The Journal of biological chemistry* **265**, 19818–23 (1990).

151. Flamand, N., Luo, M., Peters-Golden, M. & Brock, T. G. Phosphorylation of serine 271 on 5-lipoxygenase and its role in nuclear export. *The Journal of biological chemistry* **284**, 306–13 (2009).

152. Boudreau, L. H. *et al.* Novel 5-lipoxygenase isoforms affect the biosynthesis of 5-lipoxygenase products. *FASEB journal : official publication of the Federation of American Societies for Experimental Biology* **25**, 1097–105 (2011).

153. Rådmark, O., Werz, O., Steinhilber, D. & Samuelsson, B. 5-Lipoxygenase: regulation of expression and enzyme activity. *Trends in biochemical sciences* **32**, 332–41 (2007).

154. Mahshid, Y. *et al.* High expression of 5-lipoxygenase in normal and malignant mantle zone B lymphocytes. *BMC immunology* **10**, 2 (2009).

155. Rouzer, C. A., Ford-Hutchinson, A. W., Morton, H. E. & Gillard, J. W. MK886, a potent and specific leukotriene biosynthesis inhibitor blocks and reverses the membrane association of 5-lipoxygenase in ionophore-challenged leukocytes. *The Journal of biological chemistry* **265**, 1436–42 (1990).

156. Ford-Hutchinson, A. W., Gresser, M. & Young, R. N. 5-Lipoxygenase. *Annual review of biochemistry* **63**, 383–417 (1994).

157. Burkert, E. Cell type-dependent activation of 5-lipoxygenase by arachidonic acid. *Journal of Leukocyte Biology* **73**, 191–200 (2003).

158. Rakonjac, M. *et al.* Coactosin-like protein supports 5-lipoxygenase enzyme activity and up-regulates leukotriene A4 production. *Proceedings of the National Academy of Sciences of the United States of America* **103**, 13150–5 (2006).

159. Gilbert, N. C. *et al.* Conversion of human 5-lipoxygenase to a 15-lipoxygenase by a point mutation to mimic phosphorylation at Serine-663. *FASEB journal : official publication of the Federation of American Societies for Experimental Biology* **26**, 3222–9 (2012).

160. Ochi, K., Yoshimoto, T., Yamamoto, S., Taniguchi, K. & Miyamoto, T. Arachidonate 5-lipoxygenase of guinea pig peritoneal polymorphonuclear leukocytes. Activation by adenosine 5'-triphosphate. *The Journal of biological chemistry* **258**, 5754–8 (1983).

161. Zhang, Y. Y. *et al.* Analysis of a nucleotide-binding site of 5-lipoxygenase by affinity labelling: binding characteristics and amino acid sequences. *The Biochemical journal* **351 Pt 3**, 697–707 (2000).

162. Werz, O., Klemm, J., Samuelsson, B. & Rådmark, O. 5-lipoxygenase is phosphorylated by p38 kinase-dependent MAPKAP kinases. *Proceedings of the*

National Academy of Sciences of the United States of America **97**, 5261–6 (2000).

163. Werz, O., Szellas, D., Steinhilber, D. & Rådmark, O. Arachidonic acid promotes phosphorylation of 5-lipoxygenase at Ser-271 by MAPK-activated protein kinase 2 (MK2). *The Journal of biological chemistry* **277**, 14793–800 (2002).

164. Werz, O. *et al.* Extracellular signal-regulated kinases phosphorylate 5-lipoxygenase and stimulate 5-lipoxygenase product formation in leukocytes. *FASEB journal : official publication of the Federation of American Societies for Experimental Biology* **16**, 1441–3 (2002).

165. Luo, M. *et al.* Protein kinase A inhibits leukotriene synthesis by phosphorylation of 5-lipoxygenase on serine 523. *The Journal of biological chemistry* **279**, 41512–20 (2004).

166. Pande, A. H. *et al.* Modulation of human 5-lipoxygenase activity by membrane lipids. *Biochemistry* **43**, 14653–66 (2004).

167. Serio, K. J., Reddy, K. V. & Bigby, T. D. Lipopolysaccharide induces 5-lipoxygenase-activating protein gene expression in THP-1 cells via a NF-kappaB and C/EBP-mediated mechanism. *American journal of physiology. Cell physiology* **288**, C1125–33 (2005).

168. Pergola, C. *et al.* Testosterone suppresses phospholipase D, causing sex differences in leukotriene biosynthesis in human monocytes. *FASEB journal : official publication of the Federation of American Societies for Experimental Biology* **25**, 3377–87 (2011).

169. Pergola, C. & Werz, O. 5-Lipoxygenase inhibitors: a review of recent developments and patents. *Expert opinion on therapeutic patents* **20**, 355–75 (2010).

170. Peskar, B. M., Weiler, H. & Peskar, B. A. Effect of BW755C on prostaglandin synthesis in the rat stomach. *Biochemical pharmacology* **31**, 1652–3 (1982).

171. Skold, A., Cosco, D. L. & Klein, R. Methemoglobinemia: pathogenesis, diagnosis, and management. *Southern medical journal* **104**, 757–61 (2011).

172. Connolly, P. J. *et al.* N-Hydroxyurea and hydroxamic acid inhibitors of cyclooxygenase and 5-lipoxygenase. *Bioorganic & Medicinal Chemistry Letters* **9**, 979–984 (1999).

173. Hawthorne, A. B., Boughton-Smith, N. K., Whittle, B. J. & Hawkey, C. J. Colorectal leukotriene B4 synthesis in vitro in inflammatory bowel disease: inhibition by the selective 5-lipoxygenase inhibitor BWA4C. *Gut* **33**, 513–7 (1992).

174. Laursen, L. S., Naesdal, J., Bukhave, K., Lauritsen, K. & Rask-Madsen, J. Selective 5-lipoxygenase inhibition in ulcerative colitis. *Lancet* **335**, 683–5 (1990).

175. Sorkness, C. A. The use of 5-lipoxygenase inhibitors and leukotriene receptor antagonists in the treatment of chronic asthma. *Pharmacotherapy* **17**, 50S–54S

176. Braeckman, R. A. *et al.* The pharmacokinetics of zileuton in healthy young and elderly volunteers. *Clinical pharmacokinetics* **29 Suppl 2**, 42–8 (1995).

177. Knapp, H. R. Reduced allergen-induced nasal congestion and leukotriene synthesis with an orally active 5-lipoxygenase inhibitor. *The New England journal of medicine* **323**, 1745–8 (1990).

178. Reid, J. J. ABT-761 (Abbott). *Current opinion in investigational drugs (London, England : 2000)* **2**, 68–71 (2001).

179. Fischer, L., Steinhilber, D. & Werz, O. Molecular pharmacological profile of the nonredox-type 5-lipoxygenase inhibitor CJ-13,610. *British journal of pharmacology* **142**, 861–8 (2004).

180. Werz, O. 5-lipoxygenase: cellular biology and molecular pharmacology. *Current drug targets. Inflammation and allergy* **1**, 23–44 (2002).

181. Kusner, E. J. *et al.* The 5-lipoxygenase inhibitors ZD2138 and ZM230487 are potent and selective inhibitors of several antigen-induced guinea-pig pulmonary responses. *European journal of pharmacology* **257**, 285–92 (1994).

182. McMillan, R. M., Spruce, K. E., Crawley, G. C., Walker, E. R. & Foster, S. J. Pre-clinical pharmacology of ICI D2138, a potent orally-active non-redox inhibitor of 5-lipoxygenase. *British journal of pharmacology* **107**, 1042–7 (1992).

183. Abdel-Tawab, M., Werz, O. & Schubert-Zsilavecz, M. Boswellia serrata: an overall assessment of in vitro, preclinical, pharmacokinetic and clinical data. *Clinical pharmacokinetics* **50**, 349–69 (2011).

184. Gillard, J. *et al.* L-663,536 (MK-886) (3-[1-(4-chlorobenzyl)-3-t-butyl-thio-5-isopropylindol-2-yl]-2,2 - dimethylpropanoic acid), a novel, orally active leukotriene biosynthesis inhibitor. *Canadian journal of physiology and pharmacology* **67**, 456–64 (1989).

185. Hutchinson, J. H. *et al.* 5-lipoxygenase-activating protein inhibitors: development of 3-[3-tert-butylsulfanyl-1-[4-(6-methoxy-pyridin-3-yl)-benzyl]-5-(pyridin-2-ylmethoxy)-1H-indol-2-yl]-2,2-dimethyl-propionic acid (AM103). *Journal of medicinal chemistry* **52**, 5803–15 (2009).

186. Sampson, A. P. FLAP inhibitors for the treatment of inflammatory diseases. *Current opinion in investigational drugs (London, England : 2000)* **10**, 1163–72 (2009).

187. Hakonarson, H. *et al.* Effects of a 5-lipoxygenase-activating protein inhibitor on biomarkers associated with risk of myocardial infarction: a randomized trial. *JAMA : the journal of the American Medical Association* **293**, 2245–56 (2005).

188. Fruchtmann, R. *et al.* In vitro pharmacology of BAY X1005, a new inhibitor of leukotriene synthesis. *Agents and actions* **38**, 188–95 (1993).

189. Maier, T. J. *et al.* Celecoxib inhibits 5-lipoxygenase. *Biochemical pharmacology* **76**, 862–72 (2008).

190. Hammarström, S. Leukotrienes. *Annual review of biochemistry* **52**, 355–77 (1983).

191. Folco, G. & Murphy, R. C. Eicosanoid transcellular biosynthesis: from cell-cell interactions to in vivo tissue responses. *Pharmacological reviews* **58**, 375–88 (2006).

192. Watson, N., Magnussen, H. & Rabe, K. F. Inherent tone of human bronchus: role of eicosanoids and the epithelium. *British journal of pharmacology* **121**, 1099–104 (1997).

193. Kühn, H. & O'Donnell, V. B. Inflammation and immune regulation by 12/15-lipoxygenases. *Progress in lipid research* **45**, 334–56 (2006).

194. Blaho, V. A., Zhang, Y., Hughes-Hanks, J. M. & Brown, C. R. 5-Lipoxygenase-deficient mice infected with Borrelia burgdorferi develop persistent arthritis. *Journal of immunology (Baltimore, Md. : 1950)* **186**, 3076–84 (2011).

195. Di Gennaro, A. *et al.* Increased expression of leukotriene C4 synthase and predominant formation of cysteinyl-leukotrienes in human abdominal aortic aneurysm. *Proceedings of the National Academy of Sciences of the United States of America* **107**, 21093–7 (2010).

196. Riccioni, G., Bäck, M. & Capra, V. Leukotrienes and atherosclerosis. *Current drug targets* **11**, 882–7 (2010).

197. Antczak, A. *et al.* Exhaled eicosanoids and biomarkers of oxidative stress in exacerbation of chronic obstructive pulmonary disease. *Archives of medical science : AMS* **8**, 277–85 (2012).

198. Morin, C., Sirois, M., Echave, V., Rizcallah, E. & Rousseau, E. Relaxing effects of 17(18)-EpETE on arterial and airway smooth muscles in human lung. *American journal of physiology. Lung cellular and molecular physiology* **296**, L130–9 (2009).

199. Lauterbach, B. *et al.* Cytochrome P450-dependent eicosapentaenoic acid metabolites are novel BK channel activators. *Hypertension* **39**, 609–13 (2002).

200. Ye, D. *et al.* Cytochrome p-450 epoxygenase metabolites of docosahexaenoate potently dilate coronary arterioles by activating large-conductance calcium-activated potassium channels. *The Journal of pharmacology and experimental therapeutics* **303**, 768–76 (2002).

201. Chen, J.-K. *et al.* Identification of novel endogenous cytochrome p450 arachidonate metabolites with high affinity for cannabinoid receptors. *The Journal of biological chemistry* **283**, 24514–24 (2008).

202. Node, K. Anti-inflammatory Properties of Cytochrome P450 Epoxygenase-Derived Eicosanoids. *Science* **285**, 1276–1279 (1999).

203. Hercule, H. C. *et al.* Interaction between P450 eicosanoids and nitric oxide in the control of arterial tone in mice. *Arteriosclerosis, thrombosis, and vascular biology* **29**, 54–60 (2009).

204. Decker, M., Arand, M. & Cronin, A. Mammalian epoxide hydrolases in xenobiotic metabolism and signalling. *Archives of Toxicology* **83**, 297–318 (2009).

205. Lord, C. C., Thomas, G. & Brown, J. M. Mammalian alpha beta hydrolase domain (ABHD) proteins: Lipid metabolizing enzymes at the interface of cell signaling and energy metabolism. *Biochimica et biophysica acta* **1831**, 792–802 (2013).

206. Coller, J. K. *et al.* Distribution of microsomal epoxide hydrolase in humans: an immunohistochemical study in normal tissues, and benign and malignant tumours. *The Histochemical journal* **33**, 329–36 (2001).

207. Zeldin, D. C. *et al.* Biochemical characterization of the human liver cytochrome P450 arachidonic acid epoxygenase pathway. *Archives of biochemistry and biophysics* **330**, 87–96 (1996).

208. Morisseau, C. *et al.* Role of soluble epoxide hydrolase phosphatase activity in the metabolism of lysophosphatidic acids. *Biochemical and biophysical research communications* **419**, 796–800 (2012).

209. Zeldin, D. C. Epoxygenase pathways of arachidonic acid metabolism. *The Journal of biological chemistry* **276**, 36059–62 (2001).

210. Zeldin, D. C. *et al.* Metabolism of Epoxyeicosatrienoic Acids by Cytosolic Epoxide Hydrolase: Substrate Structural Determinants of Asymmetric Catalysis. *Archives of Biochemistry and Biophysics* **316**, 443–451 (1995).

211. Barbosa-Sicard, E. *et al.* Eicosapentaenoic acid metabolism by cytochrome P450 enzymes of the CYP2C subfamily. *Biochemical and biophysical research communications* **329**, 1275–81 (2005).

212. Fer, M. *et al.* Metabolism of eicosapentaenoic and docosahexaenoic acids by recombinant human cytochromes P450. *Archives of biochemistry and biophysics* **471**, 116–25 (2008).

213. Gomez, G. A., Morisseau, C., Hammock, B. D. & Christianson, D. W. Human soluble epoxide hydrolase: structural basis of inhibition by 4-(3-cyclohexylureido)-carboxylic acids. *Protein science : a publication of the Protein Society* **15**, 58–64 (2006).

214. Jiang, H. *et al.* Hydrolysis of cis- and trans-epoxyeicosatrienoic acids by rat red blood cells. *The Journal of pharmacology and experimental therapeutics* **326**, 330–7 (2008).

215. Cronin, A. *et al.* Insights into the catalytic mechanism of human sEH phosphatase by site-directed mutagenesis and LC-MS/MS analysis. *Journal of molecular biology* **383**, 627–40 (2008).

216. Cronin, A. *et al.* Insights into the catalytic mechanism of human sEH phosphatase by site-directed mutagenesis and LC-MS/MS analysis. *Journal of molecular biology* **383**, 627–40 (2008).

217. Hou, H.-H. *et al.* N-terminal domain of soluble epoxide hydrolase negatively regulates the VEGF-mediated activation of endothelial nitric oxide synthase. *Cardiovascular research* **93**, 120–9 (2012).

218. Zhao, Y.-Y. & Malik, A. B. A novel insight into the mechanism of pulmonary hypertension involving caveolin-1 deficiency and endothelial nitric oxide synthase activation. *Trends in cardiovascular medicine* **19**, 238–42 (2009).

219. EnayetAllah, A. E. *et al.* Opposite regulation of cholesterol levels by the phosphatase and hydrolase domains of soluble epoxide hydrolase. *The Journal of biological chemistry* **283**, 36592–8 (2008).

220. Oguro, A. & Imaoka, S. Lysophosphatidic acids are new substrates for the phosphatase domain of soluble epoxide hydrolase. *Journal of lipid research* **53**, 505–12 (2012).

221. Ingraham, R. H., Gless, R. D. & Lo, H. Y. Soluble epoxide hydrolase inhibitors and their potential for treatment of multiple pathologic conditions. *Current medicinal chemistry* **18**, 587–603 (2011).

222. Shen, H. C. & Hammock, B. D. Discovery of inhibitors of soluble epoxide hydrolase: a target with multiple potential therapeutic indications. *Journal of medicinal chemistry* **55**, 1789–808 (2012).

223. Dorrance, A. M. *et al.* An epoxide hydrolase inhibitor, 12-(3-adamantan-1-yl-ureido)dodecanoic acid (AUDA), reduces ischemic cerebral infarct size in stroke-prone spontaneously hypertensive rats. *Journal of cardiovascular pharmacology* **46**, 842–8 (2005).

224. Kim, I.-H. *et al.* 1,3-disubstituted ureas functionalized with ether groups are potent inhibitors of the soluble epoxide hydrolase with improved pharmacokinetic properties. *Journal of medicinal chemistry* **50**, 5217–26 (2007).

225. Anandan, S.-K., Do, Z. N., Webb, H. K., Patel, D. V & Gless, R. D. Non-urea functionality as the primary pharmacophore in soluble epoxide hydrolase inhibitors. *Bioorganic & medicinal chemistry letters* **19**, 1066–70 (2009).

226. Eldrup, A. B. *et al.* Structure-based optimization of arylamides as inhibitors of soluble epoxide hydrolase. *Journal of medicinal chemistry* **52**, 5880–95 (2009).

227. Lo, H. Y. *et al.* Substituted pyrazoles as novel sEH antagonist: investigation of key binding interactions within the catalytic domain. *Bioorganic & medicinal chemistry letters* **20**, 6379–83 (2010).

228. Chen, D. *et al.* Pharmacokinetics and pharmacodynamics of AR9281, an inhibitor of soluble epoxide hydrolase, in single- and multiple-dose studies in healthy human subjects. *Journal of clinical pharmacology* **52**, 319–28 (2012).

229. Fleming, I. *et al.* Endothelium-derived hyperpolarizing factor synthase (Cytochrome P450 2C9) is a functionally significant source of reactive oxygen species in coronary arteries. *Circulation research* **88**, 44–51 (2001).

230. DiDonato, J. A., Mercurio, F. & Karin, M. NF-κB and the link between inflammation and cancer. *Immunological reviews* **246**, 379–400 (2012).

231. Hwang, S. H. *et al.* Synthesis and structure-activity relationship studies of urea-containing pyrazoles as dual inhibitors of cyclooxygenase-2 and soluble epoxide hydrolase. *Journal of medicinal chemistry* **54**, 3037–50 (2011).

232. Gross, G. J. & Nithipatikom, K. Soluble epoxide hydrolase: a new target for cardioprotection. *Current opinion in investigational drugs (London, England : 2000)* **10**, 253–8 (2009).

233. Wang, Z.-H., Davis, B. B., Jiang, D.-Q., Zhao, T.-T. & Xu, D.-Y. Soluble epoxide hydrolase inhibitors and cardiovascular diseases. *Current vascular pharmacology* **11**, 105–11 (2013).

234. Ni, G.-H., Chen, J.-F., Chen, X.-P. & Yang, T.-L. Soluble epoxide hydrolase: a promising therapeutic target for cardiovascular diseases. *Die Pharmazie* **66**, 153–7 (2011).

235. Jiang, H. *et al.* Increases in plasma trans-EETs and blood pressure reduction in spontaneously hypertensive rats. *American journal of physiology. Heart and circulatory physiology* **300**, H1990–6 (2011).

236. Ai, D. *et al.* Soluble epoxide hydrolase plays an essential role in angiotensin II-induced cardiac hypertrophy. *Proceedings of the National Academy of Sciences of the United States of America* **106**, 564–9 (2009).

237. Schmelzer, K. R. *et al.* Enhancement of antinociception by coadministration of nonsteroidal anti-inflammatory drugs and soluble epoxide hydrolase inhibitors. *Proceedings of the National Academy of Sciences of the United States of America* **103**, 13646–51 (2006).

238. Pillarisetti, S. & Khanna, I. Targeting soluble epoxide hydrolase for inflammation and pain - an overview of pharmacology and the inhibitors. *Inflammation & allergy drug targets* **11**, 143–58 (2012).

239. Wagner, K. *et al.* Comparative efficacy of 3 soluble epoxide hydrolase inhibitors in rat neuropathic and inflammatory pain models. *European journal of pharmacology* **null**, (2012).

240. Senbanjo, R., Hunt, N. & Strang, J. Cessation of groin injecting behaviour among patients on oral opioid substitution treatment. *Addiction (Abingdon, England)* **106**, 376–82 (2011).

241. Neckář, J. *et al.* Inhibition of soluble epoxide hydrolase by cis-4-[4-(3-adamantan-1-ylureido)cyclohexyl-oxy]benzoic acid exhibits antihypertensive and cardioprotective actions in transgenic rats with angiotensin II-dependent hypertension. *Clinical science (London, England : 1979)* **122**, 513–25 (2012).

242. Davis, B. B. *et al.* The anti-inflammatory effects of soluble epoxide hydrolase inhibitors are independent of leukocyte recruitment. *Biochemical and biophysical research communications* **410**, 494–500 (2011).

243. Deng, Y., Theken, K. N. & Lee, C. R. Cytochrome P450 epoxygenases, soluble epoxide hydrolase, and the regulation of cardiovascular inflammation. *Journal of molecular and cellular cardiology* **48**, 331–41 (2010).

244. Iyer, A. *et al.* Pharmacological inhibition of soluble epoxide hydrolase ameliorates diet-induced metabolic syndrome in rats. *Experimental diabetes research* **2012**, 758614 (2012).

245. Morisseau, C. *et al.* Naturally occurring monoepoxides of eicosapentaenoic acid and docosahexaenoic acid are bioactive antihyperalgesic lipids. *Journal of lipid research* **51**, 3481–90 (2010).

246. Campbell, W. B. & Fleming, I. Epoxyeicosatrienoic acids and endothelium-dependent responses. *Pflügers Archiv : European journal of physiology* **459**, 881–95 (2010).

247. Fleming, I. *et al.* Epoxyeicosatrienoic acids regulate Trp channel dependent Ca2+ signaling and hyperpolarization in endothelial cells. *Arteriosclerosis, thrombosis, and vascular biology* **27**, 2612–8 (2007).

248. Behm, D. J., Ogbonna, A., Wu, C., Burns-Kurtis, C. L. & Douglas, S. A. Epoxyeicosatrienoic acids function as selective, endogenous antagonists of native thromboxane receptors: identification of a novel mechanism of vasodilation. *The Journal of pharmacology and experimental therapeutics* **328**, 231–9 (2009).

249. Spiecker, M. & Liao, J. K. Vascular protective effects of cytochrome p450 epoxygenase-derived eicosanoids. *Archives of biochemistry and biophysics* **433**, 413–20 (2005).

250. Sander, A. L. *et al.* Cytochrome P450-derived epoxyeicosatrienoic acids accelerate wound epithelialization and neovascularization in the hairless mouse ear wound model. *Langenbeck's archives of surgery / Deutsche Gesellschaft für Chirurgie* **396**, 1245–53 (2011).

251. Michaelis, U. R., Xia, N., Barbosa-Sicard, E., Falck, J. R. & Fleming, I. Role of cytochrome P450 2C epoxygenases in hypoxia-induced cell migration and

angiogenesis in retinal endothelial cells. *Investigative ophthalmology & visual science* **49**, 1242–7 (2008).

252. Panigrahy, D. *et al.* Epoxyeicosanoids stimulate multiorgan metastasis and tumor dormancy escape in mice. *The Journal of clinical investigation* **122**, 178–91 (2012).

253. Yang, S., Wei, S., Pozzi, A. & Capdevila, J. H. The arachidonic acid epoxygenase is a component of the signaling mechanisms responsible for VEGF-stimulated angiogenesis. *Archives of biochemistry and biophysics* **489**, 82–91 (2009).

254. Liu, L. *et al.* Epoxyeicosatrienoic acids attenuate reactive oxygen species level, mitochondrial dysfunction, caspase activation, and apoptosis in carcinoma cells treated with arsenic trioxide. *The Journal of pharmacology and experimental therapeutics* **339**, 451–63 (2011).

255. Cheng, L. *et al.* The epoxyeicosatrienoic acid-stimulated phosphorylation of EGF-R involves the activation of metalloproteinases and the release of HB-EGF in cancer cells. *Acta pharmacologica Sinica* **31**, 211–8 (2010).

256. Tang, C.-M. & Yu, J. Hypoxia-inducible factor-1 as a therapeutic target in cancer. *Journal of gastroenterology and hepatology* (2012).doi:10.1111/jgh.12038

257. Cheranov, S. Y. *et al.* An essential role for SRC-activated STAT-3 in 14,15-EET-induced VEGF expression and angiogenesis. *Blood* **111**, 5581–91 (2008).

258. Gerbal-Chaloin, S., Iankova, I., Maurel, P. & Daujat-Chavanieu, M. Nuclear receptors in the cross-talk of drug metabolism and inflammation. *Drug metabolism reviews* **45**, 122–44 (2013).

259. Chai, X., Zeng, S. & Xie, W. Nuclear receptors PXR and CAR: implications for drug metabolism regulation, pharmacogenomics and beyond. *Expert opinion on drug metabolism & toxicology* **9**, 253–66 (2013).

260. Caboni, L. & Lloyd, D. G. Beyond the Ligand-Binding Pocket: Targeting Alternate Sites in Nuclear Receptors. *Medicinal research reviews* (2012).doi:10.1002/med.21275

261. Gronemeyer, H., Gustafsson, J.-A. & Laudet, V. Principles for modulation of the nuclear receptor superfamily. *Nature reviews. Drug discovery* **3**, 950–64 (2004).

262. Imming, P., Sinning, C. & Meyer, A. Drugs, their targets and the nature and number of drug targets. *Nature reviews. Drug discovery* **5**, 821–34 (2006).

263. Pirat, C. *et al.* Targeting peroxisome proliferator-activated receptors (PPARs): development of modulators. *Journal of medicinal chemistry* **55**, 4027–61 (2012).

264. Michalik, L. & Wahli, W. Peroxisome proliferator-activated receptors: three isotypes for a multitude of functions. *Current Opinion in Biotechnology* **10**, 564–570 (1999).

265. Germain, P., Staels, B., Dacquet, C., Spedding, M. & Laudet, V. Overview of nomenclature of nuclear receptors. *Pharmacological reviews* **58**, 685–704 (2006).

266. Gampe, R. T. *et al.* Asymmetry in the PPARgamma/RXRalpha crystal structure reveals the molecular basis of heterodimerization among nuclear receptors. *Molecular cell* **5**, 545–55 (2000).

267. Chandra, V. *et al.* Structure of the intact PPAR-gamma-RXR- nuclear receptor complex on DNA. *Nature* **456**, 350–6 (2008).

268. Choi, J.-M. & Bothwell, A. L. M. The nuclear receptor PPARs as important regulators of T-cell functions and autoimmune diseases. *Molecules and cells* **33**, 217–22 (2012).

269. Berger, J. P., Akiyama, T. E. & Meinke, P. T. PPARs: therapeutic targets for metabolic disease. *Trends in pharmacological sciences* **26**, 244–51 (2005).

270. Shearer, B. G. & Billin, A. N. The next generation of PPAR drugs: do we have the tools to find them? *Biochimica et biophysica acta* **1771**, 1082–93 (2007).

271. Im, S.-S. *et al.* Peroxisome proliferator-activated receptor {alpha} is responsible for the up-regulation of hepatic glucose-6-phosphatase gene expression in fasting and db/db Mice. *The Journal of biological chemistry* **286**, 1157–64 (2011).

272. Steinhilber, D. & Schubert-Zsilavecz, M. [Molecular pharmacology and medicinal chemistry of fibrate]. *Pharmazie in unserer Zeit* **36**, 108–12 (2007).

273. Staels, B. *et al.* Mechanism of Action of Fibrates on Lipid and Lipoprotein Metabolism. *Circulation* **98**, 2088–2093 (1998).

274. Matsusue, K., Peters, J. M. & Gonzalez, F. J. PPARbeta/delta potentiates PPARgamma-stimulated adipocyte differentiation. *FASEB journal : official publication of the Federation of American Societies for Experimental Biology* **18**, 1477–9 (2004).

275. Sugawara, A. *et al.* Effects of PPARγ on hypertension , atherosclerosis , and chronic kidney disease. **57**, 847–852 (2010).

276. Kawai, M. & Rosen, C. J. PPARγ: a circadian transcription factor in adipogenesis and osteogenesis. *Nature reviews. Endocrinology* **6**, 629–36 (2010).

277. Abbas, A., Blandon, J., Rude, J., Elfar, A. & Mukherjee, D. PPAR- γ agonist in treatment of diabetes: cardiovascular safety considerations. *Cardiovascular & hematological agents in medicinal chemistry* **10**, 124–34 (2012).

278. Gurnell, M. The Metabolic Syndrome: Peroxisome Proliferator-Activated Receptor and Its Therapeutic Modulation. *Journal of Clinical Endocrinology & Metabolism* **88**, 2412–2421 (2003).

279. Tsai, Y.-S. & Maeda, N. PPARgamma: a critical determinant of body fat distribution in humans and mice. *Trends in cardiovascular medicine* **15**, 81–5 (2005).

280. Bensinger, S. J. & Tontonoz, P. Integration of metabolism and inflammation by lipid-activated nuclear receptors. *Nature* **454**, 470–7 (2008).

281. Nicholls, S. J. & Uno, K. Peroxisome proliferator-activated receptor (PPAR α/γ) agonists as a potential target to reduce cardiovascular risk in diabetes. *Diabetes & vascular disease research : official journal of the International Society of Diabetes and Vascular Disease* **9**, 89–94 (2012).

282. FIEVET, C., FRUCHART, J. & STAELS, B. PPARα and PPARγ dual agonists for the treatment of type 2 diabetes and the metabolic syndrome. *Current Opinion in Pharmacology* **6**, 606–614 (2006).

283. Lim, H.-J. *et al.* PPAR delta agonist L-165041 inhibits rat vascular smooth muscle cell proliferation and migration via inhibition of cell cycle. *Atherosclerosis* **202**, 446–54 (2009).

284. Fang, X. *et al.* Activation of peroxisome proliferator-activated receptor alpha by substituted urea-derived soluble epoxide hydrolase inhibitors. *The Journal of pharmacology and experimental therapeutics* **314**, 260–70 (2005).

285. Liberato, M. V. *et al.* Medium chain fatty acids are selective peroxisome proliferator activated receptor (PPAR) γ activators and pan-PPAR partial agonists. *PloS one* **7**, e36297 (2012).

286. Raman, P., Kaplan, B. L. F., Thompson, J. T., Vanden Heuvel, J. P. & Kaminski, N. E. 15-Deoxy-delta12,14-prostaglandin J2-glycerol ester, a putative metabolite of 2-arachidonyl glycerol, activates peroxisome proliferator activated receptor gamma. *Molecular pharmacology* **80**, 201–9 (2011).

287. Xu, L., Han, C., Lim, K. & Wu, T. Cross-talk between peroxisome proliferator-activated receptor delta and cytosolic phospholipase A(2)alpha/cyclooxygenase-2/prostaglandin E(2) signaling pathways in human hepatocellular carcinoma cells. *Cancer research* **66**, 11859–68 (2006).

288. Escher, P. & Wahli, W. Peroxisome proliferator-activated receptors: insight into multiple cellular functions. *Mutation Research/Fundamental and Molecular Mechanisms of Mutagenesis* **448**, 121–138 (2000).

289. Xu, H. E. *et al.* Molecular recognition of fatty acids by peroxisome proliferator-activated receptors. *Molecular cell* **3**, 397–403 (1999).

290. Eckel, R. H., Grundy, S. M. & Zimmet, P. Z. The metabolic syndrome. *Lancet* **365**, 1415–28

291. Kahn, R., Buse, J., Ferrannini, E. & Stern, M. The metabolic syndrome. *Lancet* **366**, 1921–2; author reply 1923–4 (2005).

292. Kahn, R., Buse, J., Ferrannini, E. & Stern, M. The metabolic syndrome: time for a critical appraisal: joint statement from the American Diabetes Association and the European Association for the Study of Diabetes. *Diabetes care* **28**, 2289–304 (2005).

293. Eckel, R. H., Alberti, K. G. M. M., Grundy, S. M. & Zimmet, P. Z. The metabolic syndrome. *Lancet* **375**, 181–3 (2010).

294. Page Acnp-Bc, J. Nonalcoholic fatty liver disease: The hepatic metabolic syndrome. *Journal of the American Academy of Nurse Practitioners* **24**, 345–51 (2012).

295. Grundy, S. M. *et al.* Diagnosis and management of the metabolic syndrome: an American Heart Association/National Heart, Lung, and Blood Institute scientific statement: Executive Summary. *Critical pathways in cardiology* **4**, 198–203 (2005).

296. Grundy, S. M. Metabolic syndrome: therapeutic considerations. *Handbook of experimental pharmacology* 107–33 (2005).

297. Grundy, S. M. Metabolic syndrome pandemic. *Arteriosclerosis, thrombosis, and vascular biology* **28**, 629–36 (2008).

298. Grundy, S. M. Drug therapy of the metabolic syndrome: minimizing the emerging crisis in polypharmacy. *Nature reviews. Drug discovery* **5**, 295–309 (2006).

299. Guglielmino, K. *et al.* Pharmacological inhibition of soluble epoxide hydrolase provides cardioprotection in hyperglycemic rats. *American journal of physiology. Heart and circulatory physiology* **303**, H853–62 (2012).

300. Vanella, L. *et al.* Crosstalk between EET and HO-1 downregulates Bach1 and adipogenic marker expression in mesenchymal stem cell derived adipocytes. *Prostaglandins & other lipid mediators* **96**, 54–62 (2011).

301. Kim, D. H. *et al.* Epoxyeicosatrienoic acid agonist regulates human mesenchymal stem cell-derived adipocytes through activation of HO-1-pAKT signaling and a decrease in PPARγ. *Stem cells and development* **19**, 1863–73 (2010).

302. Anandan, S.-K. *et al.* 1-(1-acetyl-piperidin-4-yl)-3-adamantan-1-yl-urea (AR9281) as a potent, selective, and orally available soluble epoxide hydrolase inhibitor with efficacy in rodent models of hypertension and dysglycemia. *Bioorganic & medicinal chemistry letters* **21**, 983–8 (2011).

303. Ng, V. Y. *et al.* Cytochrome P450 eicosanoids are activators of peroxisome proliferator-activated receptor alpha. *Drug metabolism and disposition: the biological fate of chemicals* **35**, 1126–34 (2007).

304. Fang, X. *et al.* 14,15-Dihydroxyeicosatrienoic acid activates peroxisome proliferator-activated receptor-alpha. *American journal of physiology. Heart and circulatory physiology* **290**, H55–63 (2006).

305. Cowart, L. A. *et al.* The CYP4A isoforms hydroxylate epoxyeicosatrienoic acids to form high affinity peroxisome proliferator-activated receptor ligands. *The Journal of biological chemistry* **277**, 35105–12 (2002).

306. Yuan, X. & Liu, N. Pioglitazone suppresses advanced glycation end product-induced expression of plasminogen activator inhibitor-1 in vascular smooth muscle cells. *Journal of genetics and genomics = Yi chuan xue bao* **38**, 193–200 (2011).

307. Schulman, I. G. Nuclear receptors as drug targets for metabolic disease. *Advanced drug delivery reviews* **62**, 1307–15 (2010).

308. Young, M. M., Kester, M. & Wang, H.-G. Sphingolipids: regulators of crosstalk between apoptosis and autophagy. *Journal of lipid research* **54**, 5–19 (2013).

309. Tirodkar, T. S. & Voelkel-Johnson, C. Sphingolipids in apoptosis. *Experimental oncology* **34**, 231–42 (2012).

310. Reynolds, C. P., Maurer, B. J. & Kolesnick, R. N. Ceramide synthesis and metabolism as a target for cancer therapy. *Cancer Letters* **206**, 169–180 (2004).

311. Spence, M. W. Sphingomyelinases. *Advances in lipid research* **26**, 3–23 (1993).

312. Kim, Y. M., Park, T.-S. & Kim, S. G. The role of sphingolipids in drug metabolism and transport. *Expert opinion on drug metabolism & toxicology* **9**, 319–31 (2013).

313. Van Echten-Deckert, G. & Walter, J. Sphingolipids: critical players in Alzheimer's disease. *Progress in lipid research* **51**, 378–93 (2012).

314. Santos, C. R. & Schulze, A. Lipid metabolism in cancer. *The FEBS journal* **279**, 2610–23 (2012).

315. Baran, Y., Bielawski, J., Gunduz, U. & Ogretmen, B. Targeting glucosylceramide synthase sensitizes imatinib-resistant chronic myeloid leukemia cells via endogenous ceramide accumulation. *Journal of cancer research and clinical oncology* **137**, 1535–44 (2011).

316. Senchenkov, A., Litvak, D. A. & Cabot, M. C. Targeting ceramide metabolism--a strategy for overcoming drug resistance. *Journal of the National Cancer Institute* **93**, 347–57 (2001).

317. Pattingre, S., Bauvy, C., Levade, T., Levine, B. & Codogno, P. Ceramide-induced autophagy: to junk or to protect cells? *Autophagy* **5**, 558–60 (2009).

318. Guillas, I. *et al.* Human homologues of LAG1 reconstitute Acyl-CoA-dependent ceramide synthesis in yeast. *The Journal of biological chemistry* **278**, 37083–91 (2003).

319. Stiban, J., Tidhar, R. & Futerman, A. H. Ceramide synthases: roles in cell physiology and signaling. *Advances in experimental medicine and biology* **688**, 60–71 (2010).

320. Goldkorn, T. & Filosto, S. Lung injury and cancer: Mechanistic insights into ceramide and EGFR signaling under cigarette smoke. *American journal of respiratory cell and molecular biology* **43**, 259–68 (2010).

321. Morad, S. A. F. & Cabot, M. C. Ceramide-orchestrated signalling in cancer cells. *Nature reviews. Cancer* **13**, 51–65 (2013).

322. Henry, B., M�ller, C., Dimanche-Boitrel, M.-T., Gulbins, E. & Becker, K. A. Targeting the ceramide system in cancer. *Cancer Letters* **In Press,** ,

323. Dimanche-Boitrel, M.-T., Rebillard, A. & Gulbins, E. Ceramide in chemotherapy of tumors. *Recent patents on anti-cancer drug discovery* **6**, 284–93 (2011).

324. Smyth, M. J. *et al.* prICE: a downstream target for ceramide-induced apoptosis and for the inhibitory action of Bcl-2. *The Biochemical journal* **316 (Pt 1**, 25–8 (1996).

325. Ségui, B., Andrieu-Abadie, N., Jaffrézou, J.-P., Benoist, H. & Levade, T. Sphingolipids as modulators of cancer cell death: potential therapeutic targets. *Biochimica et biophysica acta* **1758**, 2104–20 (2006).

326. Ravid, T. *et al.* Ceramide accumulation precedes caspase-3 activation during apoptosis of A549 human lung adenocarcinoma cells. *American journal of physiology. Lung cellular and molecular physiology* **284**, L1082–92 (2003).

327. Guillas, I. *et al.* C26-CoA-dependent ceramide synthesis of Saccharomyces cerevisiae is operated by Lag1p and Lac1p. *The EMBO journal* **20**, 2655–65 (2001).

328. Schorling, S., Vallée, B., Barz, W. P., Riezman, H. & Oesterhelt, D. Lag1p and Lac1p are essential for the Acyl-CoA-dependent ceramide synthase reaction in Saccharomyces cerevisae. *Molecular biology of the cell* **12**, 3417–27 (2001).

329. Koybasi, S. *et al.* Defects in cell growth regulation by C18:0-ceramide and longevity assurance gene 1 in human head and neck squamous cell carcinomas. *The Journal of biological chemistry* **279**, 44311–9 (2004).

330. Ogretmen, B. Sphingolipids in cancer: regulation of pathogenesis and therapy. *FEBS letters* **580**, 5467–76 (2006).

331. Hartmann, D. *et al.* Long chain ceramides and very long chain ceramides have opposite effects on human breast and colon cancer cell growth. *The international journal of biochemistry & cell biology* **44**, 620–8 (2012).

332. Pewzner-Jung, Y., Ben-Dor, S. & Futerman, A. H. When do Lasses (longevity assurance genes) become CerS (ceramide synthases)?: Insights into the regulation of ceramide synthesis. *The Journal of biological chemistry* **281**, 25001–5 (2006).

333. Kitatani, K., Idkowiak-Baldys, J. & Hannun, Y. A. The sphingolipid salvage pathway in ceramide metabolism and signaling. *Cellular signalling* **20**, 1010–8 (2008).

334. Lahiri, S. *et al.* Kinetic characterization of mammalian ceramide synthases: determination of K(m) values towards sphinganine. *FEBS letters* **581**, 5289–94 (2007).

335. Levy, M. & Futerman, A. H. Mammalian ceramide synthases. *IUBMB life* **62**, 347–56 (2010).

336. Mizutani, Y., Kihara, A. & Igarashi, Y. Mammalian Lass6 and its related family members regulate synthesis of specific ceramides. *The Biochemical journal* **390**, 263–71 (2005).

337. Riebeling, C., Allegood, J. C., Wang, E., Merrill, A. H. & Futerman, A. H. Two mammalian longevity assurance gene (LAG1) family members, trh1 and trh4, regulate dihydroceramide synthesis using different fatty acyl-CoA donors. *The Journal of biological chemistry* **278**, 43452–9 (2003).

338. Laviad, E. L. *et al.* Characterization of ceramide synthase 2: tissue distribution, substrate specificity, and inhibition by sphingosine 1-phosphate. *The Journal of biological chemistry* **283**, 5677–84 (2008).

339. Min, J. *et al.* (Dihydro)ceramide synthase 1 regulated sensitivity to cisplatin is associated with the activation of p38 mitogen-activated protein kinase and is abrogated by sphingosine kinase 1. *Molecular cancer research : MCR* **5**, 801–12 (2007).

340. Ogretmen, B. & Hannun, Y. A. Biologically active sphingolipids in cancer pathogenesis and treatment. *Nature reviews. Cancer* **4**, 604–16 (2004).

341. Grösch, S., Schiffmann, S. & Geisslinger, G. Chain length-specific properties of ceramides. *Progress in lipid research* **51**, 50–62 (2012).

342. Mesicek, J. *et al.* Ceramide synthases 2, 5, and 6 confer distinct roles in radiation-induced apoptosis in HeLa cells. *Cellular signalling* **22**, 1300–7 (2010).

343. Mullen, T. D., Hannun, Y. A. & Obeid, L. M. Ceramide synthases at the centre of sphingolipid metabolism and biology. *The Biochemical journal* **441**, 789–802 (2012).

344. Delgado, A., Fabrias, G., Bedia, C., Casas, J. & Abad, J. L. Sphingolipid modulation: a strategy for cancer therapy. *Anti-cancer agents in medicinal chemistry* **12**, 285–302 (2012).

345. Delgado, A., Casas, J., Llebaria, A., Abad, J. L. & Fabrias, G. Inhibitors of sphingolipid metabolism enzymes. *Biochimica et biophysica acta* **1758**, 1957–77 (2006).

346. Lowther, J., Naismith, J. H., Dunn, T. M. & Campopiano, D. J. Structural, mechanistic and regulatory studies of serine palmitoyltransferase. *Biochemical Society transactions* **40**, 547–54 (2012).

347. Hanada, K. Serine palmitoyltransferase, a key enzyme of sphingolipid metabolism. *Biochimica et biophysica acta* **1632**, 16–30 (2003).

348. Milhas, D., Clarke, C. J. & Hannun, Y. A. Sphingomyelin metabolism at the plasma membrane: implications for bioactive sphingolipids. *FEBS letters* **584**, 1887–94 (2010).

349. Arenz, C. Small molecule inhibitors of acid sphingomyelinase. *Cellular physiology and biochemistry : international journal of experimental cellular physiology, biochemistry, and pharmacology* **26**, 1–8 (2010).

350. Claus, R. A., Dorer, M. J., Bunck, A. C. & Deigner, H. P. Inhibition of sphingomyelin hydrolysis: targeting the lipid mediator ceramide as a key regulator of cellular fate. *Current medicinal chemistry* **16**, 1978–2000 (2009).

351. Merrill, A. H., Sullards, M. C., Wang, E., Voss, K. A. & Riley, R. T. Sphingolipid metabolism: roles in signal transduction and disruption by fumonisins. *Environmental health perspectives* **109 Suppl** , 283–9 (2001).

352. Pitman, M. R., Woodcock, J. M., Lopez, A. F. & Pitson, S. M. Molecular targets of FTY720 (fingolimod). *Current molecular medicine* **12**, 1207–19 (2012).

353. Gasperini, C. & Ruggieri, S. Development of oral agent in the treatment of multiple sclerosis: how the first available oral therapy, fingolimod will change therapeutic paradigm approach. *Drug design, development and therapy* **6**, 175–86 (2012).

354. Liu, J., Zhang, C., Tao, W. & Liu, M. Systematic Review and Meta-Analysis of the Efficacy of Sphingosine-1-Phosphate (S1P) Receptor Agonist FTY720 (Fingolimod) in Animal Models of Stroke. *The International journal of neuroscience* **123**, 163–9 (2013).

355. Radin, N. S., Shayman, J. A. & Inokuchi, J. Metabolic effects of inhibiting glucosylceramide synthesis with PDMP and other substances. *Advances in lipid research* **26**, 183–213 (1993).

356. Heitner, R., Elstein, D., Aerts, J., Weely, S. van & Zimran, A. Low-dose N-butyldeoxynojirimycin (OGT 918) for type I Gaucher disease. *Blood cells, molecules & diseases* **28**, 127–33

357. Kölzer, M., Werth, N. & Sandhoff, K. Interactions of acid sphingomyelinase and lipid bilayers in the presence of the tricyclic antidepressant desipramine. *FEBS letters* **559**, 96–8 (2004).

358. Becker, K. A. *et al.* Acid sphingomyelinase inhibitors normalize pulmonary ceramide and inflammation in cystic fibrosis. *American journal of respiratory cell and molecular biology* **42**, 716–24 (2010).

359. Orr Gandy, K. A. & Obeid, L. M. Targeting the sphingosine kinase/sphingosine 1-phosphate pathway in disease: Review of sphingosine kinase inhibitors. *Biochimica et biophysica acta* **1831**, 157–66 (2013).

360. Wolf, L. A. & Laster, S. M. Characterization of arachidonic acid-induced apoptosis. *Cell biochemistry and biophysics* **30**, 353–68 (1999).

361. Vondrácek, J. *et al.* Inhibitors of arachidonic acid metabolism potentiate tumour necrosis factor-alpha-induced apoptosis in HL-60 cells. *European journal of pharmacology* **424**, 1–11 (2001).

362. Reynolds, C. P., Maurer, B. J. & Kolesnick, R. N. Ceramide synthesis and metabolism as a target for cancer therapy. *Cancer letters* **206**, 169–80 (2004).

363. Omahen, D. A. Augmentation of chemotherapy-triggered glioma cell apoptosis by blockade of arachidonic acid metabolism--the potential role of ceramide accumulation. *Medical Hypotheses* **In Press,** ,

364. Kwon, K. J., Jung, Y.-S., Lee, S. H., Moon, C.-H. & Baik, E. J. Arachidonic acid induces neuronal death through lipoxygenase and cytochrome P450 rather than cyclooxygenase. *Journal of neuroscience research* **81**, 73–84 (2005).

365. Glaser, T. *et al.* Boswellic acids and malignant glioma: induction of apoptosis but no modulation of drug sensitivity. *British journal of cancer* **80**, 756–65 (1999).

366. Omahen, D. A. Augmentation of chemotherapy-triggered glioma cell apoptosis by blockade of arachidonic acid metabolism--the potential role of ceramide accumulation. *Medical hypotheses* **77**, 726–33 (2011).

367. Wierzba, K., Muroi, M. & Osada, H. Proteomics accelerating the identification of the target molecule of bioactive small molecules. *Current opinion in chemical biology* **15**, 57–65 (2011).

368. Lomenick, B., Olsen, R. W. & Huang, J. Identification of direct protein targets of small molecules. *ACS chemical biology* **6**, 34–46 (2011).

369. Raida, M. Drug target deconvolution by chemical proteomics. *Current opinion in chemical biology* **15**, 570–5 (2011).

370. Rau, C. *et al.* Quantitative chemical proteomics reveals mechanisms of action of clinical ABL kinase inhibitors. *Nat Biotech* **25**, 1035–1044 (2007).

371. Cong, F., Cheung, A. K. & Huang, S.-M. A. Chemical genetics-based target identification in drug discovery. *Annual review of pharmacology and toxicology* **52**, 57–78 (2012).

372. Tashiro, E. & Imoto, M. Target identification of bioactive compounds. *Bioorganic & medicinal chemistry* **20**, 1921–1910 (2011).

373. Titov, D. V & Liu, J. O. Identification and validation of protein targets of bioactive small molecules. *Bioorganic & medicinal chemistry* **20**, 1909–1902 (2011).

374. Beillard, E. & Witte, O. N. Unraveling kinase signaling pathways with chemical genetic and chemical proteomic approaches. *Cell cycle (Georgetown, Tex.)* **4**, 434–7 (2005).

375. Wan, Y. *et al.* Synthesis and target identification of hymenialdisine analogs. *Chemistry & biology* **11**, 247–59 (2004).

376. Krishnamurty, R., Brock, A. M. & Maly, D. J. Protein kinase affinity reagents based on a 5-aminoindazole scaffold. *Bioorganic & medicinal chemistry letters* **21**, 550–4 (2011).

377. Missner, E. *et al.* Off-Target Decoding of a Multitarget Kinase Inhibitor by Chemical Proteomics. *ChemBioChem* **10**, 1163–1174 (2009).

378. Hopf, C., Bantscheff, M. & Drewes, G. Pathway Proteomics and Chemical Proteomics Team Up in Drug Discovery. *Neurodegenerative Diseases* **4**, 270–280 (2007).

379. Omahen, D. A. Augmentation of chemotherapy-triggered glioma cell apoptosis by blockade of arachidonic acid metabolism-the potential role of ceramide accumulation. *Medical hypotheses* (2011).doi:10.1016/j.mehy.2011.07.025

380. Murakami, M. *et al.* Regulation of prostaglandin E2 biosynthesis by inducible membrane-associated prostaglandin E2 synthase that acts in concert with cyclooxygenase-2. *The Journal of biological chemistry* **275**, 32783–92 (2000).

381. Kamei, D. *et al.* Reduced pain hypersensitivity and inflammation in mice lacking microsomal prostaglandin e synthase-1. *The Journal of biological chemistry* **279**, 33684–95 (2004).

382. Trebino, C. E. *et al.* Impaired inflammatory and pain responses in mice lacking an inducible prostaglandin E synthase. *Proceedings of the National Academy of Sciences of the United States of America* **100**, 9044–9 (2003).

383. Engblom, D. *et al.* Microsomal prostaglandin E synthase-1 is the central switch during immune-induced pyresis. *Nature neuroscience* **6**, 1137–8 (2003).

384. Korotkova, M. & Jakobsson, P.-J. Microsomal prostaglandin e synthase-1 in rheumatic diseases. *Frontiers in pharmacology* **1**, 146 (2010).

385. Xu, D. *et al.* MF63 [2-(6-chloro-1H-phenanthro[9,10-d]imidazol-2-yl)-isophthalonitrile], a selective microsomal prostaglandin E synthase-1 inhibitor, relieves pyresis and pain in preclinical models of inflammation. *The Journal of pharmacology and experimental therapeutics* **326**, 754–63 (2008).

386. Rörsch, F. *et al.* Nonacidic inhibitors of human microsomal prostaglandin synthase 1 (mPGES 1) identified by a multistep virtual screening protocol. *Journal of Medicinal Chemistry* **53**, 911–915 (2010).

387. Rådmark, O., Werz, O., Steinhilber, D. & Samuelsson, B. 5-Lipoxygenase: regulation of expression and enzyme activity. *Trends in biochemical sciences* **32**, 332–41 (2007).

388. Tjonahen, E. *et al.* Resolvin E2: identification and anti-inflammatory actions: pivotal role of human 5-lipoxygenase in resolvin E series biosynthesis. *Chemistry & biology* **13**, 1193–202 (2006).

389. Hofmann, B. *et al.* Scaffold-hopping cascade yields potent inhibitors of 5-lipoxygenase. *ChemMedChem* **3**, 1535–8 (2008).

390. Wisniewska, J. M. *et al.* Molecular characterization of EP6--a novel imidazo[1,2-a]pyridine based direct 5-lipoxygenase inhibitor. *Biochemical pharmacology* **83**, 228–40 (2012).

391. Jung, O. *et al.* Inhibition of the soluble epoxide hydrolase promotes albuminuria in mice with progressive renal disease. *PloS one* **5**, e11979 (2010).

392. Zhang, W. *et al.* Soluble epoxide hydrolase: a novel therapeutic target in stroke. *Journal of cerebral blood flow and metabolism : official journal of the International Society of Cerebral Blood Flow and Metabolism* **27**, 1931–40 (2007).

393. Imig, J. D. & Hammock, B. D. Soluble epoxide hydrolase as a therapeutic target for cardiovascular diseases. *Nature reviews. Drug discovery* **8**, 794–805 (2009).

394. Wang, D. & Dubois, R. N. Epoxyeicosatrienoic acids: a double-edged sword in cardiovascular diseases and cancer. *The Journal of clinical investigation* **122**, 19–22 (2012).

395. Knight, Z. A., Lin, H. & Shokat, K. M. Targeting the cancer kinome through polypharmacology. *Nature reviews. Cancer* **10**, 130–7 (2010).

396. Dar, A. C., Das, T. K., Shokat, K. M. & Cagan, R. L. Chemical genetic discovery of targets and anti-targets for cancer polypharmacology. *Nature* **486**, 80–4 (2012).

397. Hopkins, A. L. Network pharmacology: the next paradigm in drug discovery. *Nature chemical biology* **4**, 682–90 (2008).

398. Voigt, T. *et al.* A Natural Product Inspired Tetrahydropyran Collection Yields Mitosis Modulators that Synergistically Target CSE1L and Tubulin. *Angewandte Chemie (International ed. in English)* **52**, 410–4 (2012).

399. Joyce, S. A. *et al.* Bacterial biosynthesis of a multipotent stilbene. *Angewandte Chemie (International ed. in English)* **47**, 1942–5 (2008).

400. Wetzel, S., Bon, R. S., Kumar, K. & Waldmann, H. Biology-oriented synthesis. *Angewandte Chemie (International ed. in English)* **50**, 10800–26 (2011).

401. Kim, D. H. *et al.* Epoxyeicosatrienoic acid agonist regulates human mesenchymal stem cell-derived adipocytes through activation of HO-1-pAKT signaling and a decrease in PPARγ. *Stem cells and development* **19**, 1863–73 (2010).

402. Rigas, B. & Williams, J. L. NO-donating NSAIDs and cancer: An overview with a note on whether NO is required for their action. *Nitric Oxide* **19**, 199–204 (2008).

403. Fiorucci, S. & Antonelli, E. NO-NSAIDs: from inflammatory mediators to clinical readouts. *Inflammation & allergy drug targets* **5**, 121–31 (2006).

404. Jain, N. K. *et al.* Pharmacological studies on nitro-naproxen (naproxen-2-nitrooxyethylester). *Drug Development Research* **61**, 66–78 (2004).

405. Chen, Y., Hu, Y., Zhang, H., Peng, C. & Li, S. Loss of the Alox5 gene impairs leukemia stem cells and prevents chronic myeloid leukemia. *Nature genetics* **41**, 783–92 (2009).

406. Anastas, J. N. & Moon, R. T. WNT signalling pathways as therapeutic targets in cancer. *Nature reviews. Cancer* **13**, 11–26 (2013).

407. Mano, T. *et al.* 5-Lipoxygenase inhibitors: convenient synthesis of 4-[3-(4-heterocyclylphenylthio)phenyl]-3,4,5,6-tetrahydro-2H-pyran-4-carboxamide analogues. *Bioorganic & Medicinal Chemistry Letters* **15**, 2611–2615 (2005).

408. Mano, T. *et al.* Efficient Synthesis of 4-(3-Fluoro-5-{[4-(2-methyl-1 H -imidazol-1-yl)benzyl]oxy}phenyl)tetrahydro-2 H -pyran-4-carboxamide, a Novel 5-Lipoxygenase Inhibitor. *Synthesis* **2004**, 2625–2628 (2004).

409. Mano, T. *et al.* Optimization of imidazole 5-lipoxygenase inhibitors and selection and synthesis of a development candidate. *Chemical & pharmaceutical bulletin* **53**, 965–73 (2005).

410. Mano, T. *et al.* 5-Lipoxygenase inhibitors: convenient synthesis of 4-[3-(4-heterocyclylphenylthio)phenyl]-3,4,5,6-tetrahydro-2H-pyran-4-carboxamide analogues. *Bioorganic & medicinal chemistry letters* **15**, 2611–5 (2005).

411. Wisniewska, J. M. *et al.* Molecular characterization of EP6--a novel imidazo[1,2-a]pyridine based direct 5-lipoxygenase inhibitor. *Biochemical pharmacology* **83**, 228–40 (2012).

412. Baviskar, A. T. *et al.* N-fused imidazoles as novel anticancer agents that inhibit catalytic activity of topoisomerase IIα and induce apoptosis in G1/S phase. *Journal of medicinal chemistry* **54**, 5013–30 (2011).

413. Groebke, K., Weber, L. & Mehlin, F. Synthesis of Imidazo[1,2-a] annulated Pyridines, Pyrazines and Pyrimidines by a Novel Three-Component Condensation. *Synlett* **1998**, 661–663 (1998).

414. Penning, T. D. *et al.* Synthesis and biological evaluation of the 1,5-diarylpyrazole class of cyclooxygenase-2 inhibitors: identification of 4-[5-(4-methylphenyl)-3-

(trifluoromethyl)-1H-pyrazol-1-yl]benze nesulfonamide (SC-58635, celecoxib). *Journal of medicinal chemistry* **40**, 1347–65 (1997).

415. Backhus, L. M. *et al.* Dimethyl celecoxib as a novel non-cyclooxygenase 2 therapy in the treatment of non-small cell lung cancer. *The Journal of thoracic and cardiovascular surgery* **130**, 1406–12 (2005).

416. Jendrossek, V. Targeting apoptosis pathways by Celecoxib in cancer. *Cancer letters* (2011).doi:10.1016/j.canlet.2011.01.012

417. Kardosh, A. *et al.* Dimethyl-celecoxib (DMC), a derivative of celecoxib that lacks cyclooxygenase-2-inhibitory function, potently mimics the anti-tumor effects of celecoxib on Burkitt's lymphoma in vitro and in vivo. *Cancer biology & therapy* **4**, 571–82 (2005).

418. Schönthal, A. H. Antitumor properties of dimethyl-celecoxib, a derivative of celecoxib that does not inhibit cyclooxygenase-2: implications for glioma therapy. *Neurosurgical focus* **20**, E21 (2006).

419. Virrey, J. J. *et al.* Antiangiogenic activities of 2,5-dimethyl-celecoxib on the tumor vasculature. *Molecular cancer therapeutics* **9**, 631–41 (2010).

420. Deckmann, K., Rörsch, F., Geisslinger, G. & Grösch, S. Dimethylcelecoxib induces an inhibitory complex consisting of HDAC1/NF-κB(p65)RelA leading to transcriptional downregulation of mPGES-1 and EGR1. *Cellular signalling* **24**, 460–7 (2012).

421. Wobst, I. *et al.* Dimethylcelecoxib inhibits prostaglandin E2 production. *Biochemical Pharmacology* **76**, 62–69 (2008).

422. Schiffmann, S. *et al.* The selective COX-2 inhibitor celecoxib modulates sphingolipid synthesis. *Journal of Lipid Research* **50**, 32–40 (2009).

423. Smith, C. J. *et al.* Pharmacological analysis of cyclooxygenase-1 in inflammation. *Proceedings of the National Academy of Sciences of the United States of America* **95**, 13313–8 (1998).

424. Lipinski, C. A. Chris Lipinski discusses life and chemistry after the Rule of Five. *Drug discovery today* **8**, 12–6 (2003).

425. Fischer, A. S. *et al.* 5-Lipoxygenase inhibitors induce potent anti-proliferative and cytotoxic effects in human tumour cells independently of suppression of 5-lipoxygenase activity. *British journal of pharmacology* **161**, 936–49 (2010).

426. Bocca, C., Bozzo, F., Bassignana, A. & Miglietta, A. Antiproliferative effects of COX-2 inhibitor celecoxib on human breast cancer cell lines. *Molecular and cellular biochemistry* **350**, 59–70 (2011).

427. Schiffmann, S. *et al.* The anti-proliferative potency of celecoxib is not a class effect of coxibs. *Biochemical pharmacology* **76**, 179–87 (2008).

428. Elojeimy, S. *et al.* New insights on the use of desipramine as an inhibitor for acid ceramidase. *FEBS letters* **580**, 4751–6 (2006).

Acknowledgement

An dieser Stelle möchte ich allen ganz herzlich danken, die mich bei der Erstellung dieser Arbeit unterstützt haben:

Junior Professor Dr. Ewgenij Proschak für die Betreuung dieser Doktorarbeit, die stete Hilfe und Unterstützung, der nicht nur in fachspezifischen, sondern auch in privaten Gesprächen immer dafür gesorgt hat, dass ich meinen Geist anstrenge.

Professor Dr. Dieter Steinhilber für die Betreuung und die Möglichkeit diese Arbeit anzufertigen.

Dr. Bettina Hofmann, für die Zusammenarbeit beim EP6-Projekt.

Dr. Joanna Wisniewska für die gute Zusammenarbeit und Unterstützung bei der Jobsuche.

Allen Kollegen und ehemaligen Kollegen der Arbeitsgruppe Steinhilber für ihre Geduld, Hilfe und die gute Stimmung.

Astrid Brüggerhoff, für die unglaubliche und fleißige Hilfe beim EP6- und Benzimidazol-Projekt.

Astrid Kaiser für die Messungen von EP6-Derivaten.

Dr. Astrid Kahnt für die Hilfe bei Zellkulturfragen, die COX-Assays und die Zusammenarbeit im Zafirlukast-Projekt.

Dr. Svenja Steinbrink für ihren Einsatz im Projekt NO-NSAIDs.

Dr. Thorsten Maier für seine Unterstützung beim Projekt NO-NSAIDs.

PD Dr. Sabine Grösch für die fachlichen Diskussionen und Unterstützung beim Ceramid-Projekt.

Flörian Rörsch für die Zusammenarbeit im Projekt mPGES-1-Inhibitoren.

Daniela Hartmann für die Ceramid-Messungen.

Allen Kollegen „unserer“ Arbeitsgruppe Proschak allgemein vielen Dank für: Feierabendbier, Kino Sessions, Eierlikör und Gedöns, „larifari, schnick schnack, weiß

der Geier“ und sonst noch mehr beibringen des umgangssprachlichen Wortschatzes, Kaffeepausen, Gans essen, grillen und Fleisch essen, etc.

Muchas gracias para: Daniel für die IT Unterstützung und tolle Zeit in Barcelona, Janosch Fernández González Pérez für die tolle Zeit, Geduld und Spaß, Steffen „for making me smile“ wenn es manchmal nicht so toll war, René für unsere tollen Labor-Diskussionen ☺ und zusammennach Hause fahren, Julia für die Dockings, Buddi für die tolle Arbeit während deiner Diplomarbeit und die ehrlichen Gespräche, Karin für die tollen Konversationen, Sandra für die gemeinsame Zeit in der Zellkultur und die Kaffeepausen. And last but not least für die Franquita…! Gracias por haber estado siempre a mi lado, por ser mi amiga y apoyarme cada día, no sólo en el Labor también en mi vida. Ich freue mich que nos veamos casi cada semana y que compartimos tantas cosas. Ohne dich wäre es alles ganz anderes gewesen!

Voldria agrair la meva família que ha estat sempre recolzant-me en totes les decisions de la meva vida, no només a nivell de carrera sinó a nivell personal. Estar tan lluny de vosaltres es fa difícil però tinc l’esperança de què algún dia podrem tornar a la nostra terra. Als meus pares que tot i les dificultats que han tingut, han sabut tirar endavant en la seva vida, per mi sempre han estat un exemple a seguir i la seva perseverància ha estat el meu company de viatge. Per la meva germaneta, ja sap que l’estimo moltíssim i que aquest treball també és un trocet seu. Per la meva vida Rafa, aquest treball no hauria estat possible sense la teva ajuda i recolzament dia a dia, per quan les coses no anaven bé i no sortien els papers fins quan anàvem a celebrar-ho al japonés que havia tret un paper. Estic molt feliç d’haver-te trobat i que durant aquesta tesi no només hagi guanyat un títol de doctor sinó el lloc de ser la teva esposa.

Eidesstattliche Erklärung

Die vorliegende Dissertation wurde selbstständig verfasst und keine anderen als die angegebenen Quellen und Hilfsmittel benutzt. Alle Stellen die wörtlich oder sinngemäß aus veröffentlichten und nicht veröffentlichten Schriften entnommen wurden, sind als solche gekennzeichnet. Die Arbeit ist in gleicher oder ähnlicher Form oder auszugsweise im Rahmen einer anderen Prüfung nicht vorgelegt worden.

Frankfurt am Main, den…… ……

(Estel·la Buscató Arsequell)

Curriculum vitae

Name:	Estel·la Buscató Arsequell
Adresse:	Ohmstraße 53
	60486 Frankfurt am Main
Telefon:	+49 15167223818
Geburtsdatum:	20.03.1985
Geburtsort:	Barcelona, Spanien
E-Mail-Adresse:	ebuscatoa@gmail.com

BERUFLICHE ERFAHRUNGEN

2013 — Bayer CropScience, Frankfurt am Main, Deutschland, *Global Chemistry Herbicide Research & Development*

- Laborleiter in der Forschung und Entwicklung

2009-2012 — Institut für Pharmazeutische Chemie, Arbeitskreis Prof. Dr. Dieter Steinhilber, Goethe Universität Frankfurt am Main
Titel der Doktorarbeit: *Synthesis and in vitro evaluation of lipid signaling modulators*

- Wirkstoffdesign (*Docking*, SAR, *Virtual Screening*), Synthese: Planung und Durchführung, Assay Entwicklung (*in vitro* und zellbasierend), Protein Expression und Zellkultur
- Betreuung von Studenten (Saalpraktika) und vier Abschlussarbeiten
- Verfassung von wissenschaftlichen Arbeiten (10 Publikationen)

2008-2009 — Internship R&D, Bayer CropScience, Frankfurt am Main, Deutschland, *Global Chemistry Herbicide Research & Development*

- Synthese Planung und Durchführung von Pflanzenschutzmitteln
- Organokatalyse, Strecker Aminosäuresynthese

AUSBILDUNG

2003-2008 — Studium der Chemie. Schwerpunkt: Organische Chemie
Institut Químic de Sarrià (IQS), Barcelona, Spanien
Abschlussnote: 2,1 (gut, 2. bester Jahrgangsabsolvent)
Abschluss: Master of Science

1989-2003 — Centre d'Estudis Àgora, Sant Cugat del Vallès, Spanien
Abschlussnote: 2,0 (gut)

WEITERBILDUNG

2012 Workshop in Drug Discovery, Erl Wood, Großbritannien, Eli Lilly

2010 Frankfurt International Research Graduate School for Translational Biomedicine (FIRST), *Basics in Medicine and Pharmacology*

2010 Grundlagen der Europäischen Zulassung von Humanarzneimitteln, Goethe Universität Frankfurt am Main

2008 Forschungspraktikum, Institut de Química Avançada (IQAC), Barcelona, Spanien
- Metallkatalyse (Suzuki-Kupplung), Festphasen-Synthese

2007 Forschungspraktikum, Scientific Park Barcelona, Asymmetric Synthesis Research Group, Barcelona, Spanien
- Prostaglandin-Synthese (Pausond-Khand-Reaktionen)

Tagungen

XXIInd International Symposium on Medicinal Chemistry, September 2012, Berlin, Deutschland

CCG European User Group Meeting, September 2011, Barcelona, Spanien

46th International Conference on Medicinal Chemistry, June 2010, Reims, Frankreich

Stipendien

2010-2012 Stipendium des DAAD (Deutscher Akademischer Austauschdienst)

2004-2008 Stipendium des spanisches Ministerium für einen Sprachkurs in Großbritannien und Irland

KENNTNISSE UND FÄHIGKEITEN

Sprachen: Spanisch, Muttersprache
Englisch, fließend in Wort und Schrift (regelmäßiger Aufenthalt in Großbritannien und Irland)
Deutsch, fließend in Wort und Schrift
Italienisch, gute Kenntnisse in Wort und Schrift
Französisch, gute Kenntnisse in Wort und Schrift
Japanisch, Fortgeschritten

EDV: MS Office (sehr gut), Molecular Operating Environment (MOE), MestRe-Nova, ChemOffice (sehr gut)

Publication list

- Key publications

Rörsch, F.; Buscató, E.; Deckmann, K.; Schneider, G.; Schubert-Zsilavecz, M.; Geisslinger, G.; Proschak, E.; Grösch, S. Structure–activity relationship of nonacidic quinazolinone inhibitors of human microsomal prostaglandin synthase 1 (mPGES 1). *Journal of Medicinal Chemistry* **55**, 3792–3803 (2012).

The autor of this thesis contributed to this publication by planning and carrying out the synthesis and evaluating another possible synthetical routes as well as spectral characterization of synthesized compounds.

Hieke, M.; Rödl, C. B.; Wisniewska, J. M.; Buscató, E.; Stark, H.; Schubert-Zsilavecz, M.; Steinhilber, D.; Hofmann, B.; Proschak, E. SAR-study on a new class of imidazo[1,2-*a*]pyridine-based inhibitors of 5-lipoxygenase. *Bioorganic & medicinal chemistry letters* **22**, 1969–75 (2012).

The autor of this thesis contributed to this publication by writing and revising the chemical part of the manuscript and structure activity relationship.

Wisniewska, J. M.; Rödl, C. B.; Kahnt, A. S.; Buscató, E.; Ulrich, S.; Tanrikulu, Y.; Achenbach, J.; Rörsch, F.; Grösch, S.; Schneider, G.; Cinatl, J.; Proschak, E.; Steinhilber, D.; Hofmann, B. Molecular characterization of EP6, a novel imidazo[1,2-*a*]pyridine based direct 5-lipoxygenase inhibitor. *Biochemical pharmacology* **83**, 228–40 (2012).

The autor of this thesis contributed to this publication by synthesizing the key compound of the publication and supporting experiments regarding cell viability.

Buscató, E.; Wisniewska J. M.; Rödl C. B.; Brüggerhoff, A.; Kaiser A.; Rörsch, F.; Kostewicz E.; Schubert-Zsilavecz M., Grösch, S.; Steinhilber D., Hofmann B. and Proschak, E., Structure activity relationship and *in vitro* pharmacological evaluation of imidazo[1,2-*a*]pyridine-based inhibitors of 5-lipoxygenase. *Future Medicinal Chemistry* (2013), *in press*.

The author of this thesis contributed to the chemical synthesis of the majority of compounds, revision of the chemical part of the manuscript, cytotoxic evaluation, metabolism assessment and pharmacological evaluation.

Buscató E.; Büttner, D.; Brüggerhoff, A.; Klingler, F.-M.; Weber J.; Scholz, B.; Živković, A.; Marschalek, R.; Stark, H.; Steinhilber D., Bode, H.B.; Proschak E.; From a multipotent stilbene to soluble epoxide hydrolase inhibitors with antiproliferative properties. *ChemMedChem* (2013), *in press*.

The author of this thesis contributed to the in-house screening, testing, protein expression and purification, chemical synthesis planning and evaluation, spectral characterization of synthesized compounds, cytotoxic evaluation and Annexin V/PI staining.

Buscató, E.; Blöcher, R.; Lamers, C.; Klingler, F.-M.; Hahn, S.; Steinhilber, D.; Schubert-Zsilavecz, M.; Proschak, E. Design and synthesis of dual modulators of soluble epoxide hydrolase and peroxisome proliferator-activated receptors. *Journal of medicinal chemistry* **55**, 10771-5 (2012).

The author of this thesis contributed to this publication by planning the synthesis and evaluating another possible synthetical routes as well as spectral characterization of synthesized compounds, protein expression as well as manuscript writing.

- Other publications

Meirer K., Rödl C., Wisniewska J.M., George S., Häfner A.-K., Buscató E., Klingler F.-M., Hahn S., Berressem D., Wittmann S.K., Steinhilber D., Hofmann B., Proschak E. Synthesis and structure-activity relationship studies of novel dual inhibitors of soluble epoxide hydrolase and 5-lipoxygenase, *Journal of medicinal chemistry* **56**, 1777–1781 (2013).

Buscató, E.; Proschak, E. (2012), 5-Lipoxygenase Inhibitors: A Patent Evaluation (WO2011161615*), Expert Opinion On Therapeutic Patents* **22** (7), 843-846 (2012).

Moser D., Achenbach J., Klingler, F.-M., Buscató, E., Hahn, S. and Proschak, E., Evaluation of structure-derived pharmacophore of soluble epoxide hydrolase inhibitors by virtual screening, *Bioorganic & Medicinal Chemistry Letters* **22** (21), 6762-6765 (2012).

Moser, D., Wisniewska, J. M., Hahn, S., Achenbach, J., Buscató, E., Klingler, F.-M., Hofmann, B., Steinhilber, D., and Proschak, E., Dual-Target Virtual Screening by Pharmacophore Elucidation and Molecular Shape Filtering, *ACS Medicinal Chemistry*, **3**, 155-158 (2012).

Hahn, S., Achenbach, J., Buscató, E., Klingler, F.-M., Schroeder, M., Meirer, K., Hieke, M., Heering, J., Barbosa-Sicard, E., Loehr, F., Fleming, I., Doetsch, V., Schubert-Zsilavecz, M., Steinhilber, D., and Proschak, E., Complementary screening techniques yielded fragments that inhibit the phosphatase activity of soluble epoxide hydrolase, *ChemMedChem* **6**, 2146-9 (2011).

Roos, J., Oancea, C., Heinßmann, M., Held, H., Kahnt, A.S., Buscató, E., Proschak, E., Steinhilber, D., Maier, T.J., Ruthardt, M., 5-lipoxygenase as a novel principle of stem cell therapy in acute myeloid leukemia, *submitted*.

Kolodziej S., Kuvardina O. N., Herglotz J., Backert, I., Böning H., Buscató, E., Karas M., Proschak, E., Lausen J., Influence of PADI4 on histone arginine methylation differentially regulates expression of the Tal1 target genes IL6ST and CTCF, *submitted*.

Publications

Journal of Medicinal Chemistry

Article

pubs.acs.org/jmc

Structure−Activity Relationship of Nonacidic Quinazolinone Inhibitors of Human Microsomal Prostaglandin Synthase 1 (mPGES 1)

Florian Rörsch,*[,†] Estel.la Buscató,[‡] Klaus Deckmann,[†] Gisbert Schneider,[§] Manfred Schubert-Zsilavecz,[‡] Gerd Geisslinger,[†] Ewgenij Proschak,[‡] and Sabine Grösch[†]

[†]Johann Wolfgang Goethe-University, Institute of Clinical Pharmacology, *pharmazentrum frankfurt*, LiFF/ZAFES, Theodor-Stern-Kai 7, D-60590 Frankfurt/Main, Germany

[‡]Johann Wolfgang Goethe-University, Institute of Pharmaceutical Chemistry, LiFF/ZAFES, Max-von-Laue-Strasse 9, D-60438 Frankfurt/Main, Germany

[§]ETH Zürich, Department of Chemistry and Applied Biosciences, Wolfgang-Pauli-Strasse 10, CH-8093 Zürich, Switzerland

Supporting Information

ABSTRACT: Microsomal prostaglandin E synthase 1 (mPGES-1) is a key enzyme of the arachidonic acid cascade. Its product PGE_2 plays an important role in various inflammatory processes, pain, fever, and cancer. Selective inhibition of mPGES-1 might be a promising step to avoid cyclooxygenase-related effects of NSAIDs. We studied a class of quinazolinone derivatives of the lead structure FR20 for their effects on the isolated human and murine enzymes, human HeLa cells, and in various settings of the whole blood assay. Novel compounds with direct enzyme inhibiting activity in the submicromolar range (IC_{50}: 0.13−0.37 μM) were designed using a bioisosteric replacement strategy and proved to be effective in both cells and human whole blood. Furthermore, pharmacological profiling of toxicity and eicosanoid screening with LC/MS-MS was applied to characterize this new class of mPGES-1 inhibitors.

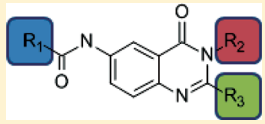

INTRODUCTION

The microsomal prostaglandin E_2-synthase 1 (mPGES-1) is an inducible enzyme of the arachidonic acid cascade and mainly coupled to the expression of cyclooxygenase-2 (COX-2).[1] Proinflammatory stimuli such as lipopolysaccharide (LPS) up-regulate the protein level of both enzymes. The major product, prostaglandin E_2 (PGE_2), plays an important role in the mediation of pain,[2,3] fever,[4] the development of various cancer types,[5] and several inflammatory diseases like rheumatoid arthritis.[6] Besides clinically relevant diseases, PGE_2 is involved in gastrointestinal protection[7,8] and the onset of wakefulness and maintenance of the circadian rhythm.[9] PGE_2 production is inhibited by nonsteroidal anti-inflammatory drugs (NSAIDs), specifically selective and nonselective COX-inhibitors. Inhibition of mPGES-1 might improve the pharmacological profile of current analgesic, anti-inflammatory, and antipyretic medication due to a reduction of side effects as compared to known NSAIDs.[10,11] Especially patients under continuous long-term treatment with NSAIDs may suffer from gastrointestinal ulcers and cardiovascular complications.[12,13] Permanent treatment, however, is indicated for treatment of chronic inflammatory diseases like rheumatoid arthritis (RA) or arteriosclerosis. Several mPGES-1 inhibitors have been tested in vitro and in vivo in different disease models (Chart 1).[14]

For mPGES-1 inhibition, two main approaches have been pursued. On the one hand, mPGES-1 can be inhibited via down-regulation of mPGES-1 expression. Benzothiophene γ-hydroxybutenolide (BTH) **1** significantly reduced PGE_2 levels in the mouse air pouch and collagen-induced arthritis (CIA) models.[15] On the other hand, mPGES-1 activity is directly affected by small-molecule inhibitors. AF3442 **2** inhibited mPGES-1 activity in LPS-stimulated human monocytes and human whole blood.[16] PF-9184 **3** exhibits high potency on recombinant human mPGES-1 with an IC_{50} of 16.5 nM but loses its potency on the rat mPGES-1 in vitro (IC_{50} of 1080 nM on recombinant rat mPGES-1) and in vivo (no effect in rat air pouch model).[17] A series of phenanthrene imidazole inhibitors around the lead compound MF63 **4** also showed high potency on the human and guinea pig enzyme and in the human whole blood assay with selectivity over several other related enzymes but lacks the ability to inhibit mouse or rat mPGES-1.[18]

These data illustrate one main problem occurring during the development of selective human mPGES-1 inhibitors, as they are inactive regarding the inhibition of the mouse or rat mPGES-1, thus rendering the application of preclinical animal models impossible. This species difference is due to several amino acid exchanges between the human and murine enzyme, leading to variations in the active site of mPGES-1. Several dual 5-lipoxygenase (5-LO)/mPGES-1 inhibitors extend the pharmacological profile of anti-inflammatory agents and exhibit activity in animal models of carrageenan-induced rat pleurisy and aortic aneurysm.[19−22] In addition, natural compounds like arzanol **5** from *Helichrysum italicum* have been reported to affect inflammation and PGE_2 levels in carrageenan-induced pleurisy in rats.[23] We recently reported a series of novel

Received: December 14, 2011
Published: March 26, 2012

Chart 1. Several Published mPGES-1 Inhibitors

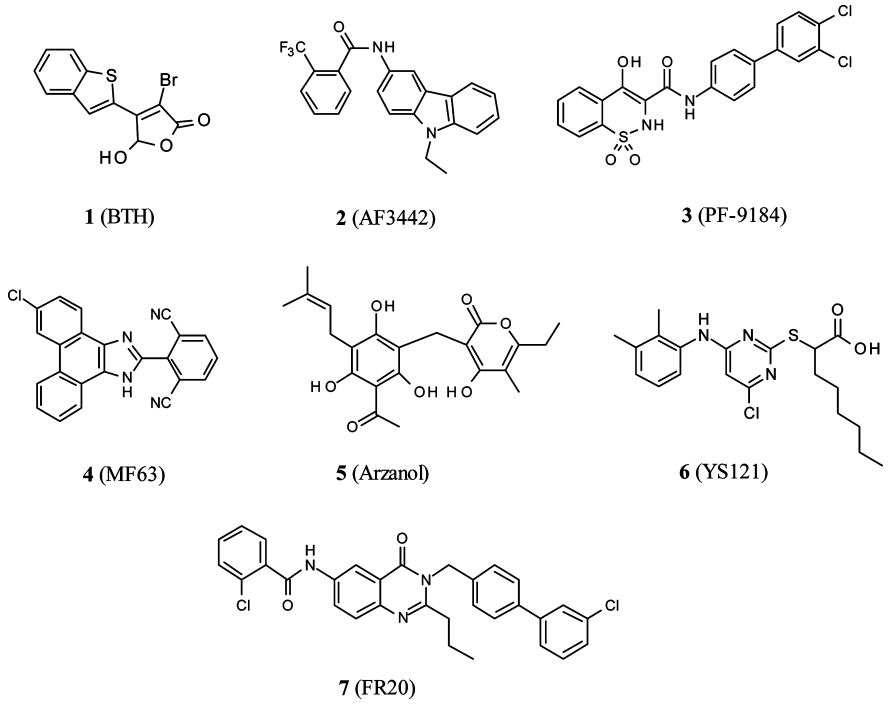

Scheme 1. Schematic Synthesis Route for Compounds Based on a Quinazolinone Scaffold[a]

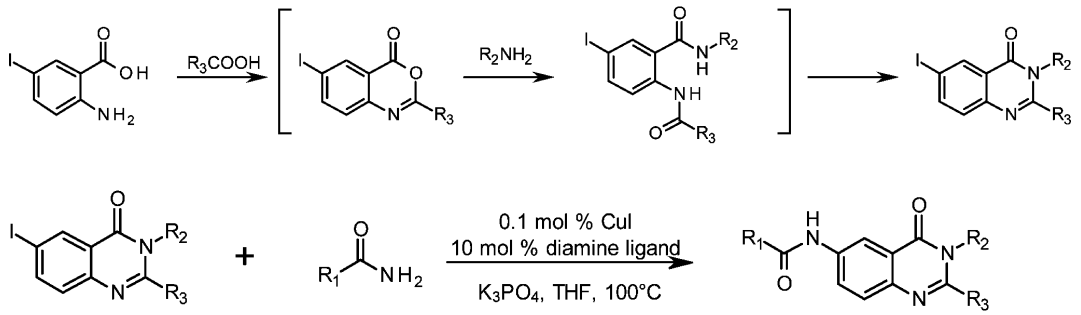

[a]Formation of 2,3-disubstituted 3*H*-quinazolin-4-one is followed by the formation of the final product by a related Goldberg reaction.

nonacidic mPGES-1 inhibitors that were found by a multistep virtual screening protocol.[24] Quinazolinone **7** (FR20) provided the starting point for an extensive structure–activity relationship study (SAR). Here we present a structure optimization approach including chemical synthesis of quinazolinone derivatives, detailed information about activity on human and murine isolated mPGES-1 enzyme, in vitro nonspecific cellular toxicity, and impact on different eicosanoids in human whole blood. As a major outcome of this study, we present a class of direct human mPGES-1 inhibitors with low nonspecific cellular toxicity and a broad whole blood eicosanoid profile.

RESULTS

Assembly of the Quinazolinone Compound Library and Development of a Synthesis Route. On the basis of the reference structure **7**, several derivatives (**7a**–**7n**, **7r**–**7x**) were purchased from Asinex (www.asinex.com, Moscow, Russia). Three novel derivatives (**7o**, **7p**, **7q**) were synthesized (Scheme 1) to extend the chemical diversity and provide a synthesis route for this scaffold class. All compounds are listed in Chart 2.

Human mPGES-1 Activity Screening. To investigate the inhibitory potency of these substances on the human mPGES-1, we compared the inhibition rate of each derivative at 1 μM on isolated protein in the mPGES-1 activity assay with the reference structure **7** (Table 1). Derivatives **7f**, **7i**, **7k**, **7l**, **7n**, **7o**, **7q**, and **7r** equipotently reduced the PGE_2-level ±5% or higher as compared to **7**. For those substances, dose–response curves (exemplary curve in Supporting Information Figure S1) and IC_{50} values with 95% confidence intervals were calculated. IC_{50} values were between 0.13 μM (**7**) and 0.37 μM (Table 1). IC_{50} values of these derivatives reveal comparable potencies.

Murine mPGES-1 Activity Screening. Because the human and murine mPGES-1 differ in their amino acid sequences, we further investigated the influence of **7** and equipotent derivatives **7f**, **7i**, **7k**, **7l**, **7n**, **7o**, **7q**, and **7r** on murine mPGES-1 in vitro. The compounds were tested on the murine mPGES-1 enzyme in the microsomal fraction of two different cell types. Mouse macrophage cells (RAW) and mouse fibroblast cells (NIH-3T3) were stimulated with either LPS or IL-1β/TNFα to upregulate mPGES-1 protein levels. Protein extracts were incubated with different concentrations of quinazolinone series compounds or the mouse mPGES-1

dx.doi.org/10.1021/jm201687d | *J. Med. Chem.* 2012, 55, 3792–3803

Chart 2. Twenty-Four Derivatives around the Lead Structure 7 Were Used for Structure–Activity Relationship Studies and Pharmacological Profiling[a]

Identifier	Structure
	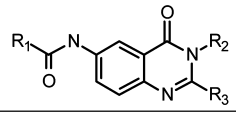
7	R_1 = 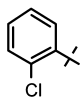 R_2 = 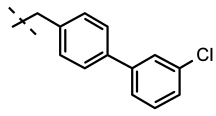 R_3= Propyl
7a	R_1 = 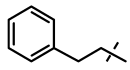 R_2 = 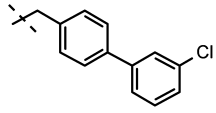 R_3= Propyl
7b	R_1 =  R_2 = 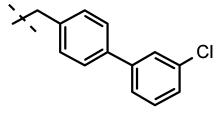 R_3= Propyl
7c	R_1 = 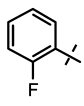 R_2 = 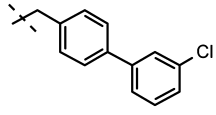 R_3= Propyl
7d	R_1 = CH_3 R_2 = 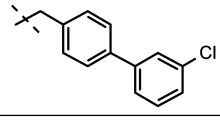 R_3= Propyl
7e	R_1 = *tert*-Butyl R_2 = 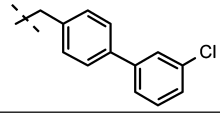 R_3= Propyl
7f	R_1 = 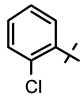 R_2 = 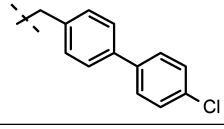 R_3= Propyl
7g	R_1 =  R_2 = 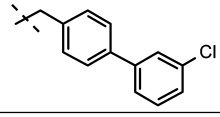 R_3= Propyl
7h	R_1 = 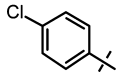 R_2 = 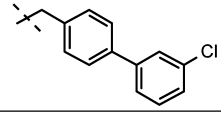 R_3= Propyl
7i	R_1 = 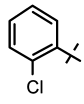 R_2 = 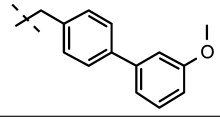 R_3= Propyl
7j	R_1 = 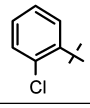 R_2 = 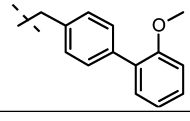 R_3= Propyl
7k	R_1 = 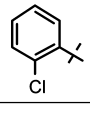 R_2 = 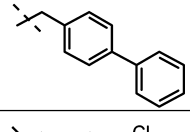 R_3= Propyl
7l	R_1 = 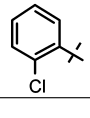 R_2 = 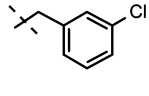 R_3= Propyl

dx.doi.org/10.1021/jm201687d | J. Med. Chem. 2012, 55, 3792–3803

Chart 2. continued

Identifier	Structure
	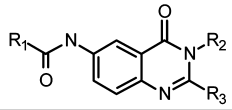
7**m**	R_1 = 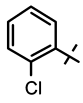 R_2 = 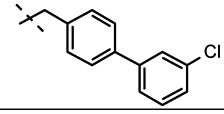 R_3= CH_3
7**n**	R_1 = 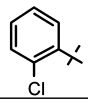 R_2 = 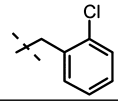 R_3= Propyl
7**o**	R_1 = 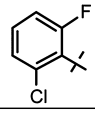 R_2 = 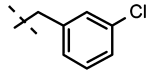 R_3= Propyl
7**p**	R_1 = 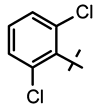 R_2 = 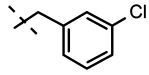 R_3= Propyl
7**q**	R_1 =  R_2 = 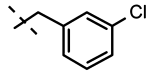 R_3= Propyl
7**r**	R_1 = 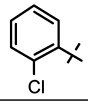 R_2 = 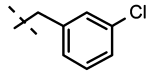 R_3= 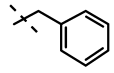
7**s**	R_1 =  R_2 = 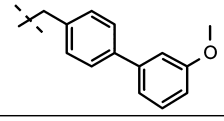 R_3= Propyl
7**t**	R_1 =  R_2 = 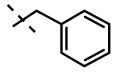 R_3= 
7**u**	R_1 = 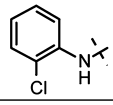 R_2 = 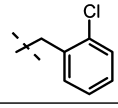 R_3= Propyl
7**v**	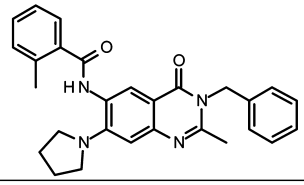
7**w**	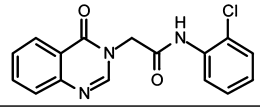
7**x**	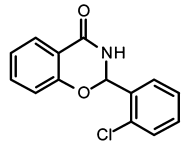

[a]Three additional compounds (**7v–x**) with slight variations were added.

inhibitor control substance **6** (YS121).[21] Neither RAW- nor NIH-derived mPGES-1 activity was impaired by quinazolinone compounds by more than 20% (Table 1), while **6** reduced the activity by more than 62%.

dx.doi.org/10.1021/jm201687d | *J. Med. Chem.* 2012, 55, 3792–3803

Table 1. Measured Activity of the Quinazolinone Series on Isolated Human and Murine (from RAW and NIH Cells) Enzyme at 1 μM Final Concentration with Standard Error of the Mean (SEM)[a]

	human				murine					
identifier unit	mPGES-1 inhibition @ 1 μM [%]	SEM [%]	IC_{50} [μM]	95% confidence interval [μM]	RAW mPGES-1 inhibition @ 1 μM [%]	SEM [%]	NIH mPGES-1 inhibition @ 1 μM [%]	SEM [%]	COX-1 inhibition @ 1 μM [%]	COX-2 inhibition @ 1 μM [%]
7	66.7	4.8	0.13	0.08−0.18	8.4	3.6	10.7	7.2	≤0	6.7
7a	32.7	6.6								
7b	15.3	6.0								
7c	30.0	4.6								
7d	14.8	5.8								
7e	18.8	10.1								
7f	**68.8**	3.1	**0.18**	0.10−0.32	12.4	3.4	17.1	2.2	2.6	≤0
7g	15.6	10.7								
7h	14.7	2.6								
7i	**71.5**	3.6	**0.21**	0.13−0.33	15.3	4.2	4.6	4.6	20.1	2.5
7j	61.3	8.4								
7k	**74.2**	0.9	**0.22**	0.13−0.38	11.8	3.5	20.3	1.9	8.4	5.8
7l	**86.3**	1.7	**0.36**	0.17−0.77	9.5	3.5	−0.8	4.5	≤0	≤0
7m	41.9	0.8								
7n	**83.6**	0.8	**0.18**	0.11−0.29	15.2	7.5	6.6	6.0	16.1	≤0
7o	**75.6**	1.3	**0.37**	0.26−0.53	−8.7	1.3	10.0	5.0	≤0	≤0
7p	61.3	2.3								
7q	63.1	3.9	**0.26**	0.16−0.42	6.0	2.3	0.9	1.5	≤0	≤0
7r	**67.2**	5.2	nd[b]		3.8	5.1	17.8	2.8	≤0	≤0
7s	15.9	7.2								
7t	≤0	16.1								
7u	14.1	13.2								
7v	37.1	10.7								
7w	≤0	22.8								
7x	≤0	7.0								
YS121					66.2 (@ 5 μM)	2.8	62.9 (@ 5 μM)	2.2		

[a]The 50% inhibitory concentration (IC_{50}) on human enzyme was calculated for each derivative showing larger inhibitory potency at 1 μM than the lead structure **7**. With 95% percent probability the IC_{50} is in the given range of the confidence interval. Cross-reactivity against COX-1/COX-2 enzymes with 1 μM inhibitor concentration was measured in vitro. Data are the mean of $n \geq 3$. [b]nd = not determined.

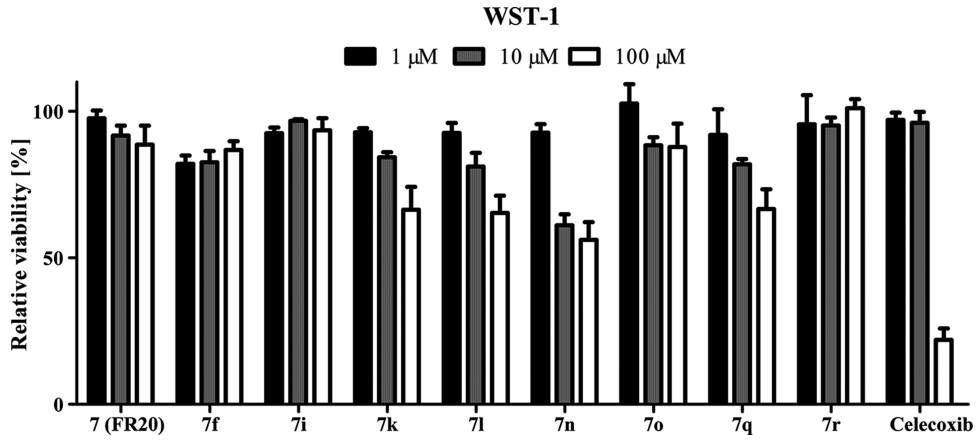

Figure 1. Cell viability assay with FR20 series compounds on stimulated human HeLa cells. Cell viability is given as percent of DMSO control with SEM after 24 h of incubation ($n \geq 3$).

COX-1 and COX-2 Cross-Reactivity. Cross-reactivity of these compounds against both COX-isoforms was tested in vitro. Neither COX-1 nor COX-2 was inhibited by any compound by more than 20% at 1 μM inhibitor concentration (Table 1).

Toxicity Assessment. To generate a toxicological profile for compound **7** and equipotent derivatives **7f**, **7i**, **7k**, **7l**, **7n**, **7o**, **7q**, and **7r**, we performed a WST-1 cell assay with human HeLa cells. Cell viability was determined after treatment of cells with IL-1β and TNFα and simultaneously with increasing concentrations of the test compounds for 24 h. Stimulation was applied to modulate an inflammatory setting. All tested derivatives showed no or only slightly decreased cell viability at 1 and 10 μM inhibitor concentration (Figure 1). At 100 μM concentration, the derivatives **7k**, **7l**, **7n**, and **7q** as well as the control substance celecoxib decreased cell viability consid-

dx.doi.org/10.1021/jm201687d | J. Med. Chem. 2012, 55, 3792−3803

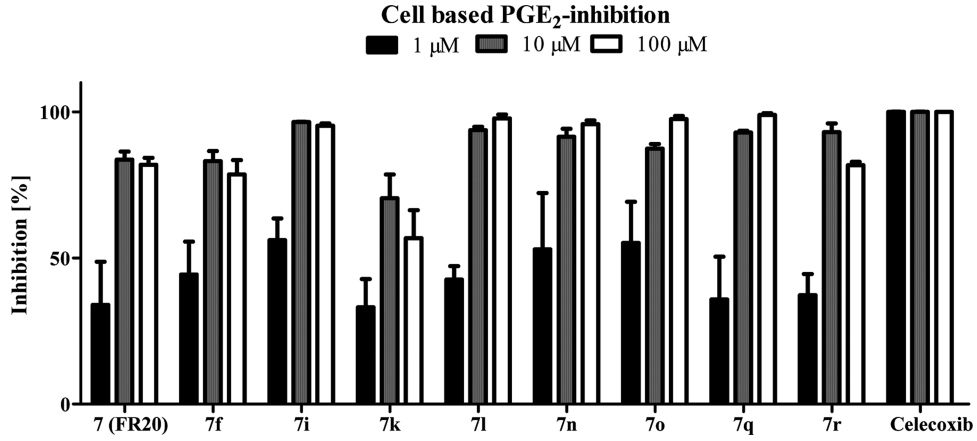

Figure 2. PGE_2 levels were measured with LC/MS-MS technique after incubation of stimulated HeLa cells with different concentrations of test compounds or DMSO. Inhibition is calculated as percent of DMSO control corrected by the background value (unstimulated control) with SEM ($n \geq 3$; **7r**, $n = 2$).

erably. The COX-2 inhibitor celecoxib is already known for its cytotoxic effects in vitro and in vivo and was used to compare the quinazolinone inhibitors with a reference compound used in clinical settings.[25−27]

Cell-Based mPGES-1 Activity Assay. To determine the PGE_2 reducing effect of the compounds on intact HeLa cells, the mPGES-1 inhibitors were simultaneously incubated with a proinflammatory stimulus (IL-1β and TNFα) for 24 h. The production of PGE_2 was determined in the extracellular supernatant and was reduced dose-dependently with all inhibitors (Figure 2). We observed a shift in inhibitory potency in comparison to isolated mPGES-1 enzyme activity of about 28% (**7i**) to 64% (**7n**) at 1 μM compound concentration.

Whole Blood Eicosanoid Profiling. To assemble a preliminary pharmacological profile and to collect first bioavailability data, we screened compound **7** and derivatives **7f**, **7i**, **7k**, **7l**, **7n**, **7o**, **7q**, and **7r** in human whole blood assays. Three different assays were selected to check their influences on (i) COX-1 mediated prostanoid production (mainly TXA_2 and PGD_2), (ii) COX-2 coupled prostanoid synthesis (mainly PGE_2 and $PGF_{2\alpha}$), and (iii) leukotriene/HETE pathways. Table 2 summarizes the remaining levels of each eicosanoid as compared to vehicle treated whole blood. COX-1 mediated prostanoid production was stimulated by platelet clotting of nonheparinized blood. Instead of the instable COX-1 related product TXA_2,[28] the stable metabolite TXB_2 was measured. In this setting, PGD_2 is also slightly up-regulated. No compound had an inhibitory or stimulating effect on the TXB_2 and PGD_2-level up to 10 μM final compound concentration (Table 2A). The selective COX-1 inhibitor SC-560 reduced both TXB_2 and PGD_2 as expected. COX-2 related prostaglandin production was induced by treatment of heparinized whole blood with LPS, which leads to an increase of mainly COX-2/mPGES-1 coupled PGE_2 levels but also to enhanced $PGF_{2\alpha}$ levels. To exclude effects mediated by COX-1, we mixed all samples with 10 μg/mL acetylsalicylic acid (in this concentration a specific COX-1 inhibitor[29]). Except for **7f**, all compounds reduced PGE_2 at 100 μM concentration (Table 2B). Celecoxib also reduced $PGF_{2\alpha}$ levels, while **7f** increased its concentration.

To assess the influence of the compounds on the leukotriene and HETE pathways, we treated heparinized whole blood with calcium-ionophore to activate the 5-lipoxygenase (5-LO)/5-lipoxygenase activating protein (FLAP) complex, leading to an increase of LTA_4 levels[30] (Table 2C−E). Beside LTB_4 (the stable metabolite of LTA_4) also enhanced levels of various hydroxyeicosatetraenoic acids (HETE) were detected after stimulation.[31] The 5-LO-inhibitor zileuton,[32] which was used as control compound, reduced LTB_4 and 5(S)-HETE. Derivative **7f** of the quinazolinone series enhanced both LTB_4 and 5(S)-HETE levels, while the residual production of 5(S)-HETE was reduced by **7i**. All other tested compounds had no influence on LTB_4 and 5(S)-HETE. 12(S)-HETE, 15(S)-HETE, and (±)11-HETE levels were not affected at all at 10 μM final concentration.

DISCUSSION

The primary aim of this study was to generate a library of quinazolinone compounds with different scaffold decorations, to investigate their influence on the mPGES-1 and other enzymes of the eicosanoid pathway, and to identify preliminary structure−activity relationships.

We were able to establish a facile synthesis route for the quinazolinone-based inhibitors of mPGES-1 (Scheme 1). The presented synthesis route is timesaving, needs small amounts of material, and enables chemical modifications of at least three residues around the quinazolinone scaffold. Together with several other compounds purchased from a commercial supplier, we investigated the structure−activity relationship of quinazolinone derivatives of the lead structure **7**. The compound set includes variations at three residue positions with (halogenated) aromatic and heterocyclic groups (like thiophene) as well as aliphatic side chains (Chart 2). It turned out that variations at R_1 in most cases considerably reduced the activity as compared to **7**. Only aromatic residues with an *ortho*-chloro-substitution (**7**, **7f**) were tolerated, which points to the importance of a hydrophobic interaction with the *ortho*-chlorine atom in contrast to unsubstituted phenyl moiety and *ortho*-fluor (**7b** and **7c** with 15% and 30% inhibition at 1 μM). Additionally, *para*-chloro substituents led to decreased activity (**7h**). Moreover, we observed reduced inhibition when R_1 is an aliphatic residue (**7d**, **7e**); larger substituents like phenethyl (**7a**) further impaired activity. Bioisosteric replacement of the *ortho*-substituted phenyl-residue R_1 by a thiophene (**7g**) resulted in a less potent inhibitor than **7**.

With 3-chlorbenzyl moiety in the R_2 position, the disubstitution at R_1 was investigated; **7o** (2-chloro-6-fluoro) and **7p** (2-chloro-6-chloro) exhibit similar inhibitory activity as

dx.doi.org/10.1021/jm201687d | J. Med. Chem. 2012, 55, 3792−3803

Table 2. Human Whole Blood Was Incubated with Quinazolinone Series Compounds[a]

A

Whole Blood COX-1 Assay	TXB_2			PGD_2		
Compound / Concentration	Residual production [%]	SEM [%]	n	Residual production [%]	SEM [%]	n
SC-560 5 μM	0.2	0.1	8	-0.2	1.1	8
7 (FR20) 10 μM	90.0	7.5	5	98.5	8.8	5
7f 10 μM	97.3	5.9	6	96.1	10.8	5
7i 10 μM	89.0	6.1	6	91.7	22.2	6
7k 10 μM	86.4	3.8	5	84.9	14.3	5
7l 10 μM	90.4	4.1	6	86.5	9.5	6
7n 10 μM	86.1	0.9	6	89.0	10.1	6
7o 10 μM	84.4	3.6	6	89.4	15.8	6
7q 10 μM	81.9	3.7	6	128.3	37.6	6

B

Whole Blood COX-2 Assay	PGE_2			PGF_{2a}		
Compound / Concentration	Residual production [%]	SEM [%]	n	Residual production [%]	SEM [%]	n
Celecoxib 5 μM	6.5	1.5	12	7.3	2.6	12
7 (FR20) 100 μM	51.2	2.0	6	94.2	5.9	6
7f 100 μM	173.8	18.0	6	234.0	34.5	6
7i 100 μM	50.0	4.9	6	92.5	10.1	6
7k 100 μM	52.1	7.1	6	92.6	7.0	6
7l 100 μM	37.4	4.5	6	81.3	10.3	6
7n 100 μM	34.2	1.7	6	73.4	7.2	6
7o 100 μM	54.7	1.5	6	97.0	8.3	6
7q 100 μM	53.0	5.8	6	93.8	10.6	6

C

Whole Blood LO/HETE Assay	LTB_4			5(S)-HETE		
Compound / Concentration	Residual production [%]	SEM [%]	n	Residual production [%]	SEM [%]	n
Zileuton 5 μM	20.4	3.1	9	19.1	2.3	9
7 (FR20) 10 μM	83.0	4.5	9	79.0	2.8	9
7f 10 μM	150.8	16.0	9	157.4	20.1	9
7i 10 μM	70.9	6.8	9	67.0	6.2	9
7k 10 μM	71.9	7.7	9	74.8	7.2	9
7l 10 μM	93.7	9.0	9	92.0	9.8	9
7n 10 μM	91.3	3.5	9	88.1	3.5	9
7o 10 μM	94.1	5.0	9	92.1	5.0	9
7q 10 μM	72.7	7.7	9	74.4	7.6	9

D

Whole Blood LO/HETE Assay	12(S)-HETE			15(S)-HETE		
Compound / Concentration	Residual production [%]	SEM [%]	n	Residual production [%]	SEM [%]	n
Zileuton 5 μM	101.3	12.7	9	95.1	7.0	9
7 (FR20) 10 μM	80.0	3.5	9	83.1	5.7	9
7f 10 μM	93.2	10.3	9	93.8	8.2	9
7i 10 μM	85.5	8.2	9	80.0	9.0	9
7k 10 μM	109.5	8.8	9	94.2	10.3	9
7l 10 μM	92.8	10.8	9	90.3	12.2	9
7n 10 μM	82.7	3.7	9	78.3	9.4	9
7o 10 μM	123.0	19.3	9	110.6	10.4	9
7q 10 μM	88.9	18.5	9	83.4	9.9	9

E

Whole Blood LO/HETE Assay	(±)11-HETE		
Compound / Concentration	Residual production [%]	SEM [%]	n
Zileuton 5 μM	93.2	11.3	6
7 (FR20) 10 μM	76.8	6.8	6
7f 10 μM	85.2	9.0	6
7i 10 μM	77.0	11.9	6
7k 10 μM	84.8	17.4	6
7l 10 μM	71.6	12.5	6
7n 10 μM	75.4	12.4	6
7o 10 μM	122.9	10.8	6
7q 10 μM	86.5	18.3	6

[a]Residual production is given in percent of control. Red color indicates a residual production ≤67% (= inhibition), yellow color between 67.1% and 132.9% (= no effect), green color ≥133% (= stimulation) (A) Blood clotting induced mainly COX-1 mediated TXB_2 production, but PGD_2 was also detected. (B) Stimulation of COX-2 and mPGES-1 with LPS upregulated PGE_2 and $PGF_{2\alpha}$-levels. (C−E) Calcium ionophore stimulated whole blood induces LTB_4 production via 5-LO/FLAP but also several HETEs.

7, implicating that a substitution at position 6 of the R_1-phenyl is tolerated. Apparently, the R_2 residue may be exchanged for a smaller substituent without losing potency. Simplification of the [1,1′-biphenyl]-4-ylmethyl- (**7**) to a benzyl-group (**7l**), as well as substitution at the [1,1′-biphenyl]-4-ylmethyl group (**7i**, **7j**) or at the benzyl-group at different positions (**7l**, **7n**) is also tolerated, with no detrimental effect on activity. Variations of the R_3 residue were only possible for some derivatives. A

dx.doi.org/10.1021/jm201687d | J. Med. Chem. 2012, 55, 3792−3803

methyl (**7m**) and a benzyl residue (**7r**) yielded comparable activities, while a replacement with cyclopropyl (**7t**) abolished inhibition. We therefore conclude that residue R_1 is critical for the activity of this class of inhibitors, while R_2 and R_3 play a minor role. These two residues may serve as a starting point for further chemical variations.

In the in vitro single concentration test on isolated human mPGES-1 protein, 13 out of 25 compounds showed an inhibition rate higher than 33%, eight of them with an enhanced potency compared to the lead structure **7** (>66%). These eight inhibitors were used in all further studies. Interestingly, no inhibitor has a lower IC_{50} than **7** (Table 1). To exclude COX-1/COX-2 related side effects, selectivity of the compounds against these two enzymes was tested in a direct inhibitor test. Neither COX-1 nor COX-2 were affected at 1 μM concentration (inhibition ≪33%). Cellular toxicology studies exhibit impaired cell viability at 100 μM inhibitor concentration for four derivatives (Figure 1). All tested compounds reduced the PGE_2 level in a cell-based assay (Figure 2) between 70% (**7k**) and 97% (**7i**) at 10 μM compound concentration. Tests with a 10-fold higher concentration (100 μM) did not enhance the inhibitory effect that was also observed on isolated enzyme. We therefore conclude that there is no major limitation in cell permeability. Whole blood eicosanoid screening revealed a distinct profile for each compound including many fatty acids of the three major arachidonic acid subcascades: the prostanoids, leukotrienes, and HETEs. It has been shown in mPGES-1-deficient mice that PGE_2 synthesis may be redirected to PGD_2, $PGF_{2\alpha}$, and 6-keto-$PGF_{1\alpha}$ (stable metabolite of PGI_2).[33] This mechanism may compensate for a loss of PGE_2 synthesis in nociceptive behavior. We therefore determined the level of other prostanoids and arachidonic acid metabolites. Besides the desired PGE_2 inhibition, no effects on TXB_2 and PGD_2 levels were observed. The role of PGD_2 in pathological conditions seems to be diverse: while exogenous PGD_2 sustains the pyrogenic effects of PGE_2[34] in brain tissue, the metabolite 15d-PGJ_2 is involved in anti-inflammatory responses.[35] Reduction of PGD_2 might therefore delay the resolution of inflammation.[36] $PGF_{2\alpha}$, which is also not affected, mediates allodynia in the spinal cord.[37] In contrast, $PGF_{2\alpha}$ contributes to resolution of inflammation in the late phase of carrageenan-induced pleurisy in rats.[38] In addition, leukotrienes and HETEs play a role in pathological conditions, but their roles are diverse and compound-dependent, suggesting no common mode of action.

While LTB_4 and 5(S)-HETE levels were only slightly affected by the tested quinazolinone substances, 12(S)-HETE, 15(S)-HETE, and (±)11-HETE were not reduced by any derivative. Compound **7f** contrarily enhanced PGE_2, $PGF_{2\alpha}$, LTB_4, and 5(S)-HETE levels, indicating a COX-2/5-LO mediated proinflammatory effect. Nevertheless, whole blood assays revealed that inhibition of mPGES-1 with our compounds is not accompanied by a redirection of COX-derived PGH_2 to other prostanoids and therefore pharmacological inhibition of mPGES-1 seems to be a promising approach for the treatment of pain and inflammation. An approximately 10-fold shift of decreased PGE_2 inhibition potency between activity assays with isolated enzyme and in whole blood was observed for all compounds. A reduced unbound fraction of the compounds due to distribution into cells, membranes, or protein binding may be responsible for this shift but does not automatically limit in vivo efficacy.[39]

CONCLUSIONS

In this study, we discovered that a *ortho*-chloro-substitued phenyl residue at position R_1 and a propyl or benzyl residue at position R_3 of the lead structure **7** promote mPGES-1 inhibition. Structural variations at position R_2 seem to be less influential on mPGES-1 inhibition. A detailed whole blood eicosanoid screening revealed that pharmacological inhibition of mPGES-1 is not accompanied by a redirection of COX derived PGH_2 to other prostanoids.

EXPERIMENTAL SECTION

Chemical Methods. Material and Reagents. Compound **7** and respective derivatives **7a−n** and **7r−x** were purchased from Asinex (Asinex, Moscow, Russia) and exhibit ≥95% purity determined by manufacturer. Compounds **7o−q** were synthesized in-house. The structures of the synthesized compounds were confirmed by ^1H , ^{13}C NMR and mass spectrometry (ESI). The purity of the synthesized compounds was determined by combustion analysis and was found to be >95%. Starting materials and solvents were purchased from Sigma-Aldrich Chemie GmbH (Steinheim, Germany) or Alfa Aesar (Ward Hill, USA) and were reagent grade and used without further purification. For the microwave synthesis, a Biotage Initiator 2.0 (300 W) was used and the products were purified using a Varian 971-FP flash purification system on silica gel with 50 μm particle size. ^1H and ^{13}C NMR spectra were measured in DMSO-d_6 or MeOD on a Bruker AV 250 (250 MHz for ^1H NMR and 63 MHz for the ^{13}C NMR). Chemical shifts are reported in parts per million (ppm) using tetramethylsilane (TMS) as internal standard. Mass spectra were obtained on an Electrospray-Ionization Fisons (VG Platform II) spectrometer measuring in the positive- or negative-ion mode (ESI-MS system). Combustion analysis was performed by the micro-analytical laboratory of the Institute of Organic Chemistry and Chemical Biology, Goethe University Frankfurt, on an Elementar Vario Micro Tube CHNO rapid elemental analyzer.

Synthesis. The compounds were synthesized in three steps (Scheme 1) involving the condensation of 5-iodoanthranilic acid with butyric acid followed by dehydration to form the intermediate benzoxazinone. Successive addition of 3-chlorbenzylamine provides 2,3-disubstituted-6-iodo-3*H*-quinazolin-4-one; these reactions were carried out under microwave conditions.[40] The third step comprises a related Goldberg reaction,[41] a copper-catalyzed *N*-arylation of amides with a heteroaryl iodide. The reaction is mediated by copper iodide, *N*,*N*′-dimethylethylenediamine, and K_3PO_4.

Synthesis of 3-(3-Chlorobenzyl)-6-iodo-2-propylquinazolin-4(3H)-one. To a conical-bottomed microwave vial, a solution of 5-iodoanthranilic acid (0.500 g, 1.901 mmol, 1 equiv), butyric acid (0.167 g, 1.901 mmol, 1 equiv), and triphenyl phosphite (0.639 g, 2.091 mmol, 1.1 equiv) in 2 mL of anhydrous pyridine was added. The mixture was irradiated in a sealed microwave vial for 10 min at 150 °C. After cooling, 3-chlorbenzylamine (0.269 g, 1.901 mmol, 1 equiv) was added and irradiated for 5 min at 230 °C. The solvent was removed, and the residue was resolved in ethyl acetate, washed with saturated $NaHCO_3$ (2 × 10 mL), 10% HCl (2 × 10 mL), and dried over $MgSO_4$. The solvent was removed under reduced pressure, and the crude product was purified by column chromatography on silica gel with hexane−ethyl acetate (50:50, v/v), obtaining 100 mg (12% yield) of an off-white solid.

^1H NMR (MeOD): δ 8.60 (br, 1H), 8.19 (dd, J = 3.4, 8.6 Hz, 1H), 7.48 (d, J = 8.6 Hz, 1H), 7.33 (m, 3H), 5.46 (s, 2H), 2.87 (t, J = 7.8 Hz, 2H), 1.73 (q, J = 7.5 Hz, 2H), 1.00 (t, J = 7.3 Hz, 3H).

MS (ESI, 70 eV) m/z (%): 439.2 (100%).

*Synthesis of 2-Chloro-N-(3-(3-chlorobenzyl)-4-oxo-2-propyl-3,4-dihydroquinazolin-6-yl)-6-fluorobenzamide (**7o**).* A round-bottomed flask was charged with CuI (1 mg, 0.005 mmol, 0.01 equiv), 2-chloro-6-fluorobenzamide (0.114 g, 0.657 mmol, 1.2 equiv), and K_3PO_4 (0.232 g, 1.094 mmol, 2 equiv), evacuated, and backfilled with argon. *N*,*N*′-Dimethylethylenediamine (4 mg, 0.055 mmol, 0.1 equiv), 3-(3-chlorobenzyl)-6-iodo-2-propylquinazolin-4(3*H*)-one (0.240 g, 0.547

dx.doi.org/10.1021/jm201687d | J. Med. Chem. 2012, 55, 3792−3803

mmol, 1 equiv), and tetrahydrofuran (10 mL) were added under argon. The reaction mixture was stirred at 110 °C for 23 h. The resulting pale-brown suspension was cooled down and filtered through a 1 cm pad of silica gel eluting with 20 mL of ethyl acetate. The filtrate was concentrated, and the residue was purified by column chromatography on silica gel with hexane−ethyl acetate (50:50, v/v) provided 189 mg (71% yield) as an off-white solid.

^{1}H NMR (DMSO-d_6): δ 11.19 (br, 1H), 8.68 (d, J = 2.4, 1H), 8.05 (dd, J = 2.4, 8.8 Hz, 1H), 7.73 (d, J = 8.7 Hz, 1H), 7.79−7.43 (m, 6H), 7.17 (d, J = 5.4 Hz, 1H), 5.43 (s, 2H), 2.76 (t, J = 14.8 Hz, 2H), 1.77 (q, J = 7.3 Hz, 2H), 0.96 (t, J = 7.3 Hz, 3H).

^{13}C NMR (DMSO-d_6): δ 163.5, 161.7, 160.5, 156.8, 156.1, 143.9, 139.7, 136.6, 133.7, 132.0, 130.9, 127.9, 126.6, 125.8, 124.9, 120.3, 115.7, 114.8, 45.2, 35.8, 19.8, 13.6.

MS (ESI, 70 eV) m/z (%): 484.5 (100%).

Anal. Calcd for $C_{25}H_{20}Cl_2FN_3O_2$: C, 61.99, H, 4.16, N, 8.68. Found: C, 61.95, H, 4.12, N, 8.64.

*Synthesis of 2,6-Dichloro-N-(3-(3-chlorobenzyl)-4-oxo-2-propyl-3,4-dihydroquinazolin-6-yl)benzamide (**7p**).* A round-bottomed flask was charged with CuI (3 mg, 0.015 mmol, 0.05 equiv), 2,6-dichlorobenzamide (0.09 g, 0.478 mmol, 1.5 equiv), and K_3PO_4 (0.132 g, 0.638 mmol, 2 equiv), evacuated, and backfilled with argon. *N*,*N*′-Dimethylethylenediamine (3 mg, 0.031 mmol, 0.1 equiv), 3-(3-chlorobenzyl)-6-iodo-2-propylquinazolin-4(3*H*)-one (0.140 g, 0.319 mmol, 1 equiv), and THF (10 mL) were added under argon. The reaction mixture was stirred at 110 °C for 23 h. The resulting pale-brown suspension was cooled down and filtered through a 1 cm pad of silica gel eluting with 20 mL of ethyl acetate. The filtrate was concentrated, and the residue was recrystallized from EtOH/water, obtaining 80 mg (50% yield) as a white solid.

^{1}H NMR (DMSO-d_6): δ 11.18 (br, 1H), 8.70 (d, J = 3.3 Hz, 1H), 8.05 (dd, J = 3.3, 9.2 Hz, 1H), 7.76−7.21 (m, 7H), 7.15 (m, 1H), 5.48 (s, 2H), 2.77 (t, J = 8.3 Hz, 2H), 1.78 (q, J = 9.6 Hz, 2H), 0.95 (t, J = 8.2 Hz, 3H).

^{13}C NMR (DMSO-d_6): 162.3, 161.3, 155.9, 143.5, 142.6, 139.4, 136.9, 136.0, 133.6, 131.9, 131.1, 128.2, 126.4, 125.3, 119.9, 115.4, 45.4, 35.7, 19.6, 13.3.

MS (ESI, 70 eV) m/z (%): 500.3 (100%).

Anal. Calcd for $C_{25}H_{20}Cl_3N_3O_2$: C, 59.96, H, 4.03, N, 8.39. Found: C, 60.19, H, 4.21, N, 8.36.

*Synthesis of N-(3-(3-Chlorobenzyl)-4-oxo-2-propyl-3,4-dihydroquinazolin-6-yl)-2-methylbenzamide (**7q**).* A round-bottomed flask was charged with CuI (43 mg, 0.228 mmol, 0.2 equiv), 2-methylbenzamide (0.185 g, 1.368 mmol, 1.2 equiv), and K_3PO_4 (0.484 g, 2.280 mmol, 2 equiv), evacuated, and backfilled with argon. *N*,*N*′-Dimethylethylenediamine (40 mg, 0.456 mmol, 0.4 equiv), 3-(3-chlorobenzyl)-6-iodo-2-propylquinazolin-4(3*H*)-one (0.5 g, 1.140 mmol, 1 equiv), and THF (10 mL) were added under argon. The reaction mixture was stirred at 110 °C for 23 h. The resulting pale-brown suspension was cooled down and filtered through a 1 cm pad of silica gel eluting with 20 mL of ethyl acetate. The filtrate was concentrated, and the residue was purified by flash chromatography on silica gel (hexane−ethyl acetate, 0→ 80% ethyl acetate, 4%/min) provided 179 mg (35% yield) as an off-white solid.

^{1}H NMR (DMSO-d_6): δ 10.69 (br, 1H), 8.74 (d, J = 2.1 Hz, 1H), 8.13 (dd, J = 2.3, 8.8 Hz, 1H), 7.70 (d, J = 8.8 Hz, 1H), 7.56 (d, J = 7.0 Hz, 1H), 7.49−7.33 (m, 6H), 7.07 (m, 1H), 5.45 (s, 2H), 2.76 (t, J = 7.4 Hz, 2H), 2.48 (s, 3H), 1.76 (q, J = 7.3 Hz, 2H), 0.96 (t, J = 7.3 Hz, 3H).

^{13}C NMR (DMSO-d_6): δ 168.2, 161.4, 155.8, 143.0, 139.4, 136.9, 135.6, 133.4, 130.7, 129.9, 129.1, 126.9, 125.8, 124.7, 120.3, 115.6, 45.3, 36.0, 19.4, 19.1, 13.6.

MS (ESI, 70 eV) m/z (%): 446.5 (100%).

Anal. Calcd for $C_{26}H_{24}ClN_3O_2$: C, 70.03, H, 5.42, N, 9.42. Found: C, 69.94, H, 5.33, N, 9.21.

Cell Biological Methods. Cells and Reagents. HeLa (human cervix carcinoma) and NIH-3T3 (Swiss mouse fibroblast) cells were purchased from Deutsche Sammlung für Mikroorganismen and Zellkulturen (DSMZ, Braunschweig, Germany). RAW 264.7 (mouse macrophage) cells were purchased from American Type Culture Collection (ATCC, Manassas, USA). HeLa were incubated in RPMI medium 1640 containing high glucose, L-glutamine, and 25 mM HEPES, NIH in Dulbecco's MEM containing 4.5 g/L glucose, and pyruvate and RAW in RPMI medium 1640, containing high glucose, GlutaMAX. All media contain 10% fetal calf serum (FCS), 100 units/mL penicillin G, and 100 μg/mL streptomycin, which were purchased from Invitrogen (Darmstadt, Germany). Cells were cultured at 37 °C in an atmosphere containing 5% CO_2. Recombinant human IL-1 β (IL-1β) and recombinant human tumor necrosis factor α (TNFα) were purchased from PeproTech (London, UK).

mPGES-1 Activity Assay. To investigate the inhibitory activity of the quinazolinone derived compounds on the mPGES-1 enzymes in vitro, the microsomal fraction of human HeLa, murine RAW, and murine NIH cells were prepared. Approximately 3 × 10^6 cells were incubated for 24 h at 37 °C in medium containing 10% FCS. The medium was removed, and HeLa/NIH cells were stimulated with IL-1β (1 ng/mL) + TNFα (5 ng/mL) for 16 h, RAW cells were stimulated with 10 mg/mL LPS for 16 h. Cells were scraped in 2 mL of phosphate buffered saline (PBS) and centrifuged at 5000 rpm for 2 min at 4 °C. Cell pellets were frozen in liquid nitrogen. After thawing the cells, they were resuspended in 800 μL of potassium phosphate buffer (Kpi buffer, 0.1 M, pH 7.4), containing 1× complete protease inhibitor cocktail (Roche Diagnostics, Mannheim, Germany), sucrose (0.25 M), and reduced glutathione (GSH, 1 mM). After sonification and centrifugation at 45000 rpm for 2 h or 53000 rpm for 1 h at 4 °C, the microsomal fraction (pellet) was stored at −80 °C. The pellet was resuspended in 100 μL Kpi buffer (0.1 M, pH 7.4) containing 1× Roche Complete and reduced GSH (2.5 mM). To homogenize the solution, a sonification step was applied and total protein content was measured using the Bradford method.[42] Activity of all quinazolinone derivates was measured at 1 μM final concentration and compared to the lead compound. The mPGES-1 activity assay was performed on the basis of Thoren et al.[43] Briefly, 0.15 mg/mL of human HeLa derived or murine NIH derived protein or 0.3 mg/mL of murine RAW derived protein was incubated with each compound for 30 min on ice. The reaction was initiated with 20 μM PGH_2 (Larodan, Malmö, Sweden) and terminated after 1 min by adding a stop solution containing 40 mM iron chloride ($FeCl_2$) and 80 mM citric acid. For the solid phase extraction procedure, 100 μL of reaction solution was mixed for 3 min with 700 μL of ultrapure water, 100 μL of 0.15 M EDTA, 20 μL of MeOH, and 20 μL of internal standard (25 ng/mL PGE_2-d_4, 50 ng/mL PGD_2-d_4), all from Cayman Chemical Company (Ann Arbor, USA), centrifuged at 1200 rpm for 3 min, and passed through a 30 mg of Bond Elut NEXUS 96 round-well plate (Agilent Technologies GmbH, Böblingen, Germany) preconditioned with 1 mL of MeOH, followed by 1 mL of ultrapure water. The cartridge was washed with 1 mL of 30% MeOH. Prostaglandins were eluted with 1 mL of hexane−ethylacetate−isopropranol (30:65:5, v/v/v). After evaporating the solvent under nitrogen atmosphere, the residue was reconstituted in 100 μL of acetonitrile−H_2O−formic acid (20:80:0.0025 v/v/v). Samples were measured by LC-MS/MS technique (LC unit: Agilent 1200 series, Agilent Technologies GmbH, Böblingen, Germany. MS/MS unit: AB SCIEX QTRAP 5500, Applied Biosystems, Foster City, USA) as described previously.[44] Compounds with improved inhibitory effect as compared to the lead structure were used for further experiments. For IC_{50} calculation, the mPGES-1 assay was performed with increasing compound concentrations. The IC_{50} was calculated using GraphPad Prism 5 software (GraphPad Software, Inc., San Diego, CA 92130 USA) by fitting the four parameter logistic curve. With 95% probability, the estimated IC_{50} is in the range of the given confidence interval.

COX-Inhibitor Screening Assay. To distinguish between mPGES-1 and COX-1 or COX-2 derived inhibition of PGE_2 production, direct inhibition of the COX-1 (ovine) and COX-2 (human recombinant) enzyme was measured using a COX inhibitor screening assay kit (Cayman Chemicals, Ann Arbor, MI, USA), according to the manufacturer's protocol. SC-560, a selective COX-1 inhibitor, and celecoxib, a selective COX-2 inhibitor, were used as positive controls. The COX assay is based on the determination of PGE_2, PGD_2, and

$PGF_{2\alpha}$ amounts produced by $SnCl_2$ reduction of COX-derived PGH_2. Then 100 μL of reaction solution was diluted with 200 μL of MeOH. Finally, 70 μL of diluted reaction solution was mixed for 3 min with 700 μL of ultrapure water, 100 μL of 0.15 M EDTA, 20 μL of MeOH, and 20 μL of internal standard (25 ng/mL PGE_2-d_4, 25 ng/mL PGD_2-d_4, 25 ng/mL TXB_2-d_4, 50 ng/mL $PGF_{2\alpha}$-d_4, 37.5 ng/mL 6-keto-$PGF_{1\alpha}$-d_4). The amount of prostaglandins was quantified by LC-MS/MS analysis after solid phase extraction as described above (see mPGES-1 activity assay).

WST-1 Cell Viability Assay. The water-soluble tetrazolium-1 salt (Roche Diagnostics, Mannheim, Germany) was used to determine the cell viability after treatment of cells with the compounds. HeLa cells were seeded at a density of 3×10^3 cells in 100 μL of culture medium containing 10% FCS into 96-well microplates and incubated for 24 h at 37 °C. Medium was removed, and HeLa cells were stimulated with IL-1β (1 ng/mL) + TNFα (5 ng/mL) and simultaneously treated with increasing concentrations of the compounds (1, 10, and 100 μM) or DMSO. After 24 h, 10 μL of WST-1 reagent was added to each well and the cells were incubated for further 90−150 min. The formation of the dye was measured at 450 nm against a reference wavelength of 620 nm using a 96-well spectrophotometric plate reader (SpectraFluor Plus, Tecan, Crailsheim, Germany).

Cell-Based mPGES-1 Activity Assay. first, 2×10^4 HeLa cells were incubated in 24-well microplates for 24 h at 37 °C. Then the medium was replaced with fresh medium containing 1 ng/mL IL-1β + 5 ng/mL TNFα (stimulated control) or an equal amount of PBS (unstimulated control) and test compound (1, 10, or 100 μM) or DMSO. After incubation for 24 h at 37 °C, cell supernatant was collected. Then 400−500 μL of supernatant was mixed with 400 μL of 45 mM H_3PO_4, 100 μL of 0.15 M EDTA, 20 μL of MeOH, and 20 μL of internal standard (25 ng/mL PGE_2-d_4, 25 ng/mL PGD_2-d_4, 25 ng/mL TXB_2-d_4, 50 ng/mL $PGF_{2\alpha}$-d_4, 37.5 ng/mL 6-keto-$PGF_{1\alpha}$-d_4). The amount of prostaglandins was quantified by LC-MS/MS analysis after solid phase extraction as described above (see mPGES-1 activity assay).

Whole Blood Eicosanoid Screening. To determine possible effects of quinazolinone derivatives on different eicosanoids levels in human whole blood, a eicosanoid profile was created for each compound. Therefore, three different experimental settings were used to stimulate the production of eicosanoid synthesis.

A stimulating effect of a compound was assumed when the relative level of an eicosanoid exceeded +33% compared to control, an inhibitory effect when levels were reduced by −33% or more, as compared to control.

Whole Blood COX-1 Assay. Because TXA_2 is the major product of the COX-1/thromboxane-A synthase-pathway (which is activated during blood clotting), this setting was used to investigate the effect of mPGES-1 inhibitors on these two enzymes. Human venous whole blood was collected in neutral monovettes without any additives (SARSTEDT AG & Co, Nümbrecht, Germany) from healthy donors who had not taken any NSAIDs for at least one week. Then 500 μL of blood per sample was directly mixed with rising concentrations of test compounds. Negative controls were immediately chilled on ice to minimize thrombocyte aggregation. All other samples were incubated at 37 °C for 1 h, and blood was allowed to clot.

Samples were chilled on ice for 5 min, and plasma was extracted by centrifugation at 4 °C with 2000 rpm for 20 min. Plasma samples were stored at −80 °C. For the extraction procedure, plasma was mixed for 3 min with 600 μL of 45 mM H_3PO_4, 100 μL of 0.15 M EDTA, 10 μL of 2 mg/mL butylated hydroxytoluene, 20 μL of MeOH, and 20 μL of internal standard (25 ng/mL PGE_2-d_4, 25 ng/mL PGD_2-d_4, 25 ng/mL TXB_2-d_4, 50 ng/mL $PGF_{2\alpha}$-d_4, 37.5 ng/mL 6-keto-$PGF_{1\alpha}$-d_4).

TXB_2 (instead of the instable TXA_2) was measured together with PGE_2, PGD_2, 6-keto-$PGF_{1\alpha}$, and PGF_{2a} after solid phase extraction as described above (see mPGES-1 activity assay).

Whole Blood COX-2 Assay. The mPGES-1 expression is mainly coupled to COX-2 and therefore many proinflammatory stimuli, activating the COX-2, also upregulate the protein level of mPGES-1. For the COX-2 assay, blood was collected in NH_4−heparin containing monovettes (SARSTEDT AG & Co, Nümbrecht, Germany) which prevent blood clotting. Then 500 μL of heparinized blood was mixed with test compounds in DMSO. Finally, 10 μg/mL acetylsalicylic acid was added to inhibit COX-1. After 15 min incubation at 37 °C, 500 μg/mL (10 μg/mL final concentration) lipopolysaccharide (LPS) in 10 μL autologous plasma was added to stimulate COX-2/mPGES-1. After 24 h incubation time at 37 °C, samples were chilled on ice for 5 min and plasma was collected and prostaglandins extracted and measured by LC-MS/MS (see Whole Blood COX-1 Assay).

Whole Blood Leukotriene/HETE Assay. To assess the influence of quinazolinone derivatives on different enzymes in the leukotriene and HETE pathway, 500 μL of human heparinized whole blood was mixed with test compounds and incubated for 15 min at 37 °C. Afterward, the whole blood was stimulated with 20 μM calcium ionophore (A23187) in autologous plasma for a further 15 min at 37 °C. Blood samples were chilled on ice for 5 min, plasma collected (centrifugation at 4 °C with 2000 rpm for 20 min), and leukotrienes and HETEs extracted by liquid−liquid extraction. Therefore, plasma was mixed with 20 μL of EtOH and 20 μL of internal standard containing 25 ng/mL LTB_4-d_4, 25 ng/mL 5(S)-HETE-d_8, 25 ng/mL 12(S)-HETE-d_8, 25 ng/mL 15(S)-HETE-d_8, and 25 ng/mL 20-HETE-d_6. Then 600 μL of ethyl acetate was added and samples were mixed and centrifuged at 13000 rpm for 3 min. The organic upper phase was extracted. Extraction of leukotrienes and HETEs was repeated once. Solvent was evaporated under nitrogen atmosphere, and the residue was reconstituted in 50 μL of MeOH−H_2O (50:50 v/v). LTB_4, 5(S)-HETE, 12(S)-HETE, 15(S)-HETE, and 20-HETE were analyzed by LC-MS/MS technique on a AB SCIEX QTRAP 5500 (Applied Biosystems, Foster City, CA, USA) operating in multiple reaction monitoring (MRM).[45] Chromatographic separation was performed on a Gemini-NX 5u C18 110A column (150 mm × 2 mm inner diameter, 5 μm particle size, Phenomenex, Aschaffenburg, Germany).

■ ASSOCIATED CONTENT

Ⓢ Supporting Information

IC_{50} dose−response curve of compound **7**. This material is available free of charge via the Internet at http://pubs.acs.org.

■ AUTHOR INFORMATION

Corresponding Author

*Phone: +49 69 6301 6086. Fax: +49 69 6301 7636. E-mail: Roersch@em.uni-frankfurt.de.

Notes

The authors declare no competing financial interest.

■ ACKNOWLEDGMENTS

This research was supported by Merz GmbH & Co. KGaA, the LOEWE Lipid Signaling Forschungszentrum Frankfurt (LiFF), the Oncogenic Signaling Frankurt (OSF), the European Graduate School "Roles of Eicosanoids in Biology and Medicine" (DFG GRK 757/1), the DAAD/Fundación Obra Social "la Caixa", and the Fonds der Chemischen Industrie.

■ ABBREVIATIONS USED

5-LO, 5-lipoxygenase; COX, cyclooxygenase; HETE, hydroxyeicosatetranoid acid; IC_{50}, half-maximal inhibitory concentration; LC-MS/MS, liquid chromatography with combined tandem mass spectrometry; LPS, lipopolysaccharide; LTB_4, leukotrien B_4; mPGES-1, microsomal prostaglandin E synthase 1; NSAIDs, nonsteroidal anti-inflammatory drugs; PGE_2, prostaglandin E_2; SAR, structure−activity relationship

■ REFERENCES

(1) Murakami, M.; Naraba, H.; Tanioka, T.; Semmyo, N.; Nakatani, Y.; Kojima, F.; Ikeda, T.; Fueki, M.; Ueno, A.; Oh, S.; Kudo, I. Regulation of prostaglandin E2 biosynthesis by inducible membrane-

associated prostaglandin E2 synthase that acts in concert with cyclooxygenase-2. *J. Biol. Chem.* **2000**, *275*, 32783−32792.
(2) Kamei, D.; Yamakawa, K.; Takegoshi, Y.; Mikami-Nakanishi, M.; Nakatani, Y.; Oh-Ishi, S.; Yasui, H.; Azuma, Y.; Hirasawa, N.; Ohuchi, K.; Kawaguchi, H.; Ishikawa, Y.; Ishii, T.; Uematsu, S.; Akira, S.; Murakami, M.; Kudo, I. Reduced pain hypersensitivity and inflammation in mice lacking microsomal prostaglandin e synthase-1. *J. Biol. Chem.* **2004**, *279*, 33684−33695.
(3) Trebino, C. E.; Stock, J. L.; Gibbons, C. P.; Naiman, B. M.; Wachtmann, T. S.; Umland, J. P.; Pandher, K.; Lapointe, J. M.; Saha, S.; Roach, M. L.; Carter, D.; Thomas, N. A.; Durtschi, B. A.; McNeish, J. D.; Hambor, J. E.; Jakobsson, P. J.; Carty, T. J.; Perez, J. R.; Audoly, L. P. Impaired inflammatory and pain responses in mice lacking an inducible prostaglandin E synthase. *Proc. Natl. Acad. Sci. U.S.A.* **2003**, *100*, 9044−9049.
(4) Engblom, D.; Saha, S.; Engstrom, L.; Westman, M.; Audoly, L. P.; Jakobsson, P. J.; Blomqvist, A. Microsomal prostaglandin E synthase-1 is the central switch during immune-induced pyresis. *Nature Neurosci.* **2003**, *6*, 1137−1138.
(5) Wang, D.; Dubois, R. N. Eicosanoids and cancer. *Nature Rev. Cancer* **2010**, *10*, 181−193.
(6) Korotkova, M.; Jakobsson, P. J. Microsomal prostaglandin E synthase-1 in rheumatic diseases. *Front. Pharmacol.* **2011**, 1.
(7) Abdel-Tawab, M.; Zettl, H.; Schubert-Zsilavecz, M. Nonsteroidal anti-inflammatory drugs: a critical review on current concepts applied to reduce gastrointestinal toxicity. *Curr. Med. Chem.* **2009**, *16*, 2042−2063.
(8) Timmers, L.; Pasterkamp, G.; de Kleijn, D. P. Microsomal prostaglandin E2 synthase: a safer target than cyclooxygenases? *Mol. Interventions* **2007**, *7* (195−199), 180.
(9) Takemiya, T. Prostaglandin E(2) produced by microsomal prostaglandin E synthase-1 regulates the onset and the maintenance of wakefulness. *Neurochem. Int.* **2011**, *59*, 922−924.
(10) Radmark, O.; Samuelsson, B. Microsomal prostaglandin E synthase-1 and 5-lipoxygenase: potential drug targets in cancer. *J. Intern. Med.* **2010**, *268*, 5−14.
(11) Scholich, K.; Geisslinger, G. Is mPGES-1 a promising target for pain therapy? *Trends Pharmacol. Sci.* **2006**, *27*, 399−401.
(12) Rahme, E.; Roussy, J. P.; Lafrance, J. P.; Nedjar, H.; Morin, S. Use of nonsteroidal antiinflammatory drugs: is there a change in patient risk profile after withdrawal of rofecoxib? *J. Rheumatol.* **2011**, *38*, 195−202.
(13) Tiliakos, A. M.; Conn, D. L. Aspirin: antiinflammatory drug of choice in 2011? *J. Rheumatol.* **2011**, *38*, 185−187.
(14) Chang, H. H.; Meuillet, E. J. Identification and development of mPGES-1 inhibitors: where we are at? *Future Med. Chem.* **2011**, *3*, 1909−1934.
(15) Guerrero, M. D.; Aquino, M.; Bruno, I.; Riccio, R.; Terencio, M. C.; Paya, M. Anti-inflammatory and analgesic activity of a novel inhibitor of microsomal prostaglandin E synthase-1 expression. *Eur. J. Pharmacol.* **2009**, *620*, 112−119.
(16) Bruno, A.; Di Francesco, L.; Coletta, I.; Mangano, G.; Alisi, M. A.; Polenzani, L.; Milanese, C.; Anzellotti, P.; Ricciotti, E.; Dovizio, M.; Di Francesco, A.; Tacconelli, S.; Capone, M. L.; Patrignani, P. Effects of AF3442 [*N*-(9-ethyl-9*H*-carbazol-3-yl)-2-(trifluoromethyl)-benzamide], a novel inhibitor of human microsomal prostaglandin E synthase-1, on prostanoid biosynthesis in human monocytes in vitro. *Biochem. Pharmacol.* **2010**, *79*, 974−981.
(17) Mbalaviele, G.; Pauley, A. M.; Shaffer, A. F.; Zweifel, B. S.; Mathialagan, S.; Mnich, S. J.; Nemirovskiy, O. V.; Carter, J.; Gierse, J. K.; Wang, J. L.; Vazquez, M. L.; Moore, W. M.; Masferrer, J. L. Distinction of microsomal prostaglandin E synthase-1 (mPGES-1) inhibition from cyclooxygenase-2 inhibition in cells using a novel, selective mPGES-1 inhibitor. *Biochem. Pharmacol.* **2010**, *79*, 1445−1454.
(18) Xu, D.; Rowland, S. E.; Clark, P.; Giroux, A.; Cote, B.; Guiral, S.; Salem, M.; Ducharme, Y.; Friesen, R. W.; Methot, N.; Mancini, J.; Audoly, L.; Riendeau, D. MF63 [2-(6-chloro-1*H*-phenanthro[9,10-*d*]imidazol-2-yl)-isophthalonitrile], a selective microsomal prostaglandin E synthase-1 inhibitor, relieves pyresis and pain in preclinical models of inflammation. *J. Pharmacol. Exp. Ther.* **2008**, *326*, 754−763.
(19) Greiner, C.; Zettl, H.; Koeberle, A.; Pergola, C.; Northoff, H.; Schubert-Zsilavecz, M.; Werz, O. Identification of 2-mercaptohexanoic acids as dual inhibitors of 5-lipoxygenase and microsomal prostaglandin E(2) synthase-1. *Bioorg. Med. Chem.* **2011**, *19*, 3394−3401.
(20) Hieke, M.; Greiner, C.; Dittrich, M.; Reisen, F.; Schneider, G.; Schubert-Zsilavecz, M.; Werz, O. Discovery and Biological Evaluation of a Novel Class of Dual Microsomal Prostaglandin E(2) Synthase-1/5-lipoxygenase Inhibitors Based on 2-[(4,6-Diphenethoxypyrimidin-2-yl)thio]hexanoic Acid. *J. Med. Chem.* **2011**, *54*, 4490−4507.
(21) Koeberle, A.; Rossi, A.; Zettl, H.; Pergola, C.; Dehm, F.; Bauer, J.; Greiner, C.; Reckel, S.; Hoernig, C.; Northoff, H.; Bernhard, F.; Dotsch, V.; Sautebin, L.; Schubert-Zsilavecz, M.; Werz, O. The molecular pharmacology and in vivo activity of 2-(4-chloro-6-(2,3-dimethylphenylamino)pyrimidin-2-ylthio)octanoic acid (YS121), a dual inhibitor of microsomal prostaglandin E2 synthase-1 and 5-lipoxygenase. *J. Pharmacol. Exp. Ther.* **2010**, *332*, 840−848.
(22) Revermann, M.; Mieth, A.; Popescu, L.; Paulke, A.; Wurglics, M.; Pellowska, M.; Fischer, A.; Steri, R.; Maier, T.; Schermuly, R.; Geisslinger, G.; Schubert-Zsilavecz, M.; Brandes, R.; Steinhilber, D. A pirinixic acid derivative (LP105) inhibits murine 5-lipoxygenase activity and attenuates vascular remodelling in a murine model of aortic aneurysm. *Br. J. Pharmacol.* **2011**, *163*, 1721−1732.
(23) Bauer, J.; Koeberle, A.; Dehm, F.; Pollastro, F.; Appendino, G.; Northoff, H.; Rossi, A.; Sautebin, L.; Werz, O. Arzanol, a prenylated heterodimeric phloroglucinyl pyrone, inhibits eicosanoid biosynthesis and exhibits anti-inflammatory efficacy in vivo. *Biochem. Pharmacol.* **2011**, *81*, 259−268.
(24) Rörsch, F.; Wobst, I.; Zettl, H.; Schubert-Zsilavecz, M.; Grosch, S.; Geisslinger, G.; Schneider, G.; Proschak, E. Nonacidic inhibitors of human microsomal prostaglandin synthase 1 (mPGES 1) identified by a multistep virtual screening protocol. *J. Med. Chem.* **2010**, *53*, 911−915.
(25) Backhus, L. M.; Petasis, N. A.; Uddin, J.; Schönthal, A. H.; Bart, R. D.; Lin, Y.; Starnes, V. A.; Bremner, R. M. Dimethyl celecoxib as a novel non-cyclooxygenase 2 therapy in the treatment of non-small cell lung cancer. *J. Thorac. Cardiovasc. Surg.* **2005**, *130*, 1406−1412.
(26) Grösch, S.; Maier, T. J.; Schiffmann, S.; Geisslinger, G. Cyclooxygenase-2 (COX-2)-independent anticarcinogenic effects of selective COX-2 inhibitors. *J. Natl. Cancer Inst.* **2006**, *98*, 736−747.
(27) Khan, Z.; Khan, N.; Tiwari, R. P.; Sah, N. K.; Prasad, G. B.; Bisen, P. S. Biology of Cox-2: an application in cancer therapeutics. *Curr. Drug Targets* **2011**, *12*, 1082−1093.
(28) Casetta, B.; Vecchione, G.; Tomaiuolo, M.; Margaglione, M.; Grandone, E. Setting up a 2D-LC/MS/MS method for the rapid quantitation of the prostanoid metabolites 6-oxo-PGF(1alpha) and TXB2 as markers for hemostasis assessment. *J. Mass. Spectrom.* **2009**, *44*, 346−352.
(29) Warner, T. D.; Giuliano, F.; Vojnovic, I.; Bukasa, A.; Mitchell, J. A.; Vane, J. R. Nonsteroid drug selectivities for cyclo-oxygenase-1 rather than cyclo-oxygenase-2 are associated with human gastrointestinal toxicity: a full in vitro analysis. *Proc. Natl. Acad. Sci. U.S.A.* **1999**, *96*, 7563−7568.
(30) Samuelsson, B.; Dahlen, S. E.; Lindgren, J. A.; Rouzer, C. A.; Serhan, C. N. Leukotrienes and lipoxins: structures, biosynthesis, and biological effects. *Science* **1987**, *237*, 1171−1176.
(31) Taylor, S. M.; Liggitt, H. D.; Laegreid, W. W.; Silflow, R.; Leid, R. W. Arachidonic acid metabolism in bovine alveolar macrophages. Effect of calcium ionophore on lipoxygenase products. *Inflammation* **1986**, *10*, 157−165.
(32) Berger, W.; De Chandt, M. T.; Cairns, C. B. Zileuton: clinical implications of 5-lipoxygenase inhibition in severe airway disease. *Int. J. Clin. Pract.* **2007**, *61*, 663−676.
(33) Brenneis, C.; Coste, O.; Schmidt, R.; Angioni, C.; Popp, L.; Nusing, R. M.; Becker, W.; Scholich, K.; Geisslinger, G. Consequences of altered eicosanoid patterns for nociceptive processing in mPGES-1-deficient mice. *J. Cell. Mol. Med.* **2008**, *12*, 639−648.

(34) Gao, W.; Schmidtko, A.; Lu, R.; Brenneis, C.; Angioni, C.; Schmidt, R.; Geisslinger, G. Prostaglandin D(2) sustains the pyrogenic effect of prostaglandin E(2). *Eur. J. Pharmacol.* **2009**, *608*, 28−31.
(35) Scher, J. U.; Pillinger, M. H. The anti-inflammatory effects of prostaglandins. *J. Invest. Med.* **2009**, *57*, 703−708.
(36) Gilroy, D. W.; Colville-Nash, P. R.; Willis, D.; Chivers, J.; Paul-Clark, M. J.; Willoughby, D. A. Inducible cyclooxygenase may have anti-inflammatory properties. *Nature Med.* **1999**, *5*, 698−701.
(37) Muratani, T.; Nishizawa, M.; Matsumura, S.; Mabuchi, T.; Abe, K.; Shimamoto, K.; Minami, T.; Ito, S. Functional characterization of prostaglandin F2alpha receptor in the spinal cord for tactile pain (allodynia). *J. Neurochem.* **2003**, *86*, 374−382.
(38) Colville-Nash, P. R.; Gilroy, D. W.; Willis, D.; Paul-Clark, M. J.; Moore, A. R.; Willoughby, D. A. Prostaglandin F2alpha produced by inducible cyclooxygenase may contribute to the resolution of inflammation. *Inflammopharmacology* **2005**, *12* (473−476), 477−480.
(39) Smith, D. A.; Di, L.; Kerns, E. H. The effect of plasma protein binding on in vivo efficacy: misconceptions in drug discovery. *Nature Rev. Drug Discovery* **2010**, *9*, 929−939.
(40) Liu, J. F.; Kaselj, M.; Isome, Y.; Ye, P.; Sargent, K.; Sprague, K.; Cherrak, D.; Wilson, C. J.; Si, Y.; Yohannes, D.; Ng, S. C. Design and synthesis of a quinazolinone natural product-templated library with cytotoxic activity. *J. Comb. Chem.* **2006**, *8*, 7−10.
(41) Klapars, A.; Huang, X.; Buchwald, S. L. A general and efficient copper catalyst for the amidation of aryl halides. *J. Am. Chem. Soc.* **2002**, *124*, 7421−7428.
(42) Bradford, M. M. A rapid and sensitive method for the quantitation of microgram quantities of protein utilizing the principle of protein−dye binding. *Anal. Biochem.* **1976**, *72*, 248−254.
(43) Thoren, S.; Jakobsson, P. J. Coordinate up- and down-regulation of glutathione-dependent prostaglandin E synthase and cyclo-oxygenase-2 in A549 cells. Inhibition by NS-398 and leukotriene C4. *Eur. J. Biochem.* **2000**, *267*, 6428−6434.
(44) Schmidt, R.; Coste, O.; Geisslinger, G. LC-MS/MS-analysis of prostaglandin E2 and D2 in microdialysis samples of rats. *J. Chromatogr., B: Anal. Technol. Biomed. Life Sci.* **2005**, *826*, 188−197.
(45) Revermann, M.; Barbosa-Sicard, E.; Dony, E.; Schermuly, R. T.; Morisseau, C.; Geisslinger, G.; Fleming, I.; Hammock, B. D.; Brandes, R. P. Inhibition of the soluble epoxide hydrolase attenuates monocrotaline-induced pulmonary hypertension in rats. *J. Hypertens.* **2009**, *27*, 322−331.

Supporting Information

Structure Activity Relationship of Non-acidic Quinazoline Inhibitors of Human Microsomal Prostaglandin Synthase 1 (mPGES 1)

Florian Rörsch, Estel.la Buscató, Klaus Deckmann, Gisbert Schneider, Manfred Schubert-Zsilavecz, Gerd Geisslinger, Ewgenij Proschak and Sabine Grösch

Figure S1 Exemplary dose-response curve for compound **7** (FR20) on isolated human mPGES-1 enzyme.

Figure S1 Exemplary dose-response curve for compound **7** (FR20) on isolated human mPGES-1 enzyme.

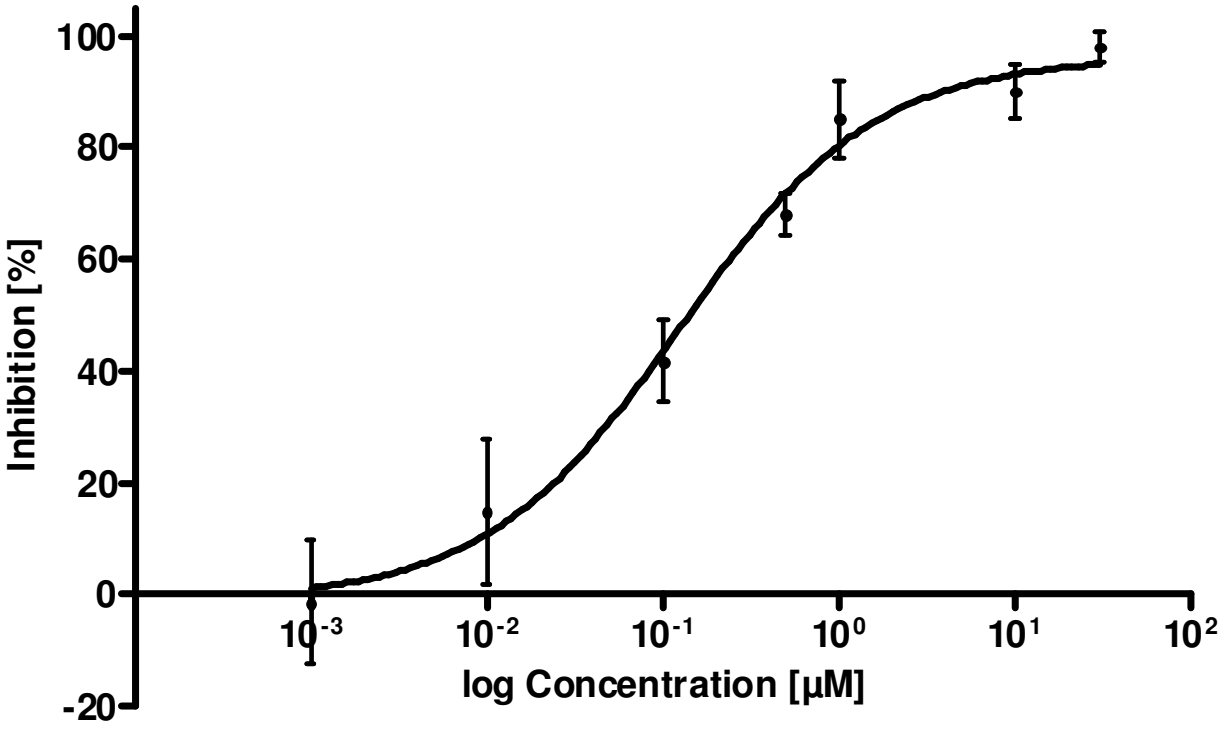

Bioorganic & Medicinal Chemistry Letters 22 (2012) 1969–1975

Contents lists available at SciVerse ScienceDirect

Bioorganic & Medicinal Chemistry Letters

journal homepage: www.elsevier.com/locate/bmcl

SAR-study on a new class of imidazo[1,2-*a*]pyridine-based inhibitors of 5-lipoxygenase

Martina Hieke [†], Carmen B. Rödl [†], Joanna M. Wisniewska, Estel. la Buscató, Holger Stark, Manfred Schubert-Zsilavecz, Dieter Steinhilber, Bettina Hofmann [*,‡], Ewgenij Proschak [*,‡]

Institute of Pharmaceutical Chemistry, ZAFES/LiFF/OSF Goethe-University Frankfurt, Max-von-Laue-Str. 9, D-60438 Frankfurt am Main, Germany

ARTICLE INFO

Article history:
Received 29 November 2011
Revised 11 January 2012
Accepted 12 January 2012
Available online 24 January 2012

Keywords:
Inflammation
5-Lipoxygenase
One-pot multicomponent reaction
Arachidonic acid cascade
Allergic diseases

ABSTRACT

A novel class of 5-lipoxygenase (5-LO) inhibitors characterized by a central imidazo[1,2-*a*]pyridine scaffold, a cyclohexyl moiety and an aromatic system, is presented. This scaffold was identified in a virtual screening study and exhibits promising inhibitory potential on the 5-LO. Here, we investigate the structure–activity relationships of this compound class. With *N*-cyclohexyl-6-methyl-2-(4-morpholinophenyl)imidazo[1,2-*a*]pyridine-3-amine (**14**), we identified a potent 5-LO inhibitor (IC_{50} = 0.16 μM (intact cells) and 0.1 μM (cell-free)), which may possess potential as an effective lead compound intervening with inflammatory diseases and certain types of cancer.

Eicosanoids are signaling lipids derived from polyunsaturated fatty acids which act as important regulators in immunity and inflammation.[1] Furthermore, diseases like rheumatoid arthritis, asthma, atherosclerosis and cancer are influenced by a subgroup of eicosanoids, the leukotrienes (LTs).[2–4] For LT biosynthesis, arachidonic acid (AA) is released from membrane phospholipids by phospholipase (PL) A_2 and transferred via the 5-lipoxygenase-activating protein (FLAP) to 5-lipoxygenase (5-LO).[5,6] 5-LO is a non-heme iron-containing enzyme and catalyzes the oxygenation of AA to 5(*S*)-hydroperoxy-6-*trans*-8,11,14-*cis*-eicosatetraenoic acid (5-HPETE). In the following, 5-HPETE gets reduced to the corresponding alcohol 5-HETE.[7] Alternatively, 5-HPETE can be dehydrated, which leads to the unstable epoxide LTA_4. LTA_4 itself is afterwards converted by LTA_4 hydrolase to LTB_4 which is a chemotactic and chemokinetic agent as well as an activator for phagocytes.[8] Furthermore, LTA_4 can be conjugated with reduced glutathione by LTC_4 synthase. The cysteinyl-containing LTs C_4, D_4 and E_4 cause bronchoconstriction and vascular permeability.[1] LTs also play a prominent role in chronic inflammation and in regulation of the adaptive immune response.[7] Though also anti-inflammatory properties of the 5-LO have recently been shown as the enzyme is involved in the biosynthesis of the resolvins, agents that trigger mechanisms of natural resolution of inflammation,[9] there are, based on the multiple pathophysiological actions of LTs, increasing therapeutic indications for 5-LO inhibitors including inflammation, allergic rhinitis, cardiovascular diseases, cancer and osteoporosis.[4,10] 5-LO as a drug target has been validated in many in vitro and in vivo studies[4] and 5-LO inhibitors are actively in clinical development. To date, the only 5-LO inhibitor that entered the market is A-64077 (zileuton),[11] which inhibits 5-LO by chelating its active site iron.[12] However, it exhibits some drawbacks, that is, the initial need to take it several times daily and the risk of hepatotoxicity.[13] Furthermore, given that many 5-LO inhibitory drug candidates lack sufficient selectivity or show mechanism-based side effects,[14–17] there is a strong need for novel 5-LO inhibitors.

Herein, we present the synthesis and SAR (structure–activity relationship) studies of a novel series of 5-LO inhibitors based on a central imidazo[1,2-*a*]pyridine scaffold (Fig. 1). Previously, we were able to identify 5-LO inhibitors containing this scaffold by ligand-based virtual screening.[18] Thereby, seven imidazo[1,2-*a*]pyridine based structures showed potent 5-LO inhibition (IC_{50} ~1 μM). Among those, compounds **1** and **2** revealed the most promising profile for inhibition of the 5-LO pathway in intact polymorphonuclear leukocytes (PMNL; IC_{50} = 0.9 and 0.6 μM, respectively (Fig. 1)) and were therefore selected as structural templates of this study.

Abbreviations: 5-H(P)ETE, 5(*S*)-hydro(pero)xy-6-*trans*-8,11,14-*cis*-eicosatetraenoic acid; 5-LO, 5-lipoxygenase; AA, arachidonic acid; FLAP, 5-lipoxygenase-activating protein; LT, leukotriene; PL, phospholipase; PMNL, polymorphonuclear leucocytes; SAR, structure–activity relationship; S100, 100,000*g* supernatant.

* Corresponding authors.
E-mail addresses: hofmann@pharmchem.uni-frankfurt.de (B. Hofmann), proschak@pharmchem.uni-frankfurt.de (E. Proschak).
† Both authors contributed equally to this work.
‡ B.H. and E.P. share senior authorship.

0960-894X/$ - see front matter © 2012 Elsevier Ltd. All rights reserved.
doi:10.1016/j.bmcl.2012.01.038

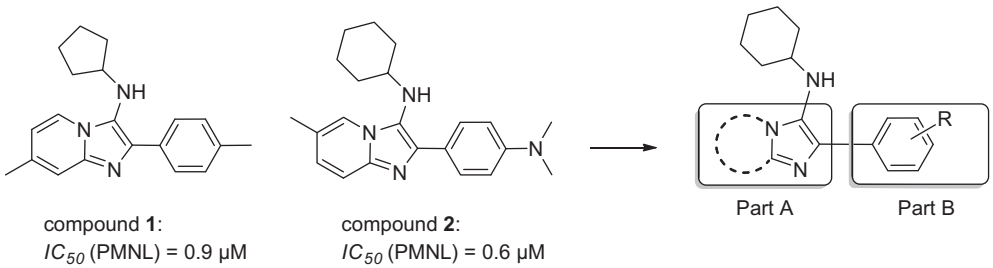

Figure 1. Lead compounds **1** and **2**[18]; general structure of presented compounds.

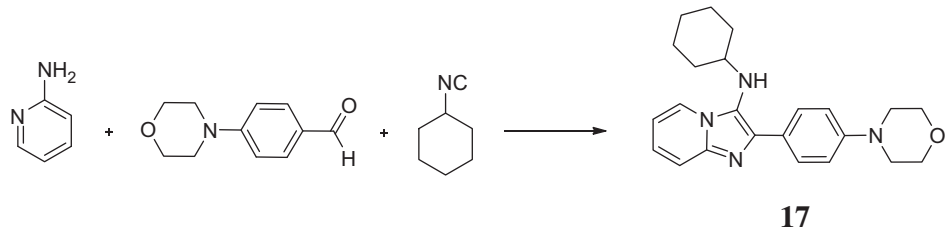

Scheme 1. Synthesis of the imidazo[1,2-*a*]pyridine derivatives, exemplified at compound **17**. Reagents and conditions: acetic acid (99%), MeOH; rt, overnight.

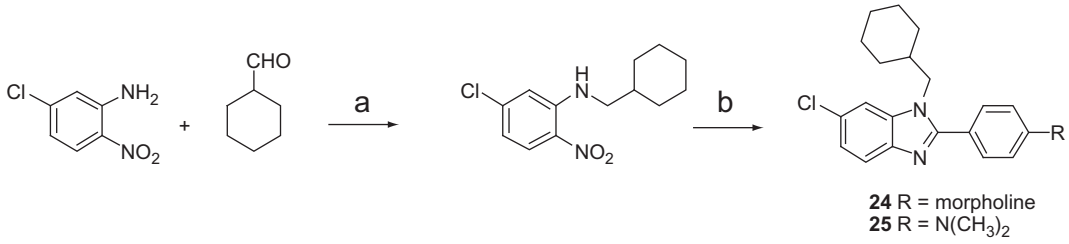

Scheme 2. Synthesis of benzimidazole derivatives **24** and **25**. Reagents and conditions: (a) nitroaniline, glacial acetic acid, $NaBH(OAc)_3$, DCE, rt, overnight. (b) N,N-substituted *p*-amino benzaldehyde, $Na_2S_2O_4$, EtOH/DMSO, 80 °C, 48 h.

The synthesis of compounds **5**, **14–23** and **26–31** follows a multicomponent procedure as outlined in Scheme 1.[19] The whole structure series was prepared by means of these multicomponent reactions, which are an excellent source for novel bioactive compounds.[20] Especially the isocyanide-based reactions have proven to provide drug-like compounds with high diversity and optimization potential. In brief, the respective benzaldehyde and aminopyridine (or structural analogs) were dissolved together in absolute methanol (MeOH). Next, cyclohexyl isonitrile and glacial acetic acid were added to the solution. Overnight stirring resulted in precipitation of the product. Purification was subsequently done by recrystallization from ethanol/ethyl acetate (EtOAc).

Benzimidazole derivatives **24** and **25** were synthesized as outlined in Scheme 2 within a modified two-step procedure described by Yang et al.[21] Briefly, 3-chloro-5-nitro-aniline reacted with cyclohexanecarboxaldehyde in a reductive amination as described by Abdel-Magid et al.[22] In the following step, a reductive cyclization with the corresponding aldehyde in presence of sodium dithionite ($Na_2S_2O_4$) was carried out. Compounds **24** and **25** were purified by recrystallization from ethanol.

The characterization of all compounds for their 5-LO inhibitory activity was carried out in intact polymorphonuclear leukocytes (PMNL) as well as in a cell-free system (S100). The PMNL assay provides cellular conditions and is useful to assess membrane permeation properties of the compounds. The latter assay (S100) was chosen to distinguish between direct inhibition of 5-LO (comparable inhibition in both assays) and indirect effects like FLAP or $cPLA_2$ interaction (lower inhibitory activity in the cell-free assay).[23] Please consider that the discussion is focused on the IC_{50} values of the PMNL assay to regard intracellular bioavailability. However, almost all compounds were equally active in both assays, indicating direct 5-LO inhibitory effects and overall, the potencies measured by both methods correlate well for most of the compounds. Outliers that diverged from this correlation (cf. correlation-plot, Supplementary data Figure S5) are discussed in each case. Detailed information about the assay conditions and dose-response curves of all tested compounds are provided as Supplementary data. BWA4C,[24] another well-established iron-ligand type 5-LO inhibitor, was used as control reference compound in both assays (IC_{50} values of 0.05 μM (PMNL S100) and 0.08 μM (intact PMNL) (Table 1), which is similar to the literature[24]).

In order to investigate the underlying SAR and to optimize the structure of compounds **1** and **2** with respect to 5-LO inhibition, we investigated the influence of different substituents at the central imidazo[1,2-*a*]pyridine core (part A) and the additional aromatic center (part B, see Fig. 1) on inhibition of 5-LO product formation. The cyclohexyl amino moiety was kept constant within the complete SAR study, due to the fact that this group has previously turned out as relevant feature for the potency of 5-LO inhibition.[18]

In the first part of our study, we performed a preliminary screening of commercially available compounds exhibiting the imidazo[1,2-*a*]pyridine core of the Asinex database (www.asinex.com, Moscow, Russia) (Table 1). Among those, compound **3** with

Table 1
Inhibition of 5-LO product formation (in intact PMNL and cell-free S100) by test compounds from the preliminary screening[a]

Compound	Structure	5-LO product formation IC_{50} (μM)	
		PMNL	S100
3*	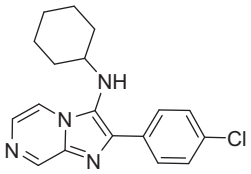	2.3	21.5
4*	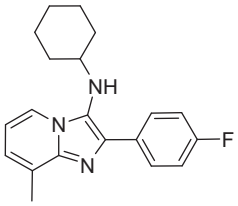	2.1	1.2
5	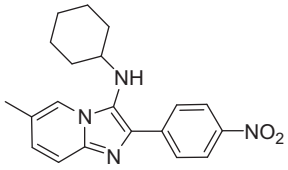	1.53	>30
6*	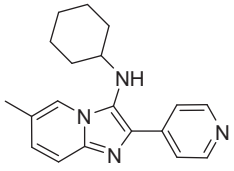	7.2	7.7
7*	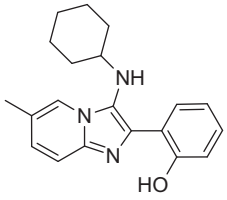	1.9	1.8
8*	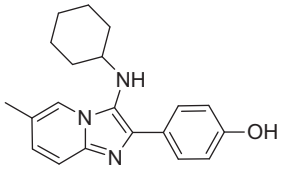	2.0	0.6
9*	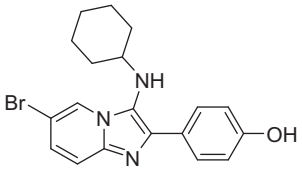	1.1	0.9
10*	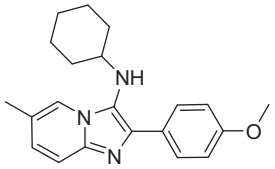	1.3	0.5
11*	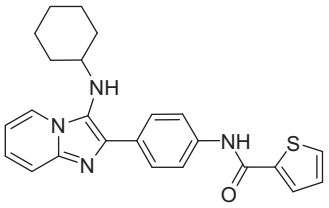	0.4	0.4

(*continued on next page*)

Table 1 (*continued*)

Compound	Structure	5-LO product formation IC_{50} (μM)	
		PMNL	S100
12*	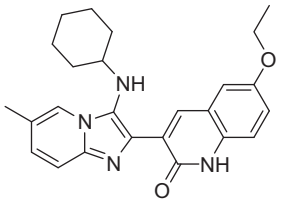	1.8	21.6
13*	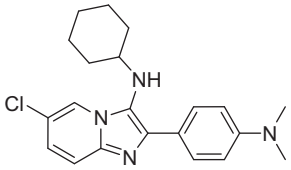	0.1	0.08
BWA4C	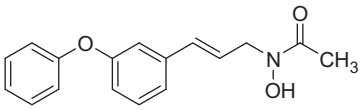	0.08	0.05

[a] The asterisk (*) indicates commercially available compounds purchased from Asinex.

an imidazo[1,2-*a*]pyrazine scaffold and an electron withdrawing *para*-chloro group in part B showed a decreased inhibitory activity of 5-LO product formation (IC_{50} = 2.3 μM) compared to compounds **1** and **2**.

The other compounds **4–13** showed broad structural variations in part B and rather marginal modifications at the central imidazo[1,2-*a*]pyridine core (part A). Within those, compound **4** features a methyl-substituted (position 8) imidazo[1,2-*a*]pyridine scaffold and a *para*-fluoro residue at part B. This compound exhibited the same decreased inhibitory potential as compound **3** (IC_{50} = 2.1 μM).

Six compounds of this screening kept a methyl group at position 6 in part A with different substituents in part B (**5**–**8**, **10**, **12**). Introduction of *para*-nitro (**5**), -hydroxyl (**8**) or -methoxy (**10**) in part B resulted in IC_{50} values of 1.53, 2.0 and 1.3 μM, respectively. The hydroxyl group in *ortho* position (**7**) did not alter the inhibitory activity (IC_{50} = 1.9 μM) at all. On the contrary, introduction of *para*-hydroxy in part B combined with a bromo moiety in part A (position 6) (**9**) resulted in a marginal higher potency (IC_{50} = 1.1 μM). Furthermore, the replacement of the phenyl moiety in part B by an unsubstituted pyridine (**6**) turned out to be even less effective (IC_{50} = 7.2 μM) but the replacement with a bulky substituent (**12**) did not alter the inhibitory potency (IC_{50} = 1.8 μM) in intact cells.

The introduction of a bulky substituent in *para*-position at part B (**11**) finally led to a potent inhibition of 5-LO product formation (IC_{50} = 0.4 μM). The most potent compound from this screening was found in **13** which displays structural similarity to the previously identified compound **2**, containing a *para*-dimethylamino group in part B. The introduction of a chloro moiety in part A (position 6) resulted in a six-fold higher potency in inhibiting 5-LO product formation (IC_{50} = 0.1 μM).

In summary, all compounds of the preliminary screening were able to inhibit 5-LO product formation at least at low micromolar ranges. The highest potency was achieved by introduction of a *para*-dimethylamino substitution in compound **13** or by the introduction of an additional bulky moiety in part B (**11**).

Considering the inhibitory activity in the cell-free S100 assay, most compounds showed a similar potency compared to the cellular assay. This led us to the conclusion that our presented compounds directly interact with 5-LO. Interestingly, three compounds **3**, **5** and **12** were dramatically less active in the cell-free assay (IC_{50} >20 μM) compared to intact cells. Compound **3** with the imidazo[1,2-*a*]pyrazine scaffold approved the importance of the imidazo[1,2-*a*]pyridine scaffold for direct 5-LO binding. Further the nitro group (**5**) or the bulky substituent of compound **12** in part B seems to disturb the binding to the 5-LO protein. The potent inhibitory activity in intact PMNL might be an indicator for indirect inhibition of 5-LO product formation possibly by an interaction with FLAP or $cPLA_2$, which has to be elucidated.

For systematic investigation of the SAR, we used a synthetic strategy based on the one-pot procedure described by Groebke et al.[19] Thereby, the most potent compounds **2** and **13** served as structural templates. Within this part of the study, we focused on the investigation of the substitution in position 6 (part A) as well as the amino group at the backbone (Table 2). As additional computational binding studies gave us a hint for the binding mode of these compounds,[25] we designed derivatives expected to provide shielding of the bound inhibitor from the solvent by extending the dimethylamino moiety in part B of compound **2** to a morpholine group. The yielded compound **14** (IC_{50} = 0.16 μM) showed a three-fold higher potency compared to compound **2** supporting our binding mode hypothesis for this compound pair.[25] Consequently, we next synthesized compound **15** combining the substituents of compound **14** (morpholine moiety in part B) and **13** (chloro residue in part A). The activity of **15** was comparable to compound **13** and **14** (IC_{50} = 0.17 μM). The replacement of chloro- by a slightly bigger bromo-moiety in compound **16** did not alter activity (IC_{50} = 0.15 μM). Removal of the halogen in this position (**17**) led only to a slightly decreased potency (IC_{50} = 0.42 μM) compared to compound **14**. Due to the promising inhibitory activity of these morpholine derivatives, we molecular pharmacologically characterized the inhibitory mode of action of the most potent representative, compound **14**, in a second study.[25] This compound shows direct, allosteric and selective inhibition of 5-LO.[25] It has distinct properties from the three known classes of 5-LO inhibitors (iron-ligand type, redox type, and non-redox type inhibitors[12]) and lacks several characteristic drawbacks known for the class of nonredox type 5-LO inhibitors: The inhibitory efficacy of compound **14** is neither influenced by the redox tone in the cell or the concentration of exogenous AA nor by the stimulus for 5-LO activation, factors crucial for the efficacy of 5-LO inhibitors in vivo.[26,27] These findings encouraged us to further investigate this scaffold class.

Table 2
Influence of imidazo[1,2-*a*]pyridine substituents on inhibition of 5-LO product formation

Compound	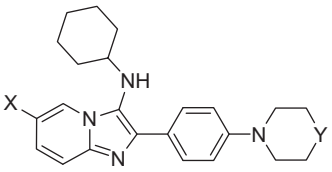			
			5-LO product formation IC_{50} (μM)	
	X	Y	PMNL	S100
14	CH_3	O	0.16	0.1
15	Cl	O	0.17	0.27
16	Br	O	0.15	0.77
17	H	O	0.42	0.51
18	Cl	CH_2	0.14	0.06
19	Cl	*N*-Boc	0.47	0.06

Table 3
Influence of heterocyclic core replacement on inhibition of 5-LO product formation

Compound	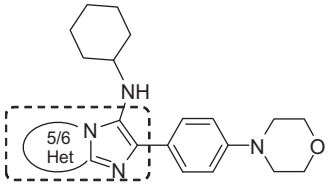	5-LO product formation IC_{50} (μM)	
		PMNL	S100
17	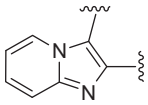	0.42	0.51
20	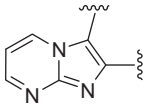	3.55	6.10
21	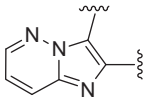	1.76	2.22
22	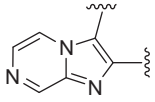	1.8	2.62
23	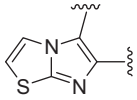	1.50	0.61
24	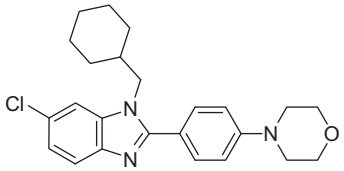	1.2	5.8
25	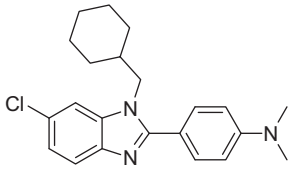	0.5	>10

To complete the sub-series based on compound **14**, we kept the chloro-residue at position 6 constant and replaced the morpholine-ring by a piperidine moiety (**18**). This resulted in a marginal increased potency (IC_{50} = 0.14 μM). In contrast, the introduction

Table 4
Influence of lipophilic backbone optimization on inhibition of 5-LO product formation

Compound	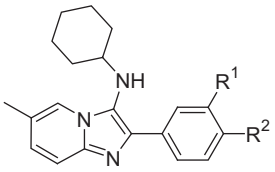		5-LO product formation IC_{50} (μM)	
	R^1	R^2	PMNL	S100
26	OMe	H	1.22	0.43
27	OMe	OMe	1.3	0.72
28	OPh	H	0.5	0.05
29	H	OBn	0.28	0.03
30	H	OPh	0.26	0.08
31	OBn	H	0.43	0.04

of *N*-Boc-piperazine instead of the morpholine-ring (**19**) caused a slight loss of activity (IC_{50} = 0.47 μM). Due to synthetic difficulties we were not able to obtain the deprotected derivative.

All tested derivatives of this sub-series were able to inhibit 5-LO product formation in submicromolar ranges, although it remains to be elucidated if these compounds show the same promising characteristics as compound **14**.

Based on the potent morpholine moiety in part A, we focused on the central imidazo[1,2-*a*]pyridine part and synthesized different bicyclic scaffolds in part A (Table 3). Therefore, we introduced an additional nitrogen resulting in imidazo[1,2-*a*]-pyrimidine (**20**), -pyridazine (**21**), -pyrazine (**22**) and -thiazole (**23**) fused scaffolds, respectively. In summary, introduction of any additional nitrogen to the bicyclic scaffold led to at least four- to eight-fold decreased activity (IC_{50} = 1.5–3.5 μM) compared to the imidazo[1,2-*a*]pyridine scaffold in **17** (IC_{50} = 0.42 μM) corroborating the promising inhibitory potential of the morpholine derivatives.

Furthermore, two benzimidazole derivatives (**24**, **25**) were synthesized as analogs to compounds **13** and **15** which showed a two- to seven-fold decrease of inhibitory activity (IC_{50} = 0.5 and 1.2 μM). Interestingly, both benzimidazole derivatives just weakly inhibited 5-LO product formation in the cell-free assay (IC_{50} >10 and 5.8 μM). Therefore we conclude that additional, indirect effects contribute to its inhibition of 5-LO product formation in the cellular assay.[23] In summary, the initial imidazo[1,2-*a*]pyridine scaffold turned out to exhibit the most potent inhibition of 5-LO product formation. Additional introduction of a methyl- or chloro-residue in position 6 resulted in an increased inhibition of 5-LO product formation.

In order to complete the study of the SAR, we focused again on the lipophilic backbone based on the structure of compound **10** (Table 4)**.** Keeping the methyl group in position 6 (part A) constant, we prepared a set of compounds featuring different ether moieties instead of amines. Introduction of 3- (**26**) or 4-methoxy at part B (**10**) as well as 3,4-dimethoxy-phenyl moieties (**27**) resulted in low micromolar inhibition of 5-LO product formation (IC_{50} = 1.2–1.3 μM). Substitution by the bulkier 3- (**28**) or 4-phenoxy (**30**) as well as 3- (**31**) or 4-benzyloxy (**29**) moieties led to a submicromolar inhibitory activity. The introduction at position 4 resulted in a nearly two-fold higher potency (IC_{50} = 0.26 and 0.28 μM) than the introduction at position 3 (IC_{50} = 0.5 and 0.43 μM). The greater flexibility of the benzyloxy moieties does not seem to have influence on the inhibitory activity compared to the phenoxy substituents. These compounds also inhibit 5-LO product formation in submicromolar concentration ranges in the S100 assay (IC_{50} = 0.03–0.72 μM). The overall correlation between the cell-free and whole cell assay is rather high (R^2 = 0.68) for all tested compounds, however, several outliers could be identified (cf. correlation-plot, Supplementary data Figure S5): Compounds **19**, **28**, **29** and **31** exhibit significantly (p >0.95) higher potency in cell-free assay system than expected. While the Boc carbamate group of compound **19** might be cleaved in whole-cell system, compounds **28**, **29** and **31** might accumulate in cell membrane due to the high lipophilicity.

In summary, we have developed a set of potent 5-LO inhibitors characterized by a central imidazo[1,2-*a*]pyridine scaffold. Starting with a preliminary screening of commercially available substances, we investigated the SAR of broad structural modifications of the imidazo[1,2-*a*]pyridine compounds. Thereby, we were able to identify a series of 5-LO inhibitors which are active in submicromolar concentrations in intact cells and a cell-free system. Imidazo[1,2-*a*]pyridines and related scaffolds were synthetically accessible by means of multicomponent one-pot Groebke reaction. We prepared a set of potent direct 5-LO inhibitors by systematic variation of the heterocyclic core, the core substituents and the phenyl substituents. The most potent compounds show a five- to 10-fold higher inhibitory potency than zileuton (IC_{50} = 0.5–1 μM[11]). This together with the promising molecular pharmacological profile in mind (demonstrated with compound **14**[25]) encourages us for further investigations to develop novel effective anti-inflammatory drugs based on this imidazo[1,2-*a*]pyridine scaffold.

Acknowledgment

The authors thank LOEWE Lipid Signaling Forschungszentrum Frankfurt (LiFF), the Oncogenic Signaling Frankfurt (OSF), the EU (LSHM-CT-2004-0050333) and Fonds der Chemischen Industrie for financial support. E.B. thanks DAAD-La Caixa (Spain) for a fellowship.

Supplementary data

Supplementary data (synthetic conditions, ^1H and ^{13}C NMR-data of intermediates and final compounds, mass spectrometry and combustion analysis data of final compounds, assay systems) associated with this article can be found, in the online version, at doi:10.1016/j.bmcl.2012.01.038.

References and notes

1. Samuelsson, B.; Dahlén, S. E.; Lindgren, J. A.; Rouzer, C. A.; Serhan, C. N. *Science* **1987**, *237*, 1171.
2. Dahlén, S. E.; Hedqvist, P.; Hammarström, S.; Samuelsson, B. *Nature* **1980**, *288*, 484.
3. Peters-Golden, M.; Henderson, W. R. *N. Engl. J. Med.* **2007**, *357*, 1841.
4. Werz, O.; Steinhilber, D. *Pharmacol. Ther.* **2006**, *112*, 701.
5. Miller, D. K.; Gillard, J. W.; Vickers, P. J.; Sadowski, S.; Léveillé, C.; Mancini, J. A.; Charleson, P.; Dixon, R. A.; Ford-Hutchinson, A. W.; Fortin, R. *Nature* **1990**, *343*, 278.
6. Woods, J. W.; Evans, J. F.; Ethier, D.; Scott, S.; Vickers, P. J.; Hearn, L.; Heibein, J. A.; Charleson, S.; Singer, I. I. *J. Exp. Med.* **1993**, *178*, 1935.
7. Rådmark, O.; Werz, O.; Steinhilber, D.; Samuelsson, B. *Trends Biochem. Sci.* **2007**, *32*, 332.
8. Ford-Hutchinson, A. W.; Bray, M. A.; Doig, M. V.; Shipley, M. E.; Smith, M. J. *Nature* **1980**, *286*, 264.
9. Tjonahen, E.; Oh, S. F.; Siegelman, J.; Elangovan, S.; Percarpio, K. B.; Hong, S.; Arita, M.; Serhan, C. N. *Chem. Biol.* **2006**, *13*, 1193.
10. Rådmark, O.; Samuelsson, B. *J. Intern. Med.* **2010**, *268*, 5.
11. Carter, G. W.; Young, P. R.; Albert, D. H.; Bouska, J.; Dyer, R.; Bell, R. L.; Summers, J. B.; Brooks, D. W. *J. Pharmacol. Exp. Ther.* **1991**, *256*, 929.
12. Ford-Hutchinson, A. W.; Gresser, M.; Young, R. N. *Annu. Rev. Biochem.* **1994**, *63*, 383.
13. Okunishi, K.; Peters-Golden, M. *Biochim. Biophys. Acta* **2011**, *1810*, 1096.
14. McMillan, R. M.; Walker, E. R. *Trends Pharmacol. Sci.* **1992**, *13*, 323.
15. Steinhilber, D. *Curr. Med. Chem.* **1999**, *6*, 71.
16. Nasser, S. M.; Bell, G. S.; Hawksworth, R. J.; Spruce, K. E.; MacMillan, R.; Williams, A. J.; Lee, T. H.; Arm, J. P. *Thorax* **1994**, *49*, 743.
17. Turner, C. R.; Smith, W. B.; Andresen, C. J.; Eggler, J. F.; Watson, J. W. *Inflamm. Res.* **1996**, *45*, 42.
18. Hofmann, B.; Franke, L.; Proschak, E.; Tanrikulu, Y.; Schneider, P.; Steinhilber, D.; Schneider, G. *ChemMedChem* **2008**, *3*, 1535.
19. Groebke, K.; Weber, L.; Mehlin, F. *Synlett* **1998**, *1998*, 661.

20. Tietze, L. F.; Modi, A. *Med. Res. Rev.* **2000**, *20*, 304.
21. Yang, D.; Fokas, D.; Li, J.; Yu, L.; Baldino, C. M. *Synthesis* **2005**, 47.
22. Abdel-Magid, A. F.; Carson, K. G.; Harris, B. D.; Maryanoff, C. A.; Shah, R. D. *J. Org. Chem.* **1996**, *61*, 3849.
23. Werz, O. *Planta Med.* **2007**, *73*, 1331.
24. Tateson, J. E.; Randall, R. W.; Reynolds, C. H.; Jackson, W. P.; Bhattacherjee, P.; Salmon, J. A.; Garland, L. G. *Br. J. Pharmacol.* **1988**, *94*, 528.
25. Wisniewska, J. M.; Rödl, C. B.; Kahnt, A. S.; Buscató, E.; Ulrich, S.; Tanrikulu, Y.; Achenbach, J.; Rörsch, F.; Grösch, S.; Schneider, G.; Cinatl, J., Jr.; Proschak, E.; Steinhilber, D.; Hofmann, B. *Biochem. Pharmacol.* **2012**, *83*, 228.
26. Werz, O.; Szellas, D.; Henseler, M.; Steinhilber, D. *Mol. Pharmacol.* **1998**, *54*, 445.
27. Fischer, L.; Szellas, D.; Rådmark, O.; Steinhilber, D.; Werz, O. *FASEB J.* **2003**, *17*, 949.

Supporting Information

SAR-study on a new class of imidazo[1,2-*a*]pyridine-based inhibitors of 5-lipoxygenase

Martina Hieke, Carmen B. Rödl, Joanna M. Wisniewska, Estel.la Buscató, Holger Stark, Manfred Schubert-Zsilavecz, Dieter Steinhilber, Bettina Hofmann and Ewgenij Proschak

Contents:

I Synthetic conditions.

The structures of all tested compounds were confirmed by ^{1}H-NMR, ^{13}C-NMR and mass spectrometry (ESI). The purities of the tested compounds were determined by combustion analysis and are 98% or higher. Commercial chemicals and solvents were reagent grade and used without further purification. ^{1}H and ^{13}C-NMR spectra were measured in DMSO-*d6* or $CDCl_3$ on a Bruker ARX 300 AV 200 spectrometer. Chemical shifts are reported in parts per million using tetramethylsilane (TMS) as internal standard. Mass spectra were obtained on a Fissous Instruments VG Platform 2 spectrometer measuring in the positive- or negative-ion mode (ESI-MS system). Combustion analysis was performed by the Microanalytical Laboratory of the Institute of Organic Chemistry and Chemical Biology, Goethe University Frankfurt, on an Elemental Vario Micro Cube. The analytical characterization of all compounds is provided in the supporting information.

General procedure for preparation of imidazo[1,2-*a*]pyridine derivatives 5, 14-23, 26-31.

The synthesis of compounds **5**, **14-23** and **26-31** follows a multi-component procedure described by Groebke *et al.*[1] N-Cyclohexyl-2-(4-morpholinophenyl)imidazo[1,2-*a*]pyridin-3-amine **17**: 0.30 g (3.1 mmol) 2-aminopyridine and 0.60 g (3.1 mmol) 4-morpholino-benzaldehyde were stirred with glacial acetic acid and 35 mL anhydrous MeOH, then 0.35 g (3.1 mmol) cyclohexyl isocyanide was added. After 18 h the reaction mixture was quenched with 5 mL 2N HCl to destroy the residual isocyanide. MeOH was removed under reduced pressure and 50 mL saturated $NaHCO_3$ solution was added. The product was extracted with EtOAc (3 x 40 mL) and the solvent was removed under reduced pressure. The purification was completed by recrystallization from EtOAc/MeOH yielding 0.50 g (42.2%) yellow solid.

Reagents and Conditions of one-pot inhibitors 5, 14-23, 26-31

	Amine in g (mmol)	Cyclohexyl-isonitrile in g (mmol)	Aldehyde in g (mmol)	Acetic acid in g (mmol)	Yield in g (%)	Product
5	0.50 (4.6)	0.42 (3.9)	0.58 (3.9)	0.48 (8.0)	0.50 (37%)	Orange solid
14	1.00 (9.2)	0.84 (7.6)	1.47 (7.6)	0.89 (14.8)	1.80 (60%)	Yellow solid
15	0.27 (2.1)	0.23 (2.1)	0.4 (2.1)	0.25 (4.2)	0.49 (56.4%)	Yellow solid
16	1.50 (8.7)	0.79 (7.2)	1.38 (7.2)	0.42 (7.2)	2.3 (70%)	Yellow solid
17	0.30 (3.1)	0.35 (3.1)	0.60 (3.1)	0.37 (6.2)	0.50 (42.2%)	Yellow solid

18	0.27 (2.1)	0.23 (2.1)	0.40 (2.1)	0.25 (4.2)	0.54 (63.1%)	Yellow solid
19	0.27 (2.1)	0.23 (2.1)	0.61 (2.1)	0.25 (4.2)	0.51 (47.9%)	Yellow solid
20	0.20 (2.1)	0.23 (2.1)	0.40 (2.1)	0.25 (4.2)	0.50 (63%)	Yellow solid
21	0.30 (3.1)	0.35 (3.1)	0.60 (3.1)	0.37 (6.2)	0.51 (43.8%)	Yellow solid
22	0.30 (3.1)	0.35 (3.1)	0.60 (3.1)	0.37 (6.2)	0.78 (67%)	White solid
23	0.16 (1.6)	0.17 (1.6)	0.30 (1.6)	0.20 (3.2)	0.15 (24.8%)	White solid
26	0.36 (3.3)	0.30 (2.7)	0.43 (2.7)	0.33 (5.5)	0.58 (64.3%)	White solid
27	0.36 (3.3)	0.30 (2.7)	0.46 (2.7)	0.33 (5.5)	0.76 (76%)	White solid
28	0.36 (3.3)	0.30 (2.7)	0.54 (2.7)	0.33 (5.5)	0.87 (80%)	White solid
29	0.36 (3.3)	0.30 (2.7)	0.58 (2.7)	0.33 (5.5)	0.82 (74.2%)	White solid
30	0.36 (3.3)	0.30 (2.7)	0.54 (2.7)	0.33 (5.5)	0.62 (57.9%)	White solid
31	0.36 (3.3)	0.30 (2.7)	0.58 (2.7)	0.33 (5.5)	0.55 (49%)	White solid

General procedure for the preparation of benzimidazole derivatives 24 and 25:

4-(6-chloro-1-(cyclohexylmethyl)-1H-benzo[d]imidazol-2-yl)-N,N-dimethylaniline **24**: 1.0 g (5.8 mmol) 5-chloro-2-nitroaniline, 1.2 g (11.0 mmol) cyclohexanecarboxaldehyde and 2.0 g (34 mmol) glacial acetic acid were dissolved in 15 mL 1,2-dichloroethane. Then 3.3 g (16.2 mmol) sodium triacetoxyborohydride was added and the mixture was stirred at RT overnight. The reaction was quenched with 10 mL saturated $NaHCO_3$ solution and the product was extracted with EtOAc (3 x 50 mL). After extraction, the residual aldehyde was removed by washing with 50 mL saturated sodium hydrogensulfite solution. The organic fraction was dried over $MgSO_4$ and the solvent was removed under reduced pressure. The orange product (0.82 g; 53 %) was recrystallized from MeOH and was used directly for the reductive cyclization. 0.27 g (1.0 mmol) of the product, 0.15 g (1.0 mmol) of 4-N,N-dimethylbenzaldehyde and 0.63 g (3.1 mmol) $Na_2S_2O_4$ were refluxed at 80 °C for 48 h in 20 mL EtOH/DMSO (1:1). The solvents were removed under reduced pressure and the reaction mixture was quenched with saturated NH_4OH and washed with water (3 x 10 mL). The purification was completed via crystallization from diethyl ether/EtOH yielding 0.12 g (32%) of an off-white solid.

II Analytical characterization by ^{1}H- and ^{13}C-NMR and mass spectrometry (ESI)

Characterization of N-cyclohexyl-6-methyl-2-(4-nitrophenyl)imidazo[1,2-*a*]pyridin-3-amine 5

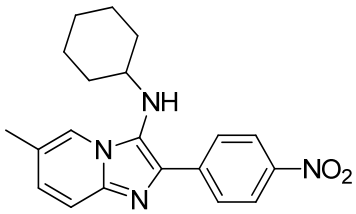

^{1}H-NMR (300.13 MHz, $(CD_3)_2SO$): δ = 1.09-1.75 (m, 10H, Cyclohex-H), 2.31 (s, 3H, Pyr-CH_3), 2.79-2.83 (m, 1H, Cyclohex-C_1H), 4.96-4.98 (d, 1H, J = 6.6Hz, NH), 7.07-7.10 (dd, 1H, J = 1.6; 9.2Hz, Pyr-C_5), 7.40-7.43 (d, 1H, J = 9.1Hz, Pyr-C_4), 8.15 (s, 1H, Pyr-C_7), 8.26-8.30 (d, 2H, J = 2.2; 7.0Hz, Ph-$C_{2/6}$), 8.44-8.47 (dd, 1H, J=1.9; 7.1Hz, Ph-$C_{3/5}$). **^{13}C-NMR** (75.44 MHz, $(CD_3)_2SO$): δ = 17.87 (Pyr-CH_3), 24.53 (2C, Cyclohex-$C_{3/5}$), 25.31 (Cyclohex-C_4), 33.79 (2C, Cyclohex-$C_{2/6}$), 56.81 (Cyclohex-C_1), 116.60 (Pyr-C_4), 120.85 (Pyr-C_7), 121.11 (Pyr-C_6), 123.66 (2C, Ph-$C_{3/5}$), 126.63 (2C, Ph-$C_{2/6}$), 127.87 (Pyr-C_5), 128.10 (Pyr-C_2), 131.94 (Pyr-C_1), 140.14 (Ph-C_1), 141.68 (Pyr-C_9), 145.40 (Ph-C_4). **MS** (ESI +) = *m/e* = 351.2 $[M+1]^+$

Characterization of N-cyclohexyl-6-methyl-2-(4-morpholinophenyl)imidazo[1,2-*a*] pyridin-3-amine 14

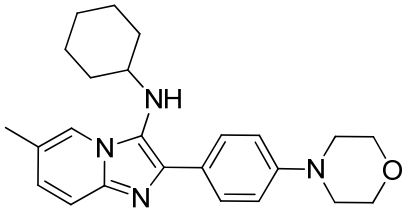

^{1}H-NMR (300.13 MHz, $(CD_3)_2SO$): δ = 1.07-1.71 (m, 10H, Cyclohex-H), 2.37 (s, 3H, -CH_3), 2.78-2.82 (m, 1H, Cyclohex-C_1H), 2.18-2.22 (t, 4H, J = 4.6Hz, Morph-$C_{2/6}H_2$), 3.79-3.83 (t, 4H, J = 4.9Hz, Morph-$C_{3/5}H_2$), 4.58-4.63 (d, 1H, J = 6.2Hz, NH), 6.95-6.98 (m, 3H, Pyr-C_6+Ph-$C_{3/5}$), 7.30-7.33 (d, 1H, J = 9.1Hz, Pyr-C_4), 8.04-8.09 (m, 3H, Pyr-C_5+Ph-$C_{2/6}$). **^{13}C-NMR** (75,44 MHz, $(CD_3)_2SO$): δ = 18.10 (Pyr-CH_3), 24.99 (2C, Cyclohex-$C_{3/5}$), 25.97 (Cyclohex-C_4), 34.04 (2C, Cyclohex-$C_{2/6}$), 48.01 (2C, Morph-$C_{2/6}$), 56.47 (Cyclohex-C_1), 66.70 (2C, Morph-$C_{3/5}$), 114.31 (2C, Ph-$C_{3/5}$), 116.08 (Pyr-C_4), 120.61 (Pyr-C_7), 120.72 (Ph-C_1), 124.15 (Pyr-C_6), 126.31 (Pyr-C_5), 126.42 (Pyr-C_2), 127.49 (2C, Ph-$C_{2/6}$), 139.69 (Pyr-C_9), 149.72 (Ph-C_4). **MS** (ESI +) = *m/e* = 391.3 $[M+1]^+$

Characterization of 6-chloro-N-cyclohexyl-2-(4-morpholinophenyl)imidazo[1,2-*a*]pyridin-3-amine 15

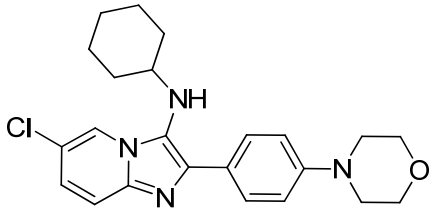

^{1}H-NMR (300.13 MHz, $(CD_3)_2SO$): δ = 1.05-1.80 (m, 10H, Cyclohex-H), 2.81-2.94 (m, 1H, Cyclohex-C_1H), 3.20-3.24 (t, 4H, J = 4.8Hz, Morph-$C_{2/6}H_2$), 3.78-3.82 (t, 4H, J = 4.7Hz, Morph-$C_{3/5}H_2$), 4.79-4.81 (d, 1H, J = 6.2Hz, NH), 7.03-7.07 (d, 2H, J = 9.0Hz, Ph-$C_{3/5}$), 7.19-7.22 (dd, 1H, J = 2.2; 9.0Hz, Pyr-C_5), 7.50-7.54 (d, 1H, J = 9.5Hz, Pyr-C_4), 8.11-8.15 (d, 2H, J = 8.9Hz, Ph-$C_{2/6}$), 8.48-8.49 (d, 1H, J = 1.5Hz, Pyr-C_7). **^{13}C-NMR** (75,44 MHz, $(CD_3)_2SO$): δ = 24.51 (2C, Cyclohex-$C_{3/5}$), 25.37 (Cyclohex-C_4), 33.46 (2C, Cyclohex-$C_{2/6}$), 47.97 (2C, Morph-$C_{2/6}$), 56.36 (Cyclohex-C_1), 66.08 (2C, Morph-$C_{3/5}$), 114.43 (2C, Ph-$C_{3/5}$), 117.14 (Pyr-C_4), 118.36 (Pyr-C_7), 120.72 (Ph-C_1), 124.02 (Pyr-C_6), 124.76 (Pyr-C_5), 125.26 (Pyr-C_2), 127.24 (2C, Ph-$C_{2/6}$), 135.86 (Pyr-C_1), 138.55 (Pyr-C_9), 149.96 (Ph-C_4). **MS** (ESI +) = *m/e* = 411.1 $[M+1]^+$

Characterization of 6-bromo-N-cyclohexyl-2-(4-morpholinophenyl)imidazo[1,2-*a*]pyridin-3-amine 16

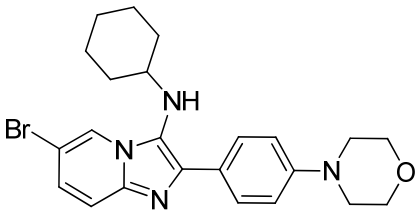

^{1}H-NMR (300.13 MHz, $(CD_3)_2SO$): δ = 1.07-1.73 (m, 10H, Cyclohex-H), 2.81-2.95 (m, 1H, Cyclohex-C_1H), 3.17-3.21 (t, 4H, J = 4.9Hz, Morph-$C_{2/6}H_2$), 3.72-3.75 (t, 4H, J = 4.8Hz, Morph-$C_{3/5}H_2$), 4.97-4.98 (d, 1H, J = 6.1Hz, NH), 7.02-7.05 (d, 2H, J = 8.9Hz, Ph-$C_{3/5}$), 7.49-7.58 (m, 2H, Pyr-$C_{4/5}$), 8.00-8.04 (d, 2H, J = 8.9Hz, Ph-$C_{2/6}$), 8.70-8.73 (d, 1H, J = 1.6Hz, Pyr-C_7). **^{13}C-NMR** (75,44 MHz, $(CD_3)_2SO$): δ = 24.51 (2C, Cyclohex-$C_{3/5}$), 25.37 (Cyclohex-C_4), 33.48 (2C, Cyclohex-$C_{2/6}$), 47.98 (2C, Morph-$C_{2/6}$), 56.38 (Cyclohex-C_1), 66.08 (2C, Morph-$C_{3/5}$), 105.17 (Pyr-C_6), 114.43 (2C, Ph-$C_{3/5}$), 117.52 (Pyr-C_4), 122.80 (Ph-C_1), 124.93 (Pyr-C_5), 125.08 (Pyr-C_2), 125.88 (Pyr-C_7), 127.25 (2C, Ph-$C_{2/6}$), 135.80 (Pyr-C_1), 138.76 (Pyr-C_9), 149.93 (Ph-C_4). **MS** (ESI +) = *m/e* = 455.2 [M+1]

Characterization of N-Cyclohexyl-2-(4-morpholinophenyl)imidazo[1,2-*a*]pyridin-3-amine 17

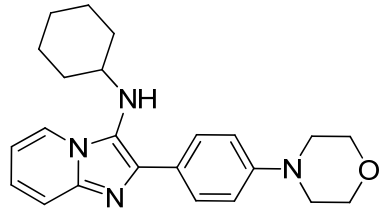

^{1}H-NMR (300.13 MHz, $(CD_3)_2SO$): δ = 1.08-1.71 (m, 10H, Cyclohex-H), 2.79-2.83 (m, 1H, Cyclohex-C_1H), 3.13-3.17 (t, 4H, J = 4.7Hz, Morph-$C_{2/6}H_2$), 3.72-3.76 (t, 4H, J = 4.6Hz, Morph-$C_{3/5}H_2$), 4.65-4.67 (d, 1H, J = 5.5Hz, NH), 6.81-6.85 (t, 1H, J = 6.6Hz, Pyr-C_6), 6.97-6.99 (d, 2H, J = 8.9Hz, Ph-$C_{3/5}$), 7.09-7.14 (t, 1H, J = 8.5Hz, Pyr-C_5), 7.39-7.42 (d, 1H, J = 8.9Hz, Pyr-C_4), 8.07-8.10 (d, 2H, J = 8.8Hz, Ph-$C_{2/6}$), 8.24-8.27 (d, 1H, J = 6.8Hz, Pyr-C_7). **^{13}C-NMR** (75.44 MHz, $(CD_3)_2SO$): δ = 24.45 (2C, Cyclohex-$C_{3/5}$), 25.43 (Cyclohex-C_4), 33.52 (2C, Cyclohex-$C_{2/6}$), 48.11 (2C, Morph-$C_{2/6}$), 56.27 (Cyclohex-C_1), 65.85 (2C, Morph-$C_{3/5}$), 110.93 (Pyr-C_4), 114.45 (2C, Ph-$C_{3/5}$), 116.31 (Pyr-C_6), 123.06 (Pyr-C_5), 123.21 (Pyr-C_7), 124.36 (Ph-C_1), 125.59 (Pyr-C_2), 127.23 (2C, Ph-$C_{2/6}$), 135.25 (Pyr-C_1), 140.33 (Pyr-C_9), 149.72 (Ph-C_4). **MS** (ESI +) = *m/e* = 377.0 $[M+1]^+$.

Characterization of 6-chloro-N-cyclohexyl-2-(4-(piperidin-1-yl)phenyl)imidazo[1,2-*a*]pyridin-3-amine 18

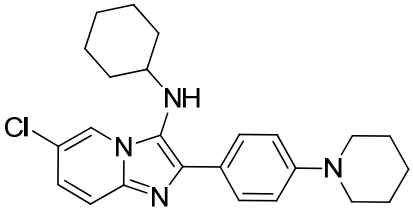

^{1}H-NMR (300.13 MHz, $(CD_3)_2SO$): δ = 0.87-2.26 (m, 17H, Cyclohex-H + Pip-$C_{3-5}H_2$), 3.21-3.25 (t, 4H, Pip-$C_{2/6}H_2$), 6.98-7.01 (d, 2H, J = 9.0Hz, Ph-$C_{3/5}$), 7.09-7.13 (dd, 1H, J = 2.0; 9.4Hz, Pyr-C_5), 7.38-7.42 (d, 2H, Pyr-C_4 + NH), 8.10-8.13 (d, 2H, J = 9.0Hz, Ph-$C_{2/6}$), 8.36 (dd, 1H, J = 2.0Hz, Pyr-C_7). **^{13}C-NMR** (75.44 MHz, $(CD_3)_2SO$): δ = 22.87 (Pip-C_4), 23.56 (2C, Cyclohex-$C_{3/5}$), 24.88 (Cyclohex-C_4), 33.22 (2C, Cyclohex-$C_{2/6}$), 47.98 (2C, Pip-$C_{2/6}$), 56.38 (Cyclohex-C_1), 66.08 (2C, Pip-$C_{3/5}$), 107.87 (Pyr-C_4), 112.84 (2C, Ph-$C_{3/5}$), 117.38 (Pyr-C_7), 120.60 (Ph-C_1), 121.48 (Pyr-C_6), 127.25 (2C, Ph-$C_{2/6}$), 128.36 (Pyr-C_5), 135.24 (Pyr-C_2), 135.80 (Pyr-C_1), 138.76 (Pyr-C_9), 149.93 (Ph-C_4). **MS** (ESI +) = *m/e* = 409.3 $[M+1]^+$

Characterization of tert-butyl 4-(4-(6-chloro-3-(cyclohexylamino)imidazo[1,2-*a*]pyridin-2-yl)phenyl)piperazine-1-carboxylate 19

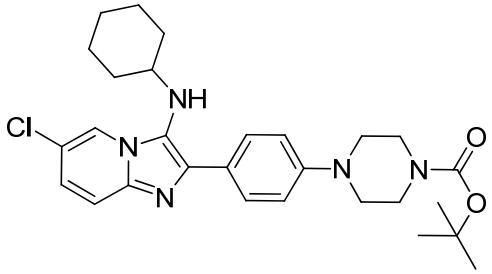

^{1}H-NMR (300.13 MHz, Acetone): δ = 1.18-1.37 (m, 1H, Cyclohex-H), 1.47 (s, 9H, Boc-CH_3), 1.50-1.85 (m, 5H, Cyclohex-H), 2.95-3.07 (m, 1H, Cyclohex-C_1H), 3.20-3.23 (t, 4H, J = 5.4Hz, Pip-$C_{3/5}$), 3.55-3.58 (t, 4H, J = 4.9Hz, Pip-$C_{2/6}$), 7.03-7.06 (d, 2H, J = 9.0Hz, Ph-$C_{2/6}$), 7.11-7.14 (dd, 1H, J = 2.0; 9.4Hz, Pyr-C_5), 7.40-7.44 (dd, 1H, J = 0.7; 9.4Hz, Pyr-C_4), 8.14-8.17 (d, 2H, J = 9.0Hz, Ph-$C_{3/5}$), 8.36 (d, 1H, J = 2.0Hz, Pyr-C_7). **^{13}C-NMR** (75.44 MHz, Acetone): δ = 25.62 (2C, Cyclohex-$C_{3/5}$), 26.54 (Cyclohex-C_4), 28.55 (3C, Boc-CH_3), 34.66 (2C, Cyclohex-$C_{2/6}$), 49.55 (2C, Pip-$C_{2/6}$), 57.37+57.46 (2C, Pip-$C_{3/5}$), 79.74 (Boc-C_1), 116.51 (2C, Ph-$C_{3/5}$), 118.34 (Pyr-C_4), 119.68 (Pyr-C_7), 121.58 (Pyr-C_6), 124.71 (Ph-C_1), 127.15 (Pyr-C_5), 128.68 (2C, Ph-$C_{2/6}$), 139.57 (Pyr-C_1), 140.78 (Pyr-C_2),151.45 (Ph-C_4) 177.10 (COO-). **MS** (ESI +) = *m/e* = 510.7 $[M+1]^+$

Characterization of N-Cyclohexyl-2-(4-morpholinophenyl)-imidazo-[1,2-*a*]pyrimidin-3-amine 20

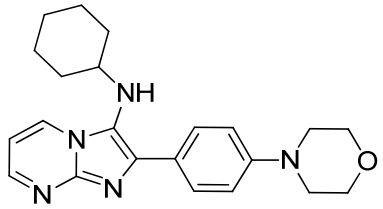

^{1}H-NMR (300.13 MHz, $(CD_3)_2SO$): δ = 1.08-1.71 (m, 10H, Cyclohex-H), 2.81 (m, 1H, Cyclohex-C_1H), 3.15-3.18 (t, 4H, J = 4.7Hz, Morph-$C_{2/6}H_2$), 3.72-3.75 (t, 4H, J = 4.5 MHz, Morph-$C_{3/5}H_2$), 4.76-4.78 (d, 1H, J = 5.7Hz, NH), 6.96-7.06 (m, 3H, Pyr-C_6 + Ph-$C_{3/5}$), 8.09-8.12 (d, 2H, J = 8.8Hz, Ph-$C_{2/6}$), 8.37-8.39 (dd, 1H, J = 1.9; 4.0Hz, Pyr-C_5), 8.65-8.68 (dd, 1H, J = 1.9; 6.7Hz, Pyr-C_7). **^{13}C-NMR** (75.44 MHz, $(CD_3)_2SO$): δ = 24.44 (2C, Cyclohex-$C_{3/5}$), 25.37 (Cyclohex-C_4), 33.49 (2C, Cyclohex-$C_{2/6}$), 47.96 (2C, Morph-$C_{2/6}$), 56.29 (Cyclohex-C_1), 65.76 (2C, Morph-$C_{3/5}$), 107.74 (Pyr-C_6), 113.71 (2C, Ph-$C_{3/5}$), 122.79 (Ph-C_1), 124.80 (Pyr-C_1), 127.60 (2C, Ph-$C_{2/6}$), 130.98 (Pyr-C_7), 136.36 (Pyr-C_2), 143.59 (Pyr-C_9), 148.41 (Ph-C_4), 150.09 (Pyr-C_5). **MS** (ESI+) = *m/e* = 378.2 $[M+1]^+$

Characterization of N-cyclohexyl-2-(4-morpholinophenyl)imidazo[1,2-*b*]pyridazin-3-amine 21

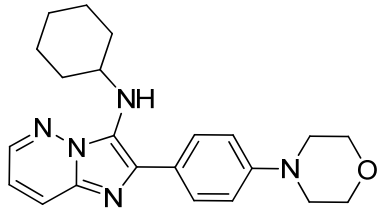

^{1}H-NMR (300.13 MHz, $(CD_3)_2SO$): δ = 1.09-1.76 (m, 10H, Cyclohex-H), 3.08-3.17 (m, 5H, Cyclohex-C_1H + Morph-$C_{2/6}H_2$), 3.72-3.75 (t, 4H, J = 4.6Hz, Morph-$C_{3/5}H_2$), 4.54-4.57 (d, 1H, J = 7.7Hz, NH), 6.99-7.06 (m, 3H, Pyr-C_4 + Ph-$C_{3/5}$), 7.90-7.94 (dd, 1H, J = 1.4; 9.0Hz, Pyr-C_5), 8.08-8.11 (d, 2H, J = 8.8Hz, Ph-$C_{2/6}$), 8.40-8.42 (dd, 1H, J = 1.4; 4.4Hz, Pyr-C_6). **^{13}C-NMR** (75.44 MHz, $(CD_3)_2SO$): δ = 24.94 (2C, Cyclohex-$C_{3/5}$), 25.87 (Cyclohex-C_4), 33.96 (2C, Cyclohex-$C_{2/6}$), 48.48 (2C, Morph-$C_{2/6}$), 55.73 (Cyclohex-C_1), 66.56 (2C, Morph-$C_{3/5}$), 114.97 (2C, Ph-$C_{3/5}$), 115.59 (Pyr-C_5), 124.75 (Ph-C_1), 125.53 (Pyr-C_4), 127.63 (2C, Ph-$C_{2/6}$), 129.08 (Pyr-C_1), 134.46 (Pyr-C_2), 134.76 (Pyr-C_9), 142.97 (Pyr-C_6), 150.50 (Ph-C_4). **MS** (ESI +) = *m/e* = 378.3 $[M+1]^+$

Characterization of N-Cyclohexyl-2-(4-morpholinophenyl)imidazo[1,2-*a*]pyrazin-3-amine 22

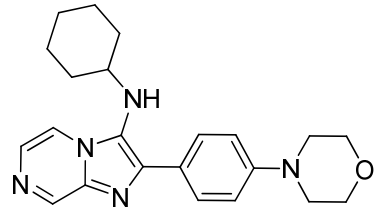

^{1}H-NMR (300.13 MHz, $(CD_3)_2SO$): δ = 1.07-1.71 (m, 10H, Cyclohex-H), 2.82-2.86 (m, 1H, Cyclohex-C_1H), 3.15-3.19 (t, 4H, J = 4.6Hz, Morph-$C_{2/6}H_2$) 3.72-3.75 (t, 4H, J = 4.6Hz, Morph-$C_{3/5}H_2$), 4.92-4.94 (t, 1H, J = 6.7Hz, NH), 6.99-7.03 (d, 2H, J = 9.0Hz, Ph-$C_{3/5}$), 7.79-7.81 (d, 1H, J = 4.6Hz, Pyr-C_7), 8.08-8.11 (d, 2H, J = 8.8Hz, Ph-$C_{2/6}$), 8.30-8.32 (dd, 1H, J = 1.2; 4.6Hz, Pyr-C_6), 8.84-8.84 (d, 1H, J = 1.0Hz, Pyr-C_4). **^{13}C-NMR** (75.44 MHz, $(CD_3)_2SO$): δ = 24.52 (2C, Cyclohex-$C_{3/5}$), 25.34 (Cyclohex-C_4), 33.58 (2C, Cyclohex-$C_{2/6}$), 47.87 (2C, Morph-$C_{2/6}$), 56.34 (Cyclohex-C_1), 66.06 (2C, Morph-$C_{3/5}$), 114.43 (2C, Ph-$C_{3/5}$), 116.05 (Pyr-C_7), 124.39 (Ph-C_1), 126.17 (Pyr-C_1), 127.51 (2C, Ph-$C_{2/6}$), 128.32 (Pyr-C_6), 135.80 (Pyr-C_2), 137.21 (Pyr-C_9), 141.80 (Pyr-C_4), 150.31(Ph-C_4). **MS** (ESI +) = *m/e* = 378.1 $[M+1]^+$

Characterization of N-Cyclohexyl-6-(4-morpholinophenyl)imidazo[2,1-*b*]thiazol-5-amine 23

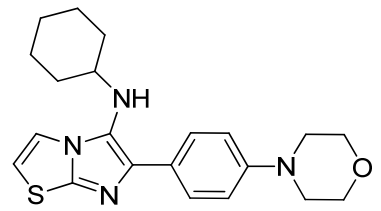

^{1}H-NMR (300.13 MHz, $(CD_3)_2SO$): δ = 1.04-1.75 (m, 10H, Cyclohex-H), 2.75-2.79 (m, 1H, Cyclohex-C_1H), 3.09-3.12 (t, 4H, J = 4.8Hz, Morph-$C_{2/6}H_2$), 3.71-3.74 (t, 4H, J = 4.8Hz, Morph-$C_{3/5}H_2$), 4.49-4.51 (d, 1H, J = 6.0Hz, NH), 6.91-6.94 (d, 2H, J = 8.9Hz, Ph-$C_{3/5}$), 7.10-7.12 (d, 1H, J = 4.5Hz, Pyr-C_5), 7.67-7.68 (d, 1H, J = 4.5Hz, Pyr-C_6), 7.89-7.92 (d, 2H, J = 8.8Hz, Ph-$C_{2/6}$). **^{13}C-NMR** (75.44 MHz, $(CD_3)_2SO$): δ = 24.44 (2C, Cyclohex-$C_{3/5}$), 25.46 (Cyclohex-C_4), 33.42 (2C, Cyclohex-$C_{2/6}$), 48.30 (2C, Morph-$C_{2/6}$), 48.30 (Cyclohex-C_1), 66.12 (2C, Morph-$C_{3/5}$), 111.52 (Pyr-C_5), 114.60 (2C, Ph-$C_{3/5}$), 118.31 (Pyr-C_1), 126.16 (2C, Ph-$C_{2/6}$), 126.76 (Ph-C_1), 135.61 (Pyr-C_2), 143.18 (Pyr-C_6), 149.10 (Ph-C_4). **MS** (ESI +) = *m/e* = 383.3 $[M+1]^+$

Characterization of 4-(6-chloro-1-(cyclohexylmethyl)-1H-benzo[d]imidazol-2-yl)-N,N-dimethylaniline 24

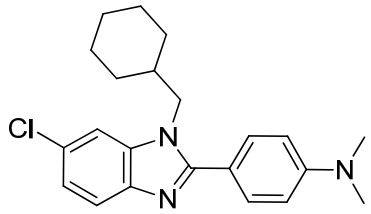

^{1}H-NMR (300.13 MHz, $(CD_3)_2SO$): δ = 0.73-1.63 (m, 11H, Cyclohex-H), 3.03 (s, 6H, N-CH_3), 4.19-4.22 (d, 2H, J = 8.7Hz, Cyclohex-CH_2), 6.80-6.83 (d, 2H, J = 10.4Hz, Ph-$C_{3/5}$), 7.15-7.20 (dd, 1H, 1.6; 9.0Hz, Pyr-C_5), 7.56-7.62 (m, 3H, Ph-$C_{2/6}$+Pyr-C_4), 7.76 (d, 1H, J = 1.8Hz, Pyr-C_7). **^{13}C-NMR** (75.44 MHz, $(CD_3)_2SO$): δ = 24.95 (2C, Cyclohex-$C_{3/5}$), 25.59 (Cyclohex-C_4), 29.77 (2C, Cyclohex-$C_{2/6}$), 37.38 (Cyclohex-C_1), 49.93 (Cyclohex-CH_2), 110.85 (Pyr-C_4), 111.55 (2C, Ph-$C_{3/5}$), 117.17 (Pyr-C_7), 119.69 (Ph-C_1), 121.75 (Pyr-C_5), 126.05 (Pyr-C_6), 129.93 (2C, Ph-$C_{2/6}$), 137.01 (Pyr-C_8), 141.35 (Pyr-C_9), 150.77 (Pyr-C_2), 155.25 (Ph-C_4). **MS** (ESI +) = *m/e* = 368.2 $[M+1]^+$.

Characterization of 4-(4-(6-chloro-1-(cyclohexylmethyl)-1H-benzo[d]imidazol-2-yl)phenyl)morpholine 25

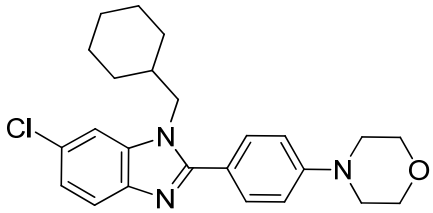

^{1}H-NMR (300.13 MHz, $(CD_3)_2SO$): δ = 1.04-1.69 (m, 10H, Cyclohex-H), 3.21-3.23 (m, 4H, Morph-$C_{2/6}H_2$), 3.80-3.83 (m, 4H, Morph-$C_{3/5}H_2$), 4.26-4.29 (d, 2H, J = 8.7Hz, Cyclohex-CH_2), 7.11-7.15 (d, 2H, J = 10.5Hz, Ph-$C_{3/5}$), 7.24-7.28 (dd, 1H, 1.6; 9.0Hz, Pyr-C_5), 7.51-7.65 (m, 3H, Ph-$C_{2/6}$+Pyr-C_4), 7.84 (d, 1H, J = 1.8Hz, Pyr-C_7). **^{13}C-NMR** (75.44 MHz, $(CD_3)_2SO$): δ = 24.93 (2C, Cyclohex-$C_{3/5}$), 25.58 (Cyclohex-C_4), 29.76 (2C, Cyclohex-$C_{2/6}$), 37.39 (Cyclohex-C_1), 47.35 (2C, Morph-$C_{2/6}$), 51.02 (Cyclohex-CH_2), 73.42 (2C, Morph-

$C_{3/5}$), 110.97 (Pyr-C_4), 114.10 (2C, Ph-$C_{3/5}$), 119.89 (Pyr-C_7), 120.20 (Ph-C_1), 121.89 (Pyr-C_5), 126.29 (Pyr-C_6), 129.97 (2C, Ph-$C_{2/6}$), 135.11 (Pyr-C_8), 136.94 (Pyr-C_9), 151.49 (Pyr-C_2), 154.79 (Ph-C_4). **MS** (ESI +) = *m/e* = 410.3 $[M+1]^+$.

Characterization of N-cyclohexyl-2-(3-methoxyphenyl)-6-methylimidazo[1,2-*a*]pyridin-3-amine 26

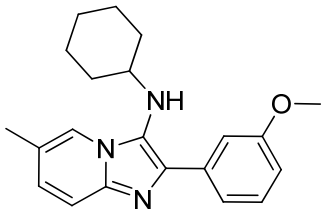

^{1}H-NMR (300.13 MHz, $(CD_3)_2SO$): δ = 1.08-1.71 (m, 10H, Cyclohex-H), 2.30 (s, 3H, Pyr-CH'), 2.85 (m, 1H, Cyclohex-C_1H), 3.80 (s, 3H, O-CH_3), 4.70-4.72 (d, 1H, J = 5.6Hz, NH), 6.99-7.03 (d, 1H, J = 9.1Hz, Pyr-C_5), 7.26-7.39 (m, 2H, Ph-$C_{2/6}$), 7.77-7.80 (m, 2H, Ph-C_5+Pyr-C_4), 8.10 (s, 1H, Pyr-C_7). **^{13}C-NMR** (75.44 MHz, $(CD_3)_2SO$): δ = 17.90 (Pyr-CH_3), 24.44 (2C, Cyclohex-$C_{3/5}$), 25.39 (Cyclohex-C_4), 33.47 (2C, Cyclohex-$C_{2/6}$), 54.91 (O-CH_3), 56.36 (Cyclohex-C_1), 111.27 (Ph-C_2), 112.70 (Ph-C_4), 116.20 (Pyr-C_4), 118.74 (Ph-C_6), 120.35 (Pyr-C_7), 120.58 (Pyr-C_1), 125.80 (Pyr-C_6), 126.77 (Ph-C_5), 129.11 (Pyr-C_5), 134.39 (Ph-C_1), 136.26 (Pyr-C_2), 139.49 (Pyr-C_9), 159.19 (Ph-C_3). **MS** (ESI +) = *m/e* = 336.0 $[M+1]^+$

Characterization of N-cyclohexyl-2-(3,4-dimethoxyphenyl)-6-methylimidazo[1,2-*a*]pyridin-3-amine 27

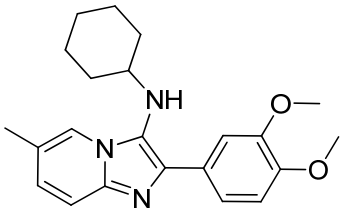

^{1}H-NMR (300.13 MHz, $(CD_3)_2SO$): δ = 1.10-1.71 (m, 10H, Cyclohex-H), 2.29 (s, 3H, Pyr-CH_3), 2.80 (m, 1H, Cyclohex-C_1H), 3.88 (s, 3H, O-CH_3), 3.81 (s, 3H, O-CH_3), 4.65-4.67 (d, 1H, J = 5.4Hz, NH), 6.97-7.0 (m, 2H, Ph-$C_{5/6}$) 7.33-7.37 (d, 1H, J = 9.1Hz, Pyr-C_5), 7.73-7.81 (m, 2H, Ph-C_2+Pyr-C_4), 8.1 (s, 1H, Pyr-C_7). **^{13}C-NMR** (75.44 MHz, $(CD_3)_2SO$): δ = 17.8 (Pyr-CH_3), 24.42 (2C, Cyclohex-$C_{3/5}$), 25.46 (Cyclohex-C_4), 33.52 (2C, Cyclohex-$C_{2/6}$), 55.33+55.49 (2C, O-CH_3), 56.23 (Cyclohex-C_1), 110.0 (Ph-C_2), 111.58 (Ph-C_5), 115.92 (Pyr-C_4), 118.89 (Ph-C_6), 120.17 (Pyr-C_7), 120.54 (Pyr-C_1), 124.43 (Pyr-C_6), 126.41 (Ph-C_1), 127.72 (Pyr-C_5), 134.81 (Pyr-C_2), 139.45 (Pyr-C_9), 147.75 (Ph-C_4), 148.41 (Ph-C_3). **MS** (ESI +) = *m/e* = 366.2 $[M+1]^+$

Characterization of N-Cycylohexyl-6-methyl-2-(3-phenoxyphenyl)imidazo[1,2-*a*]pyridin-3-amine 28

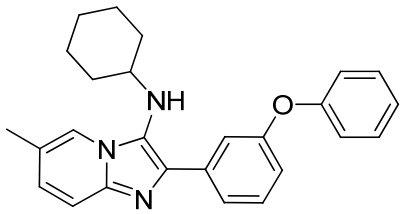

^{1}H-NMR (300.13 MHz, $(CD_3)_2SO$): δ = 1.03-1.58 (m, 10H, Cyclohex-H), 2.28 (s, 3H, Pyr-CH_3), 2.74 (m, 1H, Cyclohex-C_1H), 4.62-4.64 (d, 1H, J = 5.8Hz, NH), 6.96-7.43 (m, 9H, Ph-H+Ph'-H), 7.85 (s, 1H, Pyr-C_7), 7.96-7.99 (dd, 1H, Pyr-C_5), 8.06 (s, 1H, Pyr-C_4). **^{13}C-NMR** (75.44 MHz, $(CD_3)_2SO$): δ = 17.87 (Pyr-CH_3), 24.50 (2C, Cyclohex-$C_{3/5}$), 25.34 (Cyclohex-C_4), 33.34 (2C, Cyclohex-$C_{2/6}$), 56.35 (Cyclohex-C_1), 115.91 (Ph-C_2), 116.24 (Pyr-C_4), 117.15 (Ph-C_4), 118.77 (2C, Ph'-$C_{2/6}$), 120.45 (Ph-C_6), 120.64 (Pyr-C_1), 121.34 (Ph'-C_4), 123.35 (Pyr-C_7), 125.81 (Pyr-C_6), 126.90 (Ph-C_5), 129.76 (Pyr-C_5), 130.01 (2C, Ph'-$C_{3/5}$), 133.61 (Ph-C_1), 136.79 (Pyr-C_2), 139.53 (Pyr-C_9), 156.81 (Ph'-C_1), 156.85 (Ph-C_3). **MS** (ESI +) = *m/e* = 398.4 $[M+1]^+$

Characterization of 2-(4-(benzyloxy)phenyl)-N-cyclohexyl-6-methylimidazo[1,2-*a*]pyridin-3-amine 29

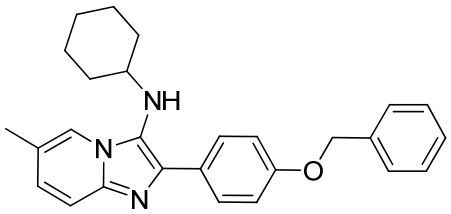

^{1}H-NMR (300.13 MHz, $(CD_3)_2SO$): δ = 1.07-1.70 (m, 10H, Cyclohex-H), 2.29 (s, 3H, Pyr-CH_3), 2.85 (m, 1H, Cyclohex-C1H), 4.62-4.64 (d, 1H, J=5.8Hz, NH), 5.12 (s, 2H, Ph-O-CH_2), 6.97-7.06 (m, 3H, Ph'-H), 7.32-7.48 (m, 6H, Ph-H+Ph'-H), 8.06-8.14 (m, 3H, Pyr-C4/5/7). **^{13}C-NMR** (75.44 MHz, $(CD_3)_2SO$): δ =17.37 (Pyr-CH_3), 24.25 (2C, Cyclohex-$C_{3/5}$), 25.00 (Cyclohex-C_4), 32.93 (2C, Cyclohex-$C_{2/6}$), 55.89 (Cyclohex-C_1), 69.34 (Ph-O-CH_2), 108.86 (Pyr-C_4), 111.48 (Pyr-C_7), 112.60 (2C, Ph-$C_{3/5}$), 115.82 (Pyr-C_6), 117.20 (2C, Ph'-$C_{2/6}$), 121.77 (2C, Ph'-$C_{3/5}$), 125.57 (Ph-C_1), 126.48 (Ph'-C_4), 127.63 (Pyr-C_5), 127.77 (Pyr-C_2), 128.23 (2C, Ph-$C_{2/6}$), 128.57 (Pyr-C_1), 134.96 (Ph'-C_1), 135.09 (Pyr-C_9), 136.62 (Ph-C_4). **MS** (ESI +) = *m/e* = 412.3 [M+1]

Characterization of N-cyclohexyl-6-methyl-2-(4-phenoxyphenyl)imidazo[1,2-*a*]pyridin-3-amine 30

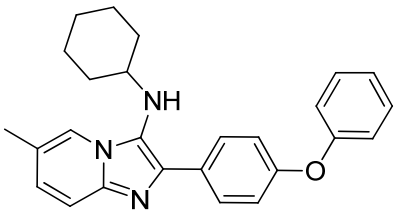

^{1}H-NMR (300.13 MHz, $(CD_3)_2SO$): δ = 1.08-1.72 (m, 10H, Cyclohex-H), 2.30 (s, 3H, Pyr-CH_3), 2.76-2.90 (m, 1H, Cyclohex-C_1H), 4.66-4.68 (d, 1H, J = 5.5Hz, NH), 6.98-7.18 (m, 6H, Ph'-H+Pyr-C_5), 7.33-7.44 (m, 3H, Ph-$C_{2/6}$+Pyr-C_4), 8.07 (s, 1H, Pyr-C_7), 8.18-8.22 (d, 2H, J = 8.7Hz, Ph-$C_{3/5}$). **^{13}C-NMR** (75.44 MHz, $(CD_3)_2SO$): δ = 17.88 (Pyr-CH_3), 24.47 (2C, Cyclohex-$C_{3/5}$), 25.40 (Cyclohex-C_4), 33.44 (2C, Cyclohex-$C_{2/6}$), 56.32 (Cyclohex-C_1), 116.10 (Pyr-C_4), 118.13 (2C, Ph-$C_{3/5}$), 118.79 (2C, Ph'-$C_{2/6}$), 120.30 (Ph'-C_4), 120.62 (Pyr-C_7), 123.48 (Pyr-C_6), 124.98 (2C, Ph-$C_{2/6}$), 126.62 (Ph-C_1), 127.91 (Ph-C_1), 130.04 (2C, Ph'-$C_{3/5}$), 130.22 (Pyr-C_5), 134.25 (Pyr-C_2), 139.56 (Pyr-C_1), 155.47 (Ph'-C_1), 156.53 (Ph-C_4). **MS** (ESI +) = *m/e* = 398.4 $[M+1]^+$

Characterization of 2-(3-(benzyloxy)phenyl)-N-cyclohexyl-6-methylimidazo[1,2-*a*]pyridin-3-amine 31

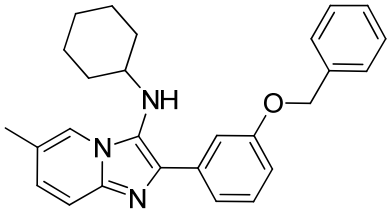

^{1}H-NMR (300.13 MHz, $(CD_3)_2SO$): δ = 1.11-1.78 (m, 10H, Cyclohex-H), 2.36 (s, 3H, Pyr-CH_3), 2.90 (m, 1H, Cyclohex-C1H), 4.77-4.79 (d, 1H, J = 5.4Hz, NH), 5.22 (s, 2H, Ph'-CH_2), 6.94-7.1 (m, 2H, Ph-C_4+Pyr-C_5), 7.34-7.56 (m, 7H, Ph'-H+Ph-$C_{5/6}$), 7.85 (d, 1H, J = 7.7Hz, Pyr-C_4), 7.94 (s, 1H, Ph-C_2), 8.16 (s, 1H, Pyr-C_7). **^{13}C-NMR** (75,44 MHz, $(CD_3)_2SO$): δ = 17.87 (Pyr-CH_3), 24.45 (2C, Cyclohex-$C_{3/5}$), 25.38 (Cyclohex-C_4), 33.47 (2C, Cyclohex-$C_{2/6}$), 56.36 (Cyclohex-C_1), 69.05 (O-CH_2), 112.35 (Ph-C_2), 113.40 (Pyr-C_4), 116.19 (Ph-C_4), 119.03 (Ph-C_6), 120.38 (Pyr-C_1), 120.80 (Ph'-C_4), 125.62 (Pyr-C_7), 126.74 (Pyr-C_6), 127.48 (2C, Ph'-$C_{2/6}$), 127.71 (Ph-C_5), 128.38 (2C, Ph'-$C_{3/5}$), 129.17 (Pyr-C_5), 134.30 (Ph-C_1), 136.38 (Pyr-C_2), 137.24 (Pyr-C_9), 139.47 (Ph'-C_1), 158.36 (Ph-C_3). **MS** (ESI +) = *m/e* = 412.3 [M+1]

III Combustion analysis

Com-pound	Molecular Formula	Expected			Found			Difference		
		C, %	H, %	N, %	C, %	H, %	N, %	C, %	H, %	N, %
5	$C_{20}H_{22}N_4O_2$	68.55	6.33	15.99	68.51	6.33	16.15	0.04	0.00	0.16
14	$C_{24}H_{30}N_4O$ x 0.35HCl	71.48	7.59	13.89	71.43	7.48	13.81	0.05	0.11	0.08
15	$C_{23}H_{27}ClN_4O_2$ x0.15 C_2H_4O	66.92	6.57	13.23	67.22	6.69	13.06	0.30	0.12	0.17
16	$C_{23}H_{27}BrN_4O$	60.66	5.98	12.30	60.41	5.90	12.36	0.25	0.08	0.06
17	$C_{23}H_{28}N_4O$	73.37	7.50	14.88	73.21	7.71	14.87	0.16	0.21	0.01
18	$C_{24}H_{29}ClN_4$	70.48	7.15	13.70	70.37	7.12	13.65	0.11	0.03	0.05
19	$C_{28}H_{36}ClN_5O_2$	65.93	7.11	13.73	65.72	7.10	13.72	0.21	0.01	0.01
20	$C_{22}H_{27}N_5O$ x0.45C_2H_4O x0.2H_20	68.45	7.53	17.43	68.48	7.50	17.39	0.03	0.03	0.04
21	$C_{22}H_{27}N_5O$	70.00	7.21	18.55	69.85	7.49	18.60	0.15	0.28	0.05
22	$C_{22}H_{27}N_5O$	70.00	7.21	18.55	69.72	7.32	18.60	0.28	0.11	0.05
23	$C_{21}H_{26}N_4OS$	65.94	6.85	14.65	65.82	7.12	14.44	0.12	0.27	0.21
24	$C_{22}H_{26}ClN_3$	71.82	7.12	11.42	71.52	7.01	11.41	0.30	0.11	0.01
25	$C_{24}H_{28}ClN_3O$	70.31	6.88	10.25	70.59	6.87	10.24	0.28	0.01	0.01
26	$C_{21}H_{25}N_3O$	75.19	7.51	12.53	75.29	7.74	12.76	0.10	0.23	0.23
27	$C_{22}H_{27}N_3O_2$	72.30	7.45	11.51	72.19	7.58	11.51	0.11	0.13	0.01
28	$C_{26}H_{27}N_3O$	78.56	6.85	10.57	78.33	6.72	10.52	0.23	0.13	0.05
29	$C_{27}H_{29}N_3O$	78.80	7.10	10.21	78.62	6.86	10.00	0.18	0.24	0.21
30	$C_{26}H_{27}N_3O$	78.56	6.85	10.57	78.29	6.87	10.50	0.27	0.02	0.07
31	$C_{27}H_{29}N_3O$	78.80	7.10	10.21	79.04	7.23	10.29	0.24	0.13	0.08

IV Assay systems.

Materials. Arachidonic acid and calcium ionophore A23187 were from Sigma (Deisenhofen, Germany). HPLC solvents were from Merck (Darmstadt, Germany). RPMI 1660 medium was purchased from Gibco/Invitrogen (Paisley, UK). Penicillin and streptomycin were purchased from PAA laboratory GmbH (Pasching, Austria). Fetal calf serum (FCS) was purchased from Biochrom AG (Berlin, Germany). Compounds **3-13** were purchased from Asinex (www.asinex.com, Moscow, Russia) and exhibited >95% purity measured by LC-MS by the manufacturer.

Cell Preparation. Human PMNL were freshly isolated from leukocyte concentrates obtained at Städtische Kliniken Frankfurt Höchst (Frankfurt, Germany). In brief, venous blood was taken from healthy adult donors with informed consent. Leukocyte concentrates were prepared by centrifugation at 4,000g for 20 min at RT. PMNLs were immediately isolated by dextran sedimentation, centrifugation on Nycoprep cushions (PAA Laboratories, Linz, Austria), and hypotonic lysis of erythrocytes as described.[2] Cells were finally resuspended in phosphate-buffered saline, pH 7.4 (PBS) containing 1 mg/mL glucose (purity > 96-97%).

Determination of 5-LO Product Formation in Intact Cells. For whole-cell assay freshly isolated PMNL (5×10^6) were resuspended in 1 mL PBS, pH 7.4, containing 1 mg/mL glucose and 1 mM $CaCl_2$. After preincubation with the test compounds for 15 min at 37 °C, 5-LO product formation was stimulated by the addition of calcium ionophore A23187 (2.5 μM) and exogenous AA (20 μM). After 10 min at 37 °C, the reaction was stopped with the addition of methanol (1 mL). HCl (30 μL, 1 N), prostaglandin B_1 (200 ng) and PBS (500 μL) were added and the 5-LO metabolites were extracted and analyzed by HPLC as described in the literature.[3] 5-LO product formation was determined as nanograms of 5-LO products per 10^6 cells, which includes leukotriene B_4 (LTB_4) and its all-*trans* isomers, and 5-H(P)ETE (5(*S*)-hydro(pero)xy-6-*trans*-8,11,14-*cis*-eicosatetraenoic acid). Cysteinyl LTs C_4, D_4 and E_4 were not detected, and oxidation products of LTB_4 were not determined. Each compound was tested at least three times, and the mean ± SE were calculated.

Determination of 5-LO Product Formation in Cell-Free Systems. For determination of the activity of 5-LO in S100 freshly isolated PMNL cells were resuspended in 1 mL of PBS

containing 1 mM EDTA and the protease inhibitors soybean trypsin inhibitor (60 µg/mL), 1 mM phenylmethylsulfonyl fluoride, and leupeptine (10 µg/mL), cooled on ice for 10 min, and sonicated (3 ×10 s) at 4 °C. The whole homogenate was then centrifuged (100,000g for 70 min at 4 °C) to obtain the S100. For determination of 5-LO activity, S100 corresponding to 7.5×10^6 PMNL was added to 1 mL of a 5-LO reaction mix (PBS, pH 7.4, 1 mM EDTA, and 1 mM ATP). After preincubation with the test compounds or vehicle (DMSO) for 15 min at 4 °C, the samples were prewarmed for 30 s at 37 °C, and 20 µM AA and 2 mM $CaCl_2$ were added to start the 5-LO reaction. The reaction was stopped after 10 min at 37 °C by addition of 1 mL ice-cold methanol and the formed metabolites were analyzed by HPLC as described for intact cells.

Cell culture. The human leukemic monocyte cells U937 were maintained in RPMI 1660 medium containing 10% FCS, 100 µg/mL streptomycin and 100 U/mL penicillin. Cells were cultured at 37 °C in an atmosphere containing 5% CO_2.

V Dose-response curves of the 5-LO activity assays

A

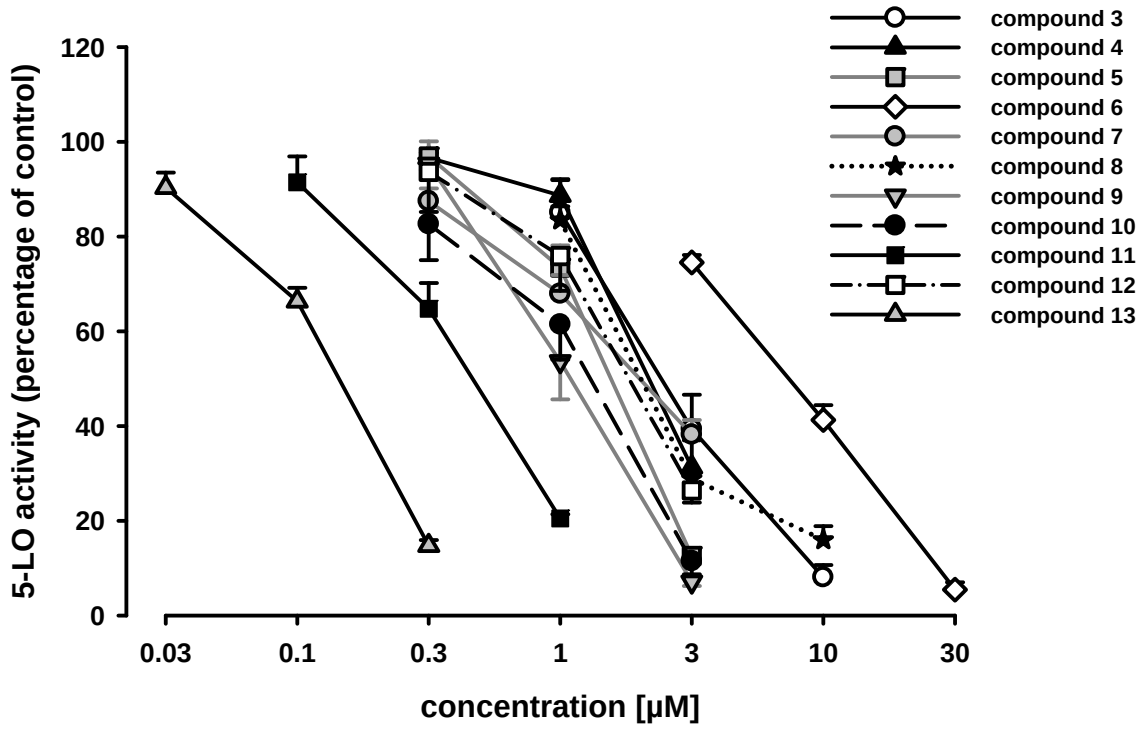

B

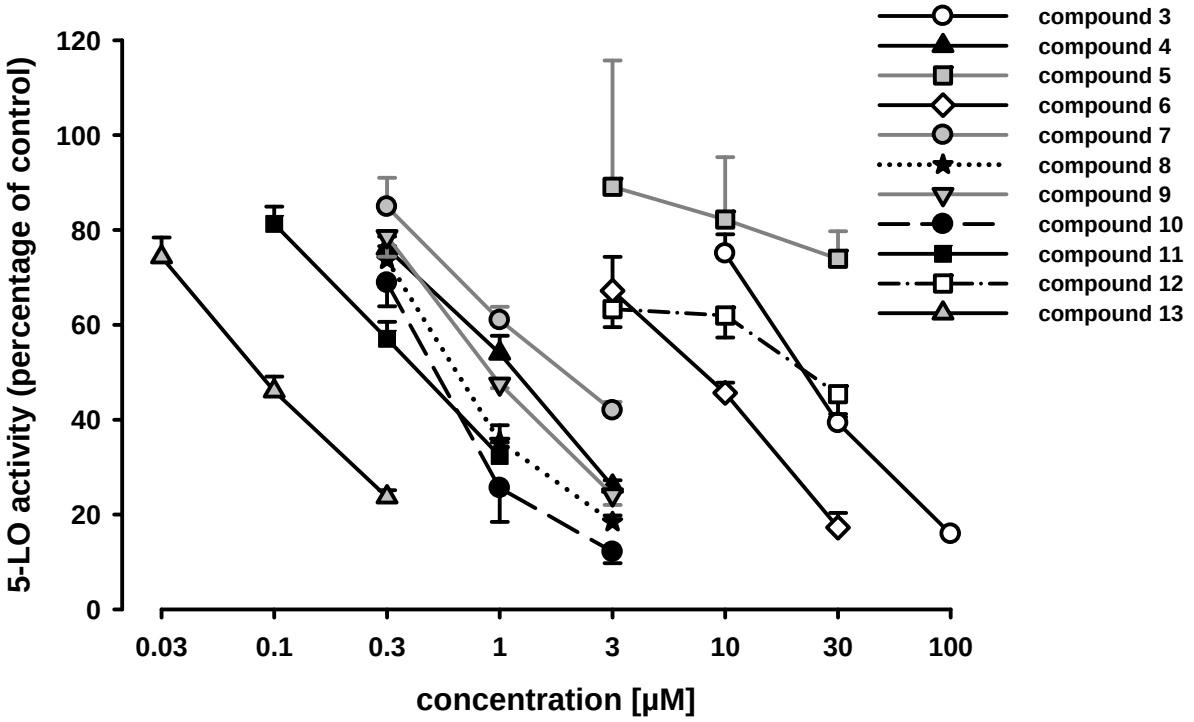

Figure S1. Dose-response curve of compounds **3** to **13** (Table 1) in intact PMNL (A) and cell-free S100 (B). Values given are the mean ± SEM of three to five independent experiments.

A

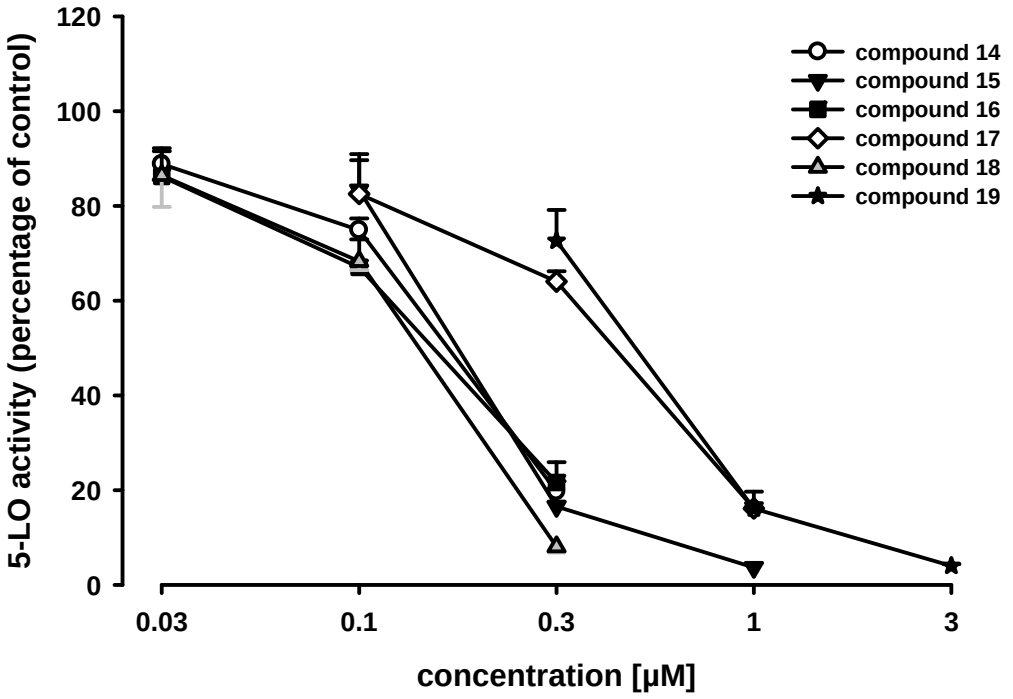

B

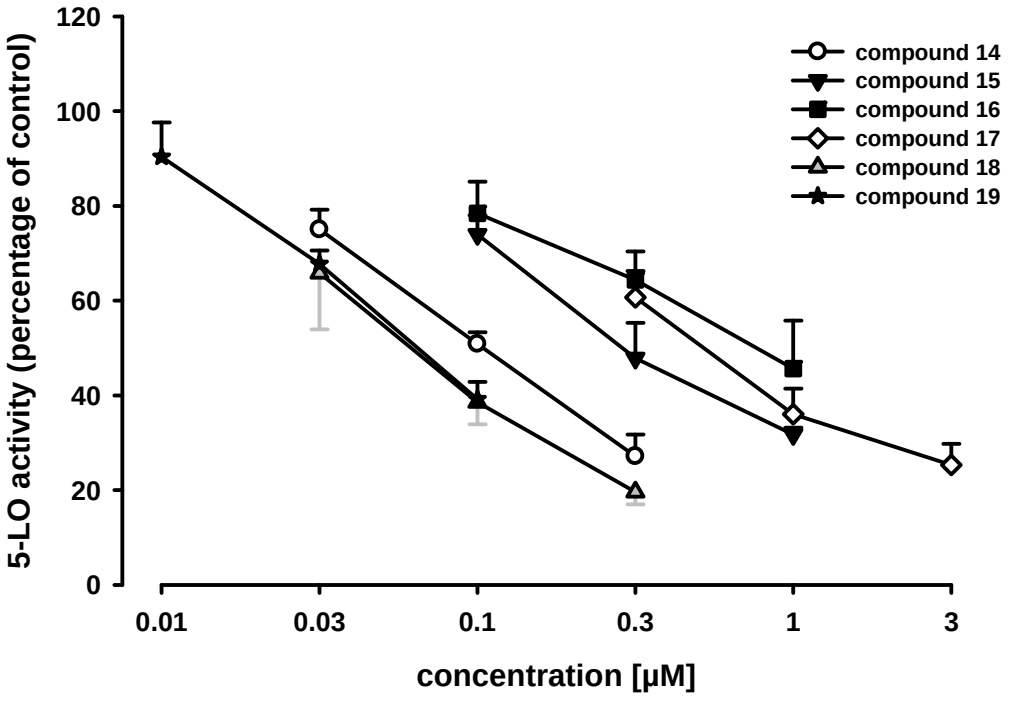

Figure S2. Dose-response curve of compounds **14** to **19** (Table 2) in intact PMNL (A) and cell-free S100 (B). Values given are the mean ± SEM of three to five independent experiments.

A

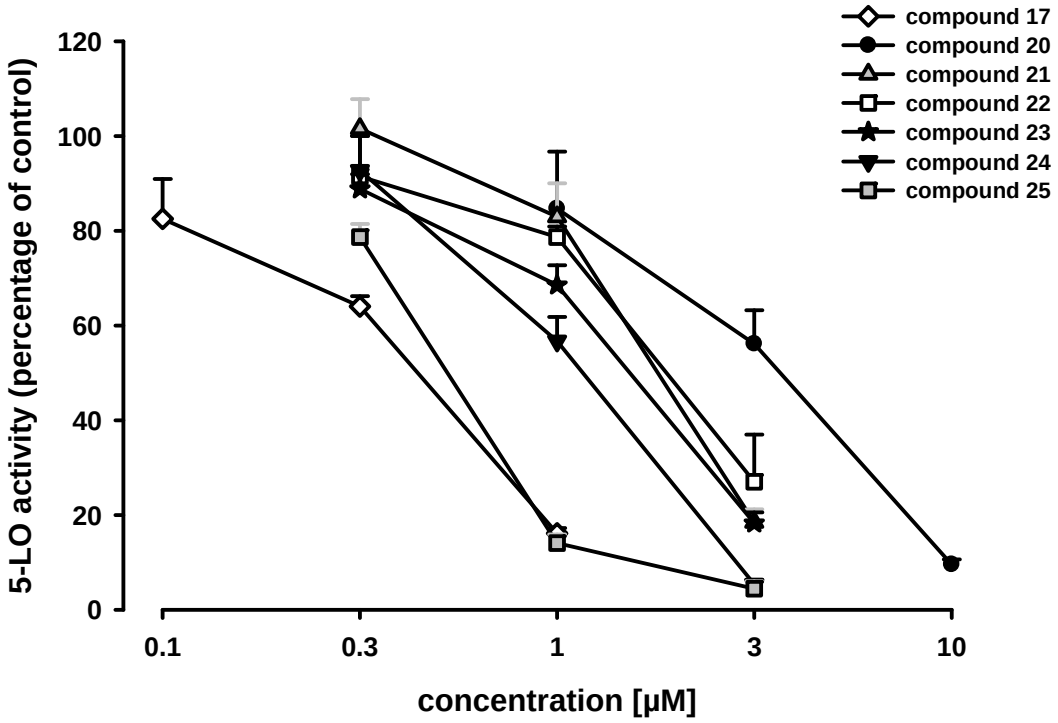

B

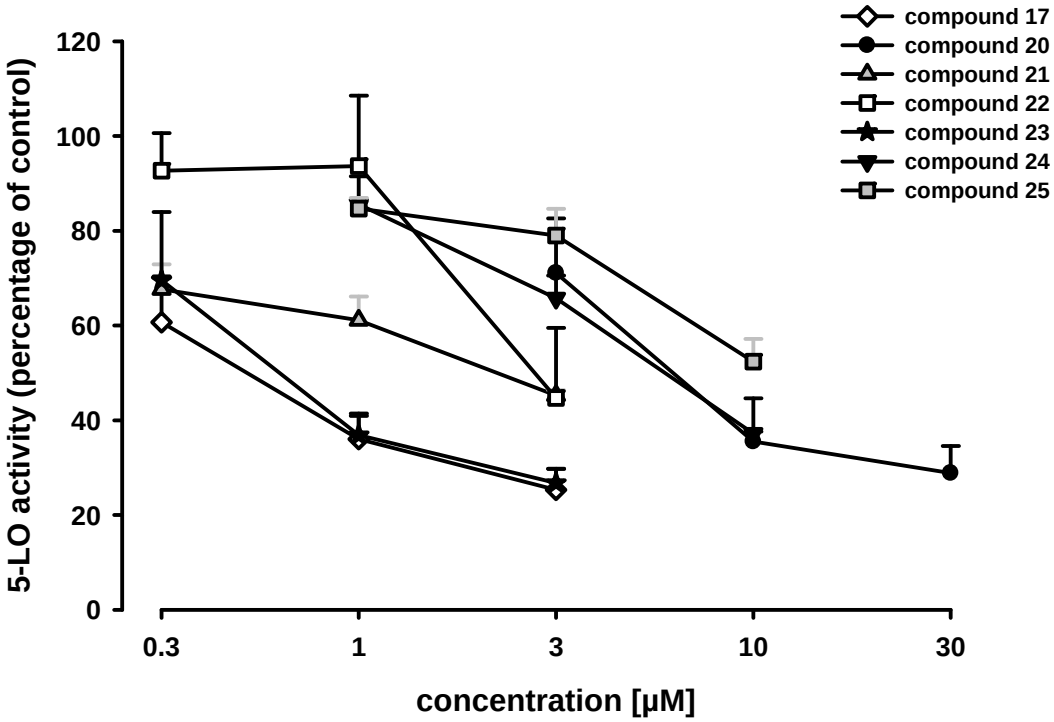

Figure S3. Dose-response curve of compounds **17** to **25** (Table 3) in intact PMNL (A) and cell-free S100 (B). Values given are the mean ± SEM of three to five independent experiments.

A

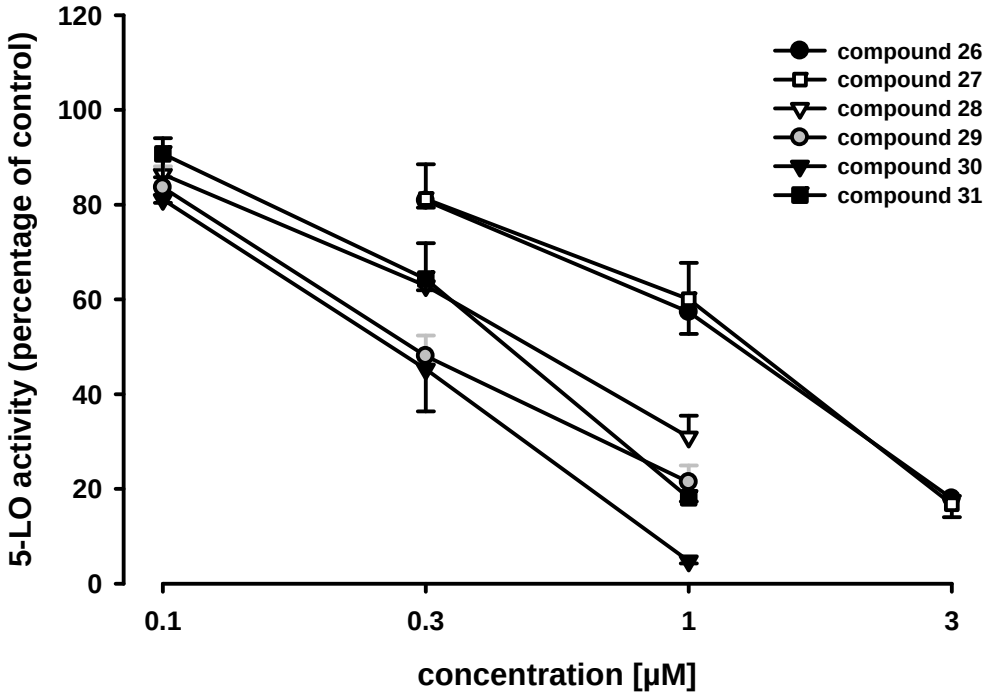

B

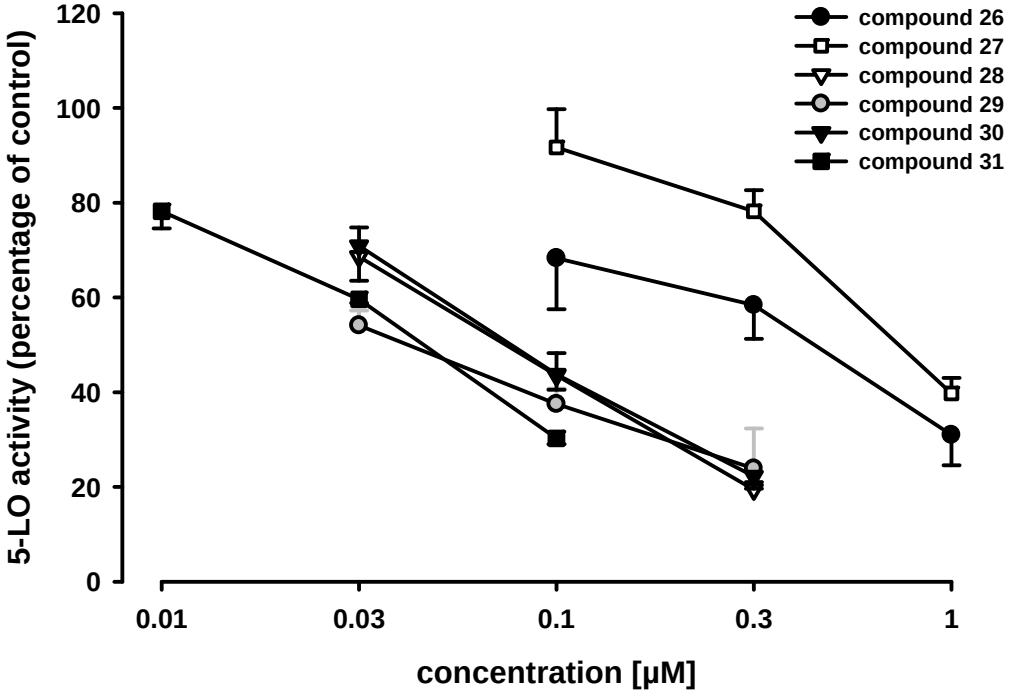

Figure S4. Dose-response curve of compounds **26** to **31** (Table 4) in intact PMNL (A) and cell-free S100 (B). Values given are the mean ± SEM of three to five independent experiments.

VI Correlation between 5-LO inhibition in S100 and PMNL assays

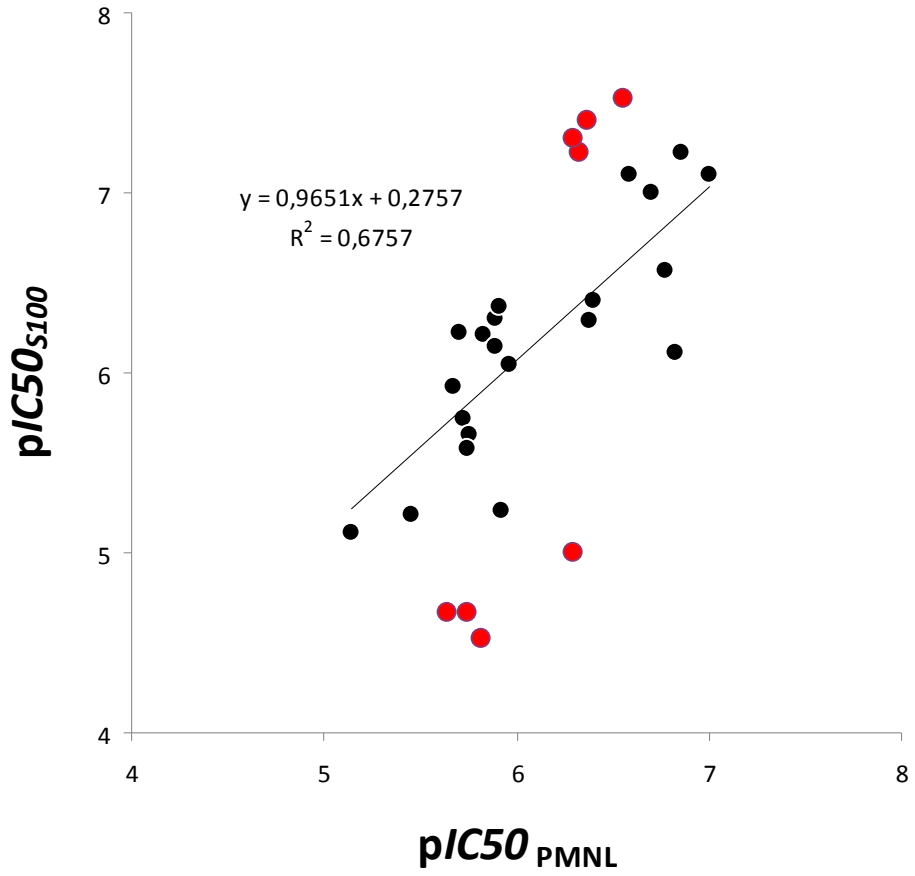

Figure S5. Correlation-plot between IC_{50} values (as $-\log IC_{50}$) measured in cell-free S100 assay and intact PMNL. Red dots represent outliers (more than 2-fold SD difference from the predicted value, p>0.95).

VII References

1. Groebke, K.; Weber, L.; Mehlin, F. *Synlett* **1998**, *1998*, 661.

2. Werz, O.; Bürkert, E.; Samuelson, B.; Rådmark, O.; Steinhilber, D. *Blood* **2002**, *99*, 1044.

3. Brungs, M.; Rådmark, O.; Samuelsson, B.; Steinhilber, D. *Proc. Natl. Acad. Sci. U. S. A.* **1995**, *92*, 107.

Biochemical Pharmacology 83 (2012) 228–240

Contents lists available at SciVerse ScienceDirect

Biochemical Pharmacology

journal homepage: www.elsevier.com/locate/biochempharm

Molecular characterization of **EP6**—A novel imidazo[1,2-*a*]pyridine based direct 5-lipoxygenase inhibitor

Joanna M. Wisniewska [a], Carmen B. Rödl [a], Astrid S. Kahnt [a], Estel.la Buscató [a], Sandra Ulrich [a], Yusuf Tanrikulu [b], Janosch Achenbach [a], Florian Rörsch [c], Sabine Grösch [c], Gisbert Schneider [d], Jindrich Cinatl Jr.[e], Ewgenij Proschak [a], Dieter Steinhilber [a], Bettina Hofmann [a,*]

[a] *Institute of Pharmaceutical Chemistry, ZAFES/LiFF, Goethe-University Frankfurt, Max-von-Laue-Str. 9, D-60438 Frankfurt/Main, Germany*
[b] *Institute of Organic Chemistry and Chemical Biology, ZAFES/CMP, Goethe-University Frankfurt, Siesmayerstr. 70, D-60323 Frankfurt/Main, Germany*
[c] *Institute of Clinical Pharmacology, ZAFES/LiFF, Goethe-University Frankfurt, Theodor-Stern-Kai 7, D-60590 Frankfurt/Main, Germany*
[d] *Institute of Pharmaceutical Sciences, ETH Zurich, Wolfgang-Pauli-Str. 10, CH-8093 Zurich, Switzerland*
[e] *Institute of Medical Virology, ZAFES/LiFF, Goethe-University Frankfurt, Paul-Ehrlich-Str. 40, D-60596 Frankfurt/Main, Germany*

ARTICLE INFO

Article history:
Received 25 July 2011
Accepted 11 October 2011
Available online 18 October 2011

Keywords:
5-Lipoxygenase
Inflammation
Inhibitor
Leukotrienes
Molecular modeling

ABSTRACT

5-Lipoxygenase (5-LO) is a crucial enzyme of the arachidonic acid (AA) cascade and catalyzes the formation of bioactive leukotrienes (LTs) which are involved in inflammatory diseases and allergic reactions. The pathophysiological effects of LTs are considered to be prevented by 5-LO inhibitors. In this study we present cyclohexyl-[6-methyl-2-(4-morpholin-4-yl-phenyl)-imidazo[1,2-*a*]pyridin-3-yl]-amine (**EP6**), a novel imidazo[1,2-*a*]pyridine based compound and its characterization in several *in vitro* assays. **EP6** suppresses 5-LO activity in intact polymorphonuclear leukocytes with an IC_{50} value of 0.16 μM and exhibits full inhibitory potency in cell free assays (IC_{50} value of 0.05 μM for purified 5-LO). The efficacy of **EP6** was not affected by the redox tone or the concentration of exogenous AA, characteristic drawbacks known for the class of nonredox-type 5-LO inhibitors. Furthermore, **EP6** suppressed 5-LO activity independently of the cell stimulus or the activation pathway of 5-LO contrary to what is known for some nonredox-type inhibitors. Using molecular modeling and site-directed mutagenesis studies, we were able to derive a feasible binding region within the C2-like domain of 5-LO that can serve as a new starting point for optimization and development of new 5-LO inhibitors targeting this site. **EP6** has promising effects on cell viability of tumor cells without mutagenic activity. Hence the drug may possess potential for intervention with inflammatory and allergic diseases and certain types of cancer including leukemia.

1. Introduction

Leukotrienes (LTs), inflammatory mediators formed from arachidonic acid (AA), are associated with inflammatory and allergic diseases like asthma and allergic rhinitis, as well as cardiovascular diseases (atherosclerosis) and certain types of cancer [1–4]. 5-Lipoxygenase (5-LO) catalyzes oxygenation of AA to 5(*S*)-hydroperoxy-6-*trans*-8,11,14-*cis*-eicosatetraenoic acid (5-HpETE) and further dehydration to the unstable epoxide leukotriene A_4 (LTA_4). The subsequent conversion of LTA_4 by LTA_4 hydrolase leads to leukotriene B_4 (LTB_4), and the conjugation of LTA_4 with GSH by LTC_4 synthase yields the cysteinyl leukotriene C_4 (LTC_4) [2,5]. Due to the role of 5-LO as a key enzyme in the biosynthesis of all LTs, 5-LO inhibitors are of therapeutic value for the treatment of asthma, allergic rhinitis, atherosclerosis as well as certain types of cancer [3,6]. Also recently, it was found that the ALOX5 gene is a critical regulator for leukemia stem cells in BCR-ABL-induced chronic

Abbreviations: 5-H(p)ETE, 5(*S*)-hydro(pero)xy-6-*trans*-8,11,14-*cis*-eicosatetraenoic acid; 12-H(p)ETE, 12(*S*)-hydro(pero)xy-6-*trans*-8,11,14-*cis*-eicosatetraenoic acid; 15-H(p)ETE, 15(*S*)-hydro(pero)xy-5,8,11-*cis*-13-*trans*-eicosatetraenoic; 5(*S*),12(*S*)-diHETE, 5(*S*),12(*S*)-dihydroxy-6,10-*trans*-8,14-*cis*-eicosatetraenoic acid; A, alanine; AA, arachidonic acid; Ada, adenosine deaminase; CML, chronic myeloid leukemia; COX, cyclooxygenase; ERK, extracellular signal-regulated kinase; FCS, fetal calf serum; FLAP, 5-LO activating protein; fMLP, N-formyl-methionine-leucine-phenylalanine; LC–MS/MS, liquid chromatography coupled with tandem mass spectrometry; LDH, lactate dehydrogenase; LO, lipoxygenase; LT, leukotriene; LPS, lipopolysaccharide; MAPK, mitogen-activated protein kinase; MBP, maltose binding protein; mPGES-1, microsomal prostaglandin E_2 synthase-1; PARP, poly ADP-ribose polymerase; PB, phosphate buffer pH 7.4; PC, phosphatidylcholine; PDB, Protein Data Bank; PG buffer, PBS containing 1 mg/ml glucose; PGC buffer, PBS containing 1 mg/ml glucose and 1 mM $CaCl_2$; PLIF, Protein Ligand Interaction Fingerprints; PMNL, polymorphonuclear leukocytes; PMSF, phenylmethylsulfonyl fluoride; RPE, retinal pigment epithelium; RT, room temperature; S100, 100 000 × *g* supernatant; SA, sodium arsenite; SDS-PAGE, SDS-polyacrylamide gel electrophoresis; W, tryptophan; WT, wild-type; Y, tyrosine.

* Corresponding author. Tel.: +49 69 798 29335; fax: +49 69 798 29323.
E-mail address: hofmann@pharmchem.uni-frankfurt.de (B. Hofmann).

0006-2952/$ – see front matter © 2011 Elsevier Inc. All rights reserved.
doi:10.1016/j.bcp.2011.10.012

myeloid leukemia (CML) [7]. Chen et al. could show, that the use of the 5-LO inhibitor zileuton [8], alone or in combination with imatinib, impairs CML (clinical trial phase I) [7]. Up to now, zileuton is the only 5-LO inhibitor that reached the market in the US for the treatment of asthma.

The reported crystal structure of a stable form of the 5-LO (Protein Data Bank (PDB), http://pdb.org [9], ID: 3o8y [10]), implies a folding of the single polypeptide chain in a two domain structure: a N-terminal regulatory C2-like domain and a C-terminal catalytic domain. The C2-like domain, organized in a β-sandwich, is important for membrane binding [11,12] or binding of diacylglycerides [13] and calcium [14], respectively. The binding site for cellular membranes or phosphatidylcholine (PC), serving as stimulating scaffolds for the 5-LO, is defined by three tryptophan residues (W13, W75 and W102) of the C2-like domain [12]. An ATP binding site formed by the C2-like domain was postulated as well [15]. The catalytic domain, primarily consisting of α-helices, contains a non-heme iron responsible for substrate conversion. In the inactive state of the enzyme, the iron is in the ferrous (Fe^{2+}) form; for entering the catalytic pathway an oxidation by hydroperoxides to the ferric (Fe^{3+}) form is necessary [16]. Reducing agents and iron-ligand inhibitors such as zileuton or BWA4C [17] stabilize the ferrous form or chelate with the central iron-atom, thereby suppressing 5-LO activity. These direct 5-LO inhibitors exhibit high inhibitory potency *in vitro*, but show unselective interactions and may interfere with cellular redox reactions [18,19]. Another group of potent and selective 5-LO inhibitors are nonredox-type inhibitors such as Rev-5901 [20], ZD2138 [21] and ZM230487 [22]. This class of inhibitors reduces acute inflammatory responses [18,23], but does not show effects on more chronic processes [24,25]. Furthermore a decreased inhibitory potency of ZM230487 in presence of elevated peroxide tone has been observed [26]. The efficacy of ZM230487 depends on the way of enzyme activation [27]. 5-LO can be activated by an increase of intracellular calcium leading to translocation of 5-LO from the cytosol to the nuclear membrane [28] or by phosphorylation via the p38 mitogen-activated protein kinase (MAPK) and the extracellular signal-regulated kinase (ERK) pathway at two serine residues [29,30]. ZM230487 exhibits impaired 5-LO inhibition after enzyme activation via phosphorylation [27]. Some inflammatory reactions, e.g. allergic asthma, various types of cancer and atherosclerosis are associated with an increased phosphorylation status of the cell [31,32], concluding that nonredox-type inhibitors such as ZM230487 are limited in their benefit. In addition, indirect 5-LO inhibition can regulate the 5-LO product formation. The membrane-bound 5-LO activating protein (FLAP), facilitates the transfer of AA within the nuclear membrane to 5-LO [33]. Targeting FLAP, the 5-LO product formation can be inhibited [34]. FLAP antagonists like MK-886 [35], MK-0591 [36] or AM103 [37] inhibit 5-LO product formation in whole cell preparation and could enter clinical phase II trials for the treatment of inflammatory diseases [38]. Therefore, there is a need for the development of new inhibitors with a different pharmacological profile which potently inhibit the enzyme activity regardless of the mode of enzyme activation. Consequently, potential drug candidates should be screened in different cellular assays where both calcium- and phosphorylation-dependent stimuli are applied.

In this study we evaluate the pharmacological profile of the novel 5-LO inhibitor cyclohexyl-[6-methyl-2-(4-morpholin-4-yl-phenyl)-imidazo[1,2-*a*]pyridin-3-yl]-amine (**EP6**) (Fig. 1A), an analogue of compound **1** and **2** (Fig. 1B) derived from a virtual screening for cyclooxygenase (COX)/5-LO dual inhibitors [39]. Compound **1** and **2**, imidazo[1,2-*a*]pyridin derivatives, inhibit 5-LO product formation in intact polymorphonuclear leukocytes (PMNL) with IC_{50} values of 0.9 μM and 0.6 μM, respectively [39]. Structural optimization led to **EP6**, which exhibits improved inhibitory potency of 5-LO. Herein, we describe the molecular pharmacology of this novel compound with a unique mode of action different to other established 5-LO inhibitors using various *in vitro* test systems.

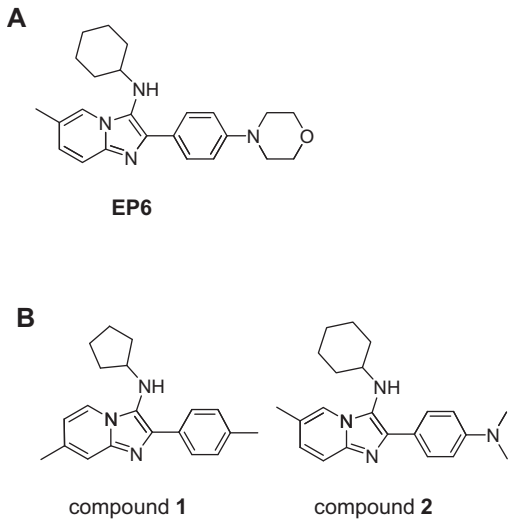

Fig. 1. Chemical structures of (A) **EP6** and (B) compound **1** and **2**.

2. Material and methods

2.1. Chemistry

Compound **EP6** was synthesized according to ref. [40] as described in the supplemental information.

2.2. Materials

AA, calcium ionophore A23187, BWA4C, DMSO, GSH, 1,2-ditetradecanoyl-*sn*-glycero-3-phosphocholine (PC) and trypan blue solution were purchased from Sigma–Aldrich (Munich, Germany), Rev-5901, zileuton and human recombinant 15-LO2 from Cayman Chemical (Ann Arbor, USA). HPLC solvents were purchased from Merck (Darmstadt, Germany), penicillin, streptomycin and IMDM medium from PAA laboratory GmbH (Pasching, Austria). Fetal calf serum (FCS) was purchased from Biochrom AG (Berlin, Germany), RPMI 1660 medium from Gibco/Invitrogen (Paisley, UK). Fresh blood cell concentrates were provided by Städtische Kliniken Frankfurt-Höchst (Frankfurt, Germany).

2.3. Cell culture

The human leukemic monocyte cells U937 and human cervix carcinoma cells HeLa were purchased from Deutsche Sammlung für Mikroorgansimen und Zellkulturen (DSMZ, Braunschweig, Germany), and mouse leukemic monocyte macrophage cells RAW 264.7 from American Type Culture Collection (ATCC, Manassas, USA). Human retinal pigment epithelium (RPE) cells were isolated as described before [41]. U937, HeLa and RAW 264.7 cells were maintained in RPMI 1640 medium containing 10% FCS, 100 μg/ml streptomycin and 100 U/ml penicillin. RPE cells were maintained in IMDM medium with 20% FCS, L-glutamine, 100 μg/ml streptomycin and 100 U/ml penicillin. Cells were cultured at 37 °C in an atmosphere containing 5% CO_2.

2.4. Isolation of PMNL and platelets from leukocyte concentrates

PMNL and platelets were freshly isolated from leukocyte concentrates obtained from Städtische Kliniken Frankfurt Höchst

(Frankfurt, Germany). Blood samples were obtained by the hospital with informed consent. In brief, cells were isolated by dextran sedimentation for 30 min, and 10 min centrifugation without deceleration at 800 × *g* on Nycoprep cushions (PAA laboratory GmbH, Pasching, Austria). For PMNL isolation the cells were re-suspended in 10 ml ice-cold water for hypotonic lysis of erythrocytes as described previously [42]. Cells were finally re-suspended in phosphate-buffered saline, pH 7.4 (PBS) containing 1 mg/ml glucose (PG buffer) (purity >96–97%). Platelets were re-suspended in PBS, pH 5.4 and centrifuged at 1849 × *g* for 15 min at room temperature (RT). The cells were re-suspended in PBS/NaCl (PBS, pH 5.4 and 0.9% NaCl, 1:1 dilution) and centrifuged at 1849 × *g* for 10 min at RT. Finally platelets were re-suspended in PBS pH 5.4.

2.5. Site-directed mutagenesis, expression and purification of 5-LO proteins and maltose binding protein (MBP) constructs

The codons for selected residues in plasmid pT3-5-LO [43] were mutated by site-directed mutagenesis polymerase chain reaction yielding the mutated 5-LO plasmids pT3-5-LO-W13/75/102A, pT3-5-LO-Y81A, pT3-5-LO-Y100A, pT3-5-LO-Y81/100A, pT3-5-LO-Y383A or pT3-5-LO-Y81/100/383A as well as in plasmid pBUF-5-LO-C2 [44] for MBP-5-LO fusion proteins yielding the mutated MBP-5-LO-C2 plasmid pBUF-5-LO-Y81/100A. The mutated DNA was confirmed by DNA-sequencing (carried out by Scientific Research and Development GmbH, Bad Homburg, Germany). *Escherichia coli* BL21 were transformed with plasmid pT3-5-LO as wild-type (WT) DNA, pBUF-5-LO-C2 DNA, pBUF1b [44] DNA and mutated DNA. The recombinant 5-LO proteins, 5-LO C2 fusion proteins with MBP or MBP itself were expressed at 22 °C (5-LO-Y81/100/383A at 16 °C) and purified from 1-l cultures according to the ATP affinity chromatography procedure as described previously [14,45] or to the MBP affinity chromatography described by Michel et al. [44]. For experiments investigating the effect of ATP or calcium, the 5-LO protein was further purified via anion exchange chromatography as described previously [46]. In brief, the ATP-eluate (10 ml) was loaded on a ResourceQ 6 ml column (GE Healthcare, Uppsala, Sweden). Buffer A was phosphate buffer (PB) 0.05 mM, pH 7.4 containing 1 mM EDTA, buffer B was buffer A plus 0.5 M NaCl. The elution of the 5-LO was performed in a gradient from 0 to 100% buffer B and the enzyme eluted at about 40% buffer B.

2.6. Determination of 5-LO product formation in intact cells

For assays in intact cells, 5×10^6 or 7.5×10^6 freshly isolated PMNL were re-suspended in 1 ml of PBS, pH 7.4 containing 1 mg/ml glucose and 1 mM $CaCl_2$ (PGC buffer). After pre-incubation with the test compound or vehicle (DMSO) at the indicated concentrations for 12 min at 37 °C, 5-LO product formation was stimulated either by pre-incubation with 300 mM NaCl for 3 min or with 10 μM sodium arsenite (SA) and addition of 20 μM AA, or stimulated with 2.5 μM calcium ionophore A23187 together with exogenous AA at the indicated concentrations after 15 min pre-incubation. For assays with stimulation via N-formyl-methionine-leucine-phenylalanine (fMLP), 7.5×10^6 or 10^7 freshly isolated PMNL were re-suspended in PGC buffer, primed for 15 min with 1 μg/ml lipopolysaccharide (LPS) and 0.2 U/ml adenosine deaminase (Ada) and incubated for 15 min with test compound or vehicle (DMSO). The 5-LO product formation was started by addition of 1 μM fMLP with or without addition of 20 μM AA. For assays with intact mouse leukemic monocyte macrophage cells (RAW 264.7), 1.5×10^7 RAW 264.7 cells were re-suspended in PGC buffer and pre-incubated with the test compound or vehicle (DMSO) at the indicated concentrations for 15 min at 37 °C, 5-LO product formation was stimulated by addition of 5 μM calcium ionophore A23187 together with 20 μM AA. After 10 min at 37 °C, the reaction was stopped with 1 ml of ice-cold methanol. 30 μl of 1 N HCl, 200 ng of prostaglandin B_1 as internal standard and 500 μl of PBS, pH 7.4 were added. 5-LO metabolites were extracted and analyzed by HPLC as described [46]. Metabolites formed via fMLP stimulation without exogenously added AA were measured by LC–MS/MS analysis as described previously [47]. 5-LO product formation was determined as ng of 5-LO products per 10^6 cells, which includes LTB_4 and its all-*trans* isomers, 5(*S*),12(*S*)-dihydroxy-6,10-*trans*-8,14-*cis*-eicosatetraenoic acid (5(S),12(S)-diHETE), and 5(*S*)-hydro(pero)xy-6-*trans*-8,11,14-*cis*-eicosatetraenoic acid (5-H(p)ETE). Cysteinyl LTs (LTC_4, D_4 and E_4) and oxidation products of LTB_4 were not determined. Each experiment was performed at least three times. Data (mean ± standard error (S.E.)) are expressed as percentage of control (DMSO).

2.7. Determination of 12-LO and 15-LO1 product formation in intact cells

Determination of 15-LO1 product formation was performed in PMNL preparations as described for 5-LO product formation in intact cells. For determination of 12-LO product formation 1×10^8 freshly isolated platelets were re-suspended in 1 ml of PGC buffer (pH 7.4) and were pre-incubated with the test compound or vehicle (DMSO) at the indicated concentrations for 15 min at 37 °C. 12-LO product formation was stimulated by addition of 10 μM AA. After 10 min at 37 °C, the reaction was stopped with 1 ml of ice-cold methanol. 12-LO products include 12(*S*)-hydro(pero)xy-6-*trans*-8,11,14-*cis*-eicosatetraenoic acid (12-H(p)ETE). 12-HETE and 12-HpETE elute as one major peak. 15-LO1 products, generated from eosinophils expressing 15-LO1, were 15(*S*)-hydro(pero)xy-5,8,11-*cis*-13-*trans*-eicosatetraenoic acid, which elute as one major peak as well. Data (mean ± S.E.; $n \geq 3$) are expressed as percentage of control (DMSO).

2.8. Determination of 5-LO product formation in cell-free systems

PMNL were re-suspended in 1 ml of PBS containing 1 mM EDTA and the protease inhibitors soybean trypsin inhibitor (60 μg/ml), 1 mM phenylmethylsulfonyl fluoride (PMSF), and leupeptin (10 μg/ml), cooled on ice for 10 min, and subsequently, the samples were sonicated for 3 × 10 s (homogenate). To obtain 100 000 × *g* supernatant (S100) the homogenate was centrifuged (100 000 × *g* for 70 min at 4 °C). For determination of 5-LO activity, cell homogenates or S100 corresponding to 7.5×10^6 PMNL were re-suspended in 1 ml of reaction mix (PBS, pH 7.4, 1 mM EDTA, and 1 mM ATP) and additional reagents were added as indicated (e.g. PC, GSH). For cell-free assays of mouse leukemic monocyte macrophage cells (RAW 264.7), 2×10^7 RAW 264.7 cells were prepared as described for PMNL S100 preparations. For determination of the activity of partially purified WT 5-LO, 5-LO-3Y mutant or S100 of WT 5-LO or S100 of 5-LO-3W mutant from *E. coli*, 2–3 μg of 5-LO were dissolved in 1 ml reaction mix. After pre-incubation with the test compounds or vehicle (DMSO) at the indicated concentrations for 15 min at 4 °C, the samples containing either homogenates, S100 or purified 5-LO were pre-warmed for 30 s at 37 °C. The reaction was started after addition of 2 mM $CaCl_2$ and 20 μM AA. After 10 min 5-LO product formation was stopped with 1 ml ice-cold methanol and the formed metabolites were analyzed by HPLC as described for intact cells. Data (mean ± S.E.; $n \geq 3$) are expressed as percentage of control (DMSO).

2.9. Determination of 15-LO2 product formation in cell-free systems

0.5 U human recombinant 15-LO2 was added to 1 ml PBS, pH 7.4. After pre-incubation with test compound or vehicle (DMSO) at the indicated concentrations for 15 min on ice, 15-LO2 product formation was stimulated with 100 μM AA. After 10 min at 37 °C, the reaction was stopped with 1 ml of ice-cold methanol. 15-LO2

metabolites were extracted and analyzed by HPLC as described for intact cells. Data (mean ± S.E.; $n \geq 3$) are expressed as percentage of control (DMSO).

2.10. C2-like domain competition assay

2–3 μg of partially purified 5-LO was dissolved in 1 ml reaction mix (PBS, pH 7.4, 1 mM EDTA, and 1 mM ATP) and increasing amounts of MBP-5-LO-C2, MBP-5-LO-C2 Y81/100A or MBP were added (0–300 μg/ml). γ-Globulin was added to adjust consistent protein concentration of 300 μg/ml. After pre-incubation with 0.3 μM **EP6** or vehicle (DMSO) for 15 min at 4 °C, the samples were pre-warmed for 30 s at 37 °C. The reaction was started after addition of 2 mM $CaCl_2$ and 20 μM AA. After 10 min 5-LO product formation was stopped with 1 ml ice-cold methanol and the formed metabolites were analyzed by HPLC as described for intact cells. For each sample in presence of **EP6**, the sample incubated with vehicle (DMSO) with the same amount of added protein construct was taken as control. Data (mean ± S.E.; $n \geq 3$) are expressed as percentage of control (DMSO).

2.11. COX and mPGES-1 assay

Inhibitory activity of **EP6** on recombinant ovine COX-1 and human COX-2 were assayed with a COX Inhibitor Screening Assay Kit (Cayman Chemical, Ann Arbor, USA) according to the manufacturer's protocol. All samples were tested in triplicate. Data (mean ± S.E.; $n = 3$) are expressed as percentage of control (DMSO).

For investigation of the inhibitory potency of **EP6** on the mPGES-1 enzyme *in vitro*, the microsomal fraction of HeLa cells was prepared. 3×10^6 cells were incubated at 37 °C and after 24 h the medium was removed and the cells where stimulated for 16 h with fresh medium containing 1 ng/ml IL-1β and 5 ng/ml TNFα. After separation into cytosolic and microsomal fraction described previously by Rörsch et al. [48], the microsomal fraction was re-suspended in 100 μl potassium phosphate buffer (0.1 M, pH 7.4), containing 1× complete protease inhibitor cocktail and reduced GSH (2.5 mM), and sonicated (1 × 10 s). The mPGES-1 activity assay was performed as described by Thorén and Jakobsson [49]. Briefly, 0.15 mg/ml protein was incubated with increasing concentrations of the test compounds for 30 min at RT. The reaction was initiated at 4 °C with 20 μM prostaglandin H_2 (Larodan, Malmö, Sweden) and terminated after 1 min by adding a stop solution containing 40 mM iron chloride and 80 mM citric acid. After solid phase extraction the amount of produced prostaglandin E_2 was measured by LC–MS/MS analysis as described previously [50].

2.12. In vitro cell viability assay

The WST-1 assay (Roche Diagnostic GmbH, Mannheim, Germany) was used to determine cell viability after treatment with test compound. U937 cells were seeded in 96-well plates at a density of 10^4 cells/well and treated with increasing concentrations of test compound or vehicle (DMSO) for 48 h in presence of 10% FCS. Cell viability was assessed according to the distributor's protocol using a microplate reader (infinite M200, Tecan Group Ltd., Crailsheim, Germany) and was calculated as a ratio of the absorbance values measured after 48 h (between test compound and vehicle (DMSO)). All experiments were tested three times and the mean ± S.E. were calculated.

2.13. Lactate dehydrogenase (LDH) cytotoxicity assay

The LDH assay (cytotoxicity detection kit; Roche Diagnostics GmbH, Roche Applied Science, Mannheim, Germany) was used to determine cell death after treatment of U937 cells with test compounds. LDH leakage was measured as an index of loss of cell membrane integrity. U937 cells were seeded in 96-well plates at a density of 1.5×10^4 cells/well and incubated with increasing concentrations of test compounds or vehicle (DMSO) for 48 h. Plates were centrifuged (250 × *g*, 4 min) and an aliquot of the supernatant was transferred to a clean microplate. Cell toxicity was assessed according to the distributor's protocol using a microplate reader (infinite M200, Tecan Group Ltd., Crailsheim, Germany). A control detergent supplied by Sigma–Aldrich (Saint Louis, MO, USA) was used for maximum LDH release and set to 100%. All experiments were tested three times and the mean ± S.E. were calculated.

2.14. Trypan blue exclusion

For investigation of effects on cell viability of test compounds in U937 and RPE cells, 1.6×10^5 cells/well were seeded in 6-well plates and treated with increasing concentrations of test compounds or vehicle (DMSO) for 24 h, 36 h or 48 h in the presence of 10% FCS. Afterwards, cell viability was measured by trypan blue exclusion by a cell counter (TC10™ Automated cell counter, Bio-Rad, Munich, Germany). For investigation of cytotoxic effects during activity assays, 5×10^6 freshly isolated PMNL were re-suspended in 1 ml of PGC buffer and incubated with the test compounds or vehicle (DMSO) at the indicated concentrations for 30 min at 37 °C. Afterwards, cell viability was measured by trypan blue exclusion.

2.15. Poly ADP-ribose polymerase (PARP) cleavage

U937 cells treated with test compounds for 24 h in medium containing 10% FCS or untreated control cells were centrifuged (1000 × *g*, 5 min). The cell pellet was washed once with ice-cold PBS. For the detection of PARP, cells were re-suspended in sonification buffer (PBS pH 7.4, protease inhibitor cocktail tablets (Complete, Mini; Roche diagnostics GmbH)), and disrupted by sonification (3 × 10 s, 4 °C). The resulting cell homogenates were centrifuged (10 000 × *g*, 10 min, 4 °C). Protein concentrations in the supernatant were determined using the Bradford method. Equal quantities of protein extracts were separated by 10% SDS-polyacrylamide gel electrophoresis (SDS-PAGE), proteins were electrophoretically blotted onto a nitrocellulose membrane (Hybond-C Extra, Amersham Biosciences Ltd., Little Chalfont, UK), and immunodetection of PARP was performed as described before [51]. Western blot analysis experiments were performed in triplicate.

2.16. Salmonella mutagenicity test

The Salmonella mutagenicity test for detecting carcinogenic and mutagenic potential was performed with the histidine auxotroph (his^-) *Salmonella typhimurium* strains TA98 and TA100 in assays conducted with and without metabolic activation (addition of S9 liver homogenate mix) as described by Maron and Ames [52].

2.17. Molecular modeling of the putative binding mode of EP6

For molecular modeling and docking calculations, the crystal structure of engineered human 5-LO (Protein Data Bank (PDB, http://pdb.org [9]), ID: 3o8y [10], chain B) was first subjected to *in silico* mutagenesis to restore the WT enzyme. For enabling crystallization and structure determination, Gilbert et al. mutated or deleted several amino acids to obtain the so called "stable 5-LO" [10]. They introduced the following mutations: W13E, F14H, W75G, L76S, C240A, C561A, $K^{653}KK^{655} \rightarrow$ ENL, and ΔP40 to D44GS. To restore the WT enzyme, we performed *in silico* mutagenesis of the modified residues and reconstruction of the missing segment using the software package MOE (version 2010.10; Chemical Computing

Group, Montreal, Canada), which uses rotamer libraries, loop prediction [53], and energy minimization to construct the missing or modified residues. Energy minimization was performed using the all-atom force field AMBER99 [54] with RMS gradient of 1. Docking calculations were performed with PLANTS (version 1.1; University of Konstanz, Germany) [55] with the scoring function chemplp with default settings and flexible amino acid side chains (supplemental information). For the docking study a set of 200 binding poses was generated. For analysis of the docking pose, so called Protein Ligand Interaction Fingerprints (PLIF) provided by the software package MOE (version 2010.10; Chemical Computing Group, Montreal, Canada) were used. PLIFs describe a receptor–ligand complex regarding the interaction between the involved amino acid residues and a bound ligand in a bit-fingerprint scheme. The fingerprint consists of six different interaction types for each residue: side chain hydrogen-bond donor and acceptor, backbone hydrogen-bond donor and acceptor, ionic interactions and surface interactions. Additionally, each type is partitioned into weak and strong interactions, described by two separate bits. For each residue only the strongest interaction between itself and the ligand is considered and regarding the interaction type no bits (0 0) for the absence of the individual interaction, the first bit for a weak (0 1) or both bits for a strong interaction (1 1) will be set. The probability of a good hydrogen-bond interaction is based on the distance and orientation of the considered atom pair regarding protein contact statistics. The ionic interactions are scored by the inverse square of the distance between two opposite formal charged atoms. The surface contact interactions are described by the difference of the solvent exposed surface area of the residues in the unbound and bound protein–ligand complex.

2.18. Statistics

Data are expressed as mean values with S.E. All IC_{50} values are means with S.E. of the IC_{50} values obtained from measurements at three to five different concentrations of the compounds in three to five independent experiments. Each IC_{50} value of an independent experiment is an approximation determined by graphical analysis (linear interpolation between the points at 50% activity) using SigmaPlot2006 (version 10.0, Systat Software Inc., Chicago, USA). Data were subjected to one- or two-way ANOVA with Tukey *post hoc* test, classification of P according to: $^{*}P \leq 0.05$; $^{**}P \leq 0.01$; $^{***}P \leq 0.001$.

3. Results

3.1. EP6 inhibits 5-LO in intact cells and cell-free systems

The inhibitory effect of **EP6** on 5-LO product formation was determined in different 5-LO preparations. **EP6** inhibited 5-LO in calcium ionophore stimulated intact PMNL, homogenates of PMNL and S100 preparations of the homogenates with comparable IC_{50} values (Fig. 2, no significant differences among the IC_{50} values). In intact cells and in homogenates, **EP6** exhibited an IC_{50} value of 0.16 μM (±0.01 μM) and 0.21 μM (±0.03 μM). The IC_{50} values for inhibition of S100 and partially purified 5-LO were 0.11 μM (±0.01 μM) and 0.05 μM (±0.01 μM), respectively. **EP6** inhibited purified 5-LO with a higher potency than in intact PMNL or homogenates ($^{*}P < 0.05$ and $^{**}P < 0.01$). Therefore, we conclude that **EP6** is a direct inhibitor of 5-LO.

3.2. Investigations of influence of substrate concentration on the inhibitory potency of EP6

To investigate the type of inhibition of **EP6**, S100 samples were stimulated with increasing substrate concentrations (1–30 μM).

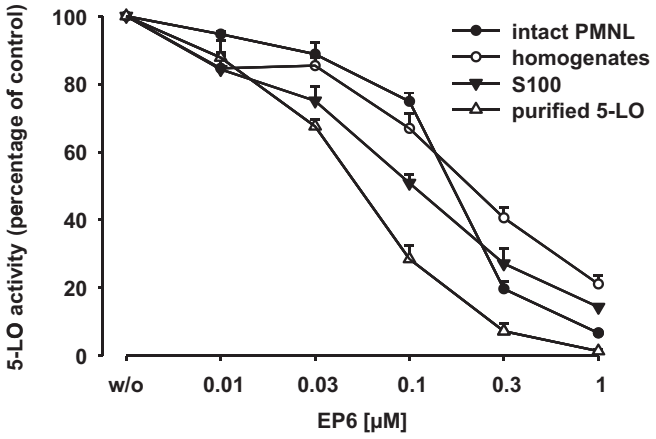

Fig. 2. Inhibition of 5-LO activity by **EP6**. 5×10^6 intact PMNL were re-suspended in PGC buffer and pre-incubated for 15 min at 37 °C with the indicated concentrations of **EP6** or vehicle (DMSO). 5-LO product formation was started by addition of 2.5 μM calcium ionophore and 20 μM AA, after 10 min 5-LO product formation was determined. For determination of 5-LO product formation in cell-free systems, homogenates and S100 preparations corresponding to 7.5×10^6 PMNL, or partially purified 5-LO were dissolved in 1 ml PBS, pH 7.4, 1 mM EDTA and 1 mM ATP and were pre-incubated for 15 min with **EP6** or vehicle (DMSO) at the indicated concentrations at 4 °C. Samples were pre-warmed at 37 °C for 30 s and 5-LO product formation was started by addition of 2 mM $CaCl_2$ and 20 μM AA. After 10 min, 5-LO product formation was determined. Data (mean ± S.E.; $n \geq 3$) are expressed as percentage of control.

AA had no direct influence on the inhibitory potency of **EP6** (Fig. 3A). Furthermore intact PMNL were stimulated via calcium ionophore A23187 without or with addition of exogenous AA (20 μM). The IC_{50} value in presence of 20 μM exogenously added AA was 0.18 μM (±0.06 μM), but in absence of exogenous substrate, an IC_{50} value of 1.14 μM (±0.32 μM) was determined (Fig. 3B). The ratio of the 5-LO products 5-H(p)ETE to LTB_4 increased in the control if exogenous AA (20 μM) was added, but the formation of the 5-LO metabolite LTB_4 and the formation of 5-H(p)ETE was thereby inhibited with a similar potency (data not shown). The FLAP antagonist MK-886 and the iron-ligand inhibitor zileuton served as controls and exhibited IC_{50} values of 0.04 μM (±0.001 μM) and 0.51 μM (±0.13 μM) without exogenously added AA, and with addition of 20 μM AA IC_{50} values of 0.03 μM (±0.003 μM) and 1.6 μM (±0.79 μM), respectively (data not shown). Moreover, zileuton did not change the ratio of 5-LO products formed, regardless the presence of exogenous AA, while MK-886 inhibited LTB_4 formation more potently than 5-H(p)ETE in presence of exogenous AA (data not shown).

3.3. Inhibition of 5-LO product formation by EP6 is stimulus-independent

The activation of 5-LO in intact cells is modulated via increase of intracellular calcium leading to translocation of the enzyme from the cytosol to the nuclear envelope [56] or by phosphorylation of the enzyme [29,30]. Moreover, the cellular redox tone regulates the enzymatic activity [57] and a certain hydroperoxide level is required for conversion of 5-LO from the ferrous to the ferric form [58]. The activity of nonredox-type inhibitors strongly depends on the mode of enzyme activation and the cellular redox tone [26]. A common *in vitro* stimulus for the evaluation of 5-LO inhibitors is the non-physiological stimulus calcium ionophore A23187 leading to cellular calcium influx. Other stimuli are cell stress such as chemical stress (sodium arsenite (SA)) or hyperosmotic stress (NaCl), which in turn activate 5-LO via phosphorylation. After stimulation of intact PMNL with 300 mM NaCl, 10 μM SA or 2.5 μM calcium ionophore A23187, the efficacy

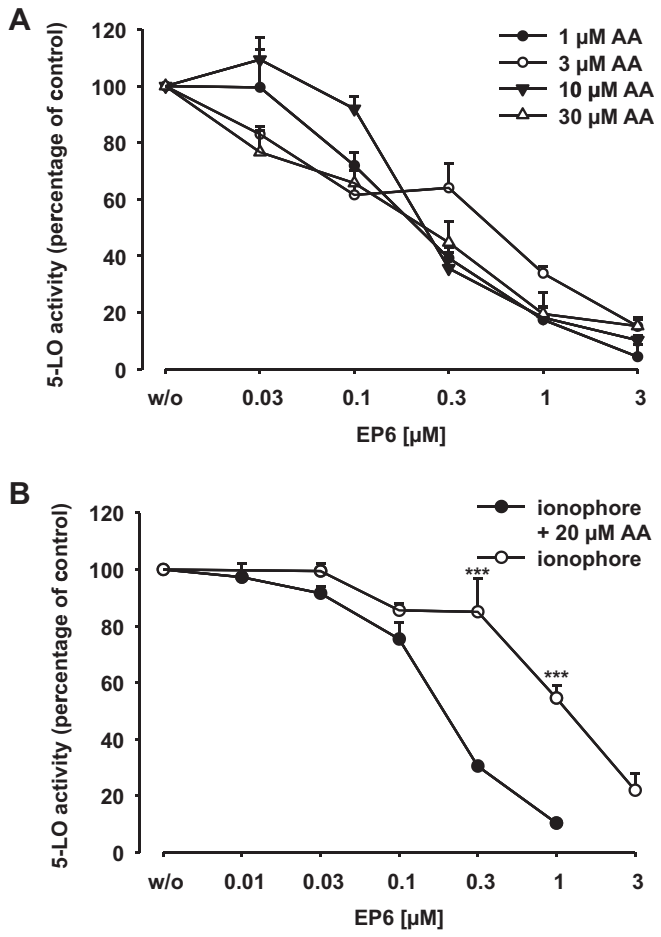

Fig. 3. Influence of substrate concentration on inhibition of 5-LO by **EP6**. (A) S100, corresponding to 7.5×10^6 PMNL were incubated as described for Fig. 2 with AA at the indicated concentrations and 5-LO product formation was determined. Data (mean ± S.E.; $n \geq 3$) are expressed as percentage of control. (B) 7.5×10^6 or 1×10^7 PMNL were incubated as described for Fig. 2 with or without 20 µM AA and 5-LO product formation was determined. Data (mean ± S.E.; $n \geq 3$) are expressed as percentage of control. $^{***}P < 0.001$ versus controls without AA addition at corresponding concentrations of test compound, two-way ANOVA + Tukey *post hoc* test.

of **EP6** was identical (Fig. 4A) and IC_{50} values of 0.2 µM were determined. **EP6** inhibits 5-LO in intact cells independently of these three stimuli for 5-LO activation. Furthermore a more physiological stimulus with LPS and fMLP was investigated. Intact PMNL were primed with 1 µg/ml LPS and 0.2 U/ml Ada and stimulated via 1 µM fMLP with or without addition of 20 µM AA (Fig. 4B). The inhibitory activity of **EP6** was reduced in intact PMNL after stimulation via LPS and fMLP compared to the other stimuli: an IC_{50} value of 0.74 µM (±0.06 µM) was determined in presence of exogenously added AA (Fig. 4B). Without exogenously added substrate the IC_{50} value even increased to 1.77 µM (±0.74 µM). Addition of exogenous AA (20 µM) led to an increase in the ratio of the 5-LO products 5-H(p)ETE to LTB_4, but both 5-LO metabolites (LTB_4 and 5-H(p)ETE) were inhibited with similar potency (data not shown). For the FLAP antagonist MK-886 IC_{50} values of 0.013 µM (±0.002 µM) in absence of exogenous AA and of 0.08 µM (±0.04 µM) in presence of exogenous AA were determined. Zileuton inhibited 5-LO product formation after stimulation via LPS and fMLP with IC_{50} values of 0.3 µM in absence of exogenous AA and of 0.66 µM (±0.07 µM) in presence of 20 µM exogenously added AA (data not shown). Again, while MK-886 inhibited LTB_4 formation more potently than 5-H(p)ETE in presence of exogenous AA, zileuton did not change the ratio of these metabolites (data not shown).

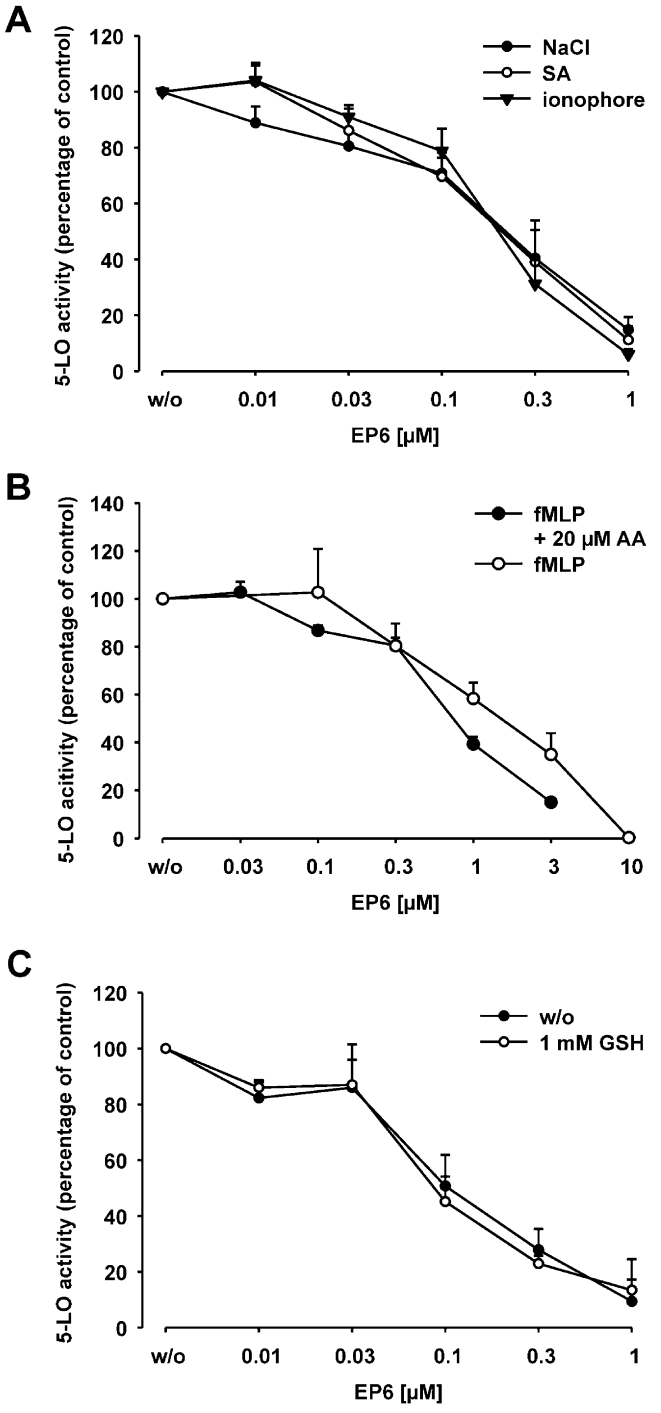

Fig. 4. Effects of different stimuli for 5-LO activation on 5-LO inhibition by **EP6**. (A) 7.5×10^6 freshly isolated PMNL were re-suspended in 1 ml PGC buffer and **EP6** or vehicle (DMSO) was added at the indicated concentrations. After 12 min at 37 °C, cells were pre-incubated with 300 mM NaCl or 10 µM SA for 3 min and 20 µM AA was added, or after 15 min at 37 °C cells were stimulated with 2.5 µM calcium ionophore A23187 together with 20 µM AA. After 10 min incubation, 5-LO product formation was determined. Data (mean ± S.E.; $n \geq 3$) are expressed as percentage of control. (B) 7.5×10^6 or 1×10^7 PMNL were primed with 1 µg/ml LPS and 0.2 U/ml Ada for 15 min at 37 °C, pre-incubated for 15 min at 37 °C with the indicated concentrations of **EP6** or vehicle (DMSO) and 5-LO product formation was stimulated by addition of 1 µM fMLP with or without addition of 20 µM AA. Data (mean ± S.E.; $n \geq 3$) are expressed as percentage of control. (C) S100, corresponding to 7.5×10^6 PMNL were incubated as described for Fig. 2 in the absence or presence of 1 mM GSH at 4 °C. Data (mean ± S.E.; $n \geq 3$) are expressed as percentage of control.

To investigate the influence of the redox tone on the potency of **EP6**, GSH, a cysteine-containing, redox-active tripeptide, was added in a cell free system. GSH serves as co-substrate of glutathione peroxidases leading to reducing conditions. The incubation of S100 samples with 1 mM GSH had no impact on the efficacy of **EP6** (Fig. 4C).

3.4. Influence of allosteric factors on the efficacy of EP6

The C2-like domain of 5-LO interacts with allosteric factors like ATP [15] and calcium [14] and mediates binding to cellular membranes [11] or phospholipid vesicles [12]. These allosteric factors are thought to induce conformational changes upon binding to 5-LO; therefore we investigated the interference of these factors with 5-LO inhibition by **EP6**. No influence on the inhibitory activity of **EP6** in cell-free systems could be measured for ATP and calcium (supplemental Fig. S1). In contrast, PC affected the inhibitory activity of **EP6**: to mimic 5-LO binding to cellular membranes, S100 of *E. coli* cultures of WT 5-LO were incubated with exogenously added PC (Fig. 5A). The presence of 20 μg/ml PC reduced the efficacy of **EP6** to an IC_{50} value of 1.04 μM (±0.28 μM). The IC_{50} value of the control, S100 of *E. coli* cultures of WT 5-LO without exogenously added PC, was 0.21 μM (±0.01 μM). In order to confirm the influence of PC on the interaction of 5-LO with **EP6**, the inhibitory potency of **EP6** in S100 of *E. coli* cultures of a 5-LO-3W mutant was investigated (Fig. 5B). Three tryptophan residues (W13, 75, 102) facilitating binding of PC [12], are mutated to alanine in this mutant. The 5-LO-3W mutant exhibits a reduced PC binding affinity thus the stimulating effect of PC is lower for the 5-LO-3W mutant in comparison to 5-LO WT [59]. For S100 of 5-LO-3W mutant, an IC_{50} value of 1.74 μM (±0.54 μM) without exogenously added PC and an IC_{50} value of 1.43 μM (±0.53 μM) with exogenously added PC was determined (Fig. 5B). **EP6** inhibited the S100 of 5-LO-3W mutant significantly less effective than the WT enzyme (Fig. 5B).

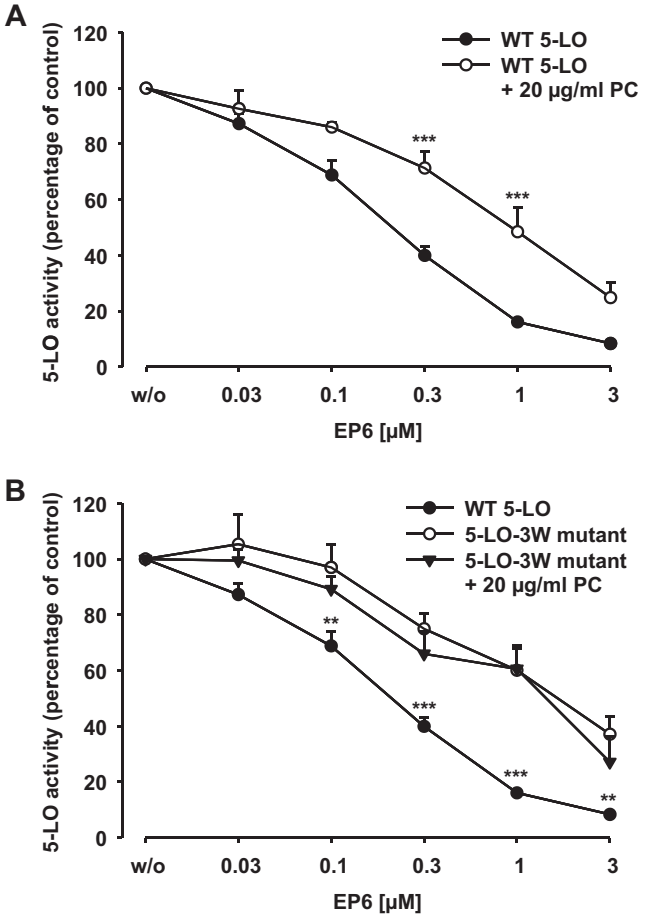

Fig. 5. Influence of allosteric factors on the inhibition of 5-LO by **EP6**. (A) S100 of WT 5-LO expressed by *E. coli* was incubated as described for Fig. 2 in the absence or presence of 20 μg/ml PC. Data (mean ± S.E.; $n \geq 3$) are expressed as percentage of control. $^{***}P < 0.001$ versus controls without PC addition at corresponding concentrations of test compound, two-way ANOVA + Tukey *post hoc* test. (B) S100 of WT 5-LO or 5-LO-3W mutant expressed by *E. coli* was incubated as described for Fig. 2. Data (mean ± S.E.; $n \geq 3$) are expressed as percentage of control. $^{**}P \leq 0.01$; $^{***}P < 0.001$ versus 5-LO-3W mutant at corresponding concentrations of test compound, two-way ANOVA + Tukey *post hoc* test.

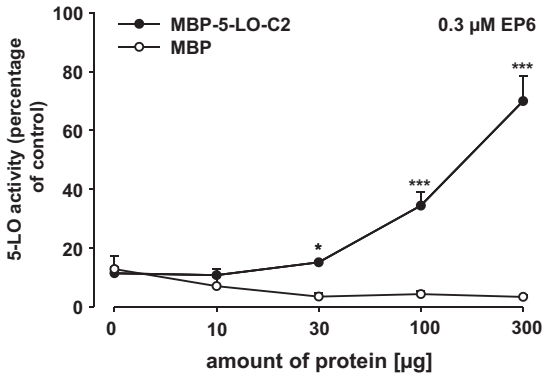

Fig. 6. C2-like domain competition assay. Increasing amounts (0–300 μg/ml) of MBP-5-LO-C2 were added to 2–3 μg partially purified 5-LO in 1 ml PBS, pH 7.4, 1 mM EDTA and 1 mM ATP. γ-Globuline was added to adjust consistent protein concentration (300 μg/ml). The samples were pre-incubated for 15 min with 0.3 μM **EP6** or vehicle (DMSO) at 4 °C. 5-LO product formation was stimulated and determined as described for Fig. 2. Data (mean ± S.E.; $n \geq 3$) are expressed as percentage of control (DMSO with the same amount of added protein). $^{*}P \leq 0.01$; $^{***}P < 0.001$ versus MBP at corresponding amounts, two-way ANOVA + Tukey *post hoc* test.

3.5. 5-LO C2-like domain: a putative binding region for EP6

To evaluate the interaction of **EP6** with the C2-like domain of 5-LO, a C2-like domain competition assay was performed. Partially purified 5-LO was incubated with 0.3 μM of **EP6** yielding a relative 5-LO activity of 13 ± 1% (Fig. 6). Increasing amounts of C2-like domain were added as fusion protein of MBP and C2-like domain (due to purification requirements). Increasing amounts of MBP alone were

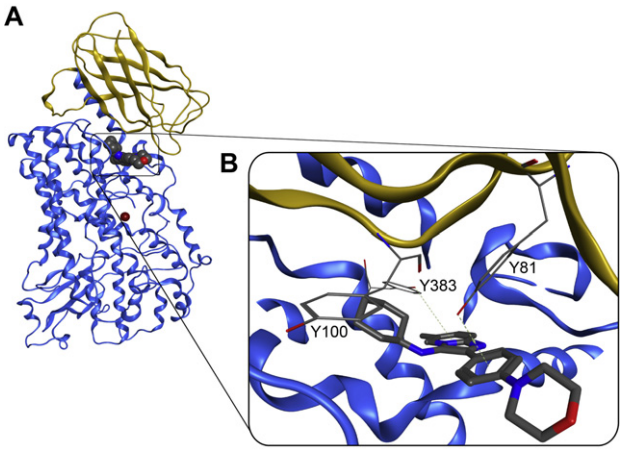

Fig. 7. (A) Structure of the restored 5-LO model of the crystal structure of engineered 5-LO [10]. Yellow: C2-like domain, blue: catalytic domain, red: active site iron, **EP6** is depicted in a spherical calotte representation. (B) Docking of **EP6** in the interface of the C2-like (yellow) and catalytic (blue) domain. Putative interacting amino acids are depicted and possible interactions are marked. **EP6** and interacting amino acids are depicted in stick representation colored by atom types.

added as control. Addition of MBP did not impair the inhibition of 5-LO by **EP6**. In contrast, the addition of MBP-5-LO-C2 led to an abolishment of the inhibition to 70 ± 8% of the relative 5-LO activity (Fig. 6). The presence of 300 μg of fusion protein of MBP and C2-like domain resulted in a low stimulation (118 ± 2% of control without MBP-C2-like domain, data not shown) of the purified 5-LO due to stabilizing scaffold properties of the C2-like domain. These results corroborate an interaction of **EP6** with the C2-like domain of 5-LO.

3.6. Docking of EP6 and mutagenesis studies for identification of a potential binding mode

For evaluation of the results of the C2-like domain competition assay, an *in silico* docking was performed for **EP6** with a restored 5-LO model of the crystal structure of engineered human 5-LO [10]. The binding pocket was defined in the interface between the catalytic and the C2-like domain of the 5-LO (Fig. 7). The docking study of **EP6** performed by a flexible side chain docking with PLANTS generated a set of 200 binding poses. The analysis of the conformations resulted in two different major orientations in which **EP6** was predicted to bind to the 5-LO.

To validate the statistical relevance of the different conformations and their underlying interactions PLIF were calculated for each pose (supplemental Fig. S2). The relative frequency of the described PLIF interactions, especially with Y81 (99.5%) and Y383 (96.5%) (supplemental Fig. S2 and Fig. 7B) is potentially indicative for the binding pose of **EP6** shown in Fig. 7B. The tyrosines are able to interact with aromatic ring systems of **EP6** via π interactions (Fig. 7B) with the imidazo[1,2-*a*]pyridine core (Y383) and the aromatic moiety neighboring the morpholine group. The morpholine group of **EP6** which is supposed to shield the bound inhibitor from the solvent, points out of the binding pocket (Fig. 7B and supplemental Fig. S3).

To verify these *in silico* results that represent a possible binding mode, two tyrosine residues within the C2-like domain (Y81, Y100) were replaced by alanine via site-directed mutagenesis. Y100 was positioned in the immediate receptor contact within the binding pocket (supplemental Fig. S3). The competition assay with the C2-like domain (*cf* Fig. 6) was repeated with a MBP-5-LO-C2 Y81/100A mutant. The addition of MBP-5-LO-C2 Y81/100A led to a much lower maximal reduction of the 5-LO inhibition (34 ± 3% remaining activity (Fig. 8)) compared to the addition of the WT C2-like domain (remaining enzyme activity: 70 ± 8% (Fig. 6)) confirming an involvement of these tyrosines in **EP6** binding. For specification of

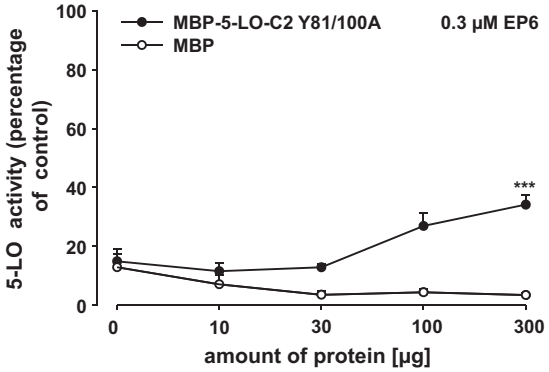

Fig. 8. C2-like domain competition assay. Increasing amounts (0–300 μg/ml) of MBP-5-LO-C2 Y81/100A were added to 2–3 μg partially purified 5-LO in 1 ml PBS, pH 7.4, 1 mM EDTA and 1 mM ATP. γ-Globuline was added to adjust consistent protein concentration (300 μg/ml). The samples were pre-incubated for 15 min with 0.3 μM **EP6** or vehicle (DMSO) at 4 °C. 5-LO product formation was stimulated and determined as described for Fig. 2. Data (mean ± S.E.; $n \geq 3$) are expressed as percentage of control (DMSO with the same amount of added protein). $^{***}P < 0.001$ versus MBP at corresponding amounts, two-way ANOVA + Tukey *post hoc* test.

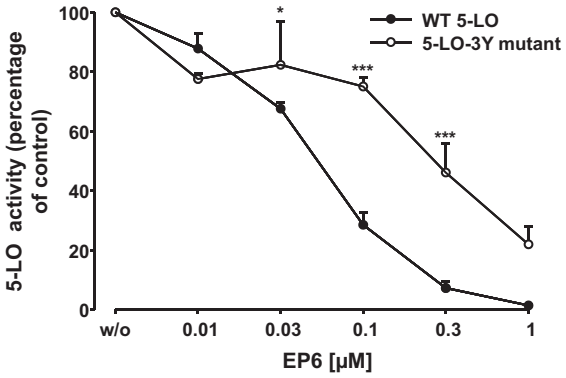

Fig. 9. Inhibition of partially purified 5-LO-3Y mutant by **EP6**. 2–3 μg partially purified 5-LO WT or 5-LO-3Y mutant were incubated as described for Fig. 2. Data (mean ± S.E.; $n \geq 3$) are expressed as percentage of control. $^{*}P \leq 0.05$; $^{**}P \leq 0.01$; $^{***}P < 0.001$ versus WT 5-LO at corresponding concentrations of test compound, two-way ANOVA + Tukey *post hoc* test.

this putative binding mode, the tyrosines (Y81, Y100, and Y383) were replaced by alanine within the whole enzyme. Single mutants (Y81A, Y100A and Y383A), a C2-like domain double mutant (Y81/100A) and a triple mutant (Y81/100/383A, 3Y) were investigated. The replacement of the tyrosines within the C2-like domain led to no change in the inhibitory efficacy of **EP6** (Table 1). The IC_{50} values were comparable (no significant differences) for the 5-LO WT and the three C2-like domain mutants (IC_{50} = 0.03 μM (±0.01 μM)–0.08 μM (± 0.04 μM), Table 1). However, the mutation of tyrosine at position 383 yielded an IC_{50} value of 0.14 μM (±0.02 μM) implying an interaction of this amino acid with the compound. Furthermore, **EP6** inhibited the 5-LO-3Y mutant with an IC_{50} value of 0.23 μM (±0.08 μM), significantly ($^{**}P < 0.01$) less potent than the 5-LO WT (IC_{50} = 0.05 μM (±0.01 μM)) (Fig. 9). The specific activities of 5-LO WT and the mutants are comparable (Table 1), implying native fold proteins with no impaired catalytic activity. The results of the 5-LO-3Y mutant confirmed an impact of the C2-like domain (via Y81 and Y100) and corroborate the results of the C2-like domain competition assay.

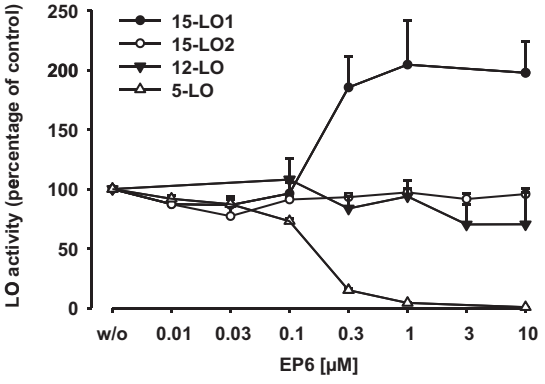

Fig. 10. Selectivity profile of **EP6**. (A) For determination of 5-, 12-LO and 15-LO1 product formation, 5×10^6 intact PMNL or 1×10^8 intact platelets were re-suspended in PGC buffer and pre-incubated for 15 min at 37 °C with the indicated concentrations of **EP6** or vehicle (DMSO). LO product formation in PMNL was started by addition of 2.5 μM calcium ionophore and 20 μM AA. For 12-LO activity in platelets 10 μM AA was added. For determination of 15-LO2 activity, 0.5 U human recombinant 15-LO2 was dissolved in 1 ml PBS, pH 7.4 and pre-incubated for 15 min on ice with the indicated concentrations of **EP6** and vehicle (DMSO). 15-LO2 activity was started by adding 100 μM AA. After 10 min, 5-, 12-LO and 15-LO product formation was determined. 12-LO products include 12(*S*)-hydro(pero)xy-6-*trans*-8,11,14-*cis*-eicosatetraenoic acid (12-H(p)ETE). 15-LO products were 15(*S*)-hydro(pero)xy-5,8,11-*cis*-13-*trans*-eicosatetraenoic acid (15-H(p)ETE). Data (mean ± S.E.; $n \geq 3$) are expressed as percentage of control.

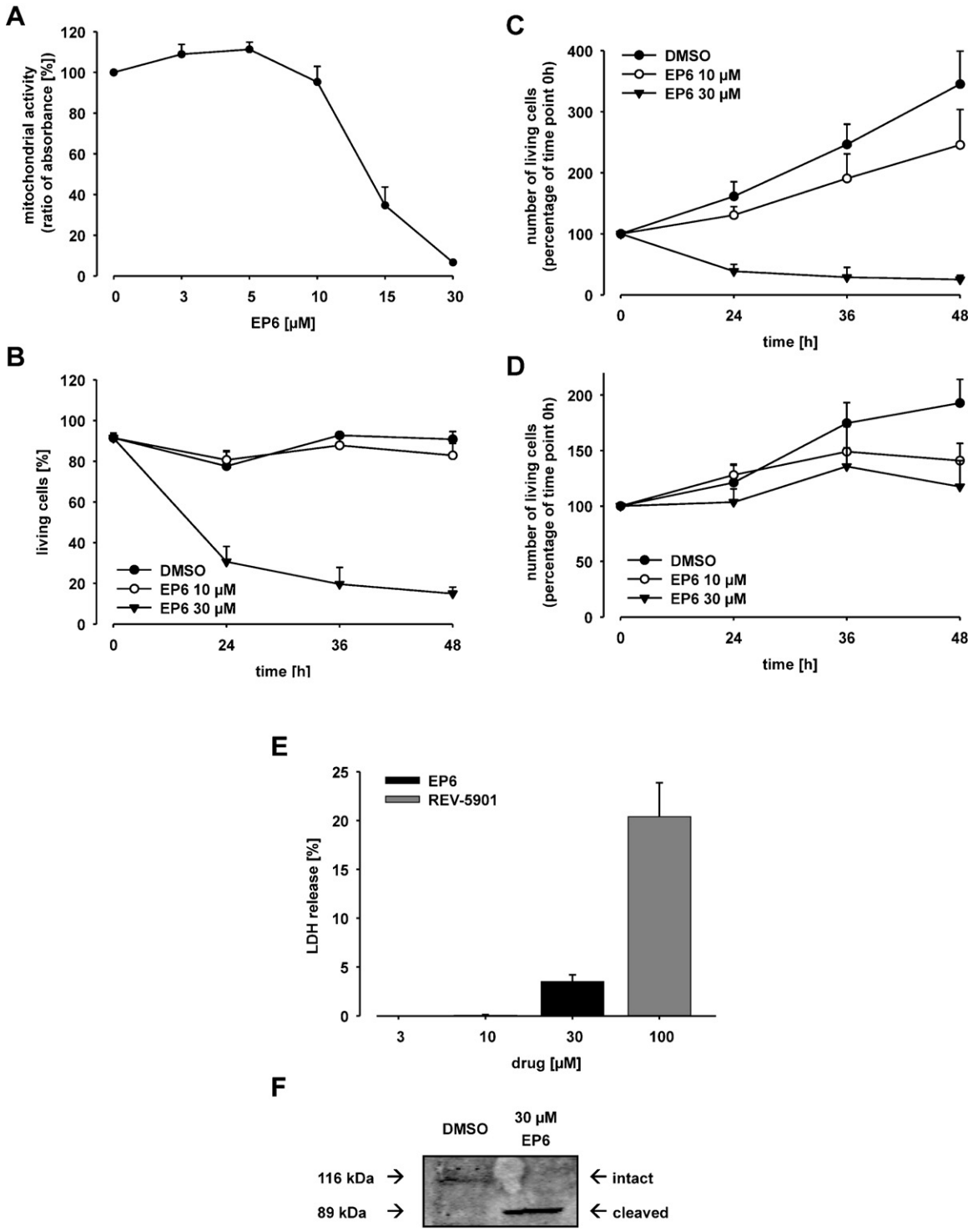

Fig. 11. Effects of **EP6** on cell viability. (A) U937 cell viability after 48 h treatment with increasing concentrations of **EP6** (3–30 μM) was assessed using a WST-1 proliferation assay. Values, measured as ratio of absorbance for a given concentration of **EP6** and the control (DMSO) after 48 h, present mean ± S.E. of three independent experiments. (B) Long-term viability assay with U937 cells. Cells were treated with 10 μM and 30 μM **EP6** for 24 h, 36 h and 48 h and the survival rates, measured as percentage of living cells compared to total cell number at a given time point, were measured by trypan blue exclusion. Values are given as mean ± S.E. of three independent experiments. (C) Long-term viability assay with U937 cells. Cells were treated with 10 μM and 30 μM **EP6** for 24 h, 36 h and 48 h and the survival rates were measured by trypan blue exclusion. The survival rates were calculated as ratio of the number of living cells at time point 0 h and a particular time point. Values are given as mean ± S.E. of three independent experiments. (D) Long-term viability assay with RPE cells. Cells were treated with 10 μM and 30 μM **EP6** for 24 h, 36 h and 48 h and the survival rates were measured by trypan blue exclusion. The survival rates were calculated as ratio of the number of living cells at time point 0 h and a particular time point. Values are given as mean ± S.E. of three independent experiments. (E) Effect of **EP6** on LDH release by U937 cells. Cells were incubated with increasing concentrations (3–30 μM) of **EP6** or 5-LO inhibitor Rev-5901 (100 μM) for 48 h. LDH release induced by a control detergent supplied by Sigma–Aldrich (Saint Louis, MO, USA) was set to 100%. Values are given as mean ± S.E. of three independent experiments. (F) Western blot analysis of PARP cleavage after treatment of U937 cells with 30 μM **EP6** for 24 h. 35 μg of total protein extract was separated on a 10% SDS-polyacrylamide gel and electroblotted onto a nitrocellulose membrane. Cleaved and intact PARP were detected using a specific antibody. One of three independent experiments is shown.

Table 1
IC_{50} values for inhibition of partially purified WT 5-LO and 5-LO-Y mutants. Mean of three experiments.

Mutant	IC_{50} value [μM]	Specific activity (ng products/μg protein)
WT	0.05 (±0.01)	361 (±151)
Y81A	0.06 (±0.02)	398 (±61)
Y100A	0.08 (±0.04)	308 (±70)
Y383A	0.14 (±0.02)	202 (±4)
Y81/100A	0.03 (±0.01)	262 (±32)
3Y	0.32 (±0.08)	260 (±85)

3.7. Investigations on pleiotropic effects and influence on cell viability of EP6

Furthermore, pleiotropic effects of **EP6** regarding several other AA binding proteins were investigated. In intact PMNL 5-LO selectivity was determined. **EP6** did not inhibit 15-LO1 (Fig. 10). The increase in 15-LO1 products could be due to the shunt of substrate to 15-LO1 when 5-LO is inhibited at least in our experimental setting where exogenous AA is present. Recombinant human 15-LO2 was not inhibited by **EP6** either (Fig. 10). In addition, the effect on platelet-type 12-LO was investigated (Fig. 10). No reduction of 12-H(p)ETE was measured. Three additional enzymes of the AA cascade, COX-1, COX-2 and mPGES-1, were investigated. COX-1 and COX-2 inhibition up to a concentration of 10 μM of **EP6** was not observed. Within the COX-1 assay, 10 μM **EP6** exhibited a residual activity of 93.6 ± 6% of control, 1 μM of the COX-1 inhibitor SC-560 [60] led to 4.4 ± 1% of control. For COX-2 residual activities of 101 ± 7% of control for 10 μM **EP6** and 21.8 ± 6% of control for 1 μM of the COX-2 inhibitor rofecoxib [61] were measured (data not illustrated). **EP6** showed no inhibitory effect on mPGES-1 activity in a cell-free assay up to 30 μM as well. For 30 μM **EP6** a residual activity of 89.4 ± 19% of control was determined (data not illustrated). For the known mPGES-1 inhibitor MD52 [62] a residual activity of 32.2 ± 13% at 0.3 μM was measured.

A salmonella mutagenicity test [52] for detecting a carcinogenic and mutagenic potential of **EP6** led to neither frameshift nor substitution mutations independent of oxidative metabolism up to 100 μM **EP6** (data not shown).

We further tested **EP6** in a murine leukemic monocyte macrophage cell line (supplemental Fig. S4). In intact RAW 264.7 cells an IC_{50} value of 2.1 μM (±0.45 μM) was determined. For cell-free S100 preparations of RAW 264.7 cells, 5-LO product formation was inhibited with an IC_{50} value of 0.36 μM (±0.07 μM).

Short-term viability in intact PMNL after incubation for 30 min with **EP6** at 37 °C, confirmed no cytotoxic effects during activity assays for concentrations up to 30 μM (supplemental Fig. S5). In contrast, when U937 mitochondrial metabolic activity was assessed after treatment with increasing concentrations of **EP6** using a WST-1 assay, a reduction in cellular viability could be seen. **EP6** reduced the number of viable cells by 50% at a concentration of 14 μM (Fig. 11A) after 48 h. The WST-1 assay does not distinguish between anti-proliferative or cytotoxic effects. Impaired cell viability in the WST-1 assay may be due to a reduction of the total number of viable cells caused by anti-proliferative properties of **EP6**. Alternatively, **EP6** may possess cytotoxic properties inducing necrosis or apoptosis. Therefore, we investigated the influence on cell viability of U937 and non-tumor RPE cells after treatment with 30 μM **EP6** for 24 h, 36 h and 48 h by trypan blue exclusion. The survival rate for U937 cells after treatment for 24 h with 30 μM **EP6** was 31 ± 8% and decreased to 15 ± 3% after 48 h (Fig. 11B) confirming the results seen in the WST-1 assay. Comparison of the number of living cells at particular time points to time point 0 h revealed a strong influence of 30 μM **EP6** on cell viability (Fig. 11C) but excluded exclusive anti-proliferative effects since the total number of living cells further decreased compared to the cell number seeded. Interestingly, **EP6** had no influence on the cell viability of the non-tumor RPE cells (overall survival rate: 94 ± 2% (data not shown)), although a slight interference with cell proliferation in these cells could be observed as the total number of viable cells did not significantly increase after treatment with the inhibitor compared to the control (Fig. 11D). To clarify whether the reduction of cellular viability in U937 resulted from cell death events like necrosis or apoptosis, we additionally investigated the loss of cell membrane integrity and PARP cleavage in **EP6** treated U937 cells. Lactate dehydrogenase (LDH) leakage is a measure for impaired membrane integrity which points to necrotic events. When treated with increasing concentrations of **EP6** up to 30 μM for 48 h, U937 cells displayed only weak LDH release (Fig. 11E). The known nonredox-type 5-LO inhibitor Rev-5901 was used as cytotoxic control [51]. Since necrotic effects could be excluded as a cause for **EP6** mediated cytotoxicity, PARP-cleavage was assessed as a marker for apoptosis. In this late apoptotic event activated caspase-3 and caspase-6 cleave the 116 kDa nuclear protein PARP specifically into a 89 kDa and 29 kDa fragment which can be detected by Western blotting. The treatment of U937 cells with 30 μM **EP6** for 24 h led to the 89 kDa cleavage product, which could not be detected in the untreated control (Fig. 11F).

4. Discussion and conclusions

In the present study we investigated the pharmacological profile of **EP6** (cyclohexyl-[6-methyl-2-(4-morpholin-4-yl-phenyl)-imidazo[1,2-*a*]pyridin-3-yl]-amine), a novel 5-LO inhibitor with distinct properties compared to compounds belonging to known classes of 5-LO inhibitors. **EP6** potently suppressed 5-LO product formation in several *in vitro* assay systems with an IC_{50} value of 0.16 μM in intact PMNL and 0.05 μM for partially purified enzyme (Fig. 2). This direct inhibitor exhibited selectivity for 5-LO and did not inhibit 12-LO, 15-LO1 and 15-LO2 (Fig. 10) or additional enzymes of the AA cascade, COX-1, COX-2 and mPGES-1. **EP6** was active in mouse leukemic monocyte macrophage cells and suppressed 5-LO in intact and cell-free assays (supplemental Fig. S4). In addition, the compound showed no mutagenic potential and did not impair the viability of normal human RPE cells up to a concentration of 30 μM, prerequisites for future in vivo investigations (Fig. 11D).

In contrast to this, impaired cell viability of human leukemic monocytic cells (U937) (Fig. 11) with overall viability being reduced by 50% at 14 μM in a WST-1 assay (Fig. 11A) and decreased cell survival (15 ± 3%) in a trypan blue exclusion assay (Fig. 11B) was seen after treatment with 30 μM of **EP6** for 48 h. Cell counts in the trypan blue exclusion assay decreased in comparison to seeded cell numbers excluding an anti-proliferative mechanism as exclusive reason for the effect on cell viability of **EP6**. LDH release was only weakly triggered in higher concentrations (3.5 ± 0.7% at 30 μM) (Fig. 11E) excluding necrosis as primary cause as well. Finally, cleavage of PARP as a marker for late apoptosis in **EP6** (30 μM) treated U937 gave a first hint to the underlying cytotoxic mechanism (Fig. 11F) which has to be investigated further in the future.

Experimental data revealed that 5-LO binds allosteric regulatory factors. These regulatory properties are mediated by the C2-like domain involving defined amino acid residues or regions within this domain. For evaluation of the binding mode and potential binding sites, the influence of these allosteric factors on the efficacy of **EP6** was tested (Fig. 5 and supplemental Fig. S1). The addition of PC to S100 of *E. coli* cultures of WT 5-LO resulted in a shift of the IC_{50} value from 0.21 μM (±0.01 μM) to 1.04 μM (±0.28 μM) (Fig. 5A). Experiments with S100 of WT 5-LO or 5-LO-3W mutant expressed by *E. coli* corroborate this result: the 5-LO-3W mutant exhibits a reduced stimulating effect of PC due to its restricted

binding affinity of PC [58] and the inhibitory potency of **EP6** for this mutant is unaffected by the addition of PC (Fig. 5B). In comparison, the 5-LO-3W mutant, which in general can be inhibited by 5-LO inhibitors [59], is less suppressed by **EP6** than the WT 5-LO (Fig. 5B). The tryptophans W13, W75 and W102 which are responsible for interaction with PC, seem to be, directly or indirectly via conformational changes, involved in the interaction of **EP6** with 5-LO. The C2-like domain competition assay confirms a binding site located at the C2-like domain (Figs. 6 and 8). Furthermore three tyrosines, two within the C2-like domain (Y81, Y100) and one in the catalytic domain (Y383) (Fig. 7), were derived from an *in silico* docking and emphasized via mutagenesis studies (Figs. 6, 8 and 9) the interface of the C2-like and the catalytic domain as a possible binding region for **EP6**. Although the single mutants and double mutant did not show impaired IC_{50} values for inhibition of 5-LO (Table 1), the 5-LO-3Y mutant did exhibit a significantly lower IC_{50} value for inhibition of 5-LO compared to WT 5-LO. The interaction of Y383 and **EP6** alone seems to be strong enough for enzyme inhibition. Together, these findings indicate a new binding site for inhibitors at the C2-like domain of the enzyme. Allosteric regulation of LOs is known [63,64] and for 5-LO, allosteric inhibitor binding could be shown for two compounds: Acetyl-11-keto-β-boswellic acid [65] and hyperforin [66] were identified to bind to the C2-like domain of 5-LO [59,67]. Targeting this allosteric site might open up a new promising approach for 5-LO inhibition.

Compound **1** [39] was assigned by Pergola and Werz to a new group of diverse 5-LO inhibitors [68]. Redox-active inhibitors with reducing properties, iron ligand inhibitors chelating the active site iron and nonredox-type inhibitors have distinct properties from **EP6** [69]. Nonredox-type inhibitors were designed as active site-directed AA mimetics [18]. A second (regulatory) fatty acid binding site [67,70] can be assumed to be located at the C2-like domain as shown for 12/15-LO [71]. Nonredox-type inhibitors like CJ-13,610 interfere with this regulatory- and with the substrate-binding cleft at the active site [72]. Characterization of **EP6** revealed no effect on the inhibitory potency by different AA concentrations (Fig. 3A). Under chronic inflammatory processes that are associated with elevated levels of lipid hydroperoxide and free AA, nonredox-type inhibitors have a reduced efficacy [26]. **EP6** might avoid this disadvantage due to its irrespective inhibitory effect in the presence of elevated AA concentrations (Fig. 3A). **EP6** indicates properties of uncompetitive inhibitors (Figs. 3B and 4B) exhibiting higher IC_{50} values in the absence of exogenous added substrate after stimulation via calcium ionophore or the more physiological stimulus fMLP. Possibly, a certain amount of AA positively modulates 5-LO activity at the second, stimulatory AA binding site [67,70] and this might be efficiently blocked by **EP6**. On the other hand, **EP6** might inhibit cytosolic 5-LO more potently than membrane-bound 5-LO: (1) in absence of exogenous AA, PMNL produce primarily membrane-mediated LTs and (2) cytosolic 5-LO needs calcium for full activation, but fMLP stimulation only causes a 4-fold lower calcium influx compared to ionophore stimulation [73]. This might explain the higher IC_{50} value for fMLP stimulation even in presence of AA and for ionophore stimulation in absence of exogenous AA. **EP6** seems to have a decreased potency at membrane-bound 5-LO. This is also in line with the observed lower IC_{50} value in presence of PC (Fig. 5A). However, we could not detect differences in the IC_{50} values for inhibition of LTB_4 and 5-H(p)ETE formation (data not shown). The same pattern was observed for zileuton, but not for the FLAP inhibitor MK-886, which inhibited LTB_4 formation more potently than 5-H(p)ETE (in presence of AA).

Another property of nonredox-type inhibitors is an impaired inhibition of purified 5-LO or 5-LO in broken cell preparations due to a dependence on a low lipid hydroperoxide tone or the presence of reducing agents like GSH or DTT [26,72]. Notably, we were able to suspend some apparent drawbacks of these inhibitors as **EP6** suppresses 5-LO independently of the addition of thiols (Fig. 4C) and has a comparable activity in intact cells and broken cell preparations (Fig. 2).

In the cellular context, 5-LO is soluble and located in the cytosol and translocates to the nuclear envelope after activation [28]. External stimuli promote an increase of intracellular calcium or phosphorylation of 5-LO by kinases of the MAPK family [29,30]. The potency of some nonredox-type inhibitors, e.g. ZM230487 and L-739.010 [22], depends on the mode of activation of the enzyme. A 10–100-fold higher inhibitor concentration is required to suppress 5-LO activity activated by phosphorylation comparable to 5-LO activated via calcium influx [27]. We were able to show that **EP6** acts independently of the mode of 5-LO activation in the cell (Fig. 4A). In this regard, the efficacy of **EP6** in vivo might be promising related to potential activity in chronic inflammatory processes associated with an increased phosphorylation status in cells [31,32]. After activation by the pathophysiologically relevant stimulus via LPS/fMLP, **EP6** inhibits 5-LO product formation although with a slightly higher IC_{50} value (Fig. 4B).

Compared to zileuton, the only 5-LO inhibitor in clinical use which inhibits 5-LO activity in various assay systems with IC_{50} values of 0.5–1 μM [8], **EP6** is up to 10-fold more potent. Furthermore, with **EP6**s molecular pharmacological profile distinct of FLAP inhibitors, which are being studied in clinical trials and benefits in respiratory diseases [74] could be demonstrated for, **EP6** might open up a novel approach for inhibition of LT formation via the hypothetical mode of action at an allosteric site of 5-LO. Besides the indication of inhibitors of LT biosynthesis in asthma, these inhibitors may have therapeutic potential in treatment of cardiovascular disease and cancer [3]. 5-LO inhibitors may be applied in these fields since the LT pathway enzymes and receptors are abundantly expressed in cancer tissues compared to healthy tissues [75]. But the underlying mechanisms through which LTs influence carcinogenesis are still incompletely understood. Effects of **EP6** on 5-LO overexpressing tumor cells were not investigated herein. However, the selectivity for 5-LO over 15-LO suggests **EP6** as a possible anticancer agent as 15-LO is known to have tumor suppressive effects [76,77]. Moreover, the tested U937 cells lack 5-LO expression and the concentrations needed to induce cytotoxic effects (50% reduction of overall viability at 14 μM) in these cells exceeded the IC_{50} value in intact PMNL (0.16 μM (±0.01 μM)) about 90-fold. Therefore, the reduction of cell viability in these cells seems to be independent of inhibition of 5-LO product formation. This has been published for a number of other 5-LO inhibitors before by our group [51] and is subject of further investigations at the moment. Interestingly, drugs based on a scaffold of N-fused imidazoles were recently recognized as novel anticancer agents with potential topoisomerase IIα inhibitory properties [78]. The promising effects of **EP6** on cell viability in 5-LO negative tumor cells and its selectivity profile, encourages further investigation of this novel 5-LO inhibitor's possible 5-LO dependent and independent anticancer properties.

Taken together, this study characterizes **EP6**, a novel direct 5-LO inhibitor exhibiting auspicious properties in various *in vitro* assays in contrast to properties of some nonredox-type inhibitors. Targeting 5-LO independently of the cellular redox tone, the substrate concentration and furthermore independent of the stimulus of 5-LO activation, **EP6** obviously possesses advantages over known 5-LO inhibitors. Our results indicate an interaction of **EP6** with the regulatory C2-like domain of the enzyme, providing a new feasible binding site for the development of novel compounds. Nevertheless, although the C2-like domain was derived as a target region, a precise binding site has not been elucidated yet. Knowledge of the precise binding mode would open up new options for structure-based optimization and development of novel compounds with the beneficial pharmacological profile of **EP6**.

Supplementary material

Synthesis procedure, molecular modeling of the putative binding mode and analysis of docking results, influence of calcium and ATP on the inhibitory potency of **EP6**, inhibitory potency in RAW 264.7 cells, and a short-term viability assay are available as supplementary material.

Acknowledgements

The authors thank Oncogenic Signaling Frankfurt (OSF), Lipid Signaling Forschungszentrum Frankfurt (LiFF), Fonds der Chemischen Industrie and the EU (LSHM-CT-2004-0050333) for financial support. The authors thank Prof. Dr. Manfred Schubert-Zsilavecz and Michaela Dittrich for the reference compound MD52. We thank Astrid Brüggerhoff for expert technical assistance.

Appendix A. Supplementary data

Supplementary data associated with this article can be found, in the online version, at doi:10.1016/j.bcp.2011.10.012.

References

[1] Dahlén SE, Hedqvist P, Hammarström S, Samuelsson B. Leukotrienes are potent constrictors of human bronchi. Nature 1980;288:484–6.
[2] Funk CD. Prostaglandins and leukotrienes: advances in eicosanoid biology. Science 2001;294:1871–5.
[3] Werz O, Steinhilber D. Therapeutic options for 5-lipoxygenase inhibitors. Pharmacol Ther 2006;112:701–18.
[4] Peters-Golden M, Henderson WR. Leukotrienes. N Engl J Med 2007;357:1841–54.
[5] Samuelsson B, Dahlén SE, Lindgren JA, Rouzer CA, Serhan CN. Leukotrienes and lipoxins: structures, biosynthesis, and biological effects. Science 1987;237:1171–6.
[6] Rådmark O, Samuelsson B. Regulation of the activity of 5-lipoxygenase, a key enzyme in leukotriene biosynthesis. Biochem Biophys Res Commun 2010;396:105–10.
[7] Chen Y, Hu Y, Zhang H, Peng C, Li S. Loss of the Alox5 gene impairs leukemia stem cells and prevents chronic myeloid leukemia. Nat Genet 2009;41:783–92.
[8] Carter GW, Young PR, Albert DH, Bouska J, Dyer R, Bell RL, et al. 5-lipoxygenase inhibitory activity of zileuton. J Pharmacol Exp Ther 1991;256:929–37.
[9] Berman HM, Battistuz T, Bhat TN, Bluhm WF, Bourne PE, Burkhardt K, et al. The Protein Data Bank. Acta Crystallogr D Biol Crystallogr 2002;58:899–907.
[10] Gilbert NC, Bartlett SG, Waight MT, Neau DB, Boeglin WE, Brash AR, et al. The structure of human 5-lipoxygenase. Science 2011;331:217–9.
[11] Chen XS, Funk CD. The N-terminal beta-barrel domain of 5-lipoxygenase is essential for nuclear membrane translocation. J Biol Chem 2001;276:811–8.
[12] Kulkarni S, Das S, Funk CD, Murray D, Cho W. Molecular basis of the specific subcellular localization of the C2-like domain of 5-lipoxygenase. J Biol Chem 2002;277:13167–74.
[13] Hörnig C, Albert D, Fischer L, Hörnig M, Rådmark O, Steinhilber D, et al. 1-Oleoyl-2-acetylglycerol stimulates 5-lipoxygenase activity via a putative (phospho)lipid binding site within the N-terminal C2-like domain. J Biol Chem 2005;280:26913–21.
[14] Hammarberg T, Provost P, Persson B, Rådmark O. The N-terminal domain of 5-lipoxygenase binds calcium and mediates calcium stimulation of enzyme activity. J Biol Chem 2000;275:38787–93.
[15] Zhang YY, Hammarberg T, Rådmark O, Samuelsson B, Ng CF, Funk CD, et al. Analysis of a nucleotide-binding site of 5-lipoxygenase by affinity labelling: binding characteristics and amino acid sequences. J Biol Chem 2000;351:3697–707.
[16] Rådmark OP. The molecular biology and regulation of 5-lipoxygenase. Am J Respir Crit Care Med 2000;161:S11–5.
[17] Tateson JE, Randall RW, Reynolds CH, Jackson WP, Bhattacherjee P, Salmon JA, et al. Selective inhibition of arachidonate 5-lipoxygenase by novel acetohydroxamic acids: biochemical assessment in vitro and ex vivo. Br J Pharmacol 1988;94:528–39.
[18] McMillan RM, Walker ER. Designing therapeutically effective 5-lipoxygenase inhibitors. Trends Pharmacol Sci 1992;13:323–30.
[19] Steinhilber D. 5-Lipoxygenase: a target for antiinflammatory drugs revisited. Curr Med Chem 1999;6:71–85.
[20] Evans JF, Lévillé C, Mancini JA, Prasit P, Thérien M, Zamboni R, et al. 5-Lipoxygenase-activating protein is the target of a quinoline class of leukotriene synthesis inhibitors. Mol Pharmacol 1991;40:22–7.
[21] Crawley GC, Dowell RI, Edwards PN, Foster SJ, McMillan RM, Walker ER, et al. Methoxytetrahydropyrans. A new series of selective and orally potent 5-lipoxygenase inhibitors. J Med Chem 1992;35:2600–9.
[22] Crawley GC, Briggs MT, Dowell RI, Edwards PN, Hamilton PM, Kingston JF, et al. 4-Methoxy-2-methyltetrahydropyrans: chiral leukotriene biosynthesis inhibitors, related to ICI D2138, which display enantioselectivity. J Med Chem 1993;36:295–6.
[23] Smith WG, Shaffer AF, Currie JL, Thompson JM, Kim S, Rao T, et al. Characterization of 5-lipoxygenase inhibitors in biochemical and functional in vivo assays. J Pharmacol Exp Ther 1995;275:1332–8.
[24] Nasser SM, Bell GS, Hawksworth RJ, Spruce KE, MacMillan R, Williams AJ, et al. Effect of the 5-lipoxygenase inhibitor ZD2138 on allergen-induced early and late asthmatic responses. Thorax 1994;49:743–8.
[25] Turner CR, Smith WB, Andresen CJ, Eggler JF, Watson JW. The effect of 5-lipoxygenase inhibition on Ascaris antigen (Ag)-induced responses in atopic monkeys. Inflamm Res 1996;45:42–9.
[26] Werz O, Szellas D, Henseler M, Steinhilber D. Nonredox 5-lipoxygenase inhibitors require glutathione peroxidase for efficient inhibition of 5-lipoxygenase activity. Mol Pharmacol 1998;54:445–51.
[27] Fischer L, Szellas D, Rådmark O, Steinhilber D, Werz O. Phosphorylation- and stimulus-dependent inhibition of cellular 5-lipoxygenase activity by nonredox-type inhibitors. FASEB J 2003;17:949–51.
[28] Peters-Golden M, Brock TG. Intracellular compartmentalization of leukotriene synthesis: unexpected nuclear secrets. FEBS Lett 2001;487:323–6.
[29] Werz O, Szellas D, Steinhilber D, Rådmark O. Arachidonic acid promotes phosphorylation of 5-lipoxygenase at Ser-271 by MAPK-activated protein kinase 2 (MK2). J Biol Chem 2002;277:14793–800.
[30] Werz O, Bürkert E, Fischer L, Szellas D, Dishart D, Samuelsson B, et al. Extracellular signal-regulated kinases phosphorylate 5-lipoxygenase and stimulate 5-lipoxygenase product formation in leukocytes. FASEB J 2002;16:1441–3.
[31] Hajjar DP, Pomerantz KB. Signal transduction in atherosclerosis: integration of cytokines and the eicosanoid network. FASEB J 1992;6:2933–41.
[32] Johnson GL, Lapadat R. Mitogen-activated protein kinase pathways mediated by ERK, JNK, and p38 protein kinases. Science 2002;298:1911–2.
[33] Mancini JA, Abramovitz M, Cox ME, Wong E, Charleson S, Perrier H, et al. 5-Lipoxygenase-activating protein is an arachidonate binding protein. FEBS Lett 1993;318:277–81.
[34] Evans JF, Ferguson AD, Mosley RT, Hutchinson JH. What's all the FLAP about?: 5-lipoxygenase-activating protein inhibitors for inflammatory diseases. Trends Pharmacol Sci 2008;29:72–8.
[35] Gillard J, Ford-Hutchinson AW, Chan C, Charleson S, Denis D, Foster A, et al. L-663,536 (MK-886) (3-[1-(4-chlorobenzyl)-3-t-butyl-thio-5-isopropylindol-2-yl]-2,2-dimethylpropanoic acid), a novel, orally active leukotriene biosynthesis inhibitor. Can J Physiol Pharmacol 1989;67:456–64.
[36] Prasit P, Belley M, Blouin M, Brideau C, Chan C, Charleson S, et al. A new class of leukotriene biosynthesis inhibitor: the development of MK-0591. J Lipid Mediat 1993;6:239–44.
[37] Hutchinson JH, Li Y, Arruda JM, Baccei C, Bain G, Chapman C, et al. 5-Lipoxygenase-activating protein inhibitors: development of 3-[3-tert-butylsulfanyl-1-[4-(6-methoxy-pyridin-3-yl)-benzyl]-5-(pyridin-2-ylmethoxy)-1H-indol-2-yl]-2,2-dimethyl-propionic acid (AM103). J Med Chem 2009;52:5803–15.
[38] Sampson AP. FLAP inhibitors for the treatment of inflammatory diseases. Curr Opin Investig Drugs 2009;10:1163–72.
[39] Hofmann B, Franke L, Proschak E, Tanrikulu Y, Schneider P, Steinhilber D, et al. Scaffold-hopping cascade yields potent inhibitors of 5-lipoxygenase. ChemMedChem 2008;3:1535–8.
[40] Groebke K, Weber L, Mehlin F. Synthesis of imidazo[1,2-a] annulated pyridines, pyrazines and pyrimidines by a novel three-component condensation. Synlett 1998;29:661–3.
[41] Cinatl JJ, Blaheta R, Bittoova M, Scholz M, Margraf S, Vogel JU, et al. Decreased neutrophil adhesion to human cytomegalovirus-infected retinal pigment epithelial cells is mediated by virus-induced up-regulation of Fas ligand independent of neutrophil apoptosis. J Immunol 2000;165:4405–13.
[42] Werz O. Activation of 5-lipoxygenase by cell stress is calcium independent in human polymorphonuclear leukocytes. Blood 2002;99:1044–52.
[43] Zhang YY, Rådmark O, Samuelsson B. Mutagenesis of some conserved residues in human 5-lipoxygenase: effects on enzyme activity. Proc Natl Acad Sci USA 1992;89:485–9.
[44] Michel AY, Steinhilber D, Werz O. Development of a method for expression and purification of the regulatory C2-like domain of human 5-lipoxygenase. Protein Expr Purif 2008;59:110–6.
[45] Hammarberg T, Zhang YY, Lind B, Rådmark O, Samuelsson B. Mutations at the C-terminal isoleucine and other potential iron ligands of 5-lipoxygenase. FEBS J 1995;230:401–7.
[46] Brungs M, Rådmark O, Samuelsson B, Steinhilber D. Sequential induction of 5-lipoxygenase gene expression and activity in Mono Mac 6 cells by transforming growth factor beta and 1,25-dihydroxyvitamin D3. Proc Natl Acad Sci USA 1995;92:107–11.
[47] Maier TJ, Tausch L, Hoernig M, Coste O, Schmidt R, Angioni C, et al. Celecoxib inhibits 5-lipoxygenase. Biochem Pharmacol 2008;76:862–72.
[48] Rörsch F, Wobst I, Zettl H, Schubert-Zsilavecz M, Grösch S, Geisslinger G, et al. Nonacidic inhibitors of human microsomal prostaglandin synthase 1 (mPGES 1) identified by a multistep virtual screening protocol. J Med Chem 2010;53:911–5.

[49] Thorén S, Jakobsson PJ. Coordinate up- and down-regulation of glutathione-dependent prostaglandin E synthase and cyclooxygenase-2 in A549 cells. Inhibition by NS-398 and leukotriene C4. FEBS J 2000;267:6428–34.
[50] Schmidt R, Coste O, Geisslinger G. LC–MS/MS-analysis of prostaglandin E2 and D2 in microdialysis samples of rats. J Chromatogr B Analyt Technol Biomed Life Sci 2005;826:188–97.
[51] Fischer A, Metzner J, Steinbrink SD, Ulrich S, Angioni C, Geisslinger G, et al. 5-Lipoxygenase inhibitors induce potent anti-proliferative and cytotoxic effects in human tumour cells independently of suppression of 5-lipoxygenase activity. Br J Pharmacol 2010;161:936–49.
[52] Maron DM, Ames BN. Revised methods for the Salmonella mutagenicity test. Mutat Res 1983;113:173–215.
[53] Fechteler T, Dengler U, Schomburg D. Prediction of protein three-dimensional structures in insertion and deletion regions: a procedure for searching data bases of representative protein fragments using geometric scoring criteria. J Mol Biol 1995;253:114–31.
[54] Wang J, Cieplak P, Kollman PA. How well does a restrained electrostatic potential (RESP) model perform in calculating conformational energies of organic and biological molecules? J Comput Chem 2000;21:1049–74.
[55] Korb O, Stützle T, Exner TE. PLANTS: application of ant colony optimization to structure-based drug design. Lect Notes Comput Sci 2006;4150:247–58.
[56] Peters-Golden M, Brock TG. Intracellular compartmentalization of leukotriene biosynthesis. Am J Respir Crit Care Med 2000;161:S36–40.
[57] Bryant RW, Simon TC, Bailey JM. Role of glutathione peroxidase and hexose monophosphate shunt in the platelet lipoxygenase pathway. J Biol Chem 1982;257:14937–43.
[58] Rouzer CA, Samuelsson B. The importance of hydroperoxide activation for the detection and assay of mammalian 5-lipoxygenase. FEBS Lett 1986;204:293–6.
[59] Feisst C, Pergola C, Rakonjac M, Rossi A, Koeberle A, Dodt G, et al. Hyperforin is a novel type of 5-lipoxygenase inhibitor with high efficacy in vivo. Cell Mol life Sci 2009;66:2759–71.
[60] Smith CJ, Zhang Y, Koboldt CM, Muhammad J, Zweifel BS, Shaffer A, et al. Pharmacological analysis of cyclooxygenase-1 in inflammation. Proc Natl Acad Sci USA 1998;95:13313–8.
[61] Prasit P, Wang Z, Brideau C, Chan CC, Charleson S, Cromlish W, et al. The discovery of rofecoxib, [MK 966, Vioxx, 4-(4′-methylsulfonylphenyl)-3-phenyl-2(5H)-furanone], an orally active cyclooxygenase-2-inhibitor. Bioorg Med Chem Lett 1999;9:1773–8.
[62] Côté B, Boulet L, Brideau C, Claveau D, Ethier D, Frenette R, et al. Substituted phenanthrene imidazoles as potent, selective, and orally active mPGES-1 inhibitors. Bioorg Med Chem Lett 2007;17:6816–20.
[63] Wecksler AT, Kenyon V, Garcia NK, Deschamps JD, van der Donk WA, Holman TR. Kinetic and structural investigations of the allosteric site in human epithelial 15-lipoxygenase-2. Biochemistry 2009;48:8721–30.
[64] Ivanov I, Heydeck D, Hofheinz K, Roffeis J, O'Donnell VB, Kuhn H, et al. Molecular enzymology of lipoxygenases. Arch Biochem Biophys 2010;503:161–74.
[65] Safayhi H, Mack T, Sabieraj J, Anazodo MI, Subramanian LR, Ammon HP. Boswellic acids: novel, specific, nonredox inhibitors of 5-lipoxygenase. J Pharmacol Exp Ther 1992;261:1143–6.
[66] Albert D, Zündorf I, Dingermann T, Müller WE, Steinhilber D, Werz O. Hyperforin is a dual inhibitor of cyclooxygenase-1 and 5-lipoxygenase. Biochem Pharmacol 2002;64:1767–75.
[67] Sailer ER, Schweizer S, Boden SE, Ammon HP, Safayhi H. Characterization of an acetyl-11-keto-beta-boswellic acid and arachidonate-binding regulatory site of 5-lipoxygenase using photoaffinity labeling. FEBS J 1998;256:364–8.
[68] Pergola C, Werz O. 5-Lipoxygenase inhibitors: a review of recent developments and patents. Expert Opin Ther Pat 2010;20:355–75.
[69] Ford-Hutchinson AW, Gresser M, Young RN. 5-Lipoxygenase. Annu Rev Biochem 1994;63:383–417.
[70] Bürkert E, Arnold C, Hammarberg T, Rådmark O, Steinhilber D, Werz O. The C2-like beta-barrel domain mediates the Ca2+-dependent resistance of 5-lipoxygenase activity against inhibition by glutathione peroxidase-1. J Biol Chem 2003;278:42846–53.
[71] Romanov S, Wiesner R, Myagkova G, Kuhn H, Ivanov I. Affinity labeling of the rabbit 12/15-lipoxygenase using azido derivatives of arachidonic acid. Biochemistry 2006;45:3554–62.
[72] Fischer L, Steinhilber D, Werz O. Molecular pharmacological profile of the nonredox-type 5-lipoxygenase inhibitor CJ-13,610. Br J Pharmacol 2004;142:861–8.
[73] Fischer L, Poeckel D, Buerckert E, Steinhilber D, Werz O. Inhibitors of actin polymerisation stimulate arachidonic acid release and 5-lipoxygenase activation by upregulation of Ca2+ mobilisation in polymorphonuclear leukocytes involving Src family kinases. Biochim Biophys Acta 2005;1736:109–19.
[74] Bain G, King CD, Rewolinski M, Schaab K, Santini AM, Shapiro D, et al. Pharmacodynamics and pharmacokinetics of AM103, a novel inhibitor of 5-lipoxygenase-activating protein (FLAP). Clin Pharmacol Ther 2010;87:437–44.
[75] Rubin P, Mollison KW. Pharmacotherapy of diseases mediated by 5-lipoxygenase pathway eicosanoids. Prostaglandins Other Lipid Mediat 2007;83:188–97.
[76] Tang DG, Bhatia B, Tang S, Schneider-Broussard R. 15-Lipoxygenase 2 (15-LOX2) is a functional tumor suppressor that regulates human prostate epithelial cell differentiation, senescence, and growth (size). Prostaglandins Other Lipid Mediat 2007;82:135–46.
[77] Cimen I, Astarci E, Banerjee S. 15-Lipoxygenase-1 exerts its tumor suppressive role by inhibiting nuclear factor-kappa B via activation of PPAR gamma. J Cell Biochem 2011;112:2490–501.
[78] Baviskar AT, Madaan C, Preet R, Mohapatra P, Jain V, Agarwal A, et al. N-fused imidazoles as novel anticancer agents that inhibit catalytic activity of topoisomerase IIα and induce apoptosis in G1/S phase. J Med Chem 2011;54:5013–30.

Supplementary Material:

Molecular Characterization of **EP6 -** a Novel Imidazo[1,2-*a*]pyridine Based Direct 5-Lipoxygenase Inhibitor

*Joanna M. Wisniewska[a], Carmen B. Rödl[a], Astrid S. Kahnt[a], Estel.la Buscató[a], Sandra Ulrich[a], Yusuf Tanrikulu[b], Janosch Achenbach[a], Florian Rörsch[c], Sabine Grösch[c], Gisbert Schneider[d], Jindrich Cinatl Jr.[e], Ewgenij Proschak[a], Dieter Steinhilber[a] and Bettina Hofmann[a]**

[a] Institute of Pharmaceutical Chemistry, ZAFES / LiFF, Goethe-University Frankfurt, Max-von-Laue-Str. 9, D-60438 Frankfurt/Main, Germany

[b] Institute of Organic Chemistry and Chemical Biology, ZAFES / CMP, Goethe-University Frankfurt, Siesmayerstr. 70, D-60323 Frankfurt/Main, Germany

[c] Institute of Clinical Pharmacology, ZAFES / LiFF, Goethe-University Frankfurt, Theodor-Stern-Kai 7, D-60590 Frankfurt/Main, Germany

[d] Institute of Pharmaceutical Sciences, ETH Zurich, Wolfgang-Pauli-Str. 10, CH-8093 Zurich, Switzerland

[e] Institute of Medical Virology, ZAFES / LiFF, Goethe-University Frankfurt, Paul-Ehrlich-Str. 40, D-60596 Frankfurt/Main, Germany

Synthesis procedure for preparation of N-cyclohexyl-6-methyl-2-(4-morpholinophenyl)imidazo[1,2-*a*]pyridin-3-amine (EP6): 1.0 g (9.2 mmol) 2-amino-5-methylpyridine and 1.47 g (9.2 mmol) 4-morpholino-benzaldehyde were stirred with 0.89 g (18.4 mmol) glacial acetic acid and 35 ml MeOH, then 0.89 g (9.2 mmol) cyclohexyl isocyanide was added. After 18 hours the reaction mixture was quenched with 10 ml 2N HCl to destroy the residual isocyanide. MeOH was removed under reduced pressure and 50 ml saturated $NaHCO_3$ solution was added. The product was extracted with EtOAc (3 x 40 ml) and crystallized as crude yellowish solid after removing the solvent under reduced pressure. The purification was completed by recrystallization from EtOAc/MeOH yielding 1.80 g (60%) yellow solid.

Molecular modeling of the putative binding mode: The following amino acid side chains were defined as flexible for docking with PLANTS (version 1.1, University of Konstanz, Germany): S-11. Q-12, Y-81, K-83, Y-100, R-101, W-102, R-165, N-166, I-167, Q-168, F-169, D-170, Y-383, V-397, A-398, V-400, R-401, F-402, T-403, I-404, A-404, E-622, H-624.

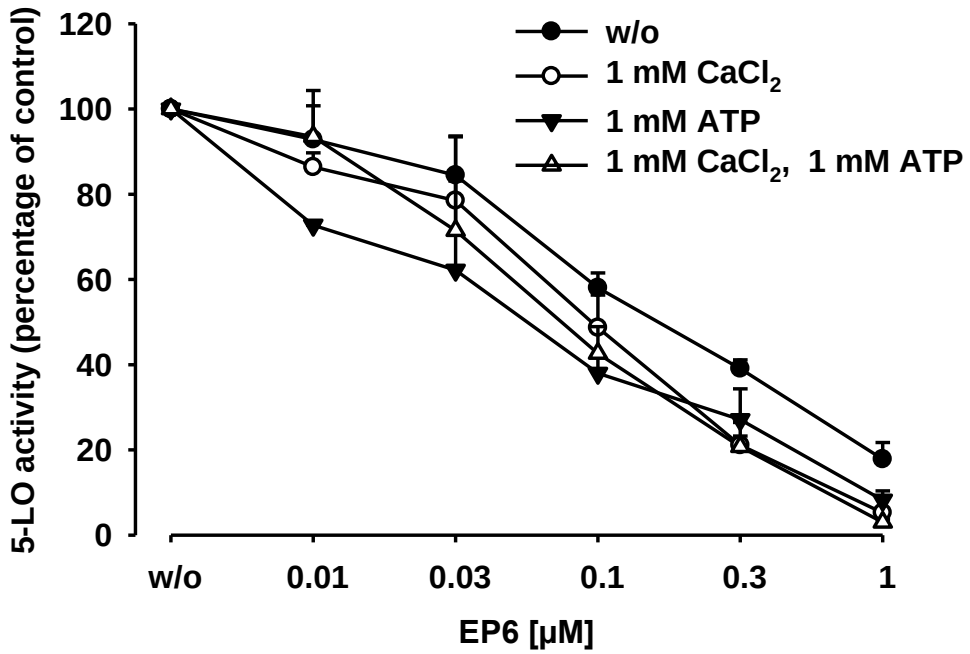

Figure S1: Influence of ATP and calcium on the inhibitory activity of **EP6**. Anion exchange chromatography purified 5-LO was set in 1 ml PB, pH 7.4 with or without 1 mM ATP and the samples were pre-incubated for 15 min with **EP6** or vehicle (DMSO) at the indicated concentrations at 4°C. Samples were pre-warmed at 37°C for 30 sec and 5-LO product formation was started by addition of 20 µM AA or 20 µM AA and 1 mM $CaCl_2$. After 10 min, 5-LO product formation was determined. Data (mean ± S.E.; $n \geq 3$) are expressed as percentage of control.

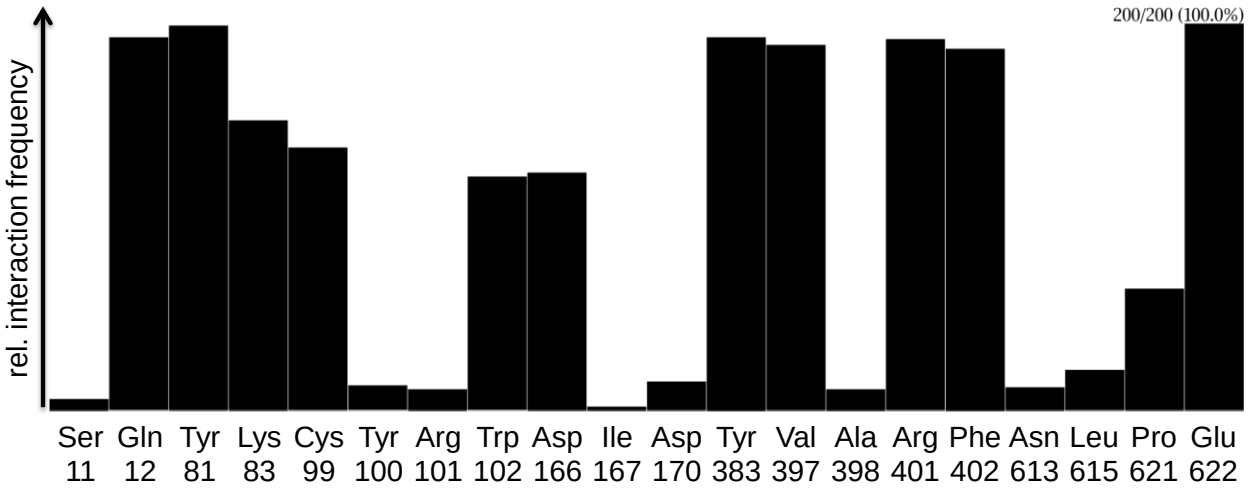

Figure S2: Statistical analysis of the Protein Ligand Interaction Fingerprints (PLIF) of 200 docking poses of **EP6**. Supplemental figure S2 shows the relative frequency of the strongest interaction type of each amino acid with the docked ligand conformation based on the PLIF.

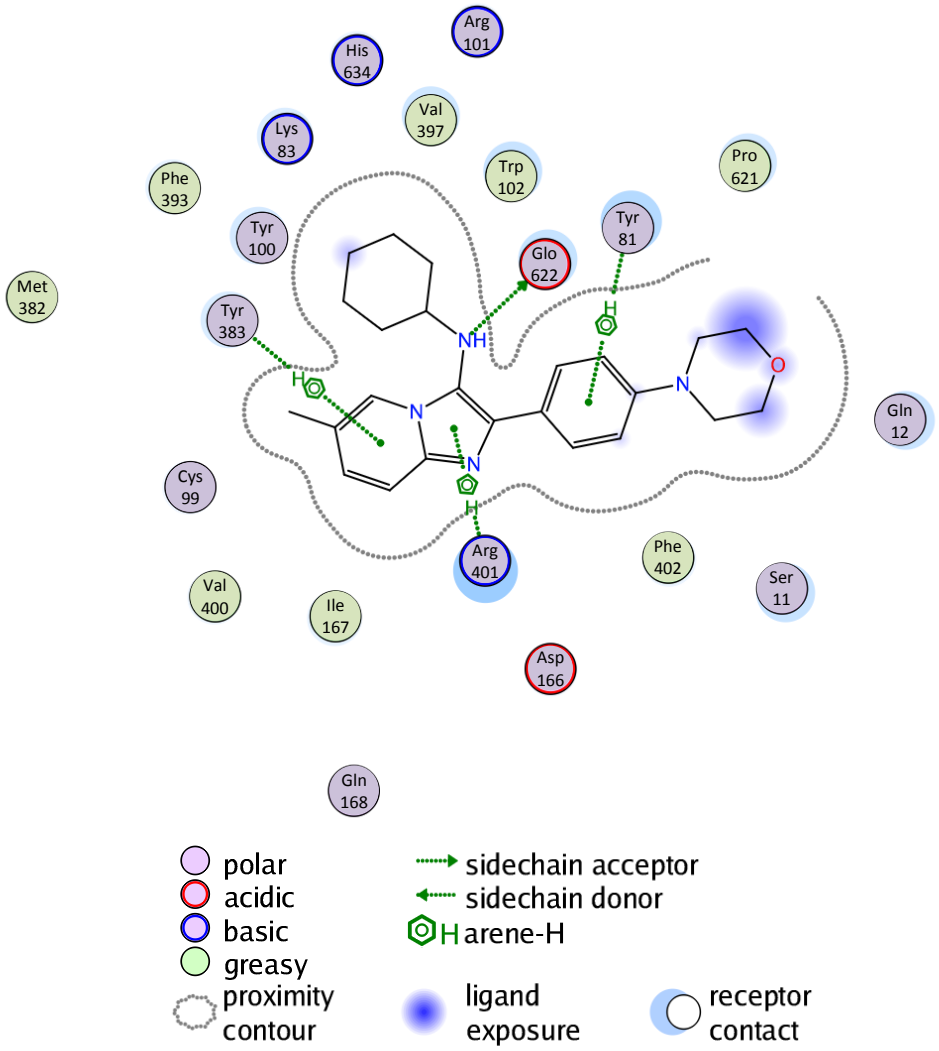

Figure S3: 2D representation of **EP6** in the binding pocket. Possible interaction amino acid side chains are depicted with the interaction type.

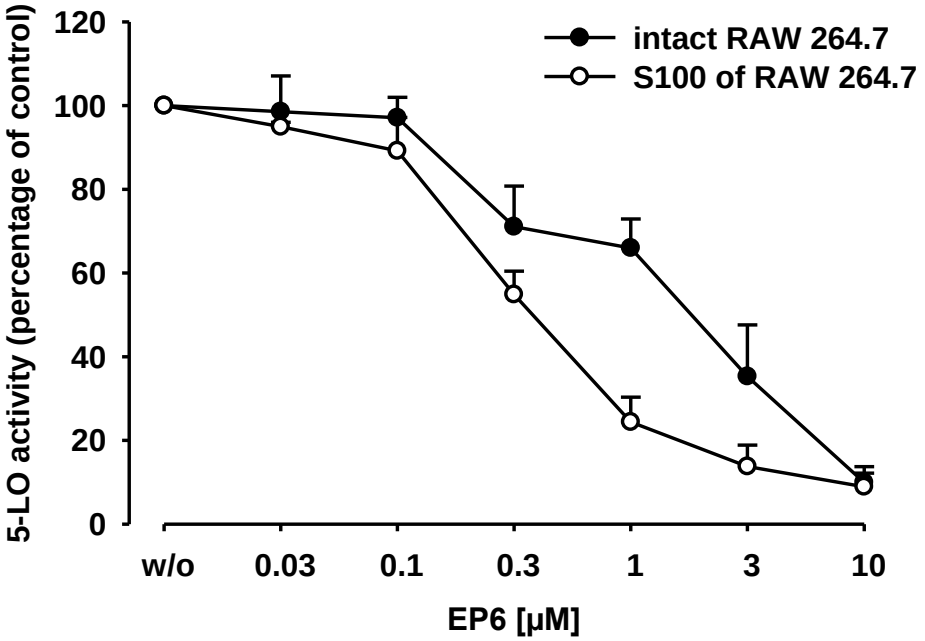

Figure S4: Inhibitory activity of **EP6** in RAW 264.7 cells. 1.5×10^7 intact RAW 264.7 cells were re-suspended in PGC buffer and pre-incubated for 15 min at 37°C with the indicated concentrations of **EP6** or vehicle (DMSO). 5-LO product formation was started by addition of 5 µM calcium ionophore and 20 µM AA, after 10 min 5-LO product formation was determined. For determination of 5-LO product formation in S100 preparations corresponding to 2×10^7 RAW 264.7 cells, samples were set in 1 ml PBS, pH 7.4, 1 mM EDTA and 1 mM ATP and were pre-incubated for 15 min with **EP6** or vehicle (DMSO) at the indicated concentrations at 4°C. Samples were pre-warmed at 37°C for 30 sec and 5-LO product formation was started by addition of 2 mM $CaCl_2$ and 20 µM AA. After 10 min, 5-LO product formation was determined. Data (mean ± S.E.; $n \geq 3$) are expressed as percentage of control.

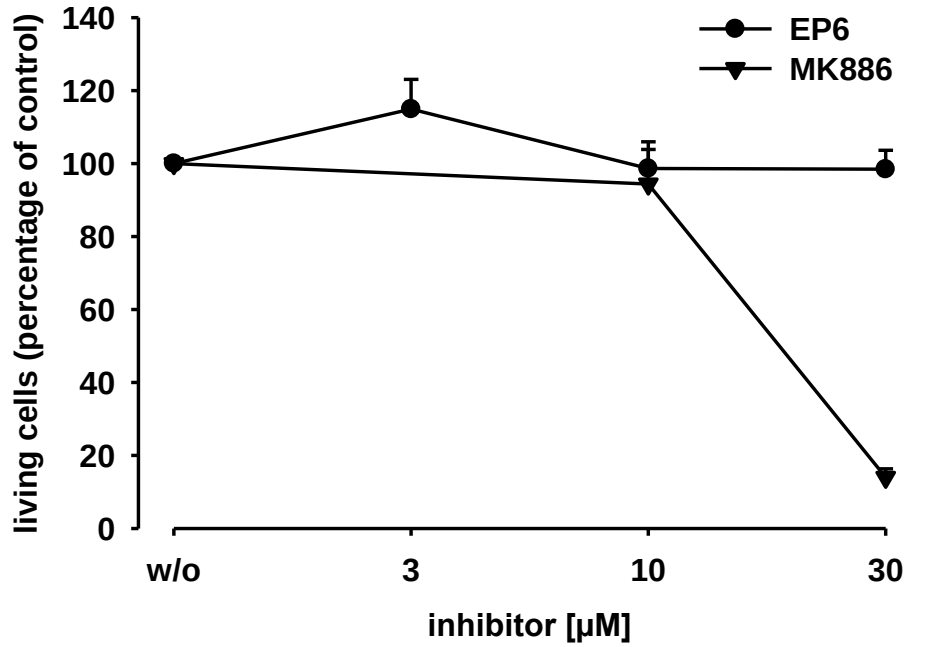

Figure S5: Short-term viability in PMNL after incubation with **EP6**. 5×10^6 intact PMNL were re-suspended in PGC buffer and were incubated for 30 min at 37°C with the indicated concentrations of **EP6**, MK886 or vehicle (DMSO). Living cells were determined. Data (mean ± S.E.; $n \geq 3$) are expressed as percentage of control.

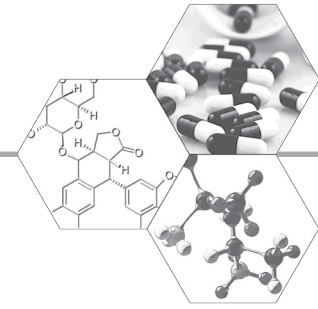

Structure–activity relationship and *in vitro* pharmacological evaluation of imidazo[1,2-*a*] pyridine-based inhibitors of 5-LO

Background: 5-LO is an important enzyme involved in the biosynthesis of leukotrienes, which are lipid mediators of immune and inflammation responses, with important roles in respiratory disease, cardiovascular disease, immune responses and certain types of cancer. Therefore, this enzyme has been investigated as a potential target for the treatment of these pathophysiological conditions. **Results:** 5-LO inhibitory potential was investigated in intact polymorphonuclear leukocytes, a cell-free assay, in human whole blood and rodent cells to both elucidate structure–activity relationships and *in vitro* pharmacological evaluation. Chemical modifications for lead optimization via straight forward synthesis was used to combine small polar groups, which led to a suitable candidate (IC_{50} [polymorphonuclear leukocytes] = 1.15 μM, IC_{50} [S100] = 0.29 μM) with desired *in vitro* biopharmaceutical profiles in terms of solubility (451.9 μg/ml) and intrinsic clearance without demonstrating any cytotoxicity. **Conclusion:** Compound **9l** is a novel, potent and selective 5-LO inhibitor with favorable preclinical drug-like properties.

Leukotrienes (LTs) are lipid mediators of immune and inflammatory responses with important roles in respiratory and cardiovascular diseases such as asthma and arteriosclerosis and certain types of cancer [1]. LTs are formed from arachidonic acid (AA), which is released from membrane phospholipids by cPLA2. AA is subsequently metabolized by **5-LO** after stimulation at the nuclear membrane by the help of the 5-LO-activating protein (FLAP), which facilitates the transfer of AA to 5-LO.

The dioxygenase 5-LO catalyzes the incorporation of both atoms of molecular oxygen into AA in two steps to give the hydroperoxide 5(*S*)-hydroperoxy-6-*trans*-8,11,14-*cis*-eicosatetraenoic acid (5-HpETE) as well as the following dehydration to the unstable epoxide LTA_4. The subsequent conversion of LTA_4 by LTA_4 hydrolase leads to LTB_4, and the conjugation with reduced glutathione by LTC_4 synthase yields the cysteinyl-containing LTs C_4, D_4 and E_4. In addition to the conversion to LTA_4, 5-HpETE can be reduced to the corresponding alcohol 5(*S*)-hydroxy-6,10-*trans*-8,14-*cis*-eicosatetraenoic acid (5(*S*)-HETE), for example, by gluthatione peroxidases. The chemotactic and chemokinetic agent LTB_4 leads to recruitment of other neutrophils and causes phagocytosis. Cysteinyl-containing LTs play a crucial role in respiratory diseases leading to bronchoconstriction and vascular permeability.

The enzyme is structured in two distinct domains: the N-terminal regulatory C2-like domain (~120 amino acids) and the larger catalytic domain containing the non-heme iron [2]. In the inactive form of the enzyme, the ferrous state of the iron (Fe^{2+}), the 5-LO is not capable of converting AA to the corresponding LTs. Fe^{2+} has to be oxidized by lipid hydroperoxides to the active Fe^{3+} in order to enable the catalytic cycle [3]. Furthermore, 5-LO has to be activated by Ca^{2+} influx or phosphorylation via the p38 MAPK or ERK pathway leading to a change of subcellular localization [4–6]. Moreover, a biosynthetic complex, located at the nuclear membrane, regulates the LT biosynthesis, with identified key proteins (i.e., $cPLA_2$, 5-LO, FLAP, LTA_4 hydrolase and LTC_4 synthase) but it is still unknown how they assemble, interact and what is the best way to interfere to inhibit LT biosynthesis [7]. The synthesis of LTs can also be found in lipid bodies [8].

5-LO plays an indisputable role in acute and chronic inflammation, asthma and rhinitis, atherosclerosis and arthritis [9], however, its contribution to carcinogenesis is under debate [10,11]. The other major LOs, 12-LO, 15-LO1 and 15-LO2 are also discussed in this field and 15-LO activity is reported to have tumor-suppressive effects [12,13]. Besides, it was recently reported that 5-LO is involved in the biosynthesis of lipoxins initiated by the 12-/15-LO pathway leading to a natural resolution of inflammation [14].

LTs are potent pathophysiological mediators and 5-LO inhibitors were developed for

Estel.la Buscató[‡1], Joanna M Wisniewska[‡1], Carmen B Rödl[1], Astrid Brüggerhoff[1], Astrid Kaiser[1], Florian Rörsch[2], Edmund Kostewicz[3], Mario Wurglics[1], Manfred Schubert-Zsilavecz[1], Sabine Grösch[2], Dieter Steinhilber[1], Bettina Hofmann*[§1] & Ewgenij Proschak[§1]

[1]Institute of Pharmaceutical Chemistry, ZAFES/LiFF/OSF Goethe-University Frankfurt, Max-von-Laue-Str. 9, D-60438 Frankfurt am Main, Germany
[2]Johann Wolfgang Goethe-University, Institute of Clinical Pharmacology, pharmazentrum frankfurt, LiFF/ZAFES, Theodor-Stern-Kai 7, D-60590 Frankfurt am Main, Germany
[3]Institute of Pharmaceutical Technology, Goethe University Frankfurt, Max-von-Laue-Str. 9, D-60438 Frankfurt am Main, Germany
*Author for correspondence:
Tel.: +49 69 798 29335
E-mail: hofmann@pharmchem.uni-frankfurt.de
[‡]Authors contributed equally
[§]Joint senior author

FUTURE SCIENCE part of fsg

Key Terms

Leukotrienes: Derivatives of the arachidonic acid and potent pro-inflammatory mediators. The different leukotrienes activate the cysteinyl leukotriene receptors CysLT1 and CysLT2 and contribute to the symptoms of asthma. Thus, inhibitors of 5-LO and CysLT1 receptor anatgonists, which prevent the leukotriene-mediated effects, can be used for asthma treatment.

5-LO: Enzyme of the arachidonic acid cascade. It catalyzes the conversion of the arachidonic acid to the corresponding peroxide 5(*S*)-hydroperoxy-6-*trans*-8,11,14-*cis*-eicosatetraenoic acid and subsequently to the leukotriene A4, which acts as a precursor for other leukotrienes. 5-LO activity is associated with asthma, atherosclerosis and various cancer types.

Multi-component reactions: Organic reactions in which the product is formed from three or more educts. Originally discovered by Ugi, multi-component reactions using isonitriles as one of the educts are very versatile and allow the preparation of a large number of complex structures from few starting materials.

many decades, although zileuton (Zyflo®; (±)-1-(1-benzo[*b*]thien-2-ylethyl)-1-hydroxyurea) is the only 5-LO inhibitor that entered the US market in 1997 for the chronic treatment and prophylaxis of various clinical phenotypes of asthma. It has also been tested in the treatment of allergic rhinitis with promising results. Nevertheless, zileuton exhibits liver toxicity and an unfavorable pharmacokinetic profile with a short half-life [15,16]; as a consequence, its clinical use is limited. Another strategy to develop inhibitors of LT production is to target FLAP, which facilitates the transfer of AA to 5-LO. These indirect inhibitors, such as MK-886 and AM103 [17], could enter clinical Phase II trials for the treatment of inflammatory diseases but are not registered yet [18]. Thus, there is a need for the design and development of new inhibitors of 5-LO. Potential drug candidates should exhibit high efficacy *in vitro* and *in vivo*; and desired pharmacological properties, such as high selectivity for 5-LO low hepatotoxicity and good oral bioavailability.

In the present study, we describe the optimization of our *in vitro* pharmacologically evaluated lead compound *N*-cyclohexyl-6-methyl-2-(4-morpholinophenyl)imidazo[1,2-*a*]pyridin-3-amine (EP6) [19], which was derived from a virtual screening study for (COX)/5-LO dual inhibitors [20]. The main advantage of EP6 over other established 5-LO inhibitors, is its stimulus-independent 5-LO inhibition. The four well-known classes [21] of 5-LO inhibitors have several drawbacks, for example, for nonredox-type 5-LO inhibitors their efficiency depends on the stimulus of 5-LO activation and the addition of exogenous AA [22]. Furthermore, imidazo[1,2-*a*]pyridines can be easily obtained by means of the Groebke–Blackburn–Bienaymé [23] **multi-component reaction** (MCR), which involves the reaction of an heteroaromatic amidine, such as 2-aminopyridine, with isonitrile and aldehyde in the presence of a catalytic amount of a protic acid such as acetic acid. N-fused imidazoles have recently gained attention because of their wide range of biological activities as antibacterial, antiviral, anti-inflammatory and anti-neoplastic agents with a high chemical stability. Herein, we present the synthesis and *in vitro* pharmacological profiling of this series of N-fused imidazoles acting as direct inhibitors of 5-LO and, thus, leukotriene biosynthesis.

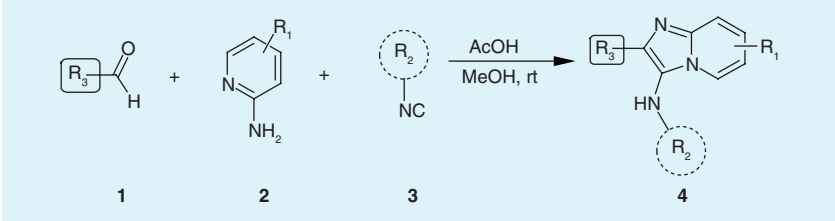

Figure 1. Groebke–Blackburn–Bienaymé multi-component reaction used to synthetize compounds with imidazo[1,2-*a*]pyridine scaffold.

Results & discussion

The imidazo[1,2-*a*]pyridine-substituted compounds were synthesized by means of a MCR (Groebke–Blackburn–Bienaymé) starting from the appropriately substituted aldehyde **1**, aminopyridine **2** and isonitrile **3** depicted in **Figure 1**. In the case of imidazo[1,2-*a*]pyridin-phenylmorpholine compounds **(4a–l)**, we started from 4-phenylmorpholine and in the case of imidazo[1,2-*a*]pyridine-3-methoxy-4-phenol, (vanillin) was used.

Structure–activity relationship of imidazo[1,2-*a*]pyridines

To understand the interactions between the ligand and the receptor (5-LO), the following 55 derivatives were tested in both a cell-free and cell-based assay. The cell-based assay was performed in intact polymorphonuclear leukocytes (PMNL) and for the cell-free assay the corresponding 100,000 × g (S100) fraction of lyzed PMNL was used. As reference 5-LO inhibitors, we used zileuton and BWA4C and as a representative compound with a imidazo[1,2-*a*]pyridine scaffold we tested zolpidem. Zolpidem was inactive, thereby suggesting that the free amine moiety is important for the inhibition of 5-LO product formation.

The N-fused imidazole-based lead compound, EP6, was discovered by means of computer-aided drug design [19]. It exhibited high inhibitory activity in both assays: IC_{50} = 0.16 μM (PMNL) and 0.21 μM (S100). The second lead (6-methyl-*N*-cyclohexyl-2-(4-phenoxyphenyl)imidazo[1,2-*a*]pyridin-3-amine) obtained in our preliminary structure–activity relationship (SAR) study [24] demonstrated slightly improved inhibition in the cell-free assay (IC_{50} = 0.08 μM [S100]). With the lead compound, EP6, exhibiting interesting biological activity, an effort was taken to study the pharmacological properties of imidazo[1,2-*a*]pyridine-based 5-LO inhibitors via the variation of substituents at different positions on the heterocyclic core. Based on our previous lead EP6, a direct 5-LO inhibitor, we began to synthesize compounds bearing an imidazo[1,2-*a*]pyridine-phenylmorpholine

scaffold **(4a–l)** depicted in TABLE 1. Introduction of chlorine at position six and a cyclopentyl **(4a)** led to a decrease in inhibition of PMNL and S100 activities (IC_{50} = 0.26 µM, IC_{50} = 0.83 µM, respectively). The combination of 6-F **(4e)** and *tert*-butyl moieties impaired the inhibition completely resulting in IC_{50} values of greater than 10 µM in both assay systems. Introduction of an adamantyl **(4b)** group on R_2 also led to a lower inhibitory potency (IC_{50} [PMNL] = 0.53 µM, IC_{50} [S100] = 0.51 µM), however, the replacement of the methyl group by a chlorine atom **(4c)**, restored the IC_{50} value for intact cells, nevertheless in the cell-free system the IC_{50} value was tenfold higher (IC_{50} = 6.98 µM). A higher IC_{50} value for the cell-free assay systems than for intact PMNL may indicate some indirect LT biosynthesis inhibition [25] such as interference with either $cPLA_2$ or FLAP, both being upstream enzymes. We explored the possibility of moving R_1 to positions five, seven and eight. Compared with our lead compound, EP6, methyl substitution at position seven **(4f)** and position five **(4h)** led to a lower inhibition in terms of PMNL and S100 (**4f**, IC_{50} [PMNL] = 4.24 µM, IC_{50} [S100] = 0.74 µM and **4h**, IC_{50} [PMNL] = 1.32 µM, IC_{50} [S100] = 0.28 µM). Similar results were obtained when compounds were replaced with a chloro or fluoro substituent at position five and seven: 7-chloro substitution (**4g**, IC_{50} [PMNL] = 1.22 µM, IC_{50} [S100] = 0.45 µM) and 5-chloro (**4i**, IC_{50} [PMNL] = 0.48 µM, IC_{50} [S100] = 0.74 µM). These substitutents at position eight **(4k, 4l)** led to similar results.

After investigating the substitutents pattern on the imidazo[1,2-*a*]pyridine-phenylmorpholine scaffold **(4a–l)**, we concluded that 6-methyl and cyclohexyl substitution were the optimal with respect of 5-LO inhibition in both, cell-based and -free assays.

Based on our previous SAR study [24], we identified a second lead structure (6-methyl-*N*-cyclohexyl-2-(4-phenoxyphenyl)imidazo[1,2-*a*]pyridin-3-amine) with an IC_{50} (S100) value of 0.08 µM, yielding to a higher inhibitory activity than EP6, consequently we used this

Table 1. Measured inhibitory activity of the imidazo[1,2-*a*]pyridine-4-phenylmorpholine series 4a–l on polymorphonuclear leukocytes and S100.

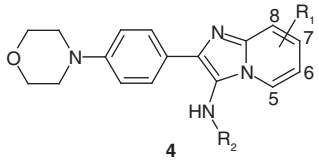

4

Entry	R_1	R_2	IC_{50} polymorphonuclear leukocytes (µM)	IC_{50} S100 (µM)	WST-1 (%)†
Zileuton	–	–	0.50	1.00	107 ± 3.9‡
BWA4C	–	–	0.08	0.05	n.t.
Zolpidem	–	–	ia.	ia.	n.t.
EP6	6-CH_3	Cyclohexyl	0.16	0.21	104 ± 2.5
4a	6-Cl	Cyclopentyl	0.26	0.83	7 ± 3.2
4b	6-CH_3	Adamantyl	0.53	0.51	99 ± 11.6
4c	6-Cl	Adamantyl	0.22	6.98	88 ± 19.1
4d	6-F	Cyclohexyl	0.42	1.54	5 ± 1.5
4e	6-F	*tert*-butyl	13.71	>30	96 ± 2.9
4f	7-CH_3	Cyclohexyl	4.24	0.74	96 ± 14.5
4g	7-Cl	Cyclohexyl	1.22	0.45	82 ± 6.3
4h	5-CH_3	Cyclohexyl	1.32	0.28	73 ± 3.9
4i	5-Cl	Cyclohexyl	0.48	0.74	84 ± 0.5
4j	5-F	Cyclohexyl	0.39	1.03	90 ± 2.0
4k	8-CH_3	Cyclohexyl	1.14	0.33	120 ± 2.9
4l	8-Cl	Cyclohexyl	1.57	1.05	22 ± 3.6

†*Cell viability (%) measured at 10 µM.*
‡*Measured at 100 µM.*
ia.: Inactive; n.t.: Not tested.

scaffold as a the second starting point for variation **(Table 2)**. Several compounds were synthetized: from halogens such as fluoro **(5a)**, chloro **(5b)**, trifluoromethyl **(5c)**, to cyano **(5d)**; compared with the previous lead they did not exhibit better inhibitory potencies in the cell-free assay system (IC_{50} from 0.33–0.57 µM), but they were comparable in terms of PMNL inhibition. Compounds **5a–d** were less effective with regards to S100 inhibition and solubility problems were faced with compounds **5c** and **5d**. R_2 was investigated and, in terms of both assay systems, a tendency could be established: big residues, such as cyclopentyl **(5e)**, were better tolerated than isopropyl **(5g)** and the bulkier *tert*-butyl (**5f**, IC_{50} [PMNL] = 1.98 µM, IC_{50} [S100] = 0.82 µM) that led to a seven-times decrease of the inhibition. The main problem of this class of compounds was their low solubility. We evaluated the solubility under conditions simulating the acidic pH of the fasted stomach using simulated gastric fluid (SGF) at pH 1.2 and in media simulating the fasting proximal intestine using simulated intestinal fluid (SIF) at pH 6.8 In the case of **5b**, its solubility in SGF was very low (6.7 µg/ml). We studied the effect on solubility, by means of reducing the size of southern substituent. Compound **5h**, comprised a small fluoro group at position six and R_2 was an isopropyl moiety; however, this substitution pattern reduced the inhibitory potency. When introducing a bigger residue, such as an adamantyl group as R_2, the inhibitory activity was restored (**5i**, IC_{50} [PMNL] = 0.58 µM). At this point we could conclude in accordance with our observation for the scaffold of EP6 that 6-methyl group and a *N*-cyclohexyl moiety at position R_2 were the optimal substituents. Therefore, we proceeded to study the SAR of the eastern part (R_3).

Our next step consisted of introduction of *N*-heterocyclic moieties in the eastern part **(Table 3)**. Compounds **6a** and **6b** did not lead to an improvement of the inhibitory activity. Replacement of the phenoxy ether found in **6a** by a 6-methylpyrazin-2-yl ring decreased the inhibitory activity seven-times (IC_{50} [PMNL] = 1.57 µM, IC_{50} [S100] = 0.38 µM). The same occurred when replacing the ring by a 6-methylpyridin-3-yl, the IC_{50} values increased two-times (**6b**, IC_{50} [PMNL] = 0.45 µM, IC_{50} [S100] = 0.19 µM).

The introduction of solubility-enhancing groups such as methylpiperazine (**6c**, IC_{50} [PMNL] = 16.56 µM, IC_{50} [S100] = 1.19 µM) resulted in loss of activity, and the introduction of solubility-enhancing groups such as morpholine through an ethoxy ether linker (**6e**, IC_{50} [PMNL] = inactive, IC_{50} [S100] = 5.2 µM) led to a compound that only inhibited moderately the S100 fraction **(Table 3)**. Compound **6d** exhibited more effective inhibitory properties (IC_{50} [PMNL] = 0.56, IC_{50} [S100] = 0.31 µM). Inhibitory activity was restored when introducing a butoxy ether linked to a phthalimide moiety (**6f**, IC_{50} [PMNL] = 0.61 µM, IC_{50} [S100] = 0.06 µM) and improved the potency of our previous lead.

Compound **6g** (IC_{50} [PMNL] = 0.55 µM, IC_{50} [S100] = 0.13 µM) reduced the molecular size of our lead compound and resulted in improved solubility (159.1 µg/ml in SGF) compared with **5b**.

We investigated possible bioisosteres of compound **6g (Table 4)** for which vanillin was the starting material. Benzo[*d*]thiazole (**7a**, IC_{50} [PMNL] = 1.17 µM, IC_{50} [S100] = 2.48 µM) did not improve the inhibitory activity and 1*H*-indazol-5-yl ring (**7b**, IC_{50} [PMNL] =14.91 µM, IC_{50} [S100] = 1.42 µM) was unable to inhibit 5-LO in the intact cell system. The same holds true for compound **7f**. The closest bioisostere to **6g**, compound **7d** with a benzo[*d*][1,3]dioxol-5-yl ring had difficulties inhibiting 5-LO in intact PMNL but led to a similar potency in the S100 fraction: IC_{50} [S100] = 0.26 µM.

Maintaining the 4-phenol scaffold **(Table 5)**, we explored *meta* substitution, replacing 3-OMe at the phenyl ring residue found in compound **6g**

Table 2. Measured inhibitory activity of the imidazo[1,2-*a*]pyridine-4-phenylphenoxy ether series 5a–m on polymorphonuclear leukocytes and S100.

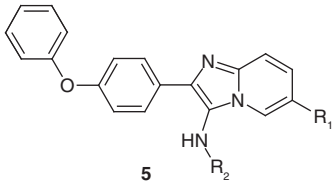

5

Entry	R_1	R_2	IC_{50} polymorphonuclear leukocytes (µM)	IC_{50} S100 (µM)	WST-1 (%)†
5a	F	Cyclohexyl	0.38	0.12	101 ± 4.4
5b	Cl	Cyclohexyl	0.33	0.26	105 ± 8.1
5c	CF_3	Cyclohexyl	0.57	n.d.	115 ± 3.3
5d	CN	Cyclohexyl	0.41	n.d.	91 ± 7.5
5e	CH_3	Cyclopentyl	0.38	0.19	89 ± 10.6
5f	CH_3	*tert*-butyl	1.98	0.82	91 ± 15.7
5g	CH_3	Isopropyl	1.07	0.35	130 ± 8.1
5h	F	Isopropyl	2.15	1.25	86 ± 8.8
5i	F	Adamantyl	0.58	n.d.	108 ± 11.3

†*Cell viability (%) measured at 10 µM.*
n.d.: Non determinable.

Table 3. Measured inhibitory activity of the imidazo[1,2-*a*]pyridine series 6a–g on polymorphonuclear leukocytes and S100.

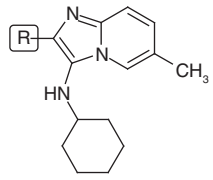

6

Entry	R	IC_{50} polymorphonuclear leukocytes (μM)	IC_{50} S100 (μM)	WST-1 (%)†
6a	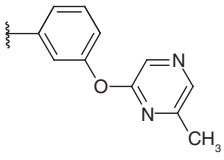	1.57	0.38	94 ± 9.4
6b	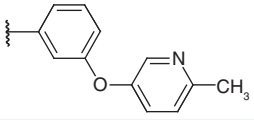	0.45	0.19	89 ± 4.4
6c	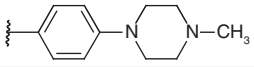	16.56	1.19	86 ± 6.5
6d	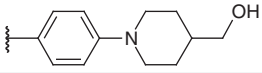	0.56	0.31	110 ± 8.5
6e	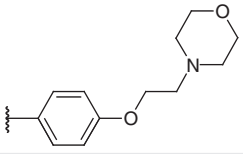	ia.	5.20	96 ± 4.4
6f	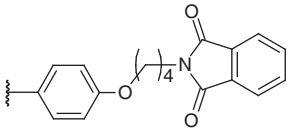	0.61	0.06	n.t.
6g	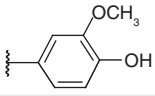	0.55	0.13	107 ± 12.1

†*Cell viability (%) measured at 10 μM.*
ia.: Inactive; n.t.: Not tested.

by a 3-OEt **(8a)**, 3-CH_3 **(8b)**, 3-Cl **(8c)**, 3-OCF_3 **(8d)**, 3-OH **(8e)**, which resulted in the decrease of IC_{50} values (PMNL) in all cases. S100 inhibitory activity was maintained compared with **6g** (IC_{50} [S100] = 0.20 μM). Therefore, we concluded that 3-OMe-4-OH-phenyl moiety was optimal and we proceeded further by investigating residues R_1 and R_2 in the presence of this scaffold.

Table 6 summarizes a list of compounds having an imidazo[1,2-*a*]pyridine-2-methoxyphenol scaffold **(9a–n)**. First, we investigated the influence of residue R_2 on 5-LO inhibition. Again cyclohexyl **(6g)** was demonstrated to be the optimal size in order to inhibit 5-LO in both assay systems, in analog to the SAR of morpholine derivatives **(Table 1)**. Slightly smaller residues, such as cyclopentyl **(9a)**, failed to inhibit in PMNL system (IC_{50} = 3.03 μM); bigger residues, such as adamantly **(9b)**, or aromatics, such as 2,6-dimethylphenyl **(9c)** or 4-methoxyphenyl **(9d)**, resulted in decreased inhibition potencies in both cases (PMNL and S100). Replacement of the methyl group at position six by a fluorine atom **(9e)** resulted in an equal potency compared with **6g**. Substitution at position seven- or eight- **(9g–j)** having either a chlorine atom or a methyl group led to higher IC_{50}

Table 4. Bioisosteric replacement of 3-methoxy-4-phenol moiety. Measured inhibitory activity of 7a–f on polymorphonuclear leukocytes and S100.

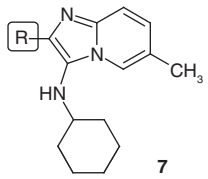

7

Entry	R	IC_{50} polymorphonuclear leukocytes (μM)	IC_{50} S100 (μM)	WST-1 (%)†
6g	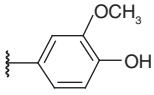	0.55	0.13	107 ± 12.1
7a	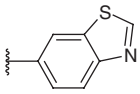	1.71	2.48	106 ± 15.8
7b	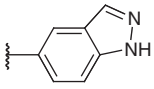	14.91	1.42	108 ± 8.1
7c	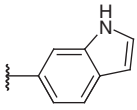	0.87	0.12	137 ± 12.1
7d	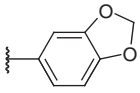	2.51	0.26	96 ± 3.1
7e	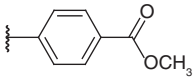	0.61	0.53	91 ± 8.6
7f	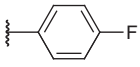	> 30.00	0.55	81 ± 3.0

†*Cell viability (%) measured at 10 μM.*

Table 5. Investigations of R substituents on 3-R-4-phenol moieties. Measured inhibitory activity of 8a–e on polymorphonuclear leukocytes and S100.

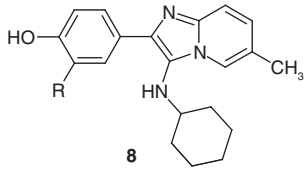

8

Entry	R	IC_{50} polymorphonuclear leukocytes (μM)	IC_{50} S100 (μM)	WST-1 (%)†
8a	OEt	1.19	0.13	90 ± 24.7
8b	CH_3	4.62	0.20	111 ± 17.5
8c	Cl	1.57	0.19	13 ± 13.6
8d	OCF_3	3.77	0.20	76 ± 30.4
8e	OH	6.08	0.23	2 ± 1.6

†*Cell viability (%) measured at 10 μM.*

(PMNL) values ranging from 1.37 to 3.77 μM, but equal S100 IC_{50} values. Similar results were obtained at position 5-CH_3 **(9k)**, 5-Cl **(9l)** and 5-F **(9m)**. Double substitution **(9n)** at the six- and eight-position increased the lipophilicity and moderately improved the inhibitory activity (logP = 2.01).

Aside from the effectiveness of the compounds to inhibit 5-LO, cytotoxicity, solubility and pharmacokinetic parameters were determined. To examine the cytotoxicity of the compounds, two assays were performed: WST-1 to assess cell viability by measuring the mitochondrial activity and to differentiate between an apoptotic and necrotic mechanism, the LDH assay was carried out to evaluate the membrane integrity and elucidate a possible necrotic effect. Regarding cytotoxic properties, most of the compounds (at 10 μM) did not affect the cell viability (>90%), only in some cases such as compounds **4a**, **4d**, **8l**, **9e**, **9f** and **9h** cell viability less than 10% was identified. Interestingly, most of them were halogenated compounds. We could determine that the imidazo[1,2-*a*]pyridine scaffold is a useful structure that does not affect the cell viability.

In vitro pharmacological evaluation

After investigating the scaffold of our previous leads and the current lead **(6g)** we found several compounds with a good inhibitory activity in both assay systems. We could also conclude that despite a flat SAR we could identify structural attributes necessary for inhibiting 5-LO **(Figure 2)**. Consequently, in order to find a candidate, we defined some selection criteria **(Figure 3)**: the compound should possess acceptable inhibitory potency; for the cell-free system, the IC_{50} (S100) value should be <0.5 μM and in intact cell formation of 5-LO products should be inhibited with an IC_{50} (PMNL) value <1 μM and, consequently, ensure sufficient potency in a cell-based system. Compounds **7d** and **9l** had IC_{50} values in intact PMNL of >1 μM **(Tables 4 & 6)**, but the IC_{50} values in the cell-free system were prospective (**7d**, IC_{50} [S100] = 0.26 μM; **9l**, IC_{50} [S100] = 0.29 μM). Cytotoxicity properties were evaluated to discard possible safety issues. To distinguish between anti-proliferative and cytotoxic mechanisms, cell viability was measure in a myeloid leukemic cell line (U937) with the help of WST-1 assay and LDH assay. The mitochondrial metabolic activity (WST-1) was assessed after treatment with 10 μM of compounds for 48 h. LDH leakage is a measure for

impaired membrane integrity pointing to necrotic events. Thus, compounds should give a high percentage of cell viability, in terms of mitochondrial metabolic activity, and a LDH release that is as little as possible (<10%). We measured only LDH leakage in compounds affecting the cell viability >50%, which was the case for 11 out of the 55 tested derivatives **(Table 7)**. Out of the 11 compounds, one **(9e)** did not demonstrate any LDH leakage. Six of our seven candidates (EP6, **5b**, **6g**, **7c**, **7d**, **9l**) obtained, did not impair cell viability of U937 cells, only **9n** reduced the mitochondrial metabolic activity to 72 ± 18.7% **(Tables 2, 3, 4 & 6)**. Then, we focused on evaluating the solubility in SGF (pH 1.2) and SIF (pH 6.8). The most soluble compounds in SGF were EP6 with 458.2 µg/ml and **9l** with 451.9 µg/ml, while **7d** (122.7 µg/ml) and **6g** (159.1 µg/ml) demonstrated moderate solubility **(Table 8)**. In contrast compound **5b** (6.7 µg/ml) was slightly soluble in SGF **(Table 8)**. Unfortunately, all compounds demonstrated poor solubility in SIF with a value <50 ng/ml [Buscató *et al.*, Unpublished Data]. In parallel, the inhibitory activity of these compounds were measured in a RBL-1 cell line. All compounds exhibited comparable IC_{50} values in intact RBL-1 cells and intact PMNL, from 0.32 µM to 2.3 µM **(Table 8; Figure 4)**. Thus, no species differences could be detected, prerequisites for future *in vivo* investigations in animal models.

Furthermore, we tested the seven compounds in a human whole blood (HWB) assay. Compound **6g** significantly inhibited the production of LTB_4 and resulted in an inhibition of 31 ± 4.1% (LTB_4) and 22 ± 4.0% (5(*S*)-HETE), respectively, at 10 µM **(Table 8; Figures 5 & 6)**. It only inhibited specifically 5-LO-derived products, remaining 8(*S*)-HETE, 9(*S*)-HETE 15(*S*)-HETE and 12(*S*)-HETE unmodified [Buscató *et al.*, Unpublished Data]. Compound **9l** inhibited the production of LTB_4 and 5(*S*)-HETE and resulted in an inhibition of 23 ± 1.0% and 8 ± 9.1%, respectively, at 10 µM. Our previous lead compound EP6 and the other candidates failed to inhibit LT biosynthesis in HWB. Although HWB activities were not as high as expected and lower compared with zileuton, which might leave the impression of questionable *in vivo* efficacy of the compounds, the lower potency in the HWB assay is very much likely due to high plasma protein binding. Importantly, it was observed that the binding of a drug to plasma proteins has little effect on the *in vivo* efficacy of that drug [26].

Table 6. Investigations of R_1 and R_2 substitutions on 3-methoxy-4-phenol moieties. Measured inhibitory activity of 9a–n on polymorphonuclear leukocytes and S100.

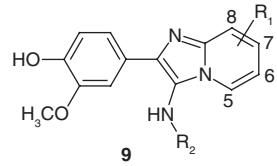

9

Entry	R_1	R_2	IC_{50} polymorphonuclear leukocytes (µM)	IC_{50} S100 (µM)	WST-1 (%)†
6g	6-CH_3	Cyclohexyl	0.55	0.13	107 ± 12.1
9a	6-CH_3	Cyclopentyl	3.03	0.30	54 ± 29.3
9b	6-CH_3	Adamantyl	2.24	0.39	100 ± 10.2
9c	6-CH_3	2,6-dimethylphenyl	4.50	0.26	89 ± 5.7
9d	6-CH_3	4-methoxyphenyl	4.18	1.35	91 ± 8.5
9e	6-F	Cyclohexyl	0.49	0.27	2 ± 2.4
9f	6-F	Isopropyl	11.60	1.38	2 ± 1.7
9g	8-CH_3	Cyclohexyl	1.69	0.28	52 ± 4.1
9h	8-Cl	Cyclohexyl	1.37	0.49	6 ± 2.4
9i	7-CH_3	Cyclohexyl	3.77	0.34	95 ± 7.8
9j	7-Cl	Cyclohexyl	1.83	0.29	42 ± 3.8
9k	5-CH_3	Cyclohexyl	1.28	0.30	88 ± 5.0
9l	5-Cl	Cyclohexyl	1.15	0.29	93 ± 11.2
9m	5-F	Cyclohexyl	1.90	0.52	78 ± 11.3
9n	6-Cl, 8-F	Cyclohexyl	0.84	0.41	72 ± 18.7

†*Cell viability (%) measured at 10 µM.*

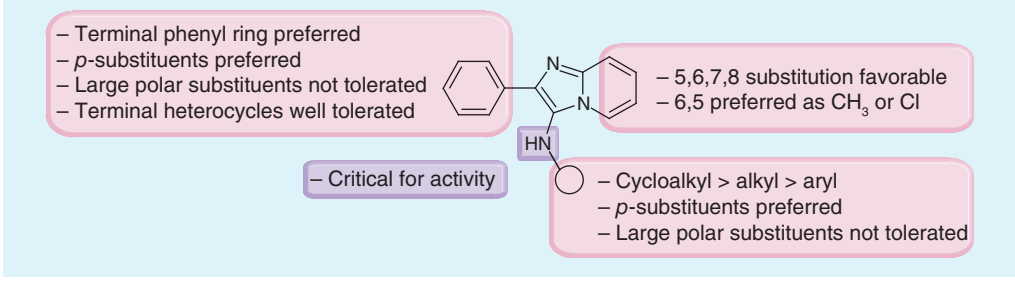

Figure 2. Structure–activity relationship summary of imidazo[1,2-*a*]pyridine 5-LO inhibitors.

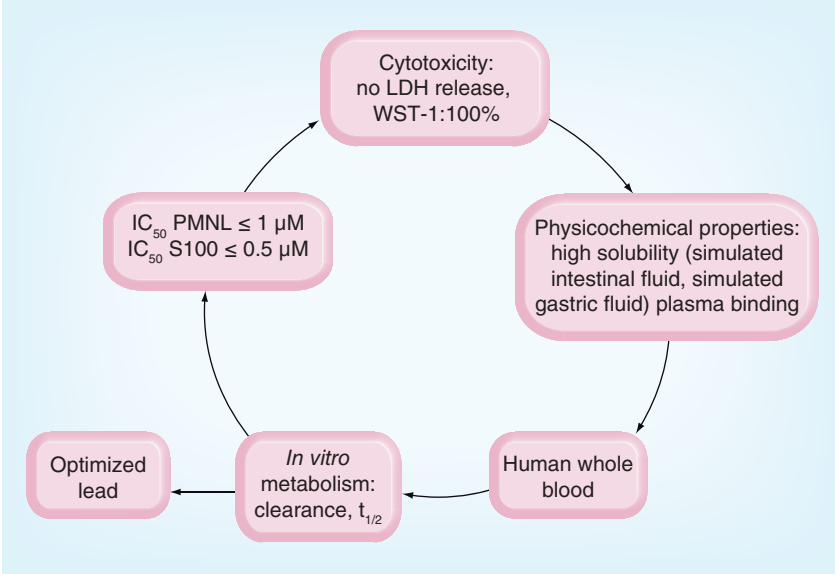

Figure 3. Evaluation criteria used to select the optimal candidate.
PMNL: Polymorphonuclear leukocytes.

We chose four candidates (EP6, **6g**, **7d**, **9l**) with the best solubility in SGF for further *in vitro* characterization. Since the selectivity of a compound is important, we investigated the inhibitory efficacy on the homolog LOs. The compounds demonstrated neither effect on the activity of platelet 12-LO nor on 15-LO1, tested in PMNL preparations **(Table 9; Figures 7A & 7B)**. For recombinant 15-LO2, only **7d** inhibited product formation with an IC_{50} value of 15 µM, which is approximately 60-times higher than for 5-LO in the cell-free system **(Table 9; Figure 7C)**. Due to the fact that 15-LO has been reported to have tumor-suppressor properties [13], inhibition of this isoform should be avoided. In addition, a pathophysiological relevant stimulus for 5-LO, lipopolysaccharide (LPS) and *N*-formyl-methionine-leucine-phenylalanine (fMLP), were investigated. This stimulus is often used in *in vivo* inflammatory animal models [27]. Intact PMNL were primed with 1 µg/ml LPS and 0.2 U/ml Ada and stimulated via 1 µM fMLP, without exogenous substrate AA, at a concentration of 10 µM of compounds. All four compounds exhibited inhibitory activity after stimulation via fMLP with residual activities between 0.9 and 20% **(Table 9)**, a necessary requirement for further investigation for possible *in vivo* studies.

Table 7. Cytotoxicity data (WST-1 and LDH assay) of compounds affecting the cell viability > 50%.

Entry	WST-1 (%)†	LDH (%)‡
4a	7 ± 3.2	35 ± 10.4
4d	5 ± 1.5	37 ± 5.5
4l	22 ± 3.6	27 ± 4.3
8c	13 ± 13.6	28 ± 6.3
8l	2 ± 1.6	28 ± 1.3
9a	54 ± 29.3	21 ± 10.1
9e	2 ± 2.4	7 ± 7.2
9f	2 ± 1.7	28 ± 3.1
9g	52 ± 4.1	20 ± 2.1
9h	6 ± 2.4	30 ± 2.0
9j	42 ± 3.8	24 ± 5.0

†*Cell viability (%) measured at 10 µM.*
‡*LDH release (%) measured at 10 µM.*

In order to examine the metabolic stability, we chose three compounds that had the best physicochemical properties: **6g**, **7d**, **9l** and these were incubated in rat liver microsomes **(Table 9; Figure 8)**. All three compounds demonstrated better metabolic stability than the control 7-ethoxycoumarin (7-EC) [28] where compounds **7d** and **9l** were more stable than **6g** (**7d**, 43% remaining after 60 min, **9l** 44% and **6g** 29%). Compared with EP6, metabolic stability could be improved as EP6 has a lower half-life and is more rapidly metabolized (20% remaining after 60 min) than the optimized compounds.

To elucidate the safety profile of our candidate compounds, a salmonella mutagenicity test for detecting carcinogenic and mutagenic potential of the compounds was performed. No substitution mutations in the histidine *Salmonella typhimurium* strain TA100 auxotroph stain up to a concentration of 100 µM were detected **(Table 9)**. Inspection of the background lawn indicated nontoxicity of the compounds, suggesting a suitable safety profile for **6g**, **7d** and **9l**.

Experimental

■ General synthetic & analytical chemistry methods

Compounds were synthesized in house. The structures of the synthesized compounds were confirmed by ^{1}H-, ^{13}C-NMR and MS (ESI). The purity of the synthesized compounds was

determined by combustion analysis or by HPLC and was found to be >95%. Starting materials and solvents were purchased from Sigma-Aldrich Chemie GmbH (Steinheim, Germany), Apollo Scientific (Stockport, UK), Acros (Nidderau, Germany) or Alfa Aesar (Ward Hill, USA) and were reagent grade and used without further purification. The products were purified using a Varian 971-FP Flash Purification System on silica gel with 50-µm particle size. ^{1}H and ^{13}C-NMR spectra were measured in DMSO-d_6 or MeOH-d_4 on a Bruker AV 250 (250 MHz for ^{1}H-NMR and 63 MHz for ^{13}C-NMR). Chemical shifts are reported in parts per million using tetramethylsilane as internal standard. Mass spectra were obtained on an Electrospray-Ionization Fisons (VG Platform II) spectrometer measuring in the positive- or negative-ion mode (ESI-MS system). Combustion analysis was performed by the microanalytical laboratory of the Institute of Organic Chemistry and Chemical Biology, Goethe University Frankfurt (Frankfurt, Germany), on an Elementar Vario Micro Tube CHNO rapid elemental analyzer. HPLC analysis was performed on a Shimadzu (Kalsruhe, Germany) LC/MS 2020 on a C18 Kinetex column (2.6 µm, 100 Å, 100 × 2.1 mm) with a 254- and 280-nm detector.

■ General procedure for the synthesis of imidazo[1,2-*a*]pyridin-3-amine derivatives

A solution of aminopyridine (1 mmol, 1 eq.), aldehyde (1.2 mmol, 1.2 eq.) and glacial acetic acid (2 mmol, 2 eq.) in 12 ml of anhydrous MeOH was stirred for 20 min at room temperature. To the reaction mixture, isocyanide (1 mmol, 1 eq.) was added in one portion. Stirring was continued at room temperature for 14 h. The reaction mixture was quenched with 1.5 ml of aqueous 10% HCl and the solvent was removed under reduced pressure. The residue was solved in 20 ml EtOAc and washed (3 × 20 ml) with saturated $NaHCO_3$. The organic phase was dried over $MgSO_4$ and the solvent was removed under reduced pressure. The crude product was recrystallized from EtOAc/EtOH or purified by flash chromatography (Hex/EtOAc) (0→80%, rate of modification 5%/min).

■ 6-chloro-*N*-cyclopentyl-2-(4-morpholinophenyl)imidazo[1,2-*a*]pyridin-3-amine **(4a)**

^{1}H-NMR (250 MHz, DMSO-d_6): δ 8.71 (s, 1H), 8.05 (d, J = 8.5 Hz, 2H), 7.78-7.65 (m, 2H), 7.14 (d, J = 9.7 Hz, 2H), 5.08 (m, 1H), 3.77 (m, 4H), 3.23 (m, 4H), 3.62 (m, 1H), 1.72 (m, 8H). ^{13}C-NMR (250 MHz, DMSO-d_6): 150.89, 148.04, 128.33, 126.52, 123.67, 122.27, 115.11, 66.37, 58.07, 47.70, 33.18, 22.81. MS (ESI, 70 eV) *m/z* 397.56 (MH^+). A yellow solid was obtained with a total mass of 172 mg (33% yield). The t_R value was 6.058 min. The HRMS calculated for $C_{22}H_{25}ClN_4O$ 397.17897 was found to be 397.17966.

Table 8. Physicochemical properties, rat hematopoietic leukemia cell line-1 inhibitory activity values and human whole blood assay data of the compounds under study.

Entry	log P	IC_{50} rat hematopoietic leukemia cell line-1 (µM)	Solubility (µg/ml)†	Human whole blood LTB_4 (%)‡	Human whole blood 5(*S*)-HETE (%)§
EP6	1.99	0.34	458.2	ia.	ia.
5b	2.36	1.06	6.7	ia.	ia.
6g	1.75	0.32	159.1	31 ± 4.1	22 ± 4.0
7c	2.15	1.23	n.t.	ia.	ia.
7d	2.17	2.30	122.7	ia.	ia.
9l	2.07	0.51	451.9	23 ± 1.0	8 ± 9.1
9n	2.01	0.61	n.t.	ia.	ia.

†*Solubility in simulated gastric fluid.*
‡*(%) LTB_4 inhibition at 10 µM in human whole blood compared with control.*
§*(%) 5(S)-HETE inhibition at 10 µM in human whole blood compared with control.*
ia.: Inactive; n.t.: Not tested.

Materials

AA, calcium ionophore A23187, BWA4C and DMSO were purchased from Sigma-Aldrich (Munich, Germany), zileuton and human recombinant 15-LO2 from Cayman Chemical

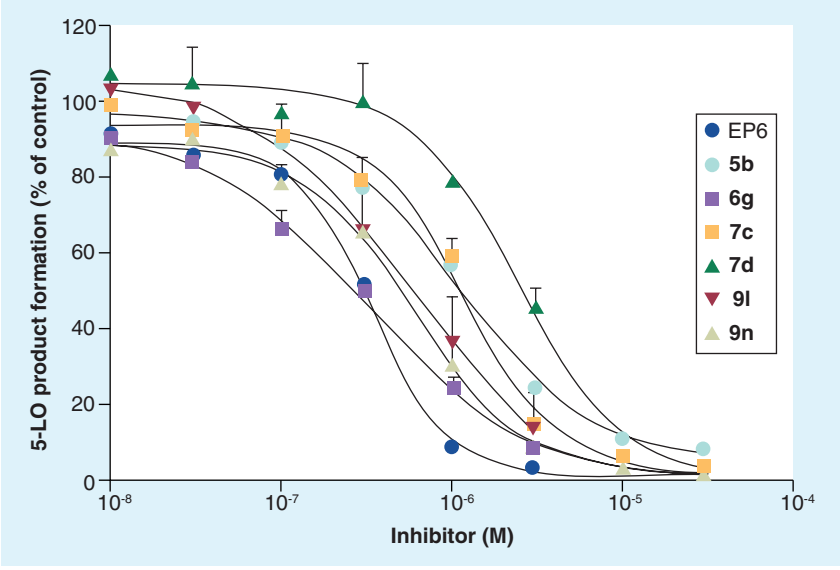

Figure 4. 5-LO product formation dose–response inhibition curves for 5b, 6g, 7c, 7d, 9l, 9n and EP6 compared with control in rat hematopoietic leukemia cell line-1 cells.

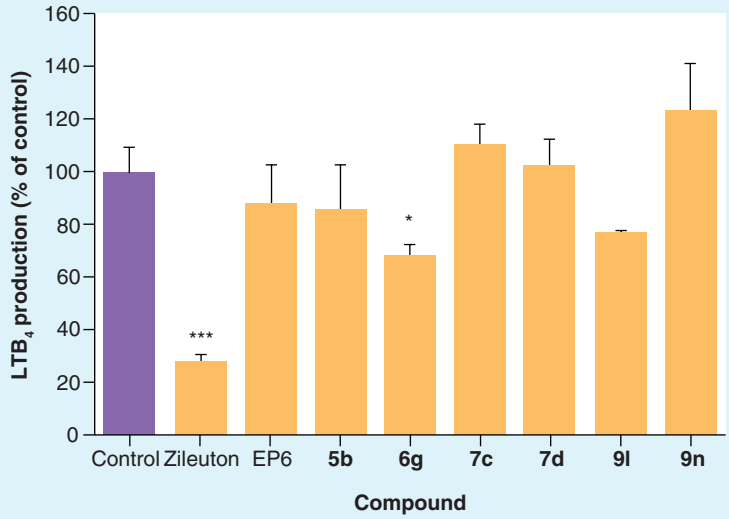

Figure 5. LTB_4 product formation after incubation with zileuton (5 µM), 5b, 6g, 7c, 7d, 9l, 9n and EP6 at 10 µM compared with control in human whole blood.
*p < 0.05.
***p < 0.001.

(MI, USA). HPLC solvents were purchased from Merck (Darmstadt, Germany), penicillin and streptomycin from PAA laboratory GmbH (Pasching, Austria). Fetal calf serum (FCS) was purchased from Biochrom AG (Berlin, Germany), RPMI 1660 medium from Gibco/Invitrogen (Paisley, UK). Fresh blood cell concentrates were kindly provided by Städtische Kliniken Frankfurt Höchst, (Frankfurt, Germany).

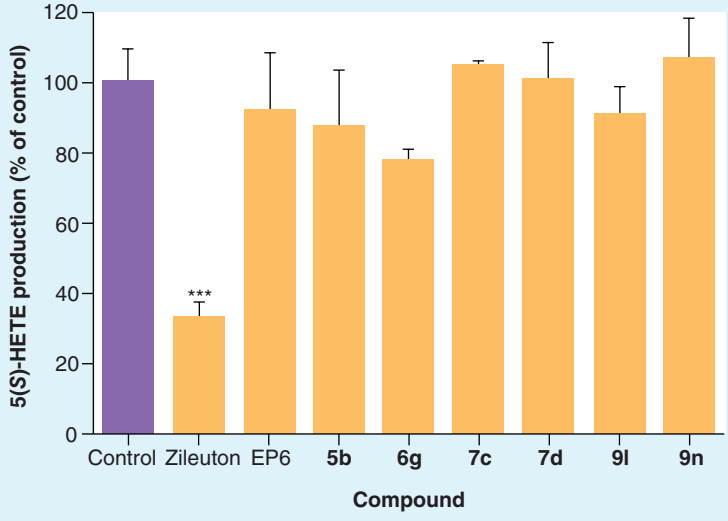

Figure 6. 5(*S*)-hydroxy-6,10-*trans*-8,14-*cis*-eicosatetraenoic acid product formation after incubation with zileuton (5 µM), 5b, 6g, 7c, 7d, 9l, 9n and EP6 at 10 µM compared with control in human whole blood.
***p < 0.001.

■ Cell culture

The human leukemic monocyte cells U937 and rat basophilic leukemia (RBL)-1 cells were purchased from Deutsche Sammlung für Mikroorganismen und Zellkulturen (DSMZ, Braunschweig, Germany). U937 were maintained in RPMI 1640 medium containing 10% FCS, 100 µg/ml streptomycin and 100 U/ml penicillin. RBL-1 cells were maintained in 1640 medium containing 10% FCS, 10 mM HEPES, pH 7.4, 100 µg/ml streptomycin, 100 U/ml penicillin, 1 mM sodium pyruvate and nonessential amino acids. Cells were cultured at 37°C in an atmosphere containing 5% CO_2.

Isolation of PMNL & platelets from leukocyte concentrates

PMNL and platelets were freshly isolated from leukocyte concentrates obtained from Städtische Kliniken Frankfurt Höchst (Frankfurt, Germany). Blood samples were obtained by the hospital with informed consent. In brief, cells were isolated by dextran sedimentation for 30 min, and 10 min centrifugation without deceleration at 800 × g on Nycoprep cushions (PAA laboratory GmbH, Pasching, Austria). For PMNL isolation the cells were resuspended in 10 ml of ice-cold water for hypotonic lysis of erythrocytes as described previously [29]. Cells were finally re-suspended in phosphate-buffered saline (PBS), pH 7.4, containing 1 mg/ml glucose (PG buffer) (purity >96–97%). Platelets were resuspended in PBS, pH 5.4 and centrifuged at 1849 × g for 15 min at room temperature. The cells were resuspended in PBS/NaCl (PBS, pH 5.4 and 0.9% NaCl, 1:1 dilution) and centrifuged at 1849 × g for 10 min at room temperature. Finally, platelets were resuspended in PBS, pH 5.4.

Determination of 5-LO product formation in intact cells

For assays in intact cells, 5×10^6 freshly isolated PMNL or 3×10^6 RBL-1 cells were resuspended in 1 ml of PBS, pH 7.4, containing 1 mg/ml glucose and 1 mM $CaCl_2$ (PGC buffer). After pre-incubation with the test compound or vehicle (DMSO) at the indicated concentrations for 15 min at 37°C, 5-LO product formation was inhibited with 2.5 µM calcium ionophore A23187 together with 20 µM AA. After 10 min at 37°C, the reaction was stopped with 1 ml of ice-cold methanol. A total of 30 µl of 1 M HCl, 200 ng of prostaglandin B1 as internal standard and 500 µl of PBS, pH 7.4, were added. 5-LO

Table 9. Selectivity properties, *in vitro* pharmacokinetic parameters and Ames test of the compounds under study.

Entry	Remaining (%)[†]	CL_{int} (ml/min/kg)	$t_{1/2}$ (min)	*N*-formyl-methionine-leucine-phenylalanine (%)[‡]	IC_{50} 12-LO[§] (μM)	IC_{50} 15-LO1[¶] (μM)	IC_{50} 15-LO2[#] (μM)	Ames
EP6	20 ± 2.2	119 ± 18.7	10.6	0.9 ±0.63	>30 μM	>30 μM	>30 μM	ia.
6g	29 ± 1.5	66 ± 1.7	18.6	15 ± 18.80	>30 μM	>30 μM	>30 μM	ia.
7d	43 ± 5.2	70 ± 20.4	18.6	20 ± 20.40	>30 μM	>30 μM	15 μM	ia.
9l	44 ± 9.1	46 ± 32.3	31.2	16 ± 18.70	>30 μM	>30 μM	>30 μM	ia.

[†](%) remaining concentration after 60 min.
[‡](%) residual activity of 5-LO after N-formyl-methionine-leucine-phenylalanine stimulation at 10 μM.
[§] Inhibition of platelet 12-LO.
[¶]Inhibition of 15-LO1 measured in polymorphonuclear leukocytes preparations.
[#]Inhibition of recombinant 15-LO2.
ia.: Inactive.

metabolites were extracted and analyzed by HPLC as described [30]. For assays with stimulation via fMLP, 10^7 freshly isolated PMNL were resuspended in PGC buffer, primed for 15 min with 1 μg/ml LPS and 0.2 U/ml Ada, and incubated for 15 min with test compound or vehicle (DMSO). The 5-LO product formation was inhibited by addition of 1 μM fMLP. Metabolites were measured by LC–MS/MS analysis as described previously [31]. 5 LO product formation was determined as ng of 5-LO products per 10^6 cells, which includes LTB_4 and its all-*trans* isomers, 5(*S*),12(*S*)-diHETE and 5-HpETE. Cysteinyl-containing LTs (LTC_4, D_4 and E_4) and oxidation products of LTB_4 were not determined. Each experiment was performed at least three times. Data (mean ± SD) are expressed as percentage of control (DMSO).

Determination of 5-LO product formation in S100

PMNL were resuspended in 1 ml of PBS containing 1 mM of EDTA, the protease inhibitors soybean trypsin inhibitor (60 μg/ml), 1 mM phenylmethylsulfonyl chloride, and leupeptin (10 μg/ml), cooled on ice for 10 min. Subsequently, the samples were sonicated for 3 × 10 s. To obtain 100,000 × g supernatant (S100), the homogenate was centrifuged (100,000 × g for 70 min at 4°C). For determination of 5-LO activity, S100 corresponding to 7.5 × 10^6 PMNL were resuspended in 1 ml of reaction mix (PBS, pH 7.4, 1 mM EDTA and 1 mM ATP). After preincubation with the test compounds or vehicle (DMSO) at the indicated concentration for 15 min at 4°C, the samples containing S100 were pre-warmed for 30 s at 37°C. The reaction was started after addition of 2 mM $CaCl_2$ and 20 μM AA. After 10 min 5-LO product formation was stopped with 1 ml ice-cold methanol and the

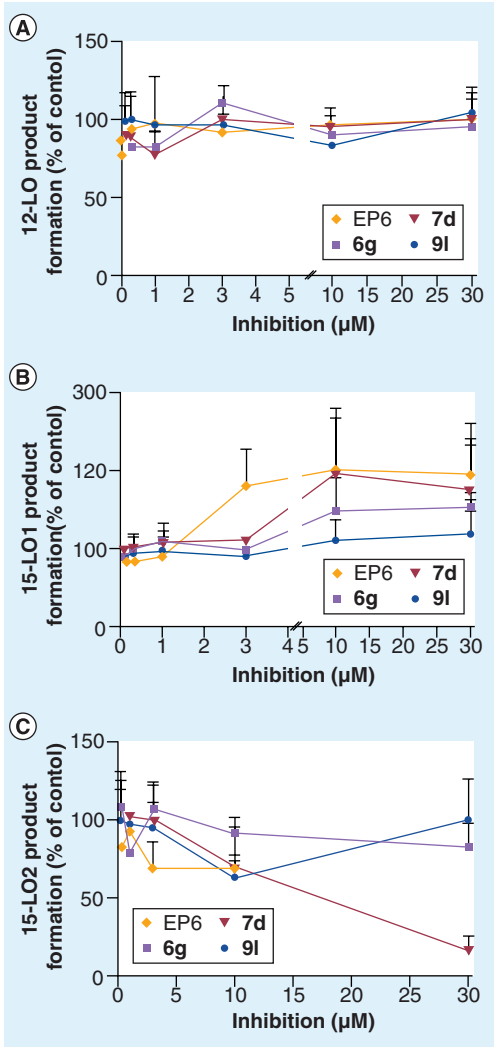

Figure 7. Selectivity of compounds towards 12-LO, 15-LO1 and 15-LO2.
(A) 12-LO activity test performed with compounds EP6, **6g**, **7d** and **9l**; **(B)** 15-LO1 activity test performed with compounds EP6, **6g**, **7d** and **9l**; and **(C)** 15-LO2 activity test performed with compounds EP6, **6g**, **7d** and **9l**.

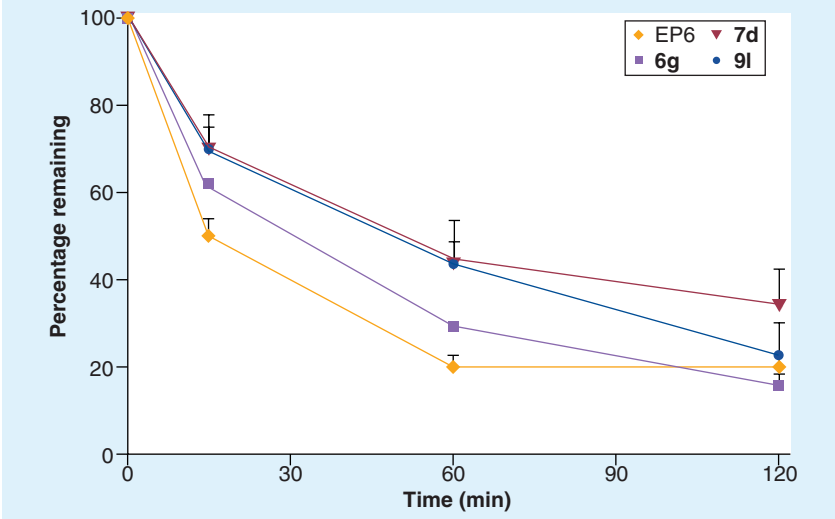

Figure 8. *In vitro* metabolism of 6g, 7d, 9l and EP6 in rat liver microsomes.

formed metabolites were analyzed by HPLC as described for intact cells. Data (mean ± SD) are expressed as percentage of control (DMSO).

Determination of 12-LO & 15-LO1 product formation in intact cells

Determination of 15-LO1 product formation was performed in PMNL preparations as described for 5-LO product formation in intact cells [19]. Here, the source for 15-LO1 products are eosinophils typically present in PMNL preparations. For determination of 12-LO product formation 1×10^8 freshly isolated platelets were re-suspended in 1 ml of PGC buffer (pH 7.4) and were pre-incubated with the test compound or vehicle (DMSO) at the indicated concentrations for 15 min at 37°C. 12-LO product formation was stimulated by addition of 10 µM AA. After 10 min at 37°C, the reaction was stopped with 1 ml of ice-cold methanol. 12-LO products include 12(*S*)-hydro(pero)xy-6-*trans*-8,11,14-*cis*-eicosatetraenoic acid (12-H(p)ETE). 12-HETE and 12-HpETE elute as one major peak. 15-LO1 products, generated from contaminating eosinophils in PMNL preparations expressing 15-LO1, were 15-H(p)ETE, which elute as one major peak as well. Data (mean ± SD; n ≥ 3) are expressed as percentage of control (DMSO).

Determination of 15-LO2 product formation in cell-free systems

A total of 0.5 U human recombinant 15-LO2 was added to 1 ml PBS, pH 7.4. After pre-incubation with test compound or vehicle (DMSO) at the indicated concentrations for 15 min on ice, 15-LO2 product formation was stimulated with 100 µM AA. After 10 min at 37°C, the reaction was stopped with 1 ml of ice-cold methanol. 15-LO2 metabolites were extracted and analyzed by HPLC as described for intact cells. Data (mean ± SD; n ≥ 3) are expressed as percentage of control (DMSO).

In vitro cell viability assay

The WST-1 assay (Roche Diagnostic GmbH, Mannheim, Germany) was used to determine cell viability after treatment with the test compound. U937 cells were seeded in 96-well plates at a density of 10^4 cells/well and treated with increasing concentrations of test compound or vehicle (DMSO) for 48 h in presence of 10% FCS. Cell viability was assessed according to the distributor's protocol using a microplate reader (infinite M200, Tecan Group Ltd, Crailsheim, Germany) and was calculated as a ratio of the absorbance values measured after 48 h (between test compound and vehicle [DMSO]). All the experiments were tested three times and the mean ± SD were calculated.

■ LDH cytotoxicity assay

The LDH assay (cytotoxicity detection kit; Roche Diagnostics GmbH, Roche Applied Science, Mannheim, Germany) was used to determine cell death after treatment of U937 cells with test compounds. LDH leakage was measured to provide an index for loss of cell membrane integrity. U937 cells were seeded in 96-well plates at a density of 1.5×10^4 cells/well and incubated with increasing concentrations of test compounds or vehicle (DMSO) for 48 h.

Plates were centrifuged (250 × g, 4 min) and an aliquot of the supernatant was transferred to a clean microplate. Cell toxicity was assessed according to the distributor's protocol using a microplate reader (infinite M200, Tecan Group Ltd, Crailsheim, Germany). A control detergent supplied by Sigma-Aldrich (MO, USA) was used for maximum LDH release and set to 100%. All experiments were tested three times and the mean ± SD were calculated.

Solubility

The solubility of EP6, **5b**, **6g**, **7d**, and **9l** was examined in SGF at pH 1.2 and SIF at pH 6.8. In each of the media, approximately 2 mg of compound was weighed directly into a UniPrep™ 0.45-µm filter device (0.45 µm PTFE, Whatman, Germany) enclosed with aluminum foil to which 3 ml of pre-warmed media was added. The UniPrep device was placed in an orbital

shaker with gentle shaking and the temperature was maintained at 37°C. After 24 h, the media was filtered and the resulting filtrate diluted in 10% DMSO (prepared in either SGF or SIF, respectively) and analyzed by HPLC (MultoHigh phenyl phase 5 µm, 250 × 4 mm and MultoHigh RP18 phase 5 µm, 250 × 4 mm and detection: 330 and 254 nm).

Metabolic stability

Test compounds were dissolved to a stock concentration of 1 mM in DMSO and diluted in phosphate buffer 0.1 M (pH 7.4) to the final concentration of 10 µM. After adding the cofactors mixture (a NADPH-regenerating system: 30 mM glucose-6-phosphate, 4 U/ml glucose-6-phosphate dehydrogenase, 10 mM NADP, 30 mM $MgCl_2$ the solution was preincubated for 5 min at 37°C. The reaction was initiated by adding 13 µl of liver rat (Sprague Dawley) microsomes (Invitrogen, Darmstadt, Germany) at a final concentration of 0.5 mg/ml. Samples were taken at times 0, 15, 60 and 120 min and 250 µl of ice-cold methanol were added to stop the reaction. After the addition of 250 µl DMSO, the samples were centrifuged (10,000 × g at 4°C). Supernatants were analyzed and quantified by HPLC (MultoHigh phenyl phase 5 µm, 250 × 4 mm [for 7-EC and **6g**] and MultoHigh RP18 phase 5 µm, 250 × 4 mm [for **7d**, **9l**] and detection: 330 and 254 nm). A control sample without cofactors was always added to check the stability of the compounds in the reaction mixture. Inactivated microsomes (at 90°C, 15 min) with cofactors were used as second control. Drug concentration was estimated by using an external calibration. Concentration data were fitted to a monoexponential equation, yielding the rate constant (k) for loss of drug, which was converted to half-life by $t_{1/2} = \ln 2/k$. Apparent intrinsic clearance was calculated [28] as $CL_{int,app}$ = (0.693/*in vitro* $t_{1/2}$)·(incubation volume/mg of microsomal protein)·(45 mg microsomal protein/gram of liver)·(20 g of liver/kg body weight).

For comparison purposes, half-live and intrinsic clearance of a standard compound (7-EC) were determined and compared with values found in the literature [32]. All experiments were performed three times and the mean ± SD calculated.

■ *Salmonella* mutagenicity test

The *Salmonella* mutagenicity test for detecting carcinogenic and mutagenic potential was performed with the histidine auxotroph (his^-) *Salmonella typhimurium* strain TA100 in assays conducted without metabolic activation as described by Maron and Ames [33].

HWB LT/HETE assay

To assess the efficacy of compounds (**5b**, **6g**, **7c**, **7d**, **9l**, **9n** and EP6) in HWB, 500 µl of human heparinized whole blood was mixed with test compounds and incubated for 15 min at 37°C. Afterwards, the whole blood was stimulated with 20 µM calcium ionophore (A23187) in autologous plasma for a further 15 min at 37°C. Blood samples were chilled on ice for 5 min, plasma collected (centrifugation at 4°C with 268 × g for 20 min), and LTs and HETEs extracted by liquid–liquid extraction. Therefore, the plasma was mixed with 20 µl of EtOH and 20 µl of internal standard containing 25 ng/ml LTB_4-d_4, 25 ng/ml 5(*S*)-HETE-d_8, 25 ng/ml 12(*S*)-HETE-d_8, 25 ng/ml 15(*S*)-HETE-d_8, and 25 ng/ml 20-HETE-d_6. Then, 600 µl of ethyl acetate was added and samples were mixed and centrifuged at 11,336 × g for 3 min. The organic upper phase was extracted. Extraction of LTs and HETEs was repeated once. Solvent was evaporated under nitrogen atmosphere, and the residue was reconstituted in 50 µl of MeOH–H_2O (50:50 v/v). LTB_4, 5(*S*)-HETE, 12(*S*)-HETE, 15(*S*)-HETE, and 20-HETE were analyzed by LC-MS/MS technique on a AB SCIEX QTRAP 5500 (Applied Biosystems, CA, USA) operating in multiple reaction monitoring. Chromatographic separation was performed on a Gemini-NX 5u C18 110A column (150 mm × 2 mm inner diameter, 5-µm particle size [Phenomenex, Aschaffenburg, Germany]). Zileuton was used as a reference at 5 µM and compounds EP6, **5b**, **6g**, **7c**, **7d**, **9l** and **9n** were tested at 10 µM. Data (mean ± SD; $n \geq 3$) are expressed as percentage of control (DMSO). Data were analyzed taking a p value < 0.05 (*) as significant (n = 3) (one way ANOVA and Dunnett's *post hoc* test).

Measurement of log P

Log P values were performed using the shake-flask method with two immiscible solvents (1-octanol/PBS, pH 7.4). Compounds (EP6, **5b**, **6g**, **7c**, **7d**, **9l** and **9n**) were first dissolved in methanol (10 mg/ml). To 6.0 ml of PBS saturated with 1-octanol, 250 µl of compound in methanol solution and 6.25 ml of 1-octanol saturated with PBS were added. The mixture was shaken for 4 h and centrifuged for 5 min at 1006 × g (Heraus Labofuge, Thermo Scientific, Schwerte, Germany). The

concentrations of the compounds in PBS and that in 1-octanol phase were measured with a Prim Spectrophotometer (Schott Instruments, Mainz, Germany) at λ_{max}=360 nm. The standard curves were obtained previously for 1-octanol and PBS and then used for measurement of concentration of compounds.

Statistics

Data are expressed as mean values with SE or SD. All IC_{50} values are means with SE of the IC_{50} values obtained from measurements at five different concentrations of the compounds in three to five independent experiments **(SUPPLEMENTARY DATA)**. IC_{50} values were determined using a sigmoidal dose response (four parameters) equation from GraphPad Prism® (GraphPad Software, LaJolla, USA) software. The accuracy of the activity assays used in this study is available as supporting information.

Conclusion

In this study, we present an extensive evaluation of imidazo[1,2-*a*]pyridines as a suitable lead structure for novel 5-LO targeting compounds. We were able to identify several parts of the structure where chemical modification for lead optimization is possible: small substituents at different positions of the imidazo[1,2-*a*]pyridine core and diverse functionalities at the eastern phenyl moiety. Although it was not possible to introduce a solubility group without impairing the 5-LO inhibitory activity, combination of small polar groups led to a more favorable solubility and, in terms of the microsomal half-life, *in vitro* metabolic stability compared with the lead EP6. Furthermore, the cytotoxic potential of the initial lead structure could be abolished and, although the effects are small, inhibitory activity in HWB was gained comparing EP6 to the final compound **9l (FIGURE 9)**. This study demonstrates that imidazo[1,2-*a*]pyridines are a versatile scaffold for the development of novel, direct and selective 5-LO inhibitors with a favorable pharmacokinetic and toxicological profile.

Future perspective

5-LO is a key enzyme that plays an important role in eicosanoid signaling in particular in LT biosynthesis. LT are involved in asthma, allergic rhinitis, glomerulonephritis, rheumatoid arthritis, inflammatory bowel disease, sepsis, cancer and atherosclerosis. Moreover, genetic variants in the genes of the 5-LO pathway have been associated with the risk of development of acute myocardial infarction and stroke [34]. Eicosanoids are increased in infectious exacerbations of chronic obstructive pulmonary disease. They are also elevated in the airways of stable chronic obstructive pulmonary disease patients [35] compared with healthy subjects. Therefore, 5-LO has created interest the scientific community as a possible therapeutic target to treat the several disease conditions listed before.

Moreover, the 5-LO gene (*Alox5*) was observed to be a critical regulator for leukemia stem cells in BCR-ABL-induced chronic myeloid leukemia (CML) [36,37]. In the absence of *Alox5* gene, BCR-ABL failed to induce CML in mice. This deficiency did not cause impairment in the function of normal hematopoietic stem cells, highlighting Alox5 and 5-LO as a possible treatment for CML stems cell that are not sensitive to BCR-ABL kinase inhibitors. Moreover, Chen *et al.* demonstrated that treatment with zileuton-suppressed leukemia stem cells in CML mice,

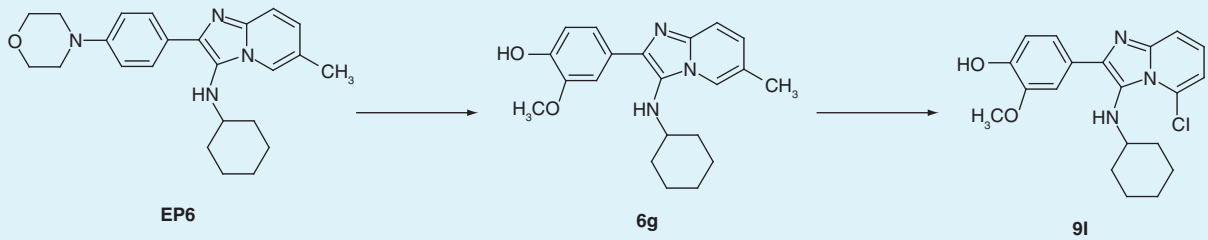

IC_{50} (PMNL) = 0.16 µM
IC_{50} (S100) = 0.21 µM
Solubility = 458.2 µg/ml
HWB (10 µM) = Inactive
$t_{1/2}$ (microsomes) = 10.6 min

IC_{50} (PMNL) = 0.55 µM
IC_{50} (S100) = 0.13 µM
Solubility = 159.1 µg/ml
HWB (10 µM) = 31%
$t_{1/2}$ (microsomes) = 18.6 min

IC_{50} (PMNL) = 1.15 µM
IC_{50} (S100) = 0.29 µM
Solubility = 451.8 µg/ml
HWB (10 µM) = 23%
$t_{1/2}$ (microsomes) = 31.2 min

Figure 9. Pharmacological evaluation of imidazo[1,2-*a*]pyridine 5-LO inhibitors and lead optimization.
HWB: Human whole blood; PMNL: Polymorphonuclear leukocytes.

inhibited *Alox5* function and coadministration with imatinib had a better therapeutic effect than zileuton or imatinib alone [37]. An *in vitro* study also supports the role of *Alox5* in CML, with the study of CML blast cell in culture with 5-LO inhibitors, which reduced cell proliferation.

Overall, the development of 5-LO inhibitors with high efficacy and selectivity *in vivo* will provide a possible treatment for patients having one of the diseases where LT biosynthesis plays an important role.

Supplementary data

To view the supplementary data that accompany this paper please visit the journal website at: **www.future-science.com/doi/full/10.4155/FMC.13.72**

Ethical conduct of research

The authors state that they have obtained appropriate institutional review board approval or have followed the principles outlined in the Declaration of Helsinki for all human or animal experimental investigations. In addition, for investigations involving human subjects, informed consent has been obtained from the participants involved.

Financial & competing interests disclosure

This research was supported by the Deutsche Forschungsgemeinschaft (DFG, Sachbeihilfe PR-1405/1) LOEWE Lipid Signaling Forschungszentrum Frankfurt (LiFF), the DAAD/Fundación Obra Social 'la Caixa' and the Fonds der Chemischen Industrie. The authors have no other relevant affiliations or financial involvement with any organization or entity with a financial interest in or financial conflict with the subject matter or materials discussed in the manuscript. This includes employment, consultancies, honoraria, stock ownership or options, expert testimony, grants or patents received or pending, or royalties.

No writing assistance was utilized in the production of this manuscript.

Executive summary

Therapeutic role of 5-LO

- 5-LO and its metabolites play an important role in different pathophysiological conditions such as cancer, allergy, inflammation and asthma.

Structure–activity relationship

- Compound **9l** was discovered through structure–activity relationship studies and empirical medicinal chemistry efforts, overcoming the poor pharmacokinetic properties of our lead compound EP6.

Selectivity

- Compound **9l** selectively inhibits 5-LO with the other lipoxygenases (15-LO1, 15-LO2, 12-LO) unaffected.

Pharmacokinetic profile

- Compound **9l** displays an improved *in vitro* pharmacokinetic profile (solubility, metabolic stability, toxicity) suitable for further *in vivo* evaluation in a rodent disease model.

References

Papers of special note have been highlighted as:
- ▪ of interest
- ▪▪ of considerable interest

1 Werz O, Steinhilber D. Therapeutic options for 5-lipoxygenase inhibitors. *Pharmacol. Ther.* 112(3), 701–718 (2006).

2 Gilbert NC, Bartlett SG, Waight MT *et al.* The structure of human 5-lipoxygenase. *Science* 331(6014), 217–219 (2011).

▪ **First human x-ray structure of 5-LO published.**

3 Rådmark OP. The molecular biology and regulation of 5-lipoxygenase. *Am. J. Respir. Crit. Care Med.* 161(2Pt 2), S11–S15 (2000).

4 Peters-Golden M, Brock TG. 5-lipoxygenase and FLAP. *Prostaglandins Leukot. Essent. Fatty Acids.* 69(2–3), 99–109 (2003).

5 Werz O, Szellas D, Steinhilber D, Rådmark O. Arachidonic acid promotes phosphorylation of 5-lipoxygenase at Ser-271 by MAPK-activated protein kinase 2 (MK2). *J. Biol. Chem.* 277(17), 14793–14800 (2002).

6 Werz O, Bürkert E, Fischer L *et al.* Extracellular signal-regulated kinases phosphorylate 5-lipoxygenase and stimulate 5-lipoxygenase product formation in leukocytes. *FASEB J.* 16(11), 1441–1443 (2002).

7 Haeggström JZ, Funk CD. Lipoxygenase and leukotriene pathways: biochemistry, biology, and roles in disease. *Chem. Rev.* 111(10), 5866–5898 (2011).

8 Melo RCN, D'Avila H, Wan H-C, Bozza PT, Dvorak AM, Weller PF. Lipid bodies in inflammatory cells: structure, function, and current imaging techniques. *J. Histochem. Cytochem.* 59(5), 540–556 (2011).

9 Blaho VA, Zhang Y, Hughes-Hanks JM, Brown CR. 5-Lipoxygenase-deficient mice infected with Borrelia burgdorferi develop persistent arthritis. *J. Immunol.* 186(5), 3076–3084 (2011).

10 Steinhilber D, Fischer AS, Metzner J *et al.* 5-lipoxygenase: underappreciated role of a pro-inflammatory enzyme in tumorigenesis. *Front. Pharmacol.* 1, 143 (2010).

▪ **Provides an overview regarding the role of 5-LO in tumorigenesis.**

11 Park S-W, Heo D-S, Sung M-W. The shunting of arachidonic acid metabolism to 5-lipoxygenase and cytochrome p450 epoxygenase antagonizes the anti-cancer effect of cyclooxygenase-2 inhibition in head and neck cancer cells. *Cell. Oncol. (Dordr.).* 35(1), 1–8 (2012).

12 Kelavkar UP, Cohen C. 15-lipoxygenase-1 expression upregulates and activates insulin-like growth factor-1 receptor in prostate cancer cells. *Neoplasia* 6(1), 41–52 2004).

13 Cimen I, Astarci E, Banerjee S. 15-lipoxygenase-1 exerts its tumor suppressive role by inhibiting nuclear factor-kappa B via activation of PPAR gamma. *J. Cell. Biochem.* 112(9), 2490–2501 (2011).

14 Duffy CD, Guiry PJ. Recent advances in the chemistry and biology of stable synthetic Lipoxin analogues. *MedChemComm* 1(4), 249 (2010).

15 Sorkness CA. The use of 5-lipoxygenase inhibitors and leukotriene receptor antagonists in the treatment of chronic asthma. *Pharmacotherapy* 17(1Pt 2), 50S–54S (1997).

16 Braeckman RA, Granneman GR, Locke CS, Machinist JM, Cavannaugh JH, Awni WM. The pharmacokinetics of zileuton in healthy young and elderly volunteers. *Clin. Pharmacokinet.* 29(Suppl. 2), 42–48 (1995).

17 Hutchinson JH, Li Y, Arruda JM *et al.* 5-lipoxygenase-activating protein inhibitors: development of 3-[3-tert-butylsulfanyl-1-[4-(6-methoxy-pyridin-3-yl)-benzyl]-5-(pyridin-2-ylmethoxy)-1H-indol-2-yl]-2,2-dimethyl-propionic acid (AM103). *J. Med. Chem.* 52(19), 5803–5815 (2009).

18 Sampson AP. FLAP inhibitors for the treatment of inflammatory diseases. *Curr. Opin. Investig. Drugs* 10(11), 1163–1172 (2009).

19 Wisniewska JM, Rödl CB, Kahnt AS *et al.* Molecular characterization of EP6 – a novel imidazo[1,2-*a*]pyridine based direct 5-lipoxygenase inhibitor. *Biochem. Pharmacol.* 83(2), 228–240 (2012).

20 Hofmann B, Franke L, Proschak E *et al.* Scaffold-hopping cascade yields potent inhibitors of 5-lipoxygenase. *ChemMedChem* 3(10), 1535–1538 (2008).

21 Pergola C, Werz O. 5-Lipoxygenase inhibitors: a review of recent developments and patents. *Expert Opin. Ther. Pat.* 20(3), 355–375 (2010).

▪▪ **Provides an optimal overview regarding the recent developments in 5-LO inhibitors.**

22 Fischer L, Steinhilber D, Werz O. Molecular pharmacological profile of the nonredox-type 5-lipoxygenase inhibitor CJ-13,610. *Br. J. Pharmacol.* 142(5), 861–868 (2004).

23 Groebke K, Weber L, Mehlin F. Synthesis of imidazo[1,2-*a*] annulated pyridines, pyrazines and pyrimidines by a novel three-component condensation. *Synlett* 1998(06), 661–663 (1998).

24 Hieke M, Rödl CB, Wisniewska JM, *et al.* SAR-study on a new class of imidazo[1,2-*a*] pyridine-based inhibitors of 5-lipoxygenase. *Bioorg. Med. Chem. Lett.* 22(5), 1969–1975 (2012).

25 Rådmark O, Werz O, Steinhilber D, Samuelsson B. 5-Lipoxygenase: regulation of expression and enzyme activity. *Trends Biochem. Sci.* 32(7), 332–341 (2007).

▪▪ **Key paper to understand 5-LO regulation.**

26 Smith DA, Di L, Kerns EH. The effect of plasma protein binding on *in vivo* efficacy: misconceptions in drug discovery. *Nat. Rev. Drug Discov.* 9(12), 929–939 (2010).

27 Huo M, Gao R, Jiang L *et al.* Suppression of LPS-induced inflammatory responses by gossypol in RAW 264.7 cells and mouse models. *Int. Immunopharmacol.* 15(2), 442–449 (2013).

28 Lu C, Li P, Gallegos R *et al.* Comparison of intrinsic clearance in liver microsomes and hepatocytes from rats and humans: evaluation of free fraction and uptake in hepatocytes. *Drug Metab. Dispos.* 34(9), 1600–1605 (2006).

29 Werz O, Bürkert E, Samuelsson B, Rådmark O, Steinhilber D. Activation of 5-lipoxygenase by cell stress is calcium independent in human polymorphonuclear leukocytes. *Blood* 99(3), 1044–1052 (2002).

30 Brungs M, Rådmark O, Samuelsson B, Steinhilber D. Sequential induction of 5-lipoxygenase gene expression and activity in Mono Mac 6 cells by transforming growth factor beta and 1,25-dihydroxyvitamin D3. *Proc. Natl Acad. Sci. USA* 92(1), 107–111 (1995).

31 Maier TJ, Tausch L, Hoernig M *et al.* Celecoxib inhibits 5-lipoxygenase. *Biochem. Pharmacol.* 76(7), 862–872 (2008).

32 Carlile DJ, Stevens AJ, Ashforth EIL, Waghela D, Houston JB. *In vivo* clearance of ethoxycoumarin and its prediction from *in vitro* systems. Use of drug depletion and metabolite formation methods in hepatic microsomes and isolated hepatocytes. *Drug Metab. Dispos.* 26(3), 216–221 (1998).

33 Maron DM, Ames BN. Revised methods for the Salmonella mutagenicity test. *Mutat. Res.* 113(3–4), 173–215 (1983).

34 Riccioni G, Bäck M, Capra V. Leukotrienes and atherosclerosis. *Curr. Drug Targets* 11(7), 882–887 (2010).

35 Antczak A, Ciebiada M, Pietras T, Piotrowski WJ, Kurmanowska Z, Górski P. Exhaled eicosanoids and biomarkers of oxidative stress in exacerbation of chronic obstructive pulmonary disease. *Arch. Med. Sci.* 8(2), 277–285 (2012).

36 Chen Y, Hu Y, Zhang H, Peng C, Li S. Loss of the Alox5 gene impairs leukemia stem cells and prevents chronic myeloid leukemia. *Nat. Genet.* 41(7), 783–792 (2009).

37 Chen Y, Li D, Li S. The Alox5 gene is a novel therapeutic target in cancer stem cells of chronic myeloid leukemia. *Cell Cycle* 8(21), 3488–3492 (2009).

Supporting information

Structure activity relationship and *in vitro* pharmacological evaluation of imidazo[1,2-*a*]pyridine-based inhibitors of 5-lipoxygenase

Estel.la Buscató[‡§], Joanna M. Wisniewska[‡§], Carmen B. Rödl[§], Astrid Brüggerhoff[§], Astrid Kaiser[§], Florian Rörsch[+], Edmund Kostewicz[§§], Mario Wurglics[§], Manfred Schubert-Zsilavecz[§], Sabine Grösch[+], Dieter Steinhilber[§], Bettina Hofmann[§]* and Ewgenij Proschak[§]*

* Authors for correspondence

[§]Institute of Pharmaceutical Chemistry, ZAFES/LiFF/OSF Goethe-University Frankfurt, Max-von-Laue-Str. 9, D-60438 Frankfurt am Main, Germany.

Tel.: +49 (0)69 798 29301

E-mail: proschak@pharmchem.uni-frankfurt.de, hofmann@pharmchem.uni-frankfurt.de

[+]Johann Wolfgang Goethe-University, Institute of Clinical Pharmacology, *pharmazentrum frankfurt*, LiFF/ZAFES, Theodor-Stern-Kai 7, D-60590 Frankfurt am Main, Germany

[§§]Institute of Pharmaceutical Technology, Goethe University Frankfurt, Max-von-Laue-Str. 9, D-60438 Frankfurt am Main, Germany

Table of Contents

N-((3s,5s,7s)-adamantan-1-yl)-6-methyl-2-(4-morpholinophenyl)imidazo[1,2-*a*]pyridin-3-amine **(4b)**

^{1}H-NMR (250 MHz, DMSO-d_6): δ 8.32 (s, 1H), 8.06 (d, J = 8.3 Hz, 2H), 7.49 (m, 1H), 7.22 (m, 2H), 7.02 (d, J = 8.2 Hz, 2H), 4.66 (m, 1H), 3.77 (m, 4H), 3.18 (m, 4H), 2.36 (s, 3H), 1.89 (m, 3H), 1.61-1.43 (m, 12H). ^{13}C-NMR (63 MHz, DMSO-d_6): δ 150.0, 128.4, 121.7, 114.1, 65.9, 55.9, 47.8, 43.2, 36.0, 29.0, 17.8. MS (ESI, 70 eV) *m/z* 443.2 (M+). Yellow solid obtained 146 mg (25 % yield). Anal. Calcd for $C_{28}H_{34}N_4O$: C, 75,98, H, 7.71, N, 12.66. Found: C, 75.70, H, 7.61, N, 12.39.

N-((3s,5s,7s)-adamantan-1-yl)-6-chloro-2-(4-morpholinophenyl)imidazo[1,2-*a*]pyridin-3-amine **(4c)**

^{1}H-NMR (250 MHz, DMSO-d_6): δ 8.99 (t, J = 1.32 Hz, 1H), 8.05 (d, J = 8.9 Hz, 2H), 7.13 (d, J=9.06 Hz, 2H), 5.16 (s, 1H, br), 3.80 (m, 4H), 3.26 (m, 4H), 1.93 (m, 3H), 1.64-1.43 (m, 12H).^{13}C-NMR (63 MHz, DMSO-d_6): δ 151.5, 135.5, 132.4, 130.9, 129.0, 123.7, 122.9, 117.1, 114.3, 112.9, 65.9, 56.9, 47.3, 42.8, 35.7, 29.2. MS (ESI, 70 eV) m/z 462.5 (100) (M+). White solid obtained 157 mg (26 % yield). Anal. Calcd for $C_{27}H_{31}ClN_4O\cdot 1HCl$: C, 64.93 H, 6.46, N, 11.16. Found: C, 64.57, H, 6.33, N, 10.99.

N-cyclohexyl-6-fluoro-2-(4-morpholinophenyl)imidazo[1,2-*a*]pyridin-3-amine (**4d**)

^{1}H-NMR (250 MHz, DMSO-d_6): δ 9.01 (s, 1H), 8.09 (d, J = 8.7 Hz, 1H), 7.99 (d, J = 6.0 Hz, 1H), 7.20 (d, J = 9.5 Hz, 1H), 3.77 (m, 4H), 3.29 (m, 4H), 2.89 (m, 1H), 1.93-1.06 (m, 10H). ^{13}C-NMR (63 MHz, DMSO-d_6): δ 150.8, 135.7, 134.2, 128.2, 126.4, 123.5, 116.5, 115.2, 113.1, 65.5, 56.1, 47.3, 33.0, 30.17, 25.2, 23.1. ^{19}F-NMR (282 MHz, DMSO-d_6): δ -134.02. MS (ESI, 70 eV) m/z (%): 395.30 (100) ($M+H^+$). A yellow solid remained 500 mg (90 % yield). t_R= 5.977 min. HRMS calculated $C_{23}H_{27}FN_4O$ 395.22417 found 395.22368

N-(tert-butyl)-6-fluoro-2-(4-morpholinophenyl)imidazo[1,2-*a*]pyridin-3-amine (**4e**)

^{1}H-NMR (250 MHz, DMSO-d_6): δ 8.71 (s, 1H), 7.99 (d, J =12.3 Hz, 2H), 7.75-7.64 (m, 2H), 7.02 (d, J =15.4 Hz, 2H), 4.83 (m, 1H), 3.77 (m, 4H), 3.22 (m, 4H), 1.00 (s, 9H). ^{13}C-NMR (63 MHz, DMSO-d_6): δ 150.6, 136.4, 128.4, 124.9, 115.7, 113.9, 65.8, 56.2, 47.9, 29.8. ^{19}F-NMR (282 MHz, DMSO-d_6): - δ 138.5. MS (ESI, 70 eV) m/z 371.3 (100) (M+3).Yellow solid remained 111 mg (23 % yield). Anal. Calcd for $C_{21}H_{25}FN_4O\cdot 0.4HCl$: C, 65.99 H, 6.65, N, 14.56. Found: C, 65,63, H, 6.44, N, 14.19.

N-cyclohexyl-7-methyl-2-(4-morpholinophenyl)imidazo[1,2-*a*]pyridin-3-amine (**4f**)
^{1}H-NMR (250 MHz, DMSO-d_6): δ 8.20 (d, J =7.7 Hz, 1H), 8.10 (d, J = 8.7 Hz, 2H), 7.17 (s, 1H), 7.01 (d, J =8.2 Hz, 2H), 6.73 (dd, J_1 =1.5 Hz, J_2 =7.0 Hz, 1H), 4.62 (d, J =7.1 Hz, 1H), 3.76 (m, 4H), 3.16 (m, 4H), 2.82 (m, 1H), 2.34 (s, 3H), 1.72-1.11 (m, 10H). ^{13}C-NMR (63 MHz, DMSO-d_6): δ 149.5, 140.6, 134.9, 133.7, 131.0, 127.7, 125.8, 123.8, 114.4, 113.1, 66.0, 56.0, 48.7, 33.6, 24.2, 23.5, 20.7. MS (ESI, 70 eV) m/z 391.7 (100) (M+) 413.5 (67) (M+Na). A white solid is obtained 150 mg (23% yield). t_R= 6.152 min. HRMS Calcd for $C_{24}H_{31}N_4O$ [M+]: 391.24924 found 391.24961

7-chloro-N-cyclohexyl-2-(4-morpholinophenyl)imidazo[1,2-*a*]pyridin-3-amine (**4g**)

^{1}H-NMR (250 MHz, DMSO-d_6): δ 8.34 (d, J = 62 Hz, 1H), 8.12 (d, J = 9.3 Hz, 2H), 7.58 (d, J = 3.1 Hz, 1H), 7.03 (d, J = 8.0 Hz, 2H), 6.92 (dd, J_1 = 2.1, J_2 = 7.3 Hz, 1H), 4.79 (d, J = 6.2 Hz, 1H), 3.79 (m, 4H), 3.20 (m, 4H), 1.78-1.09 (m, 10H). ^{13}C-NMR (63 MHz, DMSO-d_6): δ 151.1, 140.3, 128.4, 126.5, 125.0, 124.0, 120.0, 116.3, 113.9, 66.2, 54.9, 48.2, 33.9, 23.8, 13.7. MS (ESI, 70 eV) m/z 410.8 (100) (M+). A white solid is obtained 99 mg (18 % yield). Anal. Calcd for $C_{23}H_{27}ClN_4O\cdot 0.25HCl$: C, 65.76, H, 6.54, N, 13.34. Found: C, 65.99, H, 6.58, N, 13.20.

N-cyclohexyl-5-methyl-2-(4-morpholinophenyl)imidazo[1,2-*a*]pyridin-3-amine (**4h**)

^{1}H-NMR (250 MHz, DMSO-d_6): δ 8.08 (d, J = 8.5 Hz, 2H), 7.31 (d, J = 9.7 Hz, 1H), 7.06 (d, J = 6.7 Hz, 1H), 6.96 (d, J = 8.8 Hz, 2H), 6.53 (d, J = 7.1 Hz, 1H), 4.54 (d, J = 3.2 Hz, 1H), 3.82 (m, 4H), 3.19 (m, 4H), 2.94 (s, 3H), 2.73 (m, 1H), 1.53-1.02 (m, 10H). ^{13}C-NMR (63 MHz, DMSO-d_6): δ 149.6, 142.4, 138.2, 136.3, 128.2, 125.3, 123.3, 114.3, 113.0, 66.4, 57.7, 47.6, 32.3, 25.8, 24.7, 19.7. MS (ESI, 70 eV) m/z 390.86 (100) (M+). A white solid is obtained 119 mg (23 % yield). Anal. Calcd for $C_{24}H_{20}N_4O$: C, 73.81, H, 7.74, N, 14.35. Found: C, 73.74, H, 7.65, N, 14.35.

5-chloro-N-cyclohexyl-2-(4-morpholinophenyl)imidazo[1,2-*a*]pyridin-3-amine (**4i**)

^{1}H-NMR (250 MHz, DMSO-d_6): δ 8.21 (d, J = 8.4 Hz, 2H), 7.47 (dd, J_1 = 1.2 Hz, J_2 = 8.9 Hz, 1H), 7.14 (dd, J =7.0, J_2 = 8.9 Hz, 1H), 7.03 (d, J = 9.2 Hz, 2H), 6.94 (dt, J_1 = 1.5 Hz, J_2 = 7.4 Hz, 1H), 4.41 (d, J =3.3 Hz, 1H), 3.75 (m, 4H), 3.18 (m, 4H), 2.86 (m, 1H), 1.67-1.04 (m, 10H). ^{13}C-NMR (63 MHz, DMSO-d_6): δ 150.3, 143.3, 139.2, 128.1, 125.6, 124.9, 124.0, 116.0, 114.1, 113.3, 66.2, 58.5, 47.7, 32.4, 25.5, 24.1. MS (ESI, 70 eV) m/z 411.6 (100) (M+). A white solid is obtained 189 mg (35 % yield). t_R= 6.234 min. HRMS Calcd for $C_{23}H_{28}ClN_4O$ [M+]: 411.19462 found 411.19435

N-cyclohexyl-5-fluoro-2-(4-morpholinophenyl)imidazo[1,2-*a*]pyridin-3-amine (**4j**)

^{1}H-NMR (250 MHz, DMSO-d_6): δ 8.21 (d, J = 9.7 Hz, 2H), 7.30 (d, J = 9.7 Hz, 1H), 7.19 (m, 1H), 7.09 (d, J = 9.7 Hz, 2H), 6.61 (dt, J_1 = 1.2, J_2 = 7.0 Hz, 1H), 4.37 (d, J = 4.1 Hz, 1H), 3.73 (m, 4H), 3.14 (m, 4H), 2.84 (m, 10H), 1.69-1.05 (m, 10H). ^{13}C-NMR (63 MHz, DMSO-d_6): δ 152.2, 150.3, 147.8, 143.0, 137.2, 128.1, 125.2, 124.3, 123.4, 113.9, 112.7, 92.8, 66.2, 58.1, 48.3, 32.9, 25.6, 24.2. ^{19}F-NMR (282 MHz, DMSO-d_6): δ -113.45. MS (ESI, 70 eV) m/z 395.6 (100) (M+). A white solid is obtained 185 mg (35 % yield). Anal. Calcd for $C_{23}H_{27}FN_4O$: C, 70.03, H, 6.90, N, 14.20. Found: C, 69.72, H, 7.05, N, 14.19.

N-cyclohexyl-8-methyl-2-(4-morpholinophenyl)imidazo[1,2-*a*]pyridin-3-amine (**4k**)

^{1}H-NMR (250 MHz, MeOD-d_4): δ 8.08 (d, J = 7.2 Hz, 1H), 7.85 (d, J = 8.1 Hz, 2H), 6.97 (d, J = 9.1 Hz, 2H), 6.89 (m, 1H), 6.73 (t, J = 7.2 Hz, 1H), 3.78 (m, 4H), 3.12 (m, 4H), 2.45 (s, 3H), 1.65-1.05 (m, 10H). ^{13}C-NMR (250 MHz, MeOD-d_4): δ 152.1, 142.7, 137.0, 129.4, 128.4, 127.2, 124.6, 122.1, 116.7, 112.9, 67.8, 57.7, 35.1, 27.0, 26.0, 16.7. MS (ESI, 70 eV) m/z 391.6 (100) (M+). A white solid is obtained 100 mg (19 % yield). tR= min. HRMS Calcd for $C_{24}H_{31}N_4O$ [M+]: 372.391.24924 found 391.24927

8-chloro-N-cyclohexyl-2-(4-morpholinophenyl)imidazo[1,2-*a*]pyridin-3-amine (**4l**)

^{1}H-NMR (250 MHz, DMSO-d_6): δ 8.31 (d, J = 7.6 Hz, 1H), 8.13 (d, J = 8.8 Hz, 2H), 7.35 (d, J = 6.5 Hz, 1H), 7.05 (d, J = 9.4 Hz, 2H), 6.89 (d, J = 7.1 Hz, 1H), 4.83 (d, J = 5.9 Hz, 1H), 3.76 (m, 4H), 3.20 (m, 4H), 2.85 (m, 1H), 1.75-1.12 (m, 10H). ^{13}C-NMR (63 MHz, DMSO-d_6): δ 154.7, 150.0, 135.8, 127.3, 125.7, 124.7, 122.2, 120.7, 114.5, 110.8, 66.3, 56.5, 48.1, 33.8, 24.2. MS (ESI, 70 eV) m/z 411.6 (100) (M+). A yellow solid is obtained 100 mg (19 % yield). tR= 5.944 min. HRMS Calcd for $C_{23}H_{28}ClN_4O$ [M+]: 372.411.19462 found 411.19445

N-cyclohexyl-6-fluoro-2-(4-phenoxyphenyl)imidazo[1,2-*a*]pyridin-3-amine (**5a**)

^{1}H-NMR (250 MHz, DMSO-d_6): δ 8.67 (q, J = 1.4 Hz, 1H), 7.87-7.78 (m, 4H), 7.37 (t, J = 7.4 Hz, 2H), 7.08-7.00 (m, 5H), 2.90 (m, 1H), 1.73-1.08 (m, 10H). ^{13}C-NMR (63 MHz, DMSO-d_6): δ 161.0, 158.9, 157.5, 154.5, 135.9, 131.5, 130.6, 129.5, 128.6, 125.6, 122.7, 120.9, 119.3, 114.0, 113.0, 57.5, 34.8, 26.9, 25.7. ^{19}F-NMR (282 MHz, DMSO-d_6): δ -135.05.MS (ESI, 70 eV) m/z = 403.1 (M+). A white solid is obtained 184 mg (83% yield). Anal. Calcd for $C_{25}H_{24}FN_3O$•1.2HCl: C, 67.17, H, 5.69, N, 9.40. Found: C, 74.79, H, 6.03, N, 10.47.

6-chloro-N-cyclohexyl-2-(4-phenoxyphenyl)imidazo[1,2-*a*]pyridin-3-amine (**5b**)

^{1}H-NMR (250 MHz, MeOD-d_4): δ 8.86 (q, J = 0.9 Hz, 1H), 8.01-7.87 (m, 4H), 7.50 (t, J = 7.6 Hz, 2H), 7.28-7.13 (m, 5H), 3.02 (m, 1H), 1.90-1.21 (m, 10H). ^{13}C-NMR (63 MHz, MeOD-d_4): δ 161.0, 157.3, 136.9, 134.9, 131.5, 130.5, 128.1, 126.5, 125.7, 124.5, 122.2, 121.0, 119.7, 114.0, 58.2, 34.4, 26.5, 25.6. MS (ESI, 70 eV) m/z = 418.5 (M+). A yellow solid remained 226 mg (99% yield). Anal. Calcd for $C_{25}H_{24}ClN_3O$•1HCl: C, 66.08, H, 5.55, N, 9.25. Found: C, 66.06, H, 5.63, N, 9.21.

N-cyclohexyl-6-trifluoromethyl-2-(4-phenoxyphenyl)imidazo[1,2-*a*]pyridin-3-amine (**5c**)

^{1}H-NMR (250 MHz, MeOD-d_4): δ 9.03 (s, 1H), 8.06 (dd, J_1 = 1.9 Hz, J_2 = 8.9 Hz, 1H), 7.96-7.85 (m, 3H), 7.40 (t, J = 8.5 Hz, 2H), 7.14-6.99 (m, 5H), 2.90 (m, 1H), 1.75-1.04 (m, 10H). ^{13}C-NMR (63 MHz, MeOD-d_4): δ 157.3, 131.2, 129.3, 125.8, 121.9, 120.9, 119.5, 114.4, 57.7, 35.0, 26.5, 25.5. t_R

(10→20% MeOH) = 10.665 min. MS (ESI, 70 eV) m/z = 452.7 (M+). A yellow solid remained 47 mg (29% yield). ^{19}F-NMR: -60.52.

3-(cyclohexylamino)-2-(4-phenoxyphenyl)imidazo[1,2-*a*]pyridine-6-carbonitrile (**5d**)

^{1}H-NMR (250 MHz, DMSO-d_6): δ 9.12 (s, 1H), 8.33 (d, J = 8.8 Hz, 2H), 7,72 (dd, J_1 = 0.8 Hz, J_2 = 9.3 Hz, 1H), 7.53-7.48 (m, 3H), 7.28 (t, J = 7.1 Hz, 2H), 7.22 (m, 4H), 4.94 (d, J = 6.0 Hz, 1H), 2.99 (s, 1H), 1.83-1.16 (m, 10H). ^{13}C-NMR (63 MHz, DMSO-d_6): δ 155.5, 139.7, 135.9, 130.6, 129.0, 126.3, 123.9, 123.3, 119.2, 118.4, 117.6, 96.6, 56.4, 33.3, 25.4, 24.4. MS (ESI, 70 eV) m/z = 408.5 (M+). A yellow solid remained 204 mg (25%). Anal. Calcd for $C_{26}H_{24}N_4O$•0.60HCl: C, 72.56, H, 5.76, N, 13.02. Found: C, 72.56, H, 5.85, N, 12.61.

N-cyclopentyl-6-methyl-2-(4-phenoxyphenyl)imidazo[1,2-*a*]pyridin-3-amine (**5e**)

^{1}H-NMR (250 MHz, DMSO-d_6): δ 8.22 (d, J = 8.4 Hz, 2H), 8.08 (s, 1H), 7.46-7.41 (m, 3H), 7.17 (t, J = 14.0 Hz, 1H), 7.06 (m, 5H), 4.68 (d, J = 5.1 Hz, 1H), 3.58 (m, 1H), 2.33 (s, 3H), 1.73-1.47 (m, 8H). ^{13}C-NMR (63 MHz, DMSO-d_6): δ 156.5, 155.4, 139.4, 134.6, 130.2, 128.1, 126.9, 125.4, 123.3, 120.54, 118.9, 118.1, 116.1, 58.1, 32.5, 23.5, 17.9. MS (ESI, 70 eV) m/z 384.7 (100) (M+). Off-white solid remained 209 mg (50 % yield). Anal. Calcd for $C_{25}H_{25}N_3O$: C, 78.3, H, 6.57, N, 10.96. Found: C, 78.10, H, 6.59, N, 10.95.

N-(tert-butyl)-6-methyl-2-(4-phenoxyphenyl)imidazo[1,2-*a*]pyridin-3-amine (**5f**)

^{1}H-NMR (250 MHz, MeOD-d_4): δ 8.52 (s, 1H), 7.85 (d, J =7.6 Hz, 2H), 7.68 (q, J = 8.9 Hz, 2H), 7.28 (t, J =7.6 Hz, 2H), 7.06-6.97 (m, 5H), 2.42 (s, 3H), 0.98 (s, 9H). ^{13}C-NMR (63 MHz, MeOD-d_4): δ 160.9, 157.3, 137.4, 131.1, 128.8, 126.3, 125.5, 124.8, 123.5, 120.5, 119.5, 111.7, 57.0, 30.4, 18.1. A white solid remained 200 mg (98%). MS (ESI, 70 eV) m/z = 372.5 (M+). Anal. Calcd for $C_{24}H_{25}N_3O$•1.45HCl: C, 67.64, H, 6:27, N, 9.86. Found: C, 67.55, H, 6.60, N, 9.81.

N-isopropyl-6-methyl-2-(4-phenoxyphenyl)imidazo[1,2-*a*]pyridin-3-amine (**5g**)

^{1}H-NMR (250 MHz, MeOD-d_4): δ 8.30 (s, 1H), 7.90 (d, J = 9.1 Hz, 2H), 7.51 (s, 2H), 7.11 (t, J = 7.7 Hz, 2H), 7.03-6.97 (m, 5H), 2.40 (s, 3H), 1.01 (s, 3H), 0.97 (s, 3H). ^{13}C-NMR (63 MHz, DMSO-d_6): δ 156.9, 155.6, 136.9, 131.7, 130.4, 129.1, 125.7, 124.2, 122.1, 119.2, 118.2, 114.0, 48.5, 22.3, 18.4. A yellow solid remained 30 mg (13%). MS (ESI, 70 eV) m/z = 358.5 (M+). Anal. Calcd for $C_{23}H_{23}N_3O$•1.35HCl: C, 67.64, H, 6:27, N, 9.86. Found: C, 67.63, H, 6.02, N, 10.28.

6-fluoro-N-isopropyl-2-(4-phenoxyphenyl)imidazo[1,2-*a*]pyridin-3-amine (**5h**)

^{1}H-NMR (250 MHz, DMSO-d_6): δ 8.45 (m, 1H), 8.21 (d, J = 8.8 Hz, 2H), 7.58-7.38 (m, 3H), 7.29-7.08 (m, 6H), 4.78 (d, J = 5.7 Hz, 1H), 3.29 (q, J = 3.3Hz, 1H), 1.06 (s, 3H), 1.02 (s, 3H). ^{13}C-NMR (63 MHz, DMSO-d_6): δ 156.6, 155.6, 154.4, 150.5, 138.1, 136.1, 130.0, 128.4, 126.9, 123.3, 119.4, 118.26, 115.6, 110.3, 109.4, 48.4, 23.2. ^{19}F-NMR (282 MHz, DMSO-d_6): δ -141.25. Yellow solid obtained 303 mg (55% yield). MS (ESI, 70 eV) m/z (%): 362.4 (100) (M+). Anal. Calcd for $C_{22}H_{20}FN_3O$: C, 73.11, H, 5.58, N, 11.63. Found: C, 72.89, H, 5.48, N, 11.57

N-((3s,5s,7s)-adamantan-1-yl)-6-fluoro-2-(4-phenoxyphenyl)imidazo[1,2-*a*]pyridin-3-amine (**5i**)

^{1}H-NMR (250 MHz, DMSO-d_6): δ 9.06 (s, 1H), 8.17 (d, J =10.0 Hz, 2H), 7.99 (d, J = 9.2 Hz, 2H), 7.46 (t, J = 9.0 Hz, 2H), 7.26-7.12 (m, 5H), 5.22 (s, 1H, br), 1.89 (m, 3H), 1.60-1.39 (m, 12H). ^{13}C-NMR (63 MHz, DMSO-d_6): δ 158.1, 156.0, 152.5, 134.8, 130.1, 125.3, 124.1, 123.2, 119.7, 117.9, 113.7 112.7, 56.7, 42.8, 35.6, 29.2. ^{19}F-NMR (300 MHz, DMSO-d_6): -134.19. MS (ESI, 70 eV) m/z 453.5 (100) (M+). White solid obtained 364 mg (63 % yield). Anal. Calcd for $C_{29}H_{28}FN_3O$·1.1HCl: C, 70.56 H, 5.94, N, 8.51. Found: C, 70.59, H, 5.66, N, 8.49.

N-cyclohexyl-6-methyl-2-(3-((6-methylpyrazin-2-yl)oxy)phenyl)imidazo[1,2-*a*]pyridin-3-amine (**6a**)

^{1}H-NMR (250 MHz, DMSO-d_6): δ 8.33 (s, 1H), 8.31 (s, 1H), 8.10-8.07 (m, 2H), 7.99 (s, 1H), 7.49 (t, J = 7.8 Hz, 1H), 7.40 (d, J = 8.7 Hz, 1H), 7.07 (dt, J_1 = 9.8 Hz, J_2 = 2.4 Hz, 2H), 4.76 (d, J = 8 Hz, 1H), 2.79 (m, 1H), 2.36 (s, 3H), 2.31 (s, 3H), 1.62-1.03 (m, 10H). ^{13}C-NMR (63 MHz, DMSO-d_6): δ 159.0, 153.6, 151.4, 139.8, 139.0, 136.7, 133.7, 132.3, 129.8, 127.0, 125.9, 122.9, 120.8, 119.0, 116.2, 56.2, 33.6, 25.7, 24.5, 20.3, 17.7. MS (ESI, 70 eV) m/z 414.6 (100) (M+). A white solid remained 139 mg (72 % yield). Anal. Calcd for $C_{25}H_{27}N_5O \cdot 1.70HCl$: C, 63.34, H, 5.71, N, 14.35. Found: C, 63.23, H, 5.71, N, 14.34.

N-cyclohexyl-6-methyl-2-(4-((6-methylpyridin-3-yl)oxy)phenyl)imidazo[1,2-*a*]pyridin-3-amine (**6b**)

^{1}H-NMR (300 MHz, DMSO-d_6): δ 8.28 (dd, J = 2.7 Hz, 1H), 8.21 (d, J = 8.8, 2H), 8.08 (s, 1H), 7.42 (dd, J = 3.7 Hz, 1H), 7.33 (q, J = 8.8 Hz, 2H), 7.03 (m, 3H), 4.71 (d, J = 3.0 Hz, 1H), 2.81 (m, 1H), 2.48 (s, 3H), 2.32 (s, 3H), 1.75-1.08 (m, 10H).^{13}C-NMR (63 MHz, DMSO-d_6): δ 156.0, 153.4, 150.8, 141.3, 139.9, 134.7, 131.0, 128.1, 126.4, 123.8, 121.2, 120.1, 117.8, 116.3, 56.3, 33.6, 26.1, 24.7, 17.52. Off-white solid obtained 188 mg (66% yield). MS (ESI, 70 eV) m/z (%): 413.5 (100) or 413.5 [M+H$^+$]; 435.6 [M+Na$^+$] Anal. Calcd for $C_{26}H_{28}N_4O \cdot 1$ HCl: C, 69.55, H, 6.52, N, 12.48. Found: C, 69.40, H, 6.75, N, 12.45.

N-cyclohexyl-6-methyl-2-(4-(4-methylpiperazin-1-yl)phenyl)imidazo[1,2-*a*]pyridin-3-amine (**6c**)

^{1}H-NMR (250 MHz, DMSO-d_6): δ 8.06 (m, 3H), 7.34 (d, J = 8.9 Hz, 1H), 6.99 (m, 3H), 4.59 (d, J = 6.0 Hz, 1H), 3.21 (m, 4H), 3.18 (m, 4H), 2.84 (m, 1H), 2.31 (s, 3H), 2.25 (s, 3H), 1.71-1.06 (m, 10H). ^{13}C-NMR (63 MHz, DMSO-d_6): δ 149.5, 139.4, 135.2, 127.0, 126.1, 125.3, 124.0, 120.4, 119.9, 115.7, 114.6, 56.2, 54.6, 47.7, 45.7, 33.46, 24.4, 17.8. MS (ESI, 70 eV) m/z 404.2 (100) (M+) 426.2 (M+Na$^+$). A white solid is obtained 91 mg (32% yield). Anal. Calcd for $C_{25}H_{33}N_5 \cdot 0.1HCl$: C, 73.74, H, 8.19, N, 17.20. Found: C, 73.72, H, 8.24, N, 17.20.

(1-(4-(3-(cyclohexylamino)-6-methylimidazo[1,2-a]pyridin-2-yl)phenyl)piperidin-4-yl)methanol (**6d**)

^{1}H-NMR (250 MHz, DMSO-d_6): δ 8.12 (m, 3H), 7.40 (d, J = 20.7 Hz, 1H), 7.04-7.02 (m, 3H), 4.64 (d, J = 3.3 Hz, 1H), 4.54 (t, J = 4.0 Hz, 1H), 3.88 (d, J = 16.9 Hz, 2H), 3.30 (t, J = 5.6 Hz, 2H), 2.91 (m, 1H), 2.80 (t, J = 12.7 Hz, 2H), 2.39 (s, 3H), 1.86-1.58 (m, 8H), 1.41-1.18 (m, 7H). ^{13}C-NMR (63 MHz, DMSO-d_6): δ 158.2, 150.2, 146.8, 139.7, 137.6, 135.7, 127.5, 124.0, 120.1, 115.0, 107.1, 65.6, 55.8, 48.4, 33.3, 28.3, 25.9, 17.2, 17.0. White solid obtained 300 mg (52% yield). MS (ESI, 70 eV) m/z (%): 418.57 (100) (M+). Anal. Calcd for $C_{26}H_{34}N_4O \cdot 0.5$ HCl: C, 71.22, H, 7.98, N, 12.67. Found: C, 71.37, H, 7.98, N, 12.84.

N-cyclohexyl-6-methyl-2-(4-(2-morpholinoethoxy)phenyl)imidazo[1,2-*a*]pyridin-3-amine (**6e**)

^{1}H-NMR (250 MHz, MeOD-d_4): δ 7.96 (s, 1H), 7.87 (d, J = 8.3 Hz, 2H), 7.27 (d, J = 9.6 Hz, 1H), 7.02 (d, J = 12.6 Hz, 1H), 6.94 (d, J = 8.2 Hz, 2H), 4.13 (t, J = 7.0 Hz, 2H), 3.65 (m, 4H), 2.76 (m, 1 H), 2.71 (t, J = 5.3 Hz, 2H), 2.57 (m, 4H), 2.28 (s, 3H), 1.64-1.00 (m, 10H). ^{13}C-NMR (63 MHz, MeOD-d_4): δ 159.9, 129.9, 128.9, 123.3, 121.4, 115.4, 115.7, 67.7, 66.1, 58.9, 57.7, 54.9, 35.1, 27.3, 26.0, 17.9. MS (ESI, 70 eV) m/z = 435.7. A white solid was obtained 120 mg (24% yield). Anal. Calcd for $C_{26}H_{34}N_4O_2 \bullet 0.1HCl$: C, 70.97, H, 7.82, N, 12.73. Found: C, 71.06, H, 8.22, N, 12.58.

2-(4-(4-(3-(cyclohexylamino)-6-methylimidazo[1,2-*a*]pyridin-2-yl)phenoxy)butyl)isoindoline-1,3-dione (**6f**)

^{1}H-NMR (250 MHz, DMSO-d_6): δ 8.18 (d, J = 8.8 Hz, 3H), 7.95 (m, 4H), 7.42 (d, J = 9.0 Hz, 1H), 7.06 (m, 3H), 4.71 (d, J = 5.3 Hz, 1H), 4.11 (m, 2H), 3.76 (m, 2H), 2.88 (m, 1H), 2.38 (s, 3H), 1.87-1.16 (m, 14H). ^{13}C-NMR (63 MHz, DMSO-d_6): δ 168.5, 157.6, 151.86, 134.9, 131.7, 127.7, 126.2, 124.8, 122.7, 120.6, 115.8, 114.2, 102.9, 37.5, 33.3, 26.4, 24.0, 18.2. MS (ESI, 70 eV) m/z 522.6 (100) (M+). White solid obtained 255 mg (15 % yield). Anal. Calcd for $C_{32}H_{34}N_4O_3$: C, 73.54, H, 6.56, N, 10.72. Found: C, 73.45, H, 6,56, N, 10.66.

4-(3-(cyclohexylamino)-6-methylimidazo[1,2-*a*]pyridin-2-yl)-2-methoxyphenol (**6g**)

^{1}H-NMR (250 MHz, DMSO-d_6): δ 9.69 (br, 1H), 8.60 (s, 1H), 7.85-7.64 (m, 3H), 7.59 (d, J = 9.2 Hz, 1H), 7.00 (d, J = 9.2 Hz, 1H), 5.28 (m, 1H), 3.90 (s, 3H), 2.94 (m, 1H), 2.52 (s, 3H), 1.78-1.10 (m, 10H). ^{13}C-NMR (63 MHz, DMSO-d_6): δ 148.0, 135.1, 126.5, 124.9, 122.4, 120.3, 118.2, 116.1, 110.96, 33.3, 25.2, 24.6. MS (ESI, 70 eV) m/z = 352.4 (M+). Yield 500 mg (78%). Anal. Calcd for $C_{21}H_{25}N_3O_2$•1.25HCl: C, 63.53, H, 6.66, N, 10.58. Found: C, 63.62, H, 6.70, N, 11.03.

2-(benzo[d]thiazol-6-yl)-N-cyclohexyl-6-methylimidazo[1,2-*a*]pyridin-3-amine (**7a**)

^{1}H-NMR (250 MHz, DMSO-d_6): δ 9.55 (s, 1H), 8.93 (s, 1H), 8.66 (s, 1H), 8.33 (s, 2H), 7.90 (d, J=14.5 Hz, 1H), 7.75 (d, J= 14.5 Hz, 1H), 5.49 (s, 1H), 2.91 (m, 1H), 1.80-1.10 (m, 10 H). ^{13}C-NMR (63 MHz, DMSO-d_6): δ 158.2, 153.4, 135.7, 135.6, 134.6, 127.2, 126.2, 125.4, 123.6, 122.6, 121.6, 111.4, 56.2, 33.2, 25.2, 17.3. MS (ESI, 70 eV) m/z 363.7 (100) (M+). White solid obtained 264 mg (48 % yield). Anal. Calcd for $C_{21}H_{22}N_4S$·1.4HCl: C, 61.00, H, 5.82, N, 13.62, S, 8.15. Found: C, 60.93, H, 5.93, N, 13.55, S, 8.00.

N-cyclohexyl-2-(1H-indazol-5-yl)-6-methylimidazo[1,2-*a*]pyridin-3-amine (**7b**)

^{1}H-NMR (250 MHz, DMSO-d_6): δ 8.55 (s. 1H), 8.33 (d, J = 8.8 Hz, 1H), 8.10 (s, 2H), 7.58 (d, J = 8.7 Hz, 1H), 7.42 (d, J = 8.6 Hz, 1H), 7.03 (d, J = 8.6 Hz, 1H), 4.74 (d, J = 17.3 Hz, 1H), 2.87 (m, 1H), 2.32 (s, 3H), 1.77-1.05 (m, 10H). ^{13}C-NMR (63 MHz, DMSO-d_6): δ 139.7, 135.7, 133.4, 127.5, 126.5, 125.0, 124.6, 123.3, 120.6, 118.2, 116.0, 56.3, 33.8, 25.5, 24.7, 18.2. MS (ESI, 70 eV) m/z 346.5 (100) (M+). Red solid obtained 100 mg (17% yield). Anal. Calcd for $C_{21}H_{23}N_5$·1HCl: C, 66.05, H, 6.20, N, 18.32. Found: C, 66.11, H, 6.19, N, 18.20.

N-cyclohexyl-2-(1H-indol-6-yl)-6-methylimidazo[1,2-*a*]pyridin-3-amine (**7c**)

^{1}H-NMR (250 MHz, DMSO-d_6): δ 11.63 (s, 1H, br), 8.64 (s, 1H), 8.24 (s, 1H), 7.89-7.70 (m, 3H), 7.50 (s, 1H), 6.51 (s, 1H), 5.38 (d, J = 9.7 Hz, 1H), 2.95 (m, 1H), 2.49 (s, 3H), 1.82-1.09 (m, 10H). ^{13}C-NMR (63 MHz, DMSO-d_6): δ 136.0, 135.3, 134.43, 128.5, 127.7, 126.9, 126.0, 125.2, 122.8, 120.3, 117.9, 11.1, 110.5, 101.3, 55.8, 33.4, 32.3, 25.1, 24.4, 17.7. MS (ESI, 70 eV) m/z 345.2 (100) (M+). A white solid remained 100 mg (16 % yield). Anal. Calcd for $C_{22}H_{24}N_4$·1.95HCl: C, 63.59, H, 6.29, N, 13.48. Found: C, 63.64, H, 6.00, N, 13.18.

2-(benzo[d][1,3]dioxol-5-yl)-N-cyclohexyl-6-methylimidazo[1,2-*a*]pyridin-3-amine (**7d**)

^{1}H-NMR (250 MHz, DMSO-d_6): δ 8.18 (s, 1H), 7.82 (s, 1H), 7.70 (s, 1H), 7.46 (d, J = 9.9 Hz, 1H), 7.06 (dt, J_1 = 4.6 Hz, J_2 = 12.9 Hz, 2H), 6.12 (s, 2H), 4.77 (d, J = 5.8 Hz, 1H), 2.84 (m, 1H), 2.39 (s, 3H), 1.79-1.17 (m, 10H). ^{13}C-NMR (63MHz, DMSO-d_6): δ 147.1, 145.8, 139.7, 129.0, 126.3, 120.6 119.9, 116.2, 108.5, 106.8, 101.2, 56.1, 33.7, 25.5, 24.6, 17.8. MS (ESI, 70 eV) m/z 352.6 (100) (M+3). A white solid is obtained 100 mg (17% yield). Anal. Calcd for $C_{21}H_{23}N_3O_2$: C, 72.18, H, 6.63, N, 12.03. Found: C, 71.91, H, 6.55, N, 11.71.

Methyl 4-(3-(cyclohexylamino)-6-methylimidazo[1,2-*a*]pyridin-2-yl)benzoate (**7e**)

^{1}H-NMR (250 MHz, DMSO-d_6): δ 8.36 (d, J = 7.9 Hz, 2H), 8.13 (s, 1H), 8.01 (d, J = 9.2 Hz, 2H), 7.41 (d, J = 9.7 Hz, 1H), 7.08 (dd, J_1 = 2.2 Hz, J_2 = 9.2 Hz, 1H), 4.85 (d, J = 5.75 Hz, 1H), 3.85 (s, 3H), 2.81 (m, 1H), 2.31 (s, 3H), 1.73-1.07 (m, 10H). ^{13}C-NMR (63 MHz, DMSO-d_6): δ 139.8, 139.6, 132.9, 129.1, 127.1, 127.0, 126.1, 120.7, 120.6, 116.4, 56.6, 51.9, 25.3, 24.5, 17.8. MS (ESI, 70 eV) m/z 364.2 (100) (M+). A white solid is obtained 120 mg (21% yield). Anal. Calcd for $C_{22}H_{25}N_3O_2$ ·1.30HCl: C, 64.31, H, 6.45, N, 10.23. Found: C, 64.36, H, 6.57, N, 10.28.

N-cyclohexyl-2-(4-fluorophenyl)-6-methylimidazo[1,2-*a*]pyridin-3-amine (**7f**)

^{1}H-NMR (250 MHz, DMSO-d_6): δ 8.26 (dt, J_1 = 3.4Hz, J_2 = 9.7 Hz, 2H), 8.10 (m, 1H), 7.39 (d, J = 9.0Hz, 1H), 7.27 (t, J = 9.0 Hz, 2H), 7.02 (dd, J_1 = 1.6 Hz, J_2 = 9.2 Hz, 1H), 4.74 (d, J =5.8 Hz, 1H), 2.80 (m, 1H), 2.31 (s, 3H), 1.72-1.07 (m, 10H). ^{13}C-NMR (63 MHz, DMSO-d_6): δ 144.6, 139.5, 128.2, 120.8, 120.4, 116.2, 115.2, 114.6, 56.4, 33.4, 26.2, 25.2, 24.5, 18.1. ^{19}F-NMR (282 MHz, DMSO-d_6):

δ -115.23. MS (ESI, 70 eV) *m/z* 324.1 (100) (M+). A white solid is obtained 150 mg (23% yield). Anal. Calcd for $C_{20}H_{22}FN_3 \cdot 0.05HCl \cdot 0.20H_2O$: C, 73.05, H, 6.88, N, 12.78. Found: C, 73.17, H, 6.90, N, 12.50.

4-(3-(cyclohexylamino)-6-methylimidazo[1,2-*a*]pyridin-2-yl)-2-ethoxyphenol (**8a**)

^{1}H-NMR (250 MHz, DMSO-d_6): *δ* 8.09 (s, 1H), 7.78 (s, 1H), 7.65 (d, *J* = 8.3 Hz, 1H), 7.37 (d, *J* = 9.5 Hz, 1H), 7.01 (d, *J* = 8.9 Hz, 1H), 6.85 (d, *J* = 7.6 Hz, 1H), 4.62 (d, *J* = 5.9 Hz, 1H), 4.12 (q, *J* = 7.6 Hz, 2H), 2.86 (m, 1H), 2.31 (s, 3H), 1.72-1.10 (m, 10H), 1.38 (t, *J* = 7.2 Hz, 3H). ^{13}C-NMR (63 MHz, DMSO-d_6): *δ* 146.5, 145.9, 139.5, 135.2, 126.3, 123.9, 120.6, 119.3, 115.8, 11.8, 63.6, 56.0, 33.4, 25.4, 24.5, 18.0, 14.8. MS (ESI, 70 eV) m/z 364.7 (100) (M+). A white solid is obtained 185 mg (33% yield). Anal. Calcd for $C_{22}H_{27}N_3O_2 \cdot 0.2HCl$: C, 70.89, H, 7.35, N, 11.27. Found: C, 70.93, H, 7.01, N, 11.36.

4-(3-(cyclohexylamino)-6-methylimidazo[1,2-*a*]pyridin-2-yl)-2-methylphenol (**8b**)

^{1}H-NMR (250 MHz, DMSO-d_6): *δ* 8.06 (s, 1H), 7.93 (s, 1H), 7.86 (dd, J_1 = 2.7 Hz, J_2 = 8.1 Hz, 1H), 7.36 (d, *J* = 9.9 Hz, 1H), 6.99 (dd, J_1 = 2.7 Hz, J_2 = 9.0 Hz, 1H), 6.78 (d, *J* = 8.1 Hz, 1H), 4.57 (d, *J* = 6.3 Hz, 1H), 2.82 (m, 1H), 2.31 (s, 3H), 2.20 (s, 3H), 1.74-1.06 (m, 10H). ^{13}C-NMR (63 MHz, DMSO-d_6): *δ* 155.0, 139.4, 135.5, 129.0, 126.5, 125.7, 125.1, 124.2, 123.3, 120.7, 116.1, 113.8, 56.0, 34.0, 25.9, 24.5, 18.2, 15.9. MS (ESI, 70 eV) m/z 334.5 (100) (M+). A white solid is obtained 235 mg (40% yield). Anal. Calcd for $C_{21}H_{25}N_3O \cdot 0.25HCl$: C, 73.20, H, 7.39, N, 12.20. Found: C, 73.06, H, 7.27, N, 12.15.

2-chloro-4-(3-(cyclohexylamino)-6-methylimidazo[1,2-*a*]pyridin-2-yl)phenol (**8c**)

^{1}H-NMR (250 MHz, DMSO-d_6): *δ* 8.13 (d, *J* = 2.0 Hz, 1H), 8.06 (m, 1H), 7.95 (dd, J_1 = 8.5 Hz, J_2 = 2.0 Hz, 1H), 7.33 (d, *J* = 9.0 Hz, 1H), 7.0 (dd, J_1 = 9,1 Hz, J_2 = 1.6 Hz, 1H), 6.98 (d, *J* = 8. 5Hz, 1H), 4.66 (d, *J* = 5.6 Hz, 1H, NH), 2.83 (m, 1H), 2.31 (s, 3H), 1.73-1.10 (m, 10H). ^{13}C-NMR (63 MHz, DMSO-d_6): *δ* 151.7, 139.4, 133.7, 127.5, 127.1, 126.6, 125.9, 124.5, 120.5, 120.2, 119.4, 116.3, 115.9, 56.3, 33.4, 25.4, 24.4, 17.8. MS (ESI, 70 eV) m/z 354.6 (100) (M+). Off-white obtained 223 mg (39 % yield). Anal. Calcd for $C_{20}H_{22}ClN_3O$: C, 67.50, H, 6.23, N, 11.81. Found: C, 67.43, H, 6.23, N, 11.87.

4-(3-(cyclohexylamino)-6-methylimidazo[1,2-*a*]pyridin-2-yl)-2-(trifluoromethoxy)phenol (**8d**)

^{1}H-NMR (250 MHz, DMSO-d_6): *δ* 8.14 (m, 1H), 8.08 (m, 1H), 8.03 (dd, *J* = 2.1 Hz, *J* = 9.3 Hz, 1H), 7.36 (d, *J* = 9.3 Hz, 1H), 7.06 (d, *J* = 8.9 Hz, 1H), 6.99 (dd, *J* = 2.1 Hz, *J* = 9.3 Hz, 2H). 4.69 (d, *J* = 5.2 Hz, 1H), 2.78 (m, 1H), 2.29 (s, 3H), 1.71-1.06 (m, 10H). ^{13}C-NMR (63 MHz, DMSO-d_6): *δ* 148.43, 139.5, 135.9, 133.5, 126.7, 126.6, 126.1, 125.5, 124.5, 122.1, 120.6, 120.4, 120.3, 118.7, 117.3, 115.9, 56.2, 33.3, 25.3, 24.4, 20.7, 17.8. ^{19}F-NMR (282 MHz, DMSO-d_6): *δ* -56.96. MS (ESI, 70 eV) m/z 406.1 (60) (M+), 428.1 (M+23). A white solid is obtained 100 mg (50% yield). Anal. Calcd for $C_{21}H_{22}FN_3O_2 \cdot 0.35HCl \cdot 0.15H_2O$: C, 59.93, H, 5.42, N, 9.98. Found: C, 60.01, H, 5.44, N, 9.60.

4-(3-(cyclohexylamino)-6-methylimidazo[1,2-*a*]pyridin-2-yl)benzene-1,2-diol (**8e**)

^{1}H-NMR (250 MHz, DMSO-d_6): *δ* 9.68 (s, 1H), 9.33 (s, 1H), 8.59 (s, 1H), 7.79-7.60 (m, 2H), 7.54 (d, *J* = 2.9 Hz, 1H), 7.36 (dd, J_1 = 2.9 Hz, J_2 = 8.5 Hz, 1H), 6.96 (d, *J* = 7.8 Hz, 1H), 5.19 (d, *J* = 4.8 Hz, 1H), 2.92 (m, 1H), 2.31 (s, 3H), 1.78-1.50 (m, 10H). ^{13}C-NMR (63 MHz, DMSO-d_6): *δ* 147.1, 145.7, 135.1, 126.3, 125.1, 122.3, 119.0, 117.8, 115.7, 114.7, 11.0, 55.9, 33.0, 25.4, 24.5, 17.8. MS (ESI, 70 eV) m/z 338.5 (100) (M+). A white solid is obtained 200 mg (30% yield). Anal. Calcd for $C_{20}H_{23}N_3O_2 \cdot 0.9HCl \cdot 0.75H_2O$: C, 62.60, H, 6.67, N, 10.95. Found: C, 62.75, H, 6.68, N, 10.54.

4-(3-(cyclopentylamino)-6-methylimidazo[1,2-*a*]pyridin-2-yl)-2-methoxyphenol (**9a**)

^{1}H-NMR (250 MHz, DMSO-d_6): *δ* 9.68 (s, br, 1H), 8.57 (s, 1H), 7.86-7.81 (m, 4H), 7.55 (dd, J_1 = 2.1Hz, J_2 = 8.3 Hz, 1H), 7.02 (d, *J* = 8.2 Hz, 1H), 5.30 (d, *J* = 4.5 Hz, 1H), 3.87 (s, 3H), 3.39 (m, 1H), 2.47 (s, 3H), 1.69-1.45 (m, 8H). ^{13}C-NMR (63 MHz, DMSO-d_6): *δ* 148.2, 147.8, 135.0, 134.8, 126.5, 126.3, 125.3, 122.5, 120.1, 118.1, 115.8, 111.4, 111.0, 57.7, 55.7, 32.8, 23.0, 17.2. MS (ESI, 70 eV) m/z 337.2 (100) (M+). A white solid is obtained 200 mg (36 % yield). Anal. Calcd $C_{20}H_{23}N_3O_2 \cdot 1.0HCl$: C, 63.94, H, 6.45, N, 11.18. Found: C, 63.80, H, 6.37, N, 11.14.

4-(3-((3s,5s,7s)-adamantan-1-ylamino)-6-methylimidazo[1,2-*a*]pyridin-2-yl)-2-methoxyphenol (**9b**)

^{1}H-NMR (250 MHz, DMSO-d_6): δ 14.93 (br, 1H), 9.70 (s, 1H), 8.72 (s, 1H), 7.88-7-81 (m, 3H), 7.66 (d, J = 8.4 Hz, 1H), 7.04 (d, J = 10.4 Hz, 1H), 5.18 (s, 1H), 3.93 (s, 3H), 1.97 (m, 3H), 1.67-1.53 (m, 12H). ^{13}C-NMR (63 MHz, DMSO-d_6): δ 148.1, 147.0, 135.7, 129.6, 126.2, 123.5, 122.6, 121.1, 118.4, 115.9, 112.4, 110.9, 56.5, 55.62, 43.0, 35.7, 29.2, 18.1. MS (ESI, 70 eV) m/z 402.8 (100) (M+). Yellow solid remained 98 mg (13 % yield). Anal. Calcd for $C_{25}H_{29}N_3O_2 \cdot 1.15HCl$: C, 67.41, H, 6.85, N, 9.43. Found: C, 67.49, H, 6.75, N, 9.30.

4-(3-((2,6-dimethylphenyl)amino)-6-methylimidazo[1,2-*a*]pyridin-2-yl)-2-methoxyphenol (**9c**)

^{1}H-NMR (250 MHz, DMSO-d_6): δ 9.66 (s, 1H), 8.55 (s, 1H), 7.96 (d, J = 9.7 Hz, 1H), 7.91 (d, J = 9.7 Hz, 1H), 7.77 (s, 1H), 7.27 (d, J = 8.3 Hz, 2H), 6.92 (d, J = 7.6 Hz, 2H), 6.73 (dd, J_1 = 7.6 Hz, J_2 = 8.3 Hz, 2H), 3.63 (s, 3H), 2.44 (s, 3H), 1.92 (s, 3H). ^{13}C-NMR (63MHz, DMSO-d_6): δ 148.2, 139.9, 129.8, 126.2, 122.7, 121.8, 120.3, 115.7, 111.0, 55.7, 19.0, 17.1. MS (ESI, 70 eV) m/z 374.6 (100) (M+). A white solid is obtained 80 mg (13% yield). Anal. Calcd for $C_{23}H_{23}N_3O_2 \cdot 2.25HCl$: C, 60.65, H, 5.59, N, 9.23. Found: C, 60.59, H, 5.19, N, 9.25.

2-methoxy-4-(3-((4-methoxyphenyl)amino)-6-methylimidazo[1,2-*a*]pyridin-2-yl)phenol (**9d**)

^{1}H-NMR (250 MHz, DMSO-d_6): δ 9.05 (br, 1H), 7.79 (d, J = 6.1 Hz, 2H), 7.59 (d, J = 2.0 Hz, 1H), 7.48 (dd, J_1 = 2.8 Hz, J_2 = 9.3 Hz, 2H), 7.14 (dd, J_1 = 2.8 Hz, J_2 = 1.6 Hz, 1H), 6.77-6.73 (m, 3H), 6.45 (d, J = 8.8 Hz, 2H), 3.68 (s, 3H), 3.61 (s, 3H), 2.26 (s, 3H). ^{13}C-NMR (63 MHz, DMSO-d_6): δ 152.4, 147.4, 146.1, 140.6, 139.6, 137.7, 127.5, 125.2, 121.2, 120.2, 119.3, 118.4, 116.3, 115.4, 113.6, 110.8, 55.0, 17.6. MS (ESI, 70 eV) m/z (%): 376.30 (100) ($M+H^+$). A white solid remained 40 mg (6% yield). tR= 5.612 min. HRMS calculated $C_{22}H_{21}N_3O_3$: 376.16630 found: 376.16557

4-(3-(cyclohexylamino)-6-fluoroimidazo[1,2-*a*]pyridin-2-yl)-2-methoxyphenol (**9e**)

^{1}H-NMR (250 MHz, DMSO-d_6): δ 9.08 (s, 1H), 8.41 (m, 1H), 7.78 (s, 1H), 7.64 (q, J = 3.3 Hz, 1H), 7.51 (q, J = 4.9 Hz, 1H), 7.20 (m, 1H), 6.85 (d, J = 8.2 Hz, 1H) 4.78 (d, J = 5.8 Hz, 1H), 3.83 (s, 3H), 2.86 (m, 1H), 1.73-1.11 (m, 10H). ^{13}C-NMR (63 MHz, DMSO-d_6): δ 155.8, 148.1, 146.3, 143.1, 137.8, 136.25, 125.4, 119.5, 117.2, 115.6, 110.5, 56.3, 55.5, 33.8, 25.9, 24.6. ^{19}F-NMR (282 MHz, DMSO-d_6): δ -141.78. MS (ESI, 70 eV) m/z (%): 356.4 (100) (M+), 378.4 (M+23). White solid obtained 150 mg (21 % yield). Anal. Calcd for $C_{20}H_{22}FN_3O_2 \cdot 0.75$ HCl: C, 62.76, H, 5.85, N, 10.65. Found: C, 62.78, H, 5.75, N, 10.60.

4-(6-fluoro-3-(isopropylamino)imidazo[1,2-*a*]pyridin-2-yl)-2-methoxyphenol (**9f**)

^{1}H-NMR (250 MHz, DMSO-d_6): δ 9.11 (s, 1H), 8.47 (m, 1H), 7.89 (d, J = 1.8 Hz, 1H), 7.60 (dd, J = 2.2, 3.4 Hz, 1H), 7.49 (q, J = 4.9 Hz, 1H), 7.17 (dt, J_1 =2.2, J_2 = 2.9 Hz, 1H), 6.81 (d, J = 8.2Hz, 1H), 4.67 (d, J = 5.3 Hz, 1H), 3.84 (s, 3H), 3.18 (m, 1H), 1.04 (s, 3H), 0.99 (s, 3H). ^{13}C-NMR (63 MHz, DMSO-d_6): δ 154.2, 150.5, 147.3, 145.8, 137.9, 136.9, 126.2, 126.1, 125.7, 119.3, 117.2, 117.0, 115.3, 114.9, 114.5, 110.4, 109.7, 109.0, 55.4, 48.2, 22.9. ^{19}F-NMR (282 MHz, DMSO-d_6): δ -141.70. MS (ESI, 70 eV) m/z 316.1 (100) (M+). White solid obtained 300 mg (48% yield). Anal. Calcd for $C_{17}H_{18}FN_3O_2 \cdot 0.15HCl$: C, 64.10, H, 5.66, N, 13.4. Found: C, 64.26, H, 5.47, N, 13.54.

4-(3-(cyclohexylamino)-8-methylimidazo[1,2-*a*]pyridin-2-yl)-2-methoxyphenol (**9g**)

^{1}H-NMR (250 MHz, MeOD-d_4): δ 9.61 (s, 1H), 8.06 (d, J = 7.1 Hz, 1H), 7.57 (d, J = 2.6 Hz, 1H), 7.39 (dd, J_1 = 2.2 Hz, J_2 = 7.6 Hz, 1H), 6.92 (dt, J_1 = 1.2 Hz, J_2 = 6.7 Hz, 1H), 6.72 (d, J = 8.4 Hz, 1H), 6.66 (t, J = 6.6 Hz, 1H), 3.85 (s, 3H), 2.45 (s, 3H), 2.81 (m, 1H), 1.67-1.16 (m, 10H). ^{13}C-NMR (63 MHz, MeOD-d_4): δ 149.4, 147.6, 145.6, 142.6, 139.4, 137.4, 128.3, 126.8, 125.3, 122.6, 116.5, 114.5, 114.5, 113.0, 57.6, 56.1, 35.1, 27.3, 25.8, 16.3. MS (ESI, 70 eV) m/z 352.6 (100) (M+). A white solid is obtained 100 mg (17 %). tR= 5.858 min. HRMS Calcd for $C_{21}H_{26}N_3O_3$ [M+]: 352.20195 found 352.20269

4-(8-chloro-3-(cyclohexylamino)imidazo[1,2-*a*]pyridin-2-yl)-2-methoxyphenol (**9h**)

^{1}H-NMR (250 MHz, MeOD-d_4): δ 9.64 (s, 1H), 8.19 (dd, J_1 = 1.0 Hz, J_2 = 7.0 Hz, 1H), 7.58 (d, J = 1.9 Hz, 1H), 7.45 (dd, J_1 = 2.3 Hz, J_2 = 8.4 Hz, 1H), 7.21 (dd, J_1 = 1.1 Hz, J_2 = 7.2 Hz, 1H), 6.80 (d, J = 8.8 Hz, 2H), 3.83 (s, 3H), 2.81 (m, 1H), 1.67-1.00 (m, 10H). ^{13}C-NMR (63 MHz, MeOD-d_4): δ 149.1, 147.4, 139.1, 127.3, 124.6, 123.6, 122.6, 116.6, 113.1, 57.7, 55.6, 34.8, 26.8. MS (ESI, 70 eV) m/z 372.5 (100) (M+). A white solid is obtained 100 mg (16 % yield). tR= 5.741 min. HRMS Calcd for $C_{20}H_{23}ClN_3O_2$ [M+]: 372.14733 found 372.14767

4-(3-(cyclohexylamino)-7-methylimidazo[1,2-*a*]pyridin-2-yl)-2-methoxyphenol (**9i**)

^{1}H-NMR (250 MHz, DMSO-d_6): δ 9.13 (br, 1H), 8.28 (d, J = 7.0 Hz, 1H), 7.81 (d, J = 3.2 Hz, 1H), 7.68 (dd, J_1 = 2.3 Hz, J_2 = 8.4 Hz, 1H), 7.27 (s, 1H), 6.88 (d, J = 8.4 Hz, 1H), 6.83 (dd, J_1 = 1.2 Hz, J_2 = 7.0 Hz, 1H), 4.76 (d, J = 5.2 Hz, 1H), 3.86 (s, 3H), 2.82 (m, 1H), 2.37 (s, 3H), 1.76-1.09 (m, 10H). ^{13}C-NMR (63 MHz, DMSO-d_6): δ 147.3, 145.8, 140.3, 135.4, 133.4, 125.5, 123.9, 122.3, 119.3, 115.7, 113.8, 110.7, 56.2, 55.3, 33.8, 25.6, 24.6, 21.0. MS (ESI, 70 eV) m/z 352.7 (100) (M+). A white solid remained 150 mg (23% yield). tR = 5.866 min. HRMS Calcd for $C_{21}H_{26}N_3O_2$ [M+]: 352.20195 found 352.20178

4-(7-chloro-3-(cyclohexylamino)imidazo[1,2-*a*]pyridin-2-yl)-2-methoxyphenol (**9j**)

^{1}H-NMR (250 MHz, DMSO-d_6): δ 9.13 (s, 1H), 8.36 (d, J = 7.3 Hz, 1H), 7.80 (d, J = 2.0 Hz, 1H), 7.66 (dd, J_1 = 1.8 Hz, J_2 = 8.3 Hz, 1H), 7.59 (d, J = 2.1 Hz, 1H), 6.95 (dd, J_1 = 2.1 Hz, J_2 = 7.3 Hz, 1H), 6.91 (d, J = 8.1 Hz, 1H), 4.84 (d, J = 5.5 Hz, 1H), 3.84 (s, 3H), 2.86 (m 1H), 1.72-1.12 (m, 10H). ^{13}C-NMR (63 MHz, DMSO-d_6): δ 147.5, 146.1, 139.7, 136.3, 128.2, 125.6, 124.9, 124.0, 119.7, 115.7, 114.9, 112.0, 11.0, 56.6, 55.2, 33.5, 25.3, 24.5. MS (ESI, 70 eV) m/z 372.2 (100) (M+). A white solid is obtained 157 mg (25 % yield). Anal. Calcd for $C_{20}H_{22}ClN_3O_2 \cdot 1.3HCl$: C, 57.30, H, 5.60, N, 10.05. Found: C, 57.30, H, 5.24, N, 9.94.

4-(3-(cyclohexylamino)-5-methylimidazo[1,2-*a*]pyridin-2-yl)-2-methoxyphenol (**9k**)

^{1}H-NMR (250 MHz, DMSO-d_6): δ 7.74 (d, J = 2.9 Hz, 1H), 7.57 (dd, J_1 = 2.3 Hz, J_2 = 8.3 Hz, 1H), 7.33 (d, J = 7.9 Hz, 1H), 7.06 (dd, J_1 = 6.6 Hz, J_2 = 7.9 Hz, 1H), 6.82 (d, J = 8.3 Hz, 1H), 6.54 (d, J = 6.6 Hz, 1H), 4.50 (d, J = 3.7 Hz, 1H), 3.84 (s, 3H), 2.94 (s, 3H), 2.79 (m, 1H), 1.64-1.04 (m, 10H). ^{13}C-NMR (63 MHz, DMSO-d_6): δ 147.3, 145.7, 142.3, 138.5, 136.6, 126.7, 125.5, 123.9, 120.3, 115.6, 114.8, 113.0, 111.8, 58.0, 55.34, 32.7, 25.6, 24.1, 19.2. MS (ESI, 70 eV) m/z 351.8 (100) (M+). A yellow solid is obtained 100 mg (15 % yield). Anal. Calcd for $C_{21}H_{25}N_3O_2 \cdot 1.6HCl$: C, 61.55, H, 6.54, N, 10.25. Found: C, 61.56, H, 6.15, N, 10.07.

4-(5-chloro-3-(cyclohexylamino)imidazo[1,2-*a*]pyridin-2-yl)-2-methoxyphenol (**9l**)

^{1}H-NMR (250 MHz, DMSO-d_6): δ 9.30 (br, 1H), 7.90 (d, J = 1.9 Hz, 1H), 7.68 (dd, J_1 = 1.3 Hz, J_2 = 8.1 Hz, 1H), 7.56 (d, J = 8.1 Hz, 1H), 7.36 (t, J = 9.4 Hz, 1H), 7.13 (d, J = 7.2 Hz, 1H), 6.89 (d, J = 7.6 Hz, 1H), 4.59 (d, J = 3.1 Hz, 1H), 3.88 (s, 3H), 2.91 (m, 1H), 1.70-1.09 (m, 10H). ^{13}C-NMR (63 MHz, DMSO-d_6): δ 147.5, 146.4, 124.1, 120.4, 115.7, 114.8, 111.7, 58.1, 56.0, 34.0, 32.2, 25.6, 23.9. MS (ESI, 70 eV) m/z 372.2 (100) (M+). An off-white solid is obtained 370 mg (60 % yield). Anal. Calcd for $C_{20}H_{22}ClN_3O_2 \cdot 1.35HCl$: C, 57.05, H, 5.59, N, 9.98. Found: C, 57.03, H, 5.38, N, 9.78

4-(3-(cyclohexylamino)-5-fluoroimidazo[1,2-*a*]pyridin-2-yl)-2-methoxyphenol (**9m**)

^{1}H-NMR (250 MHz, DMSO-d_6): δ 7.93 (d, J = 2.1 Hz, 1H), 7.77 (dd, J_1 = 8.1 Hz, J_2 = 1.8 Hz, 1H), 7.30 (d, J = 8.1 Hz, 1H), 7.14 (m, 1H), 6.84 (d, J = 8.1 Hz, 1H), 6.61 (dt, J_1 = 2.1 Hz, J_2 = 2.1 Hz, 1H), 4.39 (d, J = 4.4 Hz, 1H), 3.81 (s, 3H), 2.83 (m, 1H), 1.70-1.04 (m, 10H). ^{13}C-NMR (63 MHz, DMSO-d_6): δ 152.1, 148.0, 147.0, 145.8, 142.7, 137.1, 125.6, 124.5, 123.7, 120.2, 115.1, 112.8, 111.1, 92.7, 57.5, 55.6, 33.2, 25.5, 24.4. ^{19}F-NMR (282 MHz, DMSO-d_6): -113.45. MS (ESI, 70 eV) m/z 354.2 (100) (M+). A white solid is obtained 328 mg (56 % yield). tR= 5.771 min. HRMS Calcd for $C_{20}H_{23}FN_3O_2$ [M+]: 356.17688 found 356.17687

4-(6-chloro-3-(cyclohexylamino)-8-fluoroimidazo[1,2-*a*]pyridin-2-yl)-2-methoxyphenol (**9n**)

^{1}H-NMR (250 MHz, DMSO-d_6): δ 9.17 (br, 1H), 8.37 (s, 1H), 7.77 (d, J = 2.5 Hz, 1H), 7.66 (dd, J_1 = 1.9 Hz, J2=8.1 Hz, 1H), 7.29 (dd, J_1 =1.4 Hz, J_2 = 10.7 Hz, 1H), 6.87 (d, J = 8.1 Hz, 1H), 4.92 (d, J = 6.2 Hz, 1H), 3.85 (s, 3H), 2.88 (m, 1H), 1.71-1.01 (m, 10H). ^{13}C-NMR (63 MHz, DMSO-d_6): δ 147.4, 146.2, 136.1, 131.1, 130.3, 126.9, 125.1, 119.7, 117.7, 116.9, 116.6, 115.4, 110.5, 108.0, 56.2, 55.2, 33.5, 25.4, 24.3. ^{19}F-NMR (282 MHz, DMSO-d_6): δ -131.15. MS (ESI, 70 eV) m/z 390.14 (100) (M+). A yellow solid is obtained 115 mg (18% yield). tR= 5.862 min. HRMS calculated $C_{20}H_{21}ClFN_3O_2$ calculated: 390.13791 found: 390.13787.

SAR tables with standard errors

Entry	*PMNL IC_{50} [µM]*	*PMNL pIC_{50}*	*SE*	*S100 IC_{50} [µM]*	*S100 pIC_{50}*	*SE*
4a	0.26	6.6	0.71	0.83	6.1	0.06
4b	0.53	6.3	0.24	0.51	6.3	0.02
4c	0.21	6.7	0.15	6.98	5.1	0.17
4d	0.42	6.4	0.02	1.54	5.8	0.18
4e	13.71	4.9	0.32	ia	-	-
4f	4.24	5.4	0.01	0.76	6.1	0.14
4g	1.22	5.9	0.05	0.48	6.3	0.18
4h	1.32	5.8	0.10	0.28	6.6	0.04
4i	0.48	6.3	0.33	0.74	6.1	0.11
4j	0.39	6.4	0.09	1.03	6.0	0.90
4k	1.14	5.9	0.03	0.33	6.5	0.15
4l	1.62	5.8	0.05	1.06	6.0	0.06
5a	0.38	6.4	0.10	0.12	6.9	0.10
5b	0.33	6.5	0.18	0.26	6.6	0.37
5c	0.57	6.2	0.24	2.22	5.7	0.53
5d	0.41	6.4	0.67	ia	-	-
5e	0.38	6.4	0.04	0.19	6.7	0.06
5f	1.99	5.7	0.42	0.82	6.1	0.71
5g	1.10	6.0	0.09	0.35	6.5	0.26
5h	2.15	5.7	0.12	1.24	5.9	0.13
5i	0.50	6.3	0.17	n.d.	n.d.	n.d.
6a	1.57	5.8	0.01	0.38	6.4	0.01
6b	0.45	6.3	0.13	0.19	6.7	0.10
6c	16.56	4.8	0.19	1.19	5.9	0.08
6d	0.56	6.3	0.15	0.31	6.5	0.37
6e	ia	-	-	5.2	5.3	0.22
6f	0.61	6.2	0.17	0.06	7.2	0.12
6g	0.52	6.3	0.12	0.13	6.9	0.21
7a	1.71	5.8	0.08	2.48	5.6	1.71
7b	14.91	4.8	0.16	1.41	5.8	0.12
7c	0.87	6.1	0.15	0.12	6.9	0.01
7d	2.50	5.6	0.23	0.26	6.6	0.10
7e	0.61	6.2	0.15	0.53	6.3	0.35
7f	22.92	4.6	0.17	0.63	6.2	0.28
8a	1.19	5.9	0.07	0.12	5.9	0.08
8b	4.62	5.3	0.10	0.19	6.7	0.10
8c	1.57	5.8	0.07	0.19	6.7	0.12
8d	3.77	5.4	0.13	0.20	6.7	0.25
8e	6.08	5.2	0.20	0.23	6.6	0.13
9a	3.03	5.5	0.04	0.30	6.5	0.15
9b	2.24	5.7	0.21	0.39	6.4	0.09
9c	4.50	5.3	0.07	0.26	6.6	0.03
9d	4.18	5.4	0.06	1.34	5.9	0.09

9e	0.49	6.3	0.14	0.27	6.6	0.12
9f	11.60	4.9	0.13	1.37	5.9	0.22
9g	1.69	5.8	0.18	0.28	6.6	0.12
9h	1.37	5.9	0.12	0.49	6.3	0.08
9i	3.77	5.4	0.24	0.34	6.4	0.12
9j	1.83	5.7	0.07	0.29	6.5	0.06
9k	1.28	5.9	0.07	0.30	6.5	0.01
9l	1.15	5.9	0.06	0.29	6.5	0.16
9m	1.91	5.7	0.03	0.52	6.3	0.20
9n	0.85	6.1	0.06	0.41	6.4	0.15

WST-1 (cell viability %) of tested compounds

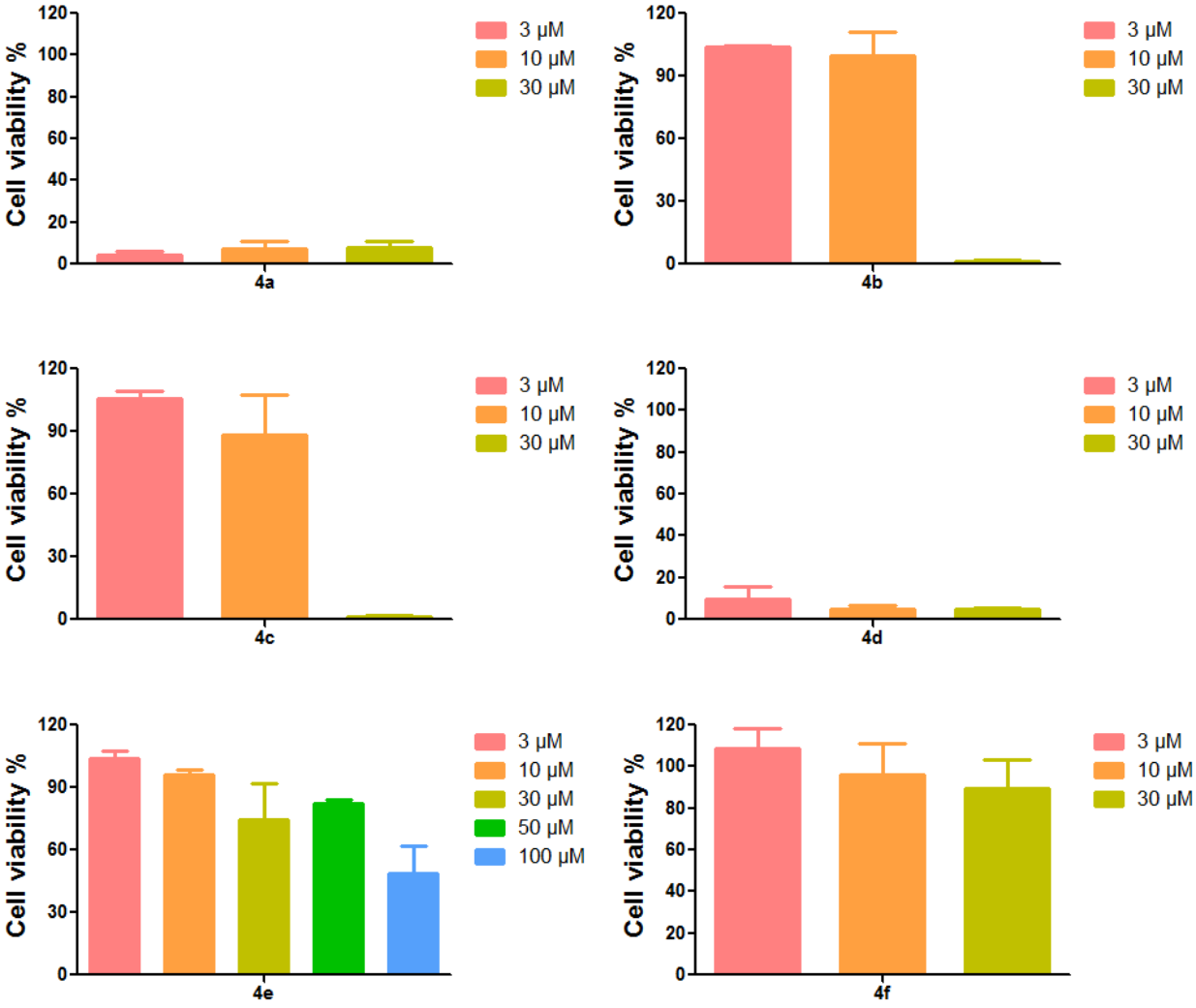

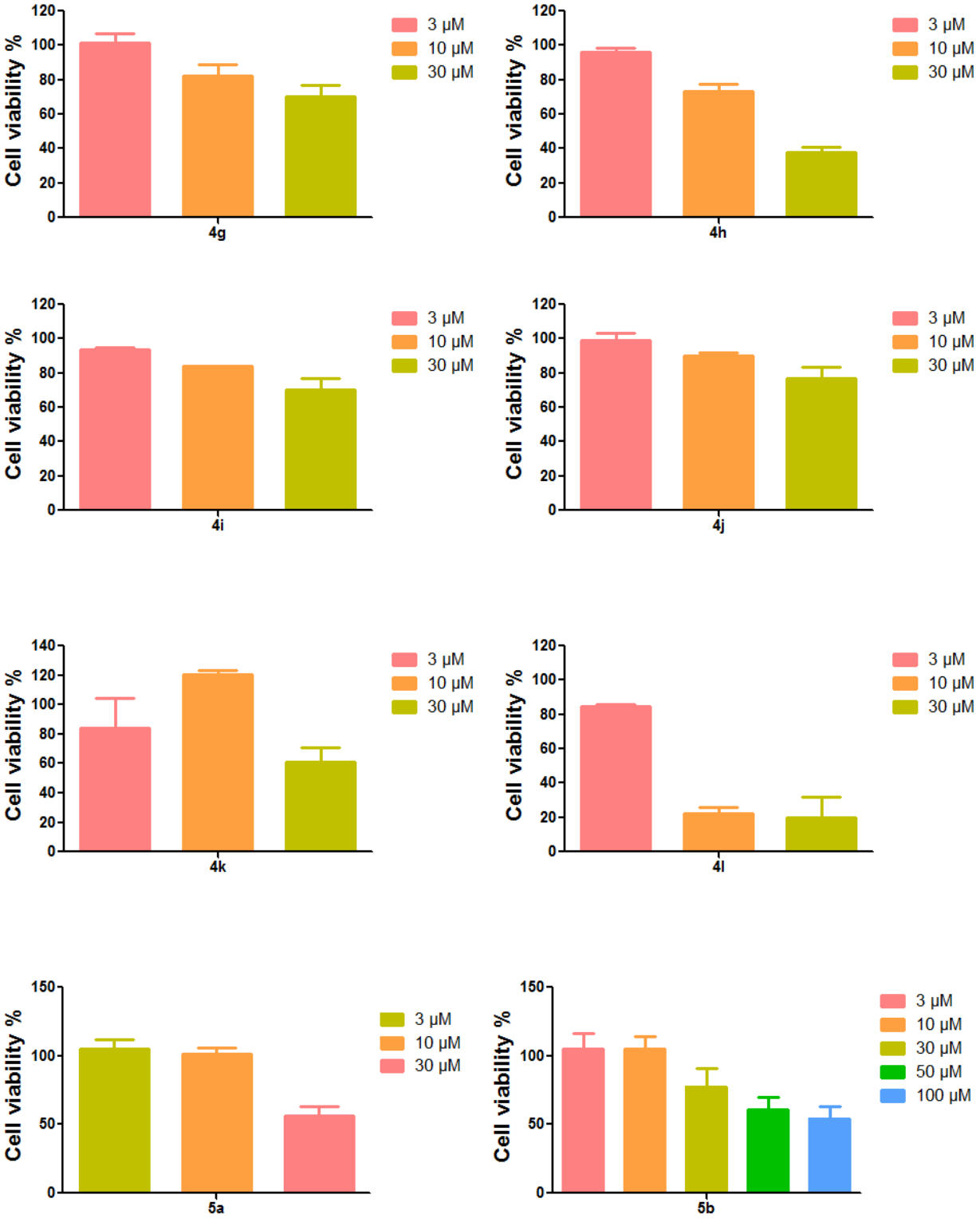
Cell viability %
120
100
80
60
40
20
0
4g
3 μM
10 μM
30 μM
Cell viability %
120
100
80
60
40
20
0
4h
3 μM
10 μM
30 μM
Cell viability %
120
100
80
60
40
20
0
4i
3 μM
10 μM
30 μM
Cell viability %
120
100
80
60
40
20
0
4j
3 μM
10 μM
30 μM
Cell viability %
140
120
100
80
60
40
20
0
4k
3 μM
10 μM
30 μM
Cell viability %
120
100
80
60
40
20
0
4l
3 μM
10 μM
30 μM
Cell viability %
150
100
50
0
5a
3 μM
10 μM
30 μM
Cell viability %
150
100
50
0
5b
3 μM
10 μM
30 μM
50 μM
100 μM

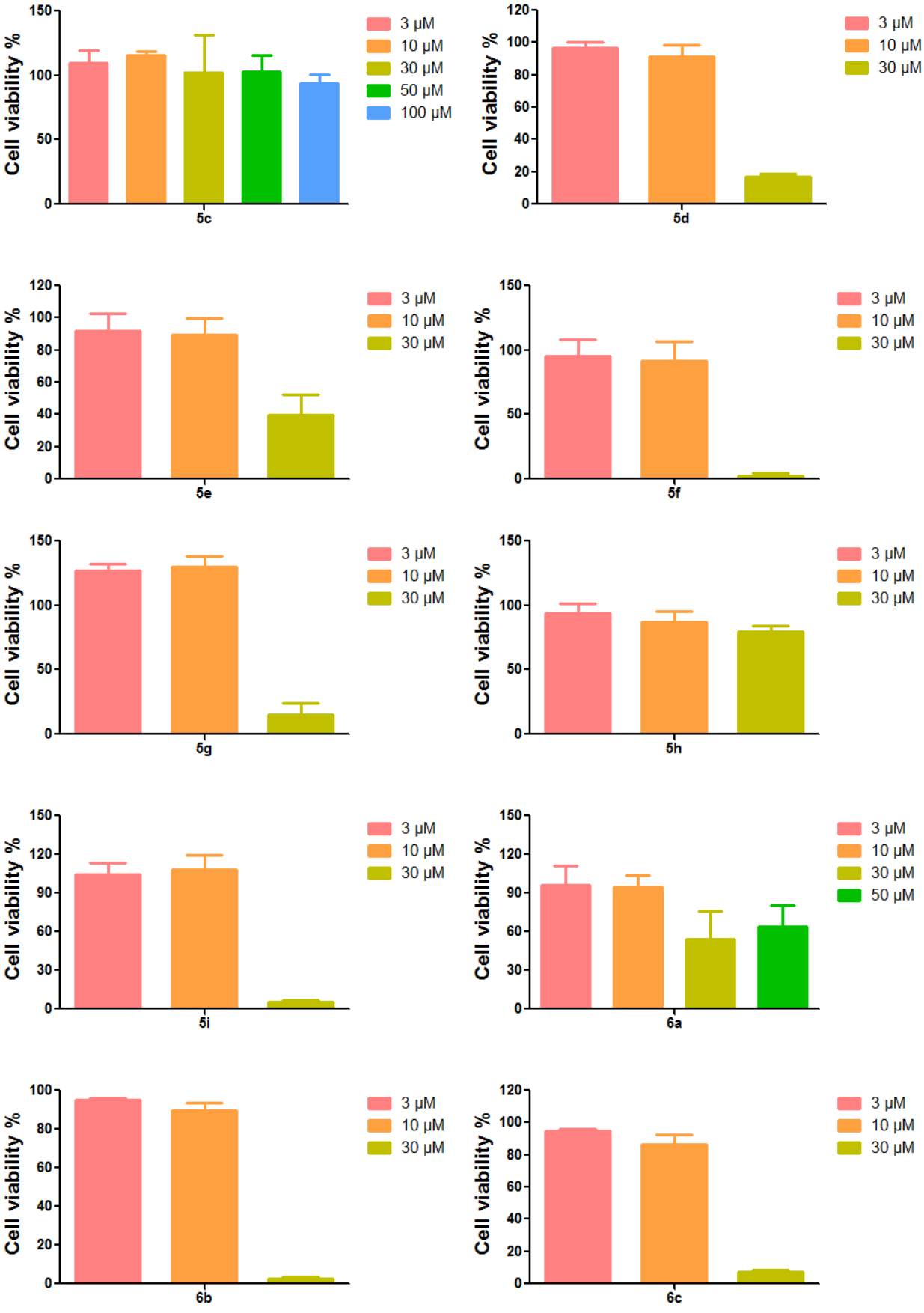
Cell viability %
150
100
50
0
5c
3 μM
10 μM
30 μM
50 μM
100 μM
Cell viability %
120
100
80
60
40
20
0
5d
3 μM
10 μM
30 μM
Cell viability %
120
100
80
60
40
20
0
5e
3 μM
10 μM
30 μM
Cell viability %
150
100
50
0
5f
3 μM
10 μM
30 μM
Cell viability %
150
100
50
0
5g
3 μM
10 μM
30 μM
Cell viability %
150
100
50
0
5h
3 μM
10 μM
30 μM
Cell viability %
150
120
90
60
30
0
5i
3 μM
10 μM
30 μM
Cell viability %
150
120
90
60
30
0
6a
3 μM
10 μM
30 μM
50 μM
Cell viability %
100
80
60
40
20
0
6b
3 μM
10 μM
30 μM
Cell viability %
120
100
80
60
40
20
0
6c
3 μM
10 μM
30 μM

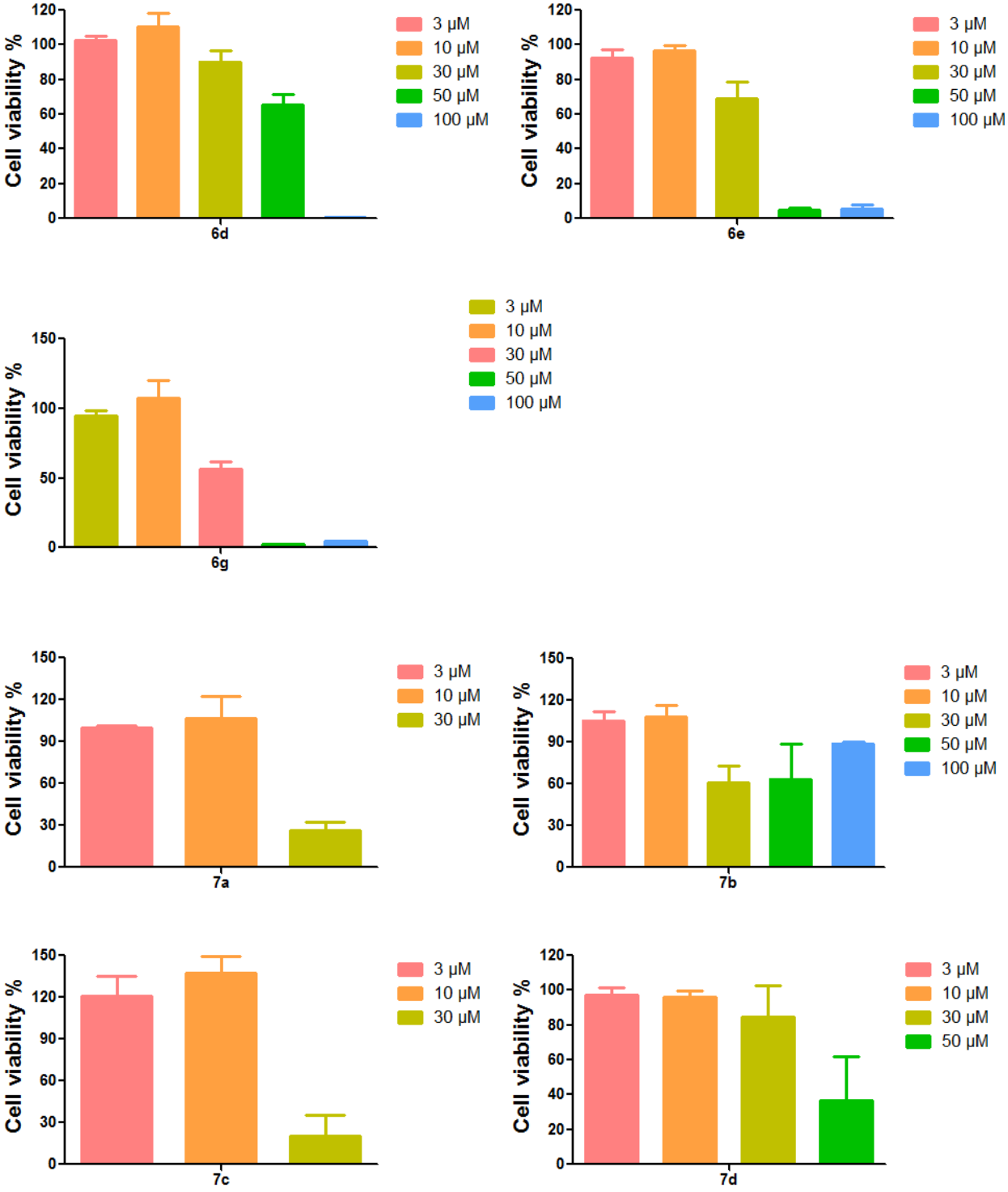
Cell viability %
120
100
80
60
40
20
0
6d
3 μM
10 μM
30 μM
50 μM
100 μM
6e
6g
150
90
30
7a
7b
7c
7d

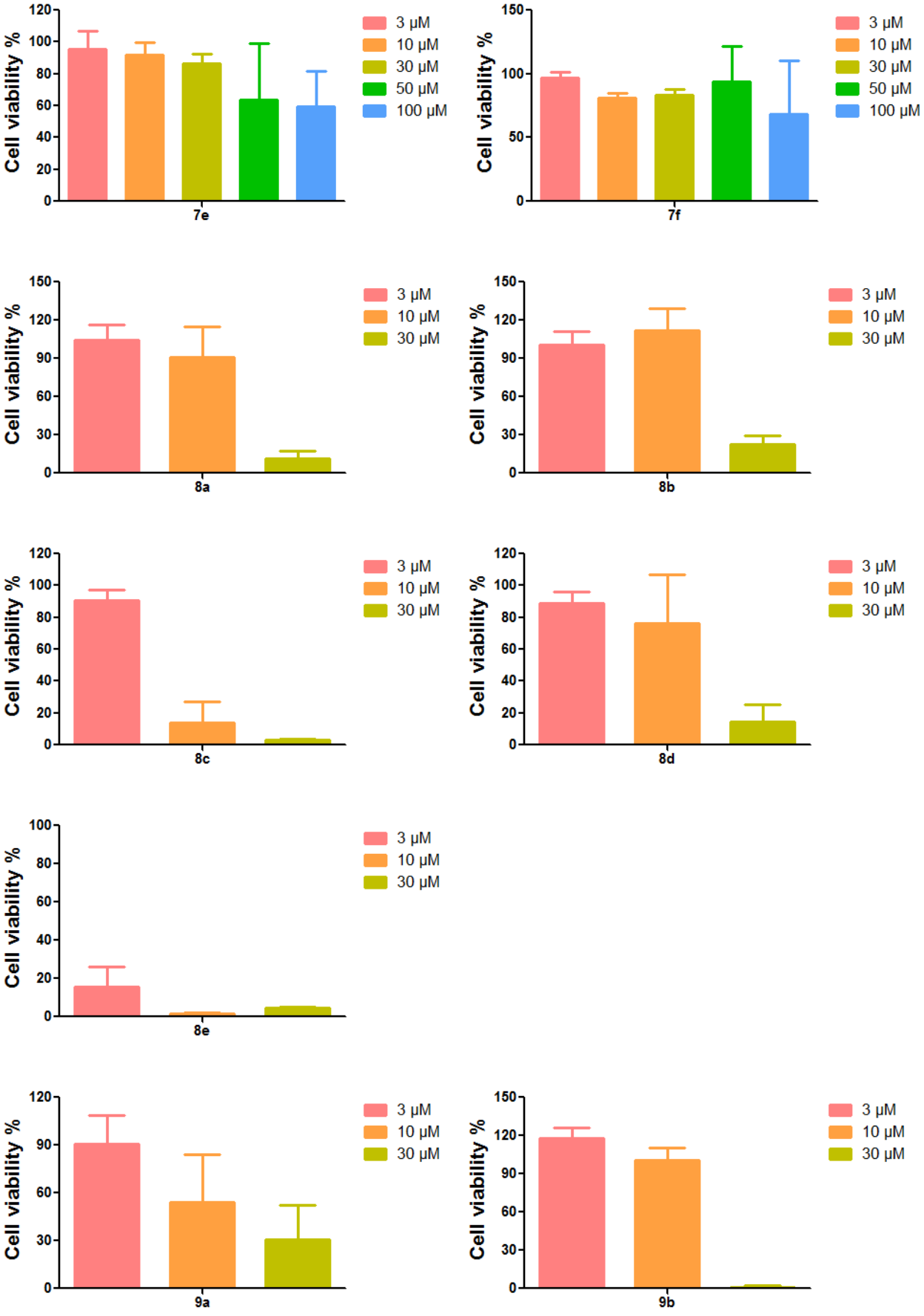
Cell viability %
120
100
80
60
40
20
0
7e
3 μM
10 μM
30 μM
50 μM
100 μM
Cell viability %
150
100
50
0
7f
3 μM
10 μM
30 μM
50 μM
100 μM
Cell viability %
150
120
90
60
30
0
8a
3 μM
10 μM
30 μM
Cell viability %
150
120
90
60
30
0
8b
3 μM
10 μM
30 μM
Cell viability %
120
100
80
60
40
20
0
8c
3 μM
10 μM
30 μM
Cell viability %
120
100
80
60
40
20
0
8d
3 μM
10 μM
30 μM
Cell viability %
100
80
60
40
20
0
8e
3 μM
10 μM
30 μM
Cell viability %
120
90
60
30
0
9a
3 μM
10 μM
30 μM
Cell viability %
150
120
90
60
30
0
9b
3 μM
10 μM
30 μM

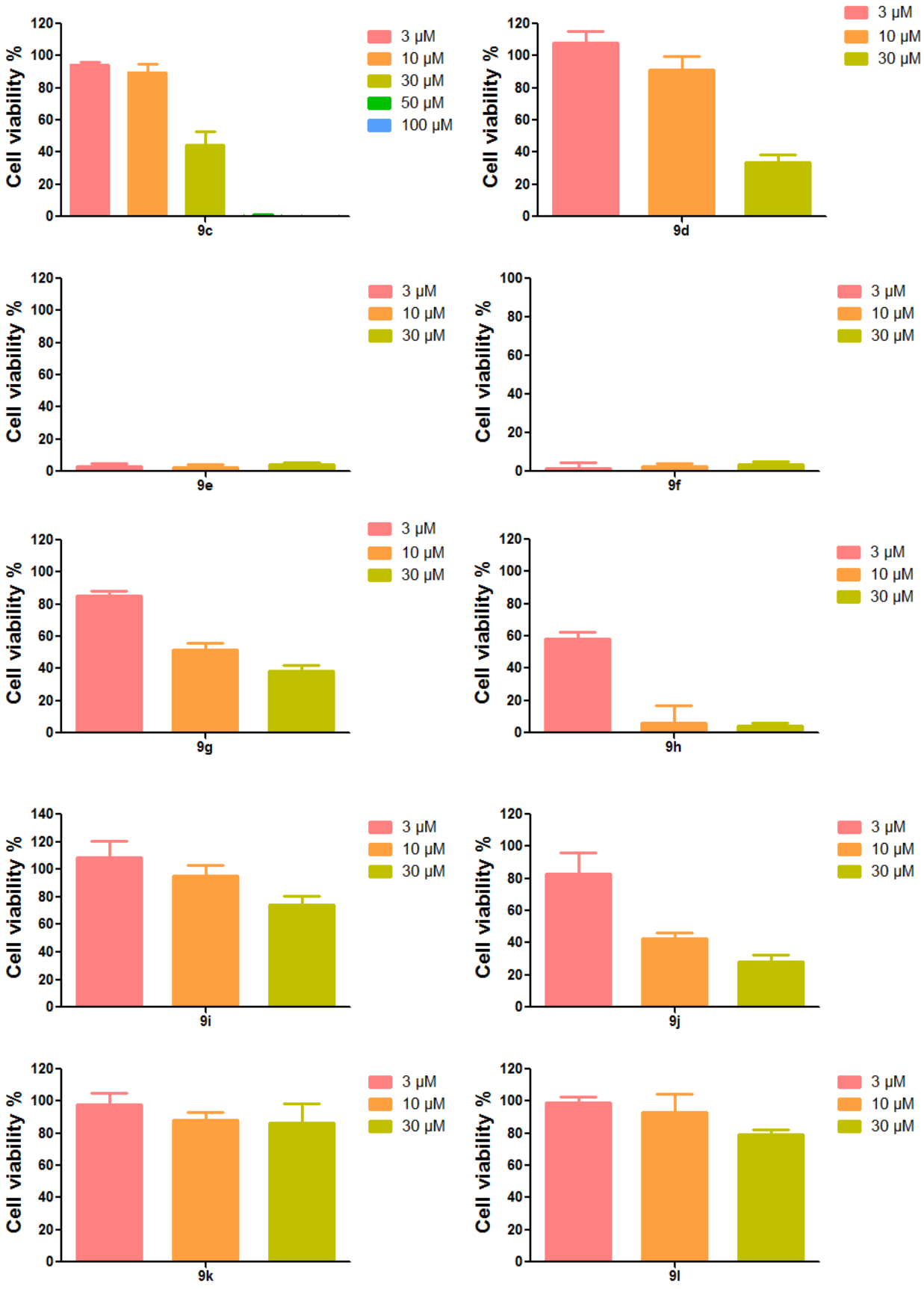
Cell viability %
9c
9d
9e
9f
9g
9h
9i
9j
9k
9l
3 μM
10 μM
30 μM
50 μM
100 μM

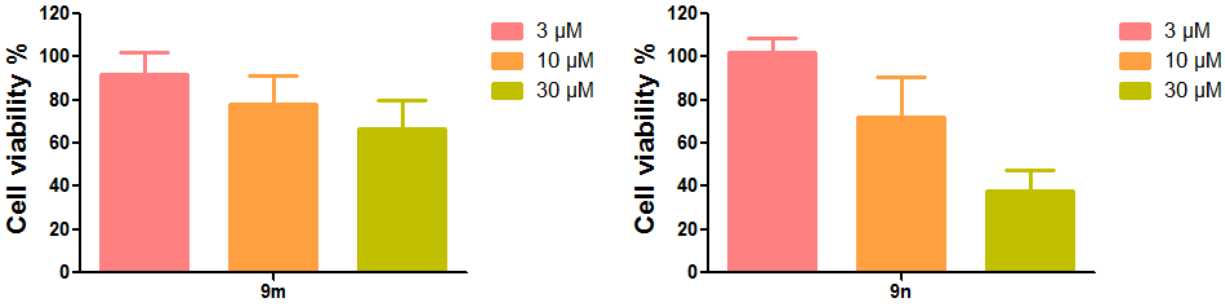

LDH release of compounds **4a**, **4d**, **4l**, **8c**, **8e**, **9a**, **9e**, **9f**, **9g**, **9h** and **9j**

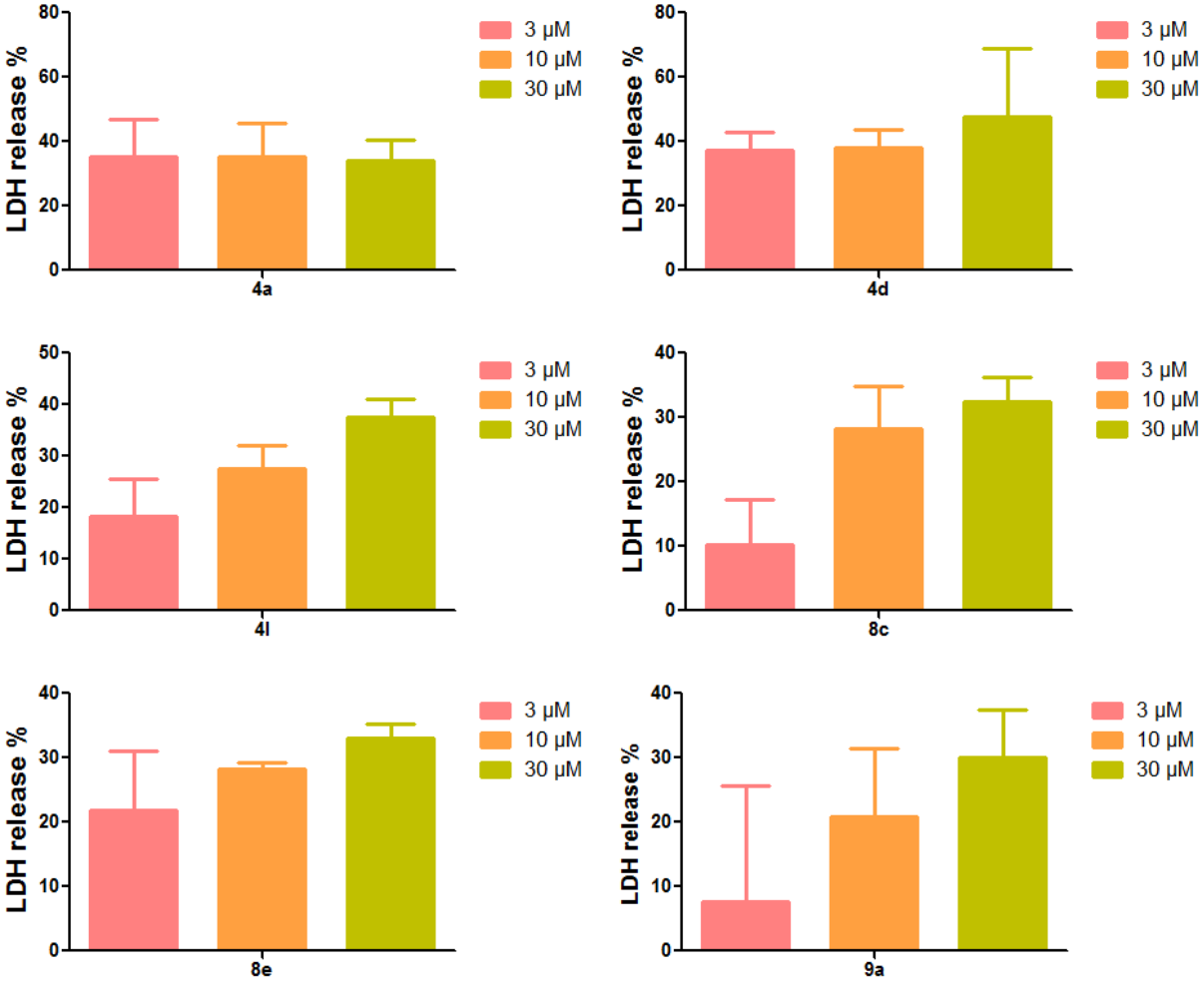

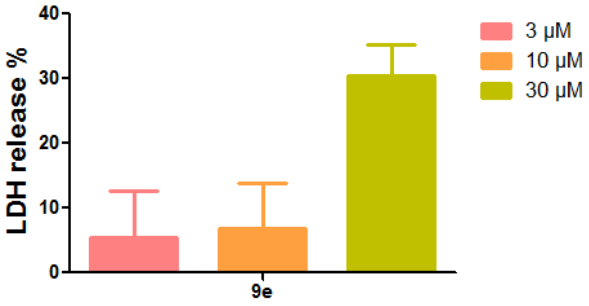
LDH release %
40
30
20
10
0
9e
3 μM
10 μM
30 μM

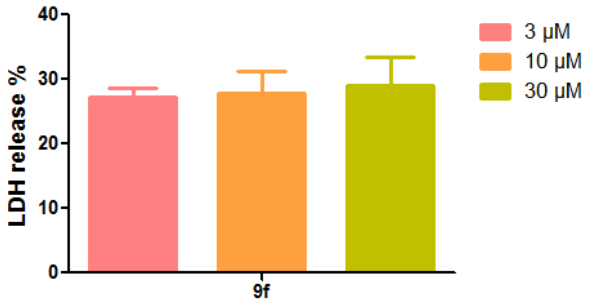
LDH release %
40
30
20
10
0
9f
3 μM
10 μM
30 μM

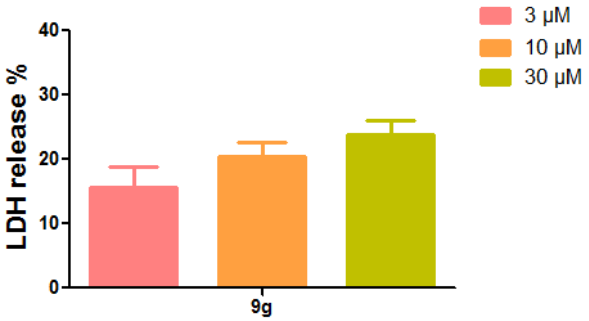
LDH release %
40
30
20
10
0
9g
3 μM
10 μM
30 μM

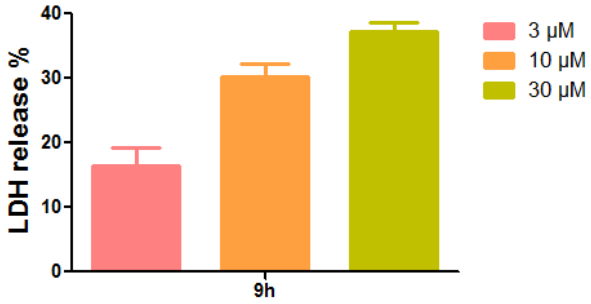
LDH release %
40
30
20
10
0
9h
3 μM
10 μM
30 μM

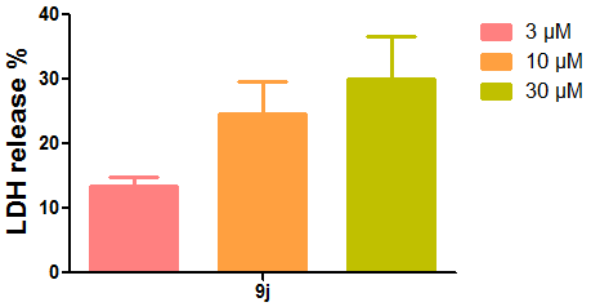
LDH release %
40
30
20
10
0
9j
3 μM
10 μM
30 μM

CHEMGX 8 (6) 865–1020 (2013) · ISSN 1860-7179 · Vol. 8 · No. 6 · June, 2013

CHEMMEDCHEM

CHEMISTRY ENABLING DRUG DISCOVERY

Soluble Epoxide Hydrolase Inhibitors
Derived from Stilbenes, Inspired by Nature

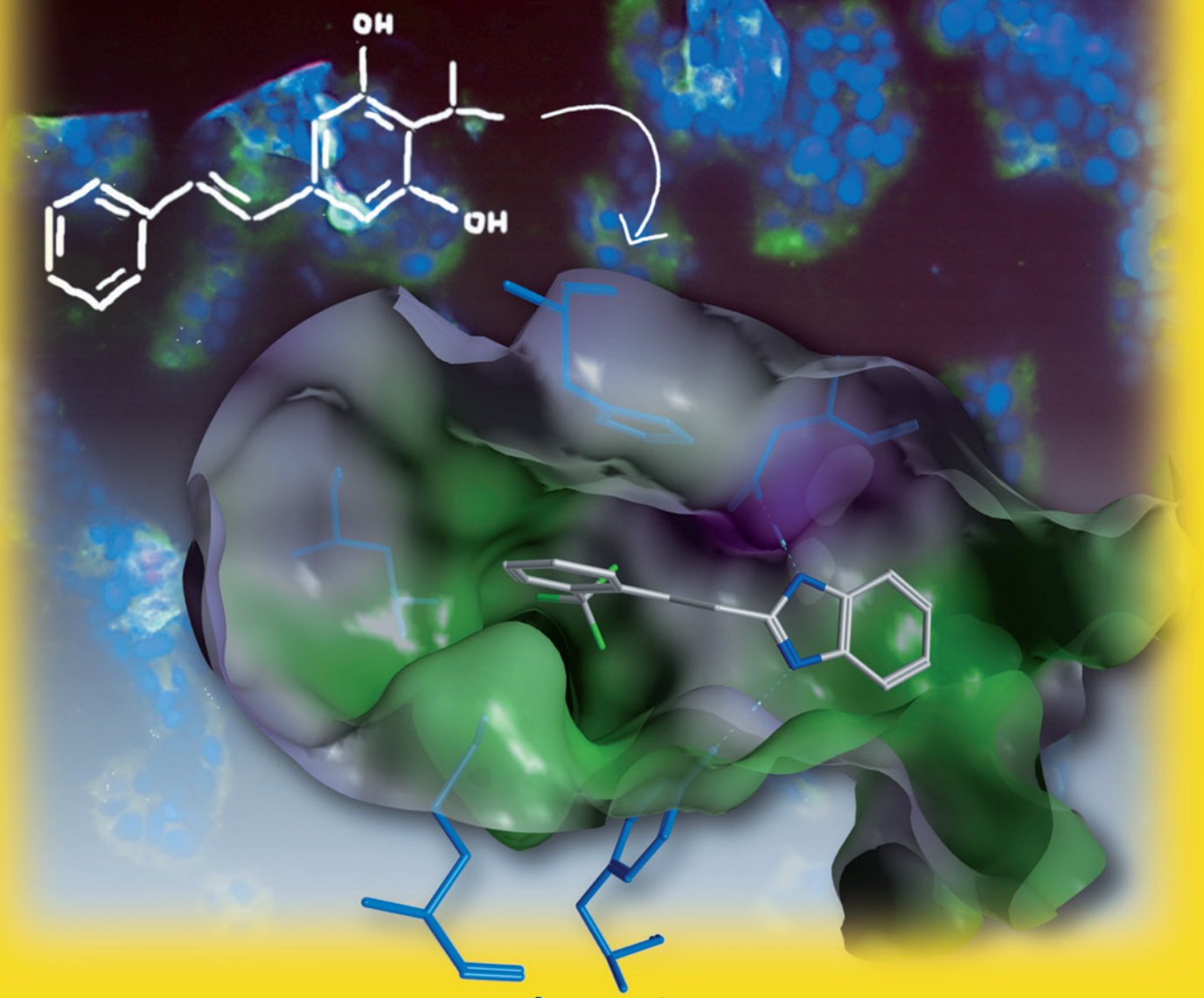

6/2013

A Journal of

ChemPubSoc Europe

Minireview: Radiolabeled Heterobivalent Peptidic Ligands (C. Wängler)

Full Paper: Triazine Nitriles as Rhodesain Inhibitors (D. W. Banner, T. Schirmeister, F. Diederich)

www.chemmedchem.org

WILEY-VCH

Cover Picture

Estel.la Buscató, Dominik Büttner, Astrid Brüggerhoff, Franca-Maria Klingler, Julia Weber, Bastian Scholz, Aleksandra Živković, Rolf Marschalek, Holger Stark, Dieter Steinhilber, Helge B. Bode, and Ewgenij Proschak*

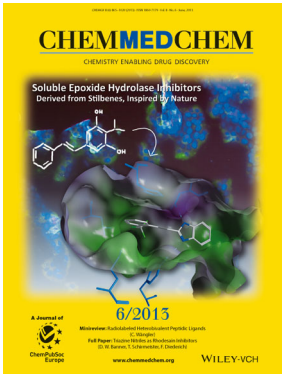

The front cover picture shows the structure of the multipotent bacterial isopropylstilbene identified as a novel soluble epoxide hydrolase (sEH) inhibitor with antiproliferative properties. This natural product served as a template for the design and synthesis of (*E*)-styryl-1*H*-benzo[*d*]imidazoles—easily accessible compounds with enhanced activity towards sEH. The modeled conformation of one of the designed compounds is shown in the foreground, and the background displays apoptotic cells after treatment with isopropylstilbene. For more details, see the Communication by Ewgenij Proschak et al. on p. 919 ff.

CHEMMEDCHEM
COMMUNICATIONS

ChemPubSoc
Europe

DOI: 10.1002/cmdc.201300057

From a Multipotent Stilbene to Soluble Epoxide Hydrolase Inhibitors with Antiproliferative Properties

Estel.la Buscató,[a] Dominik Büttner,[a] Astrid Brüggerhoff,[a] Franca-Maria Klingler,[a] Julia Weber,[a] Bastian Scholz,[b] Aleksandra Živković,[a] Rolf Marschalek,[b] Holger Stark,[a] Dieter Steinhilber,[a] Helge B. Bode,[c] and Ewgenij Proschak*[a]

Inhibitors of soluble epoxide hydrolase (sEH) are in the focus of pharmaceutical research for numerous indications including cardiovascular disorders, diabetes and inflammatory processes.[1–5] sEH is an enzyme located in the branch of the arachidonic acid cascade that hydrolyses the epoxyeicosatrienoic acids (EETs),[6] products resulting from CYP epoxygenases, into dihydroxyeicosatrienoic acids (DHETs). Although several inhibitors reached clinical trials, the role of EETs and sEH in cancer growth and metastasis remains rather ambiguous.[7] Using genetic and pharmacological alteration of EET levels, it has been demonstrated that EETs are critical for primary tumor growth and metastasis in mouse models of cancer.[8] EETs promote metastasis by triggering secretion of the vascular endothelial growth factor (VEGF) by the endothelium, which is critical for EET cancer stimulating activity. The postulated mechanism[9] for EETs to promote tumor growth is via epidermal growth factor receptor/phosphatidylinositol 3 kinase/protein kinase B (EGFR/PI3K/Akt) and EGFR/mitogen-activated protein kinase (MAPK) pathways[10] to promote cancer cell survival. However, sorafenib,[11,12] which was originally designed as a multikinase inhibitor,[13] was found to inhibit sEH in the nanomolar concentration range, which contributes to its profile in vivo.[14,15] Looking at these studies concisely, EETs act as a double-edged sword in cancer development and treatment.

Polypharmacological compounds have gained special attention in the field of cancer treatment due to the complexity of pathways involved in cancer pathogenesis.[16–18] Natural products are one of the major sources for novel antiproliferative compounds, exhibiting various modes of cytostatic action.[19] Often natural products exhibit polypharmacological activity, targeting several pathways relevant[20] for cancer pathogenesis.[21,22] The principle of addressing multiple targets by natural products can be transferred to synthetic multitarget ligands.[23] In this study, we intended to discover chemical compounds exhibiting cytotoxic profiles and simultaneously targeting sEH. We started with a small library of compounds isolated from entomopathogenic bacteria, namely *Photorhabdus* and *Xenorhabdus*.[24] These bacteria live in symbiosis with soil-dwelling nematodes and together are able to infect and kill different insect larvae[25,26] using protein toxins but also small molecules. Key compounds required to evade the insect immune system are phenoloxidase inhibitors, with rhabduscin as the most prominent example.[27] Assuming that also other insect enzymes, like juvenile hormone epoxide hydrolase (JHEH),[28] are targeted by *Photorhabdus* and *Xenorhabdus* natural products, we analyzed our in-house compound library against the JHEH-related target sEH. We found that the pluripotent isopropylstilbene (IPS, **1**) from *Photorhabdus*[29] exhibited the desired properties by inhibiting sEH with an IC_{50} value of 10 μM (Table 1, Scheme 1).

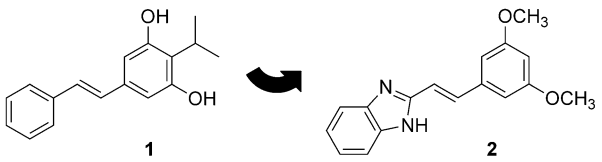

Scheme 1. Natural product inspired design of stilbene-derived sEH inhibitors.

Stilbenes like resveratrol[30,31] or erbstatin[32] are known to possess chemopreventive or antiproliferative properties. Similarly, IPS exhibited a wide range of antiproliferative properties on different cancer cell lines, including HepG2 (hepatocarcinoma), HeLa (cervical cancer), MCF-7 (breast adenocarcinoma), A498 (renal carcinoma) and U937 (histiocytic lymphoma; Table 2).

The synthesis of IPS is not straightforward;[33] therefore, we followed the natural product inspired approach and intended to identify compounds with similar properties and simple synthetic accessibility. We screened a small collection of compounds exhibiting the stilbene scaffold (chalcones and resveratrol analogues) which was available in-house (Supporting Information, SF 3). We identified (*E*)-styryl-1*H*-benzo[*d*]imidazoles as analogues of IPS that carry a benzimidazole moiety, which was previously identified as a novel sEH pharmacophore in our

[a] *E. Buscató,[+] D. Büttner,[+] A. Brüggerhoff, F.-M. Klingler, J. Weber, Dr. A. Živković, Prof. Dr. H. Stark, Prof. Dr. D. Steinhilber, Prof. Dr. E. Proschak*
Institut für Pharmazeutische Chemie, Goethe Universität Frankfurt am Main
Max-von-Laue Str. 9, 60438 Frankfurt am Main (Germany)
E-mail: proschak@pharmchem.uni-frankfurt.de

[b] *B. Scholz, Prof. Dr. R. Marschalek*
Institut für Pharmazeutische Biologie
Goethe Universität Frankfurt am Main
Max-von-Laue Str. 9, 60438 Frankfurt am Main (Germany)

[c] *Prof. Dr. H. B. Bode*
Merck Stiftungsprofessur für Molekulare Biotechnologie
Fachbereich Biowissenschaften, Goethe Universität Frankfurt am Main
Max-von-Laue Str. 9, 60438 Frankfurt am Main (Germany)

[+] *These authors contributed equally to this work.*

Supporting information for this article is available on the WWW under http://dx.doi.org/10.1002/cmdc.201300057.

Table 1. IC_{50} values of synthesized (*E*)-styryl-1*H*-benzo[*d*]imidazoles.[a]

Compd	R^1	R^2	R^3	IC_{50} [μM][b]	Compd	R^1	R^2	R^3	IC_{50} [μM][b]
AUDA	–	–	–	0.1 ± 0.01	**74**	3-(pyridin-3-yl)	H	H	0.8 ± 0.23
IPS (**1**)	–	–	–	10.0 ± 0.96	**75**	3-DHBD[c]	H	H	1.5 ± 0.36
3	H	H	H	5.9 ± 0.60	**31**	4-F	H	H	6.1 ± 0.45
7	2-CF_3	H	H	0.6 ± 0.13	**34**	4-CF_3	H	H	6.5 ± 0.50
10	2-NO_2	H	H	2.0 ± 0.39	**37**	4-OCH_3	H	H	7.5 ± 1.52
13	2-OCH_3	H	H	18.3 ± 1.35	**40**	4-NO_2	H	H	9.8 ± 3.94
16	2-Cl	H	H	1.7 ± 0.12	**43**	2-OCH_3	5-OCH_3	H	17.3 ± 3.11
19	2-F	H	H	2.6 ± 0.21	**46**	3-OCH_3	4-OCH_3	H	4.3 ± 0.57
22	2-Br	H	H	32.1 ± 10.10	**2**	3-OCH_3	5-OCH_3	H	5.4 ± 0.74
25	3-Cl	H	H	1.4 ± 0.11	**49**	4-Cl	2-Cl	H	9.7 ± 0.32
28	3-Br	H	H	4.3 ± 0.49	**52**	2-CF_3	H	3-F	1.9 ± 0.16
29	3-NO_2	H	H	4.6 ± 0.03	**55**	2-CF_3	H	3-CH_3	1.6 ± 0.37
30	3-OCH_3	H	H	5.8 ± 1.73	**58**	2-CF_3	H	3-Cl	2.7 ± 0.76
73	3-(furan-2-yl)	H	H	1.2 ± 0.16	**61**	2-CF_3	H	3-OCH_3	4.9 ± 1.10

[a] Structures are given in Schemes 2–3 and full chemical names can be found in the Supporting Information. [b] Data are the mean ± SD of sEH inhibition of three different experiments. IC_{50} values were determined with recombinant sEH using PHOME as substrate. [c] DHBD: 3-(2,3-dihydrobenzo[*b*][1,4]dioxin-6-yl).

Table 2. Cell-viability EC_{50} values of selected compounds **16**, **19**, **74**, **75** and IPS (**1**) for several cancer cell lines.

Compd	EC_{50} [μM][a]				
	HepG2	HeLa	MCF-7	A498	U937
IPS (**1**)	4.7 ± 0.94	10.4 ± 2.00	ia	n.d. (73.1 % ± 14.65)[b]	2.7 ± 0.27
16	n.d. (115.1 % ± 7.21)[b]	n.d. (63.3 % ± 28.91)[b]	n.t.	n.d. (111.8 % ± 17.09)[b]	1.1 ± 0.11
19	4.7 ± 0.25	n.d. (18.0 % ± 5.20)[b]	n.t.	n.d. (96.1 % ± 19.23)[b]	2.1 ± 0.11
74	21.8 ± 5.31	18.4 ± 5.49	15.7 ± 2.43	n.d. (26.3 % ± 1.00)[b]	10.2 ± 0.23
75	21.0 ± 2.38	19.8 ± 3.03	15.1 ± 1.04	n.d. (50.7 % ± 10.42)[b]	9.2 ± 0.51

[a] All EC_{50} values were determined by at least three independent experiments using WST-1 cell viability assay and are expressed as EC_{50} ± SD. Abbreviations: n.d. = not determinable, n.t. = not tested, ia = inactive at 30 μM. [b] Cell viability [%] at 30 μM.

group.[34] The introduction of a benzimidazole does not abolish the desired antiproliferative properties, since this class of compounds showed a wide spectrum of pharmacological characteristics,[35] including antiallergic, analgesic, anti-inflammatory and antibacterial activities. Compound **2** inhibited sEH with an IC_{50} value of 5.4 μM and was used as a starting point for further optimization.

For the synthesis of a compound collection based on an (*E*)-benzimidazole stilbene scaffold, we used a previously published[36] procedure (Scheme 2) that involves the condensation of substituted *o*-phenylenediamine **5**, **50**, **53**, **56**, or **59** with the appropriately substituted (*E*)-cinnamic acid derivative **4**, **8**, **11**, **14**, **17**, **20**, **23**, **26**, **32**, **35**, **38**, **41**, **44**, or **47** in the presence of 1-ethyl-3-(3-dimethylaminopropyl)-carbodiimide (EDC). 4-(Dimethylamino)pyridine (DMAP) and imidazole were used as catalysts. The resulting amide intermediates **6**, **9**, **12**, **15**, **18**, **21**, **24**, **27**, **33**, **36**, **39**, **42**, **45**, **48**, **51**, **54**, **57**, and **60** were cyclized by heating under microwave irradiation in the presence of hydrochloric acid to yield the target (*E*)-styryl-1*H*-benzo[*d*]imidazoles **7**, **10**, **13**, **16**, **19**, **22**, **25**, **28**, **34**, **37**, **40**, **43**, **46**, **49**, **52**, **55**, **58**, and **61** as the corresponding hydrochloric acid salt (Scheme 2). The (*E*)-geometry of the styryl double bonds was confirmed by proton–proton coupling constants (Supporting Information, SF 1). In order to introduce an aromatic residue at the *meta* position of the phenyl ring (Scheme 3), 3-bromo-(*E*)-cinnamic acid (**62**) underwent esterification (79% yield), followed by Suzuki coupling of the key intermediate **63** with the desired aryl boronic acid (26–49% yield). After hydrolysis of **64**, **65**, and **66**, the condensation with *o*-phenylenediamine (**5**) led to amide intermediates **70**–**72**, that underwent subsequent cyclization to yield compounds **73**–**75** under microwave radiation. Compounds **3**, **29**, **30** and **31** were purchased. Inhibitory activity of styryl benzimidazole derivatives was investigated on human recombinant sEH expressed in *E. coli*[37]

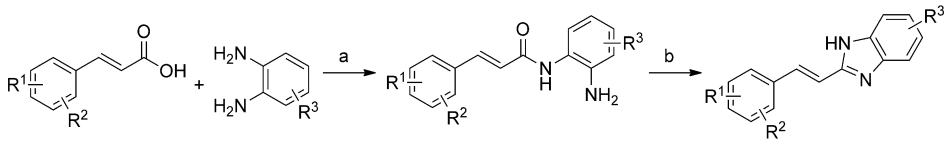

3*: R^1=H, R^2=R^3=H
4, **5**, **6**, **7**: R^1=2-CF_3, R^2=R^3=H
8, **9**, **10**: R^1=2-NO_2, R^2=R^3=H
11, **12**, **13**: R^1=2-OCH_3, R^2=R^3=H
14, **15**, **16**: R^1=2-Cl, R^2=R^3=H
17, **18**, **19**: R^1=2-F, R^2=R^3=H
20, **21**, **22**: R^1=2-Br, R^2=R^3=H
23, **24**, **25**: R^1=3-Cl, R^2=R^3=H
26, **27**, **28**: R^1=3-Br, R^2=R^3=H
29*: R^1=3-NO_2, R^2=R^3=H
30*: R^1=3-OCH_3, R^2=R^3=H
31*: R^1=4-F, R^2=R^3=H
32, **33**, **34**: R^1=4-CF_3, R^2=R^3=H
35, **36**, **37**: R^1=4-OCH_3, R^2=R^3=H
38, **39**, **40**: R^1=4-NO_2, R^2=R^3=H
41, **42**, **43**: R^1=2-OCH_3, R^2=5-OCH_3, R^3=H
44, **45**, **46**: R^1=3-OCH_3, R^2=4-OCH_3, R^3=H
47, **48**, **49**: R^1=4-Cl, R^2=2-Cl, R^3=H
50, **51**, **52**: R^1=2-CF_3, R^2=H, R^3=3-F
53, **54**, **55**: R^1=2-CF_3, R^2=H, R^3=3-CH_3
56, **57**, **58**: R^1=2-CF_3, R^2=H, R^3=3-Cl
59, **60**, **61**: R^1=2-CF_3, R^2=H, R^3=3-OCH_3

Scheme 2. Synthesis of (*E*)-styryl-1*H*-benzo[*d*]imidazoles. *Reagents and conditions*: a) EDC (1.5 equiv), DMAP (0.05 equiv), imidazole (0.05 equiv), RT, 4 h, 21–84%; b) 6 M aq HCl, EtOH, 120 °C, 10 min, MW, 20–92%. Compounds **3**, **29**, **30**, and **31** were purchased.

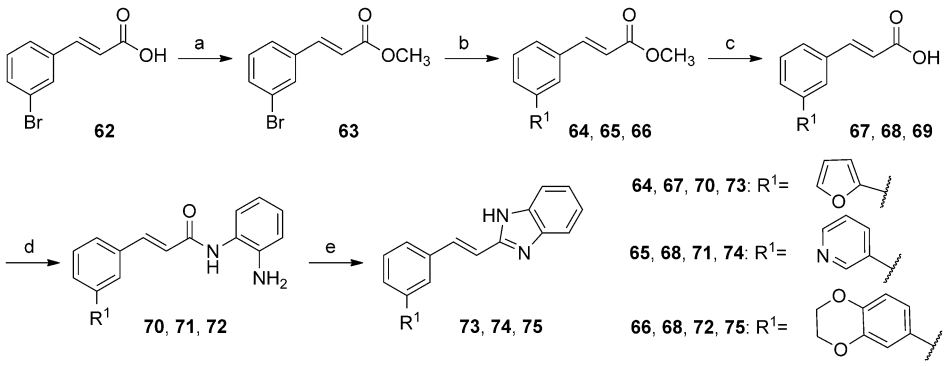

Scheme 3. Synthesis of (*E*)-styryl-1*H*-benzo[*d*]imidazoles **73**, **74** and **75** through introduction of aromatic residues at position 3. *Reagents and conditions*: a) MeOH, H_2SO_4 (0.1 equiv), reflux, 16 h, 70%; b) R^1–$B(OH)_2$ (2.0 equiv), $Pd(PPh_3)_4$ (0.1 equiv), 1 M aq Na_2CO_3, toluene/EtOH (4:1), 85 °C, 16 h, 26–49%; c) KOH (2.85 equiv), MeOH, 25 °C, 3.5 h, 64–95%; d) EDC (1.5 equiv), DMAP (0.05 equiv), *o*-phenylenediamine (1.0 equiv), imidazole (0.05 equiv), RT, 4 h, 8–32%; e) 6 M aq HCl, EtOH, 120 °C, 10 min, MW, 34–63%.

using a synthetic epoxide as a substrate (3-phenyl-cyano(6-methoxy-2-naphthalenyl)methyl ester-2-oxiraneacetic acid, PHOME).[38] As shown in Table 1, we examined the different substitutions at the phenyl ring of the styryl moiety (western part) and the substitutions at the benzimidazole scaffold (eastern part). Regarding the western part of the molecule, several compounds were synthesized bearing *ortho*, *meta* and *para* substitutions. *Ortho*-substituted compounds (**7**, **10**, **13**, **16**, **19**) yielded highest inhibitory activity, with the exception of bromo-substituted **22**. Electron-donating groups like methoxy (compound **13**) were less tolerated (IC_{50} = 18.3 μM), and the best inhibition was obtained with trifluoromethyl-substituted compound **7** (IC_{50} = 0.6 μM). Unsubstituted compound **3** resulted in a 10-fold loss of potency compared with the best compound **7**. With the exception of bromo-substituted **22** (IC_{50} = 32.1 μM), halogen groups in the *ortho* position exhibited moderate inhibition with IC_{50} values in the range of 1.7 to 2.6 μM .

Lower inhibitory activity was observed for **29** and **30**, indicating that *meta* substitution is less favored than *ortho* substitution. However, we confirmed the tendency concerning the electron-donating properties of the substituent, as compound **30** decreases the inhibitory activity (IC_{50} = 5.8 μM). The introduction of heterocyclic moieties, such as furane (**73**), pyridine (**74**) or 2,3-dihydrobenzo[*b*][1,4]dioxine (**75**), increased the inhibitory potency (**73**: IC_{50} = 1.2 μM, **74**: IC_{50} = 0.8 μM, **75**: IC_{50} = 1.5 μM, Table 1). In contrast to the positive substituent effect observed for *ortho*-substituted compounds, *para*-substitution pattern resulted in a weaker inhibitory activity regardless of the electron-donating nature of the substituent.

Additionally, double substitution at the phenyl moiety was explored and led to a decrease in the inhibitory activity. 2,5-Methoxy-substituted compound **43** (IC_{50} = 17.3 μM) exhibited the lowest inhibitory activity, which could be restored by a 3,4-dimethoxy (**46**, IC_{50} = 4.3 μM) or 3,5-dimethoxy substitution pattern (**2**, IC_{50} = 5.2 μM). The potency was not completely restored by exchanging the methoxy groups to a 3,4-dichloro pattern (**49**, IC_{50} = 9.7 μM).

After exploring the phenyl moiety, we could conclude that the best substitution pattern was *ortho*-trifluoromethyl (compound **7**, IC_{50} = 0.6 μM). Therefore, derivatives of compounds bearing altered eastern substitution were synthetized. Electron-donating groups as in methoxy-substituted **61** (IC_{50} = 4.9 μM) exhibited inhibitory activity; however, **52** (IC_{50} = 1.9 μM), **55** (IC_{50} = 1.6 μM) and **58** (IC_{50} = 2.7 μM) bearing electron-withdrawing groups partially restored the activity.

The structure–activity relationship (SAR) of the investigated styryl benzimidazoles on sEH are rather flat, which correlates with the possible binding mode proposed by the molecular docking experiment of the most potent compound **7** (Figure 1, see the Supporting Information for details). Both nitrogen atoms of the benzimidazole core seem to interact with the catalytic center of sEH (Tyr381, Asp333, Tyr465). The largest part of the benzimidazole scaffold is enclosed in the Trp334 niche (15 Å) capable for aryl interactions. The phenyl moiety showed π-stacking with Met419[39] and His524, and the benzimidazole core showed π-stacking with Trp334. The additional space around both aromatic cores correlates with the high tolerability of different substituents, as demonstrated by the SAR.

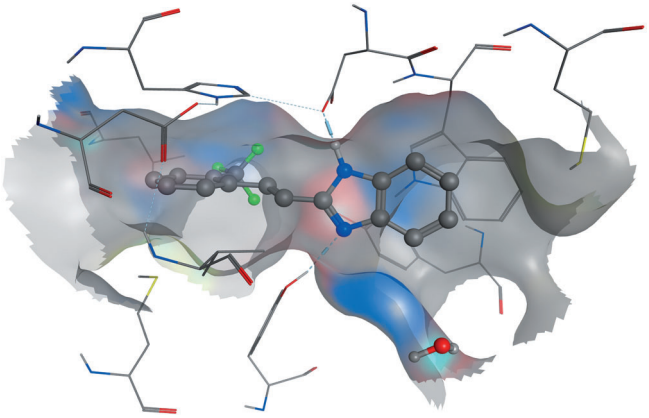

Figure 1. Docking pose of (*E*)-styryl-1*H*-benzo[*d*]imidazole **7** in the binding pocket of the catalytic domain of sEH (PDB: 3KOO).

We evaluated the effect of compounds IPS (**1**; IC_{50} = 10.0 μM), **16** (IC_{50} = 1.7 μM), **19** (IC_{50} = 2.6 μM), **74** (IC_{50} = 1.2 μM) and **75** (IC_{50} = 0.8 μM) on cell viability of several cancer lines (Table 2). IPS inhibited the proliferation activity of all cell lines except MCF-7. In the water-soluble tetrazolium salt (WST-1) assay, EC_{50} values were in the range of 2.7 to 10.4 μM. *Ortho*-substituted compounds **16** and **19** affected the proliferation

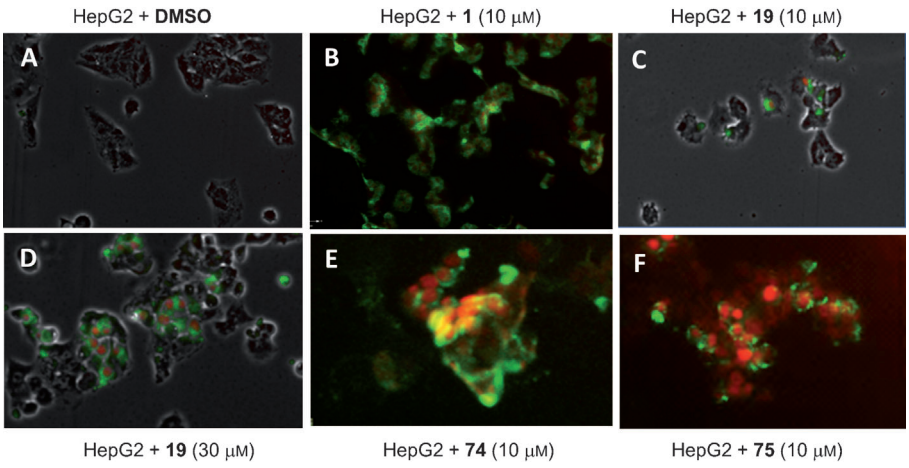

Figure 2. Annexin V/PI staining of HepG2 cells incubated with A) 1% DMSO for 48 h, B) **1** (10 μM) for 24 h, C) **19** (10 μM) for 48 h, D) **19** (30 μM) for 48 h, E) **74** (10 μM) for 24 h, F) **75** (10 μM) for 24 h.

activity of HeLa and U937 (suspension cells). *Ortho*-fluoro-substituted compound **19** inhibited cell proliferation of HepG2 (EC_{50} = 4.7 μM) and U937 (EC_{50} = 2.1 μM) and slightly of HeLa cells (30 μM, 18%).

Compounds **74** and **75** affected the cell growth of the different cancer cell lines to a lesser extent. Compound **74** inhibited the growth of HepG2 (EC_{50} = 21.8 μM), HeLa (EC_{50} = 18.4 μM), MCF-7 (EC_{50} = 15.7 μM), U937 (EC_{50} = 10.2 μM), and to some extent A498 cell lines (resulting in only 26% cell viability at 30 μM). Similarly, compound **75** displayed inhibitory activity on all cancer cell lines. EC_{50} values ranged from 9.2 to 21.5 μM (Table 2). Interestingly all compounds inhibited the cell proliferation of suspension cells U937.

In order to distinguish between an apoptotic or necrotic mechanism, we stained HepG2 cells after treatment with compounds **19**, **74** and **75** during 24–48 h with annexin V/propidium iodide (PI; Figure 2). Cells treated with **19** clearly showed apoptosis in a concentration-dependent manner compared to vehicle (dimethyl sulfoxide) after staining. With compound **74** cells showed progressing apoptosis, whereas cells treated with **75** showed a more late apoptotic/necrotic phenotype over the same time course. IPS (**1**)-treated cells were clearly early apoptotic.

In conclusion, inspired by the initial hit compound, IPS, a series of (*E*)-styryl-1*H*-benzo[*d*]imidazole derivatives were synthesized and evaluated with recombinant sEH, which led to potent sEH inhibitors exhibiting antiproliferative activities. Although the benzimidazole stilbenes presented in this work do not reach the picomolar potencies of urea-based sEH inhibitors,[3] they represent an unprecedented scaffold for further development. Following the approach of natural product inspired design recently proposed by Waldmann et al.,[40] we were able to transfer and even enhance the desired biological activity from a bacterial secondary metabolite to a synthetic compound series. The resulting compounds are accessible via a facile synthetic route and offer the possibility to investigate structure–activity relationships. The natural product inspired drug design extends the valuable role of natural products as drugs and drug precursors to templates for fully synthetic bioactive molecules.

Acknowledgements

This work was supported by the Deutsche Forschungsgemeinschaft (DFG) (PR 1405/2-1), LOEWE Schwerpunkt Insektenbiotechnologie (to H.B.B.), Oncogenic Signaling Frankfurt (OSF), Deutsches Konsortium für Translationale Krebsforschung (DKTK), and LOEWE-Schwerpunkt, Anwendungsorientierte Arzneimittelforschung. E.B. thanks the Deutscher Akademischer Austauschdienst (DAAD)-La Caixa, J.W. thanks Beilstein Institute for a fellowship.

Keywords: benzimidazoles · cancer · polypharmacology · soluble epoxide hydrolase · stilbenes

[1] A. E. EnayetAllah, A. Luria, B. Luo, H.-J. Tsai, P. Sura, B. D. Hammock, D. F. Grant, *J. Biol. Chem.* **2008**, *283*, 36592–36598.
[2] O. Jung, F. Jansen, A. Mieth, E. Barbosa-Sicard, R. U. Pliquett, A. Babelova, C. Morisseau, S. H. Hwang, C. Tsai, B. D. Hammock, L. Schaefer, G. Geisslinger, K, Amann, R. P. Brandes, *PloS One* **2010**, *5*, e11979.
[3] H. C. Shen, B. D. Hammock, *J. Med. Chem.* **2012**, *55*, 1789–1808.
[4] W. Zhang, I. P. Koerner, R. Noppens, M. Grafe, H.-J. Tsai, C. Morisseau, A. Luria, B. D. Hammock, J. R. Falck, N. J. Alkayed, *J. Cereb. Blood Flow Metab.* **2007**, *27*, 1931–1940.
[5] J. D. Imig, B. D. Hammock, *Nat. Rev. Drug Discovery* **2009**, *8*, 794–805.
[6] C. Morisseau, B. D. Hammock, *Annu. Rev. Pharmacol. Toxicol.* **2013**, *53*, 37–58.
[7] D. Wang, R. N. Dubois, *J. Clin. Invest.* **2012**, *122*, 19–22.
[8] D. Panigrahy, M. L. Edin, C. R. Lee, S. Huang, D. R. Bielenberg, C. E. Butterfield, C. M. Barnés, A. Mammoto, T. Mammoto, A. Luria et al., *J. Clin. Invest.* **2012**, *122*, 178–191.
[9] L. Liu, C. Chen, W. Gong, Y. Li, M. L. Edin, D. C. Zeldin, D. W. Wang, *J. Pharmacol. Exp. Ther.* **2011**, *339*, 451–463.
[10] L. Cheng, J. Jiang, Z. Sun, C. Chen, R. T. Dackor, D. C. Zeldin, D. Wang, *Acta Pharmacol. Sin.* **2010**, *31*, 211–218.
[11] B. I. Rini, *Expert Opin. Pharmacother.* **2006**, *7*, 453–461.
[12] S. Wilhelm, C. Carter, M. Lynch, T. Lowinger, J. Dumas, R. A. Smith, B. Schwartz, R. Simantov, S. Kelley, *Nat. Rev. Drug Discovery* **2006**, *5*, 835–844.
[13] T. Ahmad, T. Eisen, *Clin. Cancer Res.* **2004**, *10*, 6388S–6392S.
[14] H. Inoue, S. H. Hwang, A. T. Wecksler, B. D. Hammock, R. H. Weiss, *Cancer Biol. Ther.* **2011**, *12*, 827–836.
[15] J.-Y. Liu, S.-H. Park, C. Morisseau, S. H. Hwang, B. D. Hammock, R. H. Weiss, *Mol. Cancer Ther.* **2009**, *8*, 2193–2203.
[16] Z. A. Knight, H. Lin, K. M. Shokat, *Nat. Rev. Cancer* **2010**, *10*, 130–137.
[17] A. C. Dar, T. K. Das, K. M. Shokat, R. L. Cagan, *Nature* **2012**, *486*, 80–84.
[18] A. L. Hopkins, *Nat. Chem. Biol.* **2008**, *4*, 682–690.
[19] M. W. Karaman, S. Herrgard, D. K. Treiber, P. Gallant, C. E. Atteridge, B. T. Campbell, K. W. Chan, P. Ciceri, M. I. Davis, P. T. Edeen et al., *Nat. Biotechnol.* **2008**, *26*, 127–132.
[20] J. Mestres, E. Gregori-Puigjané, S. Valverde, R. V. Solé, *Mol. BioSyst.* **2009**, *5*, 1051–1057.
[21] J. Mann, *Nat. Rev. Cancer* **2002**, *2*, 143–148.
[22] A. Nagle, W. Hur, N. S. Gray, *Curr. Drug Targets* **2006**, *7*, 305–326.

[23] T. Voigt, C. Gerding-Reimers, T. T. Ngoc Tran, S. Bergmann, H. Lachance, B. Schölermann, A. Brockmeyer, P. Janning, S. Ziegler, H. Waldmann, *Angew. Chem.* **2013**, *125*, 428 – 432; *Angew. Chem. Int. Ed.* **2013**, *52*, 410 – 414.
[24] H. B. Bode, *Curr. Opin. Chem. Biol.* **2009**, *13*, 224 – 230.
[25] K. E. Murfin, A. R. Dillman, J. M. Foster, S. Bulgheresi, B. E. Slatko, P. W. Sternberg, H. Goodrich-Blair, *Biol. Bull.* **2012**, *223*, 85 – 102.
[26] N. R. Waterfield, T. Ciche, D. Clarke, *Annu. Rev. Microbiol.* **2009**, *63*, 557 – 574.
[27] J. M. Crawford, C. Portmann, X. Zhang, M. B. J. Roeffaers, J. Clardy, *Proc. Natl. Acad. Sci. USA* **2012**, *109*, 10821 – 10826.
[28] S. Debernard, C. Morisseau, T. F. Severson, L. Feng, H. Wojtasek, G. D. Prestwich, B. D. Hammock, *Insect Biochem. Mol. Biol.* **1998**, *28*, 409 – 419.
[29] S. A. Joyce, A. O. Brachmann, I. Glazer, L. Lango, G. Schwär, D. J. Clarke, H. B. Bode, *Angew. Chem.* **2008**, *120*, 1968 – 1971; *Angew. Chem. Int. Ed.* **2008**, *47*, 1942 – 1945.
[30] M. Jang, L. Cai, G. O. Udeani, K. V. Slowing, C. F. Thomas, C. W. Beecher, H. H. Fong, N. R. Farnsworth, A. D. Kinghorn, R. G. Mehta, R. C. Moon, J. M. Pezzuto, *Science* **1997**, *275*, 218 – 220.
[31] O. P. Mgbonyebi, J. Russo, I. H. Russo, *Int. J. Clin. Oncol.* **1998**, *12*, 865 – 869.
[32] M. Imoto, K. Umezawa, K. Komuro, T. Sawa, T. Takeuchi, H. Umezawa, *Jpn. J. Cancer Res.* **1987**, *78*, 329 – 332.
[33] G. Chen, J. M. Webster, J. Li, K. Hu, W. Liu, J. Zhu, *Anti-Inflammatory and Psoriasis Treatment and Protein Kinase Inhibition by Hydroxy Stilbenes and Novel Stilbene Derivatives and Analogues*, US 2005/0059733, 2004.
[34] D. Moser, J. M. Wisniewska, S. Hahn, J. Achenbach, E. Buscató, F.-M. Klingler, B. Hofmann, D. Steinhilber, E. Proschak, *ACS Med. Chem. Lett.* **2012**, *3*, 155 – 158.
[35] Y. Bansal, O. Silakari, *Bioorg. Med. Chem.* **2012**, *20*, 6208 – 6236.
[36] D. van den Berg, K. R. Zoellner, M. O. Ogunrombi, S. F. Malan, G. Terre' Blanche, N. Castagnoli, J. J. Bergh, J. P. Petzer, *Bioorg. Med. Chem.* **2007**, *15*, 3692 – 3702.
[37] S. Hahn, J. Achenbach, E. Buscató, F.-M. Klingler, M. Schroeder, K. Meirer, M. Hieke, J. Heering, E. Barbosa-Sicard, F. Loehr, I. Fleming, V. Doetsch, M. Schubert-Zsilavecz, D. Steinhilber, E. Proschak, *ChemMedChem* **2011**, *6*, 2146 – 2149.
[38] C. Morisseau, M. Bernay, A. Escaich, J. R. Sanborn, J. Lango, B. D. Hammock, *Anal. Biochem.* **2011**, *414*, 154 – 162.
[39] L. M. Salonen, M. Ellermann, F. Diederich, *Angew. Chem.* **2011**, *123*, 4908 – 4944; *Angew. Chem. Int. Ed.* **2011**, *50*, 4808 – 4842.
[40] S. Wetzel, R. S. Bon, K. Kumar, H. Waldmann, *Angew. Chem.* **2011**, *123*, 10990 – 11018; *Angew. Chem. Int. Ed.* **2011**, *50*, 10800 – 10826.

Received: February 6, 2013
Published online on ■■ ■■, 0000

COMMUNICATIONS

*E. Buscató, D. Büttner, A. Brüggerhoff, F.-M. Klingler, J. Weber, B. Scholz, A. Živković, R. Marschalek, H. Stark, D. Steinhilber, H. B. Bode, E. Proschak**

■■ – ■■

From a Multipotent Stilbene to Soluble Epoxide Hydrolase Inhibitors with Antiproliferative Properties

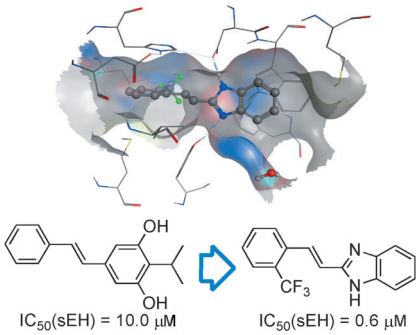

Inspired by nature: Natural product isopropylstilbene was identified as an inhibitor of soluble epoxide hydrolase exhibiting antiproliferative properties. Following the natural product inspired design approach, a library of (*E*)-styryl-1*H*-benzo[*d*]imidazoles was synthesized and evaluated with recombinant enzyme and on several cancer cell lines.

CHEMMEDCHEM
Chemistry & Drug Discovery

Supporting Information

From a Multipotent Stilbene to Soluble Epoxide Hydrolase Inhibitors with Antiproliferative Properties

Estel.la Buscató,[a] Dominik Büttner,[a] Astrid Brüggerhoff,[a] Franca-Maria Klingler,[a] Julia Weber,[a] Bastian Scholz,[b] Aleksandra Živković,[a] Rolf Marschalek,[b] Holger Stark,[a] Dieter Steinhilber,[a] Helge B. Bode,[c] and Ewgenij Proschak*[a]

cmdc_201300057_sm_miscellaneous_information.pdf

- **Chemistry**

General details

The structures of the synthesized compounds were confirmed by ^{1}H, ^{13}C NMR and mass spectrometry (ESI). The identity of the synthesized compounds was determined by high resolution mass spectrometry (HRMS), the purity by HPLC and was found > 95%. Starting materials and solvents were purchased from Sigma-Aldrich Chemie GmbH (Steinheim, Germany), Apollo Scientific (Stockport, UK) or Alfa Aesar (Ward Hill, USA) and were reagent grade and were used without further purification. For the microwave synthesis a Biotage Initiator 2.0 (300 W) was used and the products were purified using a Varian 971-FP Flash Purification System on silica gel with 50 µm particle size. Thin layer chromatography was performed on Merck aluminium backed plates, precoated with silica (0.2 mm, $60F_{254}$), which were developed using UV fluorescence (254 nm). ^{1}H and ^{13}CNMR spectra were measured in DMSO-d_6 or MeOH-d_4 on a Bruker AV 250 (250 MHz for ^{1}H-NMR and 63 MHz for ^{13}C-NMR), Bruker AMX 400 (400 MHz) (75 MHz for ^{13}C-NMR) and Bruker AV300 (282 MHz for ^{19}F-NMR). Chemical shifts (δ) are reported in parts per million (ppm) using tetramethylsilane (TMS) as internal standard. All coupling constants (J) are given in Hertz and the splitting patterns are designed as follows: s (singlet), d (doublet), dd (doublet of doublets), t (triplet), dt (doublet of triplets), q (quartet), and m (multiplet) Mass spectra were obtained on an Electrospray-Ionization Fisons (VG Platform II) spectrometer measuring in the positive- or negative-ion mode (ESI-MS system). High resolution mass spectra were measured by a MALDI LTQ Orbitrap XL spectrometer from Thermo Scientific. The purity of final compounds was determined using LC2020 (Shimadzu, Duisburg, Germany) on a Kinetex 2.6 µm C18 100 Å, 100 x 2.1 mm (Phenomenex, Aschaffenburg, Germany). The method included a water/methanol gradient run of 5-95% and detection at 254 nm and 280 nm

.

Synthetic experimental procedures and characterization

General procedure to synthesize amide intermediates (**6, 9, 12, 15, 18, 21, 24, 27, 33, 36, 39, 42, 45, 48, 51, 54, 57, 60**): To a solution of *o*-phenylenediamine (**5**) (2.31 mmol, 1 eq) and EDC (3.47 mmol, 1.5 eq) in DMF (10 mL) *(E)*-3-trifluoromethylcinnamic acid (**6**) (2.31 mmol, 1 eq) was added. 4-(dimethylamino)pyridine (0.05 mmol, 0.05 eq) and imidazole (0.05 mmol, 0.05 eq) were added as catalysts and the reaction was stirred at room temperature for 4 h. Water (30 mL) was added to the reaction mixture and the resulting precipitate was collected by filtration.

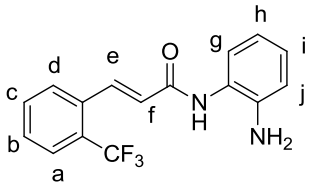

(*E*)-*N*-(2-aminophenyl)-3-(2-trifluoromethylphenyl)acrylamide (**6**): yellow powder (480 mg, 67%), R_f=0.75 (DCM/MeOH 9:1), ^{1}H NMR (DMSO-d_6) δ = 9.52 (s, 1H, *NH*), 7.77-7.93 (m, 4H, *a/c/d*), 7.64 (t, 1H, *b*, $^3J_{HH}$ = 7.7 Hz), 7.37 (dd, 1H, *g*, $^3J_{HH}$ = 7.6 Hz, $^4J_{HH}$ = 1.3 Hz), 6.92-7.02 (m, 2H, *f/i*), 6.77 (dd, 1H, *j*, $^3J_{HH}$ = 7.6 Hz, $^4J_{HH}$ = 1.3 Hz), 6.60 (dt, 1H, *h*, $^3J_{HH}$ = 7.6 Hz, $^4J_{HH}$ = 1.3 Hz), 4.98 (s, 2H, NH_2). ^{19}F NMR (DMSO-d_6) δ = -57.71. MS (ESI, 70 eV) m/z (%): 307.2 (100) $[M+H]^+$.

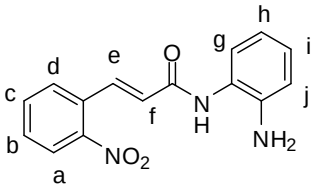

(*E*)-*N*-(2-aminophenyl)-3-(2-nitrophenyl)acrylamide (**9**): yellow solid (430 mg, 65%), R_f=0.38 (Hexan/ EtOAc 1:2), ^{1}H NMR (DMSO-d_6) δ = 9.54 (s, 1H, *NH*), 8.09 (d, 1H, *a*, $^3J_{HH}$ = 8.1 Hz), 7.80 (m, 3H, *c/d/e*), 7.69 (m, 1H, *b*), 7.36 (dd, 1H, *g*, $^3J_{HH}$ = 7.5 Hz, $^4J_{HH}$ = 1.4 Hz), 6.88-6.98 (m, 2H, *f/i*), 6.79 (dd, 1H, *j*, $^3J_{HH}$ = 7.5 Hz, $^4J_{HH}$ = 1.4 Hz), 6.60 (dt, 1H, *h*, $^3J_{HH}$ = 7.5 Hz, $^4J_{HH}$ = 1.4 Hz), 4.98 (s, 2H, NH_2). MS (ESI, 70 eV) m/z (%): 284.7 (100) $[M+H]^+$.

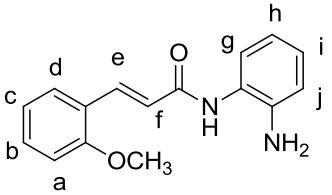

(*E*)-*N*-(2-aminophenyl)-3-(2-methoxyphenyl)acrylamide (**12**): yellow powder (250 mg, 40%), R_f=0.58 (DCM/MeOH 9:1), ^{1}H NMR (DMSO-d_6) δ = 9.39 (s, 1H, *NH*), 7.79 (d, 1H, *e*, $^3J_{HH}$ = 15.7 Hz), 7.59 (d, 1H, *d*, $^3J_{HH}$ = 7.2 Hz), 7.33-7.44 (m, 2H, *b/g*), 6.90-7.13 (m, 4H, *a/c/f/i*), 6.76 (dd, 1H, *j*, $^3J_{HH}$ = 1.4 Hz), 6.61 (dt, 1H, *h*, $^3J_{HH}$ = 7.2 Hz, ^4J = 1.4 Hz). MS (ESI, 70 eV) m/z (%):269.2 (100) $[M+H]^+$.

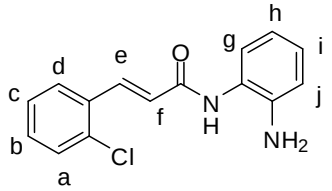

(*E*)-*N*-(2-aminophenyl)-3-(2-chlorophenyl)acrylamide (**15**): yellow powder (320 mg, 51%), R_f=0.50 (Hexan/ EtOAc 1:2), ^{1}H NMR (DMSO-d_6) δ = 9.50 (s, 1H, *NH*) , 7.85 (d, 1H, *e*, $^3J_{HH}$

= 15.6 Hz), 7.77-7.80 (m, 1H, *a*), 7.56-7.59 (m, 1H, *d*), 7.44-7.47 (m, 2H, *b/c*), 7.36 (dd, 1H, *g*, $^{3}J_{HH}$ = 7.7 Hz, $^{4}J_{HH}$ = 1.1 Hz), 6.91-7.00 (m, 2H, *f/i*), 6.77 (dd, 1H, *j*, $^{3}J_{HH}$ = 7.7 Hz, $^{4}J_{HH}$ = 1.1 Hz), 6.60 (dt, 1H, *h*, $^{3}J_{HH}$ = 7.7 Hz, $^{4}J_{HH}$ = 1.1 Hz), 4.98 (s, 2H, *NH2*). MS (ESI, 70 eV) m/z (%): 273.0 (100) $[M+H]^{+}$.

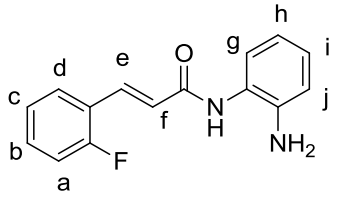

(*E*)-*N*-(2-aminophenyl)-3-(2-fluorophenyl)acrylamide (**18**): yellow powder (180 mg, 30%), R_f=0.69 (DCM/MeOH 9:1), ^{1}H NMR (DMSO-d_6) δ = 9.50 (s, 1H, NH), 7.72 (dt, 1H, *b*, $^{3}J_{HH}$ = 7.9 Hz, $^{4}J_{HH}$ = 1.5 Hz), 7.62 (d, 1H, *e*, $^{3}J_{HH}$ = 15.9 Hz), 7.44-7.52 (m, 1H, *d*), 7.28-7.37 (m, 3H, *a/c/g*,), 7.02 (d, 1H, *f*, $^{3}J_{HH}$ = 15.9 Hz), 6.94 (dt, 1H, *i*, $^{3}J_{HH}$ = 7.6 Hz, $^{4}J_{HH}$ = 1.4 Hz), 6.77 (dd, 1H, *j*, $^{3}J_{HH}$ = 7.6 Hz, $^{4}J_{HH}$ = 1.4 Hz), 6.59 (dt, 1H, *h*, $^{3}J_{HH}$ = 7.6 Hz, $^{4}J_{HH}$ = 1.4 Hz), 4.97 (s, 2H, NH_2). ^{19}F NMR (DMSO-d_6) δ = -115.70, MS (ESI, 70 eV) m/z (%): 257.8 (100) $[M+H]^{+}$.

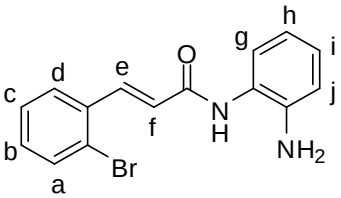

(*E*)-*N*-(2-aminophenyl)-3-(2-bromophenyl)acrylamide (**21**): yellow solid (2.54 g, 85%), R_f=0.68 (DCM/MeOH 9:1), ^{1}H NMR (DMSO-d_6) δ = 9.50 (s, 1H, NH), 7.85-7.73 (m, 3H, *a/d/e*), 7.50 (t, 1H, *c*, $^{3}J_{HH}$ = 7.5 Hz), 7.40-7.33 (m, 2H, *b/g*), 6.97-6.91 (m, 2H, *f/i*), 6.77 (dd, 1H, *j*, $^{3}J_{HH}$ = 7.9 Hz, $^{4}J_{HH}$ = 1.4 Hz), 6.60 (dt, 1H, *h*, $^{3}J_{HH}$ = 7.8 Hz, $^{4}J_{HH}$ = 1.4 Hz), 4.98 (s, 2H, NH_2). MS (ESI, 70 eV) m/z (%): 318.4 (100) $[M+H]^{+}$.

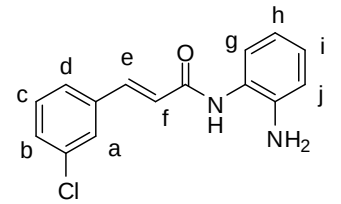

(*E*)-*N*-(2-aminophenyl)-3-(3-chlorophenyl)acrylamide (**24**): white powder (340 mg, 54 %), R_f=0.64 (Hexan/ EtOAc 1:2), ^{1}H NMR (DMSO-d_6) δ = 9.39 (s, 1H, NH), 7.71 (s, 1H, *a*), 7.60-7.63 (m, 1H, *d*), 7.55 (d, 1H, *e*, $^{3}J_{HH}$ = 15.6 Hz), 7.48-7.50 (m, 2H, *b/c*), 7.37 (d, 1H, *g*, $^{3}J_{HH}$ = 7.4 Hz), 6.91-7.00 (m, 2H, *f/i*), 6.77 (dd, 1H, *j*, $^{3}J_{HH}$ = 8.0 Hz, $^{4}J_{HH}$ = 1.1 Hz), 6.59 (dt, 1H, *h*, $^{3}J_{HH}$ = 8.0 Hz, $^{4}J_{HH}$ = 1.1 Hz), 4.97 (s, 2H, NH2). MS (ESI, 70 eV) m/z (%): 273.2 (100) $[M+H]^{+}$.

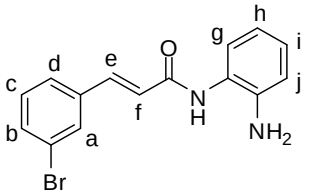

(*E*)-*N*-(2-aminophenyl)-3-(3-bromophenyl)acrylamide (**27**): white solid (2.52 g, 84%), R_f=0.67 (DCM/MeOH 9:1), ^{1}H NMR (DMSO-d_6) δ = 9.40 (s, 1H, NH), 7.85 (s, 1H, *a*), 7.66-7.57 (m, 2H, *b/d*), 7.54 (d, 1H, *e*, $^3J_{HH}$ = 15.7 Hz), 7.45-7.36 (m, 2H, *c/g*), 7.01-6.91 (m, 2H, *f/i*), 6.77 (dd, 1H, *j*, $^3J_{HH}$ = 7.9 Hz, $^4J_{HH}$ = 1.4 Hz), 6.60 (dt, 1H, *h*, $^3J_{HH}$ = 7.8 Hz, $^4J_{HH}$ = 1.4 Hz), 4.98 (s, 2H, NH_2). MS (ESI, 70 eV) m/z (%): 318.1 (100) $[M+H]^+$.

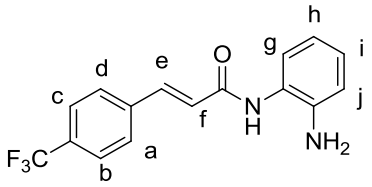

(*E*)-*N*-(2-aminophenyl)-3-(3-(4-trifluoromethyl)phenyl)acrylamide (**33**): yellow powder (470 mg, 66%), R_f=0.58 (Hexan/EtOAc 1:2), ^{1}H NMR (DMSO-d_6) δ = 9.48 (s, 1H, *NH*), 7.80-7.88 (m, 4H, *a/b/c/d*), 7.65 (d, 1H, *e*, $^3J_{HH}$ = 15.85 Hz), 7.36 (dd, 1H, *g*, $^3J_{HH}$ = 7.5 Hz, $^4J_{HH}$ = 1.4 Hz), 7.05 (d, 1H, *f*, $^3J_{HH}$ = 15.85 Hz), 6.95 (dt, 1H, *i*, $^3J_{HH}$ = 7.5 Hz, ^4J = 1.4 Hz), 6.77 (dd, 1H, *j*, $^3J_{HH}$ = 7.5 Hz, ^4J = 1.4 Hz), 6.60 (dt, 1H, *h*, $^3J_{HH}$ = 7.5 Hz, ^4J = 1.4 Hz), 4.98 (s, 2H, NH_2).^{19}F NMR (DMSO-d_6) δ = -61.16. MS (ESI, 70 eV) m/z (%):307.2 (100) $[M-H]^-$.

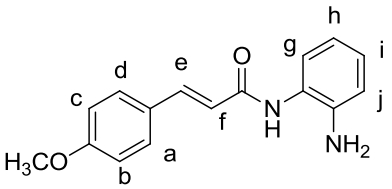

(*E*)-*N*-(2-aminophenyl)-3-(4-methoxyphenyl)acrylamide (**36**): white powder (400 mg, 65%), R_f=0.44 (Hexan/ EtOAc 1:2), ^{1}H NMR (DMSO-d_6) δ = 9.32 (s, 1H, *NH*), 7.58 (d, 2H, *b/c*, $^3J_{HH}$ = 8.8 Hz), 7.52 (d, 1H, *e*, $^3J_{HH}$ = 15.6 Hz), 7.35 (d, 1H, *g*, $^3J_{HH}$ = 7.2 Hz), 7.01 (d, 2H, *a/d*, $^3J_{HH}$ = 8.8 Hz), 6.92 (dt, 1H, *i*, $^3J_{HH}$ = 7.2 Hz, $^4J_{HH}$ = 1.4 Hz), 6.74-6.80 (m, 2H, *f/j*), 6.60 (dt, 1H, *h*, $^3J_{HH}$ = 7.2 Hz, ^4J = 1.4 Hz), 4.95 (s, 2H, NH_2), 3.82 (s, 3H, *O-CH*$_3$). MS (ESI, 70 eV) m/z (%): 269.3 (100) $[M+H]^+$.

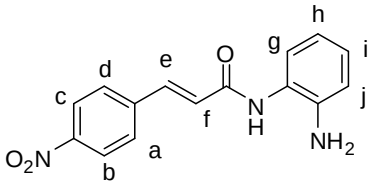

(*E*)-*N*-(2-aminophenyl)-3-(4-nitrophenyl)acrylamide (**39**): yellow solid (420 mg, 64%), R_f=0.72 (DCM/MeOH 9:1), ^{1}H NMR (DMSO-d_6) δ = 9.32 (s, 1H, NH), 8.31 (d, 2H, *b/c*, $^3J_{HH}$ = 8.7 Hz), 7.90 (d, 2H, *a/d*, $^3J_{HH}$ = 8.7 Hz), 7.68 (d, 1H, *e*, $^3J_{HH}$ = 15.9 Hz), 7.37 (dd, 1H, *g*, $^3J_{HH}$ = 7.4 Hz, $^4J_{HH}$ = 1.3 Hz), 7.10 (d, 1H, *f*, $^3J_{HH}$ = 15.9 Hz), 6.95 (dt, 1H, *i*, $^3J_{HH}$ = 7.4 Hz, $^4J_{HH}$ = 1.3 Hz), 6.78 (dd, 1H, *j*, $^3J_{HH}$ = 7.4 Hz,), 6.60 (dt, 1H, *h*, $^3J_{HH}$ = 7.4 Hz, $^4J_{HH}$ = 1.3 Hz), 4.99 (s, 2H, NH_2). MS (ESI, 70 eV) m/z (%): 284.3 (100) $[M+H]^+$.

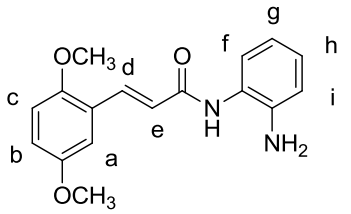

(*E*)-*N*-(2-aminophenyl)-3-(2,5-dimethoxyphenyl)acrylamide (**42**): grey powder (140 mg, 21%), R_f=0.66 (DCM/MeOH 9:1), ^{1}H NMR (DMSO-d_6) δ = 9.42 (s, 1H, NH), 7.76 (d, 1H, *d*, $^3J_{HH}$ = 16.0 Hz), 7.36 (dd, 1H, *f*, $^3J_{HH}$ = 7.6 Hz, $^4J_{HH}$ = 1.3 Hz), 7.15 (d, 1H, *b*, $^3J_{HH}$ = 2.8 Hz), 6.89-7.01 (m, 4H, *a/c/e/h*), 6.76 (dd, 1H, *i*, $^3J_{HH}$ = 7.6 Hz, $^4J_{HH}$ = 1.3 Hz), 6.59 (dt, 1H, *g*, $^3J_{HH}$ = 7.6 Hz, $^4J_{HH}$ = 1.3 Hz), 4.97 (s, 2H, NH2), 3.84 (s, 3H, *B*), 3.77 (s, 3H, *A*). MS (ESI, 70 eV) m/z (%): 299.3 (100) $[M+H]^+$.

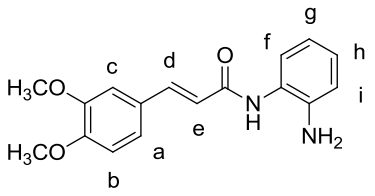

(*E*)-*N*-(2-aminophenyl)-3-(3,4-dimethoxyphenyl)acrylamide (**45**): red powder (230 mg, 33%), R_f=0.54 (DCM/MeOH 9:1), ^{1}H NMR (DMSO-d_6) δ = 9.33 (s, 1H, NH), 7.49 (d, 1H, *d*, $^3J_{HH}$ = 15.6 Hz), 7.34 (dd, 1H, *f*, $^3J_{HH}$ = 7.5 Hz, $^4J_{HH}$ = 1.4 Hz), 7.15-7.20 (m, 2H, *a/c*), 7.00 (d, 1H, *b*, $^3J_{HH}$ = 8.4 Hz), 6.91 (dt, 1H, *h*, $^3J_{HH}$ = 7.5 Hz, $^4J_{HH}$ = 1.4 Hz), 6.74-6.80 (m, 2H, *e/i*), 6.60 (dt, 1H, *g*, $^3J_{HH}$ = 7.5 Hz, $^4J_{HH}$ = 1.4 Hz), 4.97 (s, 2H, NH_2), 3.80 (s, 3H, *B*), 3.79 (s, 3H, *A*). MS (ESI, 70 eV) m/z (%): 307.2 (100) $[M+H]^+$.

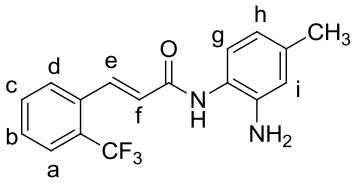

(*E*)-*N*-(2-amino-4-methylphenyl)-3-(2-(trifluoromethyl)phenyl)acrylamide (**48**): yellow solid (360 mg, 55%), R_f=0.66 (DCM/MeOH 9:1), ^{1}H NMR (DMSO-d_6) δ = 9.47 (s, 1H, *NH*), 7.92-7.77 (m, 4H, *a/c/d/e*), 7.63 (t, 1H, *b*, $^3J_{HH}$ = 7.6 Hz), 7.23 (d, 1H, *g*, $^3J_{HH}$ = 7.8 Hz), 6.98 (d, 1H, *f*, $^3J_{HH}$ = 15.4 Hz), 6.59 (s, 1H, *i*), 6.41 (dd, 1H, *h*, $^3J_{HH}$ = 8.2 Hz), 4.91 (s, 2H, NH_2), 2.19 (s, 3H, CH_3). ^{19}F NMR (DMSO-d_6) δ = -57.71. MS (ESI, 70 eV) m/z (%): 321.2 (100) $[M+H]^+$.

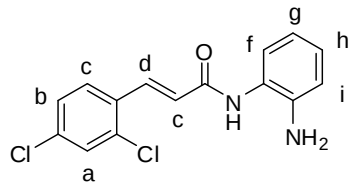

(*E*)-*N*-(2-aminophenyl)-3-(2,4-dichlorophenyl)acrylamide (**51**): yellow powder (400 mg, 56%), R_f=0.54 (DCM/MeOH 9:1), ^{1}H NMR (DMSO-d_6) δ = 9.32 (s, 1H, *NH*), 7.84 (s, 1H, *a*), 7.65 (d, 1H, *c*, $^3J_{HH}$ = 8.1 Hz), 7.55 (d, 1H, *b*, $^3J_{HH}$ = 8.1 Hz), 7.47 (d, 1H, *d*, $^3J_{HH}$ = 15.7 Hz), 7.28 (d, 1H, *f*, $^3J_{HH}$ = 7.6 Hz), 6.82-6.93 (m, 2H, *e/h*), 6.68 (d, 1H, *i*, $^3J_{HH}$ = 7.6 Hz), 6.51 (t, 1H, *g*, $^3J_{HH}$ = 7.6 Hz), 4.89 (s, 2H, NH_2). MS (ESI, 70 eV) m/z (%): 306.9 (100) $[M+H]^+$.

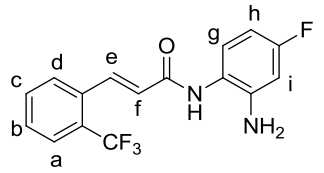

(*E*)-*N*-(2-amino-4-fluorophenyl)-3-(2-(trifluoromethyl)phenyl)acrylamide (**54**): white solid (510 mg, 80%), R_f=0.59 (DCM/MeOH 9:1), ^{1}H NMR (DMSO-d_6) δ = 9.39 (s, 1H, *NH*), 7.84-7.69 (m, 4H, *a/c/d/e*), 7.56 (t, 1H, *b*, $^3J_{HH}$ = 7.5 Hz), 7.26-7.20 (dd, 1H, *g*, $^3J_{HH}$ = 8.3 Hz, $^4J_{HH}$ = 3 Hz), 6.88 (d, 1H, *f*, $^3J_{HH}$ = 15.7 Hz), 6.47 (dd, 1H, *i*, $^3J_{HH}$ = 8.3 Hz, $^4J_{HH}$ = 3.0 Hz), 6.29 (dt, 1H, *h*, $^3J_{HH}$ = 8.3 Hz, $^4J_{HH}$ = 3.0 Hz), 5.23 (s, 2H, NH_2). ^{19}F NMR (DMSO-d_6) δ = -57.71, -116.78. MS (ESI, 70 eV) m/z (%): 325.3 (100) $[M+H]^+$.

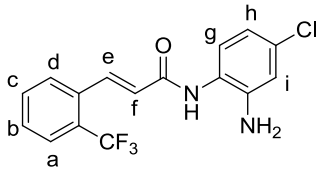

(*E*)-*N*-(2-amino-4-chlorophenyl)-3-(2-(trifluoromethyl)phenyl)acrylamide (**57**): white solid (330 mg, 55%), R_f=0.71 (DCM/MeOH 9:1), ^{1}H NMR (DMSO-d_6) δ = 9.43 (s, 1H, *NH*), 7.84-7.69 (m, 4H, *a/c/d/e*), 7.56 (t, 1H, *b*, $^3J_{HH}$ = 7.5 Hz), 7.32 (d, 1H, *g*, $^3J_{HH}$ = 8.5 Hz), 6.89 (d, 1H, *f*, $^3J_{HH}$ = 15.6 Hz), 6.73 (d, 1H, *i*, $^4J_{HH}$ = 2.5 Hz), 6.52 (dd, 1H, *h*, $^3J_{HH}$ = 8.5 Hz, $^4J_{HH}$ = 2.5 Hz), 5.24 (s, 2H, NH_2). ^{19}F NMR (DMSO-d_6) δ = -57.71. MS (ESI, 70 eV) m/z (%): 341.0 (100) $[M+H]^+$.

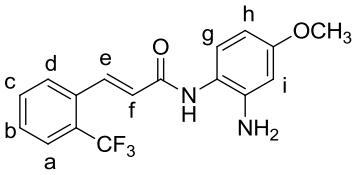

(*E*)-*N*-(2-amino-4-methoxyphenyl)-3-(2-(trifluoromethyl)phenyl)acrylamide (**60**): white solid (330 mg, 55%), R_f=0.55 (DCM/MeOH 9:1), ^{1}H NMR (DMSO-d_6) δ = 9.41 (s, 1H, *NH*), 7.91-7.77 (m, 4H, *a/c/d/e*), 7.63 (t, 1H, *b*, $^3J_{HH}$ = 7.6 Hz), 7.19 (d, 1H, *g*, $^3J_{HH}$ = 8.5 Hz), 6.95 (d, 1H, *f*, $^3J_{HH}$ = 15.5 Hz), 6.35 (d, 1H, *i*, $^4J_{HH}$ = 2.9 Hz), 6.19 (dd, 1H, *h*, $^3J_{HH}$ = 8.5 Hz, $^4J_{HH}$ = 2.9 Hz), 5.01 (s, 2H, NH_2), 3.69 (s, 3H, OCH_3). ^{19}F NMR (DMSO-d_6) δ = -57.71. MS (ESI, 70 eV) m/z (%): 337.0 (100) $[M+H]^+$.

General procedure to synthesize (*E*)-styryl 1*H*-benzo[*d*]imidazoles (**7, 13, 16, 19, 22, 25, 28, 34, 37, 40, 43, 46, 49, 52, 55, 58, 61**):

(*E*)-*N*-(2-aminophenyl)-3-(2-trifluoromethylphenyl)acrylamide (**6**) was suspended in 2 mL of 6 M aqueous hydrochloric acid and 2 ml EtOH. The reaction mixture was heated under microwave irradiation (300 W) during 10 min at 120°C. The reaction was cooled at 4°C and the precipitate formed filtered off and washed with 10 ml water. The crude was purified by recrystallization from EtOH/water 1:1. A yellow solid was obtained as hydrochloride salt.

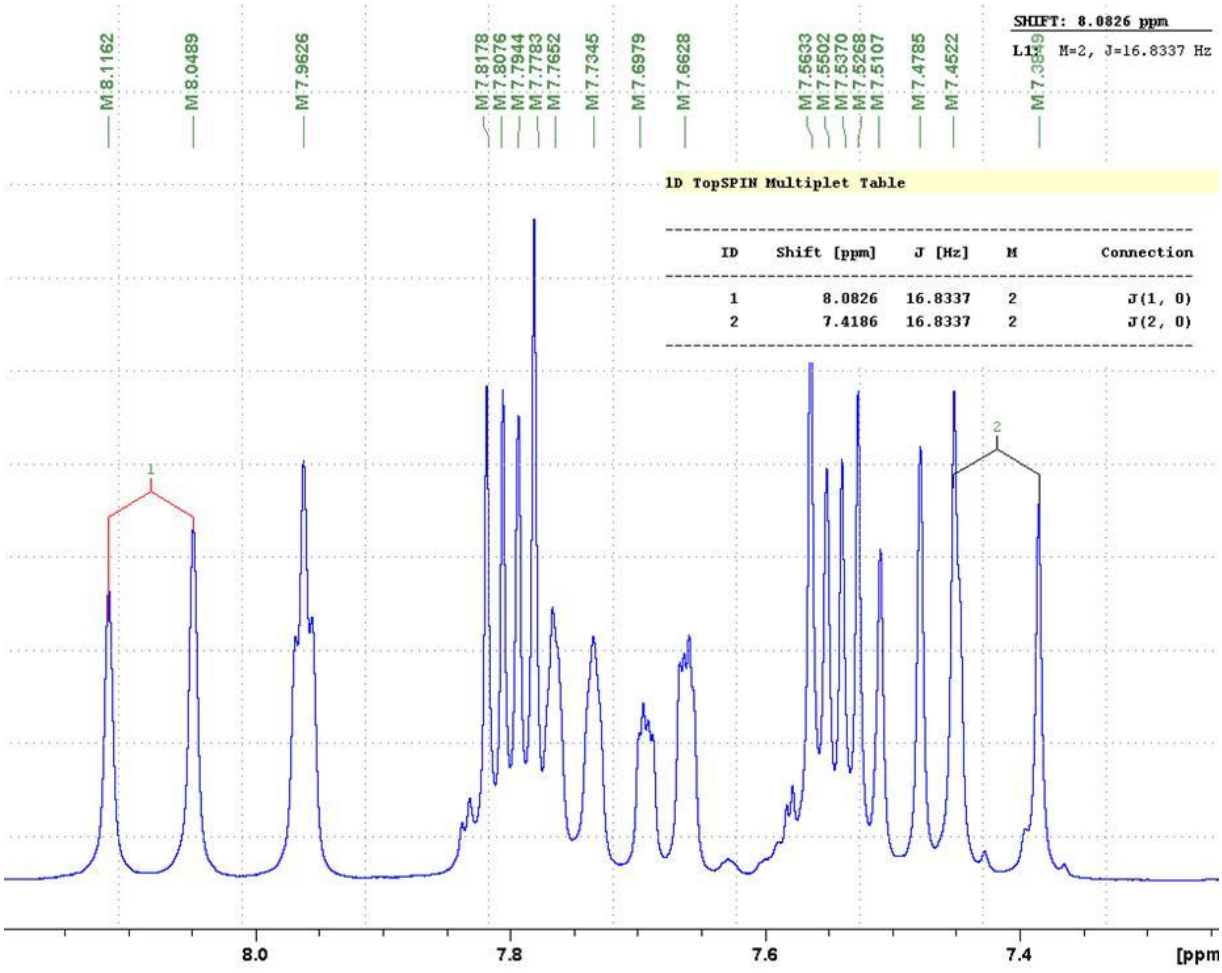

SF 1. *(E)*- geometry of (*E*)-styryl-1*H*-benzo[*d*]imidazoles (as example compound **28**)

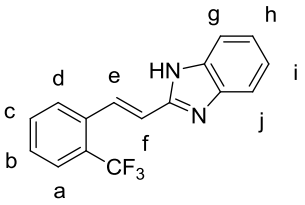

(*E*)-2-(2-(trifluoromethyl)styryl)-1*H*-benzo[*d*]imidazole (**7**): yellow solid (78 mg, 83%), R_f=0.70 (DCM/MeOH 9:1), ^{1}H NMR (DMSO-d_6) δ = 8.09 (dd, 1H, *e*, $^3J_{HH}$ = 16.4 Hz, $^4J_{HH}$ = 2.1 Hz), 8.02 (d, 1H, *a*, $^3J_{HH}$ = 7.7 Hz), 7.82-7.73 (m, 2H, *c/d*), 7.72-7.68 (m, 2H, *g/j*), 7.61 (t, 1H, *b*, $^3J_{HH}$ = 7.7 Hz), 7.42-7.38 (m, 2H, *h/i*), 7.29 (d, 1H, *f*, $^3J_{HH}$ = 16.4 Hz). ^{13}C NMR (DMSO-d_6) δ = 147.45, 135.25, 133.26, 133.08, 130.33, 128.27, 127.22, 126.74, 126.27, 125.47, 121.88, 116.60, 114.27. ^{19}F NMR (DMSO-d_6) δ = -57.44. HRMS-FAB *m/z* calcd for $C_{16}H_{11}F_3N_2$: 289.0947, found: 289.0952. t_R = 5.74 min.

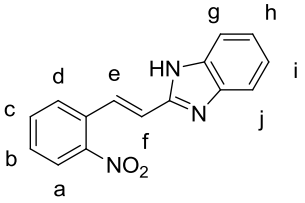

(*E*)-2-(2-nitrostyryl)-1*H*-benzo[*d*]imidazole (**10**): yellow solid (81 mg, 87%), R_f=0.54 (DCM/MeOH 9:1), ^{1}H NMR (DMSO-d_6) δ = 8.21 (d, 1H, *e*, $^3J_{HH}$ = 16.6 Hz), 8.07 (d, 1H, *a*, $^3J_{HH}$ = 7.5 Hz), 7.98 (d, 1H, *d*, $^3J_{HH}$ = 7.5 Hz), 7.83 (t, 1H, *b*, $^3J_{HH}$ = 7. 5 Hz), 7.75-7.72 (m, 2H, *g/j*), 7.68 (t, 1H, *c*, $^3J_{HH}$ = 7.5), 7.48-7.44 (m, 2H, *h/i*), 7.30 (d, 1H, *f*, $^3J_{HH}$ = 16.6 Hz). ^{13}C NMR (DMSO-d_6) δ = 148.27, 147.09, 136.10, 134.11, 132.11, 131.24, 129.15, 128.84, 125.87, 124.80, 115.44, 114.12. HRMS-FAB *m/z* calcd for $C_{15}H_{11}N_3O_2$: 266.0924, found: 266.0925. t_R = 5.70 min.

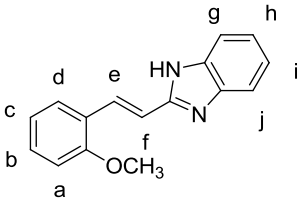

(*E*)-2-(2-methoxystyryl)-1*H*-benzo[*d*]imidazole (**13**): yellow solid (19 mg, 20%), R_f=0.65 (DCM/MeOH 9:1), ^{1}H NMR (DMSO-d_6) δ = 8.19 (d, 1H, *e*, $^3J_{HH}$ = 16.8 Hz), 7.66 (dd, 1H, *d*, $^3J_{HH}$ = 7.5 Hz, $^4J_{HH}$ = 1.3 Hz), 7.48-7.41 (m, 3H, *b/h/i*), 7.33 (d, 1H, *f*, $^3J_{HH}$ = 16.8 Hz), 7.13 (d, 1H, *a*, $^3J_{HH}$ = 8.3 Hz), 7.04 (t, 1H, *c*, $^3J_{HH}$ = 7.5 Hz), 3.89 (s, 3H, *OCH$_3$*). ^{13}C NMR (DMSO-d_6) δ = 158.20, 149.03, 137.37, 132.23, 129.17, 125.42, 122.78, 121.12, 113.89, 112.37, 111.25, 55.84. HRMS-FAB *m/z* calcd for $C_{16}H_{14}N_2O$: 251.1179, found: 251.1186. t_R = 5.77 min.

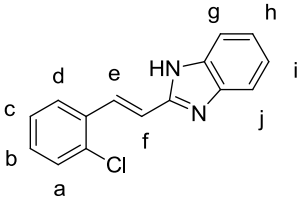

(*E*)-2-(2-chlorostyryl)-1*H*-benzo[*d*]imidazole (**16**): yellow solid (40 mg, 43%), R_f=0.67 (DCM/MeOH 9:1), ^{1}H NMR (DMSO-d_6) δ = 8.12 (d, 1H, *e*, $^3J_{HH}$ = 16.5 Hz), 7.96-7.92 (m, 1H, *a*), 7.68-7.65 (m, 2H, *g/j*), 7.56-7.52 (m, 1H, *d*), 7.44-7.40 (m, 2H, *b/c*), 7.38-7.34 (m, 2H, *h/i*), 7.28 (d, 1H, *f*, $^3J_{HH}$ = 16.5 Hz). ^{13}C NMR (DMSO-d_6) δ =148.33, 137.29, 134.88, 133.94, 133.46, 132.54, 131.60, 130.17, 127.94, 127.27, 124.90, 115.53, 114.26. HRMS-FAB *m/z* calcd for $C_{15}H_{11}ClN_2$: 255.0684, found: 255.0693. t_R = 5.85 min.

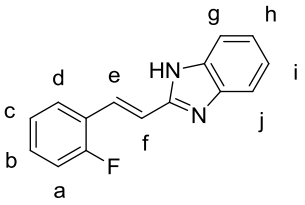

(*E*)-2-(2-fluorostyryl)-1*H*-benzo[*d*]imidazole (**19**): yellow solid (75 mg, 81%), R_f=0.80 (DCM/MeOH 9:1), ^{1}H NMR (DMSO-d_6) δ = 8.14 (d, 1H, *e*, $^3J_{HH}$ = 16.7 Hz), 7.90 (dt, 1H, *b*, $^3J_{HH}$ = 7.7 Hz, $^4J_{HH}$ = 1.7 Hz), 7.79-7.76 (m, 2H, *g/h*), 7.57 (dt, 1H, *d*, $^3J_{HH}$ = 7.7 Hz, $^4J_{HH}$ = 1.7 Hz), 7.51-7.47 (m, 2H, *h/i*), 7.44-7.35 (m, 3H, *a/c/f*). ^{13}C NMR (DMSO-d_6) δ = 162.67, 158.64, 147.89, 134.66, 132.89, 131.76, 129.14, 125.89, 125.40, 121.93, 116.56, 116.27, 113.94, 112.88. ^{19}F NMR (DMSO-d_6) δ = -115.70. HRMS-FAB *m/z* calcd for $C_{15}H_{11}FN_2$: 239.0979, found: 239.0970. t_R = 5.84 min.

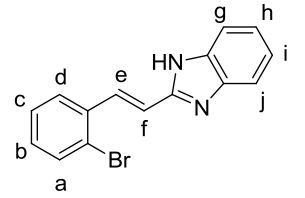

(*E*)-2-(2-bromostyryl)-1*H*-benzo[*d*]imidazole (**22**): yellow solid (1.13 g, 57%), R_f=0.82 (DCM/MeOH 9:1), ^{1}H NMR (DMSO-d_6) δ = 8.26 (d, 1H, *e*, $^3J_{HH}$ = 16.7 Hz), 7.96 (dd, 1H, *a*, $^3J_{HH}$ = 7.9Hz, $^4J_{HH}$ = 1.4 Hz), 7.77-7.81 (m, 3H, *c/g/j*), 7.48-7.58 (m, 3H, *d/h/i*), 7.34-7.45 (m, 2H, *f/b*). ^{13}C NMR (DMSO-d_6) δ = 147.95, 138.28, 134.30, 133.52, 133.28, 131.97, 128.57, 128.08, 125.31, 124.34, 115.06, 114.19. HRMS-FAB *m/z* calcd for $C_{15}H_{11}BrN_2$: 299.0178, found: 299.0185. t_R = 5.80 min.

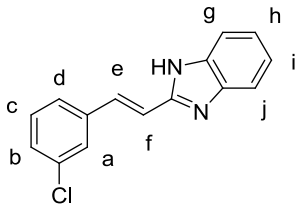

(*E*)-2-(3-chlorostyryl)-1*H*-benzo[*d*]imidazole (**25**): white solid (77 mg, 82%), R_f=0.71 (DCM/MeOH 9:1), ^{1}H NMR (DMSO-d_6) δ = 8.19 (d, 1H, *e*, $^3J_{HH}$ = 16.6 Hz), 7.75-7.74 (m, 2H, *g/j*), 7.72 (d, 1H, *b*, $^3J_{HH}$ = 3.3 Hz), 7.64-7.60 (m, 1H, *c*), 7.50-7.48 (m, 3H, *a/h/i*), 7.46 (d, 1H, *d*, $^3J_{HH}$ = 3.3 Hz), 7.38 (d, 1H, *f*, $^3J_{HH}$ = 16.6 Hz). ^{13}C NMR (DMSO-d_6) δ = 147.70, 140.77, 136.26, 134.00, 131.75, 131.11, 130.39, 127.24, 126.82, 125.86, 113.83, 112.00. HRMS-FAB *m/z* calcd for $C_{15}H_{10}Cl_2N_2$: 255.0684, found: 255.0691. t_R = 5.91 min.

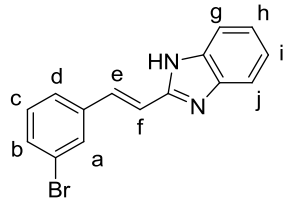

(*E*)-2-(3-bromostyryl)-1*H*-benzo[*d*]imidazole (**29**): white solid (560 mg, 85%), R_f=0.58 (DCM/MeOH 9:1), ^{1}H NMR (DMSO-d_6) δ = 8.08 (d, 1H, *e*, $^3J_{HH}$ = 16.8 Hz), 7.96 (m, 1H, *a*), 7.82-7.78 (m, 2H, *g/j*), 7.75 (d, 1H, *d*, $^3J_{HH}$ = 7.9 Hz), 7.68 (d, 1H, *b*, $^3J_{HH}$ = 7.9 Hz), 7.56-7.53 (m, 2H, *h/i*), 7.49 (d, 1H, *c*, $^3J_{HH}$ = 7.6), 7.42 (d, 1H, *f*, $^3J_{HH}$ = 16.8 Hz). ^{13}C NMR (DMSO-d_6) δ = 147.66, 140.58, 136.41, 133.33, 131.70, 131.32, 130.24, 127.16, 125.97, 122.50, 113.85, 111.84. HRMS-FAB *m/z* calcd for $C_{15}H_{11}BrN_2$: 299.0178, found: 299.0185. t_R = 5.81 min.

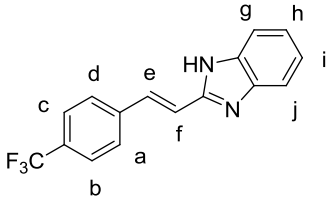

(*E*)-2-(4-(trifluoromethyl)styryl)-1*H*-benzo[*d*]imidazole (**34**): white solid (15 mg, 16%), R_f=0.59 (DCM/MeOH 9:1), ^{1}H NMR (DMSO-d_6) δ = 7.96 (d, 2H, *b/c*, $^3J_{HH}$ = 8.2 Hz), 7.86-7.76 (m, 3H, *a/d/e*), 7.65-7.61 (m, 2H, *g/j*), 7.44 (d, 1H, *f*, $^3J_{HH}$ = 16.8 Hz), 7.28-7.24 (m, 2H, *h/i*). ^{13}C NMR (DMSO-d_6) δ = 150.29, 149.37, 143.72, 132.45, 128.38, 127.59, 125.80, 125.74, 122.33, 120.53. ^{19}F NMR (DMSO-d_6) δ = -60.96. HRMS-FAB *m/z* calcd for $C_{16}H_{11}F_3N_2$: 289.0947, found: 289.0949. t_R = 5.78 min.

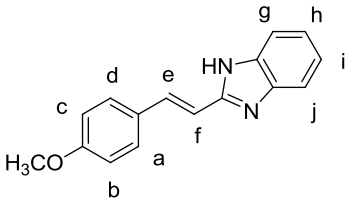

(*E*)-2-(4-methoxystyryl)-1*H*-benzo[*d*]imidazole (**37**): yellow solid (44 mg, 47%), R_f=0.63 (DCM/MeOH 9:1), ^{1}H NMR (DMSO-d_6) δ = 8.14 (d, 1H, *e*, $^3J_{HH}$ = 16.6 Hz), 7.72-7.69 (m, 2H, *g/j*), 7.64 (d, 2H, *a/d*, $^3J_{HH}$ = 7.8 Hz), 7.47-7.45 (m, 2H, *h/i*), 7.11 (d, 1H, *f*, $^3J_{HH}$ = 16.6 Hz), 7.03 (d, 2H, *b/c*, $^3J_{HH}$ = 7.8 Hz), 3.78 (s, 3H, *OCH$_3$*). ^{13}C NMR (DMSO-d_6) δ = 161.68, 148.65, 142.68, 131.47, 130.02, 126.66, 125.65, 114.88, 113.54, 107.08, 55.50. HRMS-FAB *m/z* calcd for $C_{16}H_{14}N_2O$: 251.1179, found: 251.1185. t_R = 5.78 min.

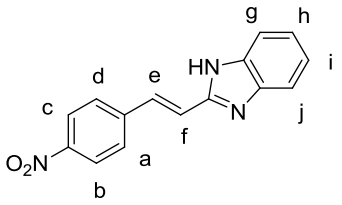

(*E*)-2-(4-nitrostyryl)-1*H*-benzo[*d*]imidazole (**40**): yellow solid (81 mg, 87%), R_f=0.64 (DCM/MeOH 9:1), ^{1}H NMR (DMSO-d_6) δ = 8.38-8.29 (m, 3H, *b/c/e*), 8.01 (d, 2H, *a/d*, $^3J_{HH}$ = 8.9 Hz), 7.85-7.81 (m, 2H, *g/j*), 7.60-7.53 (m, 3H, *f/h/i*). ^{13}C NMR (DMSO-d_6) δ = 148.09, 147.46, 140.47, 139.15, 132.35, 129.00, 125.89, 124.39, 115.06, 114.09. HRMS-FAB *m/z* calcd for $C_{15}H_{11}N_3O_2$: 266.0924, found: 266.0925.

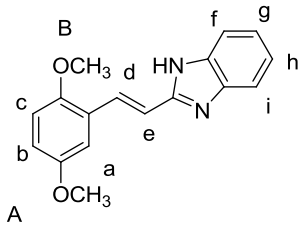

(*E*)-2-(2,5-dimethoxystyryl)-1*H*-benzo[*d*]imidazole (**43**): yellow solid (34 mg, 36%), R_f=0.77 (DCM/MeOH 9:1), ^{1}H NMR (DMSO-d_6) δ = 8.25 (d, 1H, *d*, $^3J_{HH}$ = 16.7 Hz), 7.73-7.70 (m, 2H, *f/i*), 7.48-7.37 (m, 3H, *e/g/h*), 7.16 (d, 1H, *b*, $^3J_{HH}$ = 2.4 Hz), 7.08-6.99 (m, 2H, *a/c*), 3.83 (s, 3H, *B*), 3.73 (s, 3H, *A*). ^{13}C NMR (DMSO-d_6) δ = 153.31, 152.70, 148.59, 137.88, 131.59, 125.78, 123.18, 117.98, 113.67, 113.47, 110.90, 56.31, 55.63. HRMS-FAB *m/z* calcd for $C_{17}H_{16}N_2O_2$: 281.1285, found: 281.1291. t_R = 5.76 min.

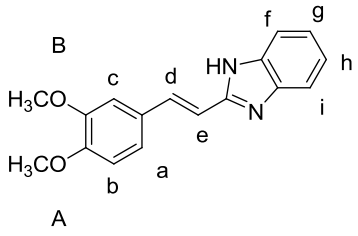

(*E*)-2-(3,4-dimethoxystyryl)-1*H*-benzo[*d*]imidazole (**46**): yellow solid (52 mg, 55%), R_f=0.82 (DCM/MeOH 9:1), ^{1}H NMR (DMSO-d_6) δ = 8.08 (d, 1H, *d*, $^3J_{HH}$ = 16.6 Hz), 7.73-7.69 (m, 2H, *f/i*), 7.44-7.47 (m, 2H, *g/h*), 7.19-7.12 (m, 3H, *a/c/e*), 7.04 (d, 1H, *b*, $^3J_{HH}$ = 8.6 Hz), 3.81 (s, 3H, *B*), 3.78 (s, 3H, *A*). ^{13}C NMR (DMSO-d_6) δ = 151.65, 149.24, 148.66, 142.96, 131.60, 126.88, 125.61, 123.23, 113.58, 111.96, 109.90, 107.39, 55.73, 55.69. HRMS-FAB *m/z* calcd for $C_{17}H_{16}N_2O_2$: 281.1285, found: 281.1290. t_R = 5.74 min.

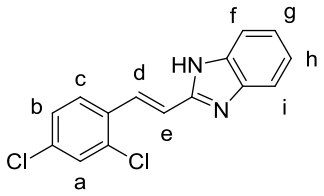

(*E*)-2-(2,4-dichlorostyryl)-1*H*-benzo[*d*]imidazole (**49**): yellow solid (44 mg, 47%), R_f=0.63 (DCM/MeOH 9:1), ^{1}H NMR (DMSO-d_6) δ = 8.04-7.98 (m, 2H, *c/d*), 7.74-7.70 (m, 3H, *a/f/i*), 7.65 (dd, 2H, *b*, $^3J_{HH}$ = 8.3 Hz, $^4J_{HH}$ = 1.7 Hz), 7.47-7.43 (m, 2H, *g/h*), 7.38 (d, 1H, *e*, $^3J_{HH}$ = 16.6 Hz). ^{13}C NMR (DMSO-d_6) δ =147.73, 134.91, 132.82, 132.43, 132.01, 131.31, 129.33, 128.12, 125.61, 114.04, 113.32. HRMS-FAB *m/z* calcd for $C_{15}H_{10}Cl_2N_2$: 289.0294, found: 289.0305. t_R = 6.06 min.

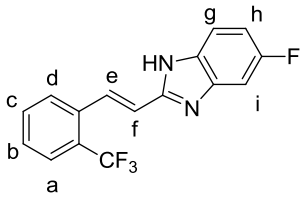

(*E*)-5-fluoro-2-(2-(trifluoromethyl)styryl)-1*H*-benzo[*d*]imidazole (**52**): white solid (87 mg, 92%), R_f=0.54 (DCM/MeOH 9:1), ^{1}H NMR (DMSO-d_6) δ = 8.16 (dd, 1H, *e*, $^3J_{HH}$ = 16.2 Hz, $^4J_{HH}$ = 2.0 Hz), 8.01 (d, 1H, *a*, $^3J_{HH}$ = 7.9 Hz), 7.82-7.72 (m, 3H, *c/d/g*), 7.63 (d, 1H, *b*, $^3J_{HH}$ = 7.9 Hz), 7.58 (dd, 1H, *i*, $^3J_{HH}$ = 8.9 Hz, $^4J_{HH}$ = 2.3 Hz), 7.35-7.27 (m, 2H, *f/h*). ^{13}C NMR (DMSO-d_6) δ = 161.56, 158.56, 148.75, 135.33, 133.31, 132.97, 130.42, 128.23, 126.83, 126.21, 125.86, 122.18, 116.39, 115.60, 113.76, 100.51. ^{19}F NMR (DMSO-d_6) δ = -57.44, -115.16. HRMS-FAB *m/z* calcd for $C_{16}H_{10}F_4N_2$: 307.0853, found: 307.0859. t_R = 5.89 min.

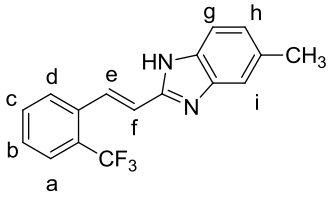

(*E*)-5-methyl-2-(2-(trifluoromethyl)styryl)-1*H*-benzo[*d*]imidazole (**55**): white solid (29 mg, 31%), R_f=0.66 (DCM/MeOH 9:1), ^{1}H NMR (MeOD-d_4) δ = 8.14 (dd, 1H, *e*, $^3J_{HH}$ = 16.5 Hz, $^4J_{HH}$ = 2.0 Hz), 7.96 (d, 1H, *a*, $^3J_{HH}$ = 7.8 Hz), 7.75 (d, 1H, *d*, $^3J_{HH}$ = 7.8 Hz), 7.69 (t, 1H, *b*, $^3J_{HH}$ = 7.8 Hz), 7.60-7.54 (m, 2H, *c/g*), 7.47 (s, 1H, *i*), 7.33 (dd, 1H, *h*, $^3J_{HH}$ = 8.4 Hz, $^4J_{HH}$ = 1.4 Hz), 7.19(d, 1H, *f*, $^3J_{HH}$ = 16.5 Hz) 2.46 (s, 3H, *CH$_3$*). ^{13}C NMR (DMSO-d_6) δ = 146.86, 135.77, 132.85, 130.40, 128.26, 126.72, 126.30, 116.25, 113.51, 21.21. ^{19}F NMR (DMSO-d_6) δ = -57.44. HRMS-FAB *m/z* calcd for $C_{17}H_{13}F_3N_2$: 303.1104, found: 303.1112. t_R = 5.78 min.

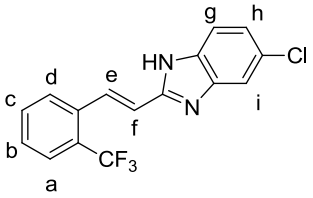

(*E*)-5-chloro-2-(2-(trifluoromethyl)styryl)-1*H*-benzo[*d*]imidazole (**58**): grey solid (62 mg, 66%), R_f=0.85 (alumina, DCM/MeOH 9:1), ^{1}H NMR (DMSO-d_6) δ = 8.21 (dd, 1H, *e*, $^3J_{HH}$ = 16.3 Hz, $^4J_{HH}$ = 2.0 Hz), 7.99 (d, 1H, *a*, $^3J_{HH}$ = 7.8 Hz), 7.82-7.72 (m, 4H, *c/d/g/i*), 7.62 (t, 1H, b, $^3J_{HH}$ = 7.8 Hz), 7.45 (dd, 1H, *h*, $^3J_{HH}$ = 8.8 Hz, $^4J_{HH}$ = 2.0 Hz), 7.33 (d, 1H, *f*, $^3J_{HH}$ = 16.3 Hz. ^{13}C NMR (DMSO-d_6) δ =148.87, 135.37, 133.26, 132.37, 130.33, 129.49, 128.24, 127.18, 126.28, 125.51, 116.76, 115.71, 114.03. ^{19}F NMR (DMSO-d_6) δ = -57.41. HRMS-FAB *m/z* calcd for $C_{16}H_{10}ClF_3N_2$: 323.0557, found: 323.0569. t_R = 5.75 min.

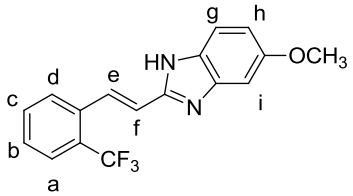

(*E*)-5-methoxy-2-(2-(trifluoromethyl)styryl)-1*H*-benzo[*d*]imidazole (**61**): green solid (30 mg, 32%), R_f=0.50 (DCM/MeOH 9:1), ^{1}H NMR (DMSO-d_6) δ = 8.18 (dd, 1H, *e*, $^3J_{HH}$ = 16.3 Hz, $^4J_{HH}$ = 1.7 Hz), 7.98 (d, 1H, *a*, $^3J_{HH}$ = 7.5 Hz), 7.82-7.75 (m, 2H, *c/d*), 7.68-7.60 (m, 2H, *b/g*), 7.32 (d, 1H, *f*, $^3J_{HH}$ = 16.3 Hz), 7.17 (d, 1H, *i*, $^4J_{HH}$ = 2.1 Hz), 7.10 (dd, 1H, *h*, $^3J_{HH}$ = 9.2 Hz, $^4J_{HH}$ = 2.1 Hz), 3.82 (s, 3H, *CH$_3$*). ^{13}C NMR (DMSO-d_6) δ = 158.10, 146.44, 135.21, 133.14, 130.44, 128.28, 126.71, 115.79, 115.07, 96.19, 55.92. ^{19}F NMR (DMSO-d_6) δ = -57.41. HRMS-FAB *m/z* calcd for $C_{17}H_{13}F_3N_2O$: 319.1053, found: 319.1057. t_R = 5.78 min.

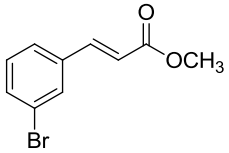

Synthesis of (*E*)-methyl 3-(3-bromophenyl)acrylate (**63**):

(*E*)-3-bromocinnamic acid 1 g (4.40 mmol, 1 eq) (**62**) was dissolved in 10 mL MeOH. To the solution 1 ml H_2SO_4 (conc) was added. The reaction was refluxed during 24 h. The reaction was neutralized with a saturated $NaHCO_3$ solution and the organic phase extracted with 15 ml x 2 EtOAc. The organic phase is washed with 25 ml brine and dried over $MgSO_4$. The solvent was removed under reduced pressure to obtain colorless oil (0.74 g, 79%). R_f=0.71 (DCM), ^{1}H NMR (DMSO-d_6) δ = 7.94 (s, 1H), 7.71 (d, 1H, $^3J_{HH}$ = 6.7 Hz), 7.64-7.57 (m, 2H), 7.35 (t, 1H, $^3J_{HH}$ = 6.7 Hz), 6.70 (d, 1H, $^3J_{HH}$ = 13.4 Hz), 3.72 (s, 3H). MS (ESI, 70 eV) m/z (%): 242.6 (100) $[M+H]^+$.

Synthesis via Suzuki coupling (**64**, **65**, **66**):

(*E*)-methyl 3-(3-bromophenyl)acrylate (**63**) 0.50 g (2.04 mmol, 1 eq) and furan-2-boronic acid 0.46 g (4.15 mmol, 2 eq) were added to a solution of 13 mL toluene, 3 mL EtOH and 3 mL aqueous 1 M Na_2CO_3 solution and stirred during 30 min at r.t. To the solution 0.24 g (0.21 mmol, 0.1 eq) of tetrakis(triphenylphosphine)palladium(0) were added. The reaction mixture was heated at 85°C overnight and after cooling to r.t. extracted with 15 mL x 3 EtOAc. The organic phase was washed with 20 ml brine and dried over $MgSO_4$. The solvent was removed under reduced pressure and the crude purified by flash (Hexane / EtOAc: 0-10 % EtOAc).

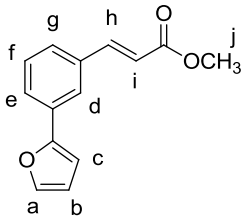

(*E*)-methyl 3-(3-(furan-2-yl)phenyl)acrylate (**64**): white solid (460 mg, 26%), R_f=0.46 (Hexane/EtOAc 5:1), ^{1}H NMR (DMSO-d_6) δ = 8.06 (s, 1H, *d*), 7.79-7.64 (m, 4H, *a/e/g/h*), 7.48 (t, 1H, *f*, $^3J_{HH}$ = 7.6 Hz), 7.09 (d, 1H, *c*, $^3J_{HH}$ = 3.1 Hz), 6.77 (d, 1H, *i*, $^3J_{HH}$ = 16.1 Hz), 6.63 (dd, 1H, *b*, $^3J_{HH}$ = 2.0 Hz), 3.76 (s, 3H, *j*). MS (ESI, 70 eV) *m/z* (%): 251.2 (100) $[M+Na]^+$.

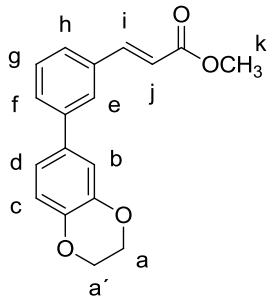

(*E*)-methyl 3-(3-(2,3-dihydrobenzo[*b*][1,4]dioxin-6-yl)phenyl)acrylate (**65**): white solid (237 mg, 29%), R_f=0.42 (Hexane/EtOAc 3:1), ^{1}H NMR (DMSO-d_6): δ = 7.95 (s, 1H, *d*), 7.72 (d, 1H, *i*, $^3J_{HH}$ = 15.7 Hz), 7.65 (dd, 2H, *f/h*, $^3J_{HH}$ = 7.9), 7.45 (t, 1H, *g*, $^3J_{HH}$ = 7.9 Hz), 7.26 (d, 1H, *b*, $^4J_{HH}$ = 2.3 Hz), 7.21, (dd, 1H, *d*, $^3J_{HH}$ = 8.1 Hz, $^4J_{HH}$ = 2.3 Hz), 6.94 (d, 1H, *c*, $^3J_{HH}$ = 8.1 Hz), 6.77 (d, 1H, *j*, $^3J_{HH}$ = 15.7 Hz), 4.28 (s, 4H, *a/a´*), 3.74 (s, 3H, *k*). MS (ESI, 70 eV) *m/z* (%): 297.2 (100) $[M+H]^+$.

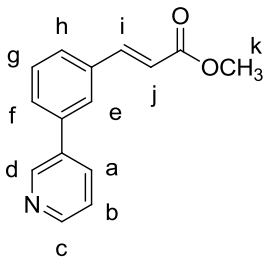

(*E*)-methyl 3-(3-(pyridin-3-yl)phenyl)acrylate (**66**): white solid (475 mg, 49%), R_f=0.53 (DCM/MeOH 9:1), ^{1}H NMR (DMSO-d_6): δ = 8.99 (s, 1H, *d*), 8.61 (dd, 1H, *c*, $^3J_{HH}$ = 4.7 Hz, $^4J_{HH}$ = 1.7 Hz), 8.20-8.14 (m, 2H, *a/e*), 7.84-7.74 (m, 3H, *b/h/i*), 7.60-7.49 (m, 2H, *f/g*), 6.85 (d, 1H, *j*, $^3J_{HH}$ = 16.1 Hz), 3.76 (s, 3H, *k*). MS (ESI, 70 eV) *m/z* (%): 240.6 (100) $[M+H]^+$.

<u>Hydrolysis of compounds **64**-**66**:</u>

120 mg (0.53 mmol, 1 eq) of (*E*)-methyl 3-(3-(furan-2-yl)phenyl)acrylate (**64**) were dissolved in 4 mL MeOH. The reaction mixture was heated at 35°C and 84 mg (1.50 mmol, 2.85 eq) KOH were added. The reaction was stirred during 3.5 h and 6 mL of water were added. The unreacted ester was eliminated by extracting with Et_2O (2 x 3 mL) and the aqueous phase was acidified to pH 2 to obtain a precipitate which was dried under vacuum.

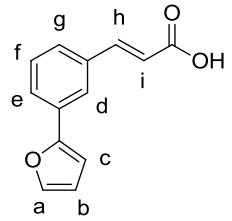

(*E*)-3-(3-(furan-2-yl)phenyl)acrylic acid (**67**): white solid (110 mg, 95%), R_f=0.05 (DCM), ^{1}H NMR (DMSO-d_6) δ = 8.02 (s, 1H, *d*), 7.79 (d, 1H, *a*, $^3J_{HH}$ = 1.9 Hz), 7.74 (d, 1H, *e*, $^3J_{HH}$ = 8.1 Hz), 7.67-7.61 (m, 2H, *g/h*), 7.48 (t, 1H, *f*, $^3J_{HH}$ = 7.6 Hz), 7.09 (d, 1H, *c*, $^3J_{HH}$ = 3.5 Hz), 6.67-6.61 (m, 2H, *b/i*). MS (ESI, 70 eV) *m/z* (%): 213.1 (100) $[M-H]^-$.

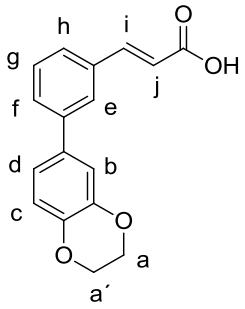

(*E*)-3-(3-(2,3-dihydrobenzo[*b*][1,4]dioxin-6-yl)phenyl)acrylic acid (**68**): white solid (197 mg, 87%), R_f=0.72 (DCM/MeOH 9:1), ^{1}H NMR (DMSO-d_6): δ = 7.96 (s, 1H, *d*), 7.73-7.66 (m, 3H, *i/f/h*), 7.50 (t, 1H, *g*, $^3J_{HH}$ = 7.6 Hz), 7.30 (d, 1H, *b*, $^4J_{HH}$ = 2.2 Hz), 7.26, (dd, 1H, *d*, $^3J_{HH}$ = 8.0 Hz, $^4J_{HH}$ = 2.2 Hz), 6.99 (d, 1H, *c*, $^3J_{HH}$ = 8.0 Hz), 6.71 (d, 1H, *j*, $^3J_{HH}$ = 16.0 Hz), 4.33 (s, 4H, *a/a´*). MS (ESI, 70 eV) *m/z* (%): 283.2 (100) $[M+H]^+$.

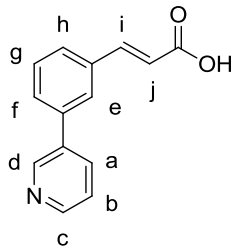

(*E*)-3-(3-(pyridin-3-yl)phenyl)acrylic acid (**69**): white solid (288 mg, 64%), R_f=0.18 (Hexane/EtOAc 1:2), ^{1}H NMR (DMSO-d_6): δ = 9.00 (d, 1H, *d*, $^4J_{HH}$ = 1.6 Hz), 8.62 (dd, 1H, *c*, $^3J_{HH}$ = 4.7 Hz, $^4J_{HH}$ = 1.6 Hz), 8.21 (dq, 1H, *a*, $^3J_{HH}$ = 8.0 Hz, $^4J_{HH}$ = 1.6 Hz), 8.10 (s, 1H, *e*), 7.79-7.69 (m, 2H, *f/g*), 7.69 (d, 1H, *i*, $^3J_{HH}$ = 15.8 Hz), 7.60-7.53 (m, 2H, *b/h*), 6.72 (d, 1H, *j*, $^3J_{HH}$ = 15.8 Hz). MS (ESI, 70 eV) *m/z* (%): 224.6 (100) $[M-H]^-$.

Compounds **70-72** were synthesized following the same procedure as with compounds **6, 9, 12, 15, 18, 21, 24, 27, 33, 36, 39, 42, 45, 48, 51, 54, 57, 60**.

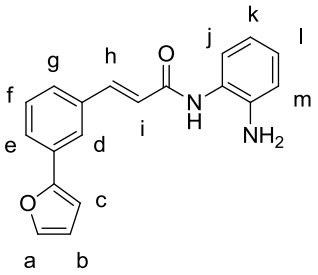

(*E*)-*N*-(2-aminophenyl)-3-(3-furanphenyl)acrylamide (**70**): yellow solid (490 mg, 32%), R_f=0.59 (DCM/MeOH 9:1),^{1}H NMR (DMSO-d_6) δ = 9.42 (s, 1H, *NH*), 7.99 (s, 1H, *d*), 7.81-7.73 (m, 2H, *a/e*), 7.64-7.51 (m, 3H, *f/g/h*), 7.39 (d, 1H, *j*, $^3J_{HH}$ = 8.2 Hz), 7.05-6.98 (m, 2H, *c/i*), 6.92 (dd, 1H, *e*, $^3J_{HH}$ = 8.2 Hz, $^4J_{HH}$ = 1.3 Hz), 6.77 (dd, 1H, *k*, $^3J_{HH}$ = 8.2 Hz, $^4J_{HH}$ = 1.3 Hz), 6.66-6.57 (m, 2H, *b/m*), 4.98 (s, 2H, NH_2). MS (ESI, 70 eV) *m/z* (%): 327.2 (100) $[M+Na]^+$.

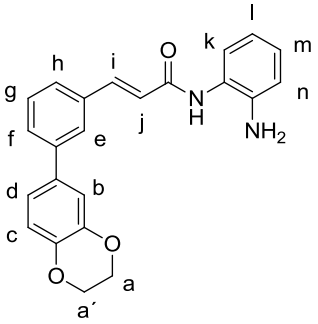

(*E*)-*N*-(2-aminophenyl)-3-(3-(2,3-dihydrobenzo[*b*][1,4]dioxin-6-yl)phenyl)acrylamide (**71**): white solid (20 mg, 8%), R_f=0.69 (Hexane/EtOAc 1:2), ^{1}H NMR (DMSO-d_6): δ = 9.44 (s, 1H, *NH*), 7.89 (s, 1H, *e*), 7.70-7.51 (m, 4H, *f/g/h/i*), 7.42 (d, 1H, *k*, *J* = 7.5 Hz), 7.27-7.24 (m, 2H, *b/d*), 7.08-6.95 (m, 3H, *c/j/m*), 6.81 (d, 1H, *n*, *J* = 8.3 Hz), 6.64 (t, 1H, *l*, *J* = 7.5 Hz), 5.01 (s, 2H, NH_2), 4.34 (s, 4H, *a/a´*). MS (ESI, 70 eV) *m/z* (%): 373.5 (100) $[M+H]^+$.

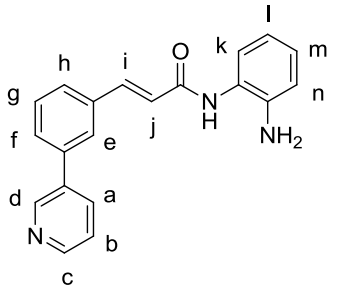

(*E*)-*N*-(2-aminophenyl)-3-(3-(pyridin-3-yl)phenyl)-acrylamide (**72**): white solid (91 mg, 23%), R_f=0.17 (Hexane/EtOAc 1:5), ^{1}H NMR (DMSO-d_6): δ = 9.40 (s, 1H, *NH*), 8.97 (d, 1H, *d*, $^4J_{HH}$ = 2.0 Hz), 8.63 (dd, 1H, *c*, $^3J_{HH}$ = 4.7 Hz, $^4J_{HH}$ = 2.0 Hz), 8.16 (dq, 1H, *a*, $^3J_{HH}$ = 8.2 Hz, $^4J_{HH}$ = 2.0Hz), 8.00 (s, 1H, *e*), 7.79 (d, 1H, *h*, $^3J_{HH}$ = 7.3 Hz), 7.72-7.51 (m, 4H, *b/f/g/i*), 7.38 (d, 1H, *k*, $^3J_{HH}$ = 7.6 Hz), 7.04 (d, 1H, *j*, $^3J_{HH}$ = 15.7 Hz), 6.94 (dt, 1H, *m*, $^3J_{HH}$ = 7.6 Hz, $^4J_{HH}$ = 1.4 Hz), 6.78 (dd, 1H, *n*, $^3J_{HH}$ = 7.6 Hz, $^4J_{HH}$ = 1.4 Hz), 6.60 (dt, 1H, *l*, $^3J_{HH}$ = 7.6 Hz, $^4J_{HH}$ = 1.4 Hz), 4.97 (s, 2H, *NH*$_2$). MS (ESI, 70 eV) *m/z* (%): 316.4 (100) $[M+H]^+$.

Compounds **73-75** were synthesized following the same procedure as with compounds **7, 13, 16, 19, 22, 25, 28, 34, 37, 40, 43, 46, 49, 52, 55, 58, 61**

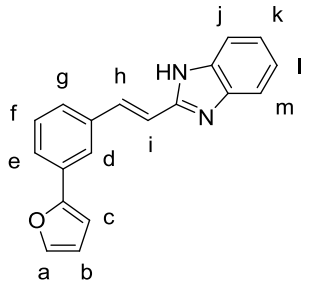

(*E*)-2-(3-(furan-2-yl)styryl)-1*H*-benzo[*d*]imidazole (**73**): orange solid (120 mg, 34%), R_f=0.38 (DCM/MeOH 9:1), ^{1}H NMR (DMSO-d_6) δ = 8.17 (d, 1H, *h*, $^3J_{HH}$ = 16.7 Hz), 8.05 (s, 1H, *d*), 7.87-7.81 (m, 4H, *a/e/j/m*), 7.69 (dd, 1H, *f*, $^3J_{HH}$ = 7.7 Hz), 7.62 (d, 1H, *g*, $^3J_{HH}$ = 7.7 Hz), 7.57-7.54 (m, 2H, *k/l*), 7.45 (d, 1H, *i*, $^3J_{HH}$ = 16.7 Hz), 7.12 (d, 1H, *c*, $^3J_{HH}$ = 3.1 Hz), 6.68 (dd, 1H, *b*, $^3J_{HH}$ = 3.1 Hz, $^3J_{HH}$ = 1.4 Hz). ^{13}C NMR (DMSO-d_6) δ = 152.13, 148.23, 143.47, 134.77, 132.09, 131.21, 129.97, 126.98, 125.71, 122.43, 113.91, 112.25, 106.92. HRMS-FAB *m/z* calcd for $C_{19}H_{14}N_2O$: 287.1179, found: 287.1185.

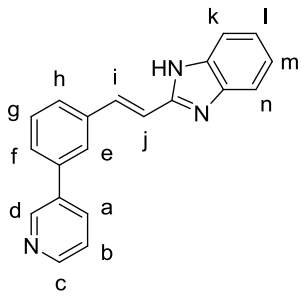

(*E*)-2-(3-(pyridin-3-yl)styryl)-1*H*-benzo[*d*]imidazole (**74**): yellow solid (50 mg, 58%), R_f=0.63 (DCM/MeOH 5:1), ^{1}H NMR (DMSO-d_6): δ = 8.93 (d, 1H, *d*, $^3J_{HH}$ = 1.9 Hz), 8.56 (dd, 1H, *c*, $^3J_{HH}$ = 4.7 Hz, $^4J_{HH}$ = 1.3 Hz), 8.12 (dt, 1H, *a*, $^3J_{HH}$ = 8.0 Hz, $^4J_{HH}$ = 1.9 Hz), 7.98 (s, 1H, *e*), 7.72 (d, 1H, *i*, $^3J_{HH}$ = 16.7 Hz), 7.69-7.66 (m, 2H, *f/h*), 7.55-7.51 (m, 3H, *g/k/n*), 7.48 (dd, 1H, *b*, $^3J_{HH}$ = 8.0 Hz, $^4J_{HH}$ = 4.7 Hz), 7.34 (d, 1H, *j*, $^3J_{HH}$ = 16.7 Hz), 7.18-7.16 (m, 2H, *l/m*). ^{13}C NMR (DMSO-d_6): δ = 150.51, 148.64, 147.71, 137.81, 136.51, 135.22, 134.91, 134.39, 129.83, 127.55, 126.87, 125.74, 123.92, 122.57, 117.65, 114.75. HRMS *m/z* calcd for $C_{20}H_{15}N_3$: 298.1339, found 298.1341. t_R = 5.79 min.

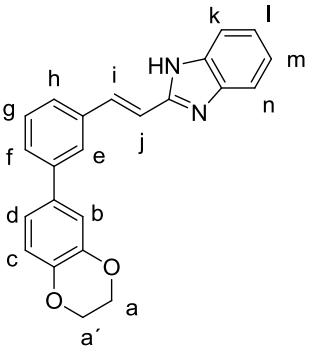

(*E*)-2-(3-(2,3-dihydrobenzo[*b*][1,4]dioxin-6-yl)styryl)-1*H*-benzo[*d*]imidazole (**75**): white solid (12 mg, 63%), R_f=0.76 (DCM/MeOH 9:1), ^{1}H NMR (DMSO-d_6): δ = 8.27 (d, 1H, *i*, $^3J_{HH}$ = 16.6 Hz), 7.99 (s, 1H, *e*), 7.89-7.85 (m, 2H, *k/n*), 7.81-7.73 (m, 2H, *g/h*), 7.67-7.59 (m, 3H, *f/l/m*), 7.52 (d, 1H. *j*, $^3J_{HH}$ = 16.6 Hz), 7.33-7.27 (m, 2H, *c/d*), 7.05 (d, 1H, $^3J_{HH}$ = 8.1 Hz), 4.36 (s, 4H, *a/a´*). ^{13}C NMR (DMSO-d_6): δ = 148.33, 143.77, 143.56, 140.59, 134.75, 132.63, 132.05, 129.82, 126.85, 125.68, 119.68, 117.62, 115.39, 113.90, 110.96, 64.21. HRMS *m/z* calcd for $C_{23}H_{18}N_2O_2$: 355.1447, found: 355.1441. t_R = 5.87 min.

Synthesis of compound **2** (ST-920)

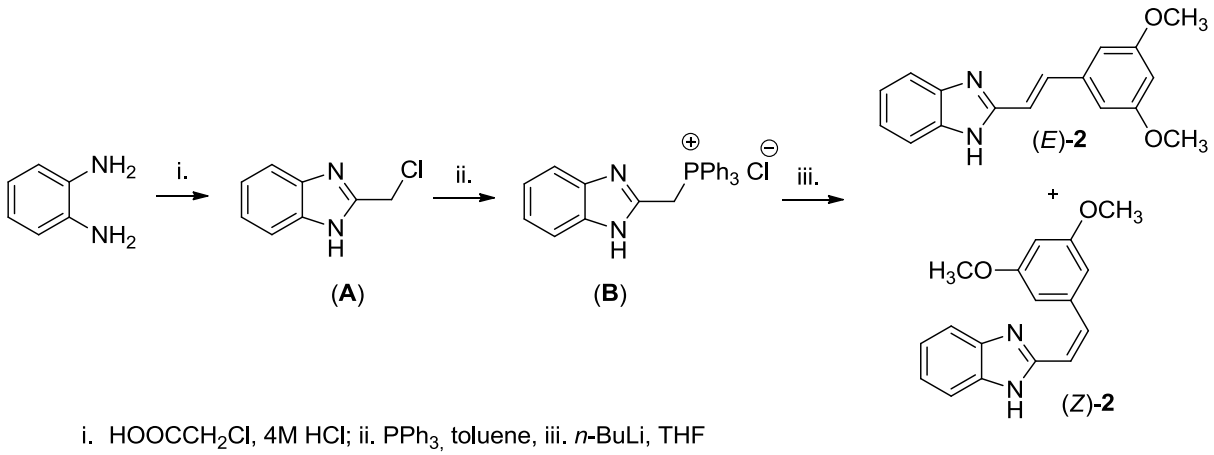

i. $HOOCCH_2Cl$, 4M HCl; ii. PPh_3, toluene, iii. *n*-BuLi, THF

SF 2. Synthesis followed for compound **2**.

The synthesis of the compound (*E*)-**2** was done following the reaction scheme shown above. The compounds A and B were synthesized following the literature procedures.[1] The isomers (*E*) and (*Z*) of compound **2** were synthesized according to the general literature procedure[2] for styrene synthesis. We describe here only analytical data for *E*-isomer, *Z*-isomer will be described elsewhere.

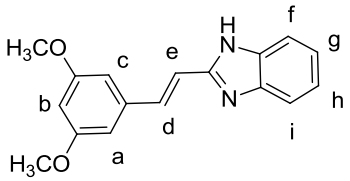

(*E*)-2-(3,5-dimethoxystyryl)-1*H*-benzo[*d*]imidazole (**2**):

A homogeneous suspension of phosphoniumchloride (**B**) (3.70 g, 8.64 mmol, 1 eq) in THF (100 mL) under argon was cooled and retained at -23 °C for 1 h. *n*-Butyllithium (5.40 mL, 8.64 mmol, 1 eq of a 1.6 M solution in hexanes) was added dropwise via syringe, and the resultant red solution was stirred at -23 °C for 60 min, at which time the 3,5-dimethoxybenzaldehyde (1.44 g, 8.64 mmol, 1 eq) in 100 mL of dry THF was added (dropwise) from an addition funnel. Stirring was continued at -23 °C for 3 h and at room temperature for 16 h. By this time, the red color had completely disappeared. Ice-water (100 mL) was added to the mixture, and the aqueous phase was washed with ether (3 x 100 mL). The combined organic phases was washed with water (100 mL) and dried. Removal of solvent *in vacuo* yielded a crude residue, which was subjected to column chromatography (silica gel; eluent 1-5% MeOH in DCM) to afford the pure isomeric product as slower migrating isomer as light yellow powder (993 mg, 41%), R_f=0.16 (DCM/MeOH 95:5), ^{1}H NMR

(DMSO-d_6) δ =12.60 (s, 1H, NH), 7.60 (d, 1H, *d*, $^3J_{HH}$ = 10.3 Hz), 7.61-7.48 (m, 2H, *f/i*), 7.30 (d, 1H, *e*, $^3J_{HH}$ = 10.4 Hz), 7.17-7.23 (m, 3H, *g/h*), 6.81 (d, 1H, *a/c*, $^3J_{HH}$ = 1.3 Hz), 6.60 (t, 21H, b^3J_{HH} = 1.5 Hz,), 3.84 (s, 6H, A/*B*); ^{13}C NMR (DMSO-d_6) δ = 154.31, 152.80, 150.59, 137.98, 131.59, 125.78, 123.18, 118.98, 113.67, 113.47, 110.90, 56.31, 55.63. MS (ESI, 70 eV) *m/z* (%): 281.1 (100) $[M+H]^+$. Elemental Analysis calcd. for $C_{17}H_{16}N_2O_2$: C (72.84), H (5.75), N (9.99), found: C (72.51), H (6.08), N (9.60).

IPS (**1**) was isolated from *Photorhabdus luminescens* strain TT01 as previously described.[3]

- In-house compounds screened

Resveratrol and Chalcone analogues

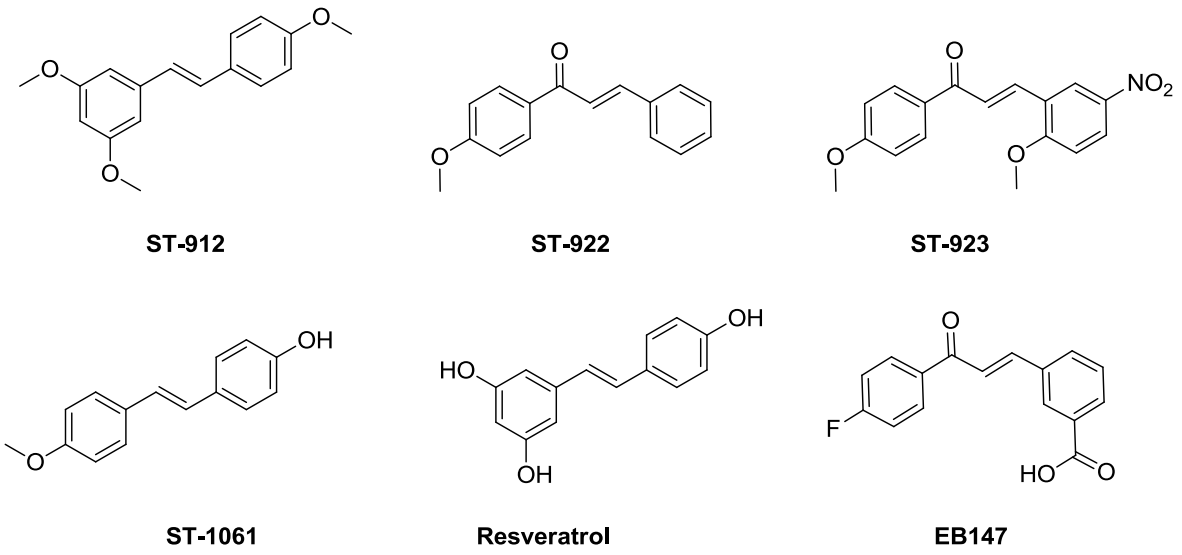

SF 3. In-house compounds screened.

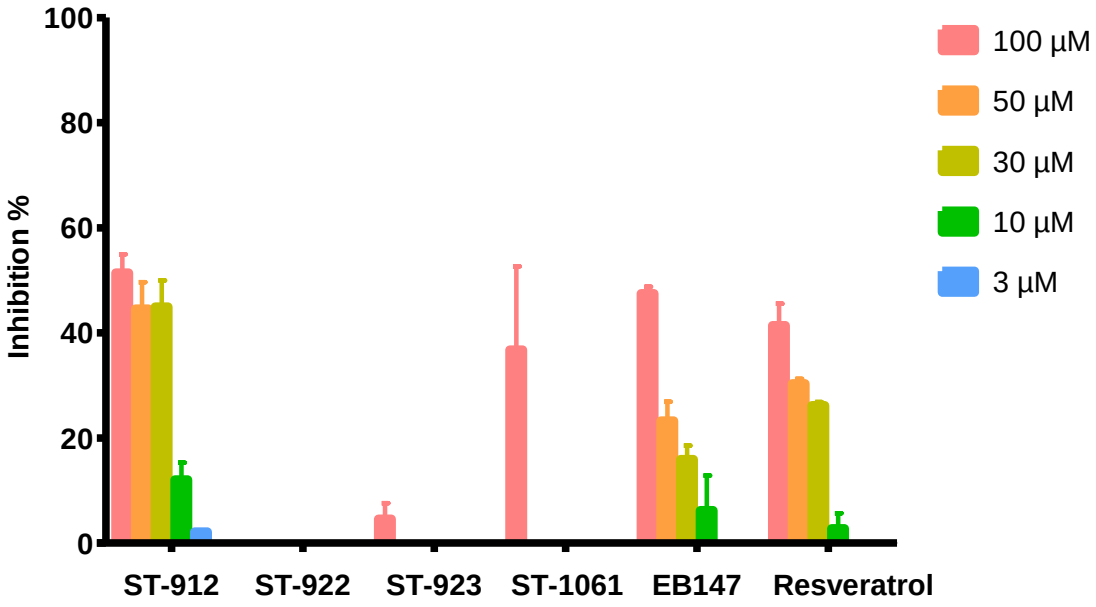

SF 4. Inhibition values of in-house compounds screened.

(*E*)-styryl-1*H*-benzo[*d*]imidazole library was purchased at (Asinex, Moscow, Russia)

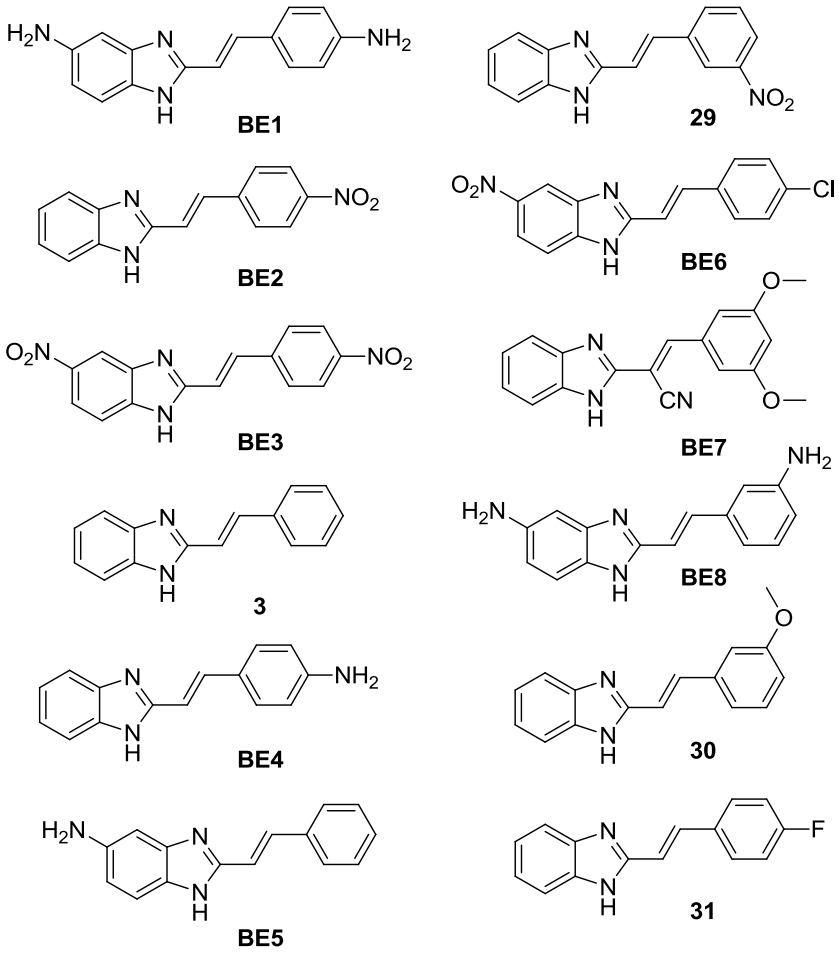

SF 5. (*E*)-styryl-1*H*-benzo[*d*]imidazole library.

.

Entry	IC_{50}	pIC_{50} ± S.E.
BE1	>100 µM	-
BE2	>100 µM	-
BE3	>100 µM	-
BE4	>100 µM	-
BE5	59.9 µM	4.2 ± 0.01
BE6	>100 µM	-
BE7	>100 µM	-
BE8	>100 µM	-

Table 1. IC_{50} values of tested compounds

- Biochemistry

sEH activity assay

sEH was expressed in *E. coli* and purified by affinity chromatography.[4] For the recombinant affinity purified sEH, we used a fluorescent-based assay[5] that uses PHOME (3-phenyl-cyano(6-methoxy-2-naphthalenyl)methyl ester-2-oxiraneacetic acid) in a 96-well format assay to determine IC_{50} values. Recombinant sEH (2 µg/well) was incubated with inhibitors for 10 min at room temperature in 25 mM Bis-Tris/HCl, 0.1 mg/mL BSA, Triton-X-100 0.01% buffer (110 µL, pH 7.0) before substrate (PHOME) was added ($[S]_{final}$ = 50 µM). Activity was evaluated by measuring the appearance of the fluorescent product 6-methoxynaphthaldehyde (λ_{em}= 330 nm, λ_{ex} = 465 nm).

Cell culture and treatment

Cell lines were obtained from the *Deutsche Sammlung von Mikroorganismen und Zellkulturen* (DSMZ). HeLa and MCF-7 cell lines were grown in Dubelcco's modified Eagle's medium (DMEM) containing 10% fetal calf serum (FCS), 100 units/mL each of penicillin and streptomycin and 1 mM sodium pyruvate. HepG2 was grown in DMEM containing 10% FCS, 0.1 mM non-essential aminoacids and 100 units/mL each of penicillin and streptomycin. U937 and A498 cell lines were grown in RPMI 1640 medium containing 10% inactivated FCS and 100 units/mL each of penicillin and streptomycin. All cell lines were grown at 37°C in an atmosphere containing 5% CO_2.

Cell viability

Cell viability in HeLa, HepG2, A498, MCF-7 and U937 was determined using the water soluble and stable tetrazolium salt WST-1 (Roche, Mannheim, Germany) which is cleaved to a soluble formazan by a complex cellular mechanism that occurs primarily at the cell surface. This bioreduction is largely dependent on the glycolytic production of NAD(P)H in viable

cells. Therefore, the amount of formazan dye formed directly correlates to the number of metabolically active cells in the culture. Cells were seeded into 96-well plates to a density of 5 x 10^3 cells/100 µL well (HeLa, HepG2, A498, MCF-7) and 100 x 10^3 cells/100 µL well (U937). After 48 h of growth to allow attachment of cells to the wells, compounds were added at various concentrations (0.1-30 µM). After 48 h of growth, 10 µL containing WST-1 reagent. Cell viability was assessed using a microplate reader (infinite M200, Tecan Group Ltd., Crailsheim, Germany) according to the manufacturer's protocol (absorbance of the formazan product at 450 nm with a reference wavelength at 620 nm). Results are expressed as a percentage relative to vehicle-treated control (1% DMSO was added to untreated cells).

Annexin V/Propidium iodide (PI) staining

HepG2 cells were seeded into 8-well chamber slide to a density of 10,000 cells /well and allowed to attach for 24h at 37°C in an atmosphere containing 5% CO_2. Cells were treated with inhibitors for 24 or 48 h in medium containing 10% FCS, followed by washing once with washing buffer. Then, cells were co-stained by covering the slips with a solution containing annexin V labeling and PI (Annexin-V-FLUOS staining kit, Roche Diagnostics, Mannheim, Germany) for 10-15 min at room temperature. Coverslips were washed with assay buffer and mounted on microscopes slides, and cell staining was visualized by fluorescence microscopy (Axio Observer.Z1, Carl Zeiss AG, Jena, Germany) and the pictures are 1344x1024 pixel, 86x96 dpi with 24 bit coloring.

- Statistics

Data are expressed as mean values with S.E. All IC_{50} and EC_{50} values are means with S.D. of the IC_{50} or EC_{50} values obtained from measurements at five different concentrations of the compounds in three to five independent experiments. IC_{50} and EC_{50} values were determined using a sigmoidal dose response (variable slope) equation from GraphPad Prism® (GraphPad Software, LaJolla, USA) software.

- Computational methods

Docking studies

We used GOLD[7–9] *(Genetic Optimisation for Ligand*Docking*)* Suite 5.1 for receptor preparation as well as for docking and scoring of the compounds. Hydrogen atoms were added to the receptor (PDBCode: 3KOO) using the Add Hydrogens function and water molecules were deleted. The binding site was defined by selecting the reference ligand, available from the co-crystallized protein-ligand complex. All remaining adjustments

selectable within the Gold Docking Wizard were kept default. The standards coring function ChemPLP[10] was used to rank the docking modes.

- References

[1] G. Ribeiro Morais, H. Vicente Miranda, I. C. Santos, I. Santos, T. F. Outeiro, A. Paulo, *Bioorganic & medicinal chemistry* **2011**, *19*, 7698–710.

[2] G. R. Pettit, M. R. Rhodes, D. L. Herald, E. Hamel, J. M. Schmidt, R. K. Pettit, *Journal of medicinal chemistry* **2005**, *48*, 4087–99.

[3] S. A. Joyce, A. O. Brachmann, I. Glazer, L. Lango, G. Schwär, D. J. Clarke, H. B. Bode, *Angewandte Chemie* **2008**, *47*, 1942–5.

[4] S. Hahn, J. Achenbach, E. Buscató, F.-M. Klingler, M. Schroeder, K. Meirer, M. Hieke, J. Heering, E. Barbosa-Sicard, F. Loehr, et al., *ChemMedChem* **2011**, *6*, 2146–9.

[5] N. M. Wolf, C. Morisseau, P. D. Jones, B. Hock, B. D. Hammock, *Analytical biochemistry* **2006**, *355*, 71–80.

[6] C. Morisseau, M. Bernay, A. Escaich, J. R. Sanborn, J. Lango, B. D. Hammock, *Analytical biochemistry* **2011**, *414*, 154–62.

[7] G. Jones, P. Willett, R. C. Glen, A. R. Leach, R. Taylor, *Journal of molecular biology* **1997**, *267*, 727–48.

[8] M. L. Verdonk, J. C. Cole, M. J. Hartshorn, C. W. Murray, R. D. Taylor, *Proteins* **2003**, *52*, 609–23.

[9] G. Jones, P. Willett, R. C. Glen, *Journal of molecular biology* **1995**, *245*, 43–53.

[10] O. Korb, T. Stützle, T. E. Exner, *Journal of chemical information and modeling* **2009**, *49*, 84–96.

Journal of Medicinal Chemistry

Brief Article

pubs.acs.org/jmc

Design and Synthesis of Dual Modulators of Soluble Epoxide Hydrolase and Peroxisome Proliferator-Activated Receptors

Estel.la Buscató,[†] René Blöcher,[†] Christina Lamers, Franca-Maria Klingler, Steffen Hahn, Dieter Steinhilber, Manfred Schubert-Zsilavecz, and Ewgenij Proschak*

Institute of Pharmaceutical Chemistry, ZAFES/LiFF/OSF Goethe-University Frankfurt, Max-von-Laue-Strasse 9, D-60438 Frankfurt am Main, Germany

Supporting Information

ABSTRACT: Metabolic syndrome is a complex condition which often requires the use of multiple medications as a treatment. The resulting problems of polypharmacy are increase in side effects, drug−drug interactions, and its high economic cost. Development of multitarget compounds is a promising strategy to avoid the complications arising from administration of multiple drugs. Modulators of peroxisome proliferator-activated receptors (PPARs) are established agents in the treatment of dyslipidaemia, hyperglycaemia, and insulin resistance. Inhibitors of soluble epoxide hydrolase (sEH) are under evaluation for their use in cardiovascular diseases. In the present study, a series of dual sEH/PPAR modulators containing a pyrrole acidic headgroup and a urea pharmacophore were designed, synthesized, and evaluated in vitro using recombinant enzyme and cell-based assays. Compounds with different activity profiles were obtained which could be used in the treatment of metabolic syndrome.

INTRODUCTION

The metabolic syndrome (MetS)[1] is a clustering of factors mainly consisting of the so-called "deadly quartet" of hyperglycaemia, hypertriglyceridemia, hypertension, and obesity. MetS results in an increased risk for atherosclerosis and diabetes. Because of its complex nature, the current therapy strategies of MetS require multiple treatments regulating lipid and glucose homeostasis as well as blood pressure and coagulation. Up-to-date treatment for MetS follows a lifestyle change of the patient to increase the physical activity, initiation of drug therapy with statins to reduce LDL, blood pressure reducing agents, oral antidiabetics, and compounds to handle obesity. Nevertheless, the combination of several drugs for individual risk factors can decrease the efficacy and enhance the toxicity of each drug. Thus, there is a strong unmet medical need in reliable and efficient drugs targeting multiple symptoms of MetS over the long term, thereby minimizing problems with polypharmacy.[2]

PPARs contribute to the regulation of glucose, lipid, and cholesterol metabolism, therefore they seem to be a valuable target to treat MetS.[3] With the hypolipidemic fibrates and the antidiabetic thiazolidindiones (TZD), two drug classes had entered the market. PPARγ agonists like troglitazone, rosiglitazone, and most recently pioglitazone were suspended by some authorities due to severe adverse events. However, a very promising finding had been made when Choi et al.[4] showed that the antidiabetic effect of the TZDs is partially mediated by the inhibition of the cyclin-dependent kinase 5 mediated phosphorylation of PPARγ. With this discovery, a promising new development regarding PPARγ as a drug target arises.

The fibrate-derived PPARα agonists (e.g., clofibrate, bezafibrate) are used in the treatment of dyslipidaemia associated with atherosclerosis and dyslipidaemia primarily linked to type 2 diabetes mellitus. The remaining subtype PPARδ stimulates fatty acid oxidation in heart and skeletal muscle and plays a role in cell differentiation and atherosclerosis. Reviewing recent patent literature implied that the development of PPARδ agonists is a promising target toward MetS associated pathologies.[5]

Soluble epoxide hydrolase (sEH) metabolizes epoxyeicosatrienoic acids (EETs), previously produced by epoxygenases, to the corresponding dihydroxyeicosatrienoic acids (DHETs). Inhibition or deletion of soluble epoxide hydrolase prevents hyperglycaemia, promotes insulin secretion, reduces islet apoptosis, and decreases adipogenesis.[6,7] On the basis of this knowledge, sEH has attired the attention as possible target to treat MetS[8] in conjunction with selective PPAR activation. This current study presents dual modulators that target sEH and PPAR, an interesting therapeutic approach to treat MetS related pathologies. PPARs and sEH are related through the modulatory action of sEH substrates and metabolites on PPAR.

Latest investigations demonstrated that EETs[9] are PPARγ and PPARα ligands. Competition as well as direct binding assays revealed that 14,15-EET[10] binds to the ligand-binding domain of PPARα.

Furthermore, latest publications discovered that DHETs have a high potency to activate PPARα,[10] suggesting that DHETs may have additional vascular actions as a result of their effect on PPARα. Figure 1 summarizes the expected mode of action of dual acting compounds which should lead to increased EETs levels due to sEH inhibition and substitute the beneficial activation of PPAR by DHETs. Fang et al. discovered an activation of PPARα by substituted urea-derived sEHIs after cellular metabolism.[11]

Received: August 28, 2012
Published: November 7, 2012

dx.doi.org/10.1021/jm301194c | J. Med. Chem. 2012, 55, 10771−10775

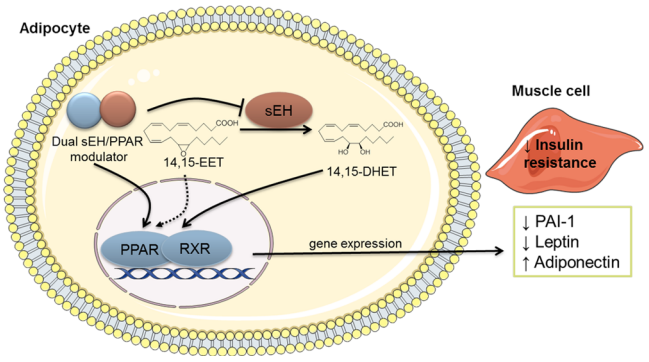

Figure 1. Mode of action of dual sEH/PPAR modulators. The sEH inhibitor leads to a decreased DHETs level, which might lead to decreased PPAR activation. This effect is compensated by the sEH/PPAR dual modulation.

In the present work, we describe novel compounds that are able to inhibit sEH and activate PPAR regardless their metabolism. Further development of these compounds could lead to agents with beneficial action on hyperglycaemia, hypertriglyceridemia, and hypertension, which can serve as a starting point for the development of polypharmacological compounds as a treatment of MetS.[12]

CHEMISTRY

We prepared the compounds **5a−i**, **6a−i** that are connected through a methylbenzyl linker between the pyrrole ring and the urea pharmacophore. An adamantyl group has been used in many sEH inhibitors[13] with high in vitro efficacy (e.g., AUDA), and Ph-*p*OCF_3 substituted moiety showed improved pharmacokinetic properties.[14] On the basis of this knowledge, we developed derivatives carrying pyrrole structures linked to urea containing compounds (sEH pharmacophore) that end in a carboxylic group needed for activation of all PPAR subtypes. We followed the previous strategy[15] to synthetize potent PPAR agonists: acidic headgroup−aromatic core−linker−hydrophobic tail.[16] In the present study, we explored the effect of the substitution pattern (*o*-, *m*-, *p*-) on the activity at the different targets. We synthesized the compounds **6a−i**, with an acidic group and **5a−i** as ethyl carboxylate esters, as seen in Scheme 1. Starting from ethyl 1*H*-pyrrole-2-carboxylate (**1**) that reacted with the *o*-, *m*-, or *p*-(bromomethyl) benzonitrile (**2**) via phase transfer catalysis using TBAI in a mixture of DCM/aqueous NaOH (1/1), we obtained the following *N*-alkylated products (**3a−c**) that underwent reduction with Raney Ni, the corresponding amines (**4a−c**) remaining which reacted with three different isocyanates: cyclohexylisocyanate, adamantylisocyanate, and *p*-OCF_3-phenylisocyanate, yielding the corresponding urea derivatives (**5a−i**). To obtain the compounds (**5a−i**) as carboxylic acid, they were solved in a mixture of THF/MeOH/water (1:1:2) and treated with KOH under microwave radiation to yield (**6a−i**).

RESULTS AND DISCUSSION

Known PPARα, γ, and δ selective agonists (GW7647,[17] pioglitazone,[18] L-165041[19]) and the sEH inhibitor AUDA[13] were evaluated and used as references. To obtain dual modulators of sEH/PPAR, it was necessary to link both pharmacophores via an aromatic spacer and maintain the lipophilic core which is characteristic of PPAR agonists. Adamantyl and cyclohexyl ureas have been shown to exhibit high sEH inhibitory properties. In terms of sEH inhibition, the ethyl ester derivatives with cyclohexyl moieties (**5a−c**) are better tolerated than adamantyl (**5d−f**) or Ph-*p*OCF_3 (**5g−i**), reaching IC_{50} values in the range from 23 to 39 nM. In general, the introduction of a Ph-*p*OCF_3 substituent decreased the inhibitory activity, yielding inactive (**5h**, **6g**) or slightly active compounds (**5g**, **5i**, **6h**, **6i**) (Table 1). The comparison of carboxylic acids with the corresponding esters in terms of sEH inhibition shows that cyclohexyl substituted esters (**5a−c**) and adamantyl (**5d−f**) are more potent than their carboxylic acids counterparts (**6a−c**, **6d−f**). Regarding the substitution pattern, the inhibitory potency of cyclohexyl carrying esters remains unaffected (**5a−c**, 23 nM < IC_{50} < 39 nM). This tendency holds true for adamantyl substituted esters (**5d−f**, 43 nM < IC_{50} < 87 nM). This behavior stands in contrast with the inhibitory potency of the acids, possibly due to an alternative binding mode which already has been described for sEH.[19] Regarding cyclohexyl acid derivatives *o*- (**6a**, IC_{50} = 747 nM) and *p*- (**6c**, IC_{50} = 252 nM), substituted compounds were more potent than the *m*-substituted moiety (**6b**, IC_{50} = 1923 nM). In the case of adamantyl, the *p*- (**6f**, IC_{50} = 73 nM) was more potent than *o*-adamantyl (**6d**, IC_{50} = 178 nM) and *m*- (**6e**, IC_{50} = 304 nM) derivatives, possibly due to sterical hindrance.

The PPAR activation potency of the compounds showed a wide diversity from modulatory effects at 10 μM to full agonistic properties with certain EC_{50} values (Table 2). Regarding the PPAR activities, only two ethyl ester derivatives showed a partial activation of PPARγ at 10 μM (**5b**, 21%; **5c**, 16%). As expected, the majority of carboxylic acids (**6a−i**) were able to activate PPARs. We observed that adamantyl derivatives (**6d−f**) were able to activate PPARγ selectively, probably due to the larger left distal ligand binding pocket compared to the other receptor subtypes.[16] The selectivity was impaired when testing Ph-*p*OCF_3 derivatives that activated both PPARα and PPARγ concerning *o*-substitution (**6g**, 38% (PPARα) and 128%, EC_{50} = 2 μM (PPARγ)). While *m*- and *p*-substituted compounds (**6h**, **6i**) yield a PPARα full agonism, only partial agonism was observed for the *o*-substituted Ph-*p*OCF_3

Scheme 1. Synthesis of sEH/PPAR Dual Modulators 5a−i, 6a−i[a]

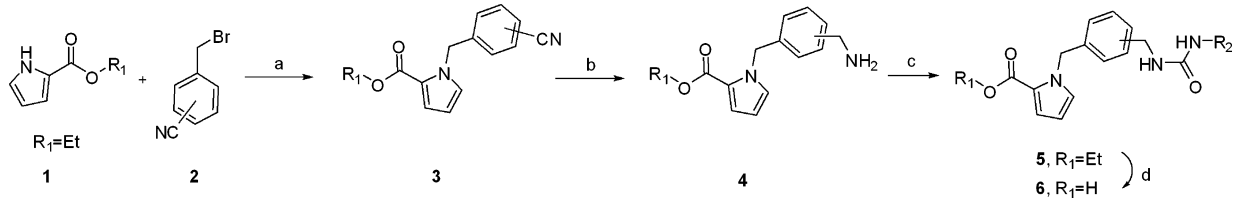

[a]Reagents and conditions: (a) tetrabutylammonium iodide, NaOH 50% aqueous, DCM, 0 °C to rt, 12 h; (b) Raney Ni, H_2, MeOH; (c) R-NCO, DIPEA, DCM, rt, 12 h; (d) THF/MeOH/H_2O (1:2:2), KOH, MW, 90 °C, 15 min.

dx.doi.org/10.1021/jm301194c | J. Med. Chem. 2012, 55, 10771−10775

Table 1. Inhibition and Activation Values of dual sEH/PPAR Modulators 5a−i, 6a−i[a]

name	R_1	R_2	subst	IC_{50} (nM) sEH	% activation @10 μM PPARα	% activation @10 μM PPARγ	% activation @10 μM PPARδ
GW7647				nt	100	nt	nt
pioglitazone				nt	nt	100	nt
L-165041				nt	nt	nt	100
AUDA				107 ± 12.8	nt	nt	nt
5a	Et	cyclohexyl	*o*-	39 ± 1.4	ia	ia	ia
5b	Et	cyclohexyl	*m*-	27 ± 8.0	ia	21 ± 4.1	ia
5c	Et	cyclohexyl	*p*-	23 ± 1.0	ia	16 ± 4.6	ia
5d	Et	adamantyl	*o*-	43 ± 10.0	ia	ia	ia
5e	Et	adamantyl	*m*-	46 ± 4.2	ia	ia	ia
5f	Et	adamantyl	*p*-	87 ± 8.4	ia	ia	ia
5g	Et	Ph-*p*OCF_3	*o*-	2009 ± 1165.6	ia	ia	ia
5h	Et	Ph-*p*OCF_3	*m*-	ia	ia	ia	ia
5i	Et	Ph-*p*OCF_3	*p*-	611 ± 248.4	ia	ia	ia
6a	H	cyclohexyl	*o*-	747 ± 194.9	ia	ia	ia
6b	H	cyclohexyl	*m*-	1923 ± 724.7	ia	ia	ia
6c	H	cyclohexyl	*p*-	252 ± 17.1	ia	ia	ia
6d	H	adamantyl	*o*-	178 ± 55.4	ia	45 ± 14.7	ia
6e	H	adamantyl	*m*-	304 ± 78.3	ia	16 ± 5.7	ia
6f	H	adamantyl	*p*-	73 ± 4.5	ia	18 ± 7.8	ia
6g	H	Ph-*p*OCF_3	*o*-	ia	38 ± 1.9	105 ± 14.4	ia
6h	H	Ph-*p*OCF_3	*m*-	943 ± 658.3	58 ± 5.7	43 ± 12.5	25 ± 4.5
6i	H	Ph-*p*OCF_3	*p*-	258 ± 48.0	67 ± 13.4	84 ± 24.1	ia

[a]nt = not tested, ia = inactive.

Table 2. EC_{50} Values of Dual sEH/PPAR Modulators[a]

name	IC_{50} (nM) sEH	EC_{50} (max activation) PPARα	EC_{50} (max activation) PPARγ	EC_{50} (max activation) PPARδ
GW7647	nt	0.2 ± 0.05 μM	nt	nt
pioglitazone	nt	nt	0.2 ± 0.05 μM	nt
L-165041	nt	nt	nt	0.039 ± 0.008 μM
AUDA	107 ± 12.8	nt	nt	nt
6d	178 ± 55.4	ia	6 ± 0.8 μM (60 ± 1.3%)	ia
6g	ia	7 ± 1.5 μM (55 ± 9.5%)	2 ± 0.4 μM (128 ± 14.4%)	ia
6h	943 ± 658.3	6 ± 0.5 μM (97 ± 38.9%)	nd	nd
6i	258 ± 48.0	5 ± 0.6 μM (90 ± 11.4%)	nd	ia

[a]nt = not tested; ia = inactive; nd = not determinable.

derivative (**6g**), which can be probably explained by the sterical hindrance. A pan-agonist was obtained (**6h**) that activated all classes of PPAR (58% on PPARα, 43% on PPARγ. and 25% on PPARδ). When considering *p*-substituted compounds, another dual PPARα/γ agonist was found (**6i**, 67% on PPARα and 84% on PPARγ at 10 μM). Surprisingly, cyclohexyl moieties (**6a−c**) did not lead to sustainable PPAR activation, indicating that this building block is not suitable for incorporation into dual acting sEH/PPAR modulators.

Regarding dual modulation of sEH/PPAR, we obtained two compounds that partially activated PPARγ (**6e**, **f**) and inhibited sEH with moderate potency (IC_{50} values of 304 and 73 nM, respectively). Compound **6h** inhibited sEH (IC_{50} = 943 nM) and activated PPARα,γ,δ (EC_{50} = 6 μM on PPARα, 43% at 10 μM on PPARγ, 25% at 10 μM on PPARδ). Compound **6i** inhibited sEH (IC_{50} = 258 nM) and activated PPARα,γ (EC_{50} = 5 μM on PPARα, 84% at 10 μM on PPARγ), resulting in an interesting compound to be evaluated in further experiments.

CONCLUSION

This work describes the synthesis of dual sEH/PPAR modulators as potential agents for the treatment of metabolic syndrome. Following a combinatorial approach, an acidic headgroup, known as a pharmacophore important for PPAR dual agonistic activity, was combined with different hydrophobic urea derivatives in order to introduce an epoxide mimetic.

The resulting compounds displayed high inhibition on sEH and different patterns of PPAR agonistic activity.

This study demonstrates that the pharmacophores of PPAR agonists and sEH inhibitors can be easily combined, resulting in a simplified blueprint of a dual sEH/PPAR modulator. Further in vivo pharmacological evaluation studies are needed in order to evaluate which pattern of PPAR activation shows the most promising profile for treatment of metabolic syndrome.

EXPERIMENTAL SECTION

General. All reagents and solvents were purchased from the suppliers Alfa-Aesar GmbH & Co. KG (Karlsruhe, Germany) and Sigma-Aldrich Chemistry GmbH (Hannover, Germany) and used without further purification. Retention factors were determined by thin layer chromatography with silica coated aluminum foil (particle size 60 μm) obtained from Merck KGaA (Darmstadt, Germany). Flash chromatography was performed on packed silica columns (particle size 50 μm) from Varian Medical Systems GmbH (Darmstadt, Germany). ^{1}H (250/400 MHz) and ^{13}C (64 MHz) spectra were measured on AV 250 and AMX 400 nuclear magnetic resonance spectrometers from

dx.doi.org/10.1021/jm301194c | J. Med. Chem. 2012, 55, 10771−10775

Bruker. Mass spectra were measured using electrospray ionization (+) with a VG Plattform II spectrometer from Fisons. High resolution mass spectra were measured by a MALDI LTQ Orbitrap XL spectrometer from Thermo Scientific. All compounds were characterized by NMR and MS. All final compounds had a purity of ≥95% as determined by HPLC (LC2020, Shimadzu, Duisburg, Germany), except for **6f** (92%). Data are expressed as mean values with SE. All IC_{50} and EC_{50} values are means with SE of the IC_{50} or EC_{50} values obtained from measurements at five different concentrations of the compounds in 3−5 independent experiments. IC_{50} and EC_{50} values were determined using a sigmoidal dose response (variable slope) equation from GraphPad Prism (GraphPad Software, LaJolla, CA) software.

General Procedure for the Preparation of Compounds 3a−c (*o*-, *m*-, *p*-). A solution of ethyl 1*H*-pyrrole-2-carboxylate (**1**) (7.2 mmol) in DCM (50 mL) was cooled to 0 °C. Tetrabutylammonium iodide (0.22 mmol) and 50 mL of sodium hydroxide solution (50%) were added. The mixture was stirred for 30 min at 0 °C before (bromomethyl)benzonitrile (**2**) (7.9 mmol) was added. The mixture was allowed to warm to room temperature and stirred vigorously overnight. The reaction was quenched by adding concentrated hydrochloric acid until a pH of 1 was reached. The aqueous layer was extracted three times with 20 mL DCM. The collected organic layers were washed twice with 10 mL of brine, dried over $MgSO_4$, and concentrated under reduced pressure. After purification by flash chromatography (Hex:EE 0−15%), white crystals remained.

General Procedure for the Preparation of the Compounds 4a−c. A mixture of ethyl (cyanobenzyl)-1*H*-pyrrole-2-carboxylate (**3a−c**) (5.9 mmol, 1 equiv) and Raney nickel (5.9 mmol) in 100 mL of dry ammoniacal methanol was stirred overnight at room temperature at H_2 atmosphere under a pressure of 6 bar. The catalyst was filtered off through Celite, and the solvent was removed under reduced pressure to give a yellow oil.

General Procedure for the Preparation of the Compounds 5a−i. A solution of ethyl 1-(aminomethyl)benzyl)-1*H*-pyrrole-2-carboxylate (**4a−c**) (0.97 mmol) and *N*,*N*-diisopropylethylamine (2.9 mmol) in 10 mL of dry DCM was stirred at room temperature under argon. An isocyanate (0.97 mmol) was added, and the mixture was stirred overnight. The solvent was evaporated under reduced pressure. The crude product was purified by hot filtration in hexane and recrystallized from ethanol.

General Procedure to Obtain Carboxylic Acid Compounds 6a−i. The ethyl ester (**5a−i**) was treated with potassium hydroxide (0.652 mmol) in a solvent mixture of THF/MeOH/H_2O (1:2:2) and accomplished under microwave irradiation at 90 °C (35 W) during 15 min. The solvent was removed under reduced pressure and the residue solved in water. For precipitation, 1 M hydrochloric acid was added. After filtration, the white solid was lyophilized. 1-(2-((3-Cyclohexylureido)methyl)benzyl)-1*H*-pyrrole-2-carboxylic acid (**6a**) was obtained from ethyl 1-(((ureido)methyl)benzyl)-1*H*-pyrrole-2-carboxylate **5a** (46 mg, 0.12 mmol) and yielded 25 mg (50% yield). ^{1}H NMR (CH_3OH-d_4): δ 7.19 (d, J = 7.2 Hz, 1H), 7.08−7.04 (m, 2H), 6.9 (m, 1H), 6.77 (m, 1H), 6.39 (d, J = 7.2 Hz, 1H), 6.09 (m, 1H), 5.54 (s, 2H), 4.29 (s, 2H), 3.39 (m 1H), 1.79 (m, 2H), 1.64 (m, 2H), 1.51 (m, 1H) and 1.25 (m, 5H) ppm. ^{13}C NMR (CH_3OH-d_4): δ 160.0, 162.6, 137.7, 135.0, 130.1, 127.3, 126.9, 125.5, 119.9, 117.3, 110.1, 55.9, 52.6, 42.5, 34.3, 31.4, 26.2, 25.3, and 24.8 ppm. HPLC (98% purity). HRMS: measured m/z [M + H$^+$] 356.1967 (theoretical, 356.1969).

Activity Assays. sEH activity assay. For the recombinant affinity purified sEH, we used a fluorescent-based assay[19] that uses PHOME (3-phenyl-cyano(6-methoxy-2-naphthalenyl)methyl ester-2-oxirane-acetic acid) in a 96-well format assay to determine IC_{50} values. Recombinant sEH (2 μg/well) was incubated with inhibitors for 10 min at room temperature in 25 mM Bis-Tris/HCl and 0.1 mg/mL BSA buffer (110 μL, pH 7.0) before substrate (PHOME) was added ($[S]_{final}$ = 50 μM). Activity was evaluated by measuring the appearance of the fluorescent product 6-methoxynaphthaldehyde (λ_{em} = 330 nm, λ_{ex} = 465 nm).

PPAR Transactivation Assay. COS7 cells were grown in DMEM supplemented with 10% FCS, sodium pyruvate, and penicillin/streptomycin at 37 °C and 5% CO_2. The day before transfection, cells were seeded in 96-well plates at a density of 30000 cells per well. Transient transfection was carried out by Lipofectamine LTX reagent (Invitrogen) according to the manufacturer's protocol with pFR-Luc (Stratagene), pRL-SV40 (Promega), and the Gal4-fusion receptor plasmids (pFA-CMV-hPPAR-LBD) of the respective subtype. Five h after transfection, the medium was changed to DMEM without phenol red and 10% FCS, containing 0.1% DMSO and the respective concentrations of the test compounds.

Following overnight incubation with the test compounds, cells were assayed for reporter gene activity using Dual-Glo luciferase assay system (Promega, Mannheim, Germany) according to the manufacturer's protocol. Luminescence was measured with a GENios Pro luminometer (Tecan Deutschland GmbH, Crailsheim, Germany). Each concentration of the compounds was tested in triplicate wells, and each experiment was repeated independently at least three times. Normalization for transfection efficacy and cell growth was done by division of the firefly luciferase data by renilla luciferase data, resulting in relative light units. Activation factors were obtained by dividing by DMSO control. EC_{50} and standard deviation values were calculated by mean values of at least three determinations by SigmaPlot 2001 (Systat Software GmbH, Erkrath, Germany) using a four-parameter logistic regression. All compounds were evaluated by comparison of the achieved maximum effect to that of the reference compound (GW 7647 for PPARα, pioglitazone for PPARγ, and L165,041 for PPARδ each with 1 μM).

■ ASSOCIATED CONTENT

Ⓢ Supporting Information

Assay protocols, purity determination method, and NMR and mass analysis data of compounds **5a−i** and **6b-i**. This material is available free of charge via the Internet at http://pubs.acs.org..

■ AUTHOR INFORMATION

Corresponding Author

*E-mail: proschak@pharmchem.uni-frankfurt.de.

Author Contributions

†These authors contributed equally. The manuscript was written through contributions of all authors. All authors have given approval to the final version of the manuscript.

Notes

The authors declare no competing financial interest.

■ ACKNOWLEDGMENTS

This work was supported by the Deutsche Forschungsgemeinschaft (DFG, Sachbeihilfe PR1405/2-1), LOEWE Lipid Signaling Forschungszentrum Frankfurt (LiFF), the Oncogenic Signaling Frankfurt (OSF), and Fonds der Chemischen Industrie. E.B. thanks DAAD-La Caixa and R.B. the Else-Kröner-Fresenius Foundation Graduiertenkolleg TRIP for a fellowship.

■ ABBREVIATIONS USED

AUDA, 12-(3-adamantan-1-yl-ureido)dodecanoic acid; DHETs, dihydroxyeicosatrienoic acids; EETs, epoxyeicosatrienoic acids; FCS, fetal calf serum; LDL, low-densitiy lipoprotein; MetS, metabolic syndrome; PPAR, peroxisome proliferator-activated receptor; sEH, soluble epoxide hydrolase; sEHI, soluble epoxide hydrolase inhibitor; TBAI, tetrabutyl ammonium iodide; TZD, thiazolidinedione

REFERENCES

(1) Eckel, R. H.; Grundy, S. M.; Zimmet, P. Z. The metabolic syndrome. *Lancet 365*, 1415−1428.

(2) Page , J. Nonalcoholic fatty liver disease: the hepatic metabolic syndrome. *J. Am. Acad. Nurse Pract.* **2012**, *24*, 345−351.

(3) Grundy, S. M. Drug therapy of the metabolic syndrome: minimizing the emerging crisis in polypharmacy. *Nature Rev. Drug Discovery* **2006**, *5*, 295−309.

(4) Pirat, C.; Farce, A.; Lebègue, N.; Renault, N.; Furman, C.; Millet, R.; Yous, S.; Speca, S.; Berthelot, P.; Desreumaux, P.; Chavatte, P. Targeting peroxisome proliferator-activated receptors (PPARs): development of modulators. *J. Med. Chem.* **2012**, *55*, 4027−4061.

(5) Choi, J. H.; Banks, A. S.; Estall, J. L.; Kajimura, S.; Boström, P.; Laznik, D.; Ruas, J. L.; Chalmers, M. J.; Kamenecka, T. M.; Blüher, M.; Griffin, P. R.; Spiegelman, B. M. Anti-diabetic drugs inhibit obesity-linked phosphorylation of PPARgamma by Cdk5. *Nature* **2010**, *466*, 451−456.

(6) Lamers, C.; Schubert-Zsilavecz, M.; Merk, D. Therapeutic modulators of peroxisome proliferator-activated receptors (PPAR): a patent review (2008−present). *Exp. Opin. Ther. Pat.* **2012**, *22*, 803−841.

(7) Vanella, L.; Kim, D. H.; Sodhi, K.; Barbagallo, I.; Burgess, A. P.; Falck, J. R.; Schwartzman, M. L.; Abraham, N. G. Crosstalk between EET and HO-1 downregulates Bach1 and adipogenic marker expression in mesenchymal stem cell derived adipocytes. *Prostaglandins Other Lipid Mediators* **2011**, *96*, 54−62.

(8) Kim, D. H.; Vanella, L.; Inoue, K.; Burgess, A.; Gotlinger, K.; Manthati, V. L.; Koduru, S. R.; Zeldin, D. C.; Falck, J. R.; Schwartzman, M. L.; Abraham, N. G. Epoxyeicosatrienoic acid agonist regulates human mesenchymal stem cell-derived adipocytes through activation of HO-1-pAKT signaling and a decrease in PPARγ. *Stem Cells Dev.* **2010**, *19*, 1863−1873.

(9) Iyer, A.; Kauter, K.; Alam, M. A.; Hwang, S. H.; Morisseau, C.; Hammock, B. D.; Brown, L. Pharmacological inhibition of soluble epoxide hydrolase ameliorates diet-induced metabolic syndrome in rats. *Exp. Diabetes Res.* **2012**, *2012*, 758614.

(10) Ng, V. Y.; Huang, Y.; Reddy, L. M.; Falck, J. R.; Lin, E. T.; Kroetz, D. L. Cytochrome P450 eicosanoids are activators of peroxisome proliferator-activated receptor alpha. *Drug Metab. Dispos.* **2007**, *35*, 1126−1134.

(11) Cowart, L. A.; Wei, S.; Hsu, M.-H.; Johnson, E. F.; Krishna, M. U.; Falck, J. R.; Capdevila, J. H. The CYP4A isoforms hydroxylate epoxyeicosatrienoic acids to form high affinity peroxisome proliferator-activated receptor ligands. *J. Biol. Chem.* **2002**, *277*, 35105−35112.

(12) Fang, X.; Hu, S.; Xu, B.; Snyder, G. D.; Harmon, S.; Yao, J.; Liu, Y.; Sangras, B.; Falck, J. R.; Weintraub, N. L.; Spector, A. A. 14,15-Dihydroxyeicosatrienoic acid activates peroxisome proliferator-activated receptor-alpha. *Am. J. Physiol., Heart Circul. Physiol.* **2006**, *290*, H55−H63.

(13) Fang, X.; Hu, S.; Watanabe, T.; Weintraub, N. L.; Snyder, G. D.; Yao, J.; Liu, Y.; Shyy, J. Y.-J.; Hammock, B. D.; Spector, A. A. Activation of peroxisome proliferator-activated receptor alpha by substituted urea-derived soluble epoxide hydrolase inhibitors. *J. Pharmacol. Exp. Ther.* **2005**, *314*, 260−270.

(14) Schulman, I. G. Nuclear receptors as drug targets for metabolic disease. *Adv. Drug Delivery Rev.* **2010**, *62*, 1307−1315.

(15) Morisseau, C.; Goodrow, M. H.; Dowdy, D.; Zheng, J.; Greene, J. F.; Sanborn, J. R.; Hammock, B. D. Potent urea and carbamate inhibitors of soluble epoxide hydrolases. *Proc. Natl. Acad. Sci. U. S. A.* **1999**, *96*, 8849−8854.

(16) Tsai, H.-J.; Hwang, S. H.; Morisseau, C.; Yang, J.; Jones, P. D.; Kasagami, T.; Kim, I.-H.; Hammock, B. D. Pharmacokinetic screening of soluble epoxide hydrolase inhibitors in dogs. *Eur. J. Pharm. Sci.* **2010**, *40*, 222−238.

(17) Proschak, E.; Sander, K.; Zettl, H.; Tanrikulu, Y.; Rau, O.; Schneider, P.; Schubert-Zsilavecz, M.; Stark, H.; Schneider, G. From molecular shape to potent bioactive agents II: fragment-based de novo design. *ChemMedChem* **2009**, *4*, 45−48.

(18) Pirard, B. Peroxisome Proliferator-Activated Receptors target family landscape: a chemometrical approach to ligand selectivity based on protein binding site analysis. *J. Comput.-Aided Mol. Des.* **2003**, *17*, 785−796.

(19) Gomez, G. A.; Morisseau, C.; Hammock, B. D.; Christianson, D. W. Human soluble epoxide hydrolase: structural basis of inhibition by 4-(3-cyclohexylureido)-carboxylic acids. *Protein Sci.* **2006**, *15*, 58−64.

Supporting Information

Design and Synthesis of Dual Modulators of Soluble Epoxide Hydrolase and Peroxisome Proliferator Activated Receptors

Estel.la Buscató and René Blöcher, Christina Lamers, Franca-Maria Klingler, Steffen Hahn, Dieter Steinhilber, Manfred Schubert-Zsilavecz and Ewgenij Proschak*

Institute of Pharmaceutical Chemistry, ZAFES/LiFF/OSF Goethe-University Frankfurt, Max-von-Laue-Str. 9, D-60438 Frankfurt am Main, Germany

Table of contents

Determination of compound purity

The purity of final compounds was determined using LC2020 (Shimadzu, Duisburg, Germany) on a Kinetex 2.6 µm C18 100 Å, 100 x 2.1 mm (Phenomenex, Aschaffenburg, Germany). The method included a water/methanol gradient run of 5-95% and detection at 254 nm and 280 nm.

Characterization of compounds 3a-c (*o*-, *m*-, *p*-):

Ethyl 1-(2-cyanobenzyl)-1H-pyrrole-2-carboxylate (**3a**). Starting from ethyl 1H-pyrrole-2-carboxylate 1g (7.2 mmol, 1 eq). Yield: 1.5 g, 82 %. ^{1}H-NMR (DMSO-d_6): δ 7.84 (d, J = 7.7 Hz, 1H), 7.59 (t, J = 6.6 Hz, 1H), 7.52 (d, J = 8.3 Hz, 1H), 7.43 (t, J = 9.6 Hz, 1H), 6.98 (d, J = 1.8 Hz, 1H), 6.56 (t, J = 7.8 Hz, 1H), 6.28 (d, J=2.7 Hz, 1H), 5.76 (s, 2H), 4.08 (q, J = 6.9 Hz, 2H) and 1.14 (t, J = 7.2 Hz, 3H) ppm. MS (ESI): m/z 277 (M + Na+).

Ethyl 1-(3-cyanobenzyl)-1H-pyrrole-2-carboxylate (**3b**). Starting from ethyl 1H-pyrrole-2-carboxylate 1g (7.2 mmol, 1 eq). Yield: 1.6 g, 88 %. ^{1}H-NMR (DMSO-d_6): δ 7.71 (d, J = 9.3 Hz, 1H), 7.52 (d, J = 6.5 Hz, 2H), 7.37 (d, J = 9.7 Hz, 2H), 6.96 (t, J = 1.8 Hz, 1H), 6.22 (t, J = 2.4 Hz, 1H), 5.61 (s, 2H), 4.14 (q, J = 7.1 Hz, 2H) and 1.19 (t, J = 7.2 Hz, 3H) ppm. MS (ESI): m/z 277 (M + Na^+).

Ethyl 1-(4-cyanobenzyl)-1H-pyrrole-2-carboxylate (**3c**). Starting from ethyl 1H-pyrrole-2-carboxylate 1g (7.2 mmol, 1 eq).Yield: 1.6 g, 88 %. ^{1}H-NMR (DMSO-d_6): δ 7.81 (d, J = 8.2 Hz, 1H), 7.42 (d, J = 2 Hz, 3H), 7.09 (d, J = 9.4 Hz, 2H), 6.24 (t, J = 2.6 Hz, 1H), 5.65 (s, 2H), 4.14 (q, J = 6.6 Hz, 2H) and 1.19 (t, J = 6.8 Hz, 3H) ppm. MS (ESI): m/z 277 (M + Na^+).

Characterization of compounds 4a-c (*o*-, *m*-, *p*-):

Ethyl 1-(2-(aminomethyl)benzyl)-1 H-pyrrole-2-carboxylate (**4a**). Starting from Ethyl 1-(2-cyanobenzyl)-1H-pyrrole-2-carboxylate (**3a**) 1 g (5.9 mmol, 1 eq). Yield: 1.3 g, 95 %. ^{1}H-NMR (DMSO-d_6): δ 7.45 (d, J = 9.3 Hz, 2H), 7.15 (d, J = 6.5 Hz, 2H), 6.99 (d, J = 9.7 Hz, 2H), 6.33 (t, J = 1.8 Hz, 1H), 6.24 (t, J = 2.4 Hz, 1H), 5.66 (s, 2H), 4.07 (q, J = 7.1 Hz, 2H) and 1.17 (t, J = 7.2 Hz, 3H) ppm. MS (ESI): m/z 281 (M + Na^+).

Ethyl 1-(3-(aminomethyl)benzyl)-1 H-pyrrole-2-carboxylate (**4b).** Starting from Ethyl 1-(3-cyanobenzyl)-1H-pyrrole-2-carboxylate (**3b**) 1 g (5.9 mmol, 1 eq). Yield: 1.5 g, 98 %. ^{1}H-NMR (DMSO-d_6): δ 7.26 (d, J = 9.3 Hz, 2H), 7.12 (d, J = 6.5 Hz, 2H), 6.92 (d, J = 9.7 Hz, 2H), 6.88 (t, J = 1.8 Hz, 1H), 6.20 (t, J = 2.4 Hz, 1H), 5.54 (s, 2H), 4.18 (q, J = 7.1 Hz, 2H) and 1.23 (t, J = 7.2 Hz, 3H) ppm. MS (ESI): m/z 281 (M + Na^+).

Ethyl 1-(4-(aminomethyl)benzyl)-1 H-pyrrole-2-carboxylate (**4c).** Starting from Ethyl 1-(4-cyanobenzyl)-1H-pyrrole-2-carboxylate (**3c**) 1 g (5.9 mmol, 1 eq). Yield: 1.5 g, 98 %. ^{1}H-NMR (DMSO-d_6): δ 7.27 (d, J = 8.2 Hz, 3H), 7.05 (d, J = 2 Hz, 2H), 6.9 (d, J = 9.4 Hz, 1H), 6.19 (t, J = 2.6 Hz, 1H), 5.52 (s, 2H), 4.18 (q, J = 6.6 Hz, 2H) and 1.22 (t, J = 6.8 Hz, 3H) ppm. MS (ESI): m/z 281 (M + Na^+).

Characterization of compounds 5a-i:

Ethyl 1-(2-((3-cyclohexylureido)methyl)benzyl)-1 H-pyrrole-2-carboxylate (**5a**)**.** Starting from Ethyl 1-(2-(aminomethyl)benzyl)-1 H-pyrrole-2-carboxylate (**4a**) 0.25 g (0.97 mmol, 1 eq).Yield: 0.25 g, 67.4 %. ^{1}H-NMR (CH_3OH-d_4): δ 7.19 (d, J = 7.2 Hz, 1H), 7.08 (m, 2H), 6.91 (m, 1H), 6.86 (m, 1H), 6.35 (d, J = 7.2 Hz, 1H), 6.11 (m, 1H), 5.54 (s, 2H), 4.3 (s, 2H), 4.07 (q, J = 7.1 Hz, 2H), 3.39 (m 1H), 1.79 (m, 2H), 1.64 (m, 2H), 1.51 (m, 1H), 1.25 (m, 5H) and 1.13 (t, J = 7.1 Hz, 3H) ppm. ^{13}C-NMR (CH_3OH-d_4): δ 160, 162.6, 137.7, 135, 130.1, 127.3, 126.9, 125.5, 119.9, 117.3, 110.1, 61.2, 55.9, 52.6, 42.5, 34.3, 31.4, 26.2, 25.3, 24.8 and 14.1 ppm. HRMS: measured m/z [M + H^+] 384.2282 (theoretical, 384.2282).

Ethyl 1-(3-((3-cyclohexylureido)methyl)benzyl)-1 H-pyrrole-2-carboxylate (**5b**). Starting from Ethyl 1-(3-(aminomethyl)benzyl)-1 H-pyrrole-2-carboxylate (**4b**) 0.25 g (0.97 mmol, 1 eq). Yield: 0.3 g, 81 %. ^{1}H-NMR (CH_3OH-d_4): δ 7.09 (m, 2H), 6.93 (m, 2H), 6.85 (m, 2H), 6.06 (m, 1H), 5.45 (s, 2H), 4.15 (s, 2H), 4.08 (q, J = 7.2 Hz, 2H), 3.38 (m 1H), 1.78 (m, 2H), 1.62 (m, 2H), 1.51 (m, 1H), 1.23 (t, J = 7.1 Hz, 3H) and 1.16 (m, 5H) ppm. ^{13}C-NMR (CH_3OH-d_4): δ 160.1, 157.4, 137.3, 135.2, 130.6, 128.7, 126.8, 125.9, 120.1, 116.9, 109.8, 60.7, 55.8, 52.9, 44.8, 34.2, 32.3, 27.1, 25.4, 24.8 and 14.7 ppm. HRMS: measured m/z [M + H^+] 384.2276 (theoretical, 384.2282)

Ethyl 1-(4-((3-cyclohexylureido)methyl)benzyl)-1 H-pyrrole-2-carboxylate (**5c**)**.** Starting from Ethyl 1-(4-(aminomethyl)benzyl)-1 H-pyrrole-2-carboxylate (**4c**) 0.25 g (0.97 mmol, 1 eq). Yield: 0.3 g, 81 %. ^{1}H-NMR (CH_3OH-d_4): δ 7.28 (d, J = 8.2 Hz, 1H), 7.18 (d, J = 8 Hz, 2H), 7.17 (d, J = 8 Hz, 2H) 6.9 (d, J = 9.4 Hz, 1H), 6.19 (t, J = 2.6 Hz, 1H), 5.52 (s, 2H), 4.16 (q, J = 7.3 Hz, 2H), 4.15 (s, 2H), 3.38 (m 1H), 1.78 (m, 2H), 1.62 (m, 2H), 1.51 (m, 1H), 1.23 (t, J = 7.1 Hz, 3H) and 1.16 (m, 5H) ppm. ^{13}C-NMR (CH_3OH-d_4): δ 160.1, 157.6, 137.5, 136, 130.3, 128.3, 126.7, 125.6, 119.7, 117.6, 109.5, 60.5, 55.7, 52.4, 44.4, 33.9, 31.8, 26.8, 25.7, 24.4 and 14.9 ppm. HRMS: measured m/z [M + H^+] 384.2286 (theoretical, 384.2282).

Ethyl 1-(2-((3-((3s,5s,7s)-adamantan-1-yl)ureido)methyl)benzyl)-1 H-pyrrole-2-carboxylate (**5d**)**.** Starting from Ethyl 1-(2-(aminomethyl)benzyl)-1 H-pyrrole-2-carboxylate (**4a**) 0.25 g (0.97 mmol, 1 eq).Yield: 0.25 g, 59.3 %**.** ^{1}H-NMR (DMSO-d_6): δ 7.22-7 (m, 3H), 6.87-6.85 (m, 1H), 6.35 (d, J = 8.1 Hz , 1H), 6.12-6.09 (m, 1H), 5.52 (s, 2H), 4.23 (s, 2H), 4.06 (q, J = 7.1 Hz, 2H), 1.82-1.97 (m, 8H), 1.6 (m, 7H), and 1.12 (t, J = 7.2 Hz, 3H) ppm. ^{13}C-NMR (CH_3OH-d_4): δ 160.2, 157, 140.3, 139.4, 135.2, 130.7, 128.5, 126.2, 121.3, 118.3, 115.9, 109.7, 60.3, 52.7 52.5, 47.6, 44.7, 42.7, 40.5, 37.6, 37.3, 32.3, 29.1 and 14.1 ppm. HRMS: measured m/z [M + H^+] 436.2584 (theoretical, 436.2595).

Ethyl 1-(3-((3-((3s,5s,7s)-adamantan-1-yl)ureido)methyl)benzyl)-1 H-pyrrole-2-carboxylate (**5e**)**.** Starting from Ethyl 1-(3-(aminomethyl)benzyl)-1 H-pyrrole-2-carboxylate (**4b**) 0.25 g (0.97 mmol, 1 eq).Yield: 0.3 g, 71.2 %. ^{1}H-NMR (DMSO-d_6): δ 7.16 (t, J = 7.6 Hz, 1H), 7.03 (d, J = 8.2 Hz, 1H), 6.96-6.91 (m, 2H), 6.87-6.82 (m, 2H), 6.08-6.05 (m, 1H), 5.46 (s, 2H), 4.1 (s, 2H), 4.09 (q, J = 7.2 Hz, 2H), 1.82-1.98 (m, 8H), 1.6 (m, 7H), and 1.16 (t, J = 7.1

Hz, 3H) ppm. ^{13}C-NMR (CH_3OH-d_4): δ 160.1, 156, 140.6, 139.7, 135.1, 130.5, 128.7, 127.3, 122.3, 119.2, 116.8, 109.6, 60.2, 52.9, 51.5, 47.6, 44.5, 41.7, 40.8, 37.7, 37.6, 32.6, 28.9 and 14.3 ppm. HRMS: measured m/z [M + H^+] 436.2586 (theoretical, 436.2595).

Ethyl 1-(4-((3-((3s,5s,7s)-adamantan-1-yl)ureido)methyl)benzyl)-1 H-pyrrole-2-carboxylate (**5f**)**.** Starting from Ethyl 1-(4-(aminomethyl)benzyl)-1 H-pyrrole-2-carboxylate (**4c**) 0.25 g (0.97 mmol, 1 eq). Yield: 0.3 g, 71.2 %. ^{1}H -NMR (DMSO-d_6): δ 7.09 (d, J = 8.6 Hz, 2H), 6.96 (s, 2H), 6.93 (d, J = 8.6 Hz, 2H), 6.86 (m, 1H), 6.06 (m, 1H), 5.44 (s, 2H), 4.1 (s, 2H), 4.08 (q, J = 7.2 Hz, 2H), 1.82-1.98 (m, 8H), 1.6 (m, 7H), and 1.16 (t, J = 7.1 Hz, 3H) ppm. ^{13}C-NMR (CH_3OH-d_4): δ 160.0, 157.0, 140.8, 139.3, 134.9, 130.8, 128.4, 126.6, 121.9, 120.2, 117.6, 109.8, 60.9, 52.5, 51.9, 46.9, 43.8, 42.7, 40.6, 37.4, 36.5, 31.6, 29 and 14.5 ppm. HRMS: measured m/z [M + H^+] 436.2585 (theoretical, 436.2595).

Ethyl 1-(2-((3-((4-(trifluoromethoxy)phenyl)ureido)methyl)benzyl)-1 H-pyrrole-2-carboxylate (**5g**). Starting from Ethyl 1-(2-(aminomethyl)benzyl)-1 H-pyrrole-2-carboxylate (**4a**) 0.25 g (0.97 mmol, 1 eq).Yield: 0.25 g, 56 %. ^{1}H-NMR (DMSO-d_6): δ 7.35 (d, J = 9.2 Hz, 2H), 7.27 (d, J = 7.3 Hz, 1H), 7.17-7.04 (m, 4H), 6.89 (d, J = 8.5 Hz, 2H), 6.4 (d, J = 7.3 Hz, 1H), 6.1 (s, 1H), 5.54 (s, 2H), 4.38 (s, 2H), 4.07 (q, J = 7.2 Hz, 2H), and 1.1 (t, J = 7.1 Hz, 3H) ppm. ^{13}C-NMR (CH_3OH-d_4): δ 160.2, 156.3, 155.1, 145.3, 140.1, 138.9, 134.7, 130.1, 127.5, 122.3, 120.5, 119.3, 114.5, 110.7, 109.2, 61.5, 52.4, 48.1, 45.5 and 14 ppm. HRMS: measured m/z [M + H^+] 462.1633 (theoretical, 462.1635).

Ethyl 1-(3-((3-((4-(trifluoromethoxy)phenyl)ureido)methyl)benzyl)-1 H-pyrrole-2-carboxylate (**5h**)**.** Starting from Ethyl 1-(3-(aminomethyl)benzyl)-1 H-pyrrole-2-carboxylate (**4b**) 0.25 g (0.97 mmol, 1 eq).Yield: 0.3 g, 67.2 %. ^{1}H -NMR (DMSO-d_6): δ 7.35 (d, J = 9.2 Hz, 2H), 7.19-7.04 (m, 4H), 6.97-6.94 (m, 2H), 6.89-6.83 (m, 2H), 6.04 (m, 1H), 5.48 (s, 2H), 4.27 (s, 2H), 4.07 (q, J = 7.2 Hz, 2H), and 1.1 (t, J = 7.2 Hz, 3H) ppm. ^{13}C-NMR (CH_3OH-d_4): δ 160, 156.7, 155.3, 146, 140.7, 139.1, 135.2, 131.1, 127.8, 122.7, 121.5, 119.6, 114.1, 110.5, 110.1, 61.1, 52.7, 48.3, 44.5 and 14.1 ppm. HRMS: measured m/z [M + H^+] 462.1634 (theoretical, 462.1635).

Ethyl 1-(4-((3-((4-(trifluoromethoxy)phenyl)ureido)methyl)benzyl)-1 H-pyrrole-2-carboxylate (**5i**). Starting from Ethyl 1-(4-(aminomethyl)benzyl)-1 H-pyrrole-2-carboxylate (**4c**) 0.25 g (0.97 mmol, 1 eq)**.** Yield: 0.3 g, 67.2 %. ^{1}H -NMR (DMSO-d_6): δ 7.33 (d, J = 9.2 Hz, 2H), 7.15 (d, J = 8.5 Hz, 2H), 7.05 (d, J = 8.5 Hz, 2H), 6.97-6.93 (m, 3H), 6.85 (m, 1H), 6.07 (m, 2H), 5.43 (s, 2H), 4.28 (s, 2H), 4.07 (q, J = 7.2 Hz, 2H) and 1.2 (t, J = 7.2 Hz, 3H) ppm. ^{13}C -NMR (CH_3OH-d_4): δ 160.1, 157.7, 154.3, 146.2, 140.1, 139.2, 134.9, 130.5, 128.7, 122.5, 121.3, 119.7, 114.5, 110.8, 109.2, 61, 52.5, 48.7, 44.3 and 14.8 ppm. HRMS: measured m/z [M + H^+] 462.1633 (theoretical, 462.1635).

Characterization of compounds 6b-i:

1-(3-((3-cyclohexylureido)methyl)benzyl)-1 H-pyrrole-2-carboxylic acid (**6b**)**.** Starting from Ethyl 1-(3-((3-cyclohexylureido)methyl)benzyl)-1 H-pyrrole-2-carboxylate (**5b**) 0.05 g (0.13 mmol, 1 eq). Yield: 25 mg, 50%. ^{1}H-NMR (CH_3OH-d_4): δ 7.16-7.03 (m, 2H), 6.93-6.91 (m, 2H), 6.88-6.84 (m, 2H), 6.07-6.04 (m, 1H), 5.49 (s, 2H), 4.14 (s, 2H), 3.38 (m 1H), 1.78 (m, 2H), 1.62 (m, 2H), 1.51 (m, 1H), and 1.16 (m, 5H) ppm. ^{13}C-NMR (CH_3OH-d_4): δ 160.1, 157.4, 137.3, 135.2, 130.6, 128.7, 126.8, 125.9, 120.1, 116.9, 109.8, 55.8, 52.9, 44.8, 34.2, 32.3, 27.1, 25.4 and 24.8 ppm. HRMS: measured m/z [M + H^+] 356.1964 (theoretical, 356.1969)

1-(4-((3-cyclohexylureido)methyl)benzyl)-1 H-pyrrole-2-carboxylic acid (**6c**). Starting from Ethyl 1-(4-((3-cyclohexylureido)methyl)benzyl)-1 H-pyrrole-2-carboxylate **(5c**) 0.05 g (0.13 mmol, 1 eq). Yield: 25 mg, 50 %. ^{1}H-NMR (CH_3OH-d_4): δ 7.23 (d, J = 8 Hz, 2H), 6.99 (d, J = 8 Hz, 2H), 6.92 (m, 1H) 6.88 (m, 1H), 6.04 (m, 1H), 5.45 (s, 2H), 4.15 (s, 2H), 3.38 (m 1H), 1.78 (m, 2H), 1.62 (m, 2H), 1.51 (m, 1H) and 1.16 (m, 5H) ppm. ^{13}C-NMR (CH_3OH-d_4): δ 160.1, 157.6, 137.5, 136, 130.3, 128.3, 126.7, 125.6, 119.7, 117.6, 109.5, 55.7, 52.4, 44.4, 33.9, 31.8, 26.8, 25.7 and 24.4 ppm. HRMS: measured m/z [M + H^+] 356.1967 (theoretical, 356.1969).

1-(2-((3-((3s,5s,7s)-adamantan-1-yl)ureido)methyl)benzyl)-1 H-pyrrole-2-carboxylic acid (**6d**)**.** Starting from Ethyl 1-(2-((3-((3s,5s,7s)-adamantan-1-yl)ureido)methyl)benzyl)-1 H-pyrrole-2-carboxylate (**5d**) 0.05 g (0.13 mmol, 1 eq). Yield: 29 mg, 98 %. ^{1}H-NMR (DMSO-d_6): δ 7-6.96 (m, 3H), 6.85-6.83 (m, 1H), 6.36 (d, J = 8.1 Hz, 1H), 6.09 (m, 1H), 5.53 (s, 2H), 4.27 (s, 2H), 1.82-1.97 (m, 8H) and 1.6 (m, 7H) ppm. ^{13}C-NMR (CH_3OH-d_4): δ 160.2, 157, 140.3, 139.4, 135.2, 130.7, 128.5, 126.2, 121.3, 118.3, 115.9, 109.7, 52.7 52.5, 47.6, 44.7, 42.7, 40.5, 37.6, 37.3, 32.3 and 29.1 ppm. HRMS: measured m/z [M + H^+] 408.2286 (theoretical, 408.2282).

1-(3-((3-((3s,5s,7s)-adamantan-1-yl)ureido)methyl)benzyl)-1 H-pyrrole-2-carboxylic acid (**6e**)**.** Starting from Ethyl 1-(3-((3-((3s,5s,7s)-adamantan-1-yl)ureido)methyl)benzyl)-1 H-pyrrole-2-carboxylate (**5e**) 0.05 g (0.13 mmol, 1 eq). Yield: 29 mg, 50 %. ^{1}H-NMR (DMSO-d_6): δ 7.15 (t, J = 7.6 Hz, 1H), 7.04 (d, , J = 8.2 Hz, 1H), 6.97-6.91 (m, 2H), 6.87-6.82 (m, 2H), 6.09-6.05 (m, 1H), 5.43 (s, 2H), 4.12 (s, 2H), 1.82-1.98 (m, 8H) and 1.6 (m, 7H) ppm. ^{13}C-NMR (CH_3OH-d_4): δ 160.1, 156, 140.6, 139.7, 135.1, 130.5, 128.7, 127.3, 122.3, 119.2, 116.8, 109.6, 52.9, 51.5, 47.6, 44.5, 41.7, 40.8, 37.7, 37.6, 32.6 and 28.9 ppm. HRMS: measured m/z [M + H^+] 408.2276 (theoretical, 408.2282).

1-(4-((3-((3s,5s,7s)-adamantan-1-yl)ureido)methyl)benzyl)-1 H-pyrrole-2-carboxylic acid (**6f**)**.** Starting from Ethyl 1-(4-((3-((3s,5s,7s)-adamantan-1-yl)ureido)methyl)benzyl)-1 H-pyrrole-2-carboxylate (**5f**) 0.05 g (0.13 mmol, 1 eq). Yield: 29 mg, 50 %. ^{1}H-NMR (DMSO-d_6): δ 7.09 (d, J = 8.6 Hz, 2H), 6.96 (s, 2H), 6.93 (d, J = 8.6 Hz, 2H), 6.88 (m, 1H), 6.07 (m, 1H), 5.44 (s, 2H), 4.1 (s, 2H), 1.82-1.98 (m, 8H) and 1.6 (m, 7H) ppm. ^{13}C-NMR (CH_3OH-d_4): δ 160, 157, 140.8, 139.3, 134.9, 130.8, 128.4, 126.6, 121.9, 120.2, 117.6, 109.8, 52.5, 51.9, 46.9, 43.8, 42.7, 40.6, 37.4, 36.5, 31.6 and 29 ppm. HRMS: measured m/z [M + H^+] 408.2283 (theoretical, 408.2282).

1-(2-((3-((4-(trifluoromethoxy)phenyl)ureido)methyl)benzyl)-1 H-pyrrole-2-carboxylate (**6g**). Starting from Ethyl 1-(2-((3-((4-(trifluoromethoxy)phenyl)ureido)methyl)benzyl)-1 H-pyrrole-2-carboxylate (**5g**) 0.05 g (0.13 mmol, 1 eq). Yield: 30 mg, 50 %. ^{1}H-NMR (DMSO-d_6): δ 7.35 (d, J = 9.2 Hz, 2H), 7.27 (d, J = 7.3 Hz, 1H), 7.1-7.02 (m, 4H), 6.89 (d, J = 8.5 Hz, 2H), 6.4 (d, J = 7.3 Hz, 1H), 6.11 (s, 1H), 5.6 (s, 2H) and 4.36 (s, 2H), ppm. ^{13}C-NMR (CH_3OH-d_4): δ 160.2, 156.3, 155.1, 145.3, 140.1, 138.9, 134.7, 130.1, 127.5, 122.3, 120.5, 119.3, 114.5, 110.7, 109.2, 52.4, 48.1 and 45.5 ppm. HRMS: measured m/z [M + H^+] 434.1315 (theoretical, 434.1322).

1-(3-((3-((4-(trifluoromethoxy)phenyl)ureido)methyl)benzyl)-1 H-pyrrole-2-carboxylic acid (**6h**). Starting from Ethyl 1-(3-((3-((4-(trifluoromethoxy)phenyl)ureido)methyl)benzyl)-1 H-pyrrole-2-carboxylate (**5h**) 0.05 g (0.13 mmol, 1 eq). Yield: 30 mg, 50 %. ^{1}H-NMR (DMSO-d_6): δ 7.36 (d, J = 9.2 Hz, 2H), 7.17-7.03 (m, 4H), 6.97-6.94 (m, 2H), 6.87-6.80 (m, 2H), 6.06 (m, 1H), 5.47 (s, 2H) and 4.24 (s, 2H) ppm. ^{13}C-NMR (CH_3OH-d_4): δ 160, 156.7, 155.3, 146, 140.7, 139.1, 135.2, 131.1, 127.8, 122.7, 121.5, 119.6, 114.1, 110.5, 110.1, 52.7, 48.3 and 44.5 ppm. HRMS: measured m/z [M + Na^+] 456.1143 (theoretical, 456.1142).

1-(4-((3-((4-(trifluoromethoxy)phenyl)ureido)methyl)benzyl)-1 H-pyrrole-2-carboxylic acid (**6i**)**.** Starting from Ethyl 1-(4-((3-((4-(trifluoromethoxy)phenyl)ureido)methyl)benzyl)-1 H-pyrrole-2-carboxylate (**5i**) 0.05 g (0.13 mmol, 1 eq). Yield: 30 mg, 50%. ^{1}H-NMR (DMSO-d_6): δ 7.33 (d, J = 9.2 Hz, 2H), 7.15 (d, J = 8.5 Hz, 2H), 7.05 (d, J = 8.5 Hz, 2H), 6.97-6.93 (m, 3H), 6.86 (m, 1H), 6.06 (m, 1H), 5.46 (s, 2H), 4.25 (s, 2H) and 1.2 (t, J = 7.2 Hz, 3H) ppm. ^{13}C-NMR (CH_3OH-d_4): δ 160.1, 157.7, 154.3, 146.2, 140.1, 139.2, 134.9, 130.5, 128.7, 122.5, 121.3, 119.7, 114.5, 110.8, 109.2, 52.5, 48.7 and 44.3 ppm. HRMS: measured m/z [M + H^+] 434.1312 (theoretical, 434.1322).

Appendix

5-LO inhibitors

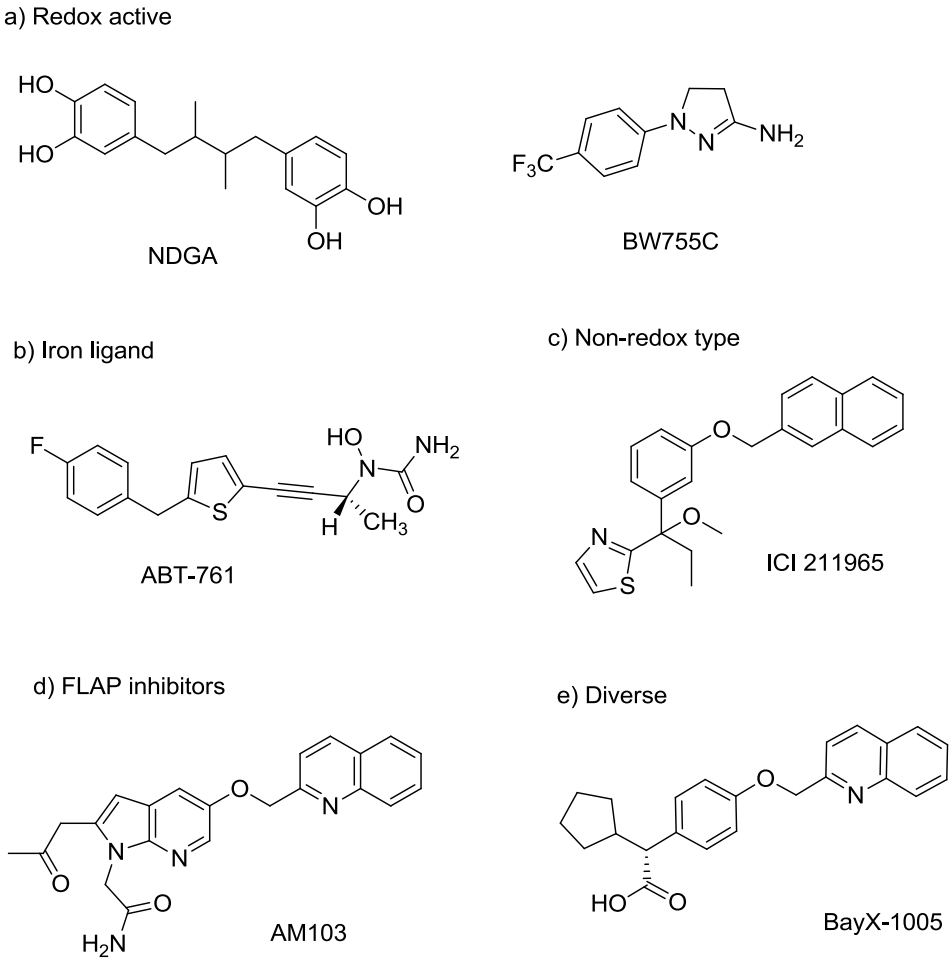

Figure 1. Chemical structures of 5-LO inhibitors.

Chemical synthesis

(*Z*)-4-bromobutyl 2-(5-fluoro-2-methyl-1-(4-(methylsulfinyl)benzylidene)-1*H*-inden-3-yl)acetate (**2**): Sulindac (**1**) (1 g, 2.8 mmol, 1 eq), potassium carbonate (0.57 g, 4.2 mmol, 1.5 eq), and 1-bromo-4-bromobutane (1 ml, 8.4 mmol, 3 eq) were dissolved in acetonitrile (15 ml) and heated to reflux during 3 h. The mixture is cooled and then filtered. The solvent from the mother liquor is evaporated under reduced pressure and dried over $MgSO_4$. The crude is purified by flash chromatography (Hex:EtOAc) obtaining a yellow solid (1.1 g, 53% yield). ^{1}H-NMR (DMSO-d_6, 250 MHz): δ 7.79 (d, J = 8.0 Hz, 2H), 7.70 (d, J= 8.0 Hz, 2H), 7.39 (s, 1H), 7.20 (q, J = 5.7 Hz, 1H), 7.04 (dd, J_1 = 2.9 Hz, J_2 = 9.7 Hz, 1H), 6.76 (dt, J_1 = 2.3 Hz, J_2 = 8.6 Hz, 1H), 4.09 (t, J = 6.4 Hz,

2 H), 3.67 (s, 2H), 3.52 (t, *J* = 8.0 Hz, 2H), 2.80 (s, 3H), 2.15 (s, 3H), 1.83-1.65 (m, 4H). MS (ESI, 70 eV) *m/z* = 493.6 ($M+H^+$).

(*Z*)-4-(nitrooxy)butyl 2-(5-fluoro-2-methyl-1-(4-(methylsulfinyl)benzylidene)-1*H*-inden-3-yl)acetate (**3**): (*Z*)-4-bromobutyl 2-(5-fluoro-2-methyl-1-(4-(methylsulfinyl)benzylidene)-1*H*-inden-3-yl)acetate (**2**) (0.25 g, 0.50 mmol, 1 eq) and silver nitrate (0.17 g, 1.07 mmol, 2 eq) were solved in 10 ml of acetonitrile and heated to 85°C for 48 h. The mixture was filtered off and the solvent removed under reduced pressure. The crude was purified by flash chromatograpy (Hex:EtOAc), a yellow solid is obtained (0.20 g, 83% yield). ^{1}H-NMR (DMSO-d_6, 250 MHz): δ 7.87 (d, *J* = 7.4 Hz, 2H), 7.80 (d, *J* = 8.9 Hz, 2H), 7.46 (s, 1H), 7.29 (q, *J* = 4.4 Hz, 1H), 7.11 (dd, J_1 = 4.4 Hz, J_2 = 8.9 Hz, 1H), 6.84 (dt, J_1 = 2.9 Hz, J_2 = 8.1 Hz, 1H), 4.54 (t, *J* = 5.7 Hz, 2H), 4.14 (t, *J* = 5.9 Hz, 2H), 3.74 (s, 2H), 2.90 (s, 3H), 2.23 (s, 3H), 1.75 (m, 4H). ^{13}C-NMR (DMSO-d_6, 63 MHz): δ 169.9, 164.5, 160.7, 146.3, 140.3, 138.4, 131.8, 131.8, 130.3, 129.1, 124.3, 123.2, 110.3, 105.7, 73.1, 63.8, 43.2, 31.1, 24.6, 22.7, 10.5. MS (ESI, 70 eV) *m/z* = 474.6 ($M+H^+$). HRMS calcd. $C_{24}H_{24}FNO_6S$ 473.13084, found 477.13861.

(*S*)-4-bromobutyl 2-(6-methoxynaphthalen-2-yl)propanoate (**5**):

Naproxen (**4**) (1.50 g, 6.5 mmol, 1 eq), potassium carbonate (1.08 g, 7.8 mmol, 2 eq), and 1-bromo-4-bromobutane (3.9 ml, 32.6 mmol, 5 eq) were dissolved in acetonitrile (20 ml) and heated to reflux during 3 h. The mixture is cooled and then filtered. The solvent from the mother liquor is evaporated under reduced pressure and dried over $MgSO_4$. The crude is purified by flash chromatography (Hex:EtOAc) obtaining a colorless oil (1.2 g, 50% yield). ^{1}H-NMR (DMSO-d_6, 250 MHz): δ 7.81 (q, *J* = 6.2 Hz, 2H), 7.74 (s, 1H), 7.39 (dd, J_1 = 2.8 Hz, J_2 = 8.2 Hz, 1H), 7.27 (d, *J* = 3.3 Hz, 1H), 7.16 (dd, J_1 = 2.5 Hz, J_2 = 9.4 Hz, 1H), 4.08 (t, *J* = 5.8 Hz, 2H), 3.93 (q, *J* = 6.9 Hz, 1H), 3.89 (s, 3H), 3.47 (t, *J* = 6.5 Hz, 2H), 1.75-1.58 (m, 4H), 1.48-1.44 (d, *J* = 7.8 Hz, 3H). MS (ESI, 70 eV) *m/z* = 389.4 ($M+Na^+$).

(*S*)-4-(nitrooxy)butyl 2-(6-methoxynaphthalen-2-yl)propanoate (**6**):

(*S*)-4-bromobutyl 2-(6-methoxynaphthalen-2-yl)propanoate (**5**) (0.25 g, 0.68 mmol, 1 eq) and silver nitrate (0.23 g, 1.37 mmol, 2 eq) were solved in 10 ml of acetonitrile and heated to 85°C for 17 h. The mixture was filtered off and the solvent removed under reduced pressure. The crude was purified by flash chromatograpy (Hex:EtOAc), a colorless oil is obtained (0.20 g, 84% yield). ^{1}H-NMR (DMSO-d_6, 250 MHz): δ ^{1}H-NMR (MeOD-d_4, 250 MHz): δ 7.83 (q, *J* = 4.7 Hz, 2H), 7.72 (s, 1H), 7.41 (dd, J_1 = 3.0 Hz, J_2 = 9.0 Hz, 1H), 7.30 (d, *J* = 2.6 Hz, 1H), 7.15 (dd, J_1 = 3.4 Hz, J_2 = 9.0 Hz, 1H), 4.43 (m,

2H), 4.07 (m, 2H), 3.96 (q, *J* = 8.5 Hz, 1H), 3.89 (s, 3H), 1.63-1.59 (m, 4H), 1.56-1.46 (d, *J* = 7.8 Hz, 3H). ^{13}C-NMR (DMSO-d_6, 63 MHz): δ 173.8, 157.0, 135.8, 133.1, 129.2, 128.2, 126.9, 126.0, 118.4, 105.3, 72.9, 63.2, 55.2, 44.4, 24.6, 22.8, 17.8. MS (ESI, 70 eV) *m/z* = 370.4 ($M+Na^+$). HRMS calcd. $C_{18}H_{21}NO_6$ 347.13689, found 347.13641.

4-(3-bromophenyl)tetrahydro-2*H*-pyran-4-carbonitrile (**8**):

3-bromophenylacetonitrile (**7**) (5.00 g, 25.5 mmol, 1 eq) and sodium hydroxide 40% (47 ml, 25.5 mmol) were stirred in THF (30 ml) to give a brown suspension. To the mixture, tetrabutylammonium hydrogen sulfate (TBAHS) (0.9 ml, 2.68 mmol, 0.1 eq) were added and set for boiling at reflux during 30 min. Later, 2-chloroethylether (3.00 ml, 25,5 mmol, 1 eq) were added dropwise. The reaction mixture was heated under reflux for 4h and then cooled. The mixture was diluted with EtOAc (40 ml), washed with 5% HCl (3 x 20 ml), water (2 x 20 ml) and saturated $NaHCO_3$ (2 x 30 ml). After drying the organic phase over $MgSO_4$, the solvent was removed under reduced pressure to provide the crude as a waxy solid. The solid was purified in a mixture of 1:1 isopropyl ether and hexanes (10 x 10 ml) to provide the desired product as a red crystal (3.85 g, 56% yield). ^{1}H-NMR (DMSO-d_6, 250 MHz): δ 7.74 (s, 1H), 7.63-7.55 (m, 2H), 7.44 (t, *J* = 8.4 Hz, 1H), 4.02 (m, 2H), 3.66 (dt, J_1 = 3.4, J_2 = 11.1 Hz, 2H), 2.17-2.02 (m, 4H). MS (ESI, 70 eV) *m/z* = 267.1 ($M+H^+$).

4-(3-bromophenyl)tetrahydro-2*H*-pyran-4-carboxamide (**9**):

4-(3-bromophenyl)tetrahydro-2*H*-pyran-4-carbonitrile (**8**) (3.85 g, 14.5 mmol, 1 eq) was stirred in sulfuric acid (12 ml) at room temperature for 48 h. The mixture was then poured onto ice and the very fine suspension was filtered and washed with water thoroughly until pH of wash is neutral. The white solid was washed with hexanes and was dried under vacuum to give a yellow solid (3.2 g, 78% yield). ^{1}H-NMR (DMSO-d_6, 250 MHz): δ 7.58 (s, 1H), 7.53-7.50 (t, *J* = 7.6 Hz, 2H), 7.46-7.37 (t, *J* = 6.2 Hz, 2H), 7.34 (s, 1H), 7.14 (s, 1H), 3.82-3.78 (m, 2H), 3.58-3.52 (m, 2H), 2.50-2.45 (m, 2H), 1.88-1.79 (m, 2H). MS (ESI, 70 eV) *m/z* = 284.3 ($M+H^+$).

4-(3-((4-fluorophenyl)thio)phenyl)tetrahydro-2*H*-pyran-4-carboxamide (**12**):

Butan-1-ol (30 ml), 4-(3-bromophenyl)tetrahydro-2*H*-pyran-4-carboxamide (**9**) (3.20 g, 11.3 mmol, 1 eq), potassium t-butoxide (2.53 g, 22.5 mmol, 2 eq), water (0.4 ml, 22.5

mmol, 2 eq), tetrakis(triphenylphosphine) palladium(0) (0.26 g, 0.22 mmol, 0.02 eq) and 4-fluorothiophenol (1.2 ml, 11.3 mmol, 2 eq) (**10**) were added to a reaction flask and set for boiling (100°C) at reflux under a nitrogen atmosphere during 8h. The reaction mixture was cooled to ambient temperature and butan-1-ol (20 ml) was added to obtain a slurry. The crude product was isolated by filtration and washed with butan-1-ol (20 ml) and sucked dry. The crude product was dissolved in methanol (20 ml) and treated with 50 mg activated carbon and heated at 60°C during 20 min. The mixture was hot filtrated through Celite ® and washed with hot methanol (20 ml). The solvent removed under reduced pressure (until 4 ml were left) and crystal formation succeeded at 4°C during 24 h. ^{1}H-NMR (DMSO-d_6, 300 MHz): δ 7.51-7.25 (m, 8H), 7.09 (m, 2H), 3.76-3.71 (m, 2H), 3.48 (m, 2H), 2.43-2.37 (m, 2H), 1.82-1.71 (m, 2H). ^{19}F-NMR (DMSO-d_6, 282 MHz): δ -113.6. MS (ESI, 70 eV) *m/z* = 370.2 ($M+K^+$).

4-(3-((4-(2-methyl-1*H*-imidazol-1-yl)phenyl)thio)phenyl)tetrahydro-2*H*-pyran-4-carboxamide (**13**):

4-(3-((4-fluorophenyl)thio)phenyl)tetrahydro-2*H*-pyran-4-carboxamide (**11**) (2.45 g, 7.4 mmol, 1 eq), 2-methyl-1*H*-imidazole (**12**) (1.2 g, 14.8 mmol, 2 eq), and cesium carbonate (4.83 g, 14.8 mmol, 2 eq) in DMSO (25 ml) were added to a reaction flask set for boiling at reflux (130°C) under nitrogen atmosphere during 20h. After the reaction was completed, it was cooled and quenched with water (25 ml), which resulted in formation of a precipitate. The product was isolated by vacuum filtration and washed with water (7x 10ml). The product was lyophilized and purified on LC-MS. 100 mg of a white solid were obtained (5% yield).

^{1}H-NMR (MeOD-d_4, 250 MHz): δ 7.56 (s, 1H), 7.46-7.34 (m, 6H), 7.20 (s, 1H), 6.99 (s, 1H), 3.87-3.79 (m, 2H), 3.73-3.63 (m, 2H), 2.48-2.44 (m, 2H), 2.36 (s, 3H), 2.05-1.95 (m, 2H). ^{13}C-NMR (MeOD-d_4, 63 MHz): δ 146.8, 146.1, 139.4, 137.9, 135.9, 132.4, 132.0, 131.7, 131.2, 130.8, 128.1, 127.2, 126.8, 122.6, 66.2, 35.7, 13.7. MS (ESI, 70 eV) *m/z* = 395.37 ($M+H^+$). t_R = 12.91 min (>95% pure).

4-(4-(hydroxymethyl)piperidin-1-yl)benzaldehyde (**16**):

In a round-bottomed flask were 4-fluorobenzaldehyde (**14**) (0.500 g, 4.03 mmol,1 eq), piperidin-4-ylmethanol (**15**) (0.557 g, 4.83 mmol, 1.2 eq), and cesium carbonate (1.313 g, 4.03 mmol, 1 eq) solved in DMF (10 ml) and the mixture was heated up to 110ºC during 23 h. The solvent is removed under reduced pressure and the residue taken up in ethyl acetate (50 ml) and washed with HCl 10% (3x20 ml); the organic phase was

dried over $MgSO_4$ and the crude purified by flash chromatography (hexane/ethyl acetate 0 → 80%) a red solid is obtained 1.3 g (73% yield).^{1}H NMR (250 MHz, DMSO-d_6): 9.68 (s, 1H), 7.68 (d, *J*=8.9 Hz, 2H), 7.02 (d, *J*=8.9 Hz, 2H), 4.50 (t, *J*=5.29 Hz, 1H), 4.01 (d, *J*=13.1 Hz, 2H), 3.28 (t, *J*=5.6 Hz, 2H), 2.89 (m, 2H), 1.68 (m, 3H), 1.17 (m, 2H). MS (ESI, 70 eV) m/z (%): 217.8 (100), 199.6 (71), 187.8 (16.6).

(1-(4-(3-(cyclohexylamino)-6-methylimidazo[1,2-*a*]pyridin-2-yl)phenyl)piperidin-4-yl)methanol (**19**, EB82):

In a round-bottom flask 4-(4-(hydroxymethyl)piperidin-1-yl)benzaldehyde (**16**) (1.000 g, 4.56 mmol, 1 eq), *N*-cyclohexylisonitrile (**18**) (0.567 ml, 4.56 mmol, 1 eq), and 5-methylpyridin-2-amine (**17**) (0.592 g, 5.47 mmol, 1.2 eq) in MeOH (10 ml) to give a yellow solution. Glacial acetic acid (0.261 ml, 4.56 mmol, 1 eq) was added and the reaction mixture stirred at rt o/n. The solvent was removed under reduced pressure and ethyl acetate was added (30 ml) and washed with (3x20 ml) $NaHCO_3$. A precipitated appeared and was kept, the organic phase was dried over $MgSO_4$ and the solvent reduced under reduced pressure to obtain a green solid obtained. The crude was purified by recrystallization from EtOH yielding 300 mg of a red solid (52% yield). ^{1}H NMR (250 MHz, DMSO-d_6): 8.12 (m, 3H), 7.40 (d, *J*=20.7 Hz, 1H), 7.04-7.02 (m, 3H), 4.64 (d, *J*=3.3 Hz, 1H), 4.54 (t, *J*=4.0 Hz, 1H), 3.88 (d, *J*= 16.9 Hz, 2H), 3.30 (t, *J*=5.6 Hz, 2H), 2.91 (m, 1H), 2.80 (t, *J*=12.7 Hz, 2H), 2.39 (s, 3H), 1.86-1.58 (m, 8H), 1.41-1.18 (m, 7H). ^{13}C-NMR (63 MHz, DMSO-d_6): 158.2, 150.2, 146.8, 139.7, 137.6, 135.7, 127.5, 124.0, 120.1, 115.0, 107.1, 65.6, 55.8, 48.4, 33.3, 28.3, 25.9, 17.2, 17.0. MS (ESI, 70 eV) m/z (%): 418.57 (100) (M+). Anal. Calcd for $C_{26}H_{34}N_4O$·0.5 HCl: C, 71.22, H, 7.98, N, 12.67. Found: C, 71.37, H, 7.98, N, 12.84.

1-(2,5-dimethylphenyl)-4,4,4-trifluorobutane-1,3-dione (**21**):

1-(2,5-dimethylphenyl)ethanone (**19**) (1.506 ml, 10.12 mmol, 1 eq) in MeOH (12 ml) to give a colorless solution. Sodium methoxide (24.29 ml, 12.15 mmol, 1.2 eq) was added and the mixture and stirred for 5 min, and then ethyl 2,2,2-trifluoroacetate (**20**) (1.208 ml, 10.12 mmol, 1 eq) was added. After refluxing for 24 h, the mixture was cooled at rt. 10% HCl (10 ml) was added to the mixture, and then extracted with EtOAc (20 ml), washed with brine and dried over $MgSO_4$. The crude was used without further purification (red oil, 1.3 g, 53%).

4-(5-(2,5-dimethylphenyl)-3-(trifluoromethyl)-1H-pyrazol-1-yl)benzenesulfonamide (**23**, DMC)

1-(2,5-dimethylphenyl)-4,4,4-trifluorobutane-1,3-dione (**21**) (1 g, 4.09 mmol, 1 eq) were solved in EtOH (15 ml) to give a colorless solution. 4-hydrazinylbenzenesulfonamide-HCl (**22**) (0.916 g, 4.09 mmol, 1 eq) was added. The mixture is stirred and refluxed for 20 h. After cooling at rt, the mixture was concentrated *in vacuo*. The residue was dissolved in EtOAc (20 ml) and washed with water (10 ml), brine (15 ml) and dried over $MgSO_4$. The crude was purified by flash chromatography (Hex/EtOAc) yielding a white solid (538 mg, 33% yield).

^{1}H-NMR (250 MHz, DMSO-d_6): δ 7.88 (d, *J*=8.2 Hz, 2H), 7.53-7.49 (m, 4H), 7.26-7.16 (m, 4H), 3.37 (s, 1H), 2.30 (s, 3H), 1.95 (s, 3H). ^{13}C-NMR (250 MHz, DMSO-d_6): δ 143.4, 142.4, 141.8, 141.1, 135.3, 133.6, 131.3, 130.8, 130.3, 128.1, 126.7, 124.6, 123.6, 119.0, 107.3, 20.4, 18.9. MS (ESI, 70 eV) *m/z* (%): 395.17 (100) (M+). Anal. Calcd for $C_{18}H_{16}F_3N_3O_2S$: C, 54.68, H, 4.08, N, 10.63, S, 8.11; found, C, 54.75, H, 4.22, N, 10.39, S, 8.06.

4,4,4-trifluoro-1-(*p*-tolyl)butane-1,3-dione (**24**):

1-(*p*-tolyl)ethanone (1.493 ml, 11.18 mmol, 1 eq) (**24**) was dissolved in MeOH (12 ml) to give a colorless solution. Sodium methoxide (26.8 ml, 13.42 mmol, 1.2 eq) was added and stirred for 5 min. Afterwards, ethyl 2,2,2-trifluoroacetate (1.335 ml, 11.18 mmol, 1 eq) (**20**) was added and refluxed during 24h. After cooling to rt, 10% HCl (10 ml) was added and extracted with EtOAc (10 ml) and washed with brine (15 ml). The crude was used without further purification.

4-(5-(*p*-tolyl)-3-(trifluoromethyl)-1H-pyrazol-1-yl)benzenesulfonamide, HCl (**25**, Cele)

4,4,4-trifluoro-1-(*p*-tolyl)butane-1,3-dione (1 g, 4.34 mmol) was disolved in EtOH (15 ml) to give a colorless solution. 4-hydrazinylbenzenesulfonamide-HCl (**22**) (0.972 g, 4.34 mmol) was added and the mixture was refluxed for 20 h. After cooling to rt, the mixture was concentrated *in vacuo*. The residue was dissolved in EtOAc (20 ml) and washed with water (10 ml), brine (15 ml) and dried over $MgSO_4$. The crude was purified by flash chromatography (Hex/EtOAc) and the obtained fraction was recrystallized from isooctane/EtOAc obtaining a white solid (151 mg, 8%).

^{1}H-NMR (250 MHz, DMSO-d_6): δ 7.91 (d, *J*=8.8 Hz, 2H), 7.58-7.54 (m, 3H), 7.23 (m, 4H), 2.34 (s, 3H). ^{13}C-NMR (250 MHz, DMSO-d_6): δ 147.4, 145.2, 143.4, 141.1, 130.8, 130.2, 128.4, 127.3, 126.9, 106.7, 21.3. MS (ESI, 70 eV) *m/z* (%): 380.3 (100) (M+). Anal. Calcd. for $C_{17}H_{14}F_3N_3O_2S$: C, 52.78, H, 3.69, N, 10.86, S, 8.29; found, C, 52.88, H, 3.60, N, 10.68, S, 8.34.

(*E*)-1-(2,5-dimethylphenyl)-3-hydroxy-3-methoxyprop-2-en-1-one (**27**):

NaH (0.89 g, 22 mmol, 1.1 eq) is solved in 25 ml absolut THF under argon atmosphere and 2,5-dimethylacetophenone (**19**) (3 g, 20 mmol, 1 eq) was added at 0°C. After 30 min stirring, a solution of THF (10 ml) and dimethyloxalate (**26**) (2.4 g, 20 mmol, 1 eq) was added. The mixture is stirred for 16 h in ultrasound bath at 45°C. The solution was cooled and to the suspension 75 ml 10% HCl were added and stirred for 1h. Eventually the solution was cooled at 0°C for 3h but no solid precipitated. THF is removed under reduced pressure and EtOAc is added to extract organic phase (3x50 ml). The organic layer is dried over $MgSO_4$. The crude product was added to a silica gel column and was eluted with EtOAc:Hex (1:2). Collected fractions were a mixture of both tautomers (3 g, 72% yield) and were used without further purification.

Methyl 5-(2,5-dimethylphenyl)-1-(4-sulfamoylphenyl)-1H-pyrazole-3-carboxylate (**28**):

In 20 ml MeOH, (*E*)-1-(2,5-dimethylphenyl)-3-hydroxy-3-methoxyprop-2-en-1-one (**27**) (1 g, 4.85 mmol, 1 eq) and 4-hydrazinylbenzenesulfonamide-HCl (**22**) (1.19 g, 5.23 mmol, 1.1 eq) were refluxed during 4h and cooled down. For 30 min the crude was stirred at 0°C, but no precipitated was obtained. MeOH was removed under reduced pressure and the organic layer was extracted with EtOAc (20 ml) and washed with brine (10 ml). The crude was purified by column chromatography with 1:1 EE/Hex as eluent obtaining a yellow solid (0.93 g, 53%).

^{1}H-NMR (250 MHz, MeOD): δ 7.87 (d, *J*=8.7 Hz, 2H), 7.47 (d, *J*=8.8 Hz, 2H), 7.13-7.11 (m, 3H), 6.96 (s, 1H), 3.96 (s, 3H), 2.30 (s, 3H), 2.02 (s, 3H). MS (ESI, 70 eV) *m/z* (%): 386.2 (100) (M+).

4-(5-(2,5-dimethylphenyl)-3-(hydroxymethyl)-1H-pyrazol-1-yl)benzenesulfonamide (**29**, DMC-OH):

Lithium aluminum hydride (3.89 ml, 7.78 mmol, 3 eq) was in THF (50 ml) dissolved to give a colorless suspension. The solution was cooled to 0°C and methyl 5-(2,5-dimethylphenyl)-1-(4-sulfamoylphenyl)-1H-pyrazole-3-carboxylate (**28**) (1.0 g, 2.59 mmol, 1 eq) in 5 ml THF was added. Eventually the reaction was stirred for 4h at room temperature. The reaction is quenched with water on an ice bath and after bubbles formation HCl concentrated was added until the solid is solved and the organic phase is extracted with EtOAc (20 ml). Eventually the crude is purified by column chromatography (EtOAc/MeOH 0→5%) to obtain 0.3928 g (42% yield).

^{1}H-NMR (250 MHz, DMSO-d_6): δ 7.77 (d, J=8.9 Hz, 2H), 7.39-7.32 (m, 4H), 7.18 (s, 2H), 7.09 (s, 1H), 6.50 (s, 1H), 5.29 (t, J=5.8 Hz, 1H), 4.58 (d, J=4.6 Hz, 2H), 2.28 (s, 3H), 2.00 (s, 3H). ^{13}C-NMR (250 MHz, DMSO-d_6):154.5, 142.8, 142.2, 141.8, 135.2, 133.1, 130.6, 130.3, 130.1, 129.9, 126.7, 126.5, 122.8, 108.2, 59.7, 57.2, 21.5, 20.4, 18.9. MS (ESI, 70 eV) *m/z* (%): 358.2 (100) (M+). Anal. Calcd. for $C_{18}H_{19}N_3O_3S$ calcd. C, 60.49, H, 5.36, N, 11.76, S, 8.97; found, C, 60.15, H, 5.56, N, 11.30, S, 8.78.

(2,2-dimethyl-1,3-dioxolan-4-yl)methanamine (**32**):

3-amino-1,2-propandiol (**30**) (3.64 g, 40.0 mmol, 1 eq) in water (10 ml) to give a yellow solution. Then 35% HCl is added until pH 1-2 is reached, and the mixture is stirred at rt for 15 minutes. The solvent is evaporated up to dryness. A suspension of the resultant residue is made in 2,2-dimethoxypropane (**31**) (24.77 ml, 200 mmol, 5 eq). *p*-toluenesulfonic anhydride (0.326 g, 0.999 mmol, 0.02 eq) was added and the mixture vigorously stirred under reflux for half an hour. The precipitated solid is filtered, washed with acetone (20 ml) and dried *in vacuo*. A mixture of R/S enantiomers are obtained 6.39 g (95% yield).

^{1}H-NMR (250 MHz, DMSO-d_6): δ 8.35 (s, br, 2H), 4.36-4.27 (q, J=6.56, 1H), 4.04-3.99 (dd, J_1= 5.5 Hz, J_2=8.7 Hz, 1H), 3.79-3.74 (dd, J_1= 5.6 Hz, J_2=8.7 Hz, 1H), 2.98-2.91 (dd, J_1= 4.5 Hz, J_2=12.7 Hz, 1H), 2.82-2.75 (dd, J_1= 7.4 Hz, J_2=12.7 Hz, 1H), 1.35 (s, 3H), 1.28 (s, 3H). MS (ESI, 70 eV) *m/z* (%): 132.2 (100) (M+).

1-(4-chlorophenyl)-3-((2,2-dimethyl-1,3-dioxolan-4-yl)methyl)urea (**34**):

(2,2-dimethyl-1,3-dioxolan-4-yl)methanamine (**32**) (0.200 g, 1.193 mmol, 1 eq) and triethylamine (0.335 ml, 2.386 mmol, 2 eq) were dissolved in DCM (5 ml) to give a white suspension. The mixture is stirred for 1h until it becomes clear and 4-chlorophenylisocyanate (**33**) (0.183 g, 1.193 mmol, 1 eq) was added. The mixture is stirred o/n at rt. The solvent is removed under reduced pressure and the crude purified by flash chromatography (Hex/EE) to yield a mixture of R/S enantiomers (269 mg, 79%)

^{1}H-NMR (250 MHz, DMSO-d_6): δ 8.77 (s, br, 1H), 7.48 (d, J= 8.8 Hz, 2H), 7.32 (d, J=8.9 Hz, 2H), 6.32 (m, 1H), 4.22 (m, 1H), 4.08 (m, 1H), 3.70 (m, 1H), 3.27 (m, 2H), 1.43 (s, 3H), 1.31 (s, 3H). MS (ESI, 70 eV) *m/z* (%): 285.0 (100) (M+).

1-(4-chlorophenyl)-3-(2,3-dihydroxypropyl)urea (**35**, EB72):

1-(4-chlorophenyl)-3-((2,2-dimethyl-1,3-dioxolan-4-yl)methyl)urea (**34**) (0.240 g, 0.843 mmol, 1 eq) was dissolved in 1,4-dioxane (5 ml) to give a colorless solution. HCl 10% (5 ml) was added and the reaction mixture was stirred o/n at rt. The reaction is followed by TLC and the solvent is removed under reduced pressure to yield a slightly yellow powder: 160 mg, (78% yield).

^{1}H-NMR (250 MHz, MeOD): *δ* 7.29 (d, *J*=8.7 Hz, 2H), 7.14 (d, *J*=8.8 Hz, 2H). 3.64 (m, 1H), 3.45 (d, *J*=5.0 Hz, 2H), 3.29 (m, 1H), 3.08 (m, 1H). ^{13}C-NMR (250 MHz, MeOD): *δ* 155.8, 139.7, 128.8, 124.1, 119.2, 70.9, 63.5, 42.3. MS (ESI, 70 eV) *m/z* (%): 244.7 (100) (M+). Anal. Calcd. for $C_{10}H_{13}ClN_2O_3$.0.20 HCl calcd. C, 47.67, H, 5.28, N, 11.12; found, C, 47.82, H, 5.14, N, 10.92

1-(2,2-dimethyl-1,3-dioxolan-4-yl)-*N*-(3-methoxy-4-((4-(trifluoromethyl)benzyl)oxy)-benzyl) methanamine (**37**):

RC3 (**36**) (0.280 g, 0.904 mmol, 1.01 eq) and (2,2-dimethyl-1,3-dioxolan-4-yl)methanamine (**32**) (0.150 g, 0.895 mmol, 1 eq) were dissolved in 1,2-dichloroethane (10 ml) to give a colorless suspension. Sodium triacetoxyborohydride (0.284 g, 1.342 mmol, 1.5 eq) was added and the reaction stirred o/n at rt. The reaction was quenched with $NaHCO_3$ and washed with brine (2 x 20 ml). The organic layer was dried over $MgSO_4$. The solvent was removed under reduced pressure and the residue solved in EtOAc (5 ml) and precipitated with oxalic acid. The solid was filtered off and dried obtaining a white powder 379 mg, 82% yield.

^{1}H-NMR (250 MHz, DMSO-d_6): *δ* 7.80-7.66 (m, 4H), 7.23 (s, 1H), 7.06-6.96 (m, 2H), 5.24 (s, 2H), 4.11 (s, 2H), 3.82 (s, 3H), 3.71 (m, 2H), 3.10 (m, 2H), 3.03 (m, 1H), 2.89 (m, 1H), 1.37 (s, 3H), 1.30 (s, 3H). MS (ESI, 70 eV) *m/z* (%): 426.6 (100) (M+).

3-((3-methoxy-4-((4-(trifluoromethyl)benzyl)oxy)benzyl)amino)propane-1,2-diol (**38**, EB143):

1-(2,2-dimethyl-1,3-dioxolan-4-yl)-*N*-(3-methoxy-4-((4-(trifluoromethyl)benzyl)oxy)benzyl) methanamine (**37**) (0.435 g, 0.844 mmol) and HCl concentrated (11.64 ml) in THF (10 mL) to give a colorless solution. The reaction mixture was stirred o/n at rt. The solvent is removed under reduced pressure and recrystallized from Hex/EtOAc 4:1.

^{1}H-NMR (250 MHz, MeOD): δ 7.57 (m, 4H), 7.11 (s, 1H), 6.95 (m, 2H), 5.12 (s, 2H), 4.09 (s, 2H), 3.82 (s, 3H), 3.50 (m, 2H), 3.20 (m, 2H), 3.03 (m, 1H), 2.89 (m, 1H). ^{13}C-NMR (250 MHz, MeOD): δ 151.7, 150.4, 143.2, 131.4, 130.6, 128.9, 126.4, 125.8, 124.0, 115.9, 114.9, 71.0, 68.2, 65.3, 56.9, 52.4, 50.7. MS (ESI, 70 eV) *m/z* (%): 386.4 (100) (M+). Anal. Calc. for $C_{19}H_{22}F_3NO_4$.1.65 HCl calcd. C, 51.22, H, 5.35, N, 3.14; found, C, 51.27, H, 5.26, N, 2.97.